Dissecting the role of ataxin-3 isoforms for the pathogenesis of Machado Joseph disease

Dissertation

zur Erlangung des Grades eines
Doktors der Naturwissenschaften

der Mathematisch-Naturwissenschaftlichen Fakultät
und
der Medizinischen Fakultät
der Eberhard-Karls-Universität Tübingen

vorgelegt
von

Daniel Weishäupl
aus Albstadt, Deutschland

2024

Tag der mündlichen Prüfung:	11.10.2023
Dekan der Math.-Nat. Fakultät:	Prof. Dr. Thilo Stehle
Dekan der Medizinischen Fakultät:	Prof. Dr. Bernd Pichler
1. Berichterstatter:	PD Dr. Thorsten Schmidt
2. Berichterstatter:	Prof. Dr. Ludger Schöls
Prüfungskommission:	PD Dr. Thorsten Schmidt
	Prof. Dr. Ludger Schöls
	Prof. Dr. Olaf Rieß
	Prof. Dr. Bernd Wissinger

Erklärung / Declaration:

Ich erkläre, dass ich die zur Promotion eingereichte Arbeit mit dem Titel: „Dissecting the role of ataxin-3 isoforms for the pathogenesis of Machado Joseph disease“ selbständig verfasst, nur die angegebenen Quellen und Hilfsmittel benutzt und wörtlich oder inhaltlich übernommene Stellen als solche gekennzeichnet habe. Ich versichere an Eides statt, dass diese Angaben wahr sind und dass ich nichts verschwiegen habe. Mir ist bekannt, dass die falsche Abgabe einer Versicherung an Eides statt mit Freiheitsstrafe bis zu drei Jahren oder mit Geldstrafe bestraft wird.

I hereby declare that I have produced the work entitled “Dissecting the role of ataxin-3 isoforms for the pathogenesis of Machado Joseph disease”, submitted for the award of a doctorate, on my own (without external help), have used only the sources and aids indicated and have marked passages included from other works, whether verbatim or in content, as such. I swear upon oath that these statements are true and that I have not concealed anything. I am aware that making a false declaration under oath is punishable by a term of imprisonment of up to three years or by a fine.

Tübingen, den ....

Datum / Date Unterschrift /Signature

Für meine Familie.

Der einzige Mensch, der sich vernünftig benimmt, ist mein Schneider.
Er nimmt jedes Mal neu Maß, wenn er mich trifft,
während alle anderen immer die alten Maßstäbe anlegen
in der Meinung, sie passten auch heute noch.

George Bernard Shaw (1856-1950)

Statement of Contributions

This section describes the personal contribution and the contribution of colleagues directly related to this dissertation.

Daniel Weishäupl is the main investigator of this whole thesis. He wrote the dissertation and designed and performed most experiments described. He analyzed data, developed required code/scripts for the analysis, visualized and interpreted the results. Individual experiments were performed in collaboration with other institutes or by students under direct supervision by Daniel Weishäupl as specified below.

Collaboration partners in the course of this project were:

German Center for Neurodegenerative Diseases (DZNE), Tübingen, Germany
Christian Johannes Gloeckner designed the interaction study, performed data processing and assisted data analysis and interpretation regarding mass spectrometry experiments for ataxin-3 interaction. Felix von Zweydorf assisted with the pulldown experiments and performed the associated mass spectrometry analysis of the ataxin-3 interaction partners (Figure 4.10).

Medizinisch-Naturwissenschaftliches Forschungszentrum, Tübingen, Germany
Hubert Kalbacher and his staff supported the generation of isoform-specific antibodies by synthesizing peptides and facilitating the immunization of rabbits and the (joint) purification of peptides and antibodies. Further, his team performed initial enzyme linked immunosorbent assay experiments to monitor the immunization process (Figure 4.25 - 4.27).

National University of Singapore, Singapore, Singapore
Christoph Winkler supervised and administrated the project regarding the generation of the Machado Joseph disease zebrafish model and provided the necessary resources and model design. Shermaine Tay generated, raised and collected samples of the Machado Joseph disease zebrafish model (Figure 4.33 and Figures 4.35 - 4.38).

The dissertation was supported by the work of Master students under direct supervision of Daniel Weishäupl:

Corinna Yilmaz (*Study on the normal and pathogenic function of ataxin-3 isoforms in HEK293 cells*) performed cell culture and quantitative polymerase chain reaction experiments regarding the trancriptional regulation of ataxin-3 (Figure 4.14).

Barbara Peixoto Pinheiro (*Study on the aggregation properties of ataxin-3 isoforms*) performed polymerase chain reaction experiments regarding the *ATXN3* integration and expression in the Machado Joseph disease zebrafish model (Figure 4.35 B/C and Figure A.6) and fluorescence microscopy aggregation experiments of ataxin-3 (Figure 4.18 A).

Heiko van Beek (*Charakterisierung Ataxin-3-isoformspezifischer Zebrafischmodelle für die spinocerebelläre Ataxie Typ 3*) performed polymerase chain reaction (Figure 4.35 D), western blot (Figure 4.36), filter trap (Figure 4.37) and immunohistochemistry (Figure 4.38) experiments regarding the *ATXN3*/ataxin-3 expression in the Machado Joseph disease zebrafish model.

Further, interns directly supervised by Daniel Weishäupl contributed to the dissertation: Alexandros Nianias, Anna Schöllhorn, Barbara Peixoto Pinheiro, Bashkim Hyseni, Corinna Yilmaz, David Skrabak, Juliane Schuhmacher, Maria-Jhaneth Prado-Carvajal, Oliver Heinzel, Sandra Maria Woerner, Svenja Wöhrle and Ziwei Li.

Acknowledgments

I would like to express my gratitude to my supervisor Thorsten Schmidt, who guided me throughout this project and always supported my ideas. I also would like to thank my doctoral adviser Olaf Rieß for his guidance and assistance during this project and my doctoral adviser Ludger Schöls for his support and the fruitful discussions during the advisory board meetings.

I wish to extend my special thanks to Christian Johannes Glöckner and Felix von Zweydorf for the support and training in performing the interaction study, Christoph Winkler and Shermaine Tay for creating, raising and housing of the zebrafish and the guidance and training during my stay at the National University of Singapore and Hubert Kalbacher and the technicians of the Medizinisch-Naturwissenschaftliches Forschungszentrum for all their work and support in generating the antibody.

I also thank the Landesgraduiertenförderung Baden-Württemberg and the Unibund Tübingen for my scholarships and the Machado-Joseph Disease Foundation for funding my participation at the first international Machado-Joseph Disease Meeting.

I would also like to thank the following people for helping me finalize the project. My students Juliane Schuhmacher, Corinna Yilmaz, Barbara Peixoto Pinheiro, Sandra Woerner, Heiko van Beek, Maria-Jhaneth Prado-Carvajal, Anna Schöllhorn, David Skrabak and all the other students which assisted the project and invested their time and energy. You did a great job and I really enjoyed supervising you. Jonasz Weber for the countless discussions, ideas, improvement of methods and so much more during the project. Priscila Pereira Sena for many discussions and all her support along the way. Ilnaz Sepahi for proof reading of this thesis and my paper and all the ideas and suggestions. My brother Matthias Weishäupl for proof reading this thesis. The whole SCA3 research group of the Institute of Medical Genetics and Applied Genomics. It has been a joy to work with you.

My thank also goes to the Landesgraduiertenförderung Baden-Württemberg and the Unibund Tübingen for funding me as a scholarship holder.

Lastly, I would like to thank my family for the support and understanding when I was allocating our most valuable resource, time, to work instead of spending it with them – thank you.

Parts of this dissertation were first published in *The Journal of Biological Chemistry*: Weishäupl, D., Schneider, J., Peixoto Pinheiro, B., Ruess, C., Dold, S. M., von Zweydorf, F., Gloeckner, C. J., Schmidt, J., Riess, O., Schmidt, T. Physiological and pathophysiological characteristics of ataxin-3 isoforms. *The Journal of Biological Chemistry*, 294(2):644-661, 2019. Available for use via `https://doi.org/10.1074/jbc.RA118.005801` under the CC BY 4.0 license (`https://creativecommons.org/licenses/by/4.0/`).

Abstract

The autosomal-dominantly inherited, neurodegenerative disorder Machado-Joseph Disease (MJD) is caused by an expanded CAG repeat in the ataxin-3 encoding gene *ATXN3*. This sequence is translated into a polyglutamine repeat in the protein. *ATXN3* is spliced alternatively leading to protein isoforms which differ in their their C-terminus and number of ubiquitin interacting motifs. Additionally, the isoforms are modified by single nucleotide polymorphisms of which one is leading to a premature stop codon. The objective of this study was to assess the influence of both, alternative splicing and the nonsense polymorphism on major aspects of ataxin-3's physiological function and main disease mechanisms.

It was found that the premature stop and alternative splicing of the *ATXN3* gene affect the physiological characteristics on multiple levels and modulate the proteins' stability enzymatic activity and subcellular localization. Interestingly, also an isoform-specific interaction of ataxin-3 with other proteins could be observed. This demonstrates that ataxin-3 isoforms are individual proteins with distinct functions and interaction networks within the cell. The modulatory effects, however, were not limited to the physiological properties of non-expanded ataxin-3. An expansion of the polyglutamine repeat entailed a stabilization of the respective isoform and caused aggregation. Surprisingly, alternative splicing and the nonsense mutation comprehensively modified the aggregation profperties. Thus ataxin-3 isoforms supposedly show a differential contribution to the pathogenesis of MJD. Further, a functional interaction between non-expanded and expanded ataxin-3 isoforms could be demonstrated for the first time. Interestingly, this cross-talk likewise modified physiological and pathophysiological properties of the protein. In order to convert the present data into a treatment strategy, the possibility of correcting the premature termination codon by translational read-through was assessed. Utilizing aminoglycoside antibiotics allowed for a partial compensation of the nonsense polymorphism and proved that it could be an interesting therapeutic intervention in order to ameliorate the disease progression. Lastly, in order to additionally verify the obtained results *in vivo*, a new isoform-specific zebrafish model was generated and initially characterized.

Altogether, alternative splicing, the nonsense polymorphism and the mutual interaction of ataxin-3 isoforms modify both, major physiological characteristics of ataxin-3 and MJD pathogenesis. However, new therapeutic strategies like stop codon read-through may allow for a compensation of the negative effects of the nonsense polymorphism. The data provided in this study stresses the importance of considering isoforms of disease causing proteins, their modification by single nucleotide polymorphisms and their interplay with the normal protein allele as disease modifiers, not only in MJD but in autosomal-dominantly inherited diseases in general.

Contents

List of Figures

List of Tables

List of abbreviations

AA	amino acid
aao	age at onset
AD	Alzheimer's disease
ALS	Amyotrophic lateral sclerosis
ANOVA	analysis of variance
bp	basepair
BSA	bovine serum albumin
CCCP	carbonyl cyanide m-chlorophenyl hydrazone
CNS	central nervous system
C-terminus	carboxyl-terminus
DAPI	4',6-diamidino-2-phenylindole
DMEM	Dulbecco's modified Eagle's medium
DPBS	Dulbecco's phosphate buffered saline
dpf	days post fertilization
DRPLA	Dentatorubral-pallidoluysian atrophy
DSB	double strand break
DTT	dithiothreitol
DUB	deubiquitination
EDTA	ethylenediaminetetraacetic acid
EGFP	enhanced green fluorescent protein
ELISA	enzyme linked immunosorbent assay
ERAD	endoplasmic-reticulum-associated protein degradation
FBS	fetal bovine serum
FTD	Frontotemporal dementia
FTDP-17	Frontotemporal dementia and parkinsonism linked to chromosome 17
GFP	green fluorescent protein
GST	glutathion-S-transferase
HD	Huntington's disease
HEK	human embryonic kidney
HPLC	high performance liquid chomatography
HR23A/B	UV excision repair protein RAD23 homolog A/B
HSD	honest significant difference
IAP	inhibitor of apoptosis
JD	Josephin domain
KEGG	Kyoto Encyclopedia of Genes and Genomes
KI	knockin
KO	knockout
LB	lysogeny broth
LC	liquid chromatography
LC3	microtubule-associated protein 1A/1B-light chain 3
MEF	mouse embryonic fibroblast
MJD	Machado Joseph disease

mpf months post fertilization

MS mass spectrometry

MSMS tandem mass spectrometry

MTOC microtubule organizing center

NES nuclear export signal

NGS next generation sequencing

NLS nuclear localization signal

NTC no template control

N-terminus amino-terminus

OD optical density

PAGE polyacrylamide gelelectrophoresis

PBS phosphate buffered saline

PBS phosphate buffered saline

PCR polymerase chain reaction

PD Parkinson's disease

polyQ polyglutamine

PTC premature termination codon

PTM posttranslational modification

RFU relative fluorescence unit

RIPA radioimmunoprecipitation assay

rpm rounds per minute

RT-PCR real-time polymerase chain reaction

SBMA Spinal and bulbar muscular atrophy

SCA Spinocerebellar ataxia

SDS sodium dodecyl sulfate

SEM standard error of the mean

SILAC stable isotope labeling by amino acids in cell culture

SNP single nucleotide polymorphism

TALEN transcription activator-like effector nuclease

TNR trinucleotide repeat

TR-FRET time-resolved Förster resonance energy transfer

UBR2 E3 ubiquitin-protein ligase UBR2

UIM ubiquitin interacting motif

UPS ubiquitin proteasome system

UTR untranslated region

VCP vasolin containing protein

WT wild type

1 | Introduction

Within the past decades vast improvements to therapies for various severe diseases were made and as a result life expectation was gradually increasing. Unfortunately, increased lifespan not necessarily signifies a healthy life of the aged (Avendano and Cylus, 2019). The increasing number of the elderly also leads to an increasing prevalence of neurodegenerative disorders (Heemels, 2014). Neurodegenerative disorders thereby is an umbrella term for a few hundred different diseases which primarily affect the central nervous system (CNS) and show a clinical and pathological overlap (Przedborski et al., 2003; Gitler et al., 2017; McLoughlin et al., 2020). The CNS is structured during embryonic development and only shows limited regeneration capacity on the cellular level (El Seblani et al., 2020; Zambusi and Ninkovic, 2020). Neurodegenerative disorders for this reason can have fatal consequences for memory, perception, personality, movement or a combination thereof (Price, 1999). Among the most well known neurodegenerative disorders are presumably Alzheimer's disease (AD) and Parkinson's disease (PD) which, from an epidemiological point of view, show a high prevalence of 5.4 % to 6.4 % (Mayeux and Stern, 2012; Haacke et al., 2006) and 1 % (Tysnes and Storstein, 2017) of the population in Europe and North America, respectively. Neurodegenerative disorders are strongly associated to the elderly and aging indeed is the number one risk factor (Przedborski et al., 2003). However, causes of neurodegenerative disorders are diverse (Harmuth et al., 2018). Genetic predisposition or mutation, environmental factors as well as their interplay can be responsible for their development (Przedborski et al., 2003; Spires and Hannan, 2005; Elbaz et al., 2007; Bradley et al., 2019).

One kind of mutations frequently causing neurodegenerative disorders are unstable repeat expansions (Tsuji, 1996; Nelson et al., 2013; Paulson, 2018; Rudich and Lamitina, 2018). This class of mutations is characterized by the expansion of a natural polymorphic repetitive DNA motif that can be found as microsatellites across the human genome. Microsatellites are short tandem repeats that cover around 3 % of the human genome (Subramanian et al., 2003) and which are characterized by a polymorphic length (Ellegren, 2004). The expanded motif can be a di-, tri-, tetra-, hexa- or dodecanucleotide repeat sequence (Paulson, 2018). The repeat-expansion itself can range from tens to several thousand repeats (Paulson, 2018) and can be localized inside non-coding sequences like introns and untranslated regions (UTRs) or inside coding exons which then also causes an amino acid (AA) repeat-expansion inside the protein. Microsatellite expansions inside the coding sequence, however, tend to be shorter and are limited to trinucleotide repeats (TNRs) (Lieberman et al., 2019).

Today, more than 40 different diseases are known from which TNR disorders were the first ones being described in 1991 (Fragile X Syndrome, Verkerk et al., 1991). Despite being clinically and pathologically diverse all diseases show a genotype-phenotype correlation between repeat

length and disease severity which is a common mechanism unique to this class of diseases (Paulson, 2018). The repeat size thereby explains around 45 % to 70 % of the age at onset (aao) while minor genetic or environmental factors may account for the rest. The repeat expansions itself are unstable and change in size from generation to generation which leads to clinical anticipation. Although these diseases are mainly inherited, the instability of the repeat also allows for *de novo* mutations (Myers et al., 1993; Stevanin et al., 1998; Laffita-Mesa et al., 2013).

The largest and most common group among TNR disorders are (Silva-Fernandes, 2010) the polyglutamine (polyQ) disorders Huntington's disease (HD) (MacDonald et al., 1993), Spinal and bulbar muscular atrophy (SBMA) (La Spada et al., 1991), Dentatorubral-pallidoluysian atrophy (DRPLA) (Koide et al., 1994), Spinocerebellar ataxia (SCA) 1 (Orr et al., 1993), SCA2 (Trottier et al., 1995; Pulst et al., 1996), SCA3/MJD (Kawaguchi et al., 1994), SCA6 (Zhuchenko et al., 1997), SCA7 (Lindblad et al., 1996) and SCA17 (Koide et al., 1999; Riley and Orr, 2006, Table 1.1). The repeat expansion thereby lies inside the coding sequence of a protein and encodes for the AA glutamine (Q) which results in an abnormally expanded polyQ stretch in the protein's primary structure (Laço et al., 2012b). Long glutamine-repeats occur in many proteins, especially within transcription factors (Perutz et al., 1994). Nonetheless, polyQ disorders are unique to humans (Lieberman et al., 2019). Although sharing the same mutation, they show a clinically diverse picture, once the pathological threshold of the polyQ stretch inside the unrelated proteins is reached (Zoghbi and Orr, 2000; Gatchel and Zoghbi, 2005; Matos et al., 2011). Despite affecting different proteins and having differing pathological polyQ expansion sizes, these diseases share similar pathological features and pathogenic mechanisms (Williams and Paulson, 2008) and all are characterized by a slowly progressive neurodegeneration with an aao of symptoms typically in midlife (Cummings, 2000; Lieberman et al., 2019).

Table 1.1. Overview of polyglutamine diseases. Although sharing a similar mutation type, the expansion of a repetitive polyQ repeat, all nine polyQ diseases have a distinctive clinical representation.

Disease	**Prevalence (per 100,000)**	**Clinics**	**Affected gene/protein**	**Repeat expansion (healthy/diseased)**	**Age at onset (years)**
Huntington's disease	4.8 - 9.7 (Harper, 1992; Ohlmeier et al., 2019)	chorea, rigidity and dementia (Pandey and Rajamma, 2018; Nguyen and Weydt, 2018)	*HTT* / huntingtin	9 - 11 / 36 -86 (Read, 1993; Duyao et al., 1993; Nguyen and Weydt, 2018)	30 – 40 (15 - 20 years prodromal phase) (Chandler et al., 1960; Heathfield, 1973; Nguyen and Weydt, 2018)
Spinal and bulbar muscular atrophy/Kennedy disease	< 1 - 3 (Giorgetti and Lieberman, 2016; Grunseich et al., 2014; Fischbeck, 1997)	muscle weakness, fasciculation of facial muscles and tongue, dysarthria and dysphagia (Kennedy et al., 1968; Harding et al., 1982; Atsuta et al., 2006; Rhodes et al., 2009)	*AR* / androgen receptor	9 - 36 / 38 - 62 (La Spada et al., 1991; Grunseich et al., 2014; Giorgetti and Lieberman, 2016)	30 -60 (Harding et al., 1982; Rhodes et al., 2009; Atsuta et al., 2006)
Dentatorubral-pallidoluysian atrophy	< 2 - 7; predominantly in the Japanese (Veneziano and Frontali; Carroll et al., 2018)	ataxia, myoclonus, seizures and intellectual disability or ataxia, cognitive impairment, psychiatric disturbance and choreoathetosis (early versus late onset, Carroll et al., 2018; Veneziano and Frontali)	*ATN1* / atrophin 1	6 - 35 / 48 - 93 (Veneziano and Frontali)	0 - 72 (Veneziano and Frontali; Rédei, 2008)
Spinocerebellar ataxia 1	1 - 4 (Martins Junior et al., 2018)	cerebellar ataxia, dysarthria and oculomotor signs (Yamada et al., 2008; Martins Junior et al., 2018)	*ATXN1* / ataxin-1	6 - 44 / 39 - 82 (Cummings, 2000; Martins Junior et al., 2018)	15 - 63 (Sasaki et al., 2009)

Continued on next page

Table 1.1. Overview of polyglutamine diseases. – *Continued from previous page*

Disease	Prevalence (per 100,000)	Clinics	Affected gene/protein	Repeat expansion (healthy/diseased)	Age at onset (years)
Spinocerebellar ataxia 2	regional 6 - 40[1] (Antenora et al., 2017; Velázquez-Pérez et al., 2017)	gait ataxia, dysmetria, dysarthria, ophthalmoplegia and peripheral neuropathy (Velázquez-Pérez et al., 2017)	*ATXN2* / ataxin-2	< 31 / 31 - 39 (up to 200 in rare cases possible, Babovic-Vuksanovic et al., 1998; Antenora et al., 2017)	11 - 86 (Moretti et al., 2004; Fernandez et al., 2000)
Spinocerebellar ataxia 3	1 - 3 (Bird, 1993; Schöls et al., 1995; Van De Warrenburg et al., 2002; Schöls et al., 2004; Riess et al., 2008)	gait and limb ataxia, dysarthria, nystagmus, dysphagia and distal sensation loss (Jardim et al., 2001)	*ATXN3* / ataxin-3	12 - 44 / 61 - 87 (Maciel et al., 1995, 2001)	4 - 78 (Carvalho et al., 2008; Maciel et al., 2001)
Spinocerebellar ataxia 6	0.02 - 0.30 (Casey and Gomez, 1998)	Cerebellar ataxia, dysarthria, intention tremor and nystagmus (Casey and Gomez, 1998)	*CACNA1A* / $Ca_v2.1$[2]	4 - 18 / 19 - 33 (Shizuka et al., 1998; Yabe et al., 1998; Katayama et al., 2000; Mariotti et al., 2001; Du and Gomez, 2018)	19 - 73 (Casey and Gomez, 1998)
Spinocerebellar ataxia 7	0.003 - 0.220 (Michalik et al., 2004)	cerebellar ataxia, dysarthria, dysphagia and retinopathy (Jonasson et al., 2000; Michalik et al., 2004)	*ATXN7* / ataxin-7	< 19 / 36 - 460 (Nardacchione et al., 1999; Van De Warrenburg et al., 2001; Michalik et al., 2004)	0 - 70 (Babovic-Vuksanovic et al., 1998; Michalik et al., 2004)
Spinocerebellar ataxia 17	0.047 - 0.160 (Maruyama et al., 2002; Craig et al., 2005)	cerebellar ataxia, dementia, chorea and dystonia (Toyoshima et al.; Toyoshima and Takahashi, 2018)	*TBP* / TATA-box-binding protein	25 - 40 / 41 - 66 (Toyoshima et al.; Maltecca et al., 2003; Toyoshima and Takahashi, 2018)	3 - 75 (Stevanin and Brice, 2008)

[1] data geographically restricted; studies do not allow a precise worldwide estimation (Velázquez-Pérez et al., 2017)
[2] voltage-dependent P/Q-type calcium channel subunit alpha-1A

1.1 Machado Joseph disease

Machado Joseph disease (MJD) is the second most frequent polyQ disorder (Paulson, 2018) and was first described in emigrants from the Azores (Portugal, Nakano et al., 1972; Woods and Schaumburg, 1972; Rosenberg et al., 1976). MJD is characterized by progressive ataxia - a lack of coordination of movement and an unsteady and uncoordinated wide-based gait (Bird, 1993). It belongs to the large group of clinically and genetically heterogeneous inheritable ataxias summarized under the term SCAs and is also known as SCA3. Meanwhile, more than 50 different SCAs were described which manifest during childhood or as an adult (Bird, 1993). Despite being clinically and genetically diverse, all SCAs are characterized by ataxia as well as cerebellar degeneration (La Spada and Taylor, 2003). Clinically, MJD itself is also characterized by strongly varying symptoms between patients, which is the reason why between 1972 and 1977 three different diseases were described in three different families (Machado, Joseph and Thomas) suffering from MJD (Nakano et al., 1972; Woods and Schaumburg, 1972; Rosenberg et al., 1976). Only 1977/1978, Romanul et al. (1977) and Coutinho and Andrade (1978) recognized that *Machado disease*, *nigro-spino-dentatal degeneration with nuclear ophthalmoplegia* and *autosomal dominant striatonigral degeneration* actually are clinical variations of the same disease and it was finally termed MJD in respect to the families studied (Gaspar et al., 2002). However, only 1995, after the exact mutation was identified by Kawaguchi et al. (1994), Haberhausen et al. (1995) confirmed the assumption of Matilla et al. (1995) that MJD and the thus far distinct disorder SCA3 are identical.

1.1.1 Epidemilogy

In Germany, and also worldwide, MJD is the most common SCA (Schöls et al., 2004; Matos et al., 2011). With a worldwide prevalence of around 1 to 3 diseased per 100,000 inhabitants, MJD belong to the group of orphan diseases (Figure 1.1 A, Bird, 1993; Schöls et al., 1995; Van De Warrenburg et al., 2002; Schöls et al., 2004; Riess et al., 2008; Coutinho et al., 2013; De Castilhos et al., 2014b; Ruano et al., 2014; Sullivan et al., 2019). Although, MJD was originally described in North American families which immigrated from the Azores (Portugal, Nakano et al., 1972; Woods and Schaumburg, 1972; Rosenberg et al., 1976), by today it can be found in many countries worldwide with strongly varying prevalence among autosomal dominant cerebellar ataxias (ADCAs). Nonetheless, the highest prevalence still can be found on the Azores (1:140, Figure 1.1 B, Sudarsky and Coutinho, 1995).

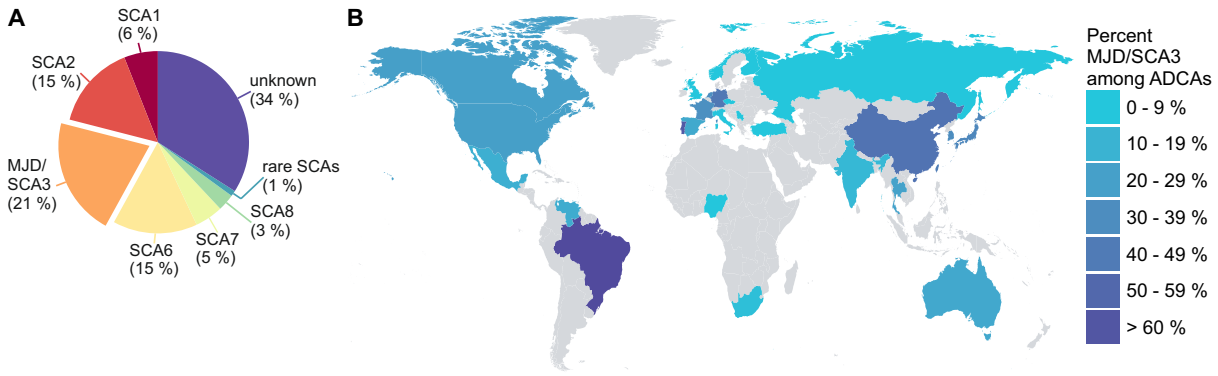

Figure 1.1. Worldwide prevalence of MJD among other autosomal dominant cerebellar ataxias. A MJD is the most frequent SCA subtype worldwide (information is based on Schöls et al., 2004). **B** The prevalence of MJD among autosomal dominant cerebellar ataxias (ADCAs), however, varies strongly depending on the country (information is based on Alluri et al., 2007; Alonso et al., 2007; Bauer et al., 2005; Brusco et al., 2004; Bryer et al., 2003; De Castilhos et al., 2014a; Chattopadhyay et al., 2003; Dragašević et al., 2006; Durr et al., 1996; Filla et al., 1996; Gan et al., 2010; Jin et al., 1999; Juvonen et al., 2005; Koht and Tallaksen, 2007; Krishna et al., 2007; Lee et al., 2003; Leggo et al., 1997; Ogun et al., 2015; Paradisi et al., 2015; Pujana et al., 1999; Ranum et al., 1995; Sasaki et al., 2003; Schöls et al., 2004; Shimizu et al., 2004; Silveira et al., 1996; Soong et al., 2001; Storey et al., 2000; Sura et al., 2009; Tang et al., 2000; Trott et al., 2006; Tsai et al., 2004a; Vale et al., 2010; Van De Warrenburg et al., 2002; Wu et al., 2004; Zhao et al., 2002; Zhou et al., 2001).

1.1.2 Neuropathology and clinical representation

The pathologic expansion of the polyQ repeat within the mutated protein ataxin-3 leads to neuronal lesions in various brain regions (Figure 1.2, reviewed in Rüb et al., 2008; Riess et al., 2008). Neuropathologically, *cerebellar dentate nucleus*, *substantia nigra*, *vestibular*, *oculumotor* and *precerebellar nuclei* are among the first that are affected in MJD (Riess et al., 2008). After a disease course of 15 years an atrophy of the *cerebellum*, *pons*, *medulla oblongata*, midbrain, spincal cord and cranial nerves III – XII as well as a depigmentation of the *substantia nigra* can be found (Riess et al., 2008; Rüb et al., 2008; Rub et al., 2006; Rüb et al., 2003; doCarmo Costa and Paulson, 2012). Neurodegeneration also leads to a lower brain weight in MJD patients (Iwabuchi et al., 1999). Damage to the described cerebral regions leads to dysfunctions in multiple components of the nervous system (Table 1.2, Rodriguez and Dymecki, 2000; Muñoz et al., 2002; Rüb et al., 2008).

Patients show mild abnormalities in magnetic resonance imaging; among others fourth ventricle enlargement, *cerebellar vermis* and hemispheres shrinking and *pontine* atrophy could be observed (Riess et al., 2008). Alterations in glucose utilization were described in cerebellum, cerebral cortex and brainstem. Interestingly, this could already be found in presymptomatic carriers (Soong and Liu, 1998). Positon emission tomography also revealed a reduced activity extending from cerebellar midline structures to pons and midbrain (Wüllner et al., 2005). A more detailed description of the MJD induced neuropathology can be found in Rüb et al. (2008).

The above described lesions well explain the observed symptoms in MJD patients. However, the fact that four different diseases were described which ultimately all reflect different clinical representations already illustrates the heterogeneity of symptoms observed in MJD. First symptoms typically appear in mid-life, but cases between four (homozygous patient, Carvalho et al., 2008) and 78 (Maciel et al., 2001) years of age were reported (Riess et al., 2008).

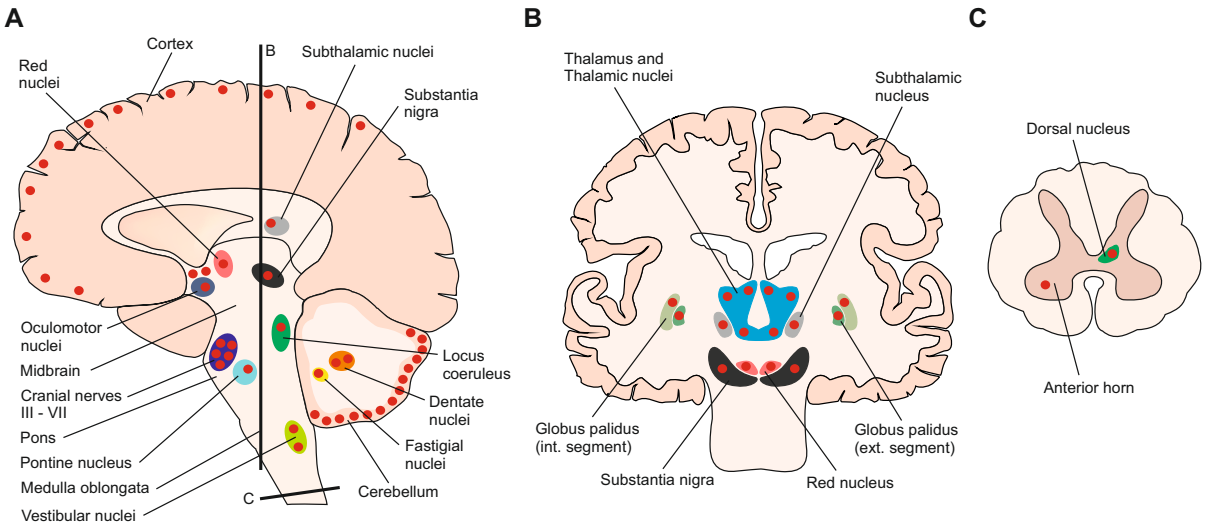

Figure 1.2. Affected brain regions in MJD. Various CNS regions are affected by neurodegeneration in MJD (red dots). *Cerebellum*, *pons* and midbrain are the primarily affected regions in MJD. **A** *Sagittal* plane of the brain. **B** *Coronal* plane of the brain. **C** Horizontal plane of the spinal cord (Information is based on Taroni and DiDonato, 2004; Rüb et al., 2008; Leisman et al., 2013; Norsk Helseinformatikk, 2016; Paulsen and Waschke, 2017).

Table 1.2. Affected CNS components in MJD and their function. Information is based on Rüb et al. (2008) and Banich and Compton (2018).

CNS component	Function
auditory system	auditory perception
basal ganglia-thalamocortical motor loop	modulation of motor control
cerebello-thalamocortical motor loop	coordination, learning and timing of movements
ingestion-related brainstem system	control of ingestion
midbrain cholinergic system	influences attention and memory
midbrain mesolimbic dopaminergic system	reward-related behavior
midbrain nigrostriatal dopaminergic system	regulation of selection, initiation and cessation in motor control
oculomotor system	control of eye movement
pontine noradrenergic system	influences attention, sleep and working memory
precerebellar brainstem system	transmission of information to the cerebellum
somatosensory system	proprioception and perception of touch, pain and temperature
vestibular system	control of balance
visual system	visual perception

Typically, gait ataxia is the first symptom and practically affects all patients. Further symptoms like limb ataxia, dysarthria, nystagmus, pyramidal signs, dysphagia and distal sensation loss are developed during the disease course (Jardim et al., 2001). Various less frequent symptoms can be found as well (reviewed in Rüb et al., 2008; Saute and Jardim, 2015). MJD is usually slowly progressing, but shows a more rapid progression in early onset patients (Riess et al., 2008). As for all polyQ disorders, the CAG repeat size is directly correlated to the disease phenotype and also explains around 40 % to 70 % of the aao (Maruyama et al., 1995; Maciel et al., 1995; Durr et al., 1996; Schöls et al., 1996; Van De Warrenburg et al., 2002; Saute and Jardim, 2015). The clinical variability led to the description of at least four distinct subtypes

which differ in their additional symptoms and their aao (Table 1.3, Riess et al., 2008). Some authors also reported three additional subtypes, V (spastic paraparesis), VI (pure cerebellar syndrome) and VII (mixed type) which are more rare (reviewed in Moro et al., 2014).

Table 1.3. Subtypes of MJD. Information is based on Schöls et al. (1996); Paulson and Bonini (2000); Riess et al. (2008); Bettencourt et al. (2011).

Subtype	Disease progression (aao)	Clinical features	Frequency	Main determinator for subtype
Type I *(Joseph / Flores)*	fast (10 – 30)	cerebellar, extrapyramidal and pyramidal deficits	13 %	early onset
Type II *(Thomas)*	intermediate (20 - 50)	cerebellar and pyramidal deficits	57 %	CAG repeat > 73 CAG
Type III *(Machado / São Miguel)*	slow (40 - 75)	cerebellar deficits and peripheral neuropathy	30 %	CAG repeat < 73 CAG
Type IV	variable	neuropathy, parkinsonism (and cerebellar deficits)	variable	n/a

Further, non-subtype specific features include ophthalmoplegia (Woods and Schaumburg, 1972), double vision (Globas et al., 2008), faciolingual fasciculations (Sudarsky and Coutinho, 1995), incontinence (Shimizu et al., 2010), restless leg syndrome (Schöls et al., 1998) and weight loss without loss of appetite (Riess et al., 2008). Possible cognitive disturbances in MJD are usually mild and do not develop into dementia (Riess et al., 2008). The mean survival after onset of MJD was calculated to be 21.18 years. However, an earlier onset was found to be related to a more severe phenotype and a shorter survival time (Kieling et al., 2007). Neurodegeneration in MJD does not directly lead to death, however, motor impairment frequently leads to aspiration pneumonia which is the primary cause of death in MJD (Rüb et al., 2013).

In addition to health-related impairments, MJD and other polyQ disorders are also a financial burden for affected families and the social system. The estimated direct medical costs are about 18 000 € to 30 000 € per year (particularly for informal care, early retirement, medications and orthopedic devices, López-Bastida et al., 2008; Lieberman et al., 2019). The loss of income and ability to work brings affected families to the border of the social ladder (Lieberman et al., 2019). This probably also contributes to the potential occurrence of depression in MJD patients, their spouses and individuals at risk (Cecchin et al., 2006; Klinke et al., 2010).

Diagnosis of MJD is raised by a patient's clinical features together with a family history showing an autosomal dominant inheritance pattern. The diagnosis is afterwards confirmed via molecular testing (Saute and Jardim, 2015). Genetic counseling of MJD patients, relatives at risk and other family members is crucial in order for them to take informed decisions and assist family/life planning (Schuler-Faccini et al., 2014). Despite intensive research, to date, MJD is incurable. Different disease-modifying and symptomatic treatments were tested in clinical trials

and other preclinical approaches targeting the cellular and molecular disease mechanisms are heavily investigated (Saute and Jardim, 2015; Matos et al., 2019). However, so far molecular treatment strategies are not available and disease-modifying treatments did not show significant beneficial effects (Yang et al., 2011; Jin et al., 2013; Saute et al., 2014) which reduces the available therapy options to various ameliorating symptomatic treatments (Saute and Jardim, 2015).

1.1.3 The *ATXN3* gene

1.1.3.1 Gene locus and properties of the poly CAG repeat

The disease-gene *ATXN3* (also *MJD1*) was found to be located on the long arm of chromosome 14 (14q32.1, Takiyama et al., 1993; Kawaguchi et al., 1994) and consists of 48 240 basepairs (bp) spread on 11 exons (Figure 1.3, Ichikawa et al., 2001). The existence of two additional exons (6a and 9a), however, was also proposed (Bettencourt et al., 2010). The 5' UTR was reported to contain a TATA-less promoter that has GC-rich regions and a CCAAT-box as well as potential binding sites for signaling protein 1 and other nuclear proteins (Schmitt et al., 2003). The *ATXN3* 3' regions are not well studied but contain at least eight different consensus sequences for polyadenylation signals (Ichikawa et al., 2001). Different single nucleotide polymorphisms (SNPs) are located inside exons, introns and the 3' UTR (Goto et al., 1997; Stevanin et al., 1997; Maciel et al., 1999; Gaspar et al., 2002; Martins et al., 2006, 2007, 2008; Bettencourt et al., 2013; Li et al., 2019).

The disease causing CAG repeat is located in exon 10 and is translated into a polyQ repeat in the protein ataxin-3 (Kawaguchi et al., 1994). Healthy people have 12 to 44 repeats whereas an unstable repeat-expansion in the range of 61 to 87 repeats can be found in MJD patients (Maciel et al., 1995, 2001). Despite showing a wide range of CAG repeats, alleles with 14 and 23 repeats are especially frequent (Stevanin et al., 1997; Maciel et al., 2001). MJD, as all other polyQ disorders, is inherited in an autosomal-dominant pattern but can show incomplete penetrance in the intermediate range and patients with 45 (Padiath et al., 2005) and 51 (Maciel et al., 2001) repeats were previously reported. The CAG repeat is interrupted by a CAA (glutamine) at position three and eventually six as well as an AAG (lysine) at position four (Kawaguchi

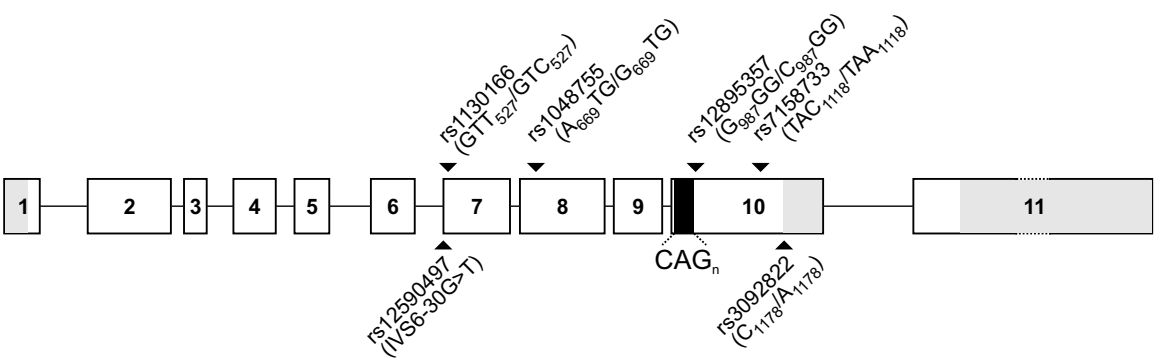

Figure 1.3. The *ATXN3* gene. The *ATXN3* gene consists of 11 exons with the poly CAG repeat (black) located in exon 10. Untranslated regions are displayed in gray. The *ATXN3* gene contains several SNPs from which six are well described in the literature. The SNPs rs1130166, rs1048755, rs12895357 and rs7158733 are located in coding regions while rs12590497 and rs 3092822 are located inside an intron and the 3' UTR of exon 10 respectively (image is based on Ichikawa et al., 2001).

et al., 1994; Limprasert et al., 1996). The CAG repeat length in the expanded allele displays an inverse correlation with the aao (Maruyama et al., 1995; Takiyama et al., 1995). However, it only explains about 50 % of its variation. Therefore, other genetic and eventually environmental factors contribute to the disease progression in MJD (Maciel et al., 1995; França et al., 2012, ; see below). The CAG repeat in the normal allele only explains about 1 % of the aao variation (França et al., 2012). As for other TNR disorders (Chong et al., 1995; Ueno et al., 1995; Telenius et al., 1994), the CAG repeat is characterized by a high meiotic and mitotic instability causing a CAG mosaic between cells and between generations which is also the basis for anticipation (Takiyama et al., 1995; Maciel et al., 1999; Saute and Jardim, 2015). Intergenerational instability thereby is especially associated with paternal transmission of the *ATXN3* gene (Maruyama et al., 1995; Takiyama et al., 1995) as well as MJD type I (Maruyama et al., 1995). The initial expansion step from a normal to an expanded CAG allele was found to be of multiple origins between different populations and can not be traced back to a single historical mutational event (Stevanin et al., 1997; Iughetti et al., 1996; Gaspar et al., 2002).

1.1.3.2 Gene lineages and haplotypes

The *ATXN3* gene is modified by various SNPs. At least six of those are well known: rs12590497 IVS6-30G>T (intron 6-7), rs1130166 GTT_{527}/GTC_{527} (exon 7), rs1048755 $A_{669}TG/\ G_{669}TG$ (exon 8), rs12895357 $G_{987}GG/C_{987}GG$ (exon 10), rs7158733 TAC_{1118}/TAA_{1118} (exon 10), rs3092822 C_{1178}/A_{1178} (3‘ UTR, see Figure 1.3, page 9, Goto et al., 1997; Stevanin et al., 1997; Maciel et al., 1999; Gaspar et al., 2002; Martins et al., 2006, 2007, 2008; Bettencourt et al., 2013; Li et al., 2019). The haplotype thereby is frequently distributed in a yin-yang pattern between the expanded and the normal allele (Zhang et al., 2003; Martins et al., 2008) and the individual SNPs are at least partially in a linkage disequilibrium (Stevanin et al., 1995, 1997; Maciel et al., 1999). Two primary haplotypes of the above mentioned SNPs, T<u>TACA</u>C[3] and G<u>TGGC</u>A, exist in MJD patients and were described to be based on distinct mutational events. However, also other haplotypes are known which presumably are mutations thereof (Martins and Sequeiros, 2018). The G<u>TGGC</u>A haplotype is most frequent on the island of São Miguel (Azores, Portugal) and along the Tagus valley in Portugal and is more or less geographically restricted (Gaspar et al., 2002; Martins et al., 2007; Martins and Sequeiros, 2018). The T<u>TACA</u>C haplotype instead is distributed worldwide and presumably originates from Asia (Martins et al., 2007). The distinct mutational events and the distribution of these two haplotypes between the families Machado and Joseph as well as the islands São Miguel and Flores led to the description of two MJD lineages known as the Joseph/Flores (T<u>TACA</u>C) and Machado/São Miguel lineage (G<u>TGGC</u>A; Table 1.4).

Among these six SNPs the exon 8 and exon 10 SNPs rs1048755, rs12895357 and rs7158733 are the most well studied in MJD patients. While the exon 8/10 GGC haplotype is associated to the normal allele (found in 72 % of alleles studied, Dengler, 2018), it was found that the haplotype ACA is strongly associated with MJD (depending on the region 72 % to 96 % of MJD patients, Figure 1.4 A, Igarashi et al., 1996; Matsumura et al., 1996; Stevanin et al., 1997; Goto et al., 1997; Maciel et al., 1999; Gaspar et al., 2002; Dengler, 2018). Further, the majority of pa-

[3] exonic SNP are underlined

Table 1.4. Lineages and haplotypes of the *ATXN3* gene. Haplotype of the two lineages Machado/São Miguel and Joseph/Flores and the location of the respective SNPs. Information is based on Goto et al. (1997); Stevanin et al. (1997); Maciel et al. (1999); Gaspar et al. (2002); Martins et al. (2006, 2007, 2008); Bettencourt et al. (2013); Li et al. (2019).

Lineage	**Reference SNP cluster ID**					
	12590497 intron 6-7	1130166 exon 7	1048755 exon 8	12895357 exon 10	7158733 exon 10	3092822 3' UTR
Machado/São Miguel	G	T	G	G	C	A
Joseph/Flores	T	T	A	C	A	C

tients worldwide carries the SNP rs7158733 TAA_{1118} in the expanded allele (Figure 1.4 B and C).

A clinical effect was reported for all three SNPs by modifying the stability of the CAG repeat and the aao (Igarashi et al., 1996; Limprasert et al., 1996; Matsumura et al., 1996; Maciel et al., 1999; Martins et al., 2008; doCarmo Costa and Paulson, 2012; Dengler, 2018). The SNPs rs12895357 $C_{998}GG$ and rs7158733 TAA_{1118} are both associated with an increased intergenerational instability of the CAG repeat in cis and generally longer CAG repeats (Matsumura et al., 1996; Limprasert et al., 1996; Martins et al., 2008; Silva-Fernandes, 2010). $G_{998}GG$ and TAC_{1118} on the other hand show an increased instability in trans (Igarashi et al., 1996; Maciel et al., 1999). The combined effects of rs12895357 in the variant combination $C_{998}GG/G_{998}GG$ (expanded/normal) and the sex of the transmitting parent (paternal) can lead to a 75-fold increase in the risk of a CAG-expansion (Igarashi et al., 1996). In general, the haplotype ACA is associated to intergenerational expansions while the haplotype GGC is more likely to cause contractions (Martins et al., 2008).

Looking at the individual SNPs, rs1048755 in a homozygous $A_{669}TG$ variant reduces the aao by 7.2 years in comparison to a homozygous $G_{669}TG$. Further, rs12895357 in a homozygous $C_{998}GG$ variant even reduces the aao by 9.7 years. The strongest effect could be observed for rs7158733 for which a homozygous TAA_{1118} reduced the aao by 11.5 years and explains about 2.7 % of the total aao variation (Dengler, 2018). Effects on aao could as well be observed for the combined exon 10 haplotype (Figure 1.4 C). Comparing the homozygous haplotype GC ($G_{998}GG/TAC_{1118}$) and CA ($C_{998}GG/TAA_{1118}$) versus the most frequent haplotype distribution with GC in the normal and CA in the expanded allele, it could be found that a homozygous CA haplotype reduces the aao by around 6 years while a homozygous GC haplotype increases the aao by around 8 years (Dengler, 2018).

1.1.4 Ataxin-3

Ataxin-3 (UniProt ID P54252) is a cysteine protease (Burnett et al., 2003; Scheel et al., 2003) with about 40 kDa to 43 kDa in size (Goto et al., 1997). It consists of an N terminal globular Josephin domain (JD) (AA 1 - 180[4]), followed by two ubiquitin interacting motifs (UIMs) (AA 224 – 243 and 244 – 263), the polyQ repeat (AA 292 – 305) and a third UIM (AA 331 – 349) at the disordered carboxyl-terminus (C-terminus) of the protein (Figure 1.5, Goto et al., 1997; Albrecht et al., 2004; The UniProt Consortium, 2019; Lambrughi et al., 2021).

[4]positions are based on the canonical ataxin-3c sequence of UniProt (The UniProt Consortium, 2019).

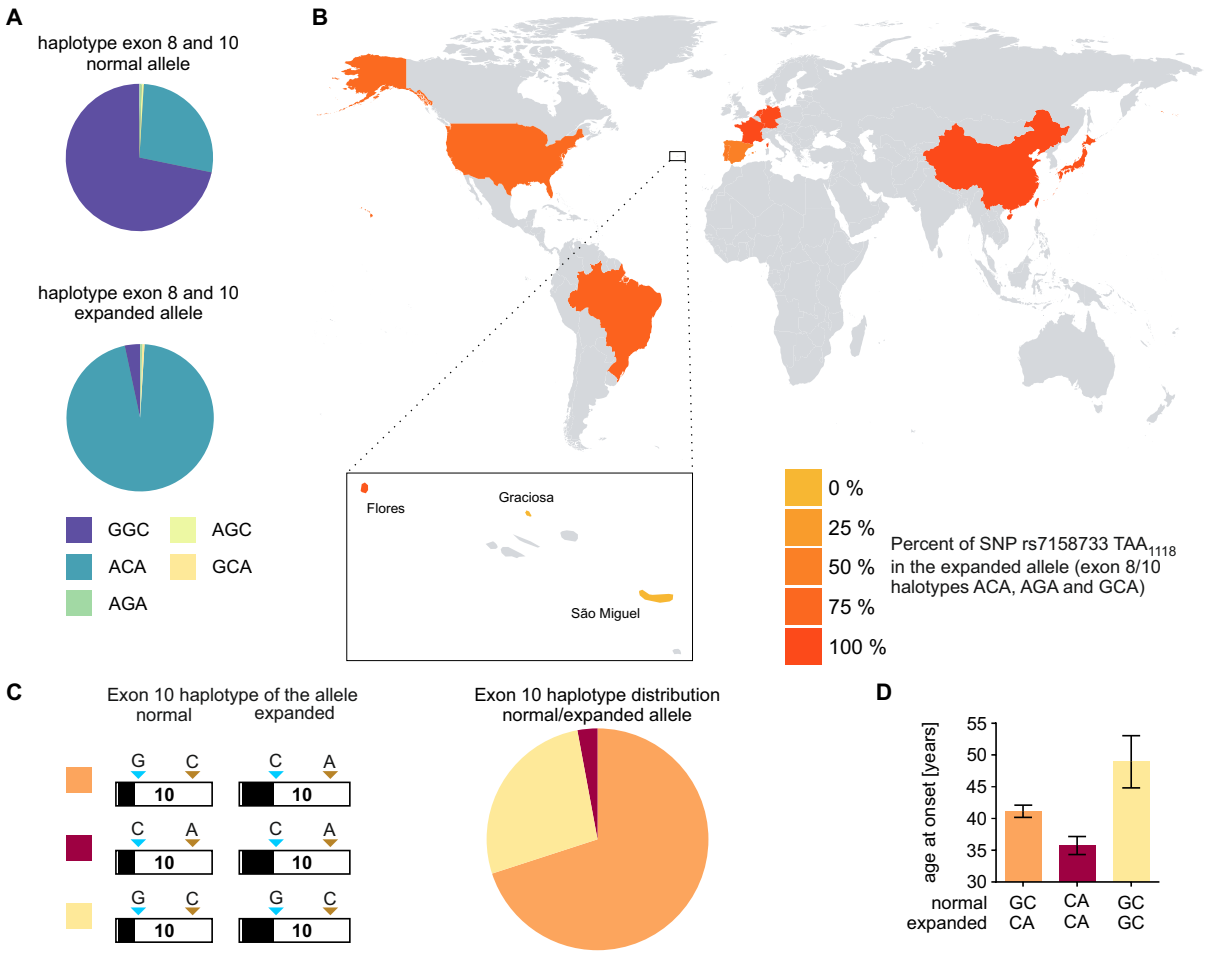

Figure 1.4. Distribution of *ATXN3* haplotypes. A The haplotype of exon 8 and 10 is differently distributed between the normal and expanded allele. While most of the normal alleles show the GGC haplotype, expanded alleles usually carry the ACA haplotype. **B** The expanded allele usually carries the TAA_{1118} variant of SNP rs7158733 in the majority of MJD patients (present in haplotype ACA, AGA and GCA). The TAC_{1118} variant (present in haplotype GGC and AGC) is geographically more restricted to islands of the Azores and the Tagus valley in Portugal (Information is based on Gaspar et al., 2002; Mittal et al., 2005; Gan et al., 2010; Ogun et al., 2015). **C** The frequency of the exon 10 haplotype is differently distributed between the normal and the expanded allele. Patients with an exon 10 haplotype of GC in the normal and CA in the expanded allele are most frequent. **D** Homozygosity of the haplotype GC increases the aao while a homozygous CA reduces the aao (Subfigures A, C and D are based on data from Dengler, 2018).

Ataxin-3 further contains one nuclear localization signals (NLSs) and two nuclear export signal (NES) (Antony et al., 2009; Albrecht et al., 2004) and is subject to posttranslational modifications (PTMs). Ataxin-3 is modified by ubiquitination, SUMOylation and phosphorylation at various sites (Fei et al., 2007; Mueller et al., 2009; Tsou et al., 2013; Almeida et al., 2015; Kristensen et al., 2017; Wan et al., 2018). Additionally, ataxin-3 is fragmented by autolytic cleavage (Mauri et al., 2006) as well as by caspases and calpains (Wellington et al., 1998; Berke et al., 2004; Haacke et al., 2006; Colomer Gould et al., 2007; Weber et al., 2017) at different positions. Ataxin-3, exhibiting its normal function, is known to interact with multiple proteins (reviewed in doCarmo Costa and Paulson, 2012) among others UV excision repair protein RAD23 homolog A/B (HR23A/B, Wang et al., 2000; Nicastro et al., 2005), parkin (Durcan et al., 2011), tubulin (Bonanomi et al., 2014a) and vasolin containing protein (VCP, also known

as transitional endoplasmic reticulum ATPase; Zhong and Pittman 2006; Boeddrich et al. 2006) seem to be important ataxin-3 interactors and could be found to interact with different regions of the protein.

1.1.4.1 The *ATNX3* gene is spliced alternatively into at least two full-length isoforms

Alternative splicing of the *ATXN3* gene is well known and happens at various splice sites (Ichikawa et al., 2001; Bettencourt et al., 2010, 2013). In total 56 different splice variants were identified for the *ATXN3* gene. Transcript diversity is thereby created by exon skipping, novel exons and usage of 5' and 3' alternative splice sites (Goto et al., 1997; Ichikawa et al., 2001; Bettencourt et al., 2010). However, it may be that most of these alternative transcripts are a result of splicing errors (Saudemont et al., 2017). Five different transcripts of the *ATXN3* gene are known to be expressed in neuronal and non-neuronal tissue (Schmitt et al., 1997; Ichikawa et al., 2001; Silva-Fernandes, 2010). These transcripts are created at the spliceosome by alternative splicing of exon 2, 10 and 11 in combination with various 3' UTR polyadenylation signals (Goto et al., 1997; Ichikawa et al., 2001; doCarmo Costa and Paulson, 2012). Four of these transcripts mainly differ in their C-terminus (Goto et al., 1997) and one shows exon skipping of exon 2 (Ichikawa et al., 2001).

Although the existence of up to 20 protein isoforms was suggested (Bettencourt et al., 2010), only two full length isoforms – ataxin-3a and ataxin-3c – have been identified and characterized

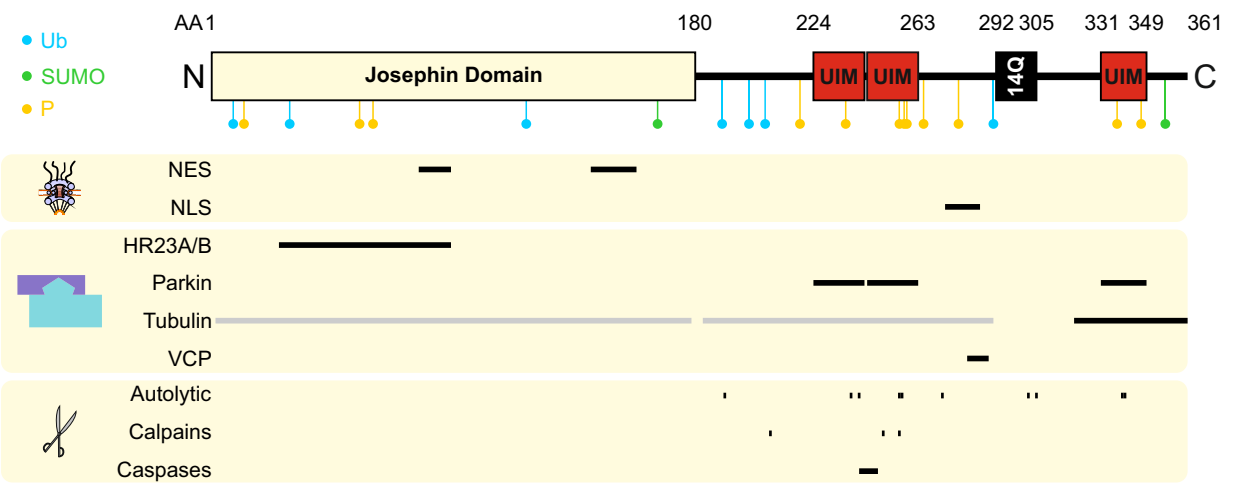

Figure 1.5. Structure and domains of ataxin-3. Ataxin-3 consists of an N terminal JD followed by two UIMs, the polyQ region and either a third UIM within an disordered C-terminus (ataxin-3c, canonical sequence) or a unstructured C-terminus (ataxin-3a). The protein is modified by different PTMs: ubiquitination (●), SUMOylation (●), phosphorylation (●), autolysis as well as calpain and caspase cleavage. Various interaction partners could be identified for ataxin-3. Among others HR23A/B (AA 25 - 89), parkin (UIMs), tubulin (tubulin binding region 1 – 3; region 3 seems to be the most important) and VCP (AA 281 - 289) could be identified as important interactors and bind different regions of the protein. All positions are based on the canonical sequence of Uniprot. (information presented is based on Albrecht et al., 2004; Berke et al., 2004; Nicastro et al., 2005; Boeddrich et al., 2006; Haacke et al., 2006; Mauri et al., 2006; Fei et al., 2007; Colomer Gould et al., 2007; Antony et al., 2009; Mueller et al., 2009; Durcan et al., 2011; Tsou et al., 2013; Bonanomi et al., 2014a; Almeida et al., 2015; Kristensen et al., 2017; Weber et al., 2017; Wan et al., 2018; The UniProt Consortium, 2019; Lambrughi et al., 2021). Protein structure modified from Weishäupl et al. (2019), available for use via `https://doi.org/10.1074/jbc.RA118.005801` under the CC BY 4.0 license (`https://creativecommons.org/licenses/by/4.0/`).

further on protein level (Kawaguchi et al., 1994; Goto et al., 1997; Harris et al., 2010; Johnson et al., 2019). The first isoform, ataxin-3a was reported by Kawaguchi et al. (1994) while ataxin-3c (the canonical isoform) was identified by Goto et al. (1997). Both isoforms consist of a globular amino-terminus (N-terminus) with the JD followed by the two UIMs and the polyQ repeat (Figure 1.6, Goto et al., 1997; Masino et al., 2003; Sicorello et al., 2018). Alternative splicing of these two isoforms happens within exon 10 at an alternative 5' donor site which leads to a partial exclusion of exon 10 (Ichikawa et al., 2001). As a consequence, both ataxin-3 isoforms differ at their C-terminus from AA 332 on. The change in the primary sequence is also accompanied by some domain changes. While isoform ataxin-3a (ID: P54252-1) contains two UIMs, ataxin-3c (ID: P54252-2) contains three UIMs (Goto et al., 1997; Kawaguchi et al., 1994). With respect to the number of UIMs these isoforms are also sometimes referred to as 2UIM and 3UIM (Harris et al., 2010).

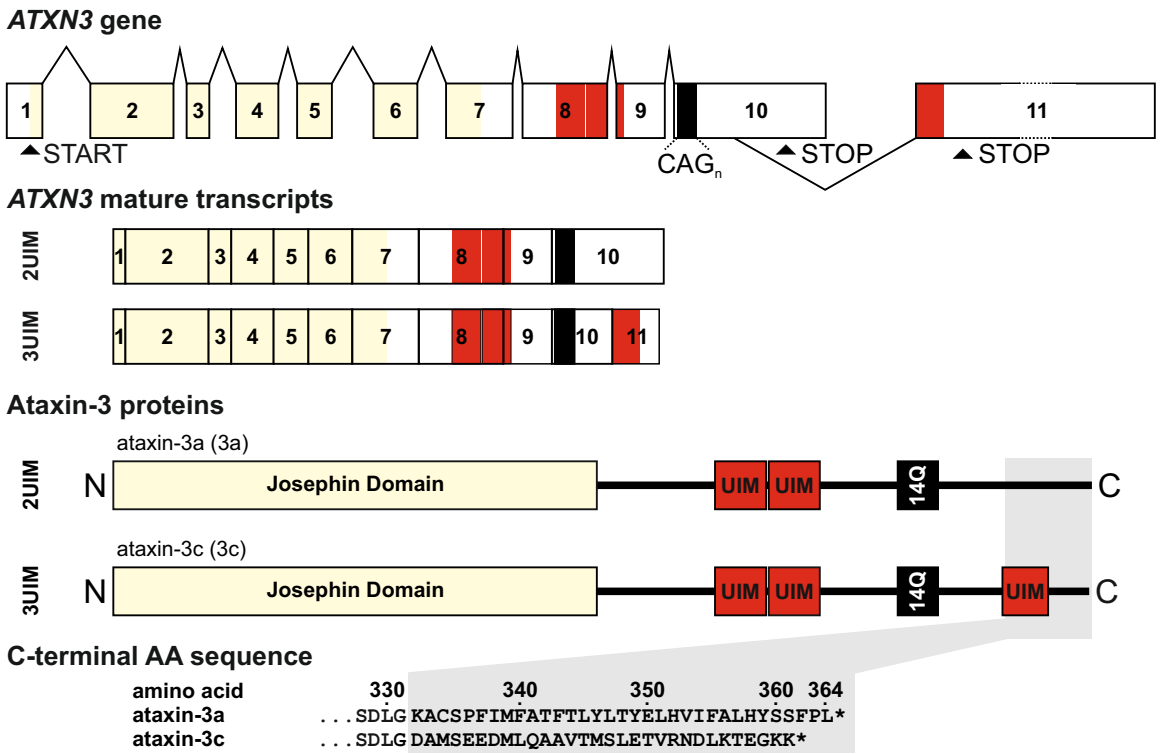

Figure 1.6. The *ATXN3* gene and ataxin-3 isoforms. Ataxin-3 is spliced alternatively into two protein isoforms named ataxin-3a and ataxin-3c which contain two or three UIMs. Both isoforms differ in their C-terminus from AA 332 on. Figure modified from Weishäupl et al. (2019) available for use via `https://doi.org/10.1074/jbc.RA118.005801` under the CC BY 4.0 license (`https://creativecommons.org/licenses/by/4.0/`).

1.1.4.2 Ataxin-3 is expressed ubiquitously

The *ATXN3* gene is expressed ubiquitously (Thul et al., 2017)[5] but is known to show regional variances within the CNS (Nishiyama et al., 1996; Paulson et al., 1997a; Schmitt et al., 1997). Although it is preferentially transcribed in neurons, it can be found in glial cells as well (Nishiyama et al., 1996). In general *pons*, *dentate* and *cerebellum* show lower protein levels. But it is unclear whether this is the result of neuronal cell death due to the involvement in MJD neurodegenera-

[5]Human Protein Atlas for *ATXN3* available from https://v18.proteinatlas.org/

tion (Trottier et al., 1998). Expression differences between normal and polyQ expanded ataxin-3 were not reported for any brain region (Paulson et al., 1997a). While it is known that cardiac and skeletal muscle express a much shorter ataxin-3 isoform (Paulson et al., 1997a), information about the expression pattern of the above mentioned ataxin-3 isoforms is hardly available. One study suggested that the canonical isoform ataxin-3c is the prominent isoform expressed in brain due to the inability of detecting ataxin-3a (Harris et al., 2010). However, data from a knockin (KI) mouse model suggests that the expansion of the polyQ repeat leads to a shift in the expression pattern towards ataxin-3a (Ramani et al., 2015).

Ataxin-3 is localized throughout the cell but seems to be mainly cytoplasmic (Paulson et al., 1997a; Wang et al., 1997; Tait et al., 1998; Trottier et al., 1998; Schmidt et al., 1998; Pozzi et al., 2008; Macedo-Ribeiro et al., 2009). The exact localization of ataxin-3 is tightly regulated by a combination of localization signals, PTMs, protein-protein interactions as well as specific cellular conditions (Trottier et al., 1998; Antony et al., 2009; Macedo-Ribeiro et al., 2009; Mueller et al., 2009; Reina et al., 2010). As mentioned before, the primary cellular localization of ataxin-3 may be the cytoplasm. However, upon proteotoxic stress, oxidative stress or heat shock ataxin-3 is translocated to the nucleus (Reina et al., 2010). The nuclear export and import of ataxin-3 is regulated by nuclear export and import signals (Figure 1.5, page 13, Antony et al., 2009; Tait et al., 1998; Albrecht et al., 2004; Macedo-Ribeiro et al., 2009). Ataxin-3 may then be transported to the nucleus by nuclear shuttling proteins which recognize the NLS. One of these proteins is karyopherin α-3 which is known to import ataxin-3 into the nucleus (Sowa et al., 2018). PTM of ataxin-3 at S335 and S347 (canonical sequence) may be a prerequisite for such a transport as phosphorylation at these positions increases the nuclear localization of ataxin-3 (Bichelmeier et al., 2007; Mueller et al., 2009).

1.1.4.3 Ataxin-3 seems to be a non-essential protein

Although ataxin-3 is a quite well studied protein, it remains unclear whether it is essential or not. A study supporting the essential role of ataxin-3 for normal cell functioning showed that a depletion of ataxin-3 using siRNA led to a cytoplasmic ubiquitin-accumulation accompanied by disorganization of the cytoskeleton and cell adhesion as well as an increased cell death (Rodrigues et al., 2010). Another study showed that a *ATXN3* knockout (KO) leads to an increase in protein ubiquitination in a mouse model (Schmitt et al., 2007). On the other hand an ataxin-3 *Caenorhabditis elegans* KO model shows no adverse phenotype (Rodrigues et al., 2007) but an improved stress-resistance (Rodrigues et al., 2011). Also, a study using lentiviruses in order to transduce shRNA into wild type rat brains did not show toxic effects (Alves et al., 2010) neither did another *ATXN3* KO model show a reduced lifespan (Switonski et al., 2011). Based on this data, ataxin-3 seems not to be essential. However, it is evolutionary conserved whereby the N-terminal part is the most highly conserved one (Scheel et al., 2003; Albrecht et al., 2004; Rodrigues et al., 2007; Schmitt et al., 2007).

1.1.4.4 Ataxin-3 has diverse molecular functions

Despite intensive research, the exact physiological function of ataxin-3 and differences between isoforms are not yet fully understood. It is known that ataxin-3 takes part in different cellular pathways and plays an important role in the ubiquitin proteasome system (UPS, Doss-Pepe et al., 2003; Zhong and Pittman, 2006; Schmitt et al., 2007) but also promotes autophagy (Ashkenazi et al., 2017; Herzog et al., 2020) and genome integrity (Tu et al., 2017; Pfeiffer et al., 2017; Singh et al., 2019). Further, it regulates the expression of different genes (Evert et al., 2001, 2003, 2006) as well as aggresome formation and shuttling (Burnett and Pittman, 2005; Mazzucchelli et al., 2009; Bonanomi et al., 2014a) and is involved in cytoskeletal organization (Rodrigues et al., 2010). The diverse molecular functions of ataxin-3 and recent experimental evidence suggest that in total it has a prominent neuroprotective character (Warrick et al., 2005; Reina et al., 2012; Tsou et al., 2013, 2015). The following paragraphs will present details on the diverse molecular functions of ataxin-3.

Ubiquitin proteasome system

Ataxin-3 is able to bind ubiquitinated proteins and acts as a deubiquitinating enzyme (Doss-Pepe et al., 2003; Burnett et al., 2003; Mao et al., 2005). Deubiquitinating enzymes are part of the protease superfamily which encompasses 561 members and can be subdivided into aspartic, metallo, serine, threonine and cysteine proteases based on their active site (reviewed in Puente and López-Otín, 2004; Puente et al., 2005). The enzymatic activity is located to the N-terminal JD (Mao et al., 2005). Ataxin-3 belongs to the cysteine proteases with a papain fold and is structurally and functionally related to two different deubiquitinating enzyme subfamilies, ubiquitin C-terminal hydrolases and ubiquitin-specific proteases (Burnett et al., 2003; Scheel et al., 2003; Evers et al., 2013a). The catalytic triad is formed by cysteine at AA position 14 (C14) which is the catalytic residue, histidin at AA position 119 (H119) which acts as a proton-donor and asparagine at AA position 134 (N134, Figure 1.7, Scheel et al., 2003). Glutamine at AA position 9 (Q9) and C14 form an oxyanion hole in order to handle the negative charge of the substrate while H119 and N134 initiate the nucleophilic attack on the peptide bond by activating the C14 side chain (Johnston et al., 1999; Albrecht et al., 2004). Generally, ataxin-3 shows a comparably slow deubiquitination (DUB) kinetic which indicates that external factors are required which could also modulate linkage specificity (Winborn et al., 2008; Reyes-Turcu and Wilkinson, 2009). Indeed, ubiquitination at AA position K117 enhances ataxin-3's enzymatic activity (Todi et al., 2009) and the binding partner VCP acts as an activator of the protein (Laço et al., 2012a).

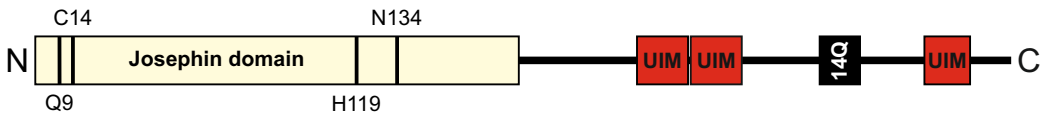

Figure 1.7. Structure of the Josephin domain. Ataxin-3's enzymatic active site is located inside the Josephin domain. The catalytic triad consists of Q9, C14, H119 and N134. While Q9 and C14 form an oxyanion hole H119 and N134 are responsible for a nucleophilic attac on the peptide bond. Figure modified from Weishäupl et al. (2019) available for use via `https://doi.org/10.1074/jbc.RA118.005801` under the CC BY 4.0 license (`https://creativecommons.org/licenses/by/4.0/`). Positions are based on the canonical sequence of UniProt (P54252, The UniProt Consortium, 2019).

Due to its JD, ataxin-3 belongs to a new family of deubiquitinases called JD-containing proteins. The family consists of two subfamilies, josephins and ataxins depending on whether they solely consist of the JD or contain additional domains (Albrecht et al., 2003; Tzvetkov and Breuer, 2007). The other family members are josephin-1 and -2 which almost solely consist of the JD and another protein sharing the JD, UIMs and the polyQ stretch called ataxin-3-like protein (Albrecht et al., 2003; Scheel et al., 2003; Matos, 2014). The N134 makes ataxin-3 more closely related to the ubiquitin-specific proteases family of deubiquitinases than the ubiquitin C-terminal hydrolases family (Scheel et al., 2003). Ubiquitin proteases of the ubiquitin C-terminal hydrolases family cleave ubiquitin from small peptides and are primarily responsible for maintaining a high level of free ubiquitins in the cell. Ubiquitin-specific proteases family members generally cleave mono-ubiquitin or ubiquitin chains from large proteins though they have a wide variety of substrates. This group is primarily responsible for editing ubiquitin chains (Chung and Baek, 1999; Wilkinson, 2000). Ataxin-3 however, was proposed to primarily shorten ubiquitin chains or edit K63-linked ubiquitin chains, topologically more complex mixed linkage ubiquitin chains or ubiquitin-like proteins (Burnett et al., 2003; Donaldson et al., 2003; Chai et al., 2004; Winborn et al., 2008). It was found that ataxin-3 indeed is capable of binding K48- and K63- linked polyubiquitin chains but preferentially cleaves K63-linked or mixed linkage chains (Burnett et al., 2003; Chai et al., 2004; Donaldson et al., 2003; Winborn et al., 2008). It thereby is able to prevent or diminish substrate delivery to the proteasome and prevent a protein's degradation (Tu et al., 2017; Liu et al., 2016; Ashkenazi et al., 2017; Pfeiffer et al., 2017; McLoughlin et al., 2020) but can also prevent removal of bound polyubiquitin chains and target misfolded proteins for proteasomal degradation (Wang et al., 2006; Li et al., 2015). Next to modulating protein turnover, ataxin-3, via its DUB activity, is also involved in regulating protein function by modulating the activity of its substrate (Scaglione et al., 2011; Durcan et al., 2012).

Ubiquitin chains are presented to the JD via ataxin-3's UIMs. UIMs are short motifs which occur in many proteins responsible for ubiquitination and ubiquitin recognition and mediate the interaction with ubiquitin (Hofmann and Falquet, 2001; Scheel et al., 2003). The UIMs thereby not only assist recruitment of substrates but also support relative positioning of those to the catalytic triad and enable trimming of polyubiquitin chains (Mao et al., 2005). Ataxin-3 preferably binds ubiquitin chains containing four or more ubiquitins via its UIMs (Burnett et al., 2003; Chai et al., 2004; Donaldson et al., 2003; Doss-Pepe et al., 2003) which is also the minimal polyubiquitin chain length for targeting proteins for proteasomal degradation (Burnett et al., 2003; Matos, 2014; Ashkenazi et al., 2017). Although, the C-terminal UIM of ataxin-3c seems to be involved in the ubiquitin presentation to the JD (Matos et al., 2011; Sicorello et al., 2018) neither a polyQ expansion nor the protein isoform was reported to have an effect on ataxin-3's activity (Tzvetkov and Breuer, 2007; Winborn et al., 2008; Harris et al., 2010).

Autophagy regulation

While it was long believed that ataxin-3 only plays a role in the UPS system recent research provided striking evidence that ataxin-3 also is a regulator of autophagy. Ataxin-3 interacts with beclin 1, a key autophagy initiator (reviewed in Maejima et al., 2016) which shows neuroprotective effects in a MJD animal model (Nascimento-Ferreira et al., 2013; Ashkenazi et al.,

2017). Ataxin-3 binds beclin 1 via the polyQ domain and deubiquitinates it. Ataxin-3-mediated stabilization of beclin 1 then leads to an increase in starvation-induced autophagy. Conversely, depletion of ataxin-3 inhibits starvation-induced autophagy (Ashkenazi et al., 2017). Further, ataxin-3 not only interacts with beclin 1 but also with microtubule-associated protein 1A/1B-light chain 3 (LC3, also known as MAP1A/MAP1B LC3 A) and gamma-aminobutyric acid receptor-associated protein via two LC3-interacting regions located within the JD in order to regulate autophagosome formation and promote the autophagic flux in an additional polyQ independent manner. The exact mechanism, however, is not yet fully understood as binding of ataxin-3 to LC3/gamma-aminobutyric acid receptor-associated protein is believed to block the enzymatic activity of the JD. Therefore, both proteins could just act as a shuttle protein or ataxin-3 could process other substrates than ubiquitin chains (Herzog et al., 2020).

Genome integrity

Ataxin-3 plays an important role in genome integrity by regulating checkpoint signaling. Ataxin-3 is known to modulate p53-mediated cell cycle arrest after DNA damage (reviewed in Menon and Povirk, 2014) by stabilizing p53 (Liu et al., 2016) but also to ensure a proper checkpoint signaling by stabilizing checkpoint kinase 1 until checkpoint termination (Tu et al., 2017). Further, ataxin-3 is also responsible for initiating the DNA repair pathway. Ataxin-3 is recruited to double strand breaks (DSBs) via DNA damage-induced SUMOylation and ensures a proper induction of the DNA damage response and DNA repair (Pfeiffer et al., 2017). Ataxin-3, however, also acts more general in the DSB signaling pathway via an ataxin-3/VCP complex which orchestrates the choice of the DNA repair pathway towards non-homologous end joining and thereby balances this pathway (Singh et al., 2019).

Transcriptional regulation

Gene expression profiling showed that ataxin-3 is able to regulate gene expression and thereby mainly suppresses the expression of various transcripts (Evert et al., 2003; Rodrigues et al., 2007). Ataxin-3 is able to bind histone proteins and represses cyclic AMP-responsive element-binding protein 1 (CREB-1)-mediated transcription and also inhibits the histone acetyltransferase activity of the major transcriptional coactivators CREB-binding protein, histone acetyltransferase p300 and P300/CBP-associated factor (PCAF) which leads to an inhibition of transcription mediated by these factors (Chai et al., 2001b; Li et al., 2002; Evert et al., 2006). Ataxin-3 also regulates the levels of heat-shock proteins (Hsp) 70, 40 and 105 (Chou et al., 2008; Reina et al., 2012). Further, ataxin-3 also seems to act as a direct inhibitor by chromatin binding. Ataxin-3 is able to directly bind chromatin regions of the matrix metalloproteinase-2 gene promoter. Transcriptional repression is then performed by recruiting histone deacetylase 3 and nuclear receptor co-repressor which leads to histone deacetylation (Evert et al., 2006). This shows that ataxin-3 is able to bind target promoter regions and acts as a direct transcriptional repressor (Evert et al., 2006; Carmo, 2011).

Aggresome formation

Ataxin-3 was also reported to be involved in aggresome formation (Burnett and Pittman, 2005). Aggresomes are membrane-free cytoplasmic inclusions that contain misfolded and ubiquitinated proteins which are surrounded by vimentin filament. Aggresomes are formed in response to an exceeded proteasome capacity and the cell's inability to degrade misfolded proteins. The transport of misfolded proteins to aggresomes in such situations therefore is crucial for cellular homeostasis (Johnston et al., 1998). It was reported that ataxin-3 is involved in trafficking misfolded proteins to aggresomes together with histone deacetylase 6 and dynein (Burnett and Pittman, 2005; Haacke et al., 2006; Mazzucchelli et al., 2009). Histone deacetylase 6 is necessary for aggresome formation and translocates polyubiquitinated proteins to dynein which facilitates the transport of misfolded proteins to the microtubule organizing center (MTOC) (Hirokawa et al., 1990; Kawaguchi et al., 2003; Burnett and Pittman, 2005; Cristofani et al., 2017). Ataxin-3 is known to interact with both proteins whereby it seems to be directly involved in the transport to the MTOC as dynein transportation requires ataxin-3's DUB activity as well as the UIMs for complex formation (Burnett and Pittman, 2005; Matos et al., 2011).

Cytoskeletal organization

Ataxin-3' interaction with histone deacetylase 6, a key regulator of the cytoskeleton (Burnett and Pittman, 2005; Valenzuela-Fernández et al., 2008) and the cytoskeletal protein tubulin (Mazzucchelli et al., 2009) also linked ataxin-3's function to the organization of the cellular cytoskeleton. A knockdown of *ATXN3* was reported to be accompanied by morphological changes, microtubule, microfilament and intermediate filament disorganization as well as loss of cell adhesion (Rodrigues et al., 2010). Even further, silencing of ataxin-3 in differentiating fibroblasts was reported to inhibit cytoskeleton development by dysregulation of integrin subunit levels (Costa et al., 2010). Such a cytoskeletal defect, however, was not reported in *ATXN3* KO animals (Schmitt et al., 2007; Rodrigues et al., 2007).

Neuroprotective function of ataxin-3

The above mentioned characteristics of ataxin-3 suggest a cell-/neuroprotective role of ataxin-3 (Warrick et al., 2005; Reina et al., 2012; Tsou et al., 2013, 2015). Indeed, different studies could show that normal ataxin-3 in *Drosophila* models protects against toxicity induced by other polyQ proteins but also by polyQ expanded ataxin-3 itself (Warrick et al., 2005; Tsou et al., 2013, 2015). The exact mechanism leading to the mitigation is not completely understood, but the neuroprotective function was reported to be mediated via the protein quality control pathway and depends on ataxin-3's DUB activity whereby ubiquitination of ataxin-3 at AA position K117 seems to be required (Warrick et al., 2005; Tsou et al., 2013). While Warrick et al. (2005) reported that the neuroprotective function is also dependent on proteasome activity, others reported that it requires UV excision repair protein RAD23 and is based on an increase in co-chaperone DnaJ-1/Hsp40 levels. Although ataxin-3 is involved in both pathways, proteasomal degradation or autophagy were not required for the neuroprotective function which suggests that the neuroprotective function is not based on modulating protein stability but on correction of protein folding and decreasing aggregates (Tsou et al., 2013, 2015). However, reports of a

neuroprotective function of ataxin-3 in higher model organisms are conflicting and could not be observed (Cemal et al., 2002; Hübener and Riess, 2010; Zeng et al., 2013).

1.1.5 Molecular Basis of Machado Joseph disease pathology

Taroni and DiDonato (2004) summarized that the polyQ expansion is disease causing because (1) there is a positive correlation between disease severity and the poly CAG expansion, (2) expression of truncated polyQ proteins or sole polyQ repeats is toxic as well and (3) introduction of a polyQ repeat into an otherwise disease-unrelated protein introduced a toxic gain of function (Maciel et al., 1995; Lerer, 1996; Ordway et al., 1997; Breuer et al., 2010; Tallaksen-Greene et al., 2003; Taroni and DiDonato, 2004; Haacke et al., 2006). The polyQ expansion may be the driving factor in neurodegeneration, but the inherited characteristics and function of the respective polyQ protein leads to an unique pathogenesis and disease. Therefore, the context of the protein and the position of the TNR repeat determines whether the underlying mutation causes a loss or a gain of function on the RNA or protein level as its function and interactions affect the pathogenesis (Gatchel and Zoghbi, 2005; Riley and Orr, 2006; Silva-Fernandes, 2010; Paulson, 2018; Lieberman et al., 2019).

The exact mechanism of MJD pathology, despite intensive research, is still not fully understood. As for all polyQ diseases, it is known that the polyQ expansion causes a neurotoxic gain of function in ataxin-3 which induces cellular dysfunctions via multiple mechanisms (Figure 1.8, Ikeda et al., 1996; Paulson et al., 1997a,b; Warrick et al., 1998; Yoshizawa et al., 2000; Paulson, 2018; Sowa et al., 2021, 2022). The toxic gain of function in all polyQ proteins is only toxic to a certain subset of neuronal cells (Cummings, 2000; Lieberman et al., 2019) which additionally highlights the importance of the protein context of the polyQ protein for the development of the individual diseases. The question of why the nervous system is selectively affected in polyQ diseases remains unknown. It was suggested that neurons may handle misfolded proteins differently from other cell types as they are highly specialized and therefore could be more sensitive to the consequences of altered protein interactions (Williams and Paulson, 2008). Further, Purkinje neurons of the *Cerebellum* are characterized by a unique metabolism and electrophysiology which could make them more susceptible to MJD neurodegeneration (Lieberman et al., 2019). Cell type-specific alternative splicing of the *ATXN3* gene and therefore the expression of certain ataxin-3 isoforms may also be a determinant for the selective toxicity (Harris et al., 2010). However, no information is available regarding the expression pattern and the contribution of ataxin-3 isoforms to the pathogenesis of MJD. Despite being a neurodegenerative disease, cellular damage is not solely restricted to neurons and toxic effects also affect neighboring cells which contributes to MJD pathogenesis (Lieberman et al., 2019). The following paragraphs will discuss the specific mechanisms that contribute to MJD pathogenesis and progression in more detail.

1.1.5.1 Aggregation

Aggregation of the polyQ expanded protein is the major hallmark of MJD (Paulson et al., 1997b; Schmidt et al., 1998) and all other polyQ diseases (Davies et al., 1997; Hayashi et al., 1998; Li et al., 1998; Skinner et al., 1997; Koyano et al., 1999; Paulson et al., 1997b; Ishikawa et al.,

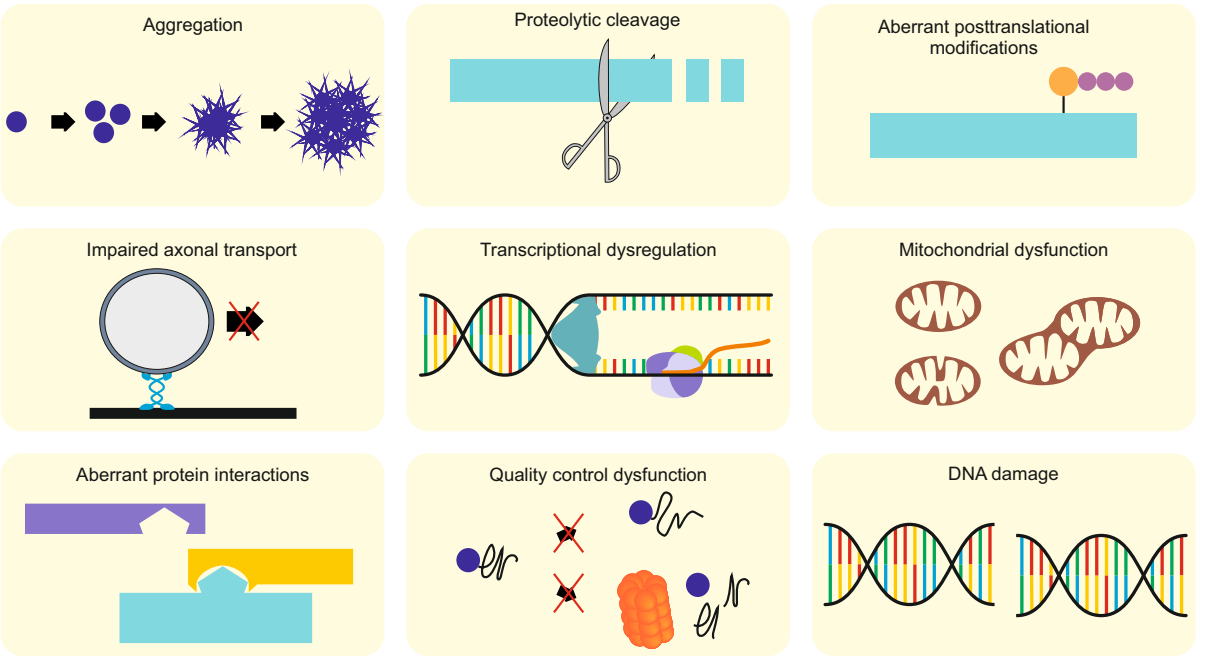

Figure 1.8. Molecular mechanisms of MJD pathology. Different mechanisms contribute to the development and progression of MJD, among others proteolytic cleavage (Miyashita et al., 1998; Wellington et al., 1998; Lunkes et al., 2002; Berke et al., 2004; Goti et al., 2004; Haacke et al., 2006; Colomer Gould et al., 2007; Haacke et al., 2007; Young et al., 2007; Breuer et al., 2010; Hübener et al., 2011, 2013; Weber et al., 2017; Weber, 2017; Weber et al., 2018; Harmuth et al., 2018) and aggregation of the disease protein ataxin-3 (Paulson et al., 1997b; Schmidt et al., 1998) as well as aberrant interactions with other proteins (Sutton et al., 2017; Lessing and Bonini, 2008) were described. Further it is known that quality control dysfunctions (Doss-Pepe et al., 2003; Zhong and Pittman, 2006; Schmitt et al., 2007; Ashkenazi et al., 2017; Herzog et al., 2020), an impaired axonal transport (Gunawardena et al., 2003; Burnett and Pittman, 2005), transcriptional dysregulation (Evert et al., 2001, 2003, 2006), mitochondrial dysfunction (Yu et al., 2009a; Kazachkova et al., 2013; Hsu et al., 2017; Harmuth et al., 2018), DNA damage (Kazachkova et al., 2013; Chatterjee et al., 2015; Tu et al., 2017; Pfeiffer et al., 2017; Singh et al., 2019) and aberrant PTMs (Fei et al., 2007; Mueller et al., 2009; Zhou et al., 2013) contribute to MJD.

1999; Holmberg et al., 1998; Nakamura, 2001). It has long been a matter of debate whether aggregates are toxic to cells or not (Davies et al., 1997; Saudou et al., 1998). Nowadays it is believed that toxicity depends on two factors, size and disease phase. Aggregates were reported to be protective in the early disease phase but become pathogenic later on (Tallaksen-Greene et al., 2003). Their toxicity then is related to their size with micro aggregates being more toxic than aggregates larger in size (Duennwald et al., 2006b; Gruber et al., 2018).

According to Masino et al. (2011) protein misfolding and aggregation has three main requirements: (1) primary structure of the protein must possess aggregation propensity information, (2) the secondary structure must have a tendency to adopt ordered or semi-ordered structures which are compatible with that of fibers (e. g. β-sheets) in a way which allows enrichment of these motifs in the tertiary structure and (3) these sequences must be accessible to the solvent and not buried inside the protein (Masino et al., 2011). Based on these assumptions, it is believed that an expansion of the polyQ repeat modifies ataxin-3's secondary structure in a way which induces misfolding of ataxin-3 and shifts the protein towards an aggregation prone conformation (Chow et al., 2004a,b; Haacke et al., 2006). Interestingly, the polyQ repeat is not involved in the first aggregation step (Masino et al., 2011). Instead, the JD plays an important role in modulating the ataxin-3 aggregation propensity by determining its stability and self-association ability (Masino et al., 2004; Matos et al., 2011) and indeed, ataxin-3 with less than 40 Q-repeats

is also able to aggregate under destabilizing conditions (e. g. thermal-, pressure- or chemically induced, Masino et al., 2011, 2004; Marchal et al., 2003; Chow et al., 2004b; Shehi et al., 2003). Although not being involved in the first aggregation step, the C-terminus of ataxin-3 modifies the aggregation phenotype and ataxin-3c was reported to show a more prominent aggregation than ataxin-3aL (Harris et al., 2010).

Aggregates were detected in the cytoplasm and axons of neurons in a variety of CNS regions (Seidel et al., 2010). However, the primary observation in MJD are nuclear inclusions in neurons of various brain regions (Paulson et al., 1997b; Schmidt et al., 1998; Seidel et al., 2012). These aggregates are highly associated with disease pathogenesis (Schmidt et al., 1998; Tait et al., 1998; Fujigasaki et al., 2000; Bichelmeier et al., 2007; Sowa et al., 2018) and in fact, the nucleus is a major site of pathogenesis in polyQ disorders (Skinner et al., 1997; Klement et al., 1998; Katsuno et al., 2002; Takeyama et al., 2002; Lieberman et al., 2019). Pathogenicity of aggregates may arise due to their localization and intrinsic sequestration properties. It is known that they sequester other proteins which are important for normal cellular functions like transcription factors, proteasome subunits and chaperones (Perez et al., 1998; McCampbell, 2000; Chai et al., 1999b,a). Further, it is known that aggregates are also able to destabilize the lipid bilayer (McLaurin and Chakrabartty, 1997; Jayasinghe and Langen, 2007; Butterfield et al., 2002; Pellistri et al., 2013; Matos, 2014; Zhang et al., 2017b). Nonetheless, there is only partial correlation between nuclear inclusions and neuronal loss which shows that either factors other than (nuclear) aggregates are contributing to cell death (Muñoz et al., 2002) or other additional factors are required in order to become toxic.

1.1.5.2 Impaired axonal transport

The sheer size of neurons requires continuous transport of cargo between e. g. soma and synapses and proper neuronal function critically depends on these processes (reviewed in Mandal and Drerup, 2019). Therefore, it was suggested that an impaired axonal transport could contribute to the pathology of polyQ disorders (Gunawardena et al., 2003). Aggregates in axons could indeed be found in several brain regions affected by MJD (Seidel et al., 2010) and due to their ability to physically impair cellular functions by inhibiting axonal transport they could be of even higher relevance for pathology than the observed nuclear inclusions (Morfini et al., 2005). Further, the fact that ataxin-3 seems to regulate dynein-dependent processes (Burnett and Pittman, 2005) shows that axonal transport could also be dysregulated in MJD as dynein is responsible for retrograde axonal transport and vesicle trafficking (Paschal and Vallee, 1987; Hirokawa et al., 1990; Martin et al., 1999).

1.1.5.3 Aberrant interactions

Ataxin-3 is expressed throughout the brain (Nishiyama et al., 1996; Paulson et al., 1997a; Schmitt et al., 1997) and the observed neuronal damage in MJD does by far not correlate with the expression pattern of ataxin-3. This clearly shows, that there must be other factors which make the MJD affected neurons susceptible to neurodegeneration upon expression of a polyQ expanded ataxin-3. Most likely these are certain interaction partners which are expressed or pathways which are activated in these neurons (Takahashi et al., 2010). Ataxin-3 is known to

interact with numerous binding partners (reviewed in doCarmo Costa and Paulson, 2012) and a few are already known to ameliorate or worsen MJD pathology. The most prominent example may be UV excision repair protein RAD23 homolog A and UV excision repair protein RAD23 homolog B (HR23A and HR23B). HR23A/B is a regulator of the ataxin-3 protein level (Blount et al., 2014) and disruption of their interaction increases the toxicity of polyQ expanded ataxin-3 (Sutton et al., 2017).

Another important protein is ataxin-2, which is the polyQ expanded protein in SCA2 (Pulst et al., 1996). It could be shown that ataxin-2 activity accelerates the formation of aggregates and neurodegeneration in a *Drosophila* model. This example prominently shows that polyQ induced toxicity of an expanded protein can be modified by the physiological function of another (polyQ) protein (Lessing and Bonini, 2008).

1.1.5.4 Proteolytic cleavage

Various studies suggest a toxic fragment hypothesis in which proteolytic fragmentation of ataxin-3 contributes to the pathogenesis of MJD and other polyQ disorders (Miyashita et al., 1998; Wellington et al., 1998; Lunkes et al., 2002; Berke et al., 2004; Goti et al., 2004; Haacke et al., 2006; Colomer Gould et al., 2007; Haacke et al., 2007; Young et al., 2007; Breuer et al., 2010; Hübener et al., 2011, 2013; Matos, 2014; Weber et al., 2017; Weber, 2017; Weber et al., 2018; Harmuth et al., 2018). Ataxin-3 is cleaved by caspases (Wellington et al., 1998; Berke et al., 2004), calpains (Haacke et al., 2007; Hübener et al., 2011, 2013; Weber et al., 2017; Weber, 2017; Weber et al., 2018) and autolytic cleavage (Mauri et al., 2006) at various positions: AA 190 (Colomer Gould et al., 2007), AA 191 (Mauri et al., 2006), AA 208 (Weber et al., 2017), AA 238 (Mauri et al., 2006), AA 241 (Mauri et al., 2006), AA 241-248 (Berke et al., 2004), AA 250 (Haacke et al., 2006), AA 256 (Weber et al., 2017; Mauri et al., 2006), AA 257 (Mauri et al., 2006), AA 272 (Mauri et al., 2006), AA 302 (Mauri et al., 2006), AA 305 (Mauri et al., 2006), AA 340 (Mauri et al., 2006) and AA 341 (Mauri et al., 2006, Figure 1.5, page 13). It is known that cleavage fragments, especially when encompassing the polyQ stretch, are misfolding whereby they undergo an aggregation-prone conformational change (Ross et al., 2003; Chiti and Dobson, 2009). Such aggregates are also capable of interacting with full-length ataxin-3, destabilize it and incorporate it into aggregates (Haacke et al., 2006). Expression of C-terminal fragments indeed was shown to increase ataxin-3 aggregation (Berke et al., 2004; Haacke et al., 2006, 2007; Hübener et al., 2013; Weber et al., 2017) and thereby presumably boost various disease pathways leading to toxicity and neurodegeneration (Goti et al., 2004; Hübener et al., 2013; Weber et al., 2017; Harmuth et al., 2018).

1.1.5.5 Transcriptional dysregulation

Ataxin-3 and other polyQ aggregates are known to be predominantly localized to the nucleus (Perez et al., 1998; Schmidt et al., 1998; Sowa et al., 2018). Transcriptional dysregulation therefore may play an important role in MJD pathogenesis and other polyQ disorders as it could be found that transcription factors are recruited to nuclear inclusions (Evers et al., 2014). Ataxin-3 is known to interact with the transcription factor TBP (TATA-box-binding protein) and the transcription co-factor CREB-binding protein which both could be detected in nuclear ataxin-3 aggregates (Perez et al., 1998; McCampbell, 2000; Riley and Orr, 2006; Matos, 2014).

Further, Evert et al. (2003) reported that differentially regulated genes involved in nuclear transcription, cell surface processes and inflammation could be identified in cells expressing normal or polyQ expanded ataxin-3. Another study revealed different membrane associated and inflammatory genes which are upregulated upon expression of expanded ataxin-3 and known to be involved in other diseases (Evert et al., 2001; Laço et al., 2012b). As mentioned before, ataxin-3 is able to recruit histone deacetylase 3 and nuclear receptor co-repressor 1/2 (N-CoR1/2) in order to suppress matrix metalloproteinase-2 transcription (Evert et al., 2006). Upon a polyQ expansion, ataxin-3 looses the ability to recruit these factors and therefor was not able to repress its transcription which shows that transcriptional dysregulation at least partly happens due to a direct loss of repressor function (Evert et al., 2006). Because non-expanded ataxin-3 is sequestered into protein aggregates, Evert et al. (2006) suggested that physiologically repressed genes may be upregulated due to the loss of a repressing function. This could support the pathogenic effect of mutant ataxin-3 which is associated to the induction of an inflammatory cascade, possibly, due to the loss of repressor function as well as the gain in activator function which leads to an altered gene expression in MJD (Evert et al., 2001, 2003, 2006).

1.1.5.6 Quality control dysfunction

Due to cellular errors, every cell produces high amount of damaged or misfolded proteins which are rapidly degraded (Schubert et al., 2000). Proper function of a quality control system regulating protein turnover therefore is important for cellular function and viability as a dysfunction causes accumulation of damaged, misfolded and aggregation prone proteins and thus contribute to polyQ pathology (reviewed in Nedelsky et al., 2008). This is especially true for neurons which are not capable of diluting toxic proteins by cell division (Nascimento-Ferreira et al., 2013).

Ataxin-3 seems to play an important role in the UPS (Doss-Pepe et al., 2003; Zhong and Pittman, 2006; Schmitt et al., 2007; Silva-Fernandes, 2010) and autophagy (Ashkenazi et al., 2017; Herzog et al., 2020) mediated protein quality control. Although the DUB activity of ataxin-3 seems not to be affected by a pathogenic expansion of the polyQ repeat and a direct loss of ataxin-3 function upon polyQ expansion was not yet described a hindrance of required interactions may be able to negatively affect this system. McLoughlin et al. (2020) suggested that already a modest UPS inhibition could have deleterious effects within neurons and MJD patients indeed show increased levels of polyubiquitinated protein aggregates (Sittler et al., 2018) and signs of an proteasomal overload (Seidel et al., 2012). Dysfunctions within this system may be induced by a depletion of important quality control proteins as sequestration of polyubiquitinated proteins, chaperones, UPS regulatory proteins and subunits was reported (Chai et al., 1999a,b; Schmidt et al., 2002; Seidel et al., 2010). Dysfunctions in protein degradation then can lead to further disturbances in other pathways, for example the O-linked β-N-acetylglucosamine cycle (Pereira Sena et al., 2021).

Next to the UPS system various autophagy proteins are known to be dysregulated in MJD *post mortem* brain. The two important autophagy proteins sequestosome 1/p62 and LC3, a ataxin-3 interactor (Herzog et al., 2020), were reported to be localized to aggregates (Sittler et al., 2018). Additionally, beclin1 levels in MJD fibroblasts were found to be reduced which causes an impaired autophagic flux and autophagosome formation (Onofre et al., 2016). Beclin 1 binding to ataxin-3 is known to promote autophagy by beclin 1 stabilization. However, the

interaction is competed by other polyQ proteins as well as polyQ expanded ataxin-3 itself which leads to reduced beclin 1 levels and subsequently impairment of the autophagic flux (Ashkenazi et al., 2017). Altogether, this data suggests a strong dysregulation of autophagy in MJD (Onofre et al., 2016; Sittler et al., 2018). This is particularly problematic as the major cellular pathway for degradation of polyQ expanded proteins was reported to be autophagy (Ravikumar et al., 2002) and an autophagy enhancement can ameliorate the MJD phenotype (Menzies et al., 2010; Watchon et al., 2017; Marcelo et al., 2019; Nóbrega et al., 2019).

Lastly, aggresomes are important deposits of misfolded and damaged proteins, when a cell is not able to degrade them (Johnston et al., 1998), however, it was reported that aggresome formation is dysfunctional in a MJD cell model which likely increases the toxicity of expanded polyQ proteins (Burnett and Pittman, 2005; Williams and Paulson, 2008).

1.1.5.7 Aberrant posttranslational modification

PTMs are an important cellular mechanism in order to regulate protein characteristics for a proper protein function, localization, interaction and turnover. It is known that PTMs modify various protein characteristics of different polyQ proteins including ataxin-3 (reviewed in Sambataro and Pennuto, 2017). Ataxin-3 is subject to ubiquitination, phosphorylation and SUMOylation (Figure 1.5, page 13, Matsumoto et al., 2004; Fei et al., 2007; Zhou et al., 2013). While ubiquitination changes ataxin-3's protein stability (Matsumoto et al., 2004; Jana et al., 2005), SUMOylation changes the stability and possibly affects various protein-protein interactions in which ataxin-3 engages (Geiss-Friedlander and Melchior, 2007; Zhou et al., 2013). Lastly, phosphorylation changes ataxin-3's stability, localization and aggregation propensity (Fei et al., 2007; Tao et al., 2008; Mueller et al., 2009). Among the afore mentioned modifications especially SUMOylation and phosphorylation may modify ataxin-3's toxicity. SUMOylation at K166 increases the protein's stability (Zhou et al., 2013), whereby SUMOylation at K356 (only present in ataxin-3c) reduces the aggregation propensity (Almeida et al., 2015). Phosphorylation at S236, S256, S260, S261. S335 and S347 (all positions based on canonical sequence) increase the stability and the nuclear translocation and aggregation of ataxin-3 with all its devastating consequences (Fei et al., 2007; Tao et al., 2008; Mueller et al., 2009).

1.1.5.8 Mitochondrial dysfunction

Mitochondrial function within neurons is of great importance in order to ensure membrane excitability and proper neurotransmission (Kann and Kovács, 2007). Therefore, it is not surprising that mitochondrial dysfunction is strongly associated with diverse neurodegenerative diseases including polyQ disorders (Johri and Beal, 2012). The normal cellular function of ataxin-3 already links ataxin-3 to mitochondria as various interaction partners could be mapped to mitochondrial function in a study by Kristensen et al. (2018). Further, ataxin-3 is involved in mitochondrial dynamics by interacting with parkin (Durcan et al., 2011) which promotes macroautophagy of mitochondria (Narendra et al., 2008). In line with its involvement in mitochondrial dynamics, mitochondrial fission and fusion was shown to be disrupted in a cell model of MJD accompanied by an increased membrane potential, reactive oxygen species and cell death (Hsu et al., 2017). Such a mitochondrial dysfunction could additionally be confirmed in an animal model (Hsu et al., 2017). Oxidative stress, as mentioned before, again increases the nuclear localiza-

tion of ataxin-3 and leads to the described adverse effects (Sowa et al., 2018). Recently also an N-terminal ataxin-3 cleavage fragment was shown to affect mitochondrial morphology, function and homeostasis and increases the cell's susceptibility for apoptosis in a cell model (Harmuth et al., 2018). Lastly, reduced mtDNA copy numbers could be found in MJD cell lines and patients showing that mutant ataxin-3 may promote mtDNA damage or depletion which leads to mitochondrial dysfunctions (Yu et al., 2009a; Tien et al., 2008; Kazachkova et al., 2013). These examples prominently show that mitochondrial dysfunction plays an important role in the pathology of MJD and other neurodegenerative disorders (Haacke et al., 2006).

1.1.5.9 DNA damage

DNA damage in MJD is not solely restricted to DNA. MJD *post mortem* brain and animal models show an accumulation of DNA damage (Kazachkova et al., 2013; Chatterjee et al., 2015) which also leads to the association of ataxin-3 to cancer (Zeng et al., 2014; Sacco et al., 2014) and liver cirrhosis (Wang et al., 2018a). It is known that normal and expanded ataxin-3 is recruited to DNA damage in a SUMOylation-dependent manner and that ataxin-3 promotes DNA repair and genome integrity by stabilizing DNA damage response signaling (Tu et al., 2017; Pfeiffer et al., 2017; Singh et al., 2019). Absence of ataxin-3 on the other hand is accompanied by a reduced repair capacity (Pfeiffer et al., 2017). The exact pathogenic mechanism leading to an increased DNA damage are not yet fully understood but it is hypothesized that either the enhanced nuclear localization could lead to an increased stabilization of DNA damage response proteins or physiological function of ataxin-3 is lost due to a sequestration-induced depletion of normal ataxin-3 (McLoughlin et al., 2020).

1.1.6 Animal models of MJD

Animal models are an important research tool for studying disease proteins due to the inability of studying pathogenesis in humans *ante mortem* and their scalable complexity. Accordingly, various models were generated in order to study MJD pathology, treatment strategies and the normal function of ataxin-3 (reviewed in Schmidt and Schmidt, 2018). Among them are diverse mouse models (Ikeda et al., 1996; Cemal et al., 2002; Goti et al., 2004; Bichelmeier et al., 2007; Colomer Gould et al., 2007; Torashima et al., 2008; Chou et al., 2008; Boy et al., 2009, 2010; Silva-Fernandes et al., 2010; Hübener et al., 2011; Silva-Fernandes et al., 2014; Switonski et al., 2015; Ramani et al., 2015; Schmidt et al., 2019; Haas et al., 2020), one rat model (Alves et al., 2008b), *D. melanogaster* (Warrick et al., 1998, 2005; Kretzschmar et al., 2005; Jung et al., 2009; Johnson et al., 2019) and *C. elegans* models (Khan et al., 2006; Teixeira-Castro et al., 2011; Christie et al., 2014) as well as the first *D. rerio* (Watchon et al., 2017) and non-human primate model (Tomioka et al., 2017). The models partially well describe the human MJD pathology with varying aao and symptoms but also show some discrepancies like an absence of symptoms in the presence of a CAG expansion and the fact that mice also seem to better tolerate expanded CAG repeats within the *ATXN3* gene than humans do (Boy et al., 2010; Silva-Fernandes et al., 2010, 2014; Ramani et al., 2015).

1.2 Alternative splicing of *ATXN3* in combination with the haplotype could modify protein characteristics and thereby act as a disease modifier in MJD

Ataxin-3 is modified by two different means, alternative splicing, i. e. the varying combination of exons and SNPs leading to AA substitutions in the protein. The modification of ataxin-3 by both factors and their possible impact on protein characteristics will be explained in the following sections.

1.2.1 Alternative splicing could modify major ataxin-3 characteristics

The *ATXN3* gene is spliced alternatively whereby at least 56 different transcripts were reported which allow for a translation of different ataxin-3 isoforms (Ichikawa et al., 2001; Bettencourt et al., 2010, 2013). Despite multiple isoforms are generated, only two - ataxin-3a and ataxin-3c - are considered to be full-length proteins (Kawaguchi et al., 1994; Goto et al., 1997) and are therefore of major interest for the protein's function. Both isoforms show a mostly identical primary sequence and only differ in their C-terminus from AA 332 on. While the C-terminus of ataxin-3a comprises of an unstructured sequence, the inclusion of exon 11 in ataxin-3c leads to a third UIM at the C-terminus of this isoform. Both isoforms therefore differ in their number of UIMs and their C terminal AA composition (see 1.1.4.1, page 13, Goto et al., 1997). Although isoforms of ataxin-3 were described shortly after the identification of the *ATXN3* gene (Goto et al., 1997), to date relatively little is known about their exact differences (Harris et al., 2010). However, as already minor changes in a proteins sequence can have a great impact on different aspects of the protein like molecular function, subcellular localization or interaction, a disparity between ataxin-3 isoforms can be expected (Tadokoro et al., 2005; Hu et al., 2009b; Asselin-Mullen et al., 2017). Indeed, initial studies presented first hints that ataxin-3 isoforms partially show differential effects in cell and animal models of MJD (Harris et al., 2010; Johnson et al., 2019), but it remains unclear why and to which extent splicing induced variations in the ataxin-3 C-terminus cause functional differences on the protein level. Goto et al. (1997) reported that due to their AA composition the C-terminus of ataxin-3a is hydrophobic while the C-terminus of ataxin-3c with the third UIM is hydrophilic which could indicate structural and functional differences. The C-terminus of ataxin-3 also contains important sites for PTM and molecular interaction (Burnett et al., 2003; Mueller et al., 2009; Durcan et al., 2011; Bonanomi et al., 2014a; Almeida et al., 2015). Based on these observations and the fact that ataxin-3 isoforms show differences in their domains it was hypothesized that ataxin-3c and ataxin-3a isoforms are two proteins which at least to some extent carry out different functions within a cell. These differences possibly affect various physiological an pathophysiological characteristics of the ataxin-3 protein like its (1) DUB activity, (2) interaction, (3) subcellular localization, (4) protein stability, (5) transcriptional regulation as well as (6) protein aggregation and (7) cleavage. The presence of a third UIM in ataxin-3c suggests that it has a special function which requires the interaction with ubiquitins. Nicastro et al. (2009) hypothesized that the third UIM increases the affinity for ubiquitin, but it was found that the C-terminus of ataxin-3c does not interact with the JD (Sicorello et al., 2018). This led to the hypothesis that ataxin-3c acts as a

molecular ruler selecting polyubiquitin chains of at least four ubiquitins whereby the C-terminus transports the ubiquitins to the JD (Sicorello et al., 2018). The presence or absence of the third UIM in ataxin-3a may also affect ataxin-3's interaction with parkin and ubiquitin which takes place via the UIMs (Burnett et al., 2003; Durcan et al., 2011). Further the major interaction site for tubulin, tubulin binding region 3, also falls in the region affected by alternative splicing and it could already be shown that ataxin-3 isoforms show a differing affinity for tubulin (Bonanomi et al., 2014a). Alternative splicing of *ATXN3* not only leads to the presence or absence of a third UIM it also affects PTMs of ataxin-3 in the alternatively spliced C-terminus. Phosphorylation of S335 and S347 (Mueller et al., 2009, S340 and S352 due to 19 glutamine repeats) can only take place in ataxin-3c. It is known that phosphorylation of these serines regulates the nuclear localization of ataxin-3, its stability, the formation of nuclear inclusions as well as ataxin-3's ability to suppress transcription (Bichelmeier et al., 2007; Mueller et al., 2009). Therefore, differences in these characteristics can be expected between ataxin-3 isoforms. Further the SUMOylation site at K356 as well is only present in ataxin-3c and known to modify ataxin-3 aggregation as well as its interaction with VCP (Almeida et al., 2015). Lastly, cleavage of ataxin-3 generates isoform-specific C terminal ataxin-3 fragments which are considered to be important for MJD pathogenesis and may affect ataxin-3 aggregation (Haacke et al., 2006; Haacke, 2006; Haacke et al., 2007; Weber et al., 2017). This data illustrates that ataxin-3 isoforms are likely to vary in their properties, but exact physiological and pathophysiological differences remain elusive so far.

Although vertebrate models comparing ataxin-3 isoforms do not exist, a recent *D. melanogaster* model published by Johnson et al. (2019) made the first attempt of directly comparing ataxin-3 protein isoforms *in vivo*. The authors found that ataxin-3aL shows a lower expression level and therefore a less pronounced aggregation phenotype than ataxin-3c which was also reported by Harris et al. (2010). However, they also stated that when the protein level is increased to the ataxin-3c level, both proteins do not differ in their aggregation phenotype (Johnson et al., 2019). Further, although ataxin-3c is believed to be the main isoform expressed in brain (Harris et al., 2010) an *ATXN3* KI mouse model suggests that splicing of the *ATXN3* gene may be dysregulated as part of the MJD disease pathology (Ramani et al., 2015). The expression level of ataxin-3a thus positively correlates with the *ATXN3* CAG repeat expansion which leads to a shift of the ataxin-3 expression towards ataxin-3a. This increase in the expression of a certain transcript upon a CAG expansion raises the question whether the characteristics of the respective isoform affect MJD pathology (Ramani et al., 2015).

1.2.2 The *ATXN3* haplotype has a major impact on one ataxin-3 isoform and could act as a modifier of MJD pathogenesis

Ataxin-3 is not only modified by alternative splicing. Additionally, SNPs within the *ATXN3* gene alter the protein sequence. At least three of them are located within exons (see 1.1.3.2, page 10) and are known to modify the primary sequence of ataxin-3 isoforms (Figure 1.9). In detail, the SNP rs1048755 in exon 8 leads to an exchange of valin to methionin at AA position 212 (p.Val212Met). SNP rs12895357 in exon 10 leads to the exchange of glycin by arginin at AA position 306 (p.Gly306Arg). SNP rs7158733 , in contrast, leads to a nonsense mutation at AA 349 instead of tyrosine and creates a premature termination codon (PTC) (c.991+56C>T). Due to the location of SNP rs7158733 3' of the alternative splice site in exon 10 the nonsense SNP is only present in the transcript of isoform ataxin-3a. Therefore, this isoform occurs in a full length (long, L) and a truncated (short, S; ID: *VAR_013690*) form.

The haplotype of the normal and the CAG expanded *ATXN3* allele follows a yin-yang pattern (Zhang et al., 2003; Martins et al., 2008). Importantly, this leads to the fact that for 72 % to 96 % of MJD patients the normal ataxin-3 can occur as isoforms ataxin-3aL and ataxin-3c (haplotype GGC) while the expanded isoforms are ataxin-3aS and ataxin-3c (haplotype ACA, Igarashi et al., 1996; Matsumura et al., 1996; Stevanin et al., 1997; Goto et al., 1997; Maciel et al., 1999; Gaspar et al., 2002; Dengler, 2018). Ataxin-3aS therefore is highly associated to MJD (Dengler, 2018).

Despite this strong association, so far it is unknown whether the haplotype of *ATXN3* has any impact on ataxin-3's function. However, it is known that it has a strong influence on the aao of MJD (see 1.1.3.2, page 10, Gaspar et al., 2002; Dengler, 2018). The haplotype ACA vs GGC reduces the mean aao from 48 years to 40 years when present in the expanded allele. Surprisingly, when it is present in the normal allele it has an even stronger effect and reduces the mean aao from 42 years to 36 years (ACA vs. GGC). It is obvious that factors which have an influence on the aao especially modify disease pathogenesis. The fact that this SNP has a strong influence on the aao and that it is only present in one isoform suggests that alternative splicing together with the patient's haplotype has a major impact on MJD pathogenesis. Despite this correlation is well understood, its mechanism remains elusive. However, the odds are that alternative splicing together with the haplotype affect physiological and pathophysiological characteristics of ataxin-3.

In summary, ataxin-3 is a deubiquitinating enzyme with two full-length isoforms that are created by alternative splicing of the *ATXN3* gene. The protein isoforms are further modified by the *ATXN3* haplotype whereby the presence of a nonsense SNP creates a truncated variant which is highly associated to MJD and known to accelerate the disease onset. Although alternative splicing between these isoforms only affects the proteins C-terminus, they differ not only in their number of UIMs but also in important domains for molecular interaction and PTM. Multiple studies render it likely that ataxin-3 isoforms differ substantially in important physiological and pathophysiological characteristics which builds the basis for the observed effects on the aao. In order to better understand the mechanisms of the haplotype impact on a patient's aao it is important to gain further knowledge about the characteristics of ataxin-3 isoforms by better understanding the physiological differences and the potential changes which are introduced by a pathological expansion of the polyQ repeat (Weishäupl et al., 2019).

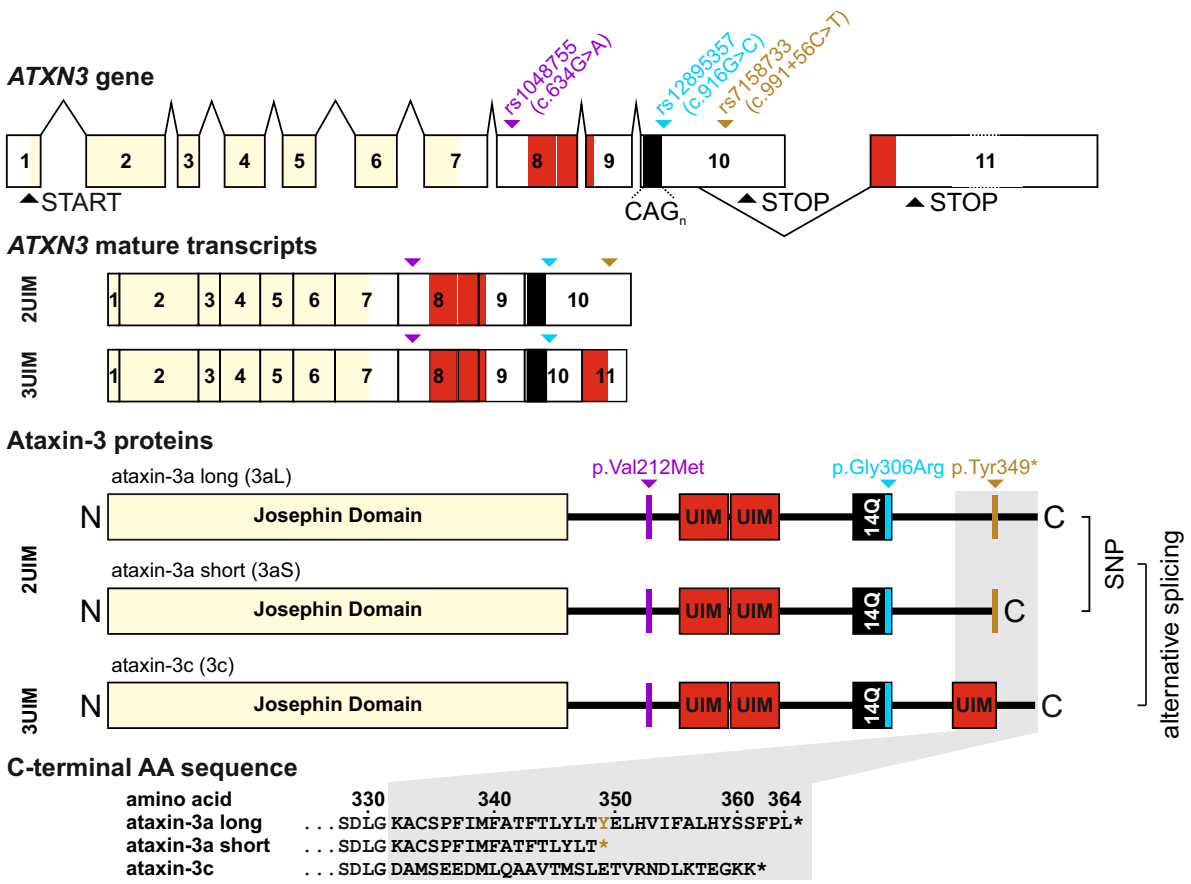

Figure 1.9. Ataxin-3 is modified by alternative splicing and the haplotype. Ataxin-3 is spliced alternatively into two protein isoforms named ataxin-3a and ataxin-3c which contain two or three UIMs. Ataxin-3a is further modified by SNPs. SNP rs1048755 (▼) and rs12895357 (▼) cause AA substitutions. SNP rs7158733 (▼) leads to a premature stop in ataxin-3a, thus this isoform exists in two variants ataxin-3aL (long) and ataxin-3aS (short) which differ in their last 16 AA. Figure was first published in Weishäupl et al. (2019), available for use via `https://doi.org/10.1074/jbc.RA118.005801` under the CC BY 4.0 license (`https://creativecommons.org/licenses/by/4.0/`).

2 | Objectives of the study

Alternative splicing and modification of the *ATXN3* gene by single nucleotide polymorphisms (SNPs) are well reported for Machado Joseph disease (MJD). Despite being a modifier of the proteins' primary sequence and the age at onset (aao), the impact of alternative splicing and the SNPs on physiological and pathophysiological characteristics of ataxin-3 remain largely elusive. Different studies indicate disparities in the physiological function of main isoforms and their impact for the pathogenesis of MJD. Therefore, the current study should focus on aspects of the proteins main function in order to clarify differences between the main isoforms on a physiological and a pathophysiological level and assess the potential of a therapeutic treatment in order to compensate for the truncation of one isoform.

Aim 1: To assess differences between the physiological characteristics of the isoforms
Differences between ataxin-3 isoforms in their physiological characteristics should be assessed using *in vitro* methods. The investigation should especially focus on stability, enzymatic activity, subcellular localization, molecular interaction and transcriptional regulation as differences between the isoforms can be expected for these characteristics.

Aim 2: To assess differences between the pathophysiological characteristics of the isoforms
After assessing the physiological characteristics of all three isoforms, next they should be examined on a pathophysiological level using *in vitro* methods. As aggregation of ataxin-3 is a hallmark of MJD this analysis will focus on the individual aggregation behavior of the isoforms.

Aim 3: To clarify whether a cross talk of ataxin-3 isoforms can modify physiological and/or pathophysiological characteristics
The presence of different combinations of ataxin-3 isoforms within a cell makes it possible that ataxin-3 isoforms have an impact on each other's physiological function or may alter pathophysiological characteristics. Therefore, the effects of a mutual ataxin-3 expression on stability and aggregation of ataxin-3 isoforms should be analyzed. In order to exclude an impact of a background expression of *ATXN3* these experiments should be performed in an *ATXN3* knockout (KO) cell line which will be verified for this purpose.

Aim 4: To generate an ataxin-3a isoform-specific antibody

The detection of a protein requires a specific antibody. To date only one isoform-specific antibody directed against ataxin-3 is available causing a lack of discrimination between ataxin-3 isoforms. In order to enable a specific detection of the other isoforms as well, a new ataxin-3-specific antibody should be created against the C-terminus of these isoforms.

Aim 5: To generate an isoform-specific MJD zebrafish model

Various animal models of MJD were described. However, these models focus on a single isoform or were designed as knockin models. One *D. melanogaster* model only compared two ataxin-3 isoforms. In order to be able to verify obtained results for all three isoforms and to enable a direct comparison of these isoforms *in vivo* the first vertebrate isoform-specific MJD zebrafish model should be created.

Aim 6: To assess the potential of a therapeutic read-through of the premature termination codon in *ATXN3*aS transcripts

One SNP of *ATXN3* causes a premature termination codon (PTC) and leads to an earlier aao in MJD patients. Therefore, a therapeutic reconstitution of the full-length isoform may be beneficial for patients carrying this SNP. The potential for a reconstitution should be assessed by translational read-through of the stop codon using aminoglycoside antibiotics. The efficiency of such a treatment should be measured by means of the relative full-length protein level and protein aggregation.

3 | Material and Methods

3.1 Devices, Consumables and Software

Devices are summarized in Table 3.1. Table 3.2 lists the used materials, chemicals and reagents. Buffers and media are shown in Table 3.3 together with their respective composition. Table 3.4 shows all enzymes. Kits used during the work are listed in Table 3.6. Table 3.7 specifies the exact primer sequences. Synthesized gBlocks are listed in Table 3.8. All primary and secondary antibodies are listed in Table 3.9. Table 3.10 summarizes the software used for obtaining and processing data and Table 3.11 specifies the exact designation of eucaryotic cells as well as the genotype of used *Escherichia coli* (*E. coli*) strains. Table 3.12 summarizes all details about animals used and Table 3.13 provides details about used expression constructs.

Table 3.1. Used devices and manufacturer. This table summarizes used devices and manufacturer details. Standard lab equipment was used in addition to the devices listed.

Device	Manufacturer
AxioCam MRm	Carl Zeiss Microscopy, Jena, Germany
Axioplan 2 Imaging System with ApoTome	Carl Zeiss Microscopy, Jena, Germany
Avanti J-30 I	Beckman Coulter, Beverley, MA, USA
BioPhotometer	Eppendorf, Wesseling-Berzdorf, Germany
CEQ 8000 Genetic Analysis System	Beckman Coulter, Beverley, MA, USA
Concentrator 5301	Eppendorf, Wesseling-Berzdorf, Germany
µCuvette G1.0	Eppendorf, Wesseling-Berzdorf, Germany
Eclipse TS100	Nikon, Düsseldorf, Germany
Ecno Pump	Bio-Rad Laboratories, Munich, Germany
EnVision Multimode Plate Reader	PerkinElmer, Rodgau, Germany
HPLC system for LC-MSMS Dionex Ultimate 3000 RSLC	Thermo Fisher Scientific, Karlsruhe, Germany
L-4000A UV Detector	Hitachi, Tokyo, Japan
L-6200 Intelligent Pump	Hitachi, Tokyo, Japan
LC-Organizer	Hitachi, Tokyo, Japan
Leica TP 1020	Leica Biosystems, Buffalo Grove, IL, USA
Light Cycler 480 II	Roche Molecular Systems, Mannheim, Germany
Magnefect-nano II	NanoTherics, Newcastle under Lyme, UK
Minifold II Slot Blot System	GE Healthcare, Munich, Germany

Continued on next page

Table 3.1. Used devices and manufacturer. – *Continued from previous page*

Device	Manufacturer
NucleoCounter NC-3000	ChemoMetec, Allerod, Denmark
Odyssey FC	LI-COR Biosciences, Bad Homburg, Germany
Paraffin embedding station EG1160	Leica Biosystems, Buffalo Grove, IL, USA
Pump P1	Pharmacia Biotech, Piscataway, NJ, USA
Q-Exactive Plus tandem mass spectrometer	Thermo Fisher Scientific, Karlsruhe, Germany
Rotor JA-10	Beckman Coulter, Beverley, MA, USA
Rotor JA-25.50	Beckman Coulter, Beverley, MA, USA
Plate reader Synergy TM HT	Bio-Tek Instruments, Bad Friedrichshall, Germany
Thermo Cycler G-Storm	AlphaMetrix Biotech, Rodermark, Germany
Ultra-Turrax disperser VDI 12 (disperser S12N-5S)	VWR International, Darmstadt, Germany
Ultrasonicator UW220 with MS73 tip	Bandelin electronic, Berlin, Germany
Universal Magnet Plate	IBA, Göttingen, Germany

Table 3.2. Used materials, chemicals and reagents. This table summarizes the used materials, chemicals and reagents which were supplied by the indicated manufacturer. Chemicals or other reagents not listed in the table were obtained from the following manufacturers in their best possible quality and purity: Carl Roth, Karlsruhe, Germany; VWR International, Leuven, Belgium; Invitrogen, Karlsruhe, Germany; Sigma-Aldrich Chemie, Taufkirchen, Germany; Merck Schuchardt, Hohenbrunn, Germany; Fresenius Kabi, Bad Homburg, Germany; Merck, Darmstadt, Germany; Becton Dickinson, Pont de Claix, France and Bio-Rad Laboratories, Munich, Germany.

Designation	Manufacturer
2,2'-azino-bis(3-ethylbenzthiazoline-6-sulphonic acid	Sigma-Aldrich Chemie, Taufkirchen, Germany
Acrylamid/Bisacrylamid (29:1)	AppliChem, Darmstadt, Germany
Agencourt AMPure PCR purification beads	Agencourt Bioscience, La Jolla, CA, USA
Amersham Hybond P 0.2 µm PVDV membrane	GE Healthcare, Munich, Germany
Amersham Hybond P 0.45 µm PVDV membrane	GE Healthcare, Munich, Germany
Amersham Protran Premium 0.2 µm nitrocellulose membrane	GE Healthcare, Munich, Germany
Amersham Protran Premium 0.45 µm nitrocellulose membrane	GE Healthcare, Munich, Germany
Amicon Ultra 0.5 centrifugal Filter Units 10K	Merck, Darmstadt, Germany
Ampuwa water	Fresenius Kabi, Bad Homburg, Germany
Attractene transfection reagent	Qiagen, Hilden, Germany

Continued on next page

Table 3.2. Used materials, chemicals and reagents. – *Continued from previous page*

Designation	Manufacturer
Avidin-Biotin Complex	Vector Laboratories, Burlingame, CA, USA
Bafilomycin A1	Invivogen, Toulouse, France
Betain	Sigma-Aldrich Chemie, Munich, Germany
Bio-Rad Protein Assay	Bio-Rad Laboratories, Munich, Germany
BSA Fraktion V	Sigma-Aldrich, Taufkirchen, Germany
C18-StageTips	Thermo Fisher Scientific, Karlsruhe, Germany
Cellulose-acetate membrane 0.45 µm	GE Healthcare, Munich, Germany
Chloroquine	Sigma-Aldrich, Munich, Germany
CNBr-Activated Sepharose 4B	GE Healthcare, Munich, Germany
cOmplete protease inhibitor without EDTA	Roche Molecular Systems, Mannheim, Germany
Dulbecco's modified Eagle's medium (DMEM)	Gibco, LifeTechnologies, Carlsbad, CA, USA
Dulbecco's phosphate buffered saline (DPBS)	Gibco, LifeTechnologies, Carlsbad, CA, USA
DTCS Quick Start Mix	Beckman Coulter, Beverley, MA, USA
Ethidiumbromide solution 1 %	Carl Roth, Karlsruhe, Germany
FBS	Gibco, LifeTechnologies, Carlsbad, CA, USA
G418-BC	Merck, Darmstadt, Germany
Gel-Red (10,000-times)	Biotium, Fremont, CA, USA
GenomeLab DNA Size Standard Kit 600	Beckman Coulter, Beverley, MA, USA
Gentamicin-sulfate	Carl Roth, Karlsruhe, Germany
GFP-trap A beads	Chromotek, Planegg-Martinsried, Germany
Glutathion-Sepharose 4B	GE Healthcare, Munich, Germany
Goat serum (normal)	Dako Deutschland, Hamburg, Germany
Lactocystin	Enzo Life Sciences, Lörrach, Germany
Leica CV Ultra Mounting Medium	Leica BIosystems, Wetzlar, Germany
Lysozyme from chicken egg white	Carl Roth, Karlsruhe, Germany
MagneGST beads	Promega, Mannheim, Germany
MATra-A Reagent	IBA, Göttingen, Germany
MG-132	Merck, Darmstadt, Germany
Microspin columns	GE Healthcare, Munich, Germany
NC-Slide-2	ChemoMetec, Allerod, Denmark
NC-Slide-8	ChemoMetec, Allerod, Denmark
NeuroMAG	OZ Biosciences SAS, Marseille, France
Non-Essential Amino Acids Solution (100-times)	Gibco, LifeTechnologies, Carlsbad, CA, USA
Nunc MaxiSorp flat bottom 96 well plate	Thermo Fisher Scientific, Karlsruhe, Germany
Opti-MEM Reduced Serum Medium	Gibco, LifeTechnologies, Carlsbad, CA, USA

Continued on next page

Table 3.2. Used materials, chemicals and reagents. – *Continued from previous page*

Designation	Manufacturer
Phosphatase Inhibitor Cocktail 1	Sigma-Aldrich Chemie, Taufkirchen, Germany
Phosphatase Inhibitor Cocktail 2	Sigma-Aldrich Chemie, Taufkirchen, Germany
Poly-L-Lysine	Sigma-Aldrich Chemie, Taufkirchen, Germany
PolyMAG	OZ Biosciences SAS, Marseille, France
Precision Plus Protein Standard Dual Color	Bio-Rad Laboratories, Munich, Germany
PreScission Protease	GE Healthcare, Munich, Germany
ProteoStat protein aggregation assay	Enzo Life Sciences, Lörrach, Germany
RapiGest	Waters, Eschborn, Germany
Sigmafast DAB tablets	Sigma-Aldrich Chemie, Taufkirchen, Germany
Skim Milk Powder	Sigma-Aldrich Chemie, Taufkirchen, Germany
Strep-Tactin Elution Buffer with Desthiobiotin (Buffer E, 10-times)	IBA, Göttingen, Germany
Strep-Tactin superflow resin	IBA, Göttingen, Germany
SYBR Green I Master	Roche Molecular Systems, Mannheim, Germany
SYPRO Ruby Protein Gel Stain	Invitrogen, Karlsruhe, Germany
TrypLE Express Enzyme, phenol red	Gibco, LifeTechnologies, Carlsbad, CA, USA
Trypsin for mass spectrometry (MS) digest	Promega, Mannheim, Germany
Ubiquitin-Rhodamine-110	LifeSensors, Malvern, PA, USA
Vectashield antifade mounting medium with DAPI	Vector Laboratories, Burlingame, CA, USA
Western Bright ECL	Advansta, Menio Park, CA, USA
Western Bright Sirius	Advansta, Menio Park, CA, USA

Table 3.3. Used buffers and solutions. This table summarizes the used solutions and buffers and their composition.

Designation	Compostition
2x YT medium	16 g/l trypton, 10 g/l yeast extract, 5 g/l NaCl, pH 7.0
Ampicillin stock soulution	100 mg/ml (working concentration 100 µg/ml)
Antibody diluent	10 mM Tris, 150 mM NaCl, 0.025 % (v/v) Triton X-100, 1 % (v/v) normal serum
Bicine/Bis-Tris transfer buffer	25 mM Bicine, 25 mM Bis-Tris pH 7.2, 1 mM EDTA, 15 % (v/v) methanol
BT gel buffer	1.25 M Bis-Tris, pH 6.68
Calpain Cleavage buffer	20 mM HEPES, pH 7.6, 10 mM KCl, 1.5 mM $MgCl_2$, 1 mM DTT

Continued on next page

Table 3.3. Used buffers and solutions. – *Continued from previous page*

Designation	Compostition
CCCP stock solution	100 µM carbonyl cyanide m-chlorophenyl hydrazone in dimethyl sulfoxide
Citrate buffer	100 mM Citric acid, pH 4.5
Coomassie destaining solution	10 % (v/v) ethanol, 2 % (v/v) ortho-Phosphpric acid
Coomassie staing solution (colloidal)	0.02 % (w/v) Coomassie-G250, 5 % (w/v) Aluminium sulfate octadecahydrate, 10 % (v/v) ethanol, 2 % (v/v) ortho-Phosphpric acid
Deyolking buffer	55 mM NaCl, 1.8 mM KCl, 1.25 mM $NaHCO_3$, cOmplete protease inhibitor without EDTA
Deyolking wash buffer	110 mM NaCl, 3.5 mM KCl, 2.7 mM $CaCl_2$, 0.4 % (v/v) 2.5 M Tris-HCl pH 8,5, cOmplete protease inhibitor without EDTA
Doxycyclin stock soulution	1 mg/ml (working concentration 1 µg/ml)
DUB assay buffer	50 mM HEPES, 500 µM EDTA, 1 mM DTT, 100 µg/ml BSA
ELISA blocking buffer	DPBS supplemented with 0.5 % (w/v) BSA Fraction V
ELISA dilution buffer	DPBS supplemented with 0.05 % (v/v) Tween-20 and 0.5 % (w/v) BSA Fraction V
ELISA substrate solution	1.8 mM 2,2'-azino-bis(3-ethylbenzthiazoline-6-sulphonic acid in 90 mM Citrate buffer
ELISA washbuffer	DPBS supplemented with 0.05 % (v/v) Tween-20
Fractionation Buffer	DPBS supplemented with 0.1 % (v/v) Nonidet P-40, cOmplete protease inhibitor without EDTA
Fractionation RIPA buffer	50 mM Tris, 150 mM NaCl, 0.2 % (v/v) Triton X-100, 25 mM EDTA, cOmplete protease inhibitor without EDTA
GFP-trap dilution buffer	10 mM Tris pH 7.5, 150 mM NaCl, 0.5 mM EDTA, cOmplete protease inhibitor without EDTA
GFP-trap lysis/wash buffer	10 mM Tris pH 7.5, 150 mM NaCl, 0.5 mM EDTA, 0.5 % (v/v) Nonidet P-40, cOmplete protease inhibitor without EDTA
GST bind/wash buffer	4.2 mM Na_2HPO_4, 2 mM KH_2PO_4, 140 mM NaCl, 10 mM KCl
GST elution buffer	50 mM Tris pH 8.0, 10 mM glutathione
GST lysis buffer	4.2 mM Na_2HPO_4, 2 mM KH_2PO_4, 140 mM NaCl, 10 mM KCl, 1 % (v/v) Nonidet P-40, cOmplete protease inhibitor without EDTA
HPLC System A	4.8 mM TFA

Continued on next page

Table 3.3. Used buffers and solutions. – *Continued from previous page*

Designation	Compostition
HPLC System B	80 % (v/v) acetonitrile, 7.1 % (v/v) TFA
In-vitro aggregation assay buffer	20 mM Tris-HCl pH 8.0, 150 mM KCl
Kanamycin stock soulution	50 mg/ml (working concentration 100 µg/ml)
LB medium	10 g/l tryptone, 5 g/l yeast extract, 10 g/l NaCl, pH 7.0
LDS sample buffer (4-times)	1 M Tris Base pH 8.5, 2 mM EDTA, 8 % (w/v) lithium dodecyl sulfate, 40 % (v/v) glycerol, 0.075 % (w/v) Coomassie Brilliant Blue G-250, 0.025 % (w/v) phenol red
Linking buffer	100 mM $NaHCO_3$, 500 mM NaCl, pH 8.0
MES buffer	50 mM MES, 50 mM Tris Base, 0.1 % (w/v) SDS, 1 mM EDTA
MOPS buffer	50 mM MOPS, 50 mM Tris Base, 0.1 % (w/v) SDS, 1 mM EDTA
Phosphate buffered saline	8 g/l NaCl, 1.44 g/l Na_2HPO_4, 0.2 g/l KCl, 0.24 g/l KH_2PO_4
Peptide solvent	25 µl H_2O, 25 µl thioanisole, 25 µl EDTA, 925 µl TFA, one spatula phenol
RIPA buffer	25 mM Tris, 150 mM NaCl, 0.1 % (w/v) SDS, 0.5 % (w/v) sodium deoxycholate, 1 % (v/v) Triton-X100, cOmplete protease inhibitor without EDTA
Sequencing buffer A	3 M Sodium Acetate pH 5.2
Sequencing buffer B	100 mM Na_2-EDTA pH 8.0
SOC medium	20 g/l tryptone, 5 g/l yeast extract, 10 mM NaCl, 2.5 mM KCl, 10 mM $MgCl_2$, 10 mM $MgSO_4$, 20 mM glucose
Sörensen buffer	106.8 mM Na_2HPO_4, 26.12 mM KH_2PO_4
Strep-Tactin lysis buffer	30 mM Tris-HCl pH 7.4, 150 mM NaCl, cOmplete protease inhibitor without EDTA, Phosphatase Inhibitor Cocktail 1, Phosphatase Inhibitor Cocktail 2, 0.5 % (v/v) Nonidet P-40
Strep-Tactin wash buffer	30 mM Tris-HCl pH 7.4, 150 mM NaCl, Phosphatase Inhibitor Cocktail 1, Phosphatase Inhibitor Cocktail 2, 0.5 % (v/v) Nonidet P-40
Stripping buffer	200 mM Glycin, 1 % (w/v) SDS, pH 2.0
SYPRO fixation solution	7 % (v/v) acetic acid, 50 % (v/v) methanol
SYPRO wash solution	7 % (v/v) acetic acid, 10 % (v/v) methanol
Tris buffered saline	10 mM Tris, 150 mM NaCl
Tetracyclin stock soulution	10 mg/ml (working concentration 10 µg/ml)

Continued on next page

Table 3.3. Used buffers and solutions. – *Continued from previous page*

Designation	Compostition
Tris-Glycin running buffer	192 mM Glycin, 25 mM Tris Base, 0.1 % (w/v) SDS
Tris-Glycin sample loading buffer (5-times)	125 mM Tris-HCl pH 6.8, 8 % (w/v) DTT, 50 % (v/v) Glycerol, 2 % (w/v) SDS, 0.05 % (w/v) Coomassie Brilliant Blue G-250
Tris-Glycin separation gel buffer	1.5 M Tris-HCl, pH 8.8
Tris-Glycin stacking gel buffer	0.5 M Tris-HCl, pH 6.8
Tris-Glycin transfer buffer	192 mM Glycin, 25 mM Tris Base, 15 % (v/v) methanol
Transformation buffer 1	100 mM RbCl, 76.3 mM $MnCl_2$, 29.5 mM KAc, 10 mM $CaCl_2$, 12 % (v/v) Glycerol, pH 5.8
Transformation buffer 2	10 mM MOPS, 1 mM RbCl, 7.5 mM $CaCl_2$, 12 % (v/v) Glycerol, pH 6.8
TAE buffer (10 times)	400 mM Tris-Base, 200 mM acetic acid, 10 mM EDTA
TBE buffer (10 times)	890 mM Tris-Base, 890 mM borate, 20 mM EDTA
TR-FRET detection buffer	50 mM NaH_2PO_4, 400 mM NaF, 0.1 % BSA, 0.05 % (v/v) Tween-20

Table 3.4. Used enzymes and manufacturer. This table summarizes the used enzymes as well as their manufacturer. All enzyme reactions were performed in the manufacturer supplied recommended buffers.

Enzyme	Manufacturer
AatII	New England Biolabs, Frankfurt a.M., Germany
AgeI	New England Biolabs, Frankfurt a.M., Germany
ApaI	New England Biolabs, Frankfurt a.M., Germany
AscI	New England Biolabs, Frankfurt a.M., Germany
BamHI	New England Biolabs, Frankfurt a.M., Germany
BglI	New England Biolabs, Frankfurt a.M., Germany
BglII	New England Biolabs, Frankfurt a.M., Germany
BsmBI	New England Biolabs, Frankfurt a.M., Germany
Bsu36I	New England Biolabs, Frankfurt a.M., Germany
EcoRI	New England Biolabs, Frankfurt a.M., Germany
NotI	New England Biolabs, Frankfurt a.M., Germany
NsiI	New England Biolabs, Frankfurt a.M., Germany
One Taq DNA Polymerase	New England Biolabs, Frankfurt a.M., Germany
PpuMI	New England Biolabs, Frankfurt a.M., Germany
PreScission Protease	GE Healthcare, Munich, Germany
Pwo Polymerase	Sigma-Aldrich Chemie, Hamburg, Germany
Qiagen Tag Polymerase	Qiagen, Hilden, Germany

Continued on next page

Table 3.4. Used enzymes and manufacturer. – *Continued from previous page*

Enzyme	Manufacturer
SalI	New England Biolabs, Frankfurt a.M., Germany
SbfI	New England Biolabs, Frankfurt a.M., Germany
SpeI	New England Biolabs, Frankfurt a.M., Germany
T4-DNA ligase	New England Biolabs, Frankfurt a.M., Germany
Taq DNA Polymerase	Roche Molecular Systems, Mannheim, Germany
XbaI	New England Biolabs, Frankfurt a.M., Germany
XhoI	New England Biolabs, Frankfurt a.M., Germany
XmnI	New England Biolabs, Frankfurt a.M., Germany

Table 3.5. Used size standards and manufacturer. This table summarizes the used size standards for DNA and protein gels as well as their manufacturer.

Standard	Manufacturer
1 kb size standard	Thermo Fisher Scientific, Karlsruhe, Germany
100 bp size standard	Thermo Fisher Scientific, Karlsruhe, Germany
Lambda/HindIII size standard	Thermo Fisher Scientific, Karlsruhe, Germany
pUC19/MspI size standard	Thermo Fisher Scientific, Karlsruhe, Germany
Precision Plus Protein Dual Color Standard	Bio-Rad Laboratories, Munich, Germany

Table 3.6. Used kits and manufacturer. This table lists all kits used for isolation, purification and staining of samples.

Kit	Manufacturer
EndoFree Plasmid Maxi Kit	Qiagen, Hilden, Germany
Expand Long Template PCR System	Roche Molecular Systems, Mannheim, Germany
High Pure PCR Template Preparation Kit	Roche Molecular Systems, Mannheim, Germany
QIAprep Spin Miniprep Kit	Qiagen, Hilden, Germany
QIAquick Gel Extraction Kit	Qiagen, Hilden, Germany
QIAquick PCR Purification Kit	Qiagen, Hilden, Germany
QIAshredder	Qiagen, Hilden, Germany
Quanti-Text Reverse Transcription Kit	Qiagen, Hilden, Germany
RNase-free DNase Kit	Qiagen, Hilden, Germany
RNeasy Mini Kit	Qiagen, Hilden, Germany
Vectastain ABC Kit	Vector Laboratories, Burlingame, CA, USA
Venor GeM Classic Mycoplasma Detection Kit	Minerva Biolabs, Berlin, Germany

Table 3.7. Used primers and sequence. This table specifies the 5' - 3' sequence of the used primers. All primers were obtained from Metabion International, Martinsried, Germany. Stock concentration was 100 µM. Primers were diluted to a 10 µM working solution and used in polymerase chain reactions in a final concentration of 320 - 400 nM.

Designation	Sequence [5' - 3']
2636_MJDpostCAG-Ppu	GCAGCGGGACCTATCAGG
5120_MJD_KO-R	CCTCGAATCGTGGATCCACTAG
5121_MJD_KO/A3R	GAGCCTCAGGACAAAGCGGGGCTG
A166_pGEXseq_r	CCGGGAGCTGCATGTGTCAGAGG
A195_MJD_Ex10b-F	AGGGGGACCTATCAGGACAGAG
E523_MJD_SA2223F	AGACAGGATTGTTCTCGCTTACC
F022_SeqRev1	TTGAGGATAATTCCACAGGGC
F023_SeqFor2	CAGGTTATAAGCAATGCCTTG
F025_SeqFor3	CTCCTGCAGATGATTAGGGT
F026_SeqRev3	GCTTCTCGTCTCTTCCGAAG
F029_SeqFor1	TGGAGTCCATCTTCCACGA
F691_pEGFP_ATX3_R	TGGACCCGTCAAGAGAGAAT
I866_preCAG-For	GCTAAGTATGCAAGGTAGTTCC
O092_pEGFP_C_Xho+Not	ATCCCGGCGGCCGCCTCGAGGGAAAGTATGAAT
O430_At3akurz_XhoI	TTTTACTCGAGTTATGTCAGATAAAGTGT
O431_At3alang_XhoI	TTTTACTCGAGTTAAAGAGGGAATGAAGA
Q385_Ataxin-3	GTTATATTTTCCACCTGCAGATAATTA
Q436_pCM327_Klon-F	GCGGGCCCGACGTCACCGGTGCCCCTAGTATGTATGTAAGTTAATAA
Q437_pCM327_Klon-R	TTACTGCACTGGATCTAGCCCTGCAGGGGCGCGCCAGATCTAA
Q439_pCS2_AatAscSalR	ACTGTCGACGGCGCGCCGACGTCTGGCGTAATAGCGAAGAGGCC
Q517_pCS2_AgeISbfI-F	ACAGCTCGAGCCTCTAGAACTATAGT
Q518_pCS2_AgeISbfI-R	CCGCGGCCGCACCGGTCCTGCAGGAATTAAAAAACCTCCCACA
Q583_pCS2_PvuI-F	GTCCTCCGATCGTTGTCAGAAGTAAGTTG
Q585_SeqPCM327L-F1	TAAGTTGGGTAACGCCAG
Q590_SeqPCM327L-R3	AATAGCAGGCATGCTGG
Q822_XbaI-ATG-AT3	GCGTCTAGAATGGAGTCCATCTTCCACGAGT
Q824_Stop-pTRE-XbaI	TGTTCTAGAGATCCGGGCCCTTA
Q941_Ex8_NSF-F	GGTACCTAAGGATCCCCCGGGCTGCAGGAATTCCGTTGCTGTCGTCGGC-GTGGGGGCCGTTGGCTCCAGACAAATAAACATGGAGTCCATCTT
Q942_Ex8:_NSF-R	CTTCTCGTCTCTTCCGAAGCTCTT
R058_At3_PpuMI-F	CAGCGGGACCTATCAGGA
R059_pBlue-TAAXbaApa	GTCGGGCCCTCTAGACTAAATTATTTTTTAAAGGTA
R100_postCAG-Rev	CAAGTGCTCCTGAACTGGTG
R161_At3aLa-Xba-Apa	AGTCGGGCCCGTATCTAGATTAAAGAGGGAATGAAG
R225_At3aKu-Xba-Apa	AGTCGGGCCCGTATCTAGATTATGTCAGATAAAGTGTG
R267_BamHIAt3XbaI-F	ACTGGGATCCCTGGAGTCCATCTT
R268_BamHIAt3XbaI-R	AGCATCTAGATTTTTTTCCTTCTGTTTTCA
R269_XbaIV5AgeI-F	AGACTTCTAGAGGTAAGCCTATCCCT

Continued on next page

Table 3.7. Used primers and sequence. – *Continued from previous page*

Designation	Sequence [5' - 3']
R270_XbaIV5AgeI-R	GTCACCGGTTTACGTAGAATCGA
R888_preCAG-For_Cy5	GCTAAGTATGCAAGGTAGTTCC-Cy5
S042_Actin beta For	CACCATGTACCCTGGCATT
S043_Actin beta Rev	GTACTTGCGCTCAGGAGGAG
S044_PGK-1_For	GACTGGCCAAGCCACTGT
S045_PGK-1_Rev	CGAGTGACAGCCTCAGCATA
S046_GAPDH_For	GCTCTCTGCTCCTCCTGTTC
S047_GAPDH_Rev	ACGACCAAATCCGTTGACTC
S048_P4HB_For	ACAAAGATGGGGTTGTCCTCT
S049_P4HB_Rev	GGCAGCTGGTTGTGTTTGA
S050_SDHA_For	GGACCTGGTTGTCTTTGGTC
S051_SDHA_Rev	CCAGCGTTTGGTTTAATTGG
S052_TBP_For	CCCATGACTCCCATGACC
S053_TBP_Rev	TTTACAACCAAGATTCACTGTGG
S054_YWHAZ_For	CAATTACTGAGAGACAACTTGACATTG
S055_YWHAZ_Rev	TGGAAGGCCGGTTAATTTT
S056_TFRC_For	CTTTGGAGTTATTAAAGGCTTTGTAGA
S057_TFRC_Rev	CTGTGCCTACACCGGATTTT
S062_PA28beta_For	ATCTAGCGACTGAAGCAGCAT
S063_PA28beta_Rev	CTCAGCCTCCTGGAAAAGATT
S064_CEBPB_For	CTGGAGACGCAGCACAAG
S065_CEBPB_Rev	ACAGCTGCTCCACCTTCTTC
S066_HSP27_For	CTCAAACACCGCCTGCTAA
S067_HSP27_Rev	ATGCTGGCTGACTCTGCTCT
S068_MKP-1_For	CGCAAGTCTTCTTCCTCAAAG
S069_MKP-1_Rev	AGTACTCAGGGGAAGGCTGAG
S100_At3_6c-myc-F	TATGGGCCCCCAGGTCCAGGTCGATAAGCTATG
S101 _At3_6c-myc-R	ATACCGGTTTAGCAGGAATTCAA
S185_MMP2_For	CGATGATGACCGCAAGTG
S186_MMP2_Rev	GGTCTTGGGAGTGCTCCAG
S281_NSF_For	TCAGTTCGAGAAGGGAGGAG
S282_NSF_Rev	ACCAGTCATGCTAGCTCCTT
T527_EGFP-N-Seq-Rev	CGTCGCCGTCCAGCTCGACCAG
T883_SV40-R	GCATTCTAGTTGTGGTT
T884_BamHIAt3LXbaI-R	AGCATCTAGAAAGAGGGAATGAAGAATAA
T885_BamHIAt3SXbaI-R	AGCATCTAGATGTCAGATAAAGTGTGAA

Table 3.8. Used gBlocks. This table lists all gBlocks (Integrated DNA Technologies B.V.B.A., Leuven, Belgium) used for cloning.

Designation	Sequence [5' - 3']
gBlock rs7158733 TAA	CAGCAGGGGGACCTATCAGGACAGAGTTCACATCCATGTGAAAGGCCAGCCACCA-GTTCAGGAGCACTTGGGAGTGATCTAGGTAAGGCCTGCTCACCATTCATCATGTT-CGCTACCTTCACACTTTATCTGACATAAGAGCTCCATGTGATTTTTGCTTTACAT-TATTCTTCATTCCCTCTTGGGCCCGGGATCC
gBlock rs1048755 GTG	AACTTGAATTCTCTCTTGACGGGTCCAGAATTAATATCAGATACATATCTTGCAC-TTTTCTTGGCTCAATTACAACAGGAAGGTTATTCTATATTTGTTGTTAAGGGTGA-TCTGCCAGATTGCGAAGCTGACCAACTCCTGCAGATGATTAGGGTCCAACAGATG-CATCGACCAAAACTTATTGGAGAAGAATTAGCACAACTAAAAGAGCAAAGAGTCC-ATAAAACAGACCTGGAACGAGTGTTAGAAGCAAATGATGGCTCAGGAATGTTAGA-CGAAGATGAGGAGGATTTGCAGAGGGCTCTGGCACTAAGTCGCCAAGAAATTGAC-ATGGAAGATGAGGAAGCAGATCTCCGCAGGGCTATTCAGCTAAGTATGCAAGGTA-GTTCCAGAAACATATCTCAAGATATGACACAGACATCAGGTACAAATCTTACTTC-AGAAGAGCTTCGGAAGAGACGAGAAG

Table 3.9. Used primary and secondary antibodies. This table lists species, dilution, batch and manufacturer of the used antibodies. Dilution of antibodies was performed in tris buffered saline (10 mM Tris, 150 mM NaCl) supplemented with 0.1 % (v/v) Tween-20. 0.02 % (w/v) NaN_3 was added for conservation. Antibodies for immunofluorescence stainings were diluted in DPBS containing 3 % (v/v) of serum.

Designation	Details	Dilution	Manufacturer
anti-ataxin-3	MAB5360 1H9	1:4000	Merck, Darmstadt, Germany
anti-ataxin-3 N-terminal region	ARP50507_P050	1:1000	Aviva Systems Biology, San Diego, CA, USA
anti-ataxin-3 center region	OAAB05835	1:500	Aviva Systems Biology, San Diego, CA, USA
anti-ataxin-3c (anti-3c)	SA3637	1:500	Schmidt et al. (1998)
anti-ataxin-3a (anti-3a)	not applicable	variable	present work
anti-β-actin	clone AC-15	1:5.000	Sigma-Aldrich, Steinheim, Germany
anti-caspase-7	#9492	1:1000	Cell Signaling Technology, Frankfurt am Main, Germany
anti-FLAG	F7425	1:2000	Sigma-Aldrich Chemie, Taufkirchen, Germany
anti-GAPDH	0411 sc-47724	1:1000	Santa Cruz Biotechnology, Heidelberg, Germany
anti-GFP	3H9	1:1000	Chromotek, Planegg-Martinsried, Germany
anti-GFP	B-2 sc-9996	1:1000	Santa Cruz Biotechnology, Heidelberg, Germany
anti-GFP	FL sc-8334	1:1000	Santa Cruz Biotechnology, Heidelberg, Germany

Continued on next page

Table 3.9. Used primary and secondary antibodies. – *Continued from previous page*

Designation	Details	Dilution	Manufacturer
anti-GST	B-14 sc-138	1:1000	Santa Cruz Biotechnology, Heidelberg, Germany
anti-histone H3	96C10 #3638	1:1000	Cell Signaling Technology, Frankfurt a.M., Germany
anti-K48 Ubiquitin	D9D5 #8081	1:1000	Cell Signaling Technology, Frankfurt a.M., Germany
anti-mouse HRP cunjugated antibody	NXA931	1:3000	GE Healthcare, Munich, Germany
anti-mouse IgG	IRDye 680LT	1:10000	LI-COR Biosciences, Bad Homburg, Germany
anti-mouse IgG	IRDye 800CW	1:10000	LI-COR Biosciences, Bad Homburg, Germany
anti-mouse IgG/IgM Alexa Fluor 488 conjugated antibody	A-10680	1:500	Thermo Fisher Scientific, Karlsruhe, Germany
anti-mouse (biotinylated)	BA-9200	1:200	Vector Laboratories, Burlingame, CA, USA
anti-parkin	#2132	1:1000	Cell Signaling Technology, Frankfurt a.M., Germany
anti-rabbit HRP conjugated antibody	ab97051	1:25000	Abcam, Cambridge, UK
anti-rabbit IgG	IRDye 680RD	1:10000	LI-COR Biosciences, Bad Homburg, Germany
anti-rabbit IgG	IRDye 800CW	1:10000	LI-COR Biosciences, Bad Homburg, Germany
anti-rabbit IgG Alexa Fluor 594 conjugated antibody	A-11012	1:500	Thermo Fisher Scientific, Karlsruhe, Germany
anti-rabbit Eu conjugated antibody	AD0082	1:60	PerkinElmer, Rodgau, Germany
anti-rabbit (biotinylated)	BA-1000	1:250	Vector Laboratories, Burlingame, CA, USA
anti-rat HRP cunjugated antibody	NA935	1:3000	GE Healthcare, Munich, Germany
anti-rat IgG	IRDye 680RD	1:10000	LI-COR Biosciences, Bad Homburg, Germany
anti-SQSTM1/p62	#5114	1:1000	Cell Signaling Technology, Frankfurt a.M., Germany
anti-α-tubulin	DM1A	1:2000	Merck, Darmstadt, Germany

Continued on next page

Table 3.9. Used primary and secondary antibodies. – *Continued from previous page*

Designation	Details	Dilution	Manufacturer
anti-α-tubulin	CP06	1:5000	Sigma-Aldrich, Steinheim, Germany
anti-TBP	T1827	1:1000	Sigma-Aldrich, Steinheim, Germany
anti-ubiquitin	Z 0458	1:1000	Dako, Glostrup, Denmark
anti-V5	R960-25	1:4.000	Thermo Fisher Scientific, Karlsruhe, Germany
anti-VCP	H-120 sc-20799	1:1.000	Cell Signaling Technology, Frankfurt a.M., Germany
anti-LC-3	clone 5F10	1:1.000	nanoTools, Teningen, Germany

Table 3.10. Used software and databases. This table specifies software and databases as well as the developer and the version.

Designation	Version	Developer
Agile Protein Interactomes DataServer (APID)	not available	Bioinformatics and Functional Genomics Research Group Cancer Research Center (CiC-IBMCC, CSIC/USAL), Salamanca, Spain (Alonso-López et al., 2019)
Biological General Repository for Interaction Datasets (BioGrid)	3.5	BioGRID Team (Chatr-Aryamontri et al., 2017)
Bokeh	0.13.0	Bokeh Development Team (Bokeh Development Team, 2018)
David Bioinformactics Resources	6.7	DAVID Bioinformatics Lab (Huang et al., 2009)
EBImage	3.6	Bioconductor (Pau et al., 2010)
Expasy ProtScale Hphob. / Kyte & Doolittle	not available	Swiss Institute of Bioinformatics, Lausanne, Switzerland (Gasteiger et al., 2003)
GenomeLab Genetic Analysis System	10.2.3	Beckman Coulter, Beverley, MA, USA
GraphPad Prism 6	6.01	GraphPad Software, La Jolla, CA, USA
Image Studio	V 4.2	LI-COR Biosciences, Bad Homburg, Germany
Integrative Genomics Viewer	2.3.11	Broad Institute, University of California, CA, USA (Robinson et al., 2011; Thorvaldsdóttir et al., 2013; Robinson et al., 2017)
LightCycler 480 software	1.5	Roche Molecular Systems, Mannheim, Germany
magick	1.6	Jeroen Ooms (Ooms, 2017)
Matlab	R2014b	MathWorks, Natick, MA, USA

Continued on next page

Table 3.10. Used software and databases. – *Continued from previous page*

Designation	Version	Developer
MaxQuant software	1.5.2.8	Max Planck Institute of Biochemistry (Cox et al., 2009)
Microsoft Excel	14.0.7208.5000	Microsoft Corporation, Munich, Germany
Perseus	1.5.4.0	Max Planck Institute of Biochemistry (Tyanova et al., 2016)
Protein Interaction Network Analysis (PINA)	2	Center for Cancer Bioinformatics, Peking University Cancer Hospital & Institute, Peking University Health Science Center, Peking, Japan (Cowley et al., 2012)
Python	2.7	Python Software Foundation
R	3.4.2	R Core Team (R Core Team, 2017)
Serial Cloner 2.6	2.6.1	Franck Perez (SerialBasics)
SnapGene Viewer	2.7.1	GLS Biotech LLC, Chicago, IL, USA
STRING	10.5	String Consortium 2017 (Snel, 2000; von Mering et al., 2003, 2005; Szklarczyk et al., 2015, 2017)
The Human Protein Atlas	V18.0	The Human Protein Atlas (Thul et al., 2017)
The Universal Protein Resource (UniProt)	UniProt release 2020_02	The Uniprot Consortium (The UniProt Consortium, 2019)

Table 3.11. Used eukaryotic and prokaryotic cells. This table lists the eucaryotic cells as wells as the strain and genotype of the prokaryotic *E. coli* cells.

Strain or celltype	Genotype, ATTC-No. or reference
E. coli ccdb Survival 2	F-mcrA δ(mrr-hsdRMS-mcrBC) ϕ80lacZδM15 δlacX74 recA1 araδ139 δ(ara-leu)7697 galU galK rpsL (StrR) endA1 nupG fhuA::IS2
E. coli DH5α	F– ϕ80lacZδM15 δ(lacZYA-argF) U169 recA1 endA1 hsdR17 (rK–, mK+) phoA supE44 λ– thi-1 gyrA96 relA1
E. coli Stop Unwanted Rearrangement Events	F'[proAB+ lacIq lacZδ M15 Tn10(TetR] endA1 glnV44 thi-1 gyrA96 relA1 lac recB recJ sbcC umuC::Tn5(KanR uvrC e14–(mcrA–) δ(mcrCB-hsdSMR-mrr)171
E. coli Stbl4	mcrA δ(mcrBC-hsdRMS-mrr) recA1 endA1 gyrA96 gal-thi-1 supE44 λ-relA1 δ(lac-proAB)/F' proAB+lacIqZδM15 Tn10 (TetR)
Human Embryonic Kidney 293T	CRL-11268
Human Embryonic Kidney 293T *ATXN3* KO	this project
Induced Pluripotent Stem Cells CO-57[a]	Weber et al. (2017)
Induced Pluripotent Stem Cells AT-36[a]	Weber et al. (2017)

[a] Protein samples kindly provided by Dr. Jonasz Weber

Table 3.12. Studied animals. This table summarizes the genotype of animals studied in this project.

Animal	***ATXN3* genotype**
Mouse C57/BL6[a]	wild type
Mouse (*ATXN3* KO, Schmitt et al., 2007)	$ATXN3^{(-/-)}$
Mouse (MJD64-84, Cemal et al., 2002)[a]	$ATXN3^{(15Q/64Q\text{-}84Q)}$
Mouse (line 2285, PrP/MJD77, Boy et al., 2009)[b]	$ATXN3^{(29/66)}$
Mouse (line 2904, PrP/MJD77, Boy et al., 2009)[b]	$ATXN3^{(60/65/80)}$
Zebrafish strain Tübingen (TU)[c]	wild type
Zebrafish *hMJD1*c18CAG$_{GG}$.1[d]	HuC:$ATXN3^{(3c18Q\text{-}VG/-)}$
Zebrafish *hMJD1*c18CAG$_{GG}$.4[d]	HuC:$ATXN3^{(3c18Q\text{-}VG/-)}$
Zebrafish *hMJD1*aL18CAG$_{GGC}$.44[d]	HuC:$ATXN3^{(3aL18Q\text{-}VGT/-)}$
Zebrafish *hMJD1*aS18CAG$_{GGA}$.1[d]	HuC:$ATXN3^{(3aS18Q\text{-}VG*/-)}$
Zebrafish *hMJD1*c73CAG$_{AC}$.2[d]	HuC:$ATXN3^{(3c73Q\text{-}MR/-)}$
Zebrafish *hMJD1*aL73CAG$_{ACC}$.1[d]	HuC:$ATXN3^{(3aL73Q\text{-}MRT/-)}$
Zebrafish *hMJD1*aS73CAG$_{ACA}$.1[d]	HuC:$ATXN3^{(3aS73Q\text{-}MR*/-)}$
Zebrafish *hMJD1*aS73CAG$_{ACA}$.16[d]	HuC:$ATXN3^{(3aS73Q\text{-}MR*/-)}$

[a] Protein samples kindly provided by Dr. Jonasz Weber

[b] gDNA samples ms-2285 and ms-2904 kindly provided by Dr. Jana Schmidt

[c] Larvae and brain samples kindly provided by Prof. Dr. Bernd Wissinger

[d] Larvae and brain samples kindly provided by Shermaine Tay and Assoc. Prof. Christoph Winkler

Table 3.13. Used expression constructs. This table summarizes the used expression constructs and their source. Constructs from intermediate cloning steps were disregard.

Plasmid	**Source**
pBluescript-XbaI-hMJD1c73CAG-AC	lab inventory
pBluescript-XbaI-hMJD1c151CAG-AC	lab inventory
pBluescript-XbaI-hMJD1c73CAG-AC-XbaI	this project
pBluescript-XbaI-hMJD1aL73CAG-ACC-XbaI	this project
pBluescript-XbaI-hMJD1aS73CAG-ACA-XbaI	this project
pBluescript-XbaI-hMJD1c151CAG-AC-XbaI	this project
pBluescript-XbaI-hMJD1aL151CAG-ACC-XbaI	this project
pBluescript-XbaI-hMJD1aS151CAG-ACA-XbaI	this project
pcDNA-6xmyc-Parkin (V380)	W. Springer Hertie-Institut, Tübingen, Germany.
pcDNA-6xmyc-Parkin (L380)	W. Springer Hertie-Institut, Tübingen, Germany.
pcDNA3.1	Thermo Fisher Scientific, Karlsruhe, Germany
pcDNA3.1-FLAG-hMJD1c18CAG-GG-V5	this project
pcDNA3.1-FLAG-hMJD1aL18CAG-GGC-V5	this project
pcDNA3.1-FLAG-hMJD1aS18CAG-GGA-V5	this project
pcDNA3.1-FLAG-hMJD1c73CAG-AC-V5	this project

Continued on next page

Table 3.13. Used expression constructs. – *Continued from previous page*

Plasmid	Source
pcDNA3.1-FLAG-hMJD1aL73CAG-ACC-V5	this project
pcDNA3.1-FLAG-hMJD1aS73CAG-ACA-V5	this project
pcDNA3.1-FLAG-hMJD1c153AG-AC-V5	this project
pcDNA3.1-FLAG-hMJD1aL153CAG-ACC-V5	this project
pcDNA3.1-FLAG-hMJD1aS153CAG-ACA-V5	this project
pcDNA3.1-FLAG-hMJD1c18CAG-GG-6xmyc	this project
pcDNA3.1-FLAG-hMJD1aL18CAG-GGC-6xmyc	this project
pcDNA3.1-FLAG-hMJD1aS18CAG-GGA-6xmyc	this project
pcDNA3.1-flag-UBR2	Alexander Varshavsky Addgene #50573
pcDNA3.1-V5-hHR23A	Steven Grossman Addgene #13054) (Brignone et al., 2004)
pcDNA3.1-V5-hHR23B	Steven Grossman Addgene #13054) (Brignone et al., 2004)
pCS2-HuC^{ATG-}:Kaede	T. Sato, RIKEN Brain Science Institute, Wakō, Japan
pDestAttB/CY	Christian Mosimann (Mosimann et al., 2013)
pDestAttB/CY-HuC-hMJD1c18CAG-GG	this project
pDestAttB/CY-HuC-hMJD1aL18CAG-GGC	this project
pDestAttB/CY-HuC-hMJD1aS18CAG-GGA	this project
pDestAttB/CY-HuC-hMJD1c73CAG-AC	this project
pDestAttB/CY-HuC-hMJD1aL73CAG-ACC	this project
pDestAttB/CY-HuC-hMJD1aS73CAG-ACA	this project
pDestAttB/CY-HuC-hMJD1c151CAG-AC	this project
pDestAttB/CY-HuC-hMJD1aL151CAG-ACC	this project
pDestAttB/CY-HuC-hMJD1aS151CAG-ACA	this project
pEGFP-C2	Takara Bio Europe, Saint-Germain-en-Laye, France
pEGFP-C2-hMJD1c18CAG-AG	lab inventory
pEGFP-C2-hMJD1aL18CAG-AGC	lab inventory
pEGFP-C2-hMJD1aS18CAG-AGA	lab inventory
pEGFP-C2-hMJD1c18CAG-GG	this project
pEGFP-C2-hMJD1aL18CAG-GGC	this project
pEGFP-C2-hMJD1aS18CAG-GGA	this project
pEGFP-C2-hMJD1c70CAG-AC	lab inventory
pEGFP-C2-hMJD1aL70CAG-ACC	lab inventory
pEGFP-C2-hMJD1aS70CAG-ACA	lab inventory
pEGFP-C2-hMJD1c151CAG-AC	lab inventory
pEGFP-C2-hMJD1aL151CAG-ACC	lab inventory
pEGFP-C2-hMJD1aS151CAG-ACA	lab inventory

Continued on next page

Table 3.13. Used expression constructs. – *Continued from previous page*

Plasmid	Source
pEGFP-N2	Takara Bio Europe, Saint-Germain-en-Laye, France
pEGFP-N2-hMJD1c18CAG-AG	lab inventory
pEGFP-N2-hMJD1aL18CAG-AGC	Schroeder (2011)
pEGFP-N2-hMJD1aL18CAG-AGA	this project
pEGFP-N2-hMJD1aS18CAG-AGA	Schroeder (2011)
pEGFP-N2-hMJD1c151CAG-AG	lab inventory
pEGFP-N2-hMJD1aL151CAG-ACC	Schroeder (2011)
pEGFP-N2-hMJD1aL151CAG-ACA	this project
pEGFP-N2-hMJD1aS151CAG-ACA	Schroeder (2011)
pGEX-6p1	GE Healthcare, Munich, Germany
pGEX-6p1-hMJD1c18CAG-987G	lab inventory
pGEX-6p1-hMJD1c73CAG-987C	lab inventory
pGEX-6p1-hMJD1c18CAG-GG	this project
pGEX-6p1-hMJD1aL18CAG-GGC	this project
pGEX-6p1-hMJD1aS18CAG-GGA	this project
pGEX-6p1-hMJD1c73CAG-AC	this project
pGEX-6p1-hMJD1aL73CAG-ACC	this project
pGEX-6p1-hMJD11aS73CAG-ACA	this project
pN-SF-TAP	Gloeckner et al. (2009)
pN-SF-TAP-hMJD1c18CAG-AG	Weber et al. (2017)
pN-SF-TAP-hMJD1c65CAG-AC	Weber et al. (2017)
pN-SF-TAP-hMJD1c18CAG-GG	this project
pN-SF-TAP-hMJD1aL18CAG-GGC	this project
pN-SF-TAP-hMJD1aS18CAG-GGA	this project
pN-SF-TAP-hMJD1c65CAG-AC	this project
pN-SF-TAP-hMJD1aL65CAG-ACC	this project
pN-SF-TAP-hMJD1aS65CAG-ACA	this project
pTRE	Takara Bio Europe, Saint-Germain-en-Laye, France
pTRE-hMJD1c18CAG-AG	Weishäupl (2012)
pTRE-hMJD1aL18CAG-AGC	Weishäupl (2012)
pTRE-hMJD1aS18CAG-AGA	Weishäupl (2012)
pTRE-hMJD1c18CAG-GG	this project
pTRE-hMJD1aL18CAG-GGC	this project
pTRE-hMJD1aS18CAG-GGA	this project
pTRE-hMJD1c73CAG-AC	Weishäupl (2012)
pTRE-hMJD1aL10CAG-ACC	Weishäupl (2012)
pTRE-hMJD1aS70CAG-ACA	Weishäupl (2012)
pTET-Off-(RCA2)	Boy et al. (2009)

Continued on next page

Table 3.13. Used expression constructs. – *Continued from previous page*

Plasmid	Source
pTRE-Parkin-V380	this project
pTRE-Parkin-L380	this project

3.2 Microbiological methods

3.2.1 Overnight cultures and glycerol stocks

In order to prepare overnight cultures of bacteria 10 ml lysogeny broth (LB) (10 g/l tryptone, 5 g/l yeast extract, 10 g/l NaCl, pH 7.0) or 2xYT (16 g/l trypton, 10 g/l yeast extract, 5 g/l NaCl, pH 7.0) media containing the appropriate antibiotic were inoculated with low amounts of a bacterial glycerol stock or colony material of a LB-agar plate by abrading. Bacterial cultures were grown over night at 37 °C.

3.2.2 Preparation of chemocompetent cells

A 200 ml day culture of *E. coli* was inoculated with 2 ml from an overnight culture and grown shaking at 37 °C. When the day culture reached an optical density $(OD)_{600}$ of 0.45 the cells were incubated on ice for 5 min. Cells were subsequently centrifuged at 1500 *g*, 4 °C, 5 min. Supernatant was discarded and bacteria were resuspended in 40 ml transformation buffer 1 (100 mM RbCl, 76.3 mM $MnCl_2$, 29.5 mM KAc, 10 mM $CaCl_2$, 12 % (v/v) Glycerol, pH 5.8) and incubated on ice for 5 min. Cells were centrifuged again and afterwards resuspended in 16 ml transformation buffer 2 (10 mM MOPS, 1 mM RbCl, 7.5 mM $CaCl_2$, 12 % (v/v) Glycerol, pH 6.8) and incubated on ice another 15 min. Afterwards, aliquots were prepared, frozen in liquid nitrogen and stored at -80 °C until use.

3.2.3 Transformation of *E. coli*

Competent cells were thawed on ice and 100 µl were added to a heat inactivated ligation mix. Suspension was incubated on ice for 30 min before a heat shock (42 °C, 45 s) was performed. Cells were cooled down on ice, 900 µl SOC medium (20 g/l tryptone, 5 g/l yeast extract, 10 mM NaCl, 2.5 mM KCl, 10 mM $MgCl_2$, 10 mM $MgSO_4$, 20 mM glucose) was added, cells were then incubated at 37 °C under constant shaking for 1.5 h. Afterwards the bacteria were pelleted by centrifugation at 600 *g* for 5 min. 800 µl of the supernatant were discarded and cells were resuspended in the remaining medium before they were spread on LB agar plates and incubated at 37 °C overnight.

3.3 Cell culture techniques

3.3.1 Culture of eucaryotic cells

Eucaryotic cells were grown in DMEM (Gibco, LifeTechnologies, Carlsbad, CA, USA) supplemented with 100 U/mL Penicillin and 100 µg/ml Streptomycin, 10 % (v/v) fetal bovine serum

(FBS, Gibco). For cells other than human embryonic kidney (HEK) 1 % (v/v) non-essential amino acids (Gibco) were added, too. Cells were cultured at 37 °C with 5 % CO_2. Media was changed every two to three days and cells were passaged at a confluency of 80 % to 90 %. Therefore, culture media was removed and cells were washed with Dulbecco's phosphate buffered saline (DPBS). Subsequently 10 % (v/v) culture volume of TrypLE Express (Gibco) was added to the cells in order to detach them form the flask. After detachment cells were resuspended in DMEM containing FBS in order to prevent cell damage. Cells remaining attached to the culture flask were washed off by pipetting. Cells were usually passaged in a 1:10 ration with fresh culture medium. Before seeding cells to plates cells were counted using a Neubauer counting chamber and cell number per ml was calculated from Equation 3.1 with total cell count C, dilution factor F and the number of counted large corner squares S.

$$\frac{cells}{ml} = \frac{C \cdot F}{S \cdot 10^{-4}\ ml} \tag{3.1}$$

3.3.2 Freezing and thawing of eucaryotic cells

Cells were passaged and pelleted. The cell pellet was resuspended in dimethyl sulfoxide supplemented with 10 % (v/v) FBS and transferred to a cryotube. Cells were frozen with 1 °C/min to -80 °C and afterwards stored in liquid nitrogen (gas phase).

In order to culture cells from a frozen stock the cryo stock was thawed at 37 °C and immediately diluted in culture medium. Cells were subsequently pelleted at 300 g for 5 min. Supernatant was removed and replaced with fresh culture medium before the cells were seeded in a culture flask and incubated at 37 °C with 5 % CO_2.

3.3.3 Transfection of eucaryotic cells

3.3.3.1 Attractene

If not stated differently cells were transfected using the nonliposomal lipid Attractene (Qiagen, Hilden, Germany). Cells were seeded in a culture plate 24 h before transfection. 1.2 µg plasmid DNA was diluted in a total volume of 100 µl Opti-MEM medium (Gibco, LifeTechnologies, Carlsbad, CA, USA). After mixing, 4.5 µl Attractene was added and the solution was mixed again and incubated for 10 min at room temperature. Afterwards the solution was applied to the cells drop wise.

3.3.3.2 NeuroMAG and PolyMAG

Transfection of mouse embryonic fibroblast (MEF) cells was performed by magnetofection using either NeuroMAG or PolyMAG (OZ Biosciences SAS, Marseille, France). Cells were seeded in a 6-well culture plate 24 h before transfection.. On the day of transfection 1 µg DNA was diluted into a total volume of 396.5 serum free medium. Afterwards 3.5 µl NeuroMAG were added and the solution was mixed and incubated for 20 min at room temperature before 1.6 ml of culture medium were added. Medium of the culture plate was removed and replaced by the transfection medium. The cells were then placed on the magnefect-nano II system (NanoTherics, Newcastle under Lyme, UK) for 30 min at 2 Hz and 0.2 mm displacement. The transfection with PolyMAG was performed with 2 µg of DNA and 1 µl of PolyMAG using a static magnet plate.

3.3.3.3 Polyethylenimine

Cells for Strep-tactin purification were seeded in 14 cm dishes and transfected with polyethylenimine 24 h post seeding. 4 µg DNA were dissolved in1 ml Opti-MEM. 8 µl of polyethylenimine (1 mg/ml in H_2O, pH 7) were added and the solution was mixed. After a 20 min incubation phase the complex was added drop-wise and cells were grown for another 72 h.

3.3.4 Generation of Mouse Embryonic Fibroblasts

A pregnant *ATXN3* KO mouse (Schmitt et al., 2007) was sacrificed 14 days post fertilization using CO_2. After disinfection in a 70 % (v/v) ethanol bath for 30 min the mouse embryos were removed surgically and transferred to sterile DPBS. Embryonic paws were isolated and transferred to sterile reaction tubes for genotyping at a later time point. Embryos without inner organs were kept in DPBS supplemented with 100 U/mL penicillin and 100 µg/ml streptomycin at 37 °C and 5 % CO_2 for 30 min. Afterwards, using a scalpel, the embryos were disintegrated in a tissue culture dish with sterile DPBS. Tissue fragments were transferred into a culture flask and dried for 10 min in order to increase the attachment of the tissue to the flask. Tissue was cultured at 37 °C, 5 % CO_2 for two days after addition of culture medium. The media was changed after 48 h and MEF cells were initially passaged at a confluency of 80 % to 90 %. The cells were kept in culture for around ten passages. Primers E523/5120 (600 bp KO allele) and E523/5121 (930 bp normal allele) were used for genotyping.

3.3.5 Mycoplasma testing

In order to ensure a mycoplasma free cell line new cultures as well as cell lines in culture (every six months) were tested for mycoplasma contaminations using the Venor GeM Mycoplasma Detection Kit (Minerva Biolabs, Berlin, Germany) according to the manufacturers protocol (V30).

3.3.6 Analysis of protein and mRNA stability

The degradation analysis was performed by using the Tet-off system. Transfection of HEK 293T *ATXN3* KO cells with pTRE -ataxin-3 responder constructs and a pTET-RCA2 promoter construct (Boy et al., 2009) was performed in a 1:1 ratio. Expression of ataxin-3 was turned off 72 h, 48 h, 32 h, 24 h, 8 h and 0 h prior to cell harvest by the addition of 4.5 µM Doxycycline. Cell lysates were prepared (3.6.1) and analyzed by sodium dodecyl sulfate (SDS)-polyacrylamide gelelectrophoresis (PAGE), western blot and immunodetection (see 3.6.9, 3.6.11 and 3.6.12, page 65 ff.). Signal intensity over time was fitted by an exponential function (Equation 3.2 with k as exponent and t as time) and protein half-life was calculated from this function following a first order kinetic (Equation 3.3, where k is the exponent of the exponential function).

$$f(t) = f(0) \cdot e^{-k \cdot t} \tag{3.2}$$

$$t_{\frac{1}{2}} = \frac{ln2}{k} \tag{3.3}$$

Ataxin-3 mRNA stability was analyzed using the Tet-off system as described above. Doxycycline treatment (4.5 µM) was performed 8 h before cell harvesting. Extraction of RNA was performed as described in 3.5.2.1 and cDNA was transcribed (see 3.5.3, page 56). Relative expression levels of 0 h and 8 h treated samples was then analyzed by real-time polymerase chain reaction (RT-PCR) normalized against the housekeeping gene GAPDH (3.5.6).

3.3.7 Analysis of the protein degradation pathway

Analysis of the degradation pathway was performed by transfection of HEK 293T *ATXN3* KO cells with pTRE-ataxin-3 responder constructs and a pTET-RCA2 promoter construct (Boy et al., 2009) in a 1:1 ratio. 24 h after transfection cells were treated with 4.5 µM Doxycycline followed by the addition of the respective inhibitors 8 h later. Proteasomal degradation was inhibited using 10 µM Lactacystin (Enzo Lifescience, Lausen, Switzerland) or 25 µM MG-132 (Merck, Darmstadt, Germany). Autophagy was inhibited by either 50 nM Bafilomycin A1 (Invivogen, Toulouse, France) or 100 µM Chloroquine (Sigma-Aldrich, Munich, Germany). Proteins were isolated (3.6.1, page 61) and samples were processed for SDS-PAGE, western blot and immunodetection (see 3.6.9, 3.6.11 and 3.6.12, page 65 ff.). Signal intensity after inhibitor treatment was then calculated relative to the Doxycycline treatment control.

3.3.8 Induction of translational read-through

Translational read-through was tested by transfecting HEK 293T *ATXN3* KO cells with the vectors pEGFP-N2-*hMJD1*a18CAG$_{\mathrm{AGC}}$ and pEGFP-N2-*hMJD1*a151CAG$_{\mathrm{ACC}}$. Cells were then grown for 24 h before they were treated with G418 (Merck, Darmstadt, Germany, 50 µg/ml to 400 µg/ml) and Gentamicin-sulfate (Carl Roth, Karlsruhe, Germany, 100 µg/ml to 500 µg/ml). EGFP expression was analyzed after an incubation time of 48 h by either fluorescence microscopy (see 3.6.22, page 71) or SDS-PAGE, western blot and immunodetection (see 3.6.9, 3.6.11 and 3.6.12, page 65 ff.).

3.3.9 Induction of proteolytic calpain cleavage

HEK 293T *ATXN3* KO cells were transfected with pEGFP-C2-ataxin-3 isoforms and grown for 24 h. Culture medium was then exchanged to Opti-MEM medium and cleavage was induced with 125 nM ionomycin and 5 mM $CaCl_2$ for 1 h. As a negative control, cells were pre-treated with calpain inhibitor III for 1 h with a final concentration of 10 mM. After the treatment, cells were grown in normal culture medium for another 48 h. Samples were then processed for filter retardation assay (see 3.6.14, page 68).

3.4 Generation of transgenic zebrafish

Generation, housing and mating of zebrafish was performed by Shermaine Tay and Assoc. Prof. Christoph Winkler at the National University of Singapore, Singapore according to standard procedures and in compliance with the local legislation. Samples of zebrafish larvae and zebrafish brain were kindly provided as described (Table 3.14).

Table 3.14. Zebrafish samples. This table summarizes the samples which were received from Shermaine Tay and Assoc. Prof. Christoph Winkler from the National University of Singapore, Singapore.

Line	Usage	Sample	n	Age	Treatment
*hMJD1*c18CAG$_{GG}$.1	DNA	Larvae	3·20	5 to 6 dpf	flash frozen
	mRNA	Larvae	3·50	5 to 6 dpf	1 ml RNAlater
	Protein	Larvae	3·70	5 to 6 dpf	100 µl RIPA buffer
	Protein	Brain	2·1	4 mpf	flash frozen
	Sectioning	Brain	2·1	4 mpf	2 ml 4 % PFA
*hMJD1*c18CAG$_{GG}$.4	DNA	Larvae	3·20	5 to 6 dpf	flash frozen
	mRNA	Larvae	3·50	5 to 6 dpf	1 ml RNAlater
	Protein	Larvae	3·70	5 to 6 dpf	100 µl RIPA buffer
	Protein	Brain	3·1	4 mpf	flash frozen
	Sectioning	Brain	2·1	4 mpf	2 ml 4 % PFA
*hMJD1*aL18CAG$_{GGC}$.44	DNA	Larvae	3·20	5 to 6 dpf	flash frozen
	mRNA	Larvae	3·50	5 to 6 dpf	1 ml RNAlater
	Protein	Larvae	3·70	5 to 6 dpf	100 µl RIPA buffer
	Protein	Brain	3·1	4 mpf	flash frozen
	Sectioning	Brain	3·1	4 mpf	2 ml 4 % PFA
*hMJD1*aS18CAG$_{GGA}$.1	DNA	Larvae	3·20	5 to 6 dpf	flash frozen
	mRNA	Larvae	3·50	5 to 6 dpf	1 ml RNAlater
	Protein	Larvae	3·70	5 to 6 dpf	100 µl RIPA buffer
	Protein	Brain	3·1	4 mpf	flash frozen
	Sectioning	Brain	3·1	4 mpf	2 ml 4 % PFA
*hMJD1*c73CAG$_{AC}$.2	DNA	Larvae	3·20	5 to 6 dpf	flash frozen
	mRNA	Larvae	3·50	5 to 6 dpf	1 ml RNAlater
	Protein	Larvae	3·70	5 to 6 dpf	100 µl RIPA buffer
	Protein	Brain	3·1	4 mpf	flash frozen
	Sectioning	Brain	3·1	4 mpf	2 ml 4 % PFA
*hMJD1*aL73CAG$_{ACC}$.1	DNA	Larvae	3·20	5 to 6 dpf	flash frozen
	mRNA	Larvae	3·50	5 to 6 dpf	1 ml RNAlater
	Protein	Larvae	3·70	5 to 6 dpf	100 µl RIPA buffer
	Protein	Brain	3·1	4 mpf	flash frozen
	Sectioning	Brain	3·1	4 mpf	2 ml 4 % PFA
*hMJD1*aS73CAG$_{ACA}$.1	DNA	Larvae	3·20	5 to 6 dpf	flash frozen
	mRNA	Larvae	3·50	5 to 6 dpf	1 ml RNAlater
	Protein	Larvae	3·70	5 to 6 dpf	100 µl RIPA buffer
	Protein	Brain	1·1	4 mpf	flash frozen
	Sectioning	Brain	3·1	4 mpf	2 ml 4 % PFA
H*hMJD1*aS73CAG$_{ACA}$.16	DNA	Larvae	3·20	5 to 6 dpf	flash frozen
	mRNA	Larvae	3·50	5 to 6 dpf	1 ml RNAlater

Continued on next page

Table 3.14. Zebrafish samples. – *Continued from previous page*

Line	Usage	Sample	n	Age	Treatment
	Protein	Larvae	3·70	5 to 6 dpf	100 µl RIPA buffer
H*hMJD1*aS73CAG$_{ACA}$.16	Protein	Brain	3·1	4 mpf	flash frozen
	Sectioning	Brain	3·1	4 mpf	2 ml 4 % PFA

3.5 Nucleic acid analytics

3.5.1 Isolation and purification of DNA

3.5.1.1 Isolation of Plasmid DNA from *E. coli*

Isolation of plasmid DNA from *E. coli* overnight cultures was performed using QIAprep Spin Miniprep Kits (Qiagen, Hilden, Germany) following the high yield protocol (02/2015). In contrast to the protocol the DNA was eluted in 40 µl instead of 50 µl of elution buffer or nuclease free water to achieve a higher DNA concentration. Isolation of plasmids for microinjections were performed using the Endo Free Plasmid Maxi Kit (Qiagen, Hilden, Germany) according to the manufactuer's protocol (01/2011).

3.5.1.2 Isolation of DNA from agarose gels

Isolation of DNA fragments from agarose gels was performed using the QIAquick Gel Isolation Kit (Qiagen, Hilden, Germany) according to the manufacturers protocol (10/2010).

3.5.1.3 Isolation of DNA from eucaryotic cells

Isolation of DNA from eucaryotic cells was performed using the High Pure polymerase chain reaction (PCR) Product Purification Kit (Roche Molecular Systems, Mannheim, Germany) according to the manufacturers protocol (version 17, 04/2017).

3.5.1.4 Isolation of DNA from zebrafish larvae

Isolation of DNA from zebrafish larvae was performed using the High Pure PCR Product Purification Kit (Roche Molecular Systems, Mannheim, Germany) according to the manufacturers protocol (version 17, 04/2017).

3.5.1.5 Purification of PCR products

PCR products were purified using the QIAquick PCR Purification Kit (Qiagen, Hilden, Germany) according to the manufacturers protocol (03/2008).

3.5.2 Isolation and purification of mRNA

3.5.2.1 Isolation of mRNA from eucaryotic cells

In order to isolate the mRNA from eucaryotic cells, the media was discarded and the cells were resuspended and washed in fresh DPBS before they were transferred to a reaction tube. Cells

were pelleted (300 *g*, 5 min, 4 °C) and kept on ice. The pellet was resuspended in lysis buffer RLT supplemented with 1 % (v/v) β-mercaptoethanol. Lysis was performed by using QIAshredder (Qiagen) columns (21.000 *g*, 2 min, 4 °C). mRNA was purified from the lysate using the RNeasy Mini Kit (Qiagen) according to the manufacturers protocol (01/2011). A digestion of genomic DNA was performed using the RNAse free DNAse Kit (Qiagen) as described in the RNeasy protocol. The purified mRNA was eluted in 30 µl of RNase free water.

3.5.2.2 Isolation of mRNA from zebrafish larvae

In order to isolate the mRNA from zebrafish larvae precipitated salts ware resolubilized after thawing and RNAlater was removed. Isolation of mRNA was then performed using the RNeasy Mini Kit (Qiagen) according to the manufacturers protocol (01/2011) whereby samples were homogenized using the Ultra-Turrax disperser after addition of 350 µl of RLT Buffer

3.5.3 Reverse transcription

Elimination of genomic DNA as well as reverse transcription of mRNA to cDNA was performed using the QuantiTect Reverse Transcription Kit (Qiagen) following the manufacturers protocol (03/2009) with 1 µg of RNA. A negative control comprising of two randomly chosen mRNA samples was only treated with the gDNA wipe-out buffer and topped to 20 µl to act as a verification of the successful elimination of gDNA in RT-PCRs.

3.5.4 Agarose gelelectrophoresis

Agarose was suspended in either 1-time TBE (analytical gels) or 1-time TAE (preparative gels) and solubilized by heating in the microwave. Lost volume was filled up with deionized water by weight-comparison. The agarose solution was cooled down a bit before the addition of Gel-Red (1:40000; Biotium, Fremont, CA, USA) or ethidium bromide (1:25000 - 1:33333; Carl Roth, Karlsruhe, Germany) and casting the gel. DNA samples were supplemented with DNA loading dye before dispensing them in the wells. Separation of DNA fragments was performed with 10 V/cm to 15 V/cm. DNA bands were documented using a gel documentation system.

3.5.5 Polymerase Chain Reaction

Two different polymerases were used for the amplification of DNA sequences. Short analytical PCR products were amplified by the OneTaq polymerase (New England Biolabs, Frankfurt a.M., Germany). The amplification of preparative PCR products for cloning purposes with increased specificity were generated by using a 3'-5' proofreading capable Pwo polymerase (Sigma-Aldrich Chemie, Hamburg, Germany). Table 3.15 shows the reaction conditions for PCRs with OneTaq and Pwo polymerases. 200 ng of gDNA or 25 ng of plasmid-DNA were used as template. PCR reactions were supplemented with 1 M Betain for the amplification of zebrafish cDNA. PCR reactions were performed with a touch-down temperature protocol, table 3.16.

Table 3.15. Composition of PCR reactions. This table specifies the composition of PCR reactions for OneTaq or Pwo polymerases.

Component	Final concentration
Polymerase	1U
Reaction buffer	1-time
dNTPs	250 µM
Forward primer	400 nM
Reverse primer	400 nM

Table 3.16. Temperature protocol of the touch down PCR. PCR reactions were performed using a touch-down temperature protocol from 65 °C to 55 °C In case of the amplification of longer templates using the Pwo polymerase, the elongation time was adjusted depending on the amplicon size according to the peqGOLD Pwo-DNA-Polymerase protocol (PEQLAB_v0116_D).

Step	Time (s)	Temperature (°C)	Repeats
Initial denaturing	300	94	
Denaturing	30	94	
Annealing	30	65 - 1 cycle	10
Elongation	60	68	
Denaturing	30	94	
Annealing	30	55	25
Elongation	60	68	
Final elongation	450	68	
Storage	∞	4	

3.5.6 Real-time Polymerase Chain Reaction

Quantification of transcript levels from cDNA was performed using real-time polymerase chain reaction (RT-PCR). All samples were thawed on ice and diluted to 2.5 ng/µl. A standard curve was created from two different cDNA samples in a serial 1:5 dilution ranging from 5 ng/µl to 8 pg/µl in the final RT-PCR reaction. Primer pairs were pre-mixed and diluted to 10 µM, whereas 1 µM was used as a final concentration in the RT-PCR. QuantiTect SYBR Green I (Qiagen), primers and Ampuwa water were mixed and distributed to a 384 well plate on ice. 2 µl of standards and samples were added to 8 µl of reaction mix. The plate was centrifuged at 800 *g* for 1 min to settle liquids at the wall of the well. Final cDNA standards were ranging vom 1 ng/µl to 1.6 pg/µl. The concentration of cDNA samples was 0.5 ng/µl. Samples were analyzed in a triplicate, standard samples in a duplicate. A no template control (NTC) as well as an negative control (no reverse transcription) were analyzed together with the standard curve and the cDNA samples for every primer pair to exclude an external contamination as well as a contamination with gDNA.

All gene of interest levels were compared to housekeeping genes (i. e. GAPDH, SDHA and TBP) using the primers S046, S047, S050, S051, S052 and S053 in order to perform a relative quantification of gene expression levels using the Advanced Relative Quantification Analysis of

the LightCycler 480 software.

Table 3.17. Temperature protocol of the RT-PCR. RT-PCR reactions were performed using optimized conditions for the QuantiTect SYBR Green I.

Step	Time (s)	Temperature (°C)	Repeats
Initial denaturing	900	95	
Denaturing	20	94	
Annealing	40	60	40
Elongation	20	72	
Melting	750	60 - 90 (0.04/s)	
Cooling	10	40	

3.5.7 Manipulation of DNA

3.5.7.1 Restriction of DNA

Restriction reactions were performed by incubating the DNA together with the respective restriction endonuclease at the optimal buffer and temperature conditions. Reactions involving more than one restriction enzyme were performed in buffer suitable for both enzymes. In case that no suitable buffer was available the reaction was performed with one restriction enzyme and the DNA was purified using the QIAquick PCR Purification Kit (Qiagen) before digesting with the second enzyme. The amount of enzyme was calculated according to the NEB unit definition to achieve an optimal digestion of the desired DNA amount in the desired time.

Usually 2 µg/ml of DNA were digested in a total reaction volume of 50 µl for three hours at the temperature optimum of the respective enzyme. If possible the reaction was heat inactivated before further processing at 65 °C or 80 °C depending on the enzyme. A purification of the desired DNA fragment was performed after an agarose gel electrophoresis using the QIAquick Gel Extraction Kit (Qiagen).

3.5.7.2 Dephosphorylation of DNA

Digestions of DNA vectors were treated with the enzyme calf intestinal phosphatase (New England Biolabs) before purification in order to prevent a religation of the vector during ligation reactions. 5 units of calf intestinal phosphatase were added to the restriction after heat inactivation if the DNA was already solubilized in a suitable buffer. Otherwise a buffer-change was performed by using the QIAquick PCR Purification Kit (Qiagen). The DNA was eluted in 45 µl of Ampuwa water and 5 µl of NEB CutSmart 10-times buffer were added before the addition of calf intestinal phosphatase. DNA samples were incubated for 2 h at 37 °C.

3.5.7.3 Ligation of DNA-fragments

In order to estimate the DNA amount for the preparation of the ligation reaction, 10 % (v/v) of the sample volume from vector and insert were loaded onto an analytical agarose gel. Band

intensities and fragment sizes were compared after the gel run. The comparison factor f was calculated according to Equation 3.4 where $Size$ is the length of the DNA fragment in bp, $Intensity$ is the signal intensity on the quantified gel, $Volume$ is the loaded volume on the gel and $Excess$ is the desired molar overage of insert compared to vector. f was usually calculated for a 3-times excess of insert DNA. The volume of insert DNA for the ligation reaction was calculated from Equation 3.5 where f is the factor from Equation 3.4 and μl_{Vector} is the volume of vector that is being used in the reaction.

$$f = \frac{Size_{Vector}}{Size_{Insert}} \cdot \frac{Intensity_{Insert}}{Intensity_{Vector}} \cdot \frac{Volume_{Vector}}{Volume_{Insert}} \cdot \frac{1}{Excess} \tag{3.4}$$

$$\mu l_{Insert} = \frac{f}{\mu l_{Vector}} \tag{3.5}$$

The ligation reaction comprising of 50 ng of vector DNA, the 3-times molar excess of insert DNA, 400 units of T4 DNA-Ligase (New England Biolabs) and 1-times T4 DNA-Ligase buffer in a total reaction volume of 20 µl was incubated either at 16 °C overnight or at an 99-times alternating sequence at 10 °C and 30 °C for 30 s each. In order to dissociate the T4 DNA-Ligase from the DNA an inactivation step at 65 °C for 15 min was performed before cooling the reaction to 4 °C.

3.5.8 Concentration measurements of nucleic acids

Measurement of the OD of DNA or RNA solutions was performed in a µCuvette (Eppendorf, Wesseling-Berzdorf, Germany) at a wavelength λof 260 nm (OD_{260}). The measured OD was used for calculation of the DNA or RNA concentration. An extinction coefficient of 1.0 corresponds to 50 mg/ml of a pure DNA solution or 40 mg/ml of a pure RNA solution. Purity of nucleic acid solutions was measured by the ratio of OD_{260}/OD_{280}. A nucleic acid preparation was considered to be pure with a ration between 1.8 and 2.0. The blank measurement was performed with the respective nucleic acid solvent.

3.5.9 Sequence analysis

Sequencing was performed on a CEQ 8000 Genetic Analysis System using a GenomeLab Quick Start Kit (both Beckman Coulter, Beverley, MA, USA). 50 fmol to 100 fmol of purified DNA were diluted to a total volume of 15.5 µl in millipore water. DNA was denatured for 1 min at 95 °C and cooled down on ice before 4 µl of DTCS quick start mix (Beckman Coulter) and 0.5 µl of the sequencing primer (10 pmol/µL) were added. The sequencing reaction was performed using the manufacturer's temperature protocol (Table 3.18).

Table 3.18. Temperature protocol of the sequencing reaction. Sequencing reactions were performed using the standard protocol for the GenomeLab Quick Start Kit.

Step	Time (s)	Temperature (°C)	Repeats
Denaturing	20	96	
Annealing	20	50	30
Elongation	240	60	
Storage	∞	10	

In the case of plasmid DNA the samples were afterwards purified by ethanol precipitation according to the manufacturer's protocol (P/N 608118 AC, 09/2004) with the following changes: Centrifugation was performed at 16 100 *g* for 30 min and afterwards twice for 15 min. The SLS solubilized samples were stored for 60 min at 4 °C before they were analyzed using the CEQ 8000 Genetic Analysis System. In the case of PCR products the samples were purified using the Agencourt AMPure PCR purification beads (Beckman Coulter) according to the manufacturers protocol (000601v024). Samples were analyzed using the CEQ 8000 Genetic Analysis System (Table 3.19). Analysis of the raw chromatogram was performed using the Standard Sequence Analysis protocol of GenomeLab Genetic Analysis System.

Table 3.19. CEQ 8000 protocol for sequencing. This table summarizes the protocol of the CEQ8000 Genetic Analysis System for the sequencing of plasmids and PCR products.

Event	Event parameters
Capillary Temperature	50 °C
Denature	90 °C, 120 s
Pause	3 min
Inject	2.0 kV, 25 s
Separate	4.2 kV, 105 min

In some cases, samples were sent for sequencing by next generation sequencing (NGS, Molecular Genetics Diagnostic department of the Institute of Medical Genetics and Applied Genomics, Tübingen).

3.5.10 Fragment length analysis

Analysis of the exact length of PCR products with CAG repeats was performed by a fragment length analysis using a 5'fluorescence labeled R888_pre-CAG-forward primer. The template DNA was diluted to a final concentration of 25 ng/µl. Table 3.20 specifies the composition of the PCR reaction. In contrast to this reaction setup the PCR reaction for the fragment length analysis of the pDestAttB-HuC-hMJD vector with 151 CAG repeats was performed using the Expand Long Template PCR System (Roche Molecular Systems) polymerase.

Table 3.20. Composition of the fragment length analysis PCR reaction. This table specifies the composition including concentrations of PCR reactions for the fragment length analysis. The setup was performed in a total volume of 20 µl.

Component	Final concentration
OneTag polymerase	1 unit
OneTag enhanced GC buffer	1-time
Betain	1 M
dNTPs	250 mM
R888_preCAG-forward	375 nM
R100_postCAG-reverse	375 nM
DNA template	1.25 ng/µl

An aliquot of the PCR product was loaded onto a 2 % (w/v) agarose gel in order to verify the specificity and purity of the amplicon. Afterwards the PCR product was diluted 1:200 and 5 µl of the dilution were mixed with 34.5 µl SLS and 0.5 µl Size Standard Kit DNA 600 (Beckman Coulter). Samples were analyzed using the CEQ 8000 Genetic Analysis System with standard parameters (Table 3.21). Raw data was analyzed using the Standard Fragment Analysis protocol of the GenomeLab Genetic Analysis System.

Table 3.21. CEQ8000 protocol for the fragment length analysis. This table summarizes the protocol of the CEQ8000 Genetic Analysis System for the fragment length analysis.

Event	Event parameters
Capillary Temperature	50 °C
Denature	90 °C, 120 s
Pause	0 min
Inject	2.0 kV, 30 s
Separate	6.0 kV, 60 min

3.6 Proteinanalytics

3.6.1 Isolation of proteins from eucaryotic cells

Protein lysates were generated after detaching cells using DPBS and pelleting at 300 *g* for 5 min. DPBS was removed and the cells were lysed in radioimmunoprecipitation assay (RIPA) buffer (25 mM Tris, 150 mM NaCl, 0.1 % (w/v) SDS, 0.5 % (w/v) sodium deoxycholate, 1 % (v/v) Triton-X100, cOmplete protease inhibitor without ethylenediaminetetraacetic acid (EDTA)) for 20 min. Samples were vortexed every 5 min during this time. Samples were cleared by centrifugation for 10 min at 16 000 *g* and 4 °C. Supernatant was supplemented with glycerol (10 % (v/v) final concentration). In the case of protein homogenates pellets were lysed using DPBS supplemented with 1 % (v/v) Triton-X100 by sonication.

3.6.2 Isolation of proteins from zebrafish larvae

Samples were lysed by addition of 125 µl fresh RIPA buffer (25 mM Tris, 150 mM NaCl, 0.1 % (w/v) SDS, 0.5 % (w/v) sodium deoxycholate, 1 % (v/v) Triton-X100, cOmplete protease inhibitor without EDTA) and sonicated 5 s at 10 % intensity. Homogenates were generated by addition of

10 % (v/v) glycerol. Lysates were centrifuged at 16 000 *g* and 4 °C for 5 min. Supernatant was supplemented with 10 % (v/v) glycerol.

Control samples of 3 days post fertilization flash frozen larvae (n = 60 - 68) from wild type (WT) zebrafish (kindly provided by Prof. Dr. Bernd Wissinger) containing the yolk sac were lysed identically. Deyolked control samples of WT zebrafish larvae were generated by addition of 1 ml deyolking buffer (55 mM NaCl, 1.8 mM KCl, 1.25 mM $NaHCO_3$) to the frozen larvae (n = 60 - 68). Deyolking was performed by pipetting of larvae samples using a 100 µl tip followed by shaking 5 min, 1000 rounds per minute (rpm). Samples were centrifuged at 300 *g* for 30 s at 4 °C and supernatant was removed. Deyolked larvae were then washed by addition of 1 ml deyolking wash buffer (110 mM NaCl, 3.5 mM KCl, 2.7 mM $CaCl_2$, 0.4 % (v/v) 2.5 M Tris-HCl pH 8.5, cOmplete protease inhibitor without EDTA) for 2 min under constant shaking at 1000 rpm. Larvae were pelleted at 300 *g* for 30 s at 4 °C and washing was repeated. Larvae were then lysed by addition of 100 µl RIPA buffer (25 mM Tris, 150 mM NaCl, 0.1 % (w/v) SDS, 0.5 % (w/v) sodium deoxycholate, 1 % (v/v) Triton-X100, cOmplete protease inhibitor without EDTA).

3.6.3 Isolation of proteins from zebrafish brains

Brain samples of zebrafish were were lysed using 150 µl RIPA buffer (25 mM Tris, 150 mM NaCl, 0.1 % (w/v) SDS, 0.5 % (w/v) sodium deoxycholate, 1 % (v/v) Triton-X100, cOmplete protease inhibitor without EDTA) and homogenization using the Ultra-Turrax disperser. Homogenate samples were supplemented with glycerol (10 % (v/v)). Lysate samples were cleared by centrifugation for 10 min at 16 000 *g* and 4 °C and supernatant was supplemented with glycerol (10 % (v/v) final concentration).

Control samples of WT zebrafish (16 months post fertilization (mpf)), n = 3, kindly provided by Prof. Dr. Bernd Wissinger) were treated identically but dissociated using ultra-sonication (5 s, 10 % intensity).

3.6.4 Concentration measurements of proteins

Protein concentration was measured using a Bradford Protein Assay (Bio-Rad Laboratories, Munich, Germany) according to the manufacturers protocol against a bovine serum albumin (BSA) Fraction V standard. OD_{495} was measured for all samples using the plate reader Synergy HT. Samples and standards were measured as duplicates.

3.6.5 Generation of polyclonal antibodies

Peptide synthesis, purification, affinity chromatography and ELISA was performed in cooperation with by Prof. Dr. Hubert Kalbacher, Medizinisch-Naturwissenschaftliches Forschungszentrum, Tübingen, Germany.

3.6.5.1 Peptide synthesis and purification

Following peptides were synthesized for either immunization of rabbits or affinity purification of antibodies from rabbit sera (Table 3.22).

Table 3.22. Peptides for the generation of isoform-specific antibodies. Peptides synthesized by Prof. Dr. Hubert Kalbacher, Medizinisch-Naturwissenschaftliches Forschungszentrum, Tübingen. All peptides carried a linker sequence. Purification peptide also carried a C-terminal solubilizer to introduce hydrophilic amino acids to the mainly hydrophobic sequence. The ataxin-3along-specific sequence is underlined.

Peptide	Application	Linker - specific sequence - solubilizer
A	immunization	KEFA-SPFIMFATFTLYLTYELHVIFALHYSSFPL
B	immunization	KEFA-SPFIMFATFTLYLT
C	immunization	KEFA-YELHVIFALHYSSFPL
1	affinity purification	KERE-SPFIMFATFTLYLTYELHVIFALHYSSFPL-EE
2	affinity purification	KERE-SPFIMFATFTLYLT-EE
3	affinity purification	KERE-YELHVIFALHYSSFPL-EE

Synthesized peptides were soaked in 1 ml dimethylformamide (DMF) for 10 min under shaking. Supernatant was removed from the filter syringe and the 9H-fluoren-9-ylmethoxycarbonyl (FMOC) protecting groups were removed under mild basic conditions by a piperidin treatment (40 % (v/v) in DMF) for 5 min. The supernatant was removed and the piperidin treatment was repeated.

Peptides were washed three times with DMF, followed by three washes with 2-propanol and ether respectively before the peptides were dried using an aspirator. The dried peptides were dissolved in 1 ml peptide solvent (25 µl H_2O, 25 µl thioanisole, 25 µl EDTA, 925 µl TFA, one spatula phenol) for 60 min at room temperature. Afterwards 25 µl bromo(trimethyl)silane were added and the peptides were incubated for 30 min under shaking. The solution was added to ice cold ether and peptides were pelleted by centrifugation for 5 min at 2000 *g*. The supernatant was removed and the washing step was repeated two times. Thereby the pellet was carefully suspended in ether before each centrifugation step. The supernatant was removed after the third wash and the pellet was dissolved in 2 ml of a 1:1 mixture of trifluoroacetic acid (TFA) and 2-methylpropan-2-ol. The sample was mixed and frozen in liquid nitrogen. Afterwards the peptides were lyophilized over night.

After lyophilization the peptide mixture was purified using high performance liquid chomatography (HPLC). Therefore 3 mg of the dried peptide was dissolved in 50 µl of dimethyl sulfoxide. Afterwards 50 µl of HPLC System B (80 % (v/v) acetonitrile, 7.1 % (v/v) TFA) buffer was added and the sample was mixed. 600 µl of HPLC System A (4.8 mM TFA) buffer was added and the solution was centrifuged at 10 000 *g* for 1 min. The sample was injected to the HPLC LC-Organizer (Hitachi, Tokyo, Japan) and separated using the L-6200 Intelligent Pump (Hitachi). Fractions were detected with a L-4000A UV Detector (Hitachi) and collected manually. The identity of those fractions showing the expected retention time was confirmed by MS. The solution was frozen in liquid nitrogen and lyophilized over night.

3.6.5.2 Immunization of rabbits

The complete immunization procedure was performed by Pineda Antikörper-Service, Berlin. The sera of six rabbits were analyzed by western blot and immunodetection for an unspecific signal in the size region of ataxin-3. Three rabbits which did not show an interfering signal were chosen and immunized with a mixture of peptides A, B and C coupled to keyhole limpet hemocyanin. Immunization was monitored every 30 days starting from day 61. by an enzyme

linked immunosorbent assay (ELISA) of the serum directed against peptides 1, 2 and 3. A boost with all three peptides was performed at the same time. All three rabbits were exsanguinated 630. days post immunization.

3.6.5.3 Preparation of the chromatography media

Affinity chromatography media was prepared by coupling of peptides to CNBr-Activated Sepharose (GE Healthcare, Munich, Germany) 4B by their amine group. Therefore 0.5 g of sepharose was swollen in 1 mM hydrogen chloride pH 3.0 for 30 min in a chromatography column. The media was washed first with millipore water followed by 100 mM sodium bicarbonate in order to remove the hydrogen chloride. The peptide was pre-dissolved in 50 µl dimethyl sulfoxide and 2 µl of 100 mM sodium bicarbonate. Afterwards the solution was added to the CNBr-Activated Sepharose. The coupling was performed over night under constant end over end shaking. The 100 mM sodium bicarbonate buffer was replaced by 100 mM Tris Base to block reactive groups of the cyanate ester for 15 min under end over end shaking. The chromatography media was washed three times with phosphate buffered saline (PBS) and stored in PBS containing 0.02 % (w/v) of sodium azide at 4 °C until its use.

3.6.5.4 Affinity chromatography

The chromatography media was washed once with PBS pH 8.0. The serum was diluted 1:1 in PBS and added to the column. Cycling was performed at 4 °C over night. The flow through was collected and the column was washed twice with PBS pH 8.0. Afterwards the affinity purified antibody was eluted in 1 ml fractions by the addition of 100 mM glycin pH 3.0. The eluate was collected in ten fractions in reaction tubes with 1 ml trisodium-phosphate in order to balance the pH. The OD_{280} of all fractions was measured to identify protein containing fractions. Those were combined and concentrated using an Amicon Ultra 10 kDa centrifugal filter (Merck, Darmstadt, Germany) with an Uracel-50 membrane for 5 min at 2000 *g*. The buffer was exchanged to PBS in three centrifugation steps using the centrifugal filter. The antibody solution was finally concentrated to 1 ml and the OD_{280} was measured for confirmation of the antibody concentration. 0.02 % (w/v) sodium azide was added for conservation.

3.6.6 Enzyme-linked Immunosorbent Assay

In order to perform an direct ELISA a 96-well MaxiSorp (Thermo Fisher Scientific, Karlsruhe, Germany) plate was coated with 100 µl of the peptide antigen at a concentration of 10 µg/ml in PBS over night at 4 °C. Wells were washed three times with ELISA wash buffer (PBS supplemented with 0.05 % (v/v) Tween-20) using a wash bottle. Afterwards the plate was blocked with 200 µl ELISA blocking buffer (PBS supplemented with 0.5 % (w/v) BSA Fraction V) and incubated for 2 h at 37 °C under constant shaking. After blocking, the plate was washed again three times using ELISA wash buffer before 100 µl of the primary antibody in ELISA dilution buffer (PBS supplemented with 0.05 % (v/v) Tween-20 and 0.5 % (w/v) BSA Fraction V) was added for 90 min under constant shaking at 37 °C. The plate was washed again five times using ELISA wash buffer. The incubation with the secondary antibody was then performed for 60 min in ELISA dilution buffer. The ELISA plate was again washed five times with ELISA wash

buffer and then incubated with 100 µl of ELISA substrate solution (1.8 mM 2,2'-azino-bis(3-ethylbenzthiazoline-6-sulphonic acid in 90 mM citrate buffer) containing 0.3 ‰ of H_2O_2 which was added just before. The plate was incubated for 15 min to 30 min in the dark. Afterwards the colorimetric reaction was quantified by measuring the OD_{405}.

A sandwich ELISA was performed according to the above mentioned direct ELISA protocol but protein A (10 µg/ml; kindly provided by Prof. Dr. Hubert Kalbacher) was coated instead of peptide antigen. Further an over night incubation at 4 °C with the capture antibody was performed after blocking of the plate.

3.6.7 Fractionation according to solubility

Fractionation was performed according to Koch and colleagues (Koch et al., 2011). The Cell pellet was resuspended in fractionation RIPA buffer (50 mM Tris, 150 mM NaCl, 0.2 % (v/v) Triton X-100, 25 mM EDTA, cOmplete protease inhibitor without EDTA) and protein concentration was measured using Bradford Protein Assay. 100 µg of sample was transferred to a new microcentrifuge tube and adjusted to a total volume of 100 µl. Samples were centrifuged at 16 000 *g* and 4 °C for 30 min. Supernatant was kept as Triton-X100 soluble fraction and pellet was suspended in fractionation RIPA buffer containing 2 % (w/v) SDS. Samples were centrifuged at 22 000 *g* for 30 min at room temperature. Supernatant was kept as SDS-soluble fraction. The remaining pellet was dissolved in 100 % formic acid for 16 h at 37 °C. Formic acid was evaporated using a Concentrator 5301 (Eppendorf). The dried pellet was solubilized in 100 µl 1-times protein loading dye. If necessary pH was adjusted with 2 M Tris Base. Equal amounts of sample were analyzed by SDS-PAGE and westen blot.

3.6.8 Fractionation according to localization

For separation of nuclear and cytoplasmic proteins the Rapid, Efficient And Practial fractionation protocol (Suzuki et al., 2010) was used with minor modifications (Weber et al., 2017). In brief cells were harvested in DPBS and pelleted at 300 *g* for 5 min. Cells were kept on ice and lysed in fractionation buffer (DPBS supplemented with 0.1 % (v/v) Nonidet P-40, cOmplete protease inhibitor without EDTA) by pipetting up and down 10 times using a 100 µl tips cut at the 10 µl mark. One third of the volume was removed and saved as whole cell homogenate. Left-over homogenate was briefly spinned at 10 000 rpm for 10 s. Supernatant was removed and saved as cytoplasmic fraction. Pellet was suspended in fractionation buffer and spinned again. Supernatant was removed and pellet was kept on ice. Samples were then supplemented with 4-times LDS sample buffer (1 M Tris Base pH 8.5, 2 mM EDTA, 8 % (w/v) lithium dodecyl sulfate, 40 % (v/v) glycerol, 0.075 % (w/v) Coomassie Brilliant Blue G-250, 0.025 % (w/v) phenol red) and 1 mM dithiothreitol (DTT).

3.6.9 Sodium dodecyl sulfate polyacrylamide gelelectrophoresis

30 µg of protein were supplemented with 4-times LDS sample buffer (1 M Tris Base pH 8.5, 2 mM EDTA, 8 % (w/v) lithium dodecyl sulfate, 40 % (v/v) glycerol, 0.075 % (w/v) Coomassie Brilliant Blue G-250, 0.025 % (w/v) phenol red) and 100 mM DTT. Samples were heat denatured for 10 min at 70 °C. SDS-PAGE was performed either using Bis-Tris gels (8 % to 12 %, Table

3.23) with MES (50 mM MES, 50 mM Tris Base, 0.1 % (w/v) SDS, 1 mM EDTA) or MOPS buffer (50 mM MOPS, 50 mM Tris Base, 0.1 % (w/v) SDS, 1 mM EDTA) or Tris-Glycin gels using Tris-Glycin running buffer (192 mM Glycin, 25 mM Tris Base, 0.1 % (w/v) SDS) (Table 3.24). In the latter case samples were supplemented with 5-times Tris-Glycin sample loading buffer (125 mM Tris-HCl pH 6.8, 8 % (w/v) DTT, 50 % (v/v) Glycerol, 2 % (w/v) SDS, 0.05 % (w/v) Coomassie Brilliant Blue G-250) instead of 4-times LDS sample buffer. Gels were run at 80 V until samples entered the separation gel. Afterwards the current was increased to 120 V until transfer.

Table 3.23. Composition of Bis-Tris gels. Bis-Tris gels were used with the following final concentrations.

Component	Separation gel	Stacking gel
Bis-Tris gel buffer	357 mM	357 mM
AA/Bis-AA (29:1)	8 % - 12 % (w/v)	6 % (w/v)
TEMED	5.25 mM	5.25 mM
Ammonium persulfate	5.25 mM	5.25 mM

Table 3.24. Composition of Tris-Glycin gels. Tris-Glycin gels were used with the following final concentrations.

Component	Separation gel	Stacking gel
Tris-Glycin stacking gel buffer pH 6.8		167 mM
Tris-Glycin separation gel buffer pH 8.8	307.5 mM	
AA/Bis-AA (29:1)	10 % (w/v)	4 % (w/v)
TEMED	4.3 mM	13.8 mM
Ammonium persulfate	71.0 mM	115.7 mM

3.6.10 Protein staining of gels

Gels were stained using a colloidal Coomassie staining according to (Kang et al., 2002, qualitative analysis) or SYPRO Ruby Protein Gel Stain (Invitrogen, Karlsruhe, Germany, quantitative analysis). In order to stain a gel using the Coomassie staining, gels were washed twice in distilled water after the gel run for 10 min before the staining solution (0.02 % (w/v) Coomassie-G250, 5 % (w/v) aluminium sulfate octadecahydrate, 10 % (v/v) ethanol, 2 % (v/v) ortho-phosphpric acid) was applied. Gels were usually stained over night. Gels were rinsed with water and afterwards destained using the Coomassie destaining solution (10 % (v/v) ethanol, 2 % (v/v) ortho-phosphpric acid) for 30 min. Finally gels were rinsed with water again in order to remove the destaining solution. SYPRO Ruby Protein gel stains were performed according to the manufacturers protocol (version 20–November–2007) and afterwards detected at 600 nm using the Li-Cor Odyssey FC (LI-COR Biosciences, Bad Homburg, Germany).

3.6.11 Western-Blot

Transfer of proteins onto Amersham Protran Premium 0.2 µm/0.45 µm nitrocellulose or Amersham Hybond P 0.2 µm PVDV membranes (both GE Healthcare) was performed using either

Bicine/Bis-Tris transfer buffer (25 mM Bicine, 25 mM Bis-Tris pH 7.2, 1 mM EDTA) or Tris-Glycin transfer buffer (192 mM Glycin, 25 mM Tris Base) depending on the type of gel. Both buffers contained 15 % (v/v) methanol. The transfer was performed at 80 V and 250 mA (Bis-Tris) or 80 V without controlling the current (Tris-Glycin).

3.6.12 Immunodetection

Membranes were blocked after the transfer with 5 % (w/v) skim milk powder for 1 h in tris buffered saline (10 mM Tris, 150 mM NaCl) at room temperature. If not stated otherwise, antibodies were diluted in tris buffered saline supplemented with 0.1 % (v/v) Tween-20. Primary antibody incubation was performed at 4°C over night. Membranes were washed three times for 5 min using tris buffered saline supplemented with 0.1 % (v/v) Tween-20 before the secondary antibody was added and membranes were incubated for 1 h at room temperature. Membranes were washed at least three more times as stated above. Signals were detected using the Odyssey FC (LI-COR Biosciences) and quantified using Image Studio (LI-COR Biosciences). For a detailed description of antibodies used see table 3.9. Membranes were stripped for 15 min using stripping buffer (200 mM Glycin, 1 % (w/v) SDS, pH 2.0) in order to remove primary and secondary antibodies from membranes. Afterwards membranes were washed twice with tris buffered saline supplemented with 0.1 % (v/v) Tween-20 for 2 min before the membrane was blocked again.

3.6.13 SILAC and Mass Spektrometry for the detection of interaction partners

The Strep co-immunoprecipitation was performed as described previously by Gloeckner et al. (2009). In brief HEK 293 cells were grown in heavy (lysine-8; aginine-10) medium (lysine-4; arginine-6) or light (lysine-0, arginine-0) stable isotope labeling by amino acids in cell culture (SILAC) medium in four 14 cm culture dishes and transfected using polyethylenimine. A robust quantification was ensured by a label switch so that every isoform was expressed in all three SILAC conditions. After 72 h the culture medium was removed and cells were washed with DPBS once. Afterwards cells were scraped off in Strep-Tactin lysis buffer (30 mM Tris-HCl pH 7.4, 150 mM NaCl, cOmplete protease inhibitor without EDTA, Phosphatase Inhibitor Cocktail 1, Phosphatase Inhibitor Cocktail 2, 0.5 % (v/v) Nonidet P-40) and lysed for 20 min under mixing. Debris was removed by centrifugation for 10 min at 10 000 g and 4 °C. Lysates were cleared by filtration through a 0.22 µm filter and then incubated with Strep-Tactin superflow resin (IBA, Göttingen, Germany) for one hour at 4 °C on a head over head tumbler. Supernatant was removed after centrifugation at 7000 g for 30 s and the resin was transferred to microspin columns. The supernatant was removed by centrifugation (5 s, 100 g) and the resin was washed thrice with Strep-Tactin wash buffer (30 mM Tris-HCl pH 7.4, 150 mM NaCl, Phosphatase Inhibitor Cocktail 1, Phosphatase Inhibitor Cocktail 2, 0.5 % (v/v) Nonidet P-40). Proteins were eluted using 1-times Strep-Tactin elution buffer (IBA) and incubated for 10 min under constant mixing. The plug of the spin column was removed and the eluate was harvested by centrifugation for 10 s at 500 g. The Strep-purified eluates were mixed in a 1:1:1 ratio prior to MS analysis and processed by chlorophorm-methanol precipitation according to Wessel and Flügge (Wessel and Flügge, 1984). Samples were re-dissolved in 50 mM ammonium bicarbonate buffer con-

taining 0.1 % (v/v) RapiGest (Waters, Eschborn, Germany). Proteolysis was performed using 0.1 mg/ml trypsin (Promega, Mannheim, Germany) over night at 37 °C. RapiGest surfactant was hydrolysed and removed. Samples were then further purified using C18-StageTips (Thermo Fisher Scientific). Samples were analysed by liquid chromatography (LC)-tandem mass spectrometry (MSMS) using a nano-flow HPLC system which was coupled to a Q-Exactive Plus tandem MS (Thermo Fisher Scientific). Raw data directly was analyzed by MaxQuant (Cox et al., 2009). The human subset of the SwissProt database (2015/05, 20198 entries) was used in the Andromeda search-engine. Carbamidomethyl (cystein) as fixed modification as well as N-terminal protein acetylation as variable modification with the heavy/medium/light (L/M/H) isotope pairs lysine-0/arinine-0, lysine-4/arinine-6 and lysine-8/arginine-10 for quantification were chosen. Trypsin was chosen as enzyme. Mass accuracy for the mass recalibration was determined to be to 20 ppm. For tandem MS spectra, 0.1 Da was set to be mass accuracy. The false discovery rate threshold was set to 1 %. Razor-peptides and peptides with N-terminal acetylation or methionine oxidation were included into protein quantification. Downstream analysis was performed in Perseus (Tyanova et al., 2016). Potential contaminations were removed and afterwards interaction rations between isoform combinations for each interaction partner were transformed by $1/x$ followed by $log_2 x$. Grouping of single experiments was performed and a t-test was used to test if the ratios differ from 0. False discovery rate threshold was set to 5 %. Cell culture and precipitation of interaction partners was assisted by Felix von Zweydorf. Proteolysis and MS analysis was performed by Felix von Zweydorf and Christian Johannes Glöckner (both German Center for Neurodegenerative Diseases, Tübingen, Germany)

3.6.14 Filter Retardation Assay

In order to analyze SDS insoluble aggregates 12.5 µg of protein homogenates were diluted in DPBS and supplemented with 2 % (w/v) SDS and 50 mM DTT. Samples were subsequently denatured at 95 °C for 5 min before they were cooled down to room temperature. In the meanwhile equilibration of a 0.45 µm cellulose-acetate membrane (GE Healthcare) was performed by the addition of 0.1 % (w/v) SDS in DPBS. Vacuum was applied using a Minifold II Slot Blot System (GE Healthcare). After equilibration samples were filtered onto the membrane and wells were washed twice with DPBS. For detection the membrane was blocked and detected as described (see 3.6.12, page 67). For zebrafish samples the cellulose-acetate membrane was substituted by a Amersham Protran Premium 0.45 µm nitrocellulose membrane (GE Healthcare).

3.6.15 Slot Blot

Slot Blots of protein lysates were performed by diluting 12.5 µg of protein homogenates in DPBS unless otherwise noted. Samples were subsequently denatured at 95 °C for 5 min before they were cooled down to room temperature. A Amersham Protran Premium 0.2 µm nitrocellulose membrane (GE Healthcare) was equilibrated using DPBS and vaccum was applied using a Minifold II Slot Blot System (GE Healthcare). After equilibration samples were filtered onto the membrane and wells were washed twice with DPBS. For detection, the membrane was blocked and detected as described in chapter 3.6.12 Immunodetection.

3.6.16 Measurement of aggreagte size

Pictures of fixed cells were taken blinded with a 10x magnification and identical exposure times of 100 ms (approximately 20 images with more than 100 aggregates in total). Image background calculation and thresholding was performed using R (R Core Team, 2017) and the EBImage (Pau et al., 2010) package. Aggregate parameters area, perimeter and position were computed and displayed using the magick package (Ooms, 2017). Objects having a perimeter smaller than 10 pixels were excluded as artefacts. After image analysis, a manual quality control was performed by comparing the original fluorescence images and the identified objects. If necessary, misidentifications were excluded. The full script for the analysis can be found in chapter B.3.

3.6.17 Purification of Glutathion-S-Transferase-ataxin-3

An *E. coli* BL21 day culture was prepared from an overnight culture and grown at 25 °C. IPTG was added in a final concentration of 100 mM at an OD_{600} of 0.6 and cells were grown another three hours. Bacteria were harvested by centrifugation at 1500 *g* for 30 min. Cells were washed with PBS and centrifuged again. Lysis was performed in glutathion-S-transferase (GST)-lysis buffer (4.2 mM Na_2HPO_4, 2 mM KH_2PO_4, 140 mM NaCl, 10 mM KCl, 1 % (v/v) Nonidet P-40, cOmplete protease inhibitor without EDTA) containing 8 mg/ml Lysozyme and 1 % (v/v) Triton-X100. Lysis was performed for 30 min in an ice bath followed by ultra-sonication (three times 30 s). The lysate was cleared twice by centrifugation for 30 min at 25 500 *g*, 4 °C. Ataxin-3 was purified by Glutathion-Sepharose 4B (GE Healthcare) according to the manufacturers protocol (10/2008). The elution (50 mM Tris pH 8.0, 10 mM glutathione) was performed three times, eluates were combined and concentrated using 10 kDa Amicon Ultra-0.5 Centrifugal Filter columns. The concentrate was supplemented with glycerol in a final concentration of 10 % (v/v).

3.6.18 Glutathion-S-transferase-Pulldown

For the GST-Pulldown the bacterial pellet with GST-ataxin-3 (see 3.6.17) was lysed in GST lysis buffer (4.2 mM Na_2HPO_4, 2 mM KH_2PO_4, 140 mM NaCl, 10 mM KCl, 1 % (v/v) Nonidet P-40, cOmplete protease inhibitor without EDTA). Suspension was ultra-sonicated twice for 30 s on ice and cleared via centrifugation (16 000 *g*, 10 min, 4 °C). Supernatant was supplemented with a glycerol (10 % (v/v) final concentration). The interaction partner was expressed in HEK 293T *ATXN3* KO cells and lysed in GST lysis buffer using a syringe. MagneGST beads (Promega) were equilibrated by adding GST bind/wash buffer (4.2 mM Na_2HPO_4, 2 mM KH_2PO_4, 140 mM NaCl, 10 mM KCl) followed by magnetic separation. Supernatant was removed and steps were repeated for a total of four washes. 500 µg GST-Ataxin-3 was added to the equilibrated GST beads. Samples were mixed by head over head rotation (2 h, 4 °C) before supernatant was removed and the beads were washed four times with GST bind/wash buffer. 500 µg of lysate containing the interaction protein was added and the samples were mixed overnight on the rotating wheel at 4 °C. The beads were magnetically separated and supernatant was removed. Beads were washed five times with GST bind/wash buffer. 1-times protein loading dye was added to the beads and proteins were denatured (70 °C for 10 min). The beads were separated from the supernatant and proteins were analyzed by SDS-PAGE and western blot.

3.6.19 Green Fluorescent Protein-Trap

enhanced green fluorescent protein (EGFP)-tagged Ataxin-3 cell pellets were lysed in GFP-trap lysis/wash buffer (10 mM Tris pH 7.5, 150 mM NaCl, 0.5 mM EDTA, 0.5 % (v/v) Nonidet P-40, cOmplete protease inhibitor without EDTA) for 35 min on ice by intensive pipetting every five minutes. Samples were then centrifuged at 16 000 *g* for 10 min at 4 °C. GFP-trap A beads were equilibrated by suspension in dilution buffer. Beads were centrifuged at 2500 *g* for two minutes at 4 °C. Supernatant was removed and beads were washed two more times with dilution buffer (10 mM Tris pH 7.5, 150 mM NaCl, 0.5 mM EDTA, cOmplete protease inhibitor without EDTA). The protein lysate was then added to the equilibrated beads and kept shaking on an head over head rotating wheel for one hour at 4 °C. Beads were settled by centrifugation at 2500 *g* for two minutes at 4 °C and washed for a total of three washes with GFP-trap lysis/wash buffer. Beads were pelleted by centrifugation at 2500 *g* for two minutes at 4 °C and then resuspended in 1-times LDS loading dye containing 1 mM DTT. Samples were denatured at 70 °C for ten minutes, beads and supernatant were separated by centrifugation (2500 *g*, 2 min). The supernatant was then processed according to the standard western blot protocol.

3.6.20 Time-resolved Förster Resonance Energy Transfer protein assays

The time-resolved Förster resonance energy transfer (TR-FRET) detection was performed as described in (Weiss et al., 2009). In brief, purified GST-ataxin-3 isoforms (see 3.6.17, page 69) were diluted in DPBS supplemented with 1 % (v/v) Triton-X100 to a final protein concentration of 1.25 µg. Antibody mixtures were prepared by diluting the D2-labeled acceptor antibody anti-ataxin-3 MAB5360 1H9 (Merck, Darmstadt, Germany), either the ataxin-3a specific antibody (anti-3a, see 3.6.5, page 62) or the antibody anti-ataxin-3c (anti-3c; Schmidt et al., 1998) and an europium-labeled LANCE Eu-W1024 anti-rabbit secondary antibody (PerkinElmer, Rodgau, Germany) in TR-FRET detection buffer (50 mM NaH_2PO_4, 400 mM NaF, 0.1 % BSA, 0.05 % (v/v) Tween-20). Samples (4 µl) were distributed onto an opaque 384-microtiter plate and 1 µl of the antibody mix and 1 µl of TR-FRET detection buffer were added to the samples and the plate was incubated for 20 h at 4 °C. The final antibody dilutions were: MAB5360 1H9 1:16.7, anti-3a 1:10, anti-3c 1:10 and LANCE Eu-W1024 anti-rabbit 1:60. The TR-FRET quantification was then performed with the EnVision Multimode Plate Reader (PerkinElmer). The europium donor fluorophore was excited at 320 nm. The emission signal of D2 was detected at 650 nm after a time-delay of 100 µs. Sample signals were then calculated as percentage signal intensity over the signal of the lysis buffer background.

3.6.21 Deubiquitination assay

2 µM Ubiquitin-Rhodamine-110 (LifeSensors, Malvern, PA, USA) and 400 nM GST-ataxin-3 in DUB assay buffer (50 mM 2-[4-(2-hydroxyethyl)piperazin-1-yl]ethanesulfonic acid (HEPES), 500 µM EDTA, 1 mM DTT, 100 µg/ml BSA) were mixed in a 1:1 ratio immediately before the assay read. Fluorescence measurement was performed at 535 nm (485 nm extinction) in an EnVision reader (PerkinElmer, Rodgau, Germany) every 10 s for 30 min. Measurements were performed in technical triplicates. The initial velocity was analyzed by fitting a linear function to the relative fluorescence unit (RFU) over the first two minutes using the Matlab script described

in B.1.

3.6.22 Fixing of EGFP expressing cells for fluorescence microscopy

Cells were prefixed by adding 0.4 % (w/v) paraformaldehyde (PFA) to the cell culture medium and incubating the cells for 10 min at 37 °C. Cells were then washed with DPBS and fixed for 15 min using 4 % (w/v) PFA in DPBS. Next, cells were washed for 5 min in DPBS and then stored in DPBS until microscopy. Cells grown on Poly-L-Lysine coated cover slips (coating for 5 min at room temperature, drying over night at 37 °C) were mounted onto a glass slide using Vectashield antifade mounting medium with 4',6-diamidino-2-phenylindole (DAPI, Vector Laboratories, Burlingame, CA, USA). The edges were sealed with nail polish.

Cells for the analysis of the read-through were additionally stained using Cyto Paint Orange (1:1000 in DPBS) for 5 min at room temperature before fixation. Solution was then removed and cells were washed with DPBS before cells were fixed using Vectashield antifade mounting medium with DAPI. Pictures of Cyto Paint Orange were all taken with an exposure time of 1000 ms and pictures of EGFP with an exposure time of 2000 ms.

3.6.23 Immunostaining of cells for fluorescence microscopy

$5 \cdot 10^4$ cells were seeded on Poly-L-Lysine coated cover slips (coating for 5 min at room temperature, drying over night at 37 °C). Cells were transfected and cultured for at least 48 h before they were transferred to ice and washed thrice for 5 min with DPBS. Fixation and permeabilization was performed using ice cold aceton:methanol (1:1) for 10 min. After fixation washing steps were repeated three times in order to remove the fixation solution. Blocking was performed afterwards by incubation with 3 % (v/v) normal goat serum in DPBS for 20 min at room temperature. Incubation with primary antibody (diluted in DPBS supplemented with 3 % (v/v) normal goat serum) was performed overnight at 4 °C. After incubation with the primary antibody cells were washed thrice with DPBS for 5 min. Incubation with the secondary antibody anti-mouse Alexa Fluor 488 or anti-rabbit Alexa Fluor 594 (both Thermo Fisher Scientific, Karlsruhe, Germany) diluted in DPBS (supplemented with 3 % (v/v) normal goat serum) was performed at room temperature for 1 h. Afterwards, cells were washed again thrice using DPBS for 5 min before mounting the cover slip onto a glass slide using Vectashield antifade mounting medium with DAPI (Vector Laboratories, Burlingame, CA, USA). The edges were sealed with nail polish.

Alternatively to the fixation and permeabilization with acetone and methanol, cells were prefixed and fixed as described in 3.6.22, before they were washed the first time. Permeabilization was then performed with 0.1 % (v/v) Triton-X100 in DPBS for 15 min. Cells were washed thrice with DPBS for 5 min before blocking.

3.6.24 Paraffin embedding of tissues

Zebrafish brain tissue was fixed in 4 % (w/v) PFA after dissection. In order to prepare the tissue for paraffin embedding the tissue was dehydrated using an ethanol, xylene and paraffin sequence (Table 3.25). The dehydration process was performed using a Leica TP 1020 (Leica Biosystems, Buffalo Grove, IL, USA). Afterwards the tissue was paraffin embedded using the

paraffin embedding station Leica EG1160 (Leica Biosystems). The paraffin blocks were cooled to -20 °C before sectioning.

Table 3.25. Dehydration of 4 % (w/v) PFA fixed tissue. This table summarizes the ethanol, xylene and paraffin sequence that was used in order to dehydrate the tissue for paraffin embedding. The treatment was performed using a Leica TP 1020.

Solution	Duration (h)
70 % (v/v) ethanol	12
96 % (v/v) ethanol	12
96 % (v/v) ethanol	12
100 % (v/v) ethanol	10
100 % (v/v) ethanol	18
100 % (v/v) ethanol	10
100 % (v/v) xylene	10
100 % (v/v) xylene	8
100 % (v/v) xylene	10
100 % (v/v) paraffin	7
100 % (v/v) paraffin	6
100 % (v/v) paraffin	8

3.6.25 Immunohistochemistry

The embedded brain tissue was cut into 7 µm sections using a microtome. Sections were mounted on a glass slide and initially dried over night at room temperature before they were dried at 50 °C for 20 min. Deparaffinization and rehydration (Table 3.26) was performed using the Leica AutoStainer XL (Leica Biosystems).

Table 3.26. Deparaffinization of paraffin embedded tissue before immunostaining. This table summarizes the xylene, ethanol and Sörensen buffer sequence that was used in order to deparaffinize and rehydrate paraffin embedded tissue sections before immunostaining. The treatment was performed using a Leica AutoStainer XL.

Solution	Duration (min)
100 % (v/v) xylene	8
100 % (v/v) xylene	8
100 % (v/v) xylene	8
100 % (v/v) ethanol	5
100 % (v/v) ethanol	5
96 % (v/v) ethanol	4
96 % (v/v) ethanol	4
80 % (v/v) ethanol	3
80 % (v/v) ethanol	3
70 % (v/v) ethanol	3
Sörensen buffer	3

The slides were kept in Sörensen buffer (106.8 mM Na_2HPO_4, 26.12 mM KH_2PO_4) until antigen retrieval by boiling in antigen retrival buffer (10 mM tri-natriumcitrate-dihydrate, 10 mM Citric acid) three times for 5 min was performed. Slides were then washed thrice with Sörensen buffer for 5 min each. Endogenous peroxidases were inhibited by a 20 min H_2O_2 treatment with a final concentration of 0.5 % (v/v). Afterwards the tissue was blocked and permeabilized for

45 min in Sörensen buffer supplemented with 0.3 % (v/v) Triton X-100 and 5 % (v/v) normal serum. Normal serum was chosen according to the species of the secondary antibody host. Slides were washed for 1 min in Sörensen buffer. The primary antibody incubation was performed in a wet chamber overnight at 4 °C in antibody diluent (Sörensen buffer supplemented with 15 % (v/v) normal serum). The antibody anti-ataxin-3 MAB5360 was diluted 1:500, the anti-ubiquitin antibody (Z 0458) was dilted 1:5000. The next day slides were washed three times for 5 min in Sörensen buffer. Secondary antibody was incubated for 60 min at room temperature (anti-mouse BA-9200, 1:200; anti-rabbit BA-1000, 1:250). Slides were washed three times for 5 min and then incubated with an avidin-biotin complex for 120 min at room temperature (Vectastain ABC Kit, Vector Laboratories, Burlingame, USA). Slides were then again washed thrice with Sörensen buffer for 5 min each. Staining was performed with diaminobenzidin (DAB, Sigma-Aldrich Chemie, Taufkirchen, Germany) for 5 min. Afterwards slides were dehydrated using an ethanol-xylene sequence (Table 3.27) before slides were mounted with a cover slip and Leica CV Ultra Mounting Medium (Leica BIosystems, Wetzlar, Germany).

Table 3.27. Dehydration of paraffin embedded tissue after immunostaining. This table summarizes the ethanol, xylene sequence that was used in order to dehydrate paraffin embedded tissue sections after immunostaining. The treatment was performed using a Leica AutoStainer XL.

Solution	Duration (min)
70 % (v/v) ethanol	5
80 % (v/v) ethanol	5
80 % (v/v) ethanol	5
96 % (v/v) ethanol	5
96 % (v/v) ethanol	5
100 % (v/v) xylene	6
100 % (v/v) xylene	6
100 % (v/v) xylene	6
100 % (v/v) xylene	8
100 % (v/v) xylene	8

3.6.26 In vitro aggregation assay

For an endpoint measurement 3 µM GST-ataxin-3 were mixed with 48 U/mL PreScission-Protease (GE Healthcare) in 100 µl *in vitro* aggregation assay buffer (20 mM Tris-HCl pH 8.0, 150 mM KCl) and incubated at 225 rpm at 37 °C for 24 h to 72 h. Afterwards 10 pmol or 20 pmol were removed and supplemented with 2 % (w/v) SDS and 100 mM DTT. Samples were boiled for 5 min at 95 °C, cooled to room temperature and processed for filter retardation assay (see 3.6.14, page 68). A life measurement was performed by adding 1 % (v/v) ProteoStat detection reagent (Enzo Life Sciences, Lörrach, Germany) to the assay buffer before incubation. Readings were performed in an EnVision reader (PerkinElmer) with an excitation at 535 nm and an emission read at 620 nm.

3.6.27 Cell cycle analysis

The cell cycle analysis was performed according to the NC-3000 (ChemoMetec, Allerod, Denmark) *Two-step cell cycle assay* protocol (No. 3001, Rev. 1.5). In brief, cells from a 6-well plate

were harvested using PBS and pelleted at 300 *g* for 5 min. Cells were washed with PBS and afterwards incubated with 250 µl lysis buffer (Solution 10) supplemented with 10 µg/ml DAPI for 5 min at 37 °C. Afterwards 250 µl stabilization buffer (Solution 11) were added and the sample was transferred to a NC-Slide before measurement. Quantification of the number of cells in a certain stage was performed by analyzing the histogram over the DAPI stain intensity.

3.6.28 Cell viability analysis

The cell viability analysis was performed by measuring the mitochondrial potential according to the NC-3000 *Mitochondrial potential assay* protocol (No. 3008, Rev. 1.8). Cells were harvested and pelleted for 5 min at 300 *g* before they were washed with DPBS. Cells were then centrifuged again and suspended in 1 ml PBS before the JC-1 (Solution 7) staining was performed for 10 min at 37 °C at a final concentration of 2.5 µg/ml. Cells were pelleted at 300 *g* for 5 min and the supernatant was removed. Cells were washed twice by resuspension in 1.5 ml PBS. After washing, the cell pellet was resuspended in 250 µl DAPI in PBS (1 µg/ml, Solution 8), transferred to a NC-Slide and analyzed immediately. Cells were gated into a polarized and depolarized/apoptotic group. Group borders were determined by a 10 µM carbonyl cyanide m-chlorophenyl hydrazone (CCCP) treatment for 2 h in order to induce depolarization.

3.7 Statistical analysis

An *a priori* definition of statistical tests and comparisons was done for all experiments whereas data was collected randomized and blinded when necessary. Analysis was performed in R version 3.4.2. Data was tested for normal distribution when $n \geq 5$ (Shapiro-Wilks test and quantile-quantile plot). A parametric test was conducted when the data was normally distributed and the requirements (i. e. variance homogeneity, sample size equality) were fulfilled. If necessary, compensations for the multiple comparison problem were performed using the family-wise error rate procedure by Hommel (Hommel, 1988). Data without independent variable was analyzed by one-sample t-test or the non-parametric one-sample Wilcoxon Signed Rank test. Groups with an independent variable of two levels were compared using the parametric two-sample t-test or the non-parametric Wilconxon-Mann Whitney test. For data sets with more than two levels either a parametric analysis of variance (ANOVA) with Tukey's honest significant difference (HSD) test or a non-parametric Kruskal-Wallis test with Dunn's Multiple Comparison test were performed. In case of multiple comparisons to a single control, Dunnett's multiple comparison test was used. Data with two independent variables was analyzed by a parametric two-way ANOVA (followed by Tukey's HSD test for main effects or estimated marginal means contrasts for simple main effects) or the non-parametric Scheirer-Ray-Hare test with Dunn's multiple comparison test. Data representing portions was analyzed by beta regression when necessary (i. e. portions equal to zero). The significance level α was defined to 5 % in all tests. If not stated differently error bars represent arithmetic mean ± standard error of the mean (SEM).

4 | Results

4.1 Physiological characteristics of ataxin-3 isoforms

4.1.1 Verification of a HEK 293T *ATXN3* knockout cell line[1]

The aim of this study was to specifically analyze the characteristic differences of ataxin-3 isoforms on a physiological and pathophysiological level as well as the effect of a mutual interplay of both ataxin-3 alleles. As multiple isoforms of ataxin-3 exist which can be expressed from both alleles, it is possible that multiple protein isoforms are expressed in the same cell. Therefore, analyzing the specific characteristics of ataxin-3 isoforms requires cells that solely express one single isoform. Otherwise, one will analyze a mixture of different proteins. Further, it is known that these ataxin-3 proteins are able to mutually interact with each other (Todi et al., 2007) and the normal allele was even reported to have a protective effect in MJD animal models (Warrick et al., 2005; Tsou et al., 2013; Burr et al., 2014; Tsou et al., 2015; Sutton et al., 2017). This raises the question whether ataxin-3 isoforms are modifying each other's physiological and pathophysiological characteristics. It was shown previously that the presence of a second ataxin-3 allele can have an influence on the stability of another ataxin-3 isoform (Weishäupl, 2012). Using a model that only expresses a single isoform allows a correct analysis of the specific characteristics of this isoform. In order to exclude the above-mentioned potential artefacts produced by an interference of endogenously expressed ataxin-3 or a mixture of ataxin-3 isoforms a KO of *ATXN3* was required and ataxin-3 isoforms should then be transfected into the cells. The absence of ataxin-3 should be ensured by two means. Either the usage of *ATXN3* KO MEF cells generated from an *ATXN3* KO mouse model (Schmitt et al., 2007) or the generation of HEK 293T *ATXN3* KO cells. Both approaches were performed in parallel.

Freshly generated MEF cells, as all primary cells, are hard to transfect (Ciftci and Levy, 2001; Hamm et al., 2002). Therefore, a physical approach using magnetic beads was tested in order to measure the transfection efficiency. MEF cells were generated from mouse embryos and cultured before transfection for two passages. Cells were then transfected with an empty EGFP-C2 vector to measure the transfection efficiency for two different reagents, polyMAG and neuroMAG. PolyMAG is a standard transfection reagent designed for a wide variety of cells, whereas neuroMAG was explicitly designed for the usage of primary neurons that show low transfection efficiencies (Karra and Dahm, 2010; Sariyer, 2013). Cells were grown for 48 h and samples were processed for western blot. Immunodetection showed that EGFP could be transfected into MEF cells (Figure 4.1). NeuroMAG showed a higher transfection efficiency than polyMAG under identical transfection conditions, 100 k MEF cells seeded, 30 min transfection

[1] Results first published in Weishäupl et al. (2019).

on the magnet. Increasing the transfection time to 60 min did not result in a stronger transfection efficiency; however increasing the number of cells also increased the amount of protein as expected.

In a parallel approach genome editing of the *ATXN3* gene was performed using transcription activator-like effector nucleases (TALENs, Dold, 2014). TALENs are fusion proteins consisting of a TAL-effector DNA-binding domain (TALE) and a nuclease (Christian et al., 2010), enabling them to specifically bind a predefined DNA region and introduce a DSB. Cells repair this damage either by homology directed repair or non-homologous end-joining of which the latter can lead to a frameshift in the genetic information and therefore cause nonsense-mediated decay which results in a functional KO of the gene (Zarraga et al., 2011).

The TALENs were designed to recognize a region 5' of exon 2 of the *ATXN3* gene (Dold, 2014). The KO was performed in HEK 293T cells which were afterwards screened for the expression of ataxin-3 in order to identify those cells carrying a frameshift mutation. One identified clone was then analyzed on DNA and protein level. Two antibodies, binding N' and C'-terminally of the expected mutation site were used to detect ataxin-3 (Figure 4.2 A). Western blot confirmed that ataxin-3 is no longer being expressed in the KO cells (Figure 4.2 B). Sequencing of the clone using the primer P158 (intron 2) showed a mixed sequence with overlapping peaks (Figure 4.2 C; Weishäupl et al., 2019). Due to the inability of an analysis of the genomic status of the cell line by sanger sequencing, an NGS approach was applied to differentiate between the respective alleles. Therefore, a PCR product was amplified using the primers P158/P159, purified and sequenced. Four alleles for ataxin-3 were found (Figure 4.2 D). Three alleles showed frameshift mutations, one allele was in frame but carried a 48 bp deletion at the beginning of exon 2. This deletion close to the intron/exon boarder possibly introduced a splice site mutation leading to a non-functional protein that undergoes degradation. The HEK 293T *ATXN3* KO clone can therefore be considered to have a fully functional KO of ataxin-3 and is therefore suitable for further experiments. Due to the good transfection efficiency (Thomas and Smart, 2005) and the human origin this cell line was used for all further experiments if not stated differently.

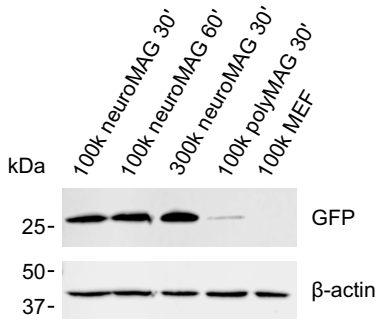

Figure 4.1. Establishment of a transfection method for MEF cells. Two different transfection reagents were tested: polyMAG and neuroMAG. MEF cells were freshly generated and cultured for a few passages before transfection. Either 100 k or 300 k cells were seeded and cells were transfected 24 h post seeding using the two reagents. 48 h post transfection cells were lysed and samples were processed for SDS-PAGE and western blot analysis. Although MEF cells could be transfected with both reagents, neuroMAG shows a stronger transfection efficiency than polyMAG. Increasing the number of seeded cells also resulted in an increased protein amount.

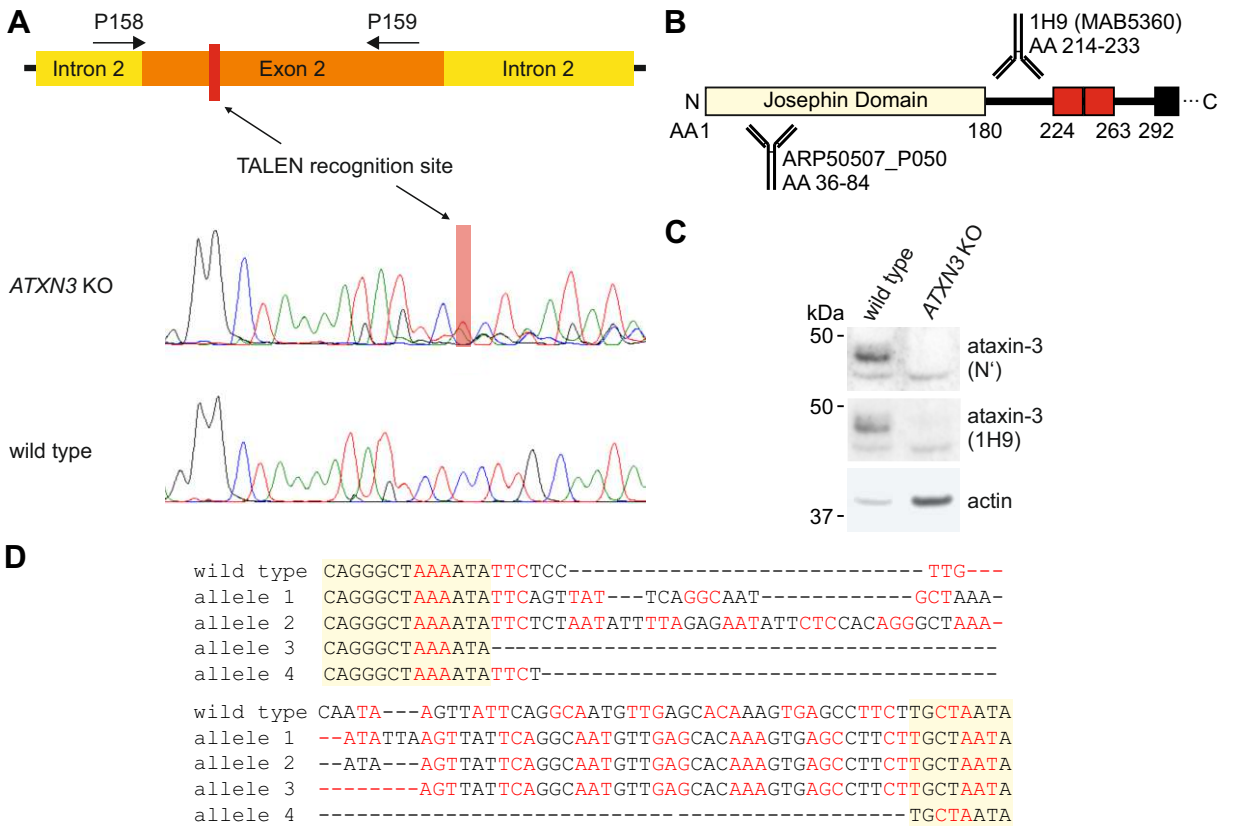

Figure 4.2. Validation of the *hMJD1* KO in HEK 293T cells. Isolated characterization of Ataxin-3 isoforms and their influence on each other requires a KO of the endogenous ataxin-3. **(A)** A KO was performed by expressing TALENs in HEK 293T cells with a recognition site in exon 2 of the *ATXN3* gene. Clonal expansion was performed and the KO was verified on DNA and protein level. Sanger sequencing of the KO clone was performed using the primer P158. The frameshift region is highlighted (red). Sequencing confirmed that a frameshift occurred in this region. **(B)** Two antibodies were used to detect the KO of ataxin-3. ARP50507 is binding in the region encoded by exon 2 (AA 36-84). The antibody 1H9 is binding at UIM1 (AA 214-233). **(C)** Western-blot of wild-type and *ATXN3* KO HEK 293T cells showed that ataxin-3 could neither be detected on protein level with 1H9 nor ARP50507. **(D)** NGS of a PCR product from P158/P159 revealed four alleles of *ATXN3*. Three carried a frameshift, one allele has a 48 bp deletion at the beginning of exon 2. Codons are displayed alternating in black and red. Intron 1-2 is underlined. Subfigure C was modified from Weishäupl et al. (2019), available for use via `https://doi.org/10.1074/jbc.RA118.005801` under the CC BY 4.0 license (`https://creativecommons.org/licenses/by/4.0/`).

4.1.2 Ataxin-3 isoforms show differences in their protein level[2]

In a first step, the differences between ataxin-3 isoforms on the physiological level were studied. It was previously reported that ataxin-3c is the main ataxin-3 isoform (Harris et al., 2010) and that ataxin-3 is expressed in many peripheral tissues and compartments of the cell (Paulson et al., 1997a; Schmidt et al., 1998; Tait et al., 1998; Trottier et al., 1998; Pozzi et al., 2008). However, nothing was known about the differences in the expression level of ataxin-3 isoforms as it was not possible so far to specifically detect ataxin-3aL or ataxin-3aS on protein level. Differences in the expression level of ataxin-3 isoforms could help to explain the observed differences in aao between the different MJD lineages. In order to analyze the physiological expression and protein level, ataxin-3 isoforms were expressed in HEK 293T *ATXN3* KO cells. The analysis, however, required the expression of ataxin-3 isoforms on a physiological level without vast overexpression. Therefore, inducible ataxin-3 expression vectors with the pTRE backbone were applied which were generated previously (Weishäupl, 2012). This vector allows an expression of ataxin-3 on a physiological level. The generated vector contained a non-appropriate combination of SNPs. Therefore the SNP rs1048755 was changed from $A_{634}TG$ to $G_{634}TG$ in order to express Val_{212} in the non-expanded 18 CAG constructs. This area was exchanged by a fragment from pGEX-hMJD1c18CAG$_{GG}$ containing the correct SNP using NsiI and BglII (Figure 4.3 A). The constructs for all three isoforms were sequence-verified using the primers F025, F026 and I866.

The expression level of ataxin-3 isoforms were analyzed on mRNA and protein level (Figure 4.3 C). Therefore, HEK 293T *ATXN3* KO cells were transfected with the pTRE-*hMJD1* vectors. Cells were lysed 48 h post transfection and mRNA was isolated and reverse transcribed to cDNA. ATXN3 mRNA levels were analyzed using quantitative RT-PCR. A non-significant trend for a higher expression level could be found for expanded ataxin-3 transcripts in comparison to the non-expanded isoform. Differences in the expression level of non-expanded ataxin-3 isoforms could not be detected. In order to analyze the ataxin-3 protein level 48 h post transfection cell homogenates were analyzed by western blot and stained with antibodies against ataxin-3 and GAPDH (Figure 4.3 D; Weishäupl et al., 2019). Differences between full-length ataxin-3 signals could be observed on the western blot. Quantification of the protein signals relative to the loading control showed that ataxin-3aS has a significantly lower protein level than non-expanded ataxin-3c and -3aL (Figure 4.3 E; Weishäupl et al., 2019). Upon an expansion of the polyQ repeat ataxin-3c has a higher protein level than both ataxin-3a isoforms. The polyQ expansion therefore has a significant influence only on the protein level of ataxin-3aL causing the expanded isoform to have a lower protein level. This lower level of expanded ataxin-3aL could at least partially be explained by the observed stronger formation of protein breakdown products lowering the level of full-length protein.

[2]Results first published in Weishäupl et al. (2019).

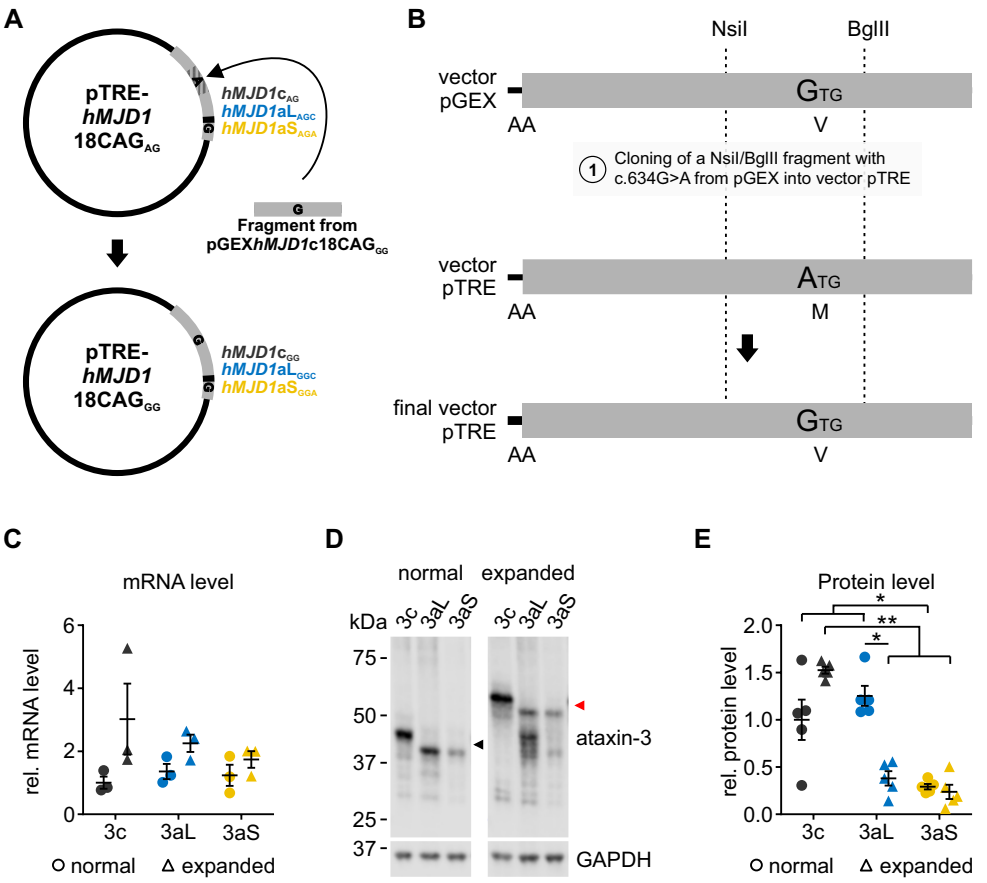

Figure 4.3. Expression levels of normal and expanded ataxin-3 isoforms. (A & B) pTRE*hMJD1*-18CAG$_{GG}$ expression constructs were generated by the introduction of a rs1048755 containing fragment from pGEX*hMJD1*c18CAG$_{GG}$ that was cloned with NsiI and BglII in order to exchange the p.Val212Met to valine ($A_{634}TG$ to $G_{634}TG$) in ataxin-3c, -3aL and -3aS. **(C)** Ataxin-3 expression was analyzed on mRNA and protein level. HEK 293T *ATXN3* KO cells were transfected with pTRE-*hMJD1* constructs and lysed 48 h post transfection. Cell lysates were processed for mRNA isolation and cDNA was then analyzed by qRT-PCR. No differences in the mRNA level could be observed between ataxin-3 isoforms using the Scheirer-Ray-Hare test. **(D)** Analysis of ataxin-3 protein level. Cell homogenates were processed for western blot and stained using antibodies against ataxin-3 (1H9) and GAPDH. Differences in the expression level of full-length ataxin-3 could be observed. Expanded ataxin-3aL shows strong signals for PBP. **(E)** Ataxin-3aS has a lower protein level independent of the polyQ expansion whereas ataxin-3c shows a higher protein level. The protein signal for ataxin-3aL however, is influenced by the polyQ region causing a weaker expression of expanded full-length ataxin-3aL, which at the same time is accompanied by the presence of multiple protein fragments. Scheirer-Ray-Hare test with Conover-Iman and Wilcoxon-Mann-Whitney posthoc tests, Hommel-adjusted, * $p < 0.05$, ** $p < 0.01$, $n = 5$. Data is represented as arithmetic mean ±SEM. Subfigures D and E were modified from Weishäupl et al. (2019), available for use via `https://doi.org/10.1074/jbc.RA118.005801` under the CC BY 4.0 license (`https://creativecommons.org/licenses/by/4.0/`).

4.1.3 Ataxin-3 isoforms differ in their stability and degradation pathway[3]

A correlation between mRNA and protein levels could not be observed, indicating that differences in protein level are caused by factors affecting the ataxin-3 protein itself. Such a factor, among many others, could be the half-life of ataxin-3. From the basis of equal expression levels, short lived proteins will not reach the same protein level as long-lived proteins as they quickly undergo degradation. Differences in the stability between ataxin-3 isoforms could therefore explain why the isoforms have different protein levels. Even further, stability differences could be a first hint that ataxin-3 isoforms have different functions resulting in different subcellular localizations and interaction networks (Alvarez-Castelao et al., 2012). Therefore, the protein stability was analyzed using the Tet-off system consisting of a Tetracycline controlled transactivator and a responder plasmid to regulate the expression of ataxin-3 dependent on the presence of Doxycycline (Figure 4.4 A).

HEK 293T *ATXN3* KO cells were transfected with the vectors and treated with Doxycycline 72 h, 48 h, 32 h, 24 h, 8 h and 0 h before cells were harvested. Samples were processed for western blot (Figure 4.4 B & C; Weishäupl et al., 2019). All ataxin-3 isoforms, independent of the polyQ repeat length, show a decreasing ataxin-3 signal over time with ataxin-3aS degrading faster than ataxin-3aL and ataxin-3c (Figure 4.4 D). The relative ataxin-3 signals were plotted over time and an exponential function was fit to the data. Half-life was then calculated from the exponent of this exponential function (Figure 4.4 E; Weishäupl et al., 2019). The half-life of ataxin-3aS (12 h) is significantly shorter than the half-life of ataxin-3c and ataxin-3aL (24 h and 26 h). This indicates that the nonsense SNP leads to a fast degradation of ataxin-3aS. As MJD is caused by an expansion of the polyQ repeat in the *MJD1* gene (Kawaguchi et al., 1994) the stability of expanded ataxin-3 was also analyzed. Interestingly, the half-life of ataxin-3 increases upon a polyQ expansion in an isoform-independent manner (3c: 53 h, 3aL: 42 h, 3aS: 20 h). Pathologically expanded ataxin-3aS however, is still less stable than ataxin-3c and ataxin-3aL (Weishäupl et al., 2019).

The observed differences on protein level can be caused by different stabilities of the ataxin-3 mRNA. If the mRNA of one is degraded more quickly, this will also lead to a reduction of the protein level as translation will be reduced. Therefore, ataxin-3 mRNA stability was analyzed using the Tet-off system 8 h after a Doxycycline treatment. Total mRNA was isolated and gDNA was removed by an on-column digestion before mRNA was reverse transcribed to cDNA and analyzed by quantitative RT-PCR (Figure 4.4 F; Weishäupl et al., 2019). No differences could be observed in the stability of alternatively spliced *ATXN3* mRNA.

Further differences in insolubility between ataxin-3 isoforms could cause differences in the levels of ataxin-3. As western blot analyzes only soluble protein fractions an increased insolubility of one isoform would strongly reduce the amount of detectable protein on the western blot and therefore lead to a false assumption of the total protein level which is the sum of soluble and insoluble proteins. In order to verify the ataxin-3 protein levels a filter retardation assay was performed. Over a 32 h treatment with Doxycycline, no differences in the stability of ataxin-3 isoforms could be found (Figure 4.4 G; Weishäupl et al., 2019). This shows that the measured reduction of ataxin-3 levels after Doxycycline treatment are caused by physiological degradation

[3]Results first published in Weishäupl et al. (2019).

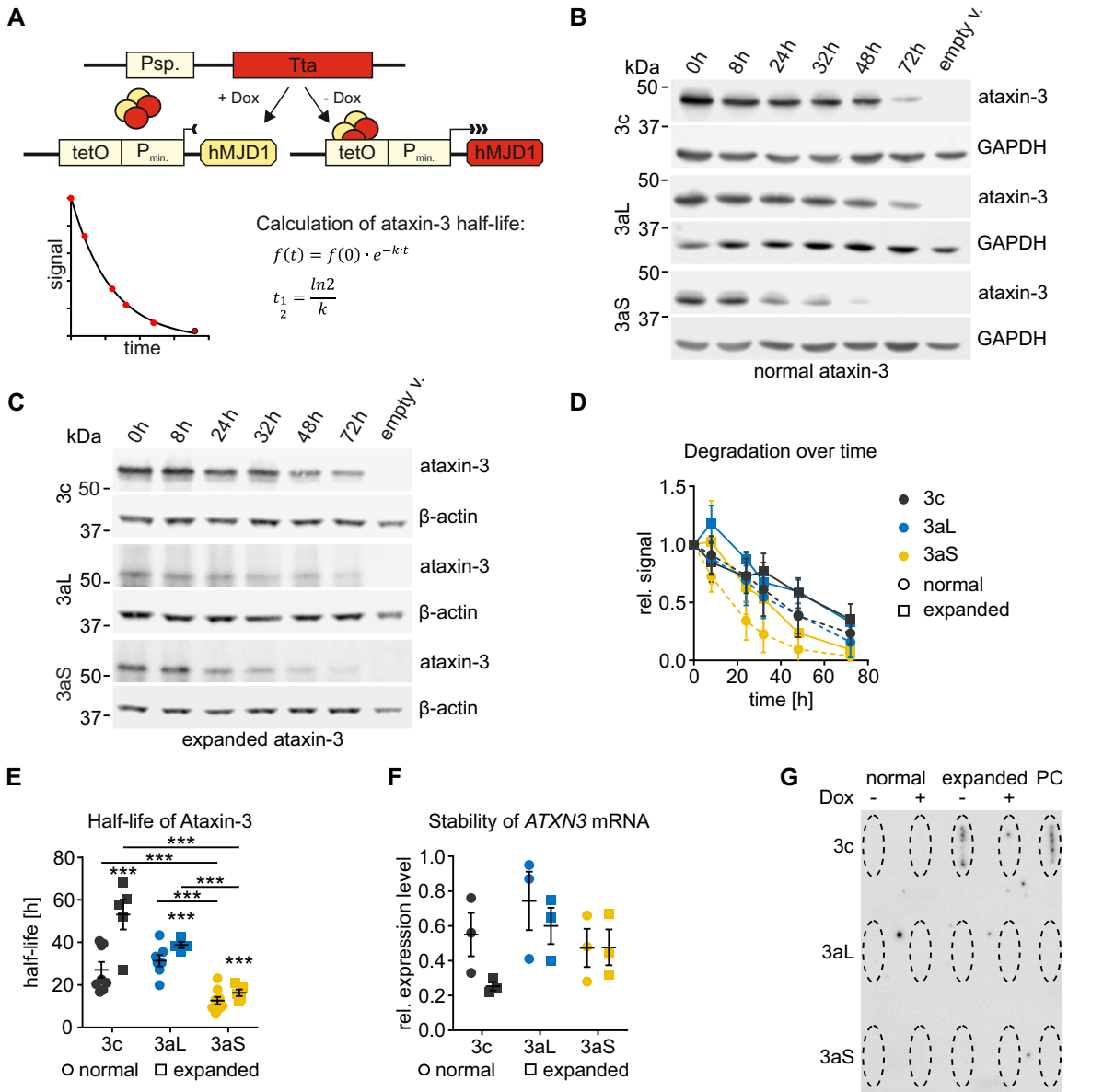

Figure 4.4. Stability of normal and expanded ataxin-3 isoforms. **(A)** The Tet-off system was used to analyze the stability of ataxin-3 isoforms. Cells were transfected with a tetracycline controlled transactivator (Tta) that regulates the expression of ataxin-3 on responder constructs dependent on the presence of Doxycycline. The expression of ataxin-3 was turned off at different time points. Ataxin-3 signals were plotted over time and an exponential function was fit to the data. Half-life calculation was performed using the exponent of the function. **(B & C)** HEK 293T *ATXN3* KO cells were transfected with either ataxin-3 isoforms and the Tta construct or an empty vector (control). Expression was abolished as indicated and cells were collected. Samples were processed for western blot and membranes were stained for ataxin-3 and GAPDH or β-actin. **(D)** Ataxin-3 signals decrease over time independent of the polyQ expansion. Ataxin-3aS shows a faster degradation rate than ataxin-3c and -3aL **(E)** The half-life of ataxin-3 was calculated from the data for a first order kinetic. The half-life of ataxin-3aS was found to be significantly lower than that of ataxin-3c or ataxin-3aL for both polyQ expansions. An expansion of the polyQ repeat increases the half-life of all isoforms. One-way ANOVA with Tukey's HSD test, *** $p < 0.001$, n = 5-9. **(F)** To ensure that the observed differences are not caused by stability differences on the mRNA level it's stability was analyzed by quantitative RT-PCR. 8 h after expression termination no differences could be found. Scheirer-Ray-Hare test, Isoform, polyQ and interaction non-significant, n = 3. **(G)** In order to ensure that the decrease over time is related to degradation and not insolubility a filter retardation assay was performed. Ataxin-3 isoforms were expressed for 24 h before a Doxycycline-induced 32 h expression termination was performed. Homogenates were analyzed by filter retardation assay stained for ataxin-3 (1H9). No differences could be found in the insolubility of ataxin-3 isoforms after a Doxycycline treatment, indicating that the decrease is caused by degradation and not insolubility. PC: positive control. Data is represented as arithmetic mean ±SEM. Subfigures B, C, E, F and G were modified from Weishäupl et al. (2019), available for use via `https://doi.org/10.1074/jbc.RA118.005801` under the CC BY 4.0 license (`https://creativecommons.org/licenses/by/4.0/`).

of the protein and not by an increasing insolubility of ataxin-3.

The stability of a protein is among others related to the underlying degradation pathway. Generally, the ubiquitin proteasome system is considered a degradation pathway for short-lived proteins while autophagy primarily degrades long-lived proteins (Nedelsky et al., 2008; Zhao et al., 2015). For this reason it was analyzed whether ataxin-3 isoforms are degraded by different pathways using the specific inhibitors Bafilomycin A1 (50 nM) and Lactacystin (10 µM). Lactacystin is an antibiotic that was isolated from *Streptomyces* and covalently modifies the N-terminal threonine of subunit X in the 20S proteasome therefore specifically inhibiting the UPS pathway irreversibly (Fenteany et al., 1995). Bafilomycin A1 instead is an active inhibitor of the late-stage autophagy pathway by preventing fusion between lysosomes and autophagosomes and therefore the maturation of autophagic vacuoles (Yamamoto et al., 1998). HEK 293T *ATXN3* KO cells were transfected with the pTRE-*hMJD1* constructs as well as the Tta construct. 24 h post transfection cells were treated with Doxycycline and again 8 h later with the inhibitors. Samples were processed for western blot and membranes were stained against ataxin-3, GAPDH, K48-linked ubiquitin and LC3-II (Figure 4.5 A; Weishäupl et al., 2019). It could be observed that ataxin-3 isoforms are indeed degraded by different pathways (Figure 4.5 B). While ataxin-3c and ataxin-3aL are degraded by autophagy, ataxin-3aS is degraded by both pathways autophagy and proteasomal degradation. This explains well the observed differences in ataxin-3 isoform stability (Weishäupl et al., 2019). Autophagy is a degradation pathway for long-lived proteins (Roberts and Deretic, 2008) whereas the UPS mainly degrades damaged and misfolded proteins tagged with ubiquitin (Lecker et al., 2006), thus explaining the shorter turn-over time of ataxin-3aS.

The degradation pathway of ataxin-3 isoforms was also verified using two other inhibitors, Chloroquine (100 µM) and MG-132 (25 µM) for autophagy and proteasomal inhibition respectively (Figure 4.5 C). Chloroquine is an antimalarial drug that inhibits autophagosome fusion with lysosomes (Mauthe et al., 2018). MG-132, a peptide aldehyde, blocks the proteolytic activity of the 26S proteasome complex and therefore inhibits proteasomal degradation effectively (Hayashi et al., 1992). Using these inhibitors the degradation of ataxin-3c by autophagy and of ataxin-3aS by the proteasome system could be verified (Figure 4.5 D). However, ataxin-3c degradation was additionally inhibited by the addition of MG-132 indicating a proteasomal degradation. For ataxin-3aL no effect of either inhibition could be observed, but this isoform also showed an reduced response using Bafilomycin A1 and Lactacystin.

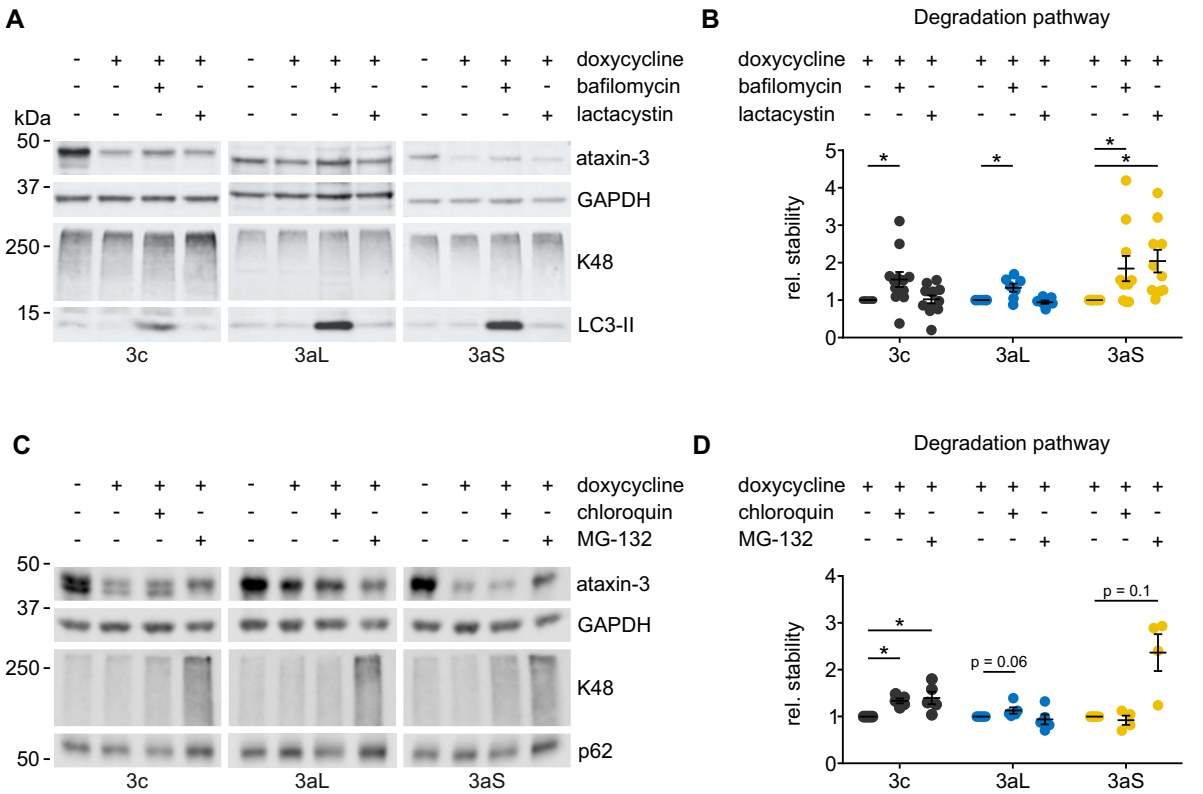

Figure 4.5. Degradation pathway of ataxin-3 isoforms. (A) HEK 293T *ATXN3* KO cells were transfected with the Tta and ataxin-3 isoforms. Expression was terminated after 24 h by the addition of Doxycycline. Inhibitors were applied 8 h after expression termination. Either autophagy (Bafilomycin A1) or the proteasome system (Lactacystin) was inhibited for 24 h before cells lysis and processing of samples for western blot. Membranes were stained for ataxin-3 (1H9), GAPDH, K48-linked ubiquitin (K48) and LC3 (LC3-II). **(B)** Ataxin-3 isoforms are degraded by different pathways. While ataxin-3aS is degraded by both pathways, ataxin-3c and -3aL are both solely degraded by autophagy. One-sided Wilcoxon Signed Rank test, * $p < 0.05$, n = 7-12. **(C)** In order to verify the results of the Bafilomycin A1 and Lactacystin treatment the assays were repeated using Chloroquine as an autophagy inhibitor and MG-132 as an inhibitor of the proteasome system. Samples were processed for western blot. Immunodetection was performed for ataxin-3 (1H9), GAPDH, K48-linked ubiquitin (K48) and sequestosome-1 (p62). **(D)** A treatment with Chloroquine caused an increase in ataxin-3c signals indicating that this isoform is degraded by autophagy. Interestingly, a significant increase could also be detected for an inhibition of the proteasome by MG-132. For ataxin-3aS an increase in the protein signal could be observed for an inhibition of the proteasome system as well. Ataxin-3aL did not respond to any treatment. One-sided Wilcoxon Signed Rank test, * $p < 0.05$, n = 4-5. Data is represented as arithmetic mean ±SEM. Subfigures A and B were modified from Weishäupl et al. (2019), available for use via `https://doi.org/10.1074/jbc.RA118.005801` under the CC BY 4.0 license (`https://creativecommons.org/licenses/by/4.0/`).

4.1.4 Ataxin-3 isoforms differ in their enzymatic deubiquitination activity[4]

It is known that Ataxin-3 is a DUB enzyme (Burnett et al., 2003; Tzvetkov and Breuer, 2007) able to remove K48 (Burnett and Pittman, 2005; Chai et al., 2004) and K63 (Winborn et al., 2008) bound ubiquitins. However, it shows a clear substrate preference for K63-linked ubiquitin chains and also preferentially cleaves longer chains over shorter ones (Winborn et al., 2008). It was reported that a polyQ expansion does not directly affect the DUB activity of ataxin-3 but increases cellular protein ubiquitination signals (Winborn et al., 2008). As alternative splicing of the ataxin-3 C-terminus leads to the presence or absence of the third UIM it can be assumed that alternative splicing has an impact on ataxin-3's enzymatic activity. Further, differences in the stability of ataxin-3 isoforms could also be explained by differences in their catalytic activity as Todi et al. (2007) described that catalytically inactive ataxin-3 is more stable than an active variant.

PTMs by ubiquitin or ubiquitin-like molecules plays an important role in virtually all aspects of cell biology. This is also reflected by the amount of DUB enzymes in the human genome. Approximately 95 genes which are encoding deubiquitinating enzymes could be identified in the human genome (Nijman et al., 2005). For this reason the DUB activity of ataxin-3 isoforms cannot be analyzed in cell culture experiments but requires purified proteins in order to exclude the influence of any other DUB protein. In order to do so, ataxin-3 expression vectors were generated that allowed an expression in *E. coli* as GST-fusion protein. The usage of an N-terminal GST tag prevents ataxin-3 aggregation (Haacke et al., 2006). Ataxin-3 isoforms were amplified from pEGFP-c2-*hMJD1*-18CAG$_{AG}$ isoform vectors using the forward primer I866 and the isoform-specific reverse primers O092 (3c), O431 (3aL) and O430 (3aS) in order to introduce an 3' XhoI site for the cloning. The isoform-specific 3' fragments of ataxin-3 cDNA were cloned into the existing pGEX-*hMJD1*c18CAG vector afterwards by a PpuMI and XhoI digestion in order to generate the new ataxin-3 isoform-specific pGEX-*hMJD1* vectors (Figure 4.6 A & B). Successful cloning was verified by Sanger sequencing with the primers A166 and I866. In the next step the G$_{634}$TG variant (Val$_{212}$) of rs1048755 was generated by creating a gBlock of the ataxin-3 cDNA with the respective SNP (Figure 4.6 C & D). The gBlock G$_{634}$TG fragment was introduced into the existing isoform-specific ataxin-3 vectors using NsiI and BglII which resulted in the final vectors pGEX-*hMJD1*c18CAG$_{GG}$, pGEX-*hMJD1*aL18CAG$_{GGC}$ and pGEX-*hMJD1*aS18CAG$_{GGA}$. The sequence was verified with the primers F025 and F026.

Ataxin-3 isoforms were overexpressed and purified from *E. coli* using the GST-tag (Figure 4.7 A). Afterwards an SDS-PAGE protein quality control was performed by analyzing the samples for integrity and purity (Figure 4.7 B). Protein samples which met the quality criteria were then quantified against a BSA standard by SDS-PAGE and a SYPRO Ruby staining.

The DUB assay uses the fluorophore Rhodamine-110 which is coupled to a single ubiquitin molecule by a peptide bond. This does not reflect the physiological situation as ubiquitins are linked by isopeptide bonds (van Nocker and Vierstra, 1993). However, using a substrate with isopeptide bond it was not possible to measure the DUB activity of ataxin-3 (data not shown). While Rhodamine-110 is bound to ubiquitin, the fluorescence signal is quenched. Upon cleavage and therefore the generation of mono-substituted Rhodamine-110 the fluorophore exhibits

[4]Results first published in Weishäupl et al. (2019).

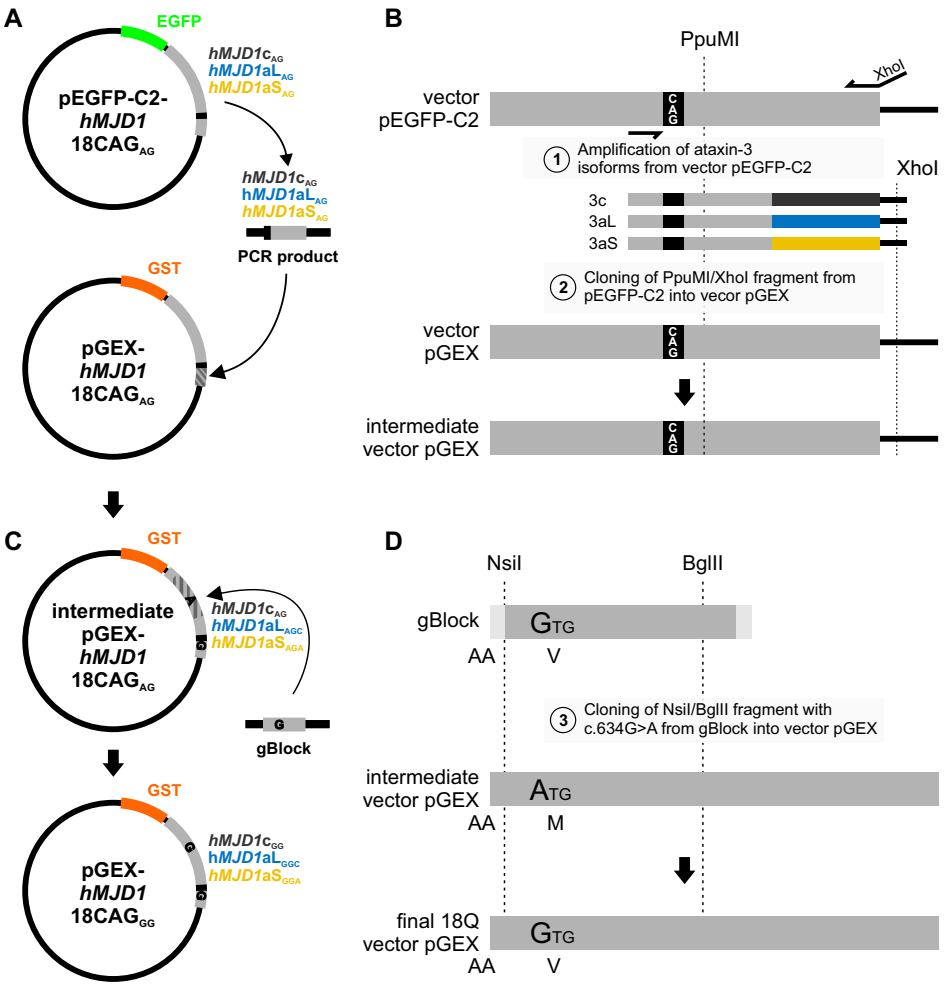

Figure 4.6. Cloning strategy for the generation of non-expanded pGEX-*hMJD1* expression constructs. (A & B) Non-expanded pGEX-*hMJD1* expression constructs were generated by amplification of ataxin-3 cDNA from pEGFP-C2 using the primer I866 in combination with the isoform-specific reverse primers O092 (3c), O431 (3aL) and O430 (3aS) in order to introduce an XhoI site. The PCR product was cloned into the PpuMI and XhoI restriction sites of the pGEX-*hMJD1*c18CAG$_{AG}$ vector resulting in intermediate isoform vectors with rs1048755 (A$_{634}$). **(C & D)** These intermediate vectors were modified by the introduction of a gBlock containing the G-variant of rs1048755 into the NsiI and BglII sites in order to exchange p.Val212Met to valine in the non-expanded isoforms.

fluorescence when excited (Figure 4.7 C). The purified protein was mixed to equimolar conditions with Ubiquitin-Rhodamine-110 and the DUB activity was measured over time. It could be observed that all ataxin-3 isoforms were able to cleave the substrate (Figure 4.7 D). Ataxin-3c however, showed a lower increase in the RFU than both ataxin-3a isoforms (Weishäupl et al., 2019). The initial velocity was then measured from the slope of a linear function fitted to the raw data of the initial two minutes (Figure 4.7 E). It could be shown that the enzymatic activity of ataxin-3 (16 734 RFU/min) was indeed significantly reduced compared to the activity of ataxin-3aL (36 510 RFU/min RFU/min) and ataxin-3aS (35 514 RFU/min, Figure 4.7 F; Weishäupl et al., 2019).

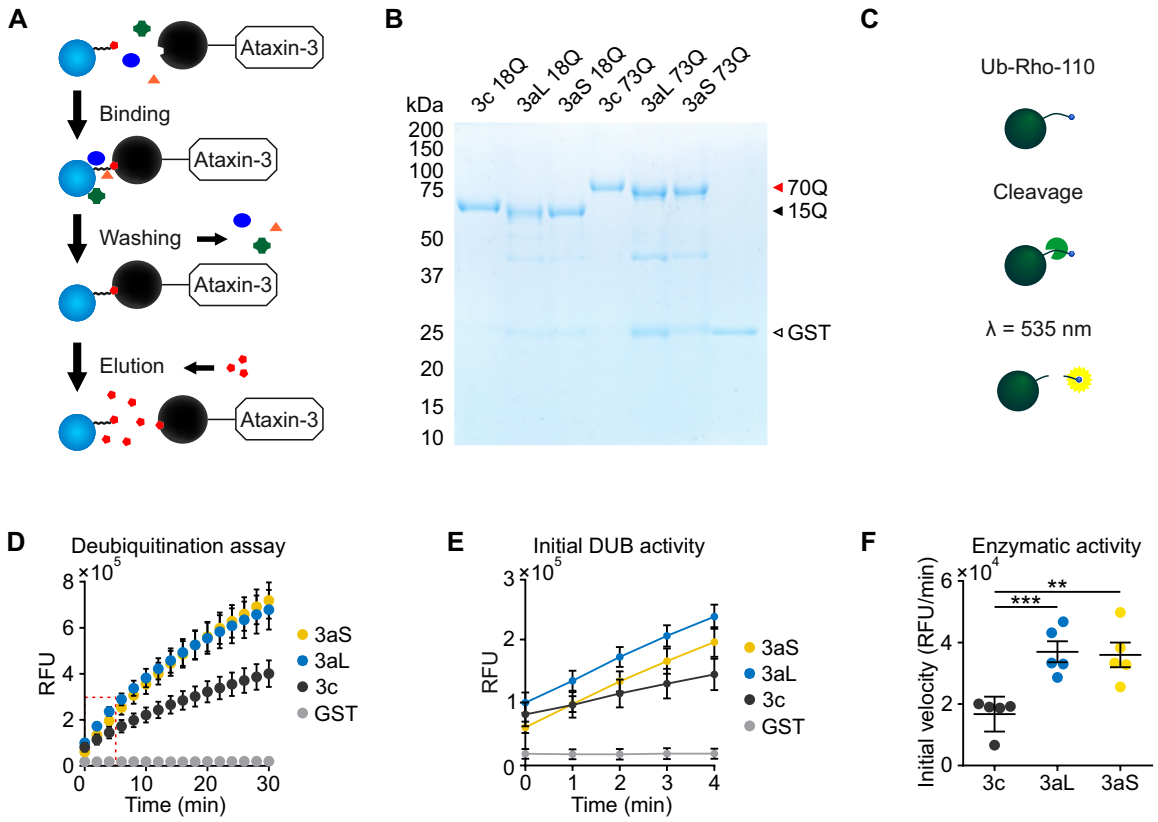

Figure 4.7. Enzymatic deubiquitination activity of ataxin-3 isoforms. **(A)** Ataxin-3 isoforms were expressed in E. coli as GST-fusion protein and purified using the GST-tag. Elution was performed using Glutathion. The GST-tag prevents ataxin-3 from aggregation. **(B)** Quality control of purified proteins. Purified ataxin-3 isoforms were analyzed by SDS-PAGE. Gels were afterwards stained with Coomassie. The expression as well as the band pattern was analyzed. **(C)** Principle of the DUB assay. The fluorophore Rhodamine-110 is linked to the C-terminus of ubiquitin leading to a quenching of the fluorescence signal. Upon cleavage and thereby separation of both molecules Rhodamine-110 can be excited and starts to emit a fluorescence signal. **(D)** Purified GST-ataxin-3 was mixed in a 1:5 ratio with Ubiquitin-Rhodamine-110. The relative fluorescence was measured every 10 s for a period of 30 min (every two minutes displayed). All ataxin-3 isoforms cleaved Ubiquitin-Rhodamine-110 leading to an increase in the RFU. **(E)** The initial velocity was calculated from the values of the first two minutes. **(F)** Ataxin-3aL and -3aS show a higher enzymatic activity than ataxin-3c as analyzed from five individual protein purifications. Kruskal Wallis test with Conover-Iman post hoc test with Hommel-adjustment, * $p < 0.05$, $n = 5$. Data is represented as arithmetic mean ±SEM. Subfigures D and F were modified from Weishäupl et al. (2019), available for use via `https://doi.org/10.1074/jbc.RA118.005801` under the CC BY 4.0 license (`https://creativecommons.org/licenses/by/4.0/`).

4.1.5 Ataxin-3 isoforms differ in their interaction with protein partners[5]

A major part of a protein's function is determined by the interaction with protein partners. Though numerous interaction partners of ataxin-3 were described before (reviewed in doCarmo Costa and Paulson, 2012), nothing was known about differences in the interaction of ataxin-3 isoforms with these binding partners. Different interactors are known to directly bind to the C-terminus of ataxin-3 (CREB-binding protein, CK2beta, PCAF, p300 and UBXN-5, Chai et al., 2002; Tao et al., 2008; Li et al., 2002; Rodrigues et al., 2009), with the UIMs (CHIP, PLIC1 and PARK2, Jana et al., 2005; Heir et al., 2006; Durcan et al., 2011) or it is known that the C-terminal polyQ stretch modifies the interaction strength (CREB-binding protein, PCAF and p300, Chai et al., 2002; Li et al., 2002). Therefore, it is likely that alternative splicing of ataxin-3's C-terminus as well as the nonsense SNP affect protein-protein interactions. Differences in the interaction with certain protein partners would not only show that ataxin-3 isoforms have specific functions. It would also allow a conclusion about pathogenic mechanisms that could be triggered by certain isoforms when specific interactions are strengthened or abolished for certain isoforms. In order to perform GST pulldown interaction assays it was necessary to generate expanded GST-ataxin-3 constructs for the ataxin-3a isoforms which were created by an exchange of the CAG repeat in the intermediate 18CAG pGEX constructs (see 4.1.4, page 84) by the CAG repeat of the existing pGEX-*hMJD1*c73CAG$_{AC}$ construct using BglI and PpuMI (Figure 4.8 A & B). This cloning step resulted in the final expanded ataxin-3 expression constructs pGEX-*hMJD1*c73CAG$_{AC}$, pGEX-*hMJD1*aL73CAG$_{ACC}$ and pGEX-*hMJD1*aS73CAG$_{ACA}$. All constructs were sequence verified using the primers A166, F025 and I866.

In order to establish all assay conditions ataxin-3's interaction with the well-known interaction partner vasolin containing protein (VCP) (Doss-Pepe et al., 2003) was analyzed using a GST pulldown and western blot. VCP is a type II member of the AAA+ ATPase family and takes part in the UPS pathway for the degradation of polyubiquitinated proteins (Zalk and Shoshan-Barmatz, 2003). VCP binds ataxin-3 at a sequence adjacent to the polyQ area and is able to modify ataxin-3 aggregation (Boeddrich et al., 2006). GST-pulldowns revealed that normal as well as expanded ataxin-3 isoforms interact with VCP while GST itself does not (Figure 4.8 C). Significant differences in the interaction could not be found between them, which however is not surprising as the VCP/ataxin-3 interaction involves the NLS of ataxin-3 (Laço et al., 2012a). Though expanded ataxin-3aL and -3aS showed a trend towards a stronger interaction with VCP the variation for the expanded isoforms was much higher than for the normal isoforms which could be a result of the increased insolubility upon a polyQ expansion. Therefore, further assays were only performed using the non-expanded ataxin-3 isoforms.

As the interaction with VCP could be verified for all ataxin-3 isoforms the interaction with parkin, another well known interaction partner, was analyzed in the next step. Parkin interacts with the UIMs of ataxin-3 and as an E3 ubiquitin ligase also takes part in the ubiquitin proteasome system (Joch et al., 2007; Hampe et al., 2006). *PARK2* mutations are one of the genetic causes of the recessive form of early-onset Parkinson's disease (Matsumine et al., 1997; Kitada et al., 1998). Interestingly, one SNP in *PARK2* is associated with a modification of the aao in MJD as well as a decrease in the interaction strength with ataxin-3 (Jeremiasz, 2011).

[5]Results first published in Weishäupl et al. (2019).

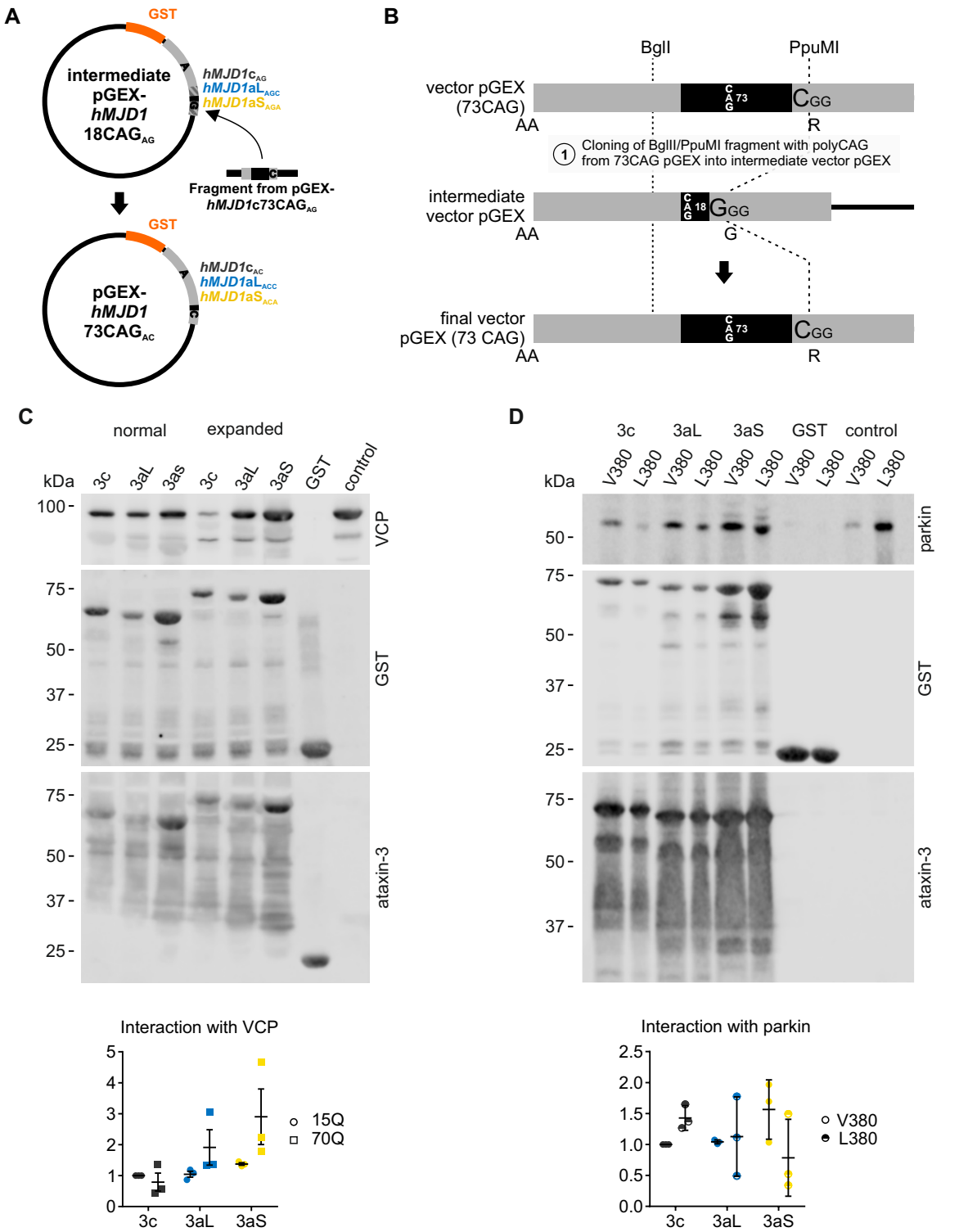

Figure 4.8. Interaction of ataxin-3 isoforms with VCP and parkin. (A & B) The poly CAG repeat as well as rs12895357 was modified by the exchange of the poly CAG region in the intermediate pGEX-*hMJD1*-18CAG vectors with a BglI/PpuMI fragment from the pGEX-*hMJD1*c73CAG$_{AC}$ vector for all three isoforms. The modified constructs express 73 glutamines followed by an arginine. **(C)** WB of a pulldown of VCP with GST-ataxin-3 isoforms. After the pulldown, all samples with ataxin-3 isoforms show a signal for VCP whereas GST does not. The GST-antibody shows clear signals for both GST-ataxin-3 and GST alone. The GST signal was confirmed by the 1H9 antibody. Comparison of the relative VCP signal in pulldown samples containing 18Q and 73Q ataxin-3 isoforms relative to the respective GST-ataxin-3c signal. Only minor differences in the interaction of VCP with 18Q ataxin-3 isoforms were found whereas the polyQ expansion increases the interaction with VCP for ataxin-3aL and ataxin-3aS compared to the 18Q ataxin-3 isoform. **(D)** WB of a pulldown of two parkin variants (p.V380L)

Figure 4.8 Interaction of ataxin-3 isoforms with VCP and parkin - *continued from previous page* with 18Q GST-ataxin-3 isoforms. All 18Q ataxin-3 isoforms show a signal for both parkin variants. The GST-control shows no signal. Comparison of the relative parkin signal normalized to the GST-ataxin-3 signal detected by the GST-antibody showed minor differences in the interaction of ataxin-3 isoforms with parkin. Due to the weak parkin signal in the western blot the error rate is proportionally high hindering a statistical analysis. Comparison of the interaction of ataxin-3c with parkin V_{380} and L_{380} did not show a statistical significance. Data is represented as arithmetic mean ±SEM.

Therefore, the interaction with parkin was analyzed with both variants of the p.V380L SNP. It could be shown that ataxin-3c, -3aL and -3aS interact with both parkin variants (Figure 4.8 D). Ataxin-3aS shows a non-significant trend towards an increased interaction with the V_{380} variant compared to ataxin-3c and ataxin-3aL. Comparing both parkin variants, the exchange from valine to leucine seems to increase the interaction strength between parkin and ataxin-3c whereas it decreases the interaction for ataxin-3aS.

Overall, the usage of GST-pulldowns involved numerous manual steps and is highly error prone. Therefore, the interactions of ataxin-3 isoforms with various interaction partners should be assessed in a high throughput manner using SILAC. SILAC is a proteomic approach that makes use of isotope-labeled amino acids which are added to cultured cells (Ong et al., 2002). Incorporation of these isotope-labeled amino acids later on allows an identification of the original culture even in a mixture of different cultures via MS. Using this technique a quantitative MS of all three ataxin-3 isoforms was possible after a pulldown. Protein partners could be identified by MS and the respective isoform which pulled the protein could be identified by the mass-shift. Combination of all samples for MS allowed a quantitative determination of the protein partners for the isoforms.

In order to perform the SILAC experiments pN-SF-Tap ataxin-3 isoforms were generated which allow for a Strep-FLAG purification as described previously (Gloeckner et al., 2009). The non-expanded SF-Tap-ataxin-3 constructs were generated by firstly exchanging the SNP rs1048755 from A_{634}TG to G_{634}TG (Figure 4.9 A & B). Therefore a fragment from pTRE-*hMJD1*c 18CAG$_{GG}$ was excised using Bsu36I and BsmBI and cloned into the pN-SF-Tap-*hMJD1*c18CAG$_{AG}$ vector generating the non-poly-expanded construct pN-SF-Tap-*hMJD1*c18-CAG$_{GG}$. Afterwards the isoform constructs (pN-SF-Tap-*hMJD1*aL18CAG$_{GGC}$ and pN-SF-Tap-*hMJD1*ashort 18CAG$_{GGA}$) were generated by exchanging the 3' end of ataxin-3 cDNA with a fragment from the pTRE-*hMJD1*-18CAG vector using PpuMI and ApaI. The expanded isoform constructs were generated the same way by introducing this fragment into the pN-SF-Tap-*hMJD1*c65CAG$_{AC}$ vector resulting into the vectors pN-SF-Tap-*hMJD1*aL65CAG$_{ACC}$ and pN-SF-Tap-*hMJD1*aS 65CAG$_{ACA}$. Clones were sequence-verified using the primers I866, F025, F023 and F029.

Successful cloning of the constructs could be confirmed by expression of the constructs in HEK 293T *ATXN3* KO cells (Figure 4.9 C). All isoforms could be detected with an antibody against ataxin-3 (1H9) as well as a FLAG-tag specific antibody. Further, ataxin-3 could be purified from the lysates using the Strep-tag (Figure 4.9 D). This confirmed that these constructs were suitable for the identification of ataxin-3 isoform-specific interaction networks using the SILAC tandem MS approach.

In order to identify ataxin-3 isoform-specific interaction partners, ataxin-3 isoforms were expressed in HEK 293 cells cultured in heavy ($^{13}C_6$,$^{15}N_2$-lysine; $^{13}C_6$,$^{15}N_4$-arginine), medium

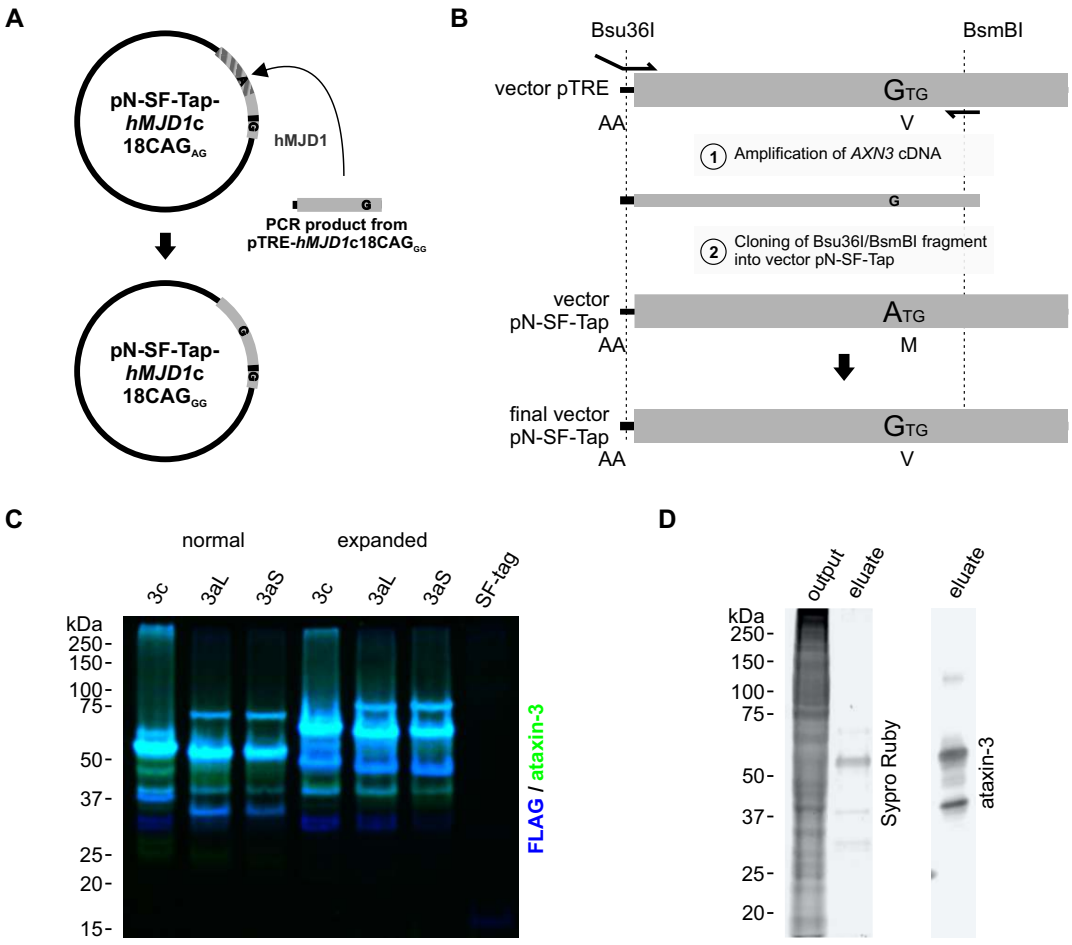

Figure 4.9. Cloning strategy for the exchange of rs1048755 in the pN-SF-Tap-*hMJD1* expression constructs. (A & B) The SNP rs1048755 in the Step-Flag-*hMJD1* expression constructs was exchanged from $A_{634}TG$ to $G_{634}TG$ in order to express valine instead of methionine in the non-expanded constructs before ataxin-3 isoforms were cloned. A 5' fragment from pTRE-*hMJD1*c18CAG$_{GG}$ was amplified using the primers Q941 and Q942 to introduce a Bsu36I recognition site 5' of the ataxin-3 cDNA. The PCR product was digested and cloned into the Bsu36I and BsmBI sites of the existing pN-SF-Tap-*hMJD1*c18CAG$_{AG}$ vector generating the vector pN-SF-Tap-*hMJD1*c18CAG$_{GG}$. **(C)** pN-SF-Tap constructs were expressed in HEK 293T *ATXN3* KO cells. All isoforms could be detected using an ataxin-3 (1H9, green) and FLAG-tag specific antibody (blue). **(D)** Ataxin-3 could be purified from cell culture lysates by the Strep-tag. While the output after purification shows multiple protein signals more specific signals could be identified for the eluate using a total protein stain (SYPRO Ruby). The identity of ataxin-3 could be confirmed by immunodetection with an ataxin-3 specific antibody (1H9).

(4,4,5,5-D4-lysine; $^{13}C_6$-arginine) or light (lysine; arginine) SILAC medium for the incorporation of isotopes into the proteome. A label switch was performed for every biological replicate in order to ensure a robust quantification without artifacts created by the isotope-label. Ataxin-3 was purified using the Strep tag and co-precipitated proteins were identified by tandem MS. Many shared interaction partners could be identified. However, multiple proteins interact stronger with one specific isoform (Figure 4.10 and Table A.1; Weishäupl et al., 2019). In general, ataxin-3c vs. ataxin-3aL/ataxin-3aS shows more differently interacting proteins than ataxin-3aL vs. ataxin-3aS. Among the proteins interacting differently with ataxin-3 isoforms, caspase-7 could be identified as a novel protein partner with a strengthened ataxin-3aS interaction compared to ataxin-3c and -3aL. Additionally, HR23B showed a stronger interaction with ataxin-3c and ataxin-3aL in comparison to ataxin-3aS. Interestingly, tubulin showed differences in the interaction with ataxin-3a and ataxin-3c isoforms, whereby the interaction with ataxin-3aL and -3aS

was increased. The results of the SILAC-MS-MS approach were verified by co-precipitation of the exemplary interactors caspase 7, HR23A, HR23B, α-tubulin, E3 ubiquitin-protein ligase UBR2 (UBR2) and VCP using GFP-traps. EGFP-ataxin-3 was expressed in HEK 293T *ATXN3* KO cells and purified using the EGFP-tag. Co-precipitated proteins were then detected by western blot (Figure 4.11). The validity of the MS approach could be confirmed as an interaction with all protein partners could be verified.

The SILAC approach delivered 330 protein interaction partners for ataxin-3 isoforms. 298 interaction partners could be identified which were not yet reported. 32 interaction partners were listed either in the BioGRID database (without two-hybrid results, Chatr-Aryamontri et al., 2017), the APID database (Alonso-López et al., 2019) or the PINA2 database (Cowley et al., 2012). This high number of interaction partners is inaccessible and hard to interpret. Therefore, proteins were clustered and structured into biological pathways. Thereby pathways should be identified where ataxin-3 isoforms presumably take part in due to the interaction with protein partners of this pathway. In order to identify proteins that are part of a common pathway all interaction partners were annotated using gene ontology. The Kyoto Encyclopedia of Genes and Genomes (KEGG) pathway annotations for all annotated proteins were obtained from the DAVID Bioinformatics Resources 6.8 (Huang et al., 2009).

KEGG pathway analysis showed that proteins which show a stronger interaction with both ataxin-3a isoforms are associated to the following pathways: Huntington's disease, oxidative phosphorylation, Parkinson's disease and Spliceosome pathway (Figure 4.12 A; Weishäupl et al., 2019). This indicates a role of ataxin-3aL and -3aS within these pathways (Weishäupl et al., 2019). NGLY1 could be identified as a new interaction partners of ataxin-3c which shows a weaker interaction with both ataxin-3a isoforms. Interestingly, ataxin-3c seems to play a role within the endoplasmic-reticulum-associated protein degradation (ERAD) pathway as four out

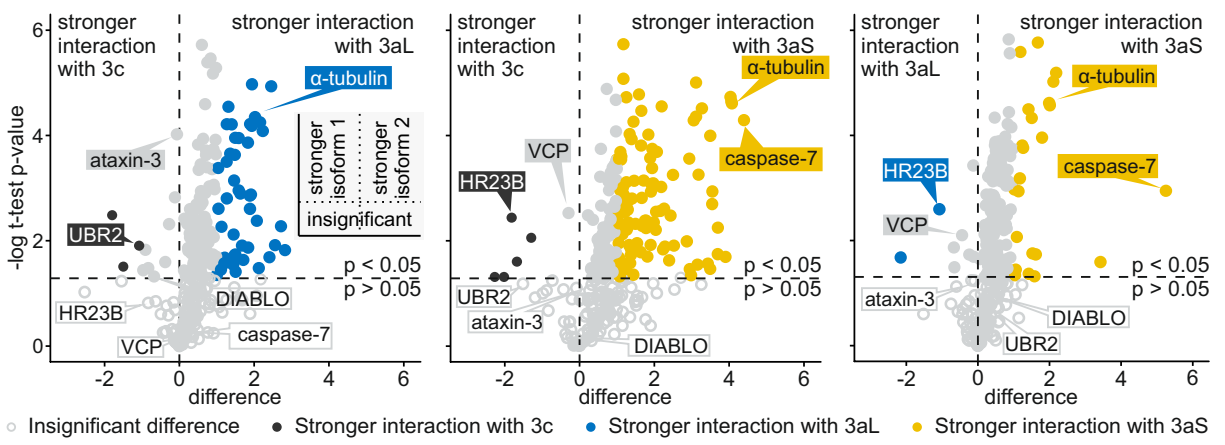

Figure 4.10. Interaction of ataxin-3 isoforms with other proteins. Volcano plot comparing the interaction of ataxin-3 isoforms. Transfected HEK 293 cells were grown in SILAC medium for 72 h and ataxin-3 purification was performed using the Strep-tag. Purifications were combined and concentrated before co-purified proteins were identified by tandem MS. Volcano plots show a direct comparison between ataxin-3c/3aL, -3c/3aS and -3aL/3aS. Interactors with a one-sample t-test $p < 0.05$ (false discovery rate 5 %) and a difference of at least ±1 were considered significant. Insignificant proteins are depicted as open circle ○. Though, ataxin-3 isoforms share numerous interaction partners (●) all isoforms have specific variations in their interaction with different proteins (3c ●, 3aL ●, 3aS ●). Figure was modified from Weishäupl et al. (2019), available for use via `https://doi.org/10.1074/jbc.RA118.005801` under the CC BY 4.0 license (`https://creativecommons.org/licenses/by/4.0/`).

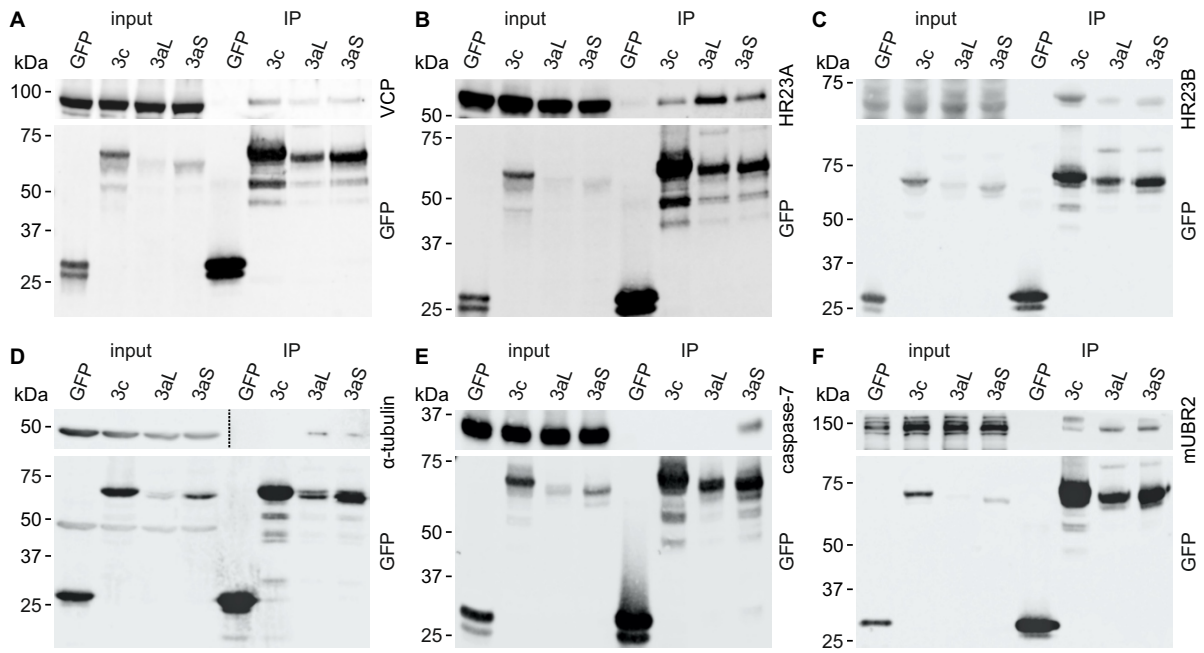

Figure 4.11. Verification of the SILAC-MS interaction analysis using GFP-traps. The SILAC-MS results were verified by GFP-trap assays using the previously described interaction partners **(A)** VCP, **(B)** HR23A and **(C)** HR23B. **(D)** α-tubulin, **(E)** caspase-7 and **(F)** E3 ubiquitin-protein ligase UBR2 (mUBR2) were used as newly identified interaction partners. An interaction with ataxin-3 could be verified for all tested proteins. Figure was modified from Weishäupl et al. (2019), available for use via `https://doi.org/10.1074/jbc.RA118.005801` under the CC BY 4.0 license (`https://creativecommons.org/licenses/by/4.0/`).

of six proteins that show a stronger interaction with ataxin-3c are associated to this pathway (Figure 4.12 B; Weishäupl et al., 2019). HR23B and NGLY1 are both part of the ERAD pathway (Park et al., 2001; Medicherla et al., 2004). UBR2 and heterogeneous nuclear ribonucleoprotein L (hnRNP L) are interactors of ERAD proteins (Havugimana et al., 2012; Wood et al., 2003).

After observing major differences in the interactomes of ataxin-3 isoforms, additional specific questions should be answered using GFP-traps for individual protein partners. Ataxin-3 is a deubiquitinating enzyme and differences in the enzymatic activity between the ataxin-3 isoforms could be identified (see 4.1.4, page 84). Therefore, ataxin-3's affinity against ubiquitin-conjugated proteins was analyzed by GFP-trap and western blot. It was found that ataxin-3aL and -3aS co-precipitated higher amounts of high molecular weight ubiquitinated proteins than ataxin-3c (Figure 4.13 A & B; Weishäupl et al., 2019). These results match the observed lower DUB activity of ataxin-3c indicating a more specific DUB function of this isoform.

The E3 ubiquitin ligase parkin unfortunately could not be identified by the SILAC-MS approach. This possibly is due to a low expression level in HEK 293T cells. In order to study the interaction of parkin with ataxin-3 isoforms GFP-traps were also performed for this interaction partner. Western blotting verified the results of the GST pulldown showing that all isoforms interact with wild-type parkin (Figure 4.13 C & D). Interestingly, the interaction strength was increased for ataxin-3aL and -3aS indicating that the C-terminus indeed is involved in the binding between these two proteins (Weishäupl et al., 2019).

Ataxin-3 isoforms showed an interaction with diablo homolog and caspase 7. Both are taking part in apoptosis regulation (Vucic et al., 2002; Lakhani et al., 2006). Therefore, it should be

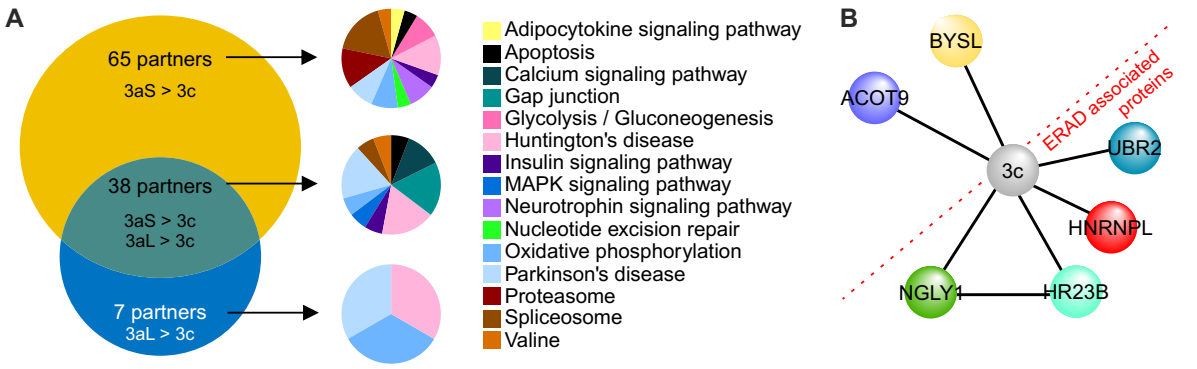

Figure 4.12. Ataxin-3 isoforms take part in different cellular pathways. (A) Venn diagram for the comparison of proteins interacting stronger with ataxin-3aL and ataxin-3aS. In total, 65 proteins interact stronger with ataxin-3aS, whereas 38 show a strengthened interaction with ataxin-3aL and ataxin-3aS. Seven proteins have a strengthened interaction with ataxin-3aL. These proteins take part in different pathways according to the KEGG pathways analysis. However, proteins from the Huntington's disease and Parkinson's disease pathways could be found for all groups. GO annotation was performed using the DAVID Bioinformatics Resources 6.8. **(B)** Proteins interacting stronger with ataxin-3c do not show a common interaction network. However, four out of six proteins were associated to the ERAD pathway which suggests that ataxin-3c plays a role in this pathway. Depicted information about the interaction between the proteins is based on their STRING interaction network (Szklarczyk et al., 2017). Figure was modified from Weishäupl et al. (2019), available for use via `https://doi.org/10.1074/jbc.RA118.005801` under the CC BY 4.0 license (`https://creativecommons.org/licenses/by/4.0/`).

analyzed if ataxin-3 also interacts with X-linked inhibitor of apoptosis protein (XIAP). XIAP is a protein that is capable of stopping the apoptotic cell death by binding to and inhibiting caspase 3, 7 and 9 (Deveraux et al., 1997) by its BIR2 and BIR3 domain (Deveraux and Reed, 1999). On the other hand, XIAP is negatively regulated by diablo homolog, which can bind to XIAP and prevent it from binding to caspases (Du et al., 2000; Srinivasula et al., 2001; Creagh et al., 2004; Morizane et al., 2005). An interaction of ataxin-3 with the so far undescribed interaction partner XIAP could be confirmed for all ataxin-3 isoforms (Figure 4.13 E). Ataxin-3 thereby shows an interaction with both, XIAP and diablo homolog (Figure 4.13 F). Further, ataxin-3aS also interacts with caspase 7 indicating that ataxin-3 may also play a functional role in apoptosis regulation, which partially could explain the observed earlier aao in patients with a stop SNP in the normal allele. Altogether, the interaction analysis of ataxin-3 isoforms showed that ataxin-3 isoforms differ in their interaction networks.

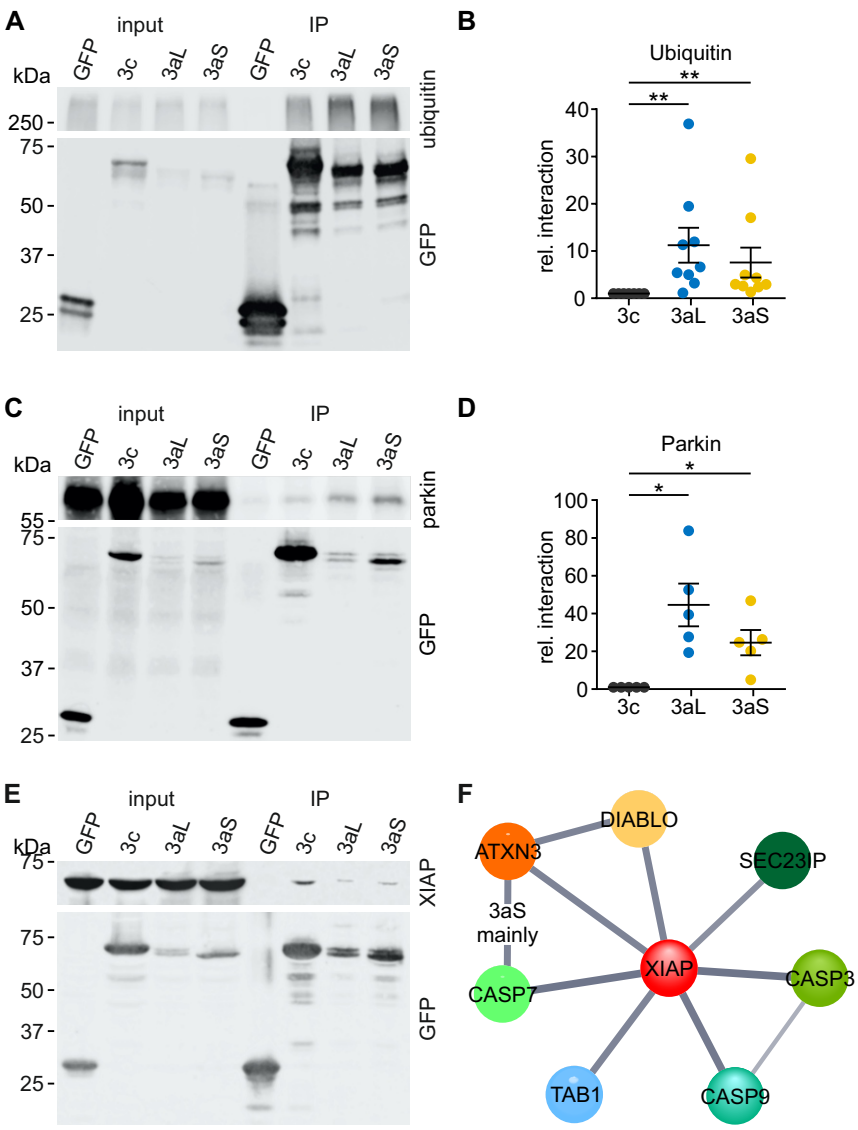

Figure 4.13. Interaction of ataxin-3 isoforms with ubiquitin, parkin and XIAP. (A & B) GFP-trap assay for ataxin-3 and high molecular weight ubiquitinated proteins. Ataxin-3aL and -3aS were able to precipitate higher amounts of high molecular weight ubiquitinated proteins than ataxin-3c which indicates a higher ubiquitin-affinity of these isoforms. One sample t-test, Hommel adjusted, * $p < 0.05$, $n = 9$ **(C & D)** GFP-trap assay for ataxin-3 and parkin. Ataxin-3aL and ataxin-3aS show a significantly stronger interaction with parkin than ataxin-3c. One sample t-test, Hommel adjusted, * $p < 0.05$, $n = 5$. Data is represented as arithmetic mean ±SEM. **(E)** GFP-trap assay for ataxin-3 and XIAP. It could be shown that all ataxin-3 isoforms are able to interact with XIAP. **(F)** STRING (Szklarczyk et al., 2017) interaction network of XIAP. XIAP is an inhibitor of apoptosis that interacts with caspase 3, 7 and 9. It is negatively regulated by diablo homolog (DIABLO). Ataxin-3 isoforms showed to interact with both, XIAP and DIABLO and ataxin-3aS also interacted with caspase 7 indicating a functional role of ataxin-3 in apoptosis regulation. Subfigures A - D were modified from Weishäupl et al. (2019), available for use via `https://doi.org/10.1074/jbc.RA118.005801` under the CC BY 4.0 license (`https://creativecommons.org/licenses/by/4.0/`).

4.1.6 Ataxin-3 isoforms do not differ in their transcriptional regulation

Ataxin-3 is known to be a transcriptional regulator. Ataxin-3 is able to repress the expression of main transcriptional coactivators (e. g. CREB-binding protein and p300) by inhibiting histone acetyltransferase (HAT) activity (Li et al., 2002; Evert et al., 2006). Further ataxin-3 is able to directly bind the MMP-2 promoter and represses transcription by recruitment of other proteins leading to the deacetylation of bound histones (Evert et al., 2006). Evert et al. (2003) reported that mutant ataxin-3 changes the expression level of various genes in a rat mesencephalic cell line. Among others those genes are transcription factors, nuclear proteins, inflammatory cytokines, signal transducers and proteasome proteins.

To assess the transcriptional regulation by ataxin-3 isoforms quantitative RT-PCRs with normal and expanded ataxin-3 isoforms was performed in HEK 293T *ATXN3* KO cells. Genes of interest (*HSPB1*, *DUSP1*, *PSME2*, *MMP2*, *CEBPB*, *SNCA*) were selected from different pathways based upon previously reported genes by Evert et al. (2003). Heat shock protein beta-1/heat shock 27 kDa protein (*HSPB1*) was chosen as a heat shock protein. These proteins belong to an important group that mediates the response to various kinds of cellular stress (Bouillet and Strasser, 2002; Stetler et al., 2010, reviewed in). *HSPB1* is known to suppress polyQ-mediated toxicity in a cellular Huntington's disease model (Wyttenbach et al., 2002) and therefore could also play a role in MJD pathology. It was found that *HSPB1* is insignificantly upregulated by around 25 % in ataxin-3 expressing cells compared to an empty vector control (Figure 4.14). Differences between ataxin-3 isoforms or normal and expanded polyQ repeat could not be found.

A proper transformation of information within the cell is crucial for its function and can cause severe diseases when dysfunctioning, among others Parkinson's disease (Timmons et al., 2009), schizophrenia (Hakak et al., 2001; McGuire et al., 2017), Donnai-Barrow (Kantarci et al., 2007), Laron's syndrome (Laron et al., 1966; Amselem et al., 1989) and autosomal recessive tetraamelia (Niemann et al., 2004). In order to assess the modulating effects of ataxin-3 on

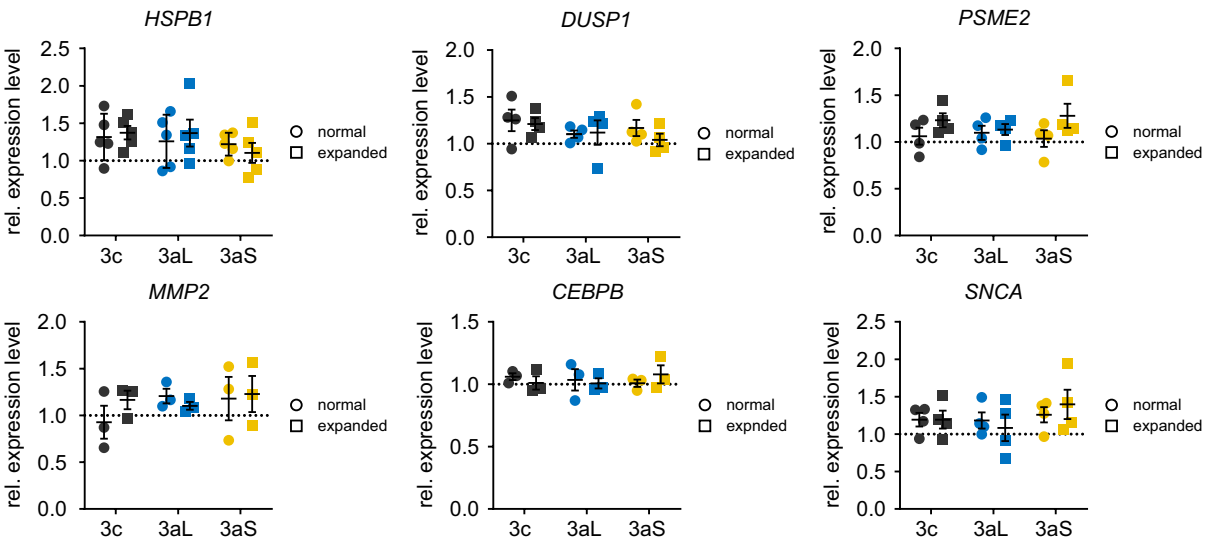

Figure 4.14. Transcriptional regulation by ataxin-3 isoforms. HEK 293T *ATXN3* KO cells were transfected with pN-SF-Tap ataxin-3 isoforms and cultured for 48 h before samples were processed for RNA isolation and gene expression levels of *HSPB1*, *DUSP1*, *PSME2*, *MMP2*, *CEBP* and *SNCA* were analyzed by quantitative RT-PCR. No differences could be found between ataxin-3 isoforms. Kruskal-Wallis test and ANOVA (HSP27). Data is represented as arithmetic mean ±SEM.

signal transduction the *DUSP1* transcription levels were measured after expression of ataxin-3 isoforms. *DUSP1* encodes for the dual specificity phosphatase 1 that regulates the activity of *MAPK1* during the meiotic cell cycle by dephosphorylation resulting in a negative regulation of cellular proliferation (Slack et al., 2001; Calvisi et al., 2008). The protein is considered to play an important role in stress response (Liu et al., 2008). It was found that *DUSP1* is slightly upregulated upon ataxin-3 expression, whereas no statistically significant difference could be found between the isoforms or polyQ expansion.

The proteasome activator PA28 (*PSME2*) is important for the immunoproteasome assembly (Preckel et al., 1999) and necessary for antigen processing (Macagno et al., 1999). It alternates the cleavage pattern of the proteasome and therefore enhances the generation of class I binding peptides (Dick et al., 1996). A slight upregulation for expanded ataxin-3 isoforms could be found compared to the empty vector control. However, this effect did not reach statistical significance.

Matrix metalloproteinase-2 (*MMP2*), a ubiquitous Ca^{2+} and Zn^{2+} dependent endopeptidases involved in various cellular processes such as tissue remodeling and organ development (Wiseman et al., 2003; Page-McCaw et al., 2007), inflammation (Parks et al., 2004), tumor invasion and angiogenesis (Bergers et al., 2000; Fang et al., 2000; Egeblad and Werb, 2002; Rojiani et al., 2010) as well as degradation of extracellular matrix proteins (Allan et al., 1995; Monaco et al., 2006) and the *CEBPB* encoded CCAAT/enhancer-binding protein beta, a transcription factor for genes involved in immune and inflammatory response (Kinoshita et al., 1992; Chinery et al., 1997; Roy et al., 2002; Pless et al., 2008), both did not show a significant upregulation upon expression of ataxin-3 isoforms.

Lastly the effect of ataxin-3 isoforms on *SNCA* was analyzed. The gene encodes α-synuclein, an important protein involved in familial Parkinson's disease (Polymeropoulos et al., 1997; Krüger et al., 1998; Zarranz et al., 2004; Appel-Cresswell et al., 2013; Lesage et al., 2013) which can be found in lewy bodies (Spillantini et al., 1997). It enhances the toxic effects of tau strains in Alzheimer's disease (Castillo-Carranza et al., 2018) and is responsible for dopamine release and transport in dopaminergic neurons (Abeliovich et al., 2000). Upon expression of ataxin-3 a insignificant upregulation could be observed which reached 40 % in ataxin-3aS expressing cells compared to empty vector transfected cells.

4.1.7 Ataxin-3 isoforms differ in their subcellular localization[6]

Ataxin-3 is localized to different compartments of the cell and it was reported to be a cytoplasmic (Paulson et al., 1997a; Schmidt et al., 1998; Trottier et al., 1998; Pozzi et al., 2008), a nuclear (Tait et al., 1998; Pozzi et al., 2008) and a mitochondrial protein (Pozzi et al., 2008). A protein's localization is dependent on protein-intrinsic factors (e. g. localization signals, PTMs) as well as its cellular context. Ataxin-3 itself has NES as well as a NLSs (Tait et al., 1998; Albrecht et al., 2004; Antony et al., 2009) and is known to be able to translocate to the nucleus (Fujigasaki et al., 2000; Pozzi et al., 2008; Macedo-Ribeiro et al., 2009; Sowa et al., 2018; Wang et al., 2018b). An interaction with nuclear import or export proteins, however, could not be found yet. Mueller et al. (2009) reported that phosphorylation of two serines by casein kinase 2 is responsible for the nuclear localization of ataxin-3. As ataxin-3 isoforms differ in their stability, activity and interaction network, it is possible that they show a differing subcellular localization as they carry out different functions and/or shown an isoform-specific interaction with shuttling proteins. Further, the two phosphorylation sites important for ataxin-3 localization are only present in ataxin-3c. Alternative splicing therefore makes differences in localization very likely. In order to clarify if ataxin-3 isoforms show a preferred localization to a certain compartment subcellular fractionation assays were performed with EGFP-ataxin-3 transfected HEK 293T *ATXN3* KO cells. Before the experiments could be performed, the SNP rs1048755 needed to be exchanged from $A_{634}TG$ to $G_{634}TG$ in the 18CAG pEGFP-C2 constructs. A fragment from pGEX-*hMJD1*c18CAG$_{GG}$ was introduced into the pEGFP-C2 ataxin-3 isoform vectors using NotI and PpuMI (Figure 4.15 A & B). The cloning was sequence-verified using the primers F022, F023, F025 and F029.

Performing subcellular fractionation assays it could be found that ataxin-3aL and ataxin-3aS, independent of the polyQ expansion, show an enhanced nuclear localization in comparison to ataxin-3c (Figure 4.15 C & D). This suggests that these isoforms play a more important role in this compartment. However, to exclude any influence of the EGFP tag which could modulate the localization of the protein these experiments were validated using untagged ataxin-3 isoforms which were expressed from the pTRE vector in HEK 293T *ATXN3* KO cells. The usage of untagged constructs confirmed the enrichment of ataxin-3aS in the nuclear fraction (Figure 4.15 E & F; Weishäupl et al., 2019). However, the enrichment of ataxin-3aL could not be confirmed indicating that the protein tag influences the subcellular localization. The nuclear localization was independent of the polyQ repeat. Even more interesting, the pTRE-ataxin-3 isoforms showed a fragmentation pattern which allowed the analysis of the localization. One fragment of ataxin-3 was strongly enriched in the nuclear fraction (Figure 4.15 G; Weishäupl et al., 2019). This is of special importance as Bichelmeier et al. (2007) and Sowa et al. (2018) previously observed a link between ataxin-3's nuclear localization and it's toxicity. The fragment observed is an N-terminal fragment of ataxin-3 and was described to cause mitochondrial deficits (Harmuth et al., 2018; Weishäupl et al., 2019).

[6]Results first published in Weishäupl et al. (2019).

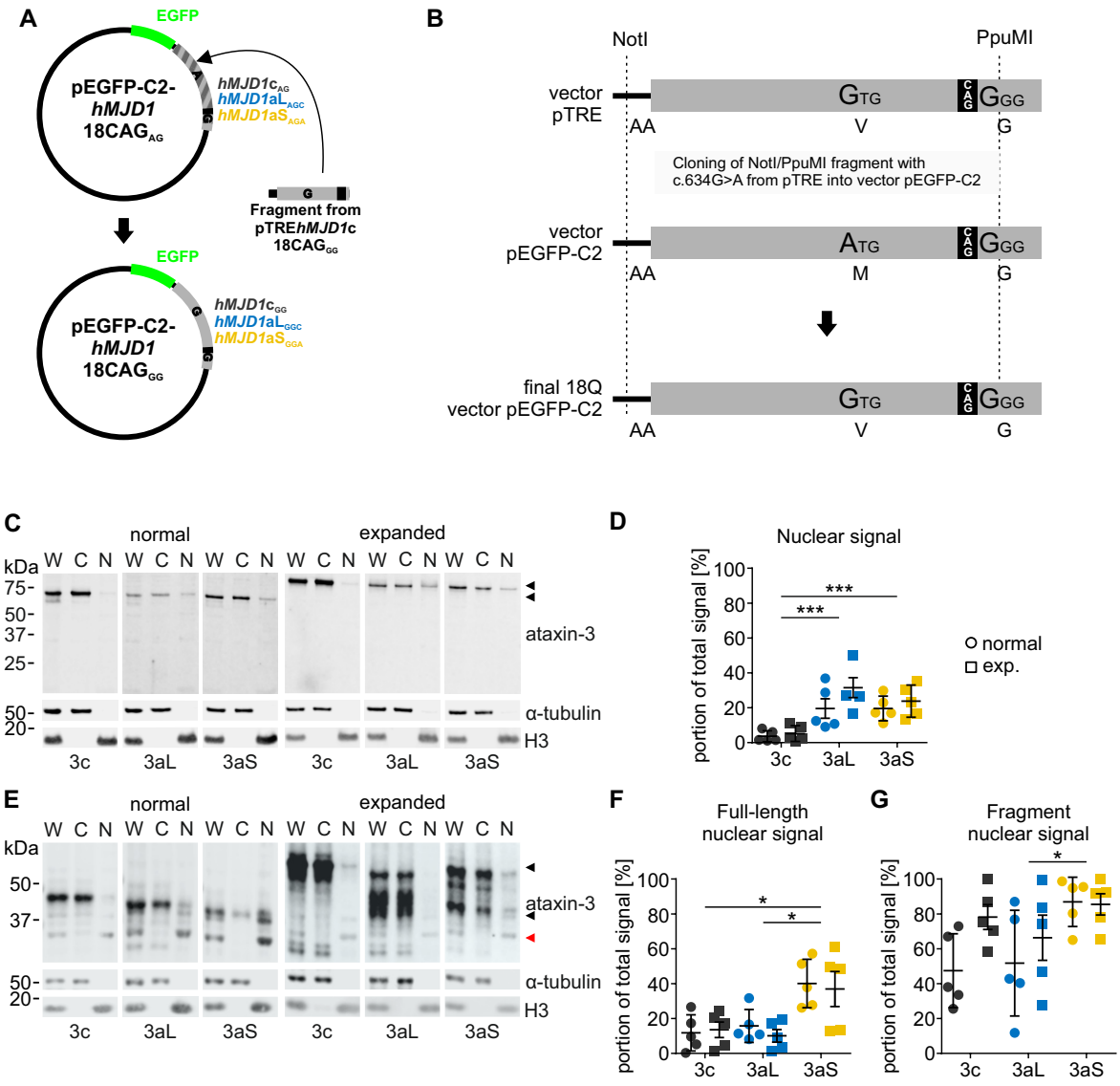

Figure 4.15. Analysis of ataxin-3's subcellular localization. (A & B) The SNP rs1048755 in the pEGFP-C2 vector was exchanged by insertion of a NotI/PpuMI fragment from the vector pGEX-*hMJD1*c18CAG$_{GG}$ into the pEGFP-C2-*hMJD1*-18CAG vectors creating isoform-specific vectors expressing Val_{212} instead of Met_{212}. **(C)** Subcellular location of ataxin-3 was analyzed by a nuclear-cytoplasmatic fractionation followed by western blot analysis. *ATXN3* KO cells were transfected with ataxin-3 isoforms and cultured for 48 h before fractionation into whole cell (W), cytoplasmatic (C) and nuclear (N) fraction was performed. Ataxin-3 was detected using the antibody 1H9. Tubulin was used as cytoplasmatic, H3 as nuclear marker proteins in order to estimate the identity and purity of the fractions. **(D)** Ataxin-3aL and -3aS show an increased presence in the normal and polyQ expanded nuclear fraction. Two-way ANOVA, *** $p < 0.001$. Data is represented as arithmetic mean ±SEM. **(E)** Fractionation into whole cell (W), cytoplasmic (C) and nuclear (N) fractions was performed 48 h post transfection of HEK 293T *ATXN3* KO cells with ataxin-3 isoforms. Samples were processed for western blot and immunostaining was performed for ataxin-3 (1H9) as well as α-tubulin (cytoplasmic marker) and H3 (nuclear marker). Full length ataxin-3 (◀) as well as ataxin-3 breakdown products (◀) could be detected. **(F & G)** Ataxin-3aS showed a polyQ-independent increased nuclear localization. The fragment of ataxin-3aS was more nuclear than the fragment of ataxin-3aL. Two-way ANOVA with Tukey's HSD test, * $p < 0.05$, $n = 5$. Data is represented as arithmetic mean ±SEM. Subfigures E, F and G were modified from Weishäupl et al. (2019), available for use via `https://doi.org/10.1074/jbc.RA118.005801` under the CC BY 4.0 license (`https://creativecommons.org/licenses/by/4.0/`).

4.2 Pathophysiological characteristics of ataxin-3 isoforms

4.2.1 Ataxin-3 isoforms show differences in protein aggregation[7]

After observing major differences between the ataxin-3 isoforms on a physiological level, next the contribution of ataxin-3 isoforms to pathological mechanisms of the neurodegenerative disorder MJD was assessed. As for other polyQ diseases aggregation of ataxin-3 is one of the hallmarks of MJD (Paulson et al., 1997b; Schmidt et al., 1998). It was previously reported that N- and C-terminal regions of polyQ stretches affect aggregation and that alternative splicing of the C-terminus indeed modifies ataxin-3's aggregation behavior (Harris et al., 2010; Sicorello et al., 2018). However, nothing is known about the aggregation behavior of ataxin-3aS. Protein aggregation was analyzed for all ataxin-3 isoforms to assess whether the isoforms aggregate the same way or show specific differences which could cause them to be more or less harmful.

Purified GST-ataxin-3 was used for the aggregation assays. The GST-tag inhibits aggregation during expression and purification (Haacke et al., 2006). In order to induce aggregation, the GST-tag was cleaved from ataxin-3 using PreScission protease. This enzyme was able to fully cleave GST-ataxin-3 within one hour of incubation at 37 °C as reported previously (Figure 4.16 A, Haacke et al., 2006). Ataxin-3 isoforms were kept aggregating under constant shaking at 37 °C for 24 h. Afterwards samples were analyzed for SDS-insoluble aggregates using an filter retardation assay. Aggregates could be detected well in a loading range between 375 ng and 6 µg of purified protein (Figure 4.16 B). Normal ataxin-3 did not form aggregates whereas all polyQ-expanded isoforms formed SDS-insoluble aggregates within 24 h (Figure 4.16 C). While ataxin-3c and -3aL showed comparable amounts of aggregates (100 % vs. 80 %) ataxin-3aS formed 2.5-times more aggregates (Figure 4.16 D). This suggests that ataxin-3aS undergoes a stronger aggregate formation than ataxin-3c and ataxin-3aL or forms aggregates that are less soluble to SDS.

In a next step the ataxin-3 aggregation kinetics were analyzed using the *in vitro* aggregation assay combined with an aggregate specific dye that binds aggregated proteins and emits a fluorescence signal after excitation. Protein aggregation starts with misfolding of the native protein in an initial lag phase which is followed by a growth phase where the misfolded proteins form oligomers and protofibrils. When most of the proteins are aggregated to fibrils a saturation phase is reached in which no aggregates are formed anymore (reviewed in Morris et al., 2009). Expanded 73Q ataxin-3 isoforms from five individual protein preparations were incubated for 72 h and aggregation was analyzed in real-time (Figure 4.16 E). All ataxin-3 isoforms show an increasing aggregation signal over time. The initial lag phase lasted about 3 h. Growth phase started at around 4 h and lasted until the end of the assay. Within the 72 h measured, saturation phase was not reached. In general, ataxin-3aL showed a lower signal increase and a slower inclination than ataxin-3c and -3aS. Fitting a linear function to the initial linear growth phase (4 h to 27 h) and the linear end-phase (50 h to 72 h) revealed that the aggregation is faster in the beginning than in the end-phase indicating that protein aggregation is about to reach the saturation phase at this time (Figure 4.16 F). Further ataxin-3aS shows an increased slope compared to ataxin-3aL indicating that the nonsense SNP causes the protein to aggregate faster than ataxin-3aL.

[7] Results first published in Weishäupl et al. (2019).

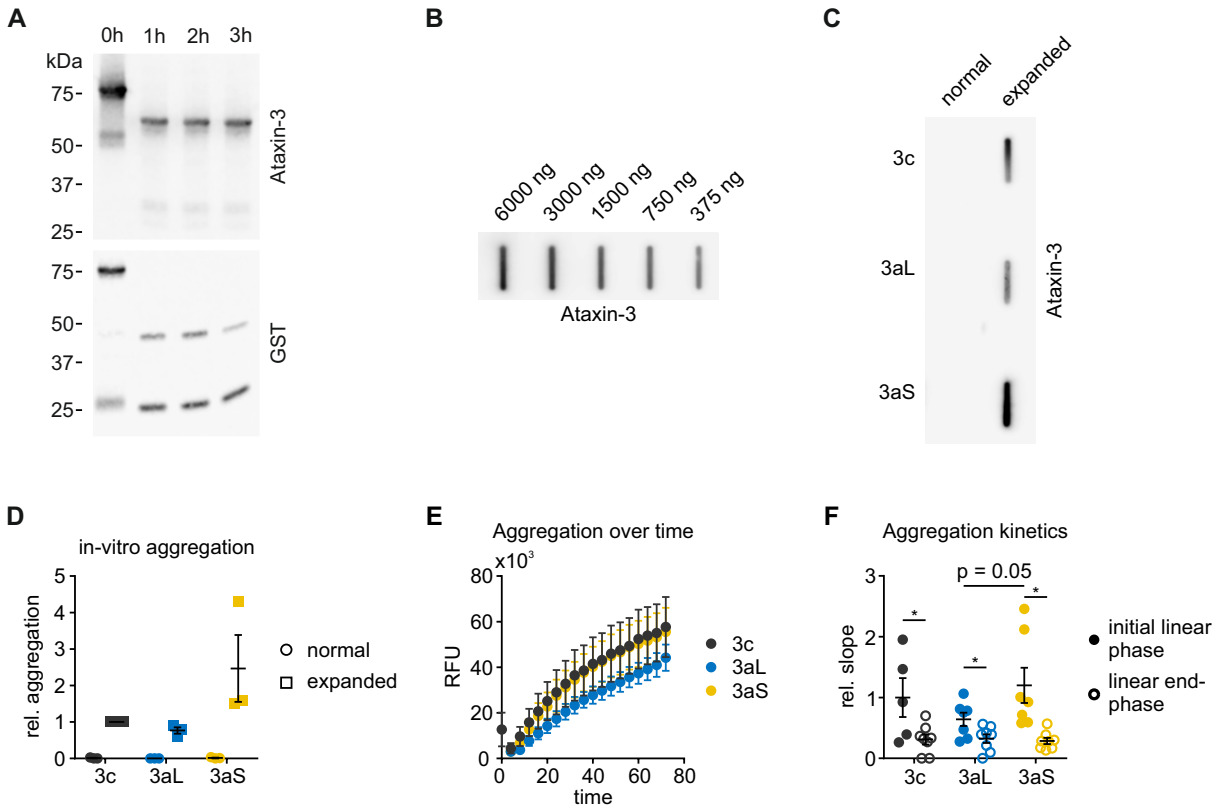

Figure 4.16. ***In vitro*** **aggregation of ataxin-3 isoforms.** **(A)** The GST tag was cleaved from GST-ataxin-3 using PreScission protease in order to initiate ataxin-3 aggregation. The protease was able to fully cleave its specific recognition sequence within 1 h of incubation resulting in expanded ataxin-3 and a free GST tag. Ataxin-3 was detected with the antibody 1H9. **(B)** Different amounts of aggregated ataxin-3 isoforms were loaded in a filter retardation assay stained for ataxin-3 (1H9). Aggregates could be detected in a range between 375 ng and 6 µg. **(C)** Non polyQ-expanded ataxin-3 isoforms did not form SDS-insoluble aggregates. Upon a polyQ expansion the isoforms start to form aggregates. 750 ng of protein were loaded onto the membrane and ataxin-3 was detected using the antibody 1H9. **(D)** While ataxin-3c and ataxin-3aL form comparable amounts of aggregates ataxin-3aS forms 2.5-times more insoluble aggregates. Wilcoxon Signed Rank test, $p > 0.05$, $n = 3$. Data is represented as arithmetic mean ±SEM. **(E)** *In-vitro* real time aggregation assay for ataxin-3 isoforms. Aggregation was induced by cleavage of the GST-tag using PreScission protease and incubation of 73Q ataxin-3 isoforms with an aggregate specific dye. Aggregation was measured over a period of 72 h once per hour. Displayed are the values in a sequence of 4 h. Ataxin-3 isoforms formed aggregates over time. Ataxin-3aL showed a lower inclination speed and in general a lower signal increase over time compared to ataxin-3aS and -3c. **(F)** Quantification of the initial linear growth phase (4 – 27 h) and the linear end phase (50 – 72 h) slope revealed that all isoforms show a faster aggregation speed at the beginning of aggregation than at the end of the growth phase. Further ataxin-3aS showed a faster aggregation speed than ataxin-3aL in the initial growth phase. Two-way ANOVA with Tukey's HSD test, * $p < 0.05$, $n = 5$. Data is represented as arithmetic mean ±SEM.

After analyzing the aggregation properties of ataxin-3 isoforms *in vitro*, ataxin-3 aggregation was assessed in the generated *ATXN3* KO cell culture model. It was tested if alternative splicing or the nonsense SNP have an influence on ataxin-3 solubility. Therefore, homogenates of transfected cells were separated into Triton X-100 soluble (soluble), SDS-soluble and SDS-insoluble fractions of proteins using the fractionation method described by Koch et al. (2011). All ataxin-3 isoforms were found to be present in the soluble and SDS-soluble fraction whereas only highly expanded ataxin-3 and fragments showed to be SDS-insoluble indicating late stage fibrils (Figure 4.17 A; Weishäupl et al., 2019). Further, ataxin-3aL showed a comparably weaker

signal in the SDS-insoluble fraction but at the same time a comparably stronger signal in the SDS-soluble fraction. This suggests that ataxin-3aL forms less insoluble aggregates but more soluble ones. This reduced formation of SDS-insoluble aggregates could also be confirmed by filter retardation assay of ataxin-3 transfected cells 72 h post transfection (Figure 4.17 B & C). Ataxin-3aL showed a relative aggregation signal of 45 % compared to ataxin-3c and ataxin-3aS (100 % and 90 % respectively). 151Q ataxin-3 isoforms formed more aggregates than 18Q and 73Q isoforms as expected (Weishäupl et al., 2019).

As differences in the aggregation kinetics could already be observed using the *in vitro* aggregation assay, also cell culture kinetic experiments were performed over a period of 72 h. Ataxin-3aL again showed to aggregate slower and to form fewer aggregates than ataxin-3c and ataxin-3aL (Figure 4.17 D). Although, ataxin-3c showed the strongest aggregation signal at 72 h,

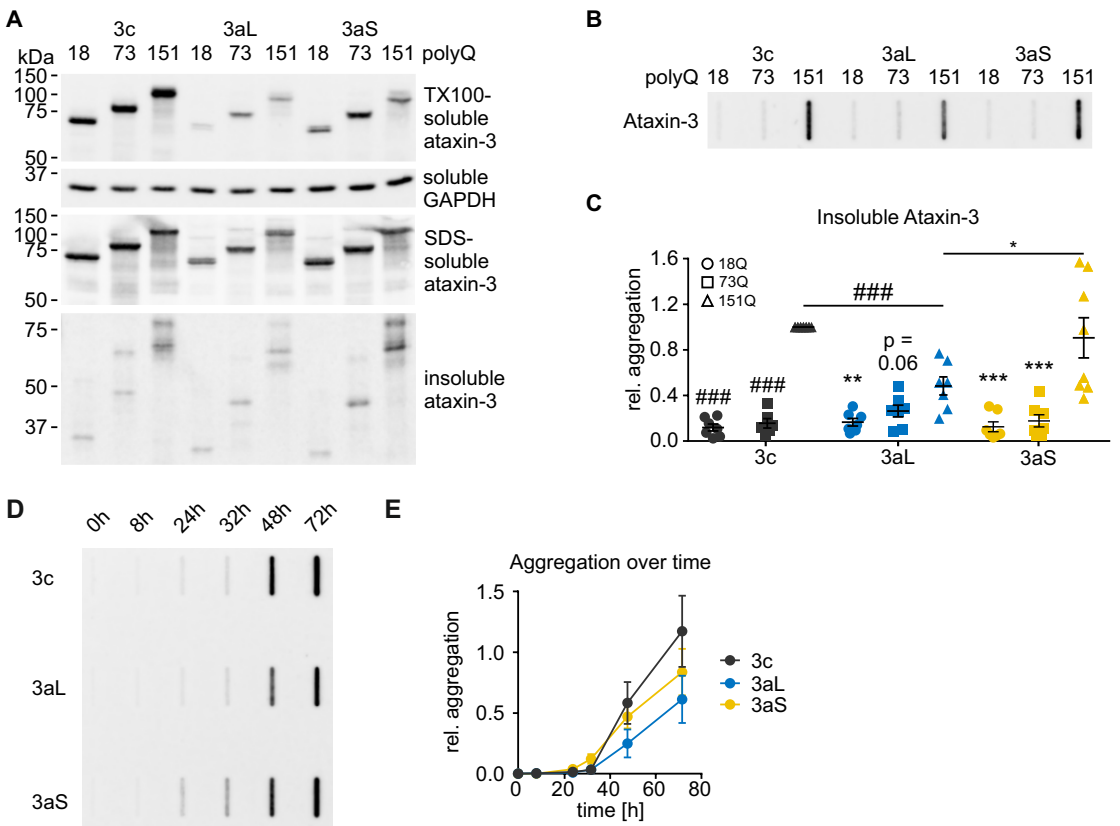

Figure 4.17. *In-vitro* aggregation properties of ataxin-3 isoforms. (A) Fractionation of cellular proteins into fractions of varying solubility (Triton X-100 soluble, SDS-soluble and SDS-insoluble). Ataxin-3 was found in the soluble and SDS-soluble fraction. Ataxin-3 fragments and ataxin-3 with an expansion size of 151Q also was able to formed SDS-insoluble aggregates whereby ataxin-3aL formed fewer of these aggregates than ataxin-3c and ataxin-3aS. **(B & C)** The lower amount of SDS-insoluble ataxin-3aL aggregates could be confirmed by a filter retardation assay (one-sample t-test, ♯♯♯ $p < 0.001$ and two-sample t-test, * $p < 0.05$, p-values were Hommel-corrected for multiple comparison, n = 7-8). Equal protein amounts were loaded onto the membrane. The amount of ataxin-3 aggregates increases with the polyQ expansion size independent of the isoform. One-sample t–test, ### $p < 0.001$, p-values were Hommel-corrected and one-way ANOVA with Tukey's HSD test, ** $p < 0.01$, *** $p < 0.001$, n = 6-8). **(D & E)** Aggregation of ataxin-3 isoforms in cell culture over a period of 72 h. Ataxin-3aL showed a reduced formation of SDS-insoluble aggregates as well as a slower kinetic than ataxin-3c and -3aS. Though ataxin-3c formed the highest amount of protein aggregates, ataxin-3aS started to form SDS-insoluble aggregates faster. First aggregates were visible after 24 h. Data is represented as arithmetic mean ±SEM. Subfigures A, B and C were modified from Weishäupl et al. (2019), available for use via `https://doi.org/10.1074/jbc.RA118.005801` under the CC BY 4.0 license (`https://creativecommons.org/licenses/by/4.0/`).

SDS-insoluble ataxin-3aS aggregates could already be detected after 24 h. It therefore started to form fibrils faster than ataxin-3c. This data again shows that the introduction of the PTC by the nonsense SNP leads to an increased aggregation propensity in ataxin-3a.

After analyzing the aggregation characteristics of ataxin-3 isoforms using filter retardation assay HEK 293T *ATXN3* KO cells were transfected and aggregate formation was inspected visually. Upon a pathological expansion of the polyQ tract ataxin-3 formed visible aggregates within 72 h of expression independent of the isoform as assessed by the GFP signal (Figure 4.18 A). Visually, ataxin-3c and ataxin-3aS formed larger but fewer aggregates per cell than ataxin-3aL. Counting the number of transfected cells with at least one aggregate revealed that the fraction of cells with aggregates is lower when they were transfected with ataxin-3c 48 h post transfection (Figure 4.18 B). After 72 h, no differences between the isoforms could be found anymore. It can be concluded that under *in vitro* conditions ataxin-3c undergoes a slower aggregation process with a longer nucleation phase. However, when seeds are formed ataxin-3c starts to aggregate fast. Counting of the aggregate number per cell revealed that ataxin-3aL formed multiple aggregates per cell (Figure 4.18 C). For ataxin-3c and ataxin-3aS 3 % to 7 % of all cells showed more than 5 aggregates. For ataxin-3aL the number of cells carrying at least six aggregates was increased to 20 %. At the same time the number of cells with only one aggregate was reduced for ataxin-3aL.

Microscopic inspection revealed that ataxin-3aL aggregates visually were different in appearance compared to ataxin-3aS and ataxin-3c aggregates. Therefore, the size of aggregates was measured (see B.3, page B11). All isoforms formed aggregates of various sizes. In general ataxin-3aL formed more aggregates of a smaller size than the other isoforms (Figure 4.18 D). 48 h as well as 72 h post transfection the median aggregate size of ataxin-3aL (40 µm^2 and 43 µm^2) was smaller than that of ataxin-3c (99 µm^2 and 94 µm^2) and ataxin-3aS (66 µm^2 and 79 µm^2) (Figure 4.18 E). While ataxin-3aS initially formed smaller aggregates, after 72 h the aggregates size was similar to ataxin-3c aggregates.

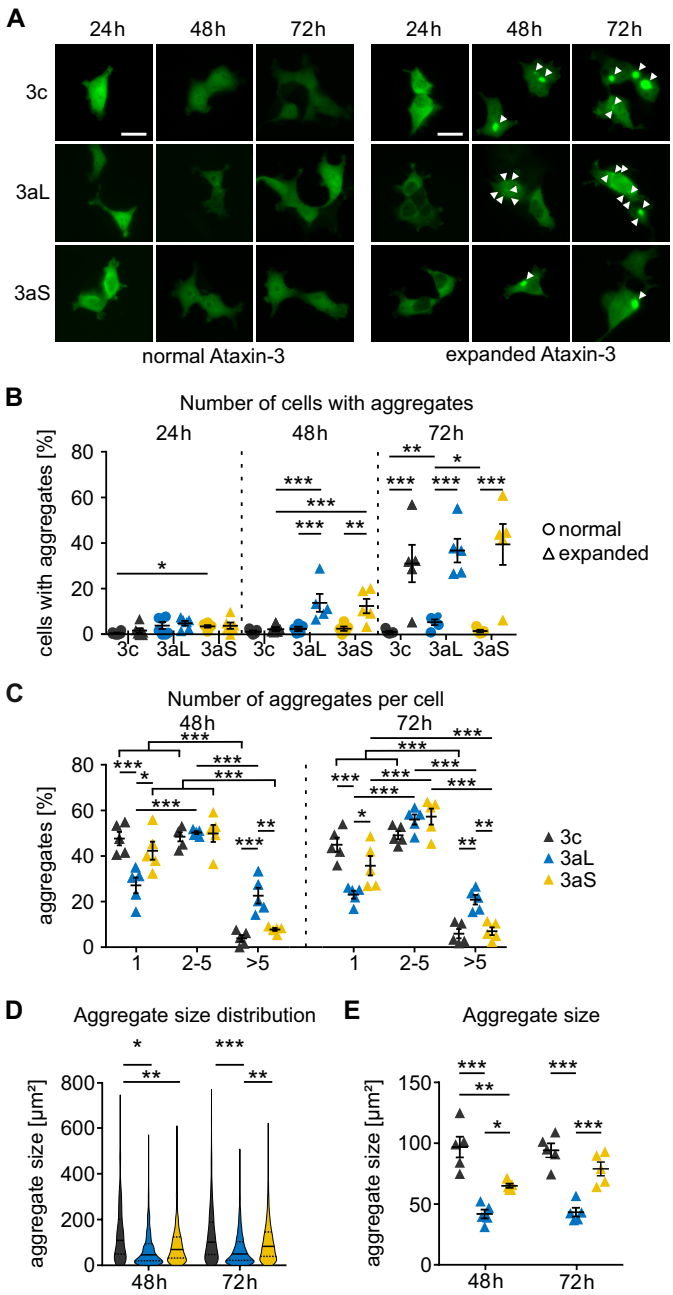

Figure 4.18. Microscopic analysis of ataxin-3 aggregation. **(A)** HEK 293T *ATXN3* KO cells were transfected with EGFP-ataxin-3 isoforms either expressing 18Q or 151Q repeats. Cells were grown for 24 h, 48 h and 72 h before they were fixed and the relative number of cells carrying an aggregate was counted from the GFP signal. For every biological replicate at least 200 GFP positive cells were counted. Aggregates are marked with an arrowhead, bar represents 100 µm. **(B)** 48 h post transfection first differences in the number of cells showing ataxin-3 aggregates could be observed. Cells expressing ataxin-3aL or ataxin-3aS showed more cells with aggregates than those expressing ataxin-3c. Further, both expanded ataxin-3a isoforms showed more aggregates than the respective non-expanded isoform. 72 h post transfection the observed differences were no longer present. All ataxin-3 isoforms showed comparable amounts of aggregates whereby an expansion of the polyQ repeat led to a stronger aggregation. Beta-regression with estimated marginal means contrasts for each time point, n = 5, * $p < 0.05$. **(C)** Counting the numbers of aggregates per cell for all expanded ataxin-3 isoforms revealed that ataxin-3aL shows fewer cells with one aggregate but at the same time more cells with at least six aggregates. Two-way ANOVA with estimated marginal means contrasts, * $p < 0.05$, ** $p < 0.01$, *** $p < 0.001$, n = 5. Data is represented as arithmetic mean ±SEM. **(D)** The area for aggregate signals was measured on microscopic pictures for around 100 aggregates per isoform. 48 h post transfection the size distribution of ataxin-3c aggregates differs significantly from the size distribution of ataxin-3aL and -3aS. At 72 h the size distribution of ataxin-3aS aggregates changed so that ataxin-3aL aggregates are now

Continued on next page

Figure 4.18 Microscopic analysis of ataxin-3 aggregation - *continued from previous page*
different from both other ataxin-3 isoforms. Kolmogorov-Smirnoff test with Hommel-adjustment for multiple comparison, * $p < 0.05$, ** $p < 0.01$, *** $p < 0.001$, $n = 5$. At both time-points the size distribution shows that ataxin-3aL produces higher numbers of small aggregates but shows comparable numbers of large aggregates. Quartils are indicated as solid (50 %) and dashed lines (25 % and 75 %). **(E)** Comparison of the median aggregate size. At both time points aggregates formed by ataxin-3aL were smaller than those of ataxin-3c and -3aS. 48 h post transfection aggregates from ataxin-3c were larger than those from ataxin-3aS. This effect was lost after 72 h. Two-way ANOVA with Tukey's HSD test, * $p < 0.05$, ** $p < 0.01$, *** $p < 0.001$, $n = 5$. Data is represented as arithmetic mean ±SEM. Subfigures A - E were modified from Weishäupl et al. (2019), available for use via `https://doi.org/10.1074/jbc.RA118.005801` under the CC BY 4.0 license (`https://creativecommons.org/licenses/by/4.0/`).

4.2.2 Ataxin-3 isoforms show minor differences in aggregation after cleavage

Cleavage of ataxin-3 is discussed to be a main factor of the pathogenesis of MJD (Hübener et al., 2013). According to the toxic fragment hypothesis especially fragments of mutant ataxin-3 may harbor toxic characteristics and therefore may be important for the pathogenesis of MJD (Ikeda et al., 1996; Haacke et al., 2006). Ataxin-3 was previously described to be cleaved by calpain-1 (Hübener et al., 2013) as well as caspases (Berke et al., 2004). Due to the different AA composition at the C-terminus harboring also the polyQ area, it can be assumed that ataxin-3 isoforms are cleaved differently by proteases. In order to analyze differences in cleavage, the likelihood of a calpain cleavage was predicted using GPS-CCD 1.0 (Liu et al., 2011). It could be found that the C-terminus of ataxin-3c is more likely to be cleaved at the very terminal area resulting in smaller polyQ harboring fragments than the C-terminus of both ataxin-3a isoforms (Figure 4.19 A). These fragments may be especially toxic as the C-terminus of ataxin-3c is hydrophilic. Therefore, a loss of those soluble AA may result in insoluble polyQ containing fragments.

In order to determine this, the calpain-cleavage influence on aggregation of ataxin-3 isoforms was assessed upon expression in HEK 293T *ATXN3* KO cells. Cleavage was induced by the addition of ionomycin, a ionophore produced by *Streptomyces conglobatus* that is capable of raising the intracellular Ca^{2+} levels (Liu et al., 1978; Gil-Parrado et al., 2002). After 24 h cells were treated with 125 nM ionomycin and 5 mM $CaCl_2$ for 1 h in Opti-MEM medium. As a negative control, cells were pre-treated with calpain inhibitor III (CI3) for 1 h with a final concentration of 10 mM. After the treatment, cells were grown in normal culture medium for another 48 h. Homogenates were analyzed by filter retardation assay (Figure 4.19 B). Quantification showed that the addition of ionomycin increased the aggregation of ataxin-3c whereas the treatment did not have an effect on ataxin-3aL and -3aS (Figure 4.19 C). The addition of CI3 again decreased the aggregation signal for ataxin-3c showing that ionomycin indeed activated calpain cleavage that led to the increase in aggregation.

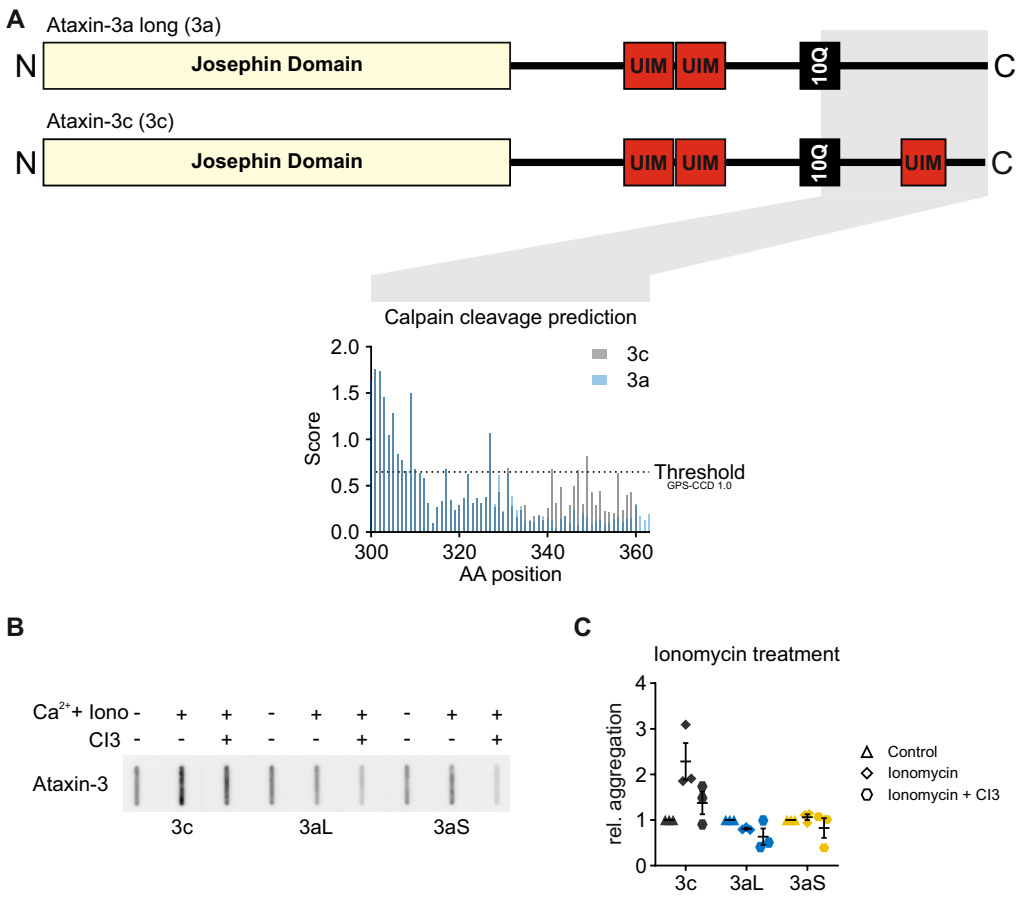

Figure 4.19. **(A)** Prediction of calpain cleavage of ataxin-3 isoforms using GPS-CCD 1.0. The C-terminus of ataxin-3c is more likely to be cleaved in the last 30 AA than for ataxin-3a. This may result in smaller polyQ harboring fragments for ataxin-3c lacking the hydrophilic AA of the C-terminus which is causing these fragments to be more insoluble. **(B)** HEK 293T *ATXN3* KO cells were transfected with pEGFP-C2-ataxin-3 isoforms and grown for 24 h. Controls were pre-treated with calpain inhibitor III (CI3) for 1 h. Ionomycin was then added to the culture for 2 h and cells were afterwards grown for another 48 h. Samples were processed for filter retardation assay and membranes were stained for ataxin-3 aggregates using the antibody 1H9. **(C)** Ataxin-3c showed a non-significant increase of aggregation after induction of calpain cleavage. Inhibition of calpains by CI3 reduced the amount of aggregates. Treatments did not have an effect for ataxin-3aL and -3aS (one-sample Wilcoxon Signed Rank test, Hommel-adjustment for multiple comparisons). Data is represented as arithmetic mean ±SEM. Subfigure A was modified from Weishäupl et al. (2019), available for use via `https://doi.org/10.1074/jbc.RA118.005801` under the CC BY 4.0 license (`https://creativecommons.org/licenses/by/4.0/`

4.2.3 Ataxin-3 isoforms do not affect the mitochondrial potential and cell cycle

MJD pathology is characterized by a loss of neurons mainly in *cerebellum*, *putamen*, *cingulate cortex*, *precentral gyrus* and *parietal lobe* (Lopes et al., 2013). The exact mechanism which is leading to the toxic gain of function in ataxin-3 remains unknown so far. Due to the variation of MJD pathology and aao between different genetic subtypes (Gaspar et al., 2002), it can be assumed that the SNP combination in ataxin-3 has an effect on ataxin-3 toxicity. In order to prove this hypothesis, ataxin-3 isoforms were characterized regarding their toxicity in the HEK 293T *ATXN3* KO model.

The toxicity of ataxin-3 isoforms was measured using a mitochondrial potential assay where the depolarization of mitochondria was analyzed as a measure of toxicity. EGFP-ataxin-3 transfected cells were stained with the mitochondrial membrane potential probe JC-1 48 h post transfection. In its monomeric form JC-1 emits green fluorescence; however, in high concentrations JC-1 starts to form aggregates changing the emission spectrum of the dye to an emission in the red area of the visible spectrum. JC-1 can be used to assess the membrane potential of mitochondria as JC-1 accumulates in polarized (high membrane potential) mitochondria. Upon depolarization (lower membrane potential), the monomeric form of JC-1 can be detected leading to a decrease in the red fluorescence measurement. The mitochondrial membrane potential of cells transfected with ataxin-3 isoforms was measured and compared to empty vector transfected cells (negative control) and cells treated with 10 µM CCCP (positive control) for two hours (Figure 4.20 A). Cell populations were gated based on their red and green JC-1 fluorescence signal into a healthy cell population and a depolarized population whereat the positive and negative control were used to define both populations. Differences in the mitochondrial potential of HEK 293T *ATXN3* KO cells transfected with ataxin-3 isoforms could not be found (Figure 4.20 B). 10 % of the ataxin-3 transfected cells as well as the empty vector transfected cells were depolarized. The polyQ expansion did not have an influence on this depolarization. The CCCP treatment strongly increased the fraction of depolarized cells to around 90 %.

Minor toxic effects which do not lead to a certain mitochondrial stress cannot be analyzed using this mitochondrial potential assay. However, if ataxin-3 stresses the cell, expression of a toxic ataxin-3 isoform presumably impacts cell cycle progression. One possibility to analyze the cell cycle distribution of a certain cell population is to measure the DNA content (Tobey and Crissman, 1972; Krishan, 1975). This is usually performed by a microfluidic approach after a DNA staining with DAPI or propidium iodite. This DNA staining also allows for the assessment of DNA fragmentation which can occur during apoptosis (Wyllie, 1980; Gorczyca et al., 1992). Therefore, the assay can be also used to measure apoptosis by analyzing the $SubG_1$ population which corresponds to cells that have a lower DNA content than cells in the G_0/G_1 phase (Riccardi and Nicoletti, 2006).

To analyze the potential toxic effects of ataxin-3 isoforms, KO cells were transfected with EGFP-ataxin-3 isoforms and grown for 48 h. Afterwards individual cells were screened for their nucleic acid content after a DAPI staining in order to determine the current step in the cell cycle using the NucleoCounter NC-3000. Cell count was plotted over the DAPI staining intensity and cells were gated into $SubG_1$, G_1, S and G_2m subpopulations according to their staining intensity (Figure 4.20 C). As expected the majority of cells showed a diploid chromosome content

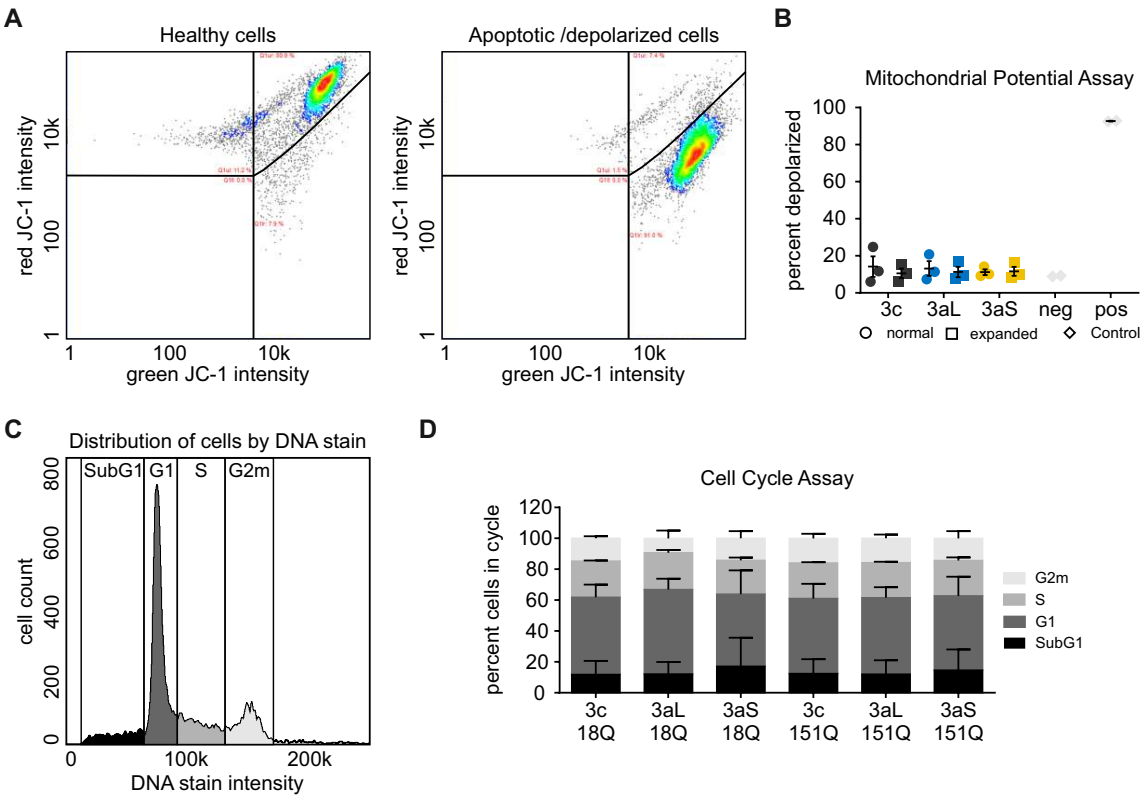

Figure 4.20. Toxicity of ataxin-3 isoforms. (A) Representative example of the cell cycle analysis for EGFP-ataxin-3 transfected cells after DAPI staining and gating of cells into SubG1-, G1-, S- and G2m-phase. The majority of cells showed the diploid chromosome content of the G1-phase. 20 % of the cells were in the S-phase, another 10 % to 15 % showed the double diploid chromosome content of the G2m phase. **(B)** No differences could be found between ataxin-3 isoforms, independent of the polyQ expansion (Kolmogorov-Smirnoff test with Hommel-adjustment for multiple comparisons). Normal as well as expanded ataxin-3aS showed a mild increase in the SubG1 population accompanied by a decrease in the G1 population. **(C)** Example of the negative (no treatment) and positive control (10 µM CCCP treatment for 2 h) of the mitochondrial potential assay used to assess differences in the toxicity of ataxin-3 isoforms. Healthy cells show an intense green and red JC-1 fluorescence. Upon depolarization of mitochondria, the signal of the red JC-1 fluorescence decreases. **(D)** No differences in the mitochondrial membrane potential could be found for EGFP-ataxin-3 isoform transfected cells 48 h post transfection. All cells show a comparable amount of depolarization that was also observed in empty vector transfected cells. Data is represented as arithmetic mean ±SEM.

associated with the G1 phase (approximately 50 %, Figure 4.20 D). Around 20 % of the cells were undergoing replication of the DNA in the S-phase and another 10 % to 15 % showed a double diploid DNA content associated with the G2m-phase. No differences in the subpopulations could be found between ataxin-3 isoforms or normal and expanded ataxin-3. Ataxin-3aS however, showed a mild increase in the SubG1 population that is associated with apoptotic cells (Gao et al., 2016) and at the same time shows a reduced population size of cells in the G1 phase. This slight increase in SubG1 could be observed for normal as well as expanded ataxin-3aS.

4.3 Mutual interaction of ataxin-3 isoforms

4.3.1 Ataxin-3 isoforms can have an influence on each other's stability[8]

For all characterizations described, only one specific ataxin-3 isoform was analyzed. However, in patients, two alleles of the *ATXN3* gene are present, i. e. a normal and an expanded allele. Therefore it was tested if both influence each other mutually as it was previously described that ataxin-3 is able to interact with itself (Todi et al., 2007). It was of special interest to test if this mutual interaction specifically depends on the isoform-combination. Therefore, combinations that are frequently observed in patients (Gaspar et al., 2002; Martins et al., 2006; Dengler, 2018) were used.

In order to analyze if a simultaneous expression of two ataxin-3 proteins of different isoform has an effect on ataxin-3 stability, co-transfections of isoforms were performed. This required constructs which allow a differentiation between ataxin-3 isoforms. Therefore, pcDNA3.1-FLAG-*hMJD1*-V5 constructs were created by introducing the *hMJD1* cDNA into the pcDNA-FLAG-PrePro-*hMJD1*-001-060-V5-His vector (Figure 4.21 A & B). Ataxin-3 was amplified from pTRE-*hMJD1*c18CAG$_{GG}$ using the primers R267 and R268 in order to introduce a 3' XbaI site. The PCR product was then subcloned using BamHI and XbaI generating a pcDNA3.1-FLAG-*hMJD1*c18CAG$_{GG}$-V5-His construct which was verified using the primers 2636, F023, F691 and I866. In the second step the C-terminal His-tag was removed by introduction of an ochre stop codon at the end of the V5-tag (Figure 4.21 C & D). The V5-tag of this construct was amplified using R269 and R270 in order to introduce the TAA signal. The product was then subcloned using XbaI and AgeI resulting in the final construct pcDNA3.1-FLAG-*hMJD1*c18CAG$_{GG}$-V5. Ataxin-3 isoforms from pEGFP-C2-*hMJD1* were cloned into this vector using PpuMI and XbaI and sequenced using the primer I866. Lastly, expanded constructs were generated by an exchange of the poly CAG region and the SNP rs1048755 from G$_{634}$TG to A$_{634}$TG using EcoRI and PpuMI fragments from pEGFP-C2-*hMJD1*-73CAG and -151CAG vectors. Sequence verification was performed using I866.

The expression of one protein was regulated using the Tet-off system while the other isoform was expressed constitutively. Both isoforms could be expressed in HEK 293T *ATXN3* KO cells and the allelic variants could be distinguished by their respective protein size (Figure 4.22 A). However, for technical reasons it was not possible to separate the untagged ataxin-3c from the FLAG-ataxin-3-V5. Therefore, ataxin-3c stability was analyzed under co-expression of Strep-FLAG-tagged ataxin-3 isoforms. The usage of a different backbone vector did not affect the outcome of the experiment (see A.2, page A16). The presence of a second ataxin-3 protein allele had a stabilizing effect on ataxin-3 degradation depending on the isoform combination (Figure 4.22 B). This clearly shows that ataxin-3 isoforms can mutually change their own physiological characteristics (Weishäupl et al., 2019).

[8] Results first published in Weishäupl et al. (2019).

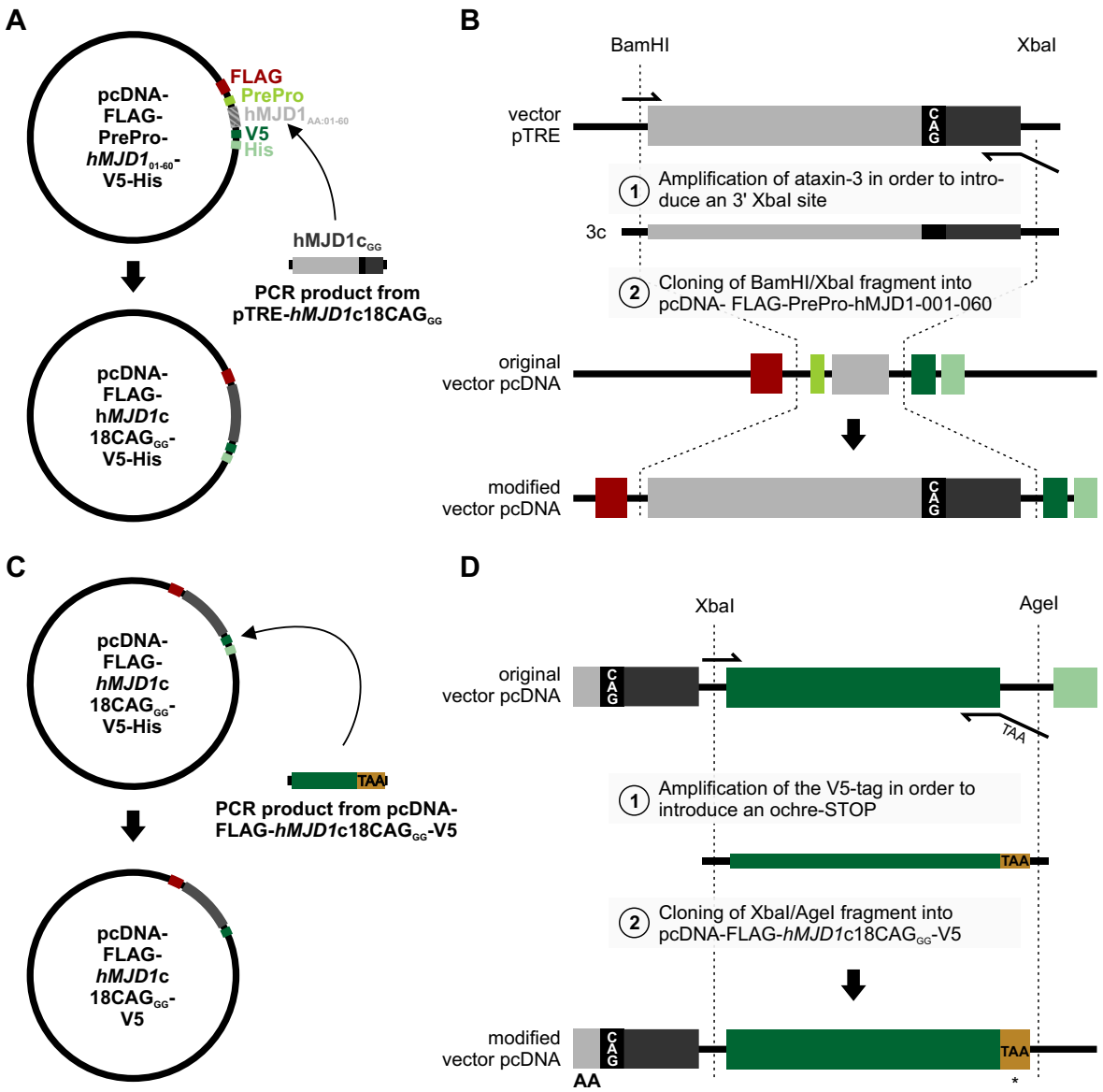

Figure 4.21. Cloning strategy for the generation of pcDNA3.1-FLAG-*hMJD1*-V5 constructs. (A & B) In order to generate FLAG-*hMJD1*-V5 constructs, AAs 01-60 of the pcDNA-FLAG-PrePro-*hMJD1*-001-060-V5-His construct were replaced by a PCR product of the full ataxin-3c cDNA that was amplified using R267 and R268. The PCR product was cloned into the vector after BamHI and XbaI digestion resulting in the expression construct pcDNA-FLAG-*hMJD1*c18CAG$_{AG}$-V5-His. **(C & D)** Afterwards, the His-tag was removed by the introduction of an ochre stop signal that was added using the primers R269 and R270. After amplification of the V5 tag from the construct, the tag was replaced by the V5-stop PCR product using XbaI and AgeI resulting in the pcDNA-FLAG-*hMJD1*c18CAG$_{AG}$-V5 vector.

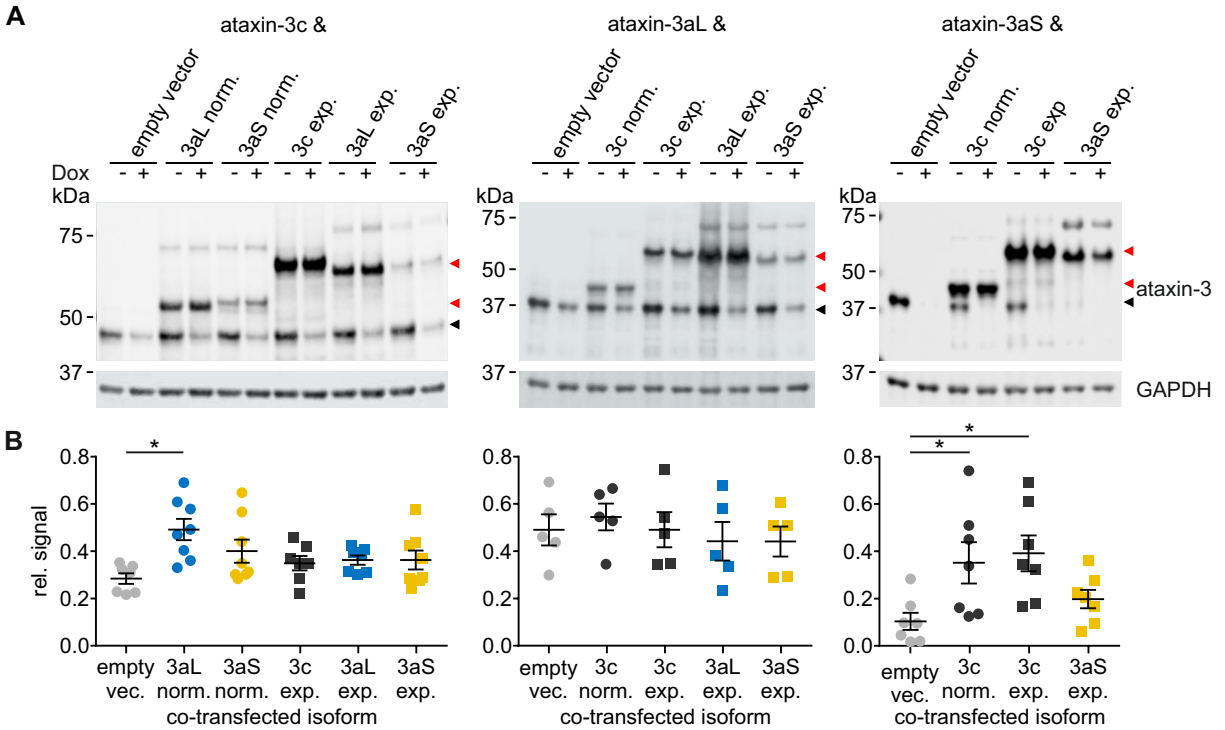

Figure 4.22. Stability of normal ataxin-3 under co-expression of ataxin-3 isoforms.
(A) Co-expression of ataxin-3 isoforms was performed in HEK 293T *ATXN3* KO cells in order to analyze the stability. Strep-FLAG-ataxin-3 (3c) or FLAG-ataxin-3-V5 (3a) were expressed constitutively whereas the expression of untagged ataxin-3 could be controlled using the Tet-off system. A usage of identical vector backbones was not possible due to technical reasons. However, no differences between the vector backbone could be observed in previous experiments. Cells were Doxycycline treated 24 h post transfection and cells were harvested and processed for western blot after a 32 h treatment. Immunostaining was performed against ataxin-3 (1H9) and GAPDH. **(B)** Relative ataxin-3 stability was calculated for the individual isoforms under co-expression with an empty vector as well as for specific combinations of isoforms. Ataxin-3c was stabilized under co-expression of non-expanded ataxin-3aL compared to the empty vector control. A stabilizing effect could also be found for ataxin-3aS under co-expression with ataxin-3c independent of the polyQ expansion. The stability of ataxin-3aL was not modified by the presence of another ataxin-3 protein allele. One-way ANOVA with Tukey's HSD test, * $p < 0.05$, $n = 5$-7. Data is represented as arithmetic mean ±SEM. Figure was modified from Weishäupl et al. (2019), available for use via `https://doi.org/10.1074/jbc.RA118.005801` under the CC BY 4.0 license (`https://creativecommons.org/licenses/by/4.0/`).

4.3.2 Ataxin-3 isoforms have an influence on each other's aggregation[9]

Observing a mutual influence of ataxin-3 isoforms on physiological characteristics raised the question if such an interplay between ataxin-3 isoforms also exists for pathophysiological characteristics. Therefore, 151Q ataxin-3 isoforms were co-expressed with normal 18Q ataxin-3 isoforms for 72 h. Filter retardation assay indeed revealed a reduced amount of aggregates in the presence of a non-expanded ataxin-3 allele (Figure 4.23 A). This effect however, was not specific for a certain combination of ataxin-3 isoforms but could be observed for all combinations (Figure 4.23 B). This confirms a protective function of the normal ataxin-3 protein allele as it was previously described (Warrick et al., 2005).

These two experiments confirm that a mutual influence of ataxin-3 isoforms exists that is modifying physiological as well as pathophysiological characteristics of the protein. This clearly suggests that ataxin-3 isoforms are playing a differential role in their physiological function and are contributing differently to the pathogenesis of MJD (Weishäupl et al., 2019).

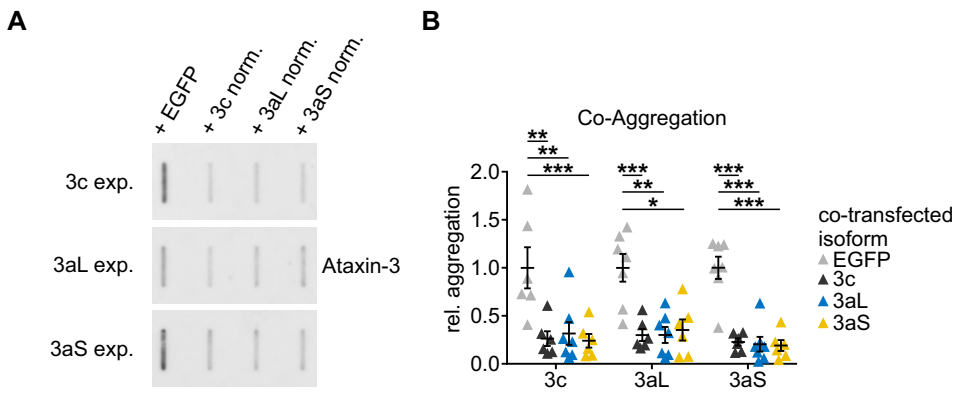

Figure 4.23. Aggregation behavior of ataxin-3 under co-expression of ataxin-3 isoforms. (A) Expanded 151Q ataxin-3 was co-expressed with non-expanded 18Q ataxin-3 isoforms or EGFP in HEK 293T *ATXN3* KO cells for 72 h and homogenates were analyzed by filter retardation assay stained for ataxin-3 (1H9). **(B)** Co-transfection of expanded together with non-expanded ataxin-3 led to a reduction in the amount of aggregates compared to a co-expression of EGFP in an isoform independent manner. One sample t-test with Hommel-correction, ** $p < 0.01$, *** $p < 0.001$, n = 6-7. Data is represented as arithmetic mean ±SEM. Figure was modified from Weishäupl et al. (2019), available for use via `https://doi.org/10.1074/jbc.RA118.005801` under the CC BY 4.0 license (`https://creativecommons.org/licenses/by/4.0/`).

[9]Results first published in Weishäupl et al. (2019).

4.4 Generation of an ataxin-3a isoform-specific antibody

Specific detection and identification of ataxin-3 isoforms requires specific antibodies which are able to distinguish the individual variants by their C-terminus. A multitude of ataxin-3 antibodies is available; however, none of these is directed against the ataxin-3a C termini (Table 4.1).

Table 4.1. Frequently used anti-ataxin-3 antibodies. This table summarizes frequently used anti-ataxin-3 antibodies and their binding epitope. C-terminal antibodies are both directed against the C-terminus of ataxin-3c.

Antibody	Epitope	Immunogen	Source
anti-3c (SA3637)	C-terminus	peptide	Schmidt et al. 1998
ABIN2205691	C-terminus	peptide	antibodies-online, Aachen, Germany
MJ2-5-3	center	protein	Wang et al. 1997
AK A-5 (sc-393193)	center	peptide	Santa Cruz Biotechnology, Heidelberg, Germany
AK A-7 (sc-398114)	center	peptide	Santa Cruz Biotechnology, Heidelberg, Germany
MAB5360 (1H9)	center	peptide	Merck, Darmstadt, Germany
OAAB05835	center	peptide	Aviva Systems Biology, San Diego, CA, USA
PAB1728	N-terminus	peptide	Abnova, Taipei City, Taiwan
ARP50507	N-terminus	peptide	Aviva Systems Biology, San Diego, CA, USA
ab96316	N-terminus	fragment	Abcam, Cambridge, UK
13H9L9	n. d.	protein	Thermo Fisher Scientific, Karlsruhe Germany
Anti-ataxin-3	n. d.	protein	Paulson et al. 1997a
anti-ATXN3	n. d.	protein	Breuer et al. 2010
Thio-At-3 Q20	n. d.	protein	Doss-Pepe et al. 2003
Z46	n. d.	protein	Shehi et al. 2003
5TF1-1C2	polyQ	TBP	Merck, Darmstadt
MW1	polyQ	DRPLA	Ko et al. 2001

Ataxin-3 isoforms only differ in their last 15 - 30 AA (Figure 4.24 A). An isoform-specific antibody was previously generated against the C-terminus of ataxin-3c (Schmidt et al., 1998). However, the C-terminal amino acid sequence of both ataxin-3a isoforms is highly hydrophobic with a mean hydrophobicity score of around 1 – 1.5 as analyzed by Expasy using the Kyte and Doolittle method (Kyte and Doolittle, 1982; Gasteiger et al., 2003, Figure 4.24 B). This is in great contrast to the mainly hydrophilic C-terminus of ataxin-3c. In regard to immunization and the generation of an antibody, hydrophobic sequences are highly problematic as they are (I) insoluble and unstable in the blood, (II) not exposed in aqueous solutions and therefore (III) poor antigens. However, due to the high sequence homogeneity of all three isoforms, these differing peptide sequences had to be used as an immunogen for the immunization of rabbits in

order to create antibodies that allow a discrimination of all three ataxin-3 isoforms. In order to achieve this, three different peptides should be used for immunization, the whole ataxin-3aL C terminal sequence (peptide A, composed of the 3aL and 3aS sequence), the ataxin-3aL (peptide B) and the ataxin-3aS C-terminus (peptide C). Antibodies raised against the shared ataxin-3aS C-terminal sequence are expected to detect both, ataxin-3aL and ataxin-3aS, while antibodies directed against the whole C-terminus and the ataxin-3aL-specific peptide are able to recognize ataxin-3aL (Figure 4.24 C). Peptide synthesis, purification, generation and purification of the antibody was performed in cooperation with Dr. Kalbacher from Medizinisch-Naturwissenschaftliches Forschungszentrum (Tübingen). The C-terminal peptides coupled to keyhole limpet hemocyanin were insoluble and needed to be synthesized coupled to a highly hydrophilic sequence to keep them in solution for the peptide purification and immunization.

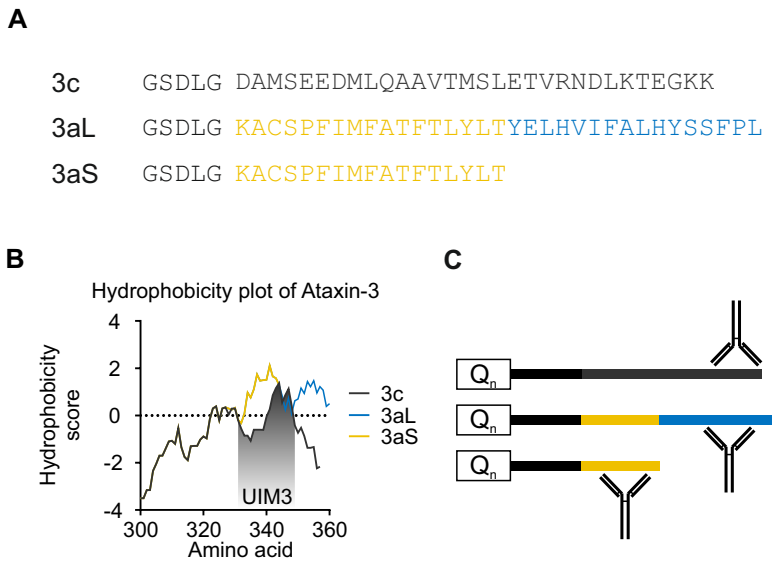

Figure 4.24. Strategy for the generation of a anti-3a-specific ataxin-3 antibody. **(A)** Ataxin-3 isoforms only differ in their last 15 AA to 30 AA. **(B)** For ataxin-3aL and ataxin-3aS this peptide sequence contains highly hydrophobic amino acids, which is especially true for the C-terminus of ataxin-3aS. The C-terminus of ataxin-3c shows a mixture of hydrophobic and hydrophilic peptides and is in general hydrophilic. **(C)** Antibodies should be generated against these C-terminal peptides of ataxin-3aL and -3aS. One antibody should be capable of recognizing both ataxin-3aL and ataxin-3aS (3aS-specific). The other antibody was directed against the 3aL-specific peptide and therefore should only recognize ataxin-3aL.

In order to choose rabbits that do not show an unspecific signal at the respective size of ataxin-3 in a western blot, six rabbits were analyzed preliminary to the immunization. This analysis of antisera should allow for the detection of an appearing signal during immunization. Two cell lines as well as a brain lysate of 148Q SCA3 mice (Boy et al., 2010) were analyzed by SDS-PAGE and western blot. Immunostaining was performed with a 1:200 dilution of the rabbit antisera in TBS supplemented with 0.1 % (v/v) Tween-20. Three animals (3, 4 and 5) showed multiple bands in the size range of ataxin-3 between 37 kDa and 50 kDa (Figure 4.25). Animals 1, 2 and 6 did not show signals in this range. Therefore, these rabbits were chosen for an immunization. Rabbits were immunized with a mixture of all three peptides. Differentiation between the antibodies should be achieved post immunization by affinity chromatography against the individual peptides.

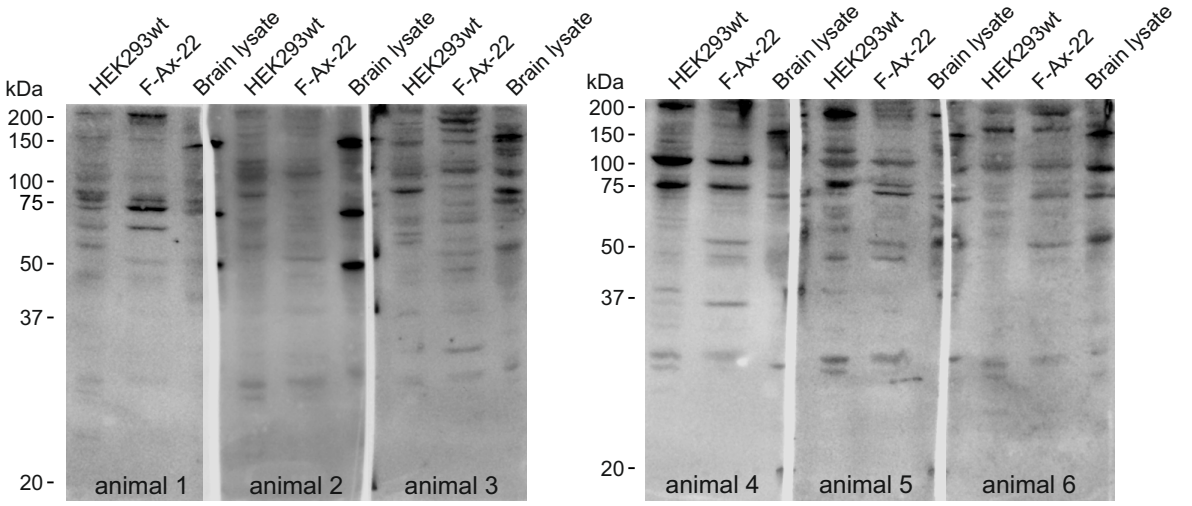

Figure 4.25. Analysis of rabbit antisera before immunization. Rabbit antisera were analyzed before immunization in order to exclude a background signal in the size range of ataxin-3 so that an appearing signal during immunization can be detected. Two cell lines as well as a brain lysate of MJD mice were analyzed after SDS-PAGE and western blot with a 1:200 dilution of the rabbit antisera in TBS supplemented with Tween-20. Three animals (3, 4 and 5) showed multiple bands in the size range of ataxin-3 between 37 to 50 kDa. Animals 1, 2 and 6 did not show such signals and were therefore chosen for the immunization.

The rabbit immunization was performed by Pineda Antibody Service (Berlin). The immune-reaction was boosted every 30 days starting from day 61. post immunization. Exsanguination was performed at day 630 before antibodies were purified from the rabbit antisera (Figure 4.26 A). The immunization process was verified by both, ELISA and western blot. ELISA was performed against the immunization peptides which were coupled to the plate and detected using the diluted rabbit antisera as well as an HRP-coupled secondary antibody. ELISA confirmed that the animals show an immune-response against the peptides at later stages of the immunization (exemplary shown for rabbit 1 and peptide B, Figure 4.26 B). However, this immune-response could not be observed on western-blot against whole cell lysates of FLAG-ataxin-3-V5 transfected HEK 293T *ATXN3* KO cells which were detected with the rabbit antisera (Figure 4.26 C). Pre- and post immunization antisera of all three animals showed multiple protein bands and none of these bands corresponded to ataxin-3aL or ataxin-3aS. Further, no specific signal appeared after the immunization. Differences in signal intensities or position could only be found between animals and time points but not between ataxin-3 isoforms.

Rabbit antisera from day 630. were tested in an ELISA for their immune-reaction against all three immunization peptides. All rabbits showed a strong affinity reaction against the 3a-specific peptide B (Figure 4.27 A). Animals 2 and 3 also showed a weaker reaction against the 3aL-specific C and 3a-specific peptide A. Based on these results the antibodies were purified using the 3a-peptide. Purification peptides carried a modified linker sequence in order to prevent a cross-purification of antibodies directed against the hydrophilic linker sequence (KERE-peptide-EE instead of KEFA-peptide). Peptides were purified by HPLC and fractions were collected manually. Dilution of peptides in HPLC system A buffer was problematic and only possible when the peptides were predissolved in DMSO. In order to prevent a precipitation of peptides, the volume of HPLC system A buffer needed to be optimized for every single peptide slightly. HPLC showed a clear peak at the expected retention time of peptide 2 (Figure 4.27 B). Other

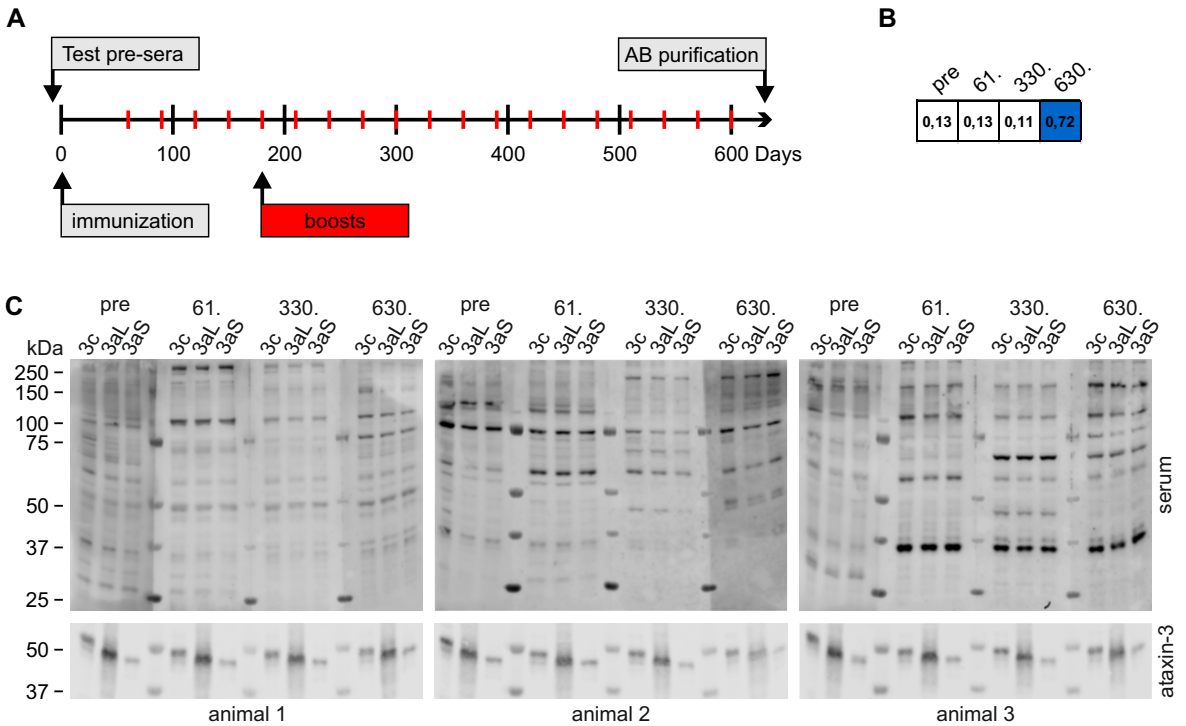

Figure 4.26. Immunization analysis of rabbit antisera. **(A)** Schematic representation of the immunization process. Immunization of the rabbits was performed on day 0 followed by a first boost after 61 days. Boosts were repeated every 30 days. **(B)** The immunization process was followed by ELISA throughout the 630 days until exsanguination and purification of antibodies. A signal against the 3aS-specific peptide (4/9) was obtained after the immunization process as shown exemplary for rabbit 1 antisera in a dilution of 1:1000. **(C)** Rabbit antisera were tested in western blot for their specificity against ataxin-3 isoforms at the different time points throughout the immunization process. No specific signal could be obtained for the antisera of rabbit 1, 2 and 3 before or after the immunization.

peaks next to the respective peptide could be detected additionally. Those signals were associated to oxidized peptides or shorter peptides lacking single AAs. The identity of peptide 2 could be confirmed by measuring its mass using MS (Figure 4.27 C). The mass of 2451.80 Da equates to the AA sequence with a monoisotopic weight of 2451.21 Da. An affinity matrix was created by coupling the peptide to CNBr activated sepharose. Purification of the antibody from rabbit serum was performed by affinity chromatography using this chromatography medium overnight at 4 °C. The eluted antibody was then concentrated and afterwards tested by ELISA against the respective immunization peptide. The ELISA showed that the antibody could be purified from the serum and that purification increased the reactivity against the peptide (Figure 4.27 D).

Affinity purification of the rabbit antisera should result in a specificity-increase of the antibody as undesired immunoglobulins are depleted so that they cannot cause an unspecific background signal. In order to test the specificity of the purified anti-3a antibody, it was tested against whole cell lysates from FLAG-ataxin-3-V5 transfected HEK 293T *ATXN3* KO cells. Membrane was immunodetected using different antibody dilutions ranging from 1:200 to 1:5000 as well as two different detergents, Tween-20 and Triton X-100 (Figure 4.28 A). All dilutions showed multiple protein bands comparable to the original rabbit serum. Higher dilutions of the antibody resulted in a reduction of background signal but did not reduce the vast number of unspecific bands. In general, the usage of Triton X-100 instead of Tween-20 changed band intensities but did not increase specificity. Further, it did not result in the appearance of other signals.

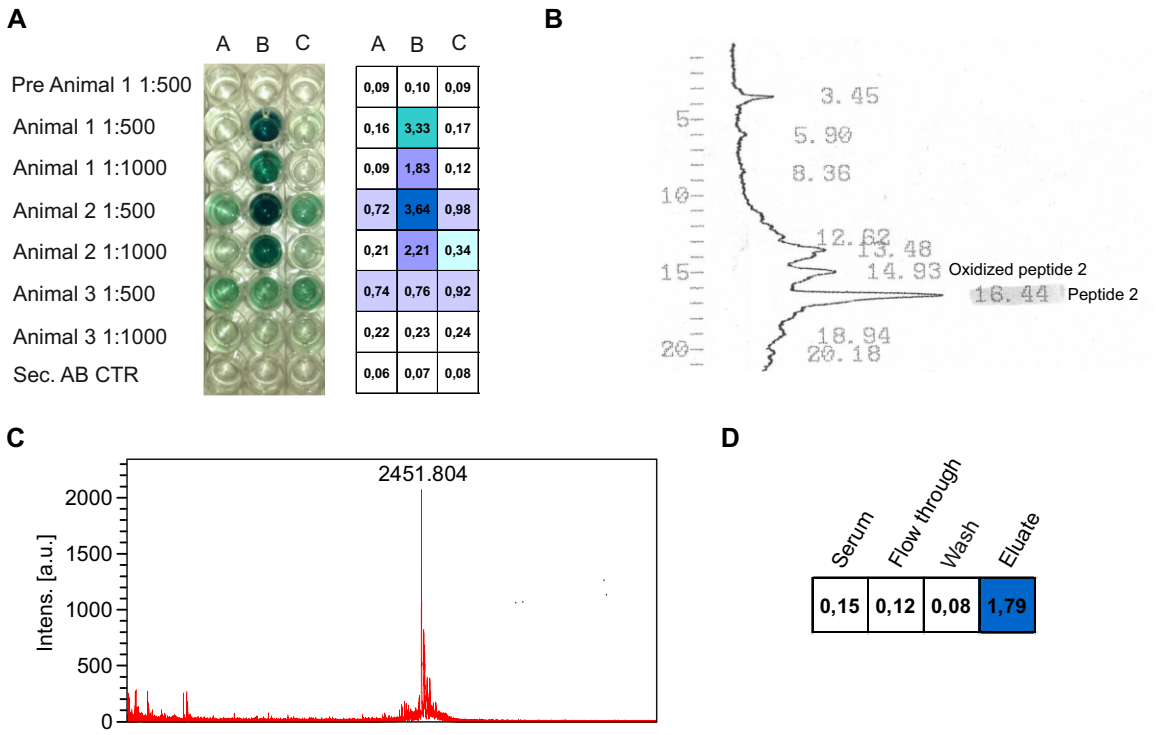

Figure 4.27. Purification of the anti-3a-specific antibody. **(A)** Rabbit antisera were tested before purification by ELISA against the peptides used for immunization. All rabbits show a strong signal against the 3aS-specific peptide (B). Rabbit 2 and rabbit 3 also show a weak affinity against the 3aL-specific (C) and 3a-specific (A) peptides in higher concentrations. **(B)** Due to the strong response of the post-immunization antisera, antibodies against peptide B were HPLC purified. A new peptide (2) was synthesized carrying a modified hydrophilic sequence in order to prevent the purification of antibodies against the former hydrophilic linker. HPLC fractions were collected manually dependent on their retention time. The predicted retention time for peptide 2 was around 16 min. A second peak caused by oxidized peptide 2 was found next to the specific peak of the peptide. **(C)** The identity of peptide 2 was verified using MS. The measured mass equates to the mass of the peptide. **(D)** The antibody was purified from the rabbit antisera against peptide 2. The purified anti-3a-antibody was then tested in an ELISA against peptide B. Concentrated eluate of the antibody anti-3a shows a strong affinity against the 3a-specific peptide.

In the next step it was tested if the antibody is directed against the C-terminal peptide sequence of ataxin-3aL and ataxin-3aS. Therefore, the specific paratopes of the antibody should be blocked with the epitope prior to an immunodetection. This blocking should result in an absence or weakening of the specific signal. A 1:200 anti-3a antibody dilution was therefore preincubated with the purification peptide 2 for 24 h before a dot blot of purified GST-ataxin-3 was immunodetected (Figure 4.28 B). It could be shown that the ataxin-3aL and ataxin-3aS signal was reduced after pre-absorption of the antibody compared to the original anti-3a antibody. Therefore, it can be concluded that the antibody is capable of recognizing the ataxin-3aL and ataxin-3aS C-terminal peptide sequence.

As the purified antibody showed a reaction against the immunization peptide but no specific reactivity against crude cell culture lysates in western blot, it was tested if the antibody is able to specifically dissect the ataxin-3 isoforms by ELISA (Figure 4.29 A). It was found that the anti-3a antibody shows a strong reactivity against GST-purified ataxin-3aS and a weaker reaction against ataxin-3aL. An unspecific reaction against ataxin-3c could not be observed.

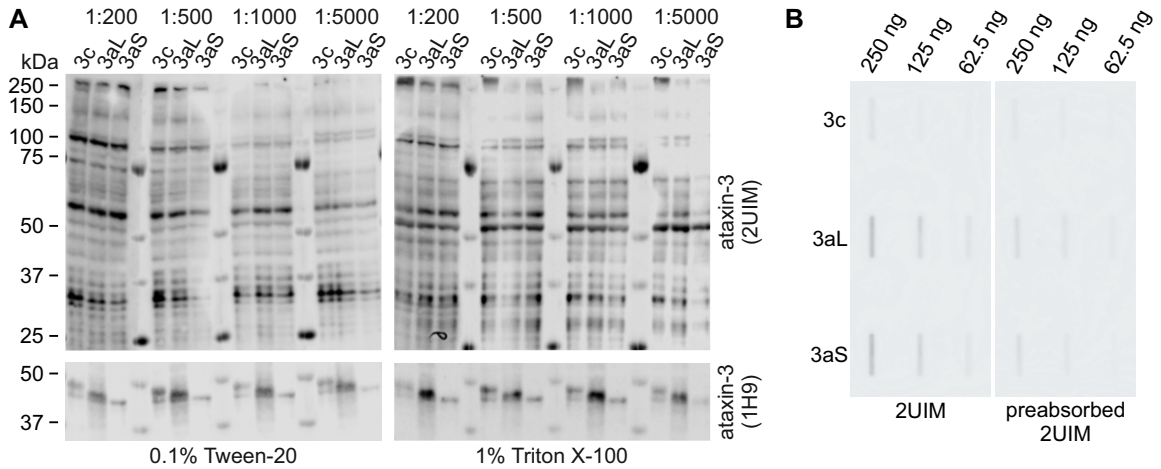

Figure 4.28. Evaluation of anti-3a antibody specificity. (A)HEK 293T *ATXN3* KO cells were transfected with pcDNA3.1-FLAG-ataxin-3-V5 constructs and samples were processed for western blot. The anti-3a-specific antibody was diluted in TBS supplemented with 0.1 % (v/v) Tween-20 or 1 % (v/v) Triton X-100 in a range between 1:200 and 1:5.000. Neither a variation of the dilution factor, nor a change of the detergent allowed a specific detection of ataxin-3aL or ataxin-3aS. **(B)** The anti-3a-specific antibody was preabsorbed with the purification peptide syro 2 for 24 h in order to specifically block the paratopes of the antibody. Slot blotting with 250 ng to 62.5 ng of purified GST-ataxin-3 isoforms and staining for ataxin-3 showed that the preincubation reduced the antibody binding. Antibodies were diluted 1:200.

Purification of the antibody generally reduced the absolute signal in the ELISA compared to the raw rabbit antisera.

Purified proteins for ELISA stay natively folded and are not denatured during the assay procedure. Therefore, it was tested, if ataxin-3aL and ataxin-3aS can be specifically detected in ataxin-3 transfected HEK 293T *ATXN3* KO lysates and GST-purified ataxin-3 samples in a slot blot where proteins are neither denatured. Immunodetection showed that the anti-3a antibody was able to detect ataxin-3aS in the GST-purified samples (Figure 4.29 B). Using Triton X-100 instead of Tween-20 also allowed the detection of ataxin-3aL but reduced the signal intensities. However, the antibody did not show an isoform-specific signal for the ataxin-3 transfected cell culture lysates.

Purified GST-ataxin-3aS could be detected in ELISA and slot blot. Therefore, it was next tested if this specificity can also be observed for purified but denatured and electrophoretically separated ataxin-3 samples in a western blot. Immunostaining of ataxin-3 using the anti-3a antibody confirmed that the antibody was able to detect ataxin-3aS together with multiple protein breakdown products harboring the C-terminus in GST-purified ataxin-3 samples (Figure 4.29 C). The antibody did not show this specificity in cell culture lysates from EGFP-N2-ataxin-3 and FLAG-ataxin-3-V5 transfected HEK 293T *ATXN3* KO cells. Multiple unspecific bands could be detected in these samples.

Next to the purity of ataxin-3, one major difference between the whole cell lysates and the GST-ataxin-3 samples is the protein host. EGFP-N2-ataxin-3 and FLAG-ataxin-3-V5 isoforms were expressed in eukaryotic cell culture samples while GST-ataxin-3 was expressed in a prokaryotic system. Therefore, native PTMs may be present in the cell culture samples which prevent the anti-3a antibody from binding to the ataxin-3 C-terminus. In order to exclude this possibility Strep-FLAG-ataxin-3 was purified from HEK 293T *ATXN3* KO cells after transfection using the Strep-tag. Purified proteins were blotted onto a membrane using a slot blot system.

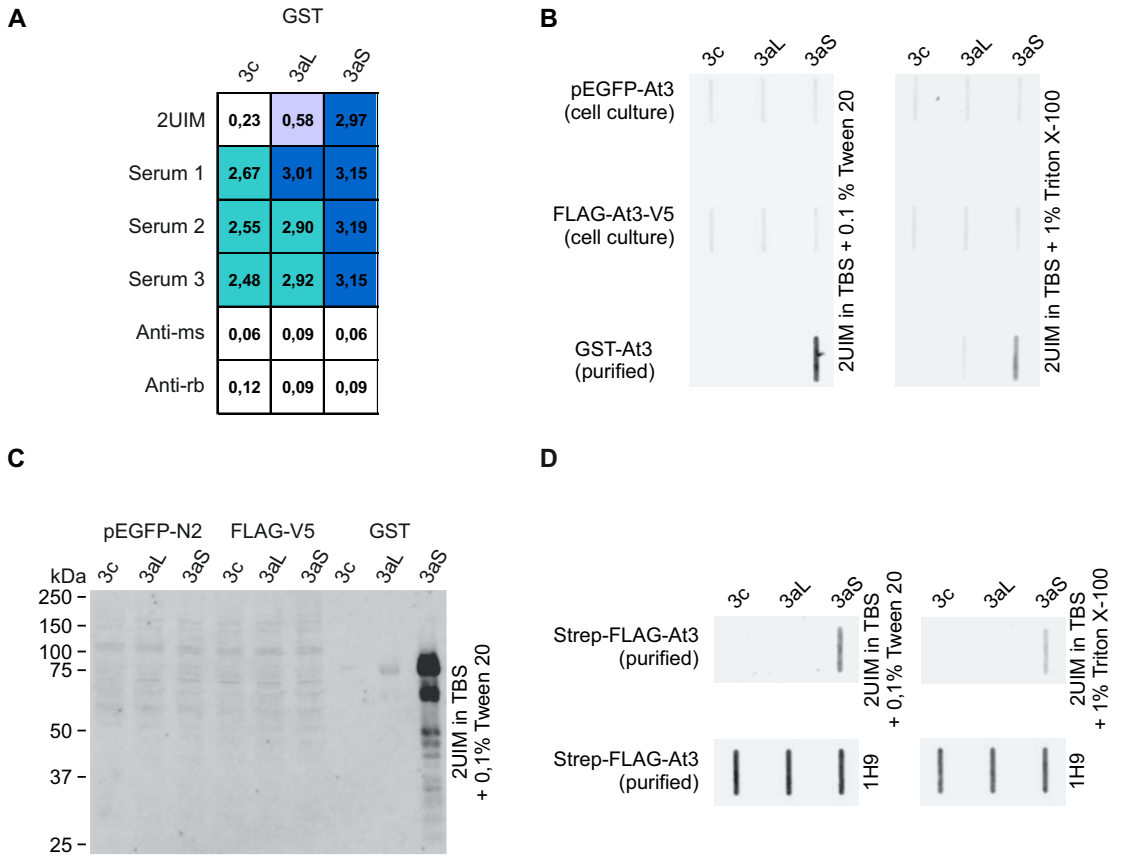

Figure 4.29. Evaluation of the specificity of the purified anti-3a antibody. (A) The purified anti-3a antibody was tested in an ELISA with immobilized GST-ataxin-3 isoforms (250 ng). The anti-3a antibody specifically detected ataxin-3aS in the purified ataxin-3 samples. Ataxin-3aL could also be detected but the signal intensity was weaker. The purification strongly improved the signal-to-noise ratio. **(B)** Slot blot with ataxin-3 isoforms from cell culture transfections (30 µg) and purified GST-ataxin-3 (250 ng, prokaryotic culture). Nitrocellulose membrane was stained for ataxin-3 using the purified anti-3a antibody (1:200). Ataxin-3aS could be detected in the GST-purified samples independent of the detergent used. However, the usage of Triton X-100 allowed the detection of ataxin-3aL but reduced the signal intensity for ataxin-3aS. **(C)** Western-blot of the cell culture and purified ataxin-3 samples. The anti-3a antibody was able to specifically detect prokaryotic GST-purified ataxin-3aS. The antibody did not show a specific signal in the cell culture samples. **(D)** Slot blot with Strep-FLAG-purified ataxin-3 isoforms from eukaryotic samples. Purified ataxin-3aS could specifically be detected with the anti-3a antibody independent of the detergent used.

Immunodetection with the anti-3a antibody showed that it also recognizes eukaryotic ataxin-3aS specifically (Figure 4.29 D). The usage of Triton X-100 again reduced the signal intensity for this detection. Therefore, it can be concluded that the antibody would require purified protein in order to specifically distinguish ataxin-3 isoforms but is not able to perform this task in a crude mixture of different proteins.

The inability of a specific detection of the ataxin-3aL/ataxin-3aS C-terminus in lysates raised the question if the C-terminus of these isoforms can be detected at all. Binding of proteins to the western blot membrane depends on the physical, chemical and physio-chemical characteristics of the membrane. Proteins are bound to nitrocellulose membranes by hydrophobic and electrostatic interactions while binding to polyvinylidene difluoride membranes is solely hydrophobic (Gershoni and Palade, 1982, 1983; Tovey and Baldo, 1989). Nylon membranes bind proteins by ionic, hydrophobic (Beeskow et al., 1997), and electrostatic interactions (Gershoni and Palade,

1983). Protein binding by hydrophobic interactions could result in embedding of hydrophobic regions on the membrane which detracts its accessibility for an antibody. Therefore, it was tested if FLAG-ataxin-3-V5 isoforms can be detected in cell culture samples by their C-terminal V5 tag on nitrocellulose, polyvinylidene difluoride and nylon membranes. Immunodetection showed that the tag can only be detected for ataxin-3c but not for the ataxin-3aL and ataxin-3aS isoforms independent of the membrane type (Figure 4.30 A). While nitrocellulose showed the strongest protein signal, nylon showed a generally high background staining. Interestingly, a bigger C-terminal EGFP tag could be detected in all three isoforms (Figure 4.30 B).

In a next step it was tested if the usage of a different buffer system as well as two different protein loading dyes improves the detectability of the V5 tag for both ataxin-3a isoforms. While electrophoresis in the so far used bis-tris gels is performed at a neutral pH, this time electrophoretic separation of proteins was performed under alkaline conditions in a tris-glycine gel. Proteins were denatured with a loading dye containing either dithiothreitol or β-mercaptoethanol prior to samples analysis by SDS-PAGE and western blot. Immunodetection using the V5 antibody and two different detergents (Tween-20 or Triton X-100) showed that neither of the modifications allowed a detection of V5 in ataxin-3aL or -3aS (Figure 4.30 C).

After inspecting the anti-3a antibody performance in immunodetections, next the antibody was evaluated using immunocytochemistry. As proteins are not bound to a blotting membrane, the antibody could show more reliable results by directly staining cells. HEK 293T *ATXN3* KO cells were transfected with pcDNA3.1-FLAG-ataxin-3-V5 isoforms before they were fixed by two different methods using either 4 % (v/v) paraformaldehyde or a 1:1 mixture of acetone and methanol. Paraformaldehyde is a commonly used fixation method (Leduc et al., 1969) as it well preserves antigenicity; however, the ultrastructure preservation is not good (McLean and Nakane, 1974). On the other hand, acetone-methanol is a denaturing fixative. While acetone permeabilizes cells, they are fixed by methanol. It is known that the tertiary structure of proteins is modified but the secondary structure is preserved using this fixative (St-Laurent et al., 2006). The fixation method therefore needs to be chosen dependent on the cellular marker studied (St-Laurent et al., 2006). As rabbits were immunized with a small peptide, a preservation of the protein tertiary structure is likely not necessary. A preservation of the cell ultrastructure however, is only necessary when subcellular ultrastructures are analyzed. Both fixation methods therefore could be used to test the anti-3a antibody.

Performing immunostainings of the fixed cells with three different anti-3a antibody dilutions and 1H9 showed that the antibody stained cells independent of ataxin-3 expression and the isoform (Figure 4.31). The counter staining for total ataxin-3 using 1H9 usually did not overlap with the anti-3a staining which shows that the anti-3a staining is unspecific. Further, cells expressing ataxin-3c were also stained by the anti-3a antibody. Comparing the paraformaldehyde and acetone-methanol fixation, it was found that an acetone-methanol fixation provides sharper and less blurry fluorescence pictures.

The previous experiments showed, that the antibody raised against ataxin-3aL and ataxin-3aS shows minor specificity against the their C-terminus. Hence, it is not suitable for application with complex protein mixtures. Therefore, it would be beneficial to either reduce sample com-

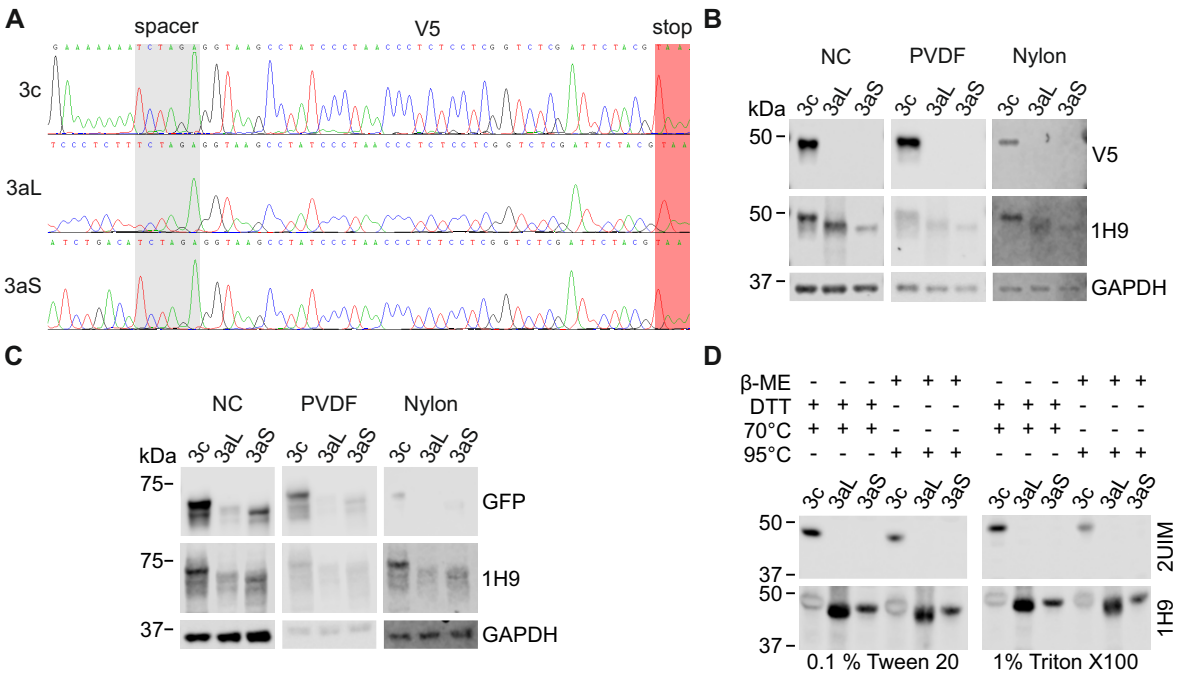

Figure 4.30. Evaluation of C-terminal ataxin-3 detections. (A) Sequence analysis of the pcDNA-FLAG-ataxin-3-V5 constructs. No frame-shift mutation could be found between the 3' end of ataxin-3 (before spacer) and the V5-tag. **(B)** HEK 293T *ATXN3* KO cells were transfected with pcDNA3.1-FLAG-ataxin-3-V5 isoforms. Cells were lysed and processed for SDS-PAGE and western-blot using bis-tris gels. Transfer was performed onto either nitrocellulose (NC), polyvinylidene difluoride (PVDF) or a nylon membrane. Membranes were stained for the V5-tagged ataxin-3 C-terminus (V5), ataxin-3 (1H9) and GAPDH. The ataxin-3 C-terminus could only be detected for ataxin-3c. In general, the NC membrane shows the strongest signal while nylon shows a high background. **(C)** In order to improve the solubility of the ataxin-3aL/ataxin-3aS C-terminus pEGFP-N2-ataxin-3 isoforms were used and membranes were stained for the C-terminal GFP-tag (GFP), ataxin-3 (1H9) and GAPDH. The big GFP-tag allowed the specific detection of the C-terminus for all ataxin-3 isoforms. **(D)** The FLAG-ataxin-3-V5 samples were also analyzed using tris-glycin gels and two different loading dyes. Samples were either denatured in β-mercaptoethanol, 95 °C, 5 min or dithiothreitol, 70 °C, 5 min. Membranes were stained for the ataxin-3 C-terminus (V5) and total ataxin-3 (1H9). V5 could only be detected for ataxin-3c using either 0.1 % (v/v) Tween-20 or 1 % (v/v) Triton X-100.

plexity, i. e. by purification or apply a second antibody to increase total specificity. Further, the antibody probably is not suitable for western blot applications. Therefore, a TR-FRET assay was performed which utilizes two different antibodies which both bind to ataxin-3 in close spatial proximity in order to generate a FRET signal which can be measured by a plate reader. This assay combines the advantages of both, time resolved measurement and FRET. Upon excitation, the donor (i. e. europium) excites a signal which itself excites the acceptor (i. e. D2). The acceptor emits a fluorescence signal that can be measured by the plate reader. A time delay between excitation and measurement reduces the overall background fluorescence (Figure 4.32 A).

FLAG-ataxin-3-V5 isoforms were expressed in HEK 293T *ATXN3* KO cells and lysates were mixed with different antibody combinations in order to allow a specific detection of either ataxin-3c, ataxin-3aL and ataxin-3aS or total ataxin-3. Measurement of the MW1/1H9 fluorescence emission signal showed that total ataxin-3 could be detected in all three lysates. Further, the anti-3c-specific antibody in combination with the antibody 1H9 allowed a specific detection of ataxin-3c. The combination of the newly generated anti-3a antibody and 1H9 however, did not allow a detection of ataxin-3 in the cell culture lysates (Figure 4.32 B).

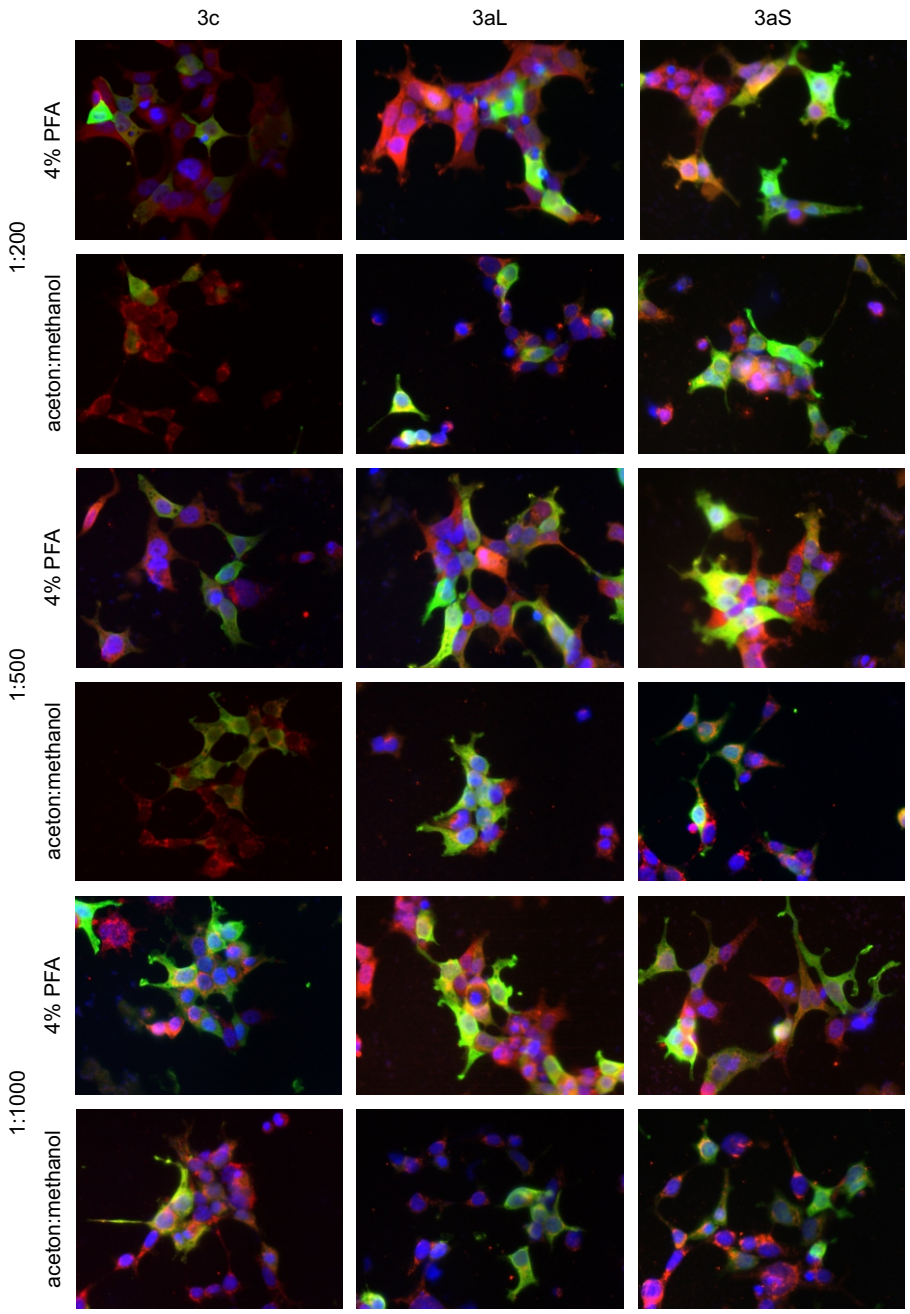

Figure 4.31. Evaluation of the anti-3a antibody using fluorescence microscopy. HEK 293T *ATXN3* KO cells were transfected with 18Q pcDNA3.1-FLAG-*hMJD1*-V5 isoforms and grown for 48 h. Cells were either fixed using 4 % (v/v) paraformaldehyde or a 1:1 solution of acetone and methanol. Cells were then stained for ataxin-3aL and ataxin-3aS using the anti-3a antibody (red) in dilutions of 1:200, 1:500 and 1:1000 and total ataxin-3 (1H9, 1:1000, green) and the nucleus (DAPI, blue). 1H9 stained ataxin-3 expressing cells while the anti-3a antibody does not show an isoform-specific staining. A anti-3a signal could be observed for all isoform conditions as well as for cells that were negative for the 1H9 staining. The staining pattern shows that the anti-3a antibody did not stain ataxin-3aL and ataxin-3aS specifically. Pictures were taken with identical exposure times for all three isoforms.

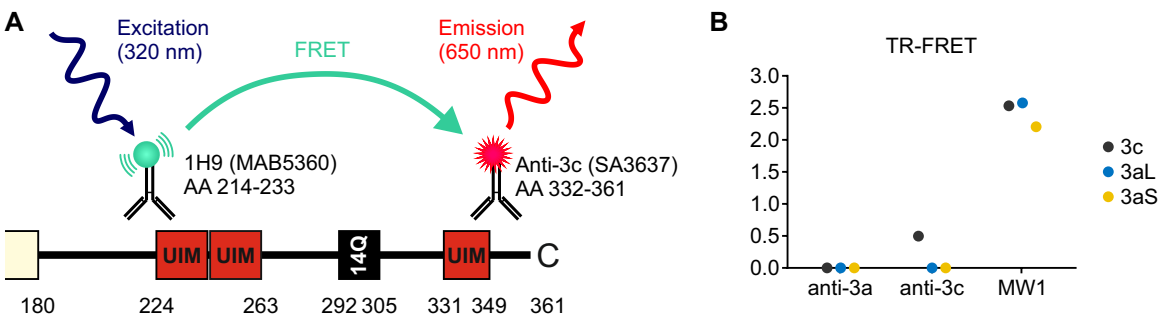

Figure 4.32. TR-FRET assay for the detection of the ataxin-3 C-terminus. (A) Principle of the TR-FRET assay using the example of ataxin-3c. Europium (coupled to 1H9) is excited at 320 nm. Upon excitation, FRET occurs between the donor fluorophore europium and the acceptor D2 (coupled to anti-3c) whose emission signal can be detected at 650 nm after a time-delay of 100 µs. FRET thereby requires a close spatial proximity of donor and acceptor and ensures that an emission can only be detected upon binding of both antibodies. **(B)** The TR-FRET assay against all ataxin-3 isoforms was performed using three antibody combinations MW1/1H9, anti-3a/1H9 and anti-3c/1H9. Due to the polyQ-binding of MW1 this antibody combination detects total ataxin-3. While the anti-3a antibody raised against the ataxin-3aL/ataxin-3aS C-terminus did not show a specific signal, the anti-3c antibody allowed a specific detection ataxin-3c. Protein structure in Subfigure A modified from Weishäupl et al. (2019), available for use via `https://doi.org/10.1074/jbc.RA118.005801` under the CC BY 4.0 license (`https://creativecommons.org/licenses/by/4.0/`

4.5 Generation of an isoform-specific MJD zebrafish model

In addition to the *in vitro* and cell culture experiments the effect of ataxin-3 isoforms should be studied in an *in vivo* MJD model. Therefore the first isoform-specific zebrafish model for MJD was generated in cooperation with the lab of Assoc. Prof. Christoph Winkler at the National University of Singapore. The Winkler lab has various established zebrafish models for several human neurodegenerative diseases (e. g. Spinal Muscular Atrophy, See and Winkler, 2013) as well as all the technology, necessary to generate transgenic zebrafish and study the pathology. Generation, housing, raising and mating of zebrafish therefore was performed by Shermaine Tay and Assoc. Prof. Christoph Winkler. The MJD zebrafish should express ataxin-3 isoforms of 18Q, 73Q and 151Q in the nervous system.

The sole expression of ataxin-3 isoforms in nervous tissue is achieved by the usage of the neuron-specific promoter HuC (*elavl3*) that is regulating the expression of a neuronal RNA-binding protein in zebrafish (Park et al., 2000). In order to allow an equal expression of ataxin-3 isoforms, a site-directed integration of the expression vector is necessary. This site-directed integration is achieved by the usage of a special line that harbors an AttP site within the zebrafish genome (Mosimann et al., 2013). The usage of a special pDestAttB vector allows a site directed integration when it is injected into fertilized eggs together with phiC31 mRNA. Transgene AttP fish are characterized by an EGFP expression in the heart, while the pDestAttB vector allows an eye-lens specific expression of venus under control of the α-crystalline promoter (Figure 4.33).

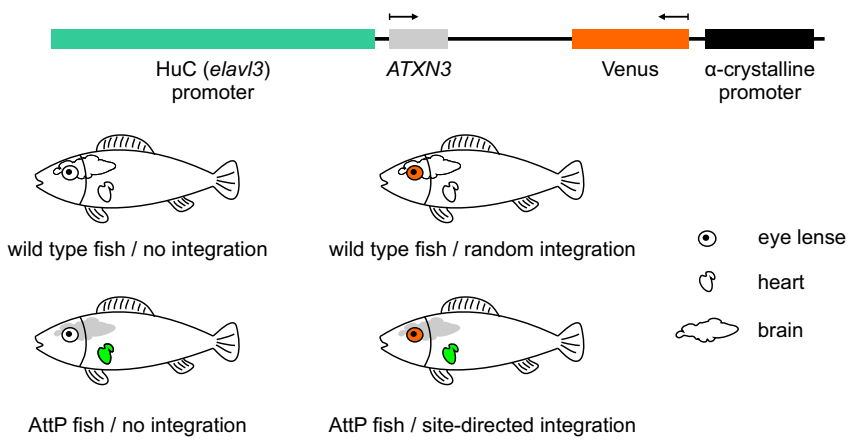

Figure 4.33. Generation of MJD zebrafish. MJD zebrafish were generated by the injection of the pDestAttB expression vector together with phiC31 mRNA into a fertilized zebrafish egg. The vector allows a neuronal expression of *ATXN3* (■) under control of the HuC promoter and an α-crystalline controlled expression of venus (■) in the eye lens. The transgene AttP zebrafish line expresses EGFP (■) in the heart. Fish positive for both, venus expression in the eye lens and EGFP expression in the heart were raised.

Generation of the zebrafish as described above required the creation of special constructs that allow the expression of *ATXN3* under control of the HuC promoter as well as of venus under α-crystalline promoter control. In order to achieve this, the HuC promoter needed to be subcloned from a pCS2-HuC:Kaede construct into the pDestAttB vector (Figure 4.34). Afterwards, ataxin-3 isoforms of 18Q, 73Q and 151Q were inserted under control of HuC.

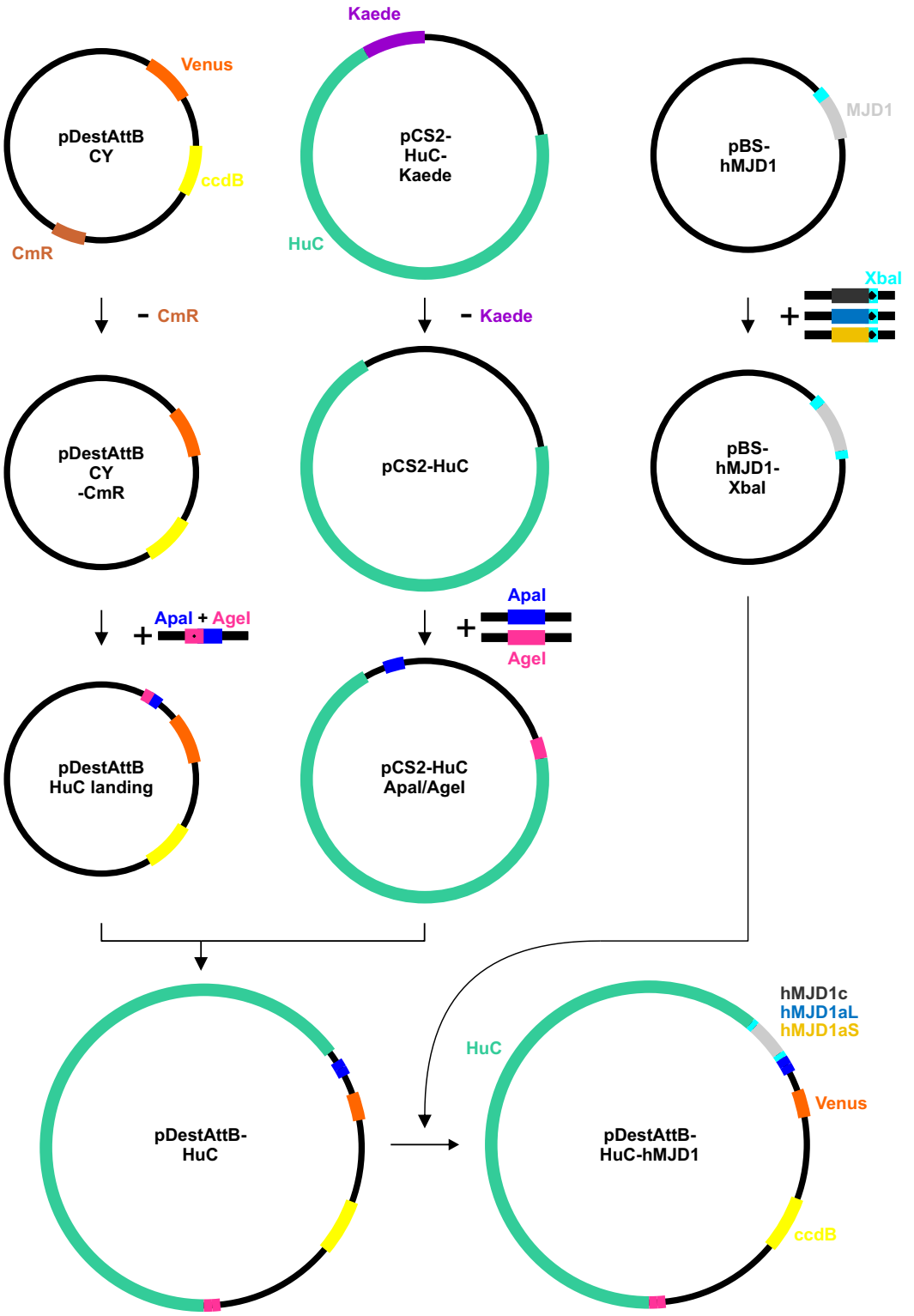

Figure 4.34. Cloning strategy for the generation of *hMJD1* AttB integration constructs. The site directed integration of the expression vector into the zebrafish genome should be achieved by the usage of the vector pDestAttB in combination with the PhiC31 integrase zebrafish line. Ataxin-3 was expressed pan-neuronally under control of the HuC (*elavl3*) promoter. An XbaI site in the pDestAttB vector was destroyed by the removal of the CmR resistance in order to allow a later cloning of ataxin-3 cDNA using XbaI. The fluorescent protein kaede was removed from the pCS2-HuC-Kaede vector and restriction enzyme recognition sites were introduced in both vectors in order to facilitate the integration of the HuC promoter and

Continued on next page

Figure 4.34 Cloning strategy for the generation of *hMJD* AttB integration constructs - *continued from previous page*
polyA region into the pDestAttB vector using ApaI and AgeI creating the final vector for the introduction of ataxin-3 pDestAtt-HuC. Ataxin-3 isoforms were cloned into the pBluescript vector with an additional 3' XbaI recognition site that allowed the undirected integration of ataxin-3 into the pDestAttB-HuC vector. All three ataxin-3 isoforms with 73 and 151CAG repeats were cloned into this vector.

The pCS2-HuC:Kaede construct containing the HuC promoter was received from the RIKEN Brain Science Institute, Japan. The pDestAttB/CY vector for the targeted integration of HuC:ataxin-3 into the zebrafish genome was received from Dr. Mosimann (Mosimann et al., 2013). A detailed cloning procedure can be found in A.3 (Figures A.2, A.3, A.4 and A.5, page A17 ff.). Final expression vectors were sequenced by sanger sequencing and one vector in addition by NGS to clarify the whole vector structure. NGS sequencing confirmed the successful generation of the constructs. The new vector pDestAttB-HuC-*hMJD1* allows the integration of the whole vector into the AttP landing site of the zebrafish offspring, the easy identification of transgene-carriers by the tissue-specific expression of venus in the eye lens as well as the neuron-specific expression of ataxin-3 isoforms to study MJD pathology in detail.

Offspring from the crossing of the AttP lines and WT zebrafish were injected with phiC31 integrase mRNA together with the respective pDestAttB-HuC-*hMJD1* vector. The newly generated transgene offspring with an expression of venus in the eye lens as well as an expression of EGFP in the heart was raised. The expression of venus in the lens is a marker for the integration of the vector into the genome and the expression of EGFP in the heart is a marker for an AttP harboring fish. Fish just positive for either venus or EGFP were put down as well as fish that did not show a fluorescence expression. 18Q as well as 73Q founders could be identified for all isoforms.

In order to confirm the correct insertion of the pDestAttB-HuC-*hMJD1* construct, DNA was isolated from 5 days post fertilization (dpf) to 6 dpf zebrafish larvae followed by PCR amplification of four different main regions of the vector: (1) 5' HuC, (2) 3'HuC/ataxin-3, (4) α-crystalline/venus and (4) ataxin-3 (Figure 4.35 A). The PCR confirmed the integration of the HuC promoter, of ataxin-3 and of the α-crystalline promoter and venus in all MJD zebrafish lines (Figure 4.35 B). Further, all lines carry the full ataxin-3 cDNA.

After confirming an integration of the full pDestAttB-HuC-*hMJD1* construct into the zebrafish genome, the length of the CAG repeat was verified for all lines. Therefore, the CAG repeat was amplified using two different primers flanking this region (R100 and R888). Agarose gelelectrophoresis of the PCR-products confirmed the CAG-repeat length for all 18Q lines (Figure 4.35 C) with an amplicon size of approximately 240 bp. The lines expressing expanded 73Q ataxin-3c and ataxin-3aL also carry a CAG repeat of the correct size (approximately 420 bp). Both founder lines for polyQ-expanded ataxin-3aS however, show a CAG-repeat length of various sizes with a maximum length of the expected 73 CAG repeats.

Fragment length analysis of these PCR-products confirmed the results of the agraose gelelectrophoresis (Figure A.6). A PCR-product carrying a CAG-repeat with 18 triplets has a size of approximately 229 nucleotides whereas CAG expanded amplicons have a size of 382 nucleotides. All lines with 18CAG repeats show a peak at the expected size. Expanded ataxin-3c and -

3aL show a comparably weaker peak at 381 nucleotides and 382 nucleotides, respectively. Both 73CAG lines for ataxin-3aS show multiple peaks for the CAG repeat length. Line 3aS73.1 shows two peaks (263 nucleotides and 382 nucleotides) whereas line 3aS73.16 shows three peaks (207 nucleotides, 301 nucleotides and 379 nucleotides). The peak size of this line shows that it carries 72 instead of 73CAG repeats.

After confirming the CAG repeat size of all lines, the expression of ataxin-3 transcripts was analyzed using by PCR. mRNA was isolated from 5 days to 6 days old zebrafish larvae and cDNA was reverse transcribed before transcripts were amplified using the primers R100 and R888. Expression of a CAG containing transcript could be confirmed for all lines. Non-expanded zebrafish 3c18.1, 3c18.4, 3aL18.44 and 3aS18.1 showed transcripts of identical sizes (around 240 bp) without a CAG expansion. Expanded lines 3aL73.1, 3aS73.1 and 3aS73.18 showed two or more transcript amplicons. The maximum size for all three lines was approximately 420 bp. The expression analysis thereby generally confirmed the analysis of the CAG size and shows that the CAG-expanded lines show a CAG mosaic. Interestingly, the line 3c73.2 showed a weak amplicon of smaller size than the non-expanded lines. This is in huge contrast to the analysis of the CAG repeat size (Figure 4.35 C and A.6) which both confirmed the integration of the expanded pDestAttB-HuC-*hMJD1* construct. The amplified PCR products are specific for the transgenic ataxin-3 transcripts as an primer BLAST showed that unspecific amplification of reverse-transcribed zebrafish cDNA results in amplicons of different sizes (van Beek, 2019). Therefore, it remains unclear, why the results for the CAG repeat length of line 3c73.2 differ between the DNA and mRNA/cDNA level.

In the next step the expression of the transgene ataxin-3 was analyzed in 5 to 6 dpf old larvae using SDS-PAGE and western blot. Immunodetection of the larvae lysates mainly showed unspecific protein bands which could not only be found in the eight newly generated zebrafish lines but also in a control line (3 dpf, Figure 4.36 A). Expression of ataxin-3 in line 3c18.1 could be confirmed with both antibodies 1H9 and SA3637. Full-length ataxin-3 as well as fragments could be found in this line. The identified fragments are presumably created by cleavage at the C-terminus because they could not be detected using the ataxin-3c specific antibody SA3637 (Schmidt et al., 1998). Such protein fragments could also be detected *in vitro* (Figure 4.15) and are well known for ataxin-3 (Hübener et al., 2013; Weber et al., 2017; Weber, 2017; Harmuth et al., 2018). The most prominent fragment (30 kDa) seems to be identical to the fragment which was shown to be an N-terminal calpain cleavage fragment which causes a mitochondrial phenotype in MJD (Figure 4.15, page 98, Harmuth et al., 2018).

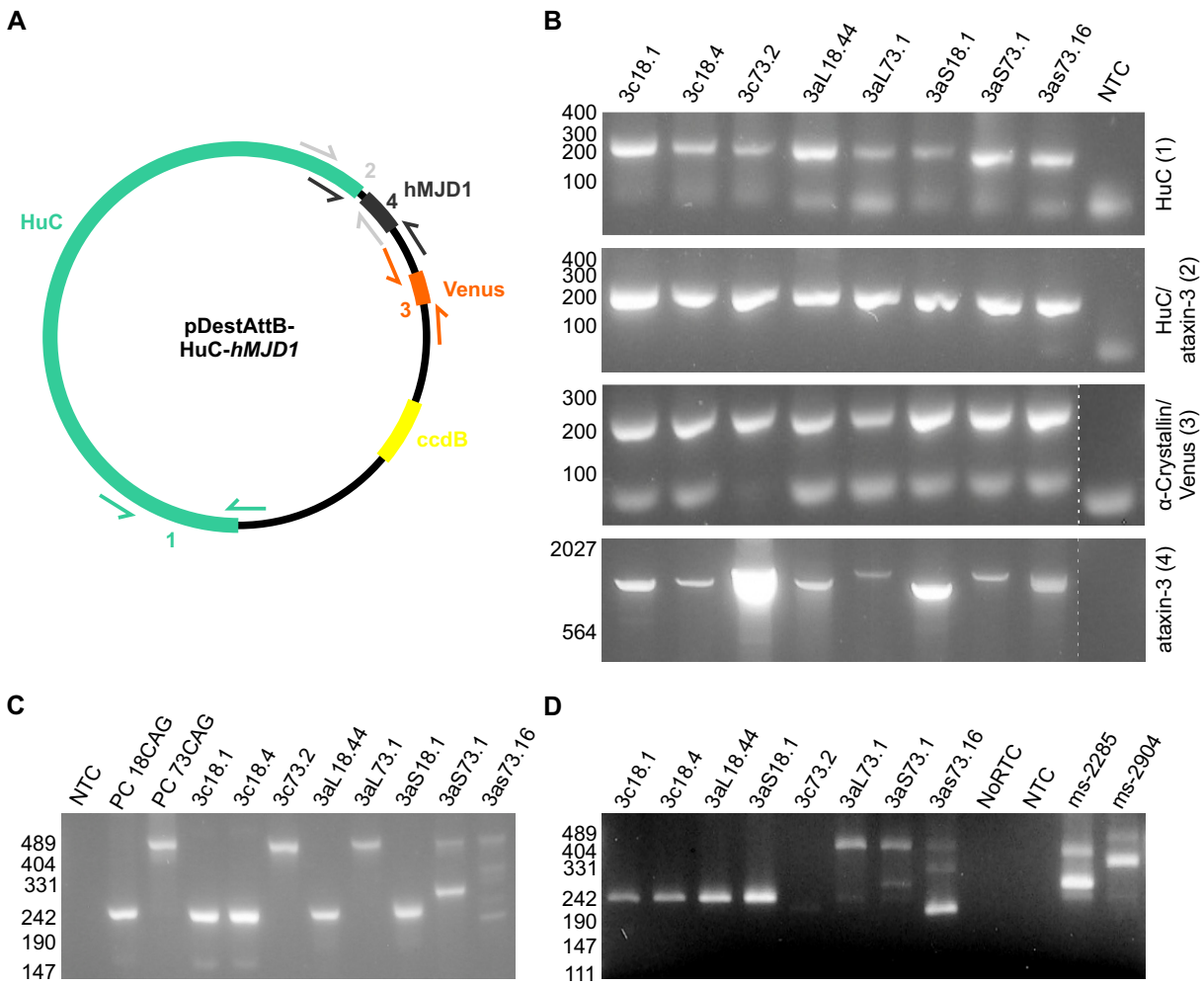

Figure 4.35. Integreation-verification of pDest-AttB-HuC-*hMJD1* into the zebrafish genome. **(A)** Schematic representation of primer binding sites of primers used for the verification of the pDestAttB-HuC-*hMJD1*-integration into the zebrafish genome. **(B)** An amplification of the 5' HuC (*elavl3*) region (pair 1), the 3' HuC/ataxin-3 region (pair 2), the α-crystallin/venus region (pair 3) and ataxin-3 (pair 4) confirmed the integration of the expression construct in all zebrafish lines. NTC was moved from the beginning of the gel to the end for primer pairs 3 and 4 in order to achieve an equal representation. **(C)** The CAG repeat length was determined for all zebrafish lines using the primers R100 and R888 resulting in an amplification of the CAG region of ataxin-3. Amplicons from pEGFP-C2-*hMJD1*c18CAG and -73CAG constructs were used as a positive control. Generally, the zebrafish lines show the expected CAG repeat length. However, both expanded 73CAG ataxin-3aS lines show multiple bands for the CAG repeat length which could indicate a CAG-mosaic in this line. **(D)** Expression of ataxin-3 transcripts was confirmed by PCR amplification of cDNA from 5 dpf to 6 dpf old larvae after reverse transcription of mRNA. Amplification of the CAG repeat in exon 10 was performed using the human-specific primers R100 and R888. Expression of the ataxin-3 transcript could be confirmed for all isoforms after loading the sample onto an agarose gel. Zebrafish lines 3c18.1, 3c18.4, 3aL18.44 and 3aS18.1 show a single amplicon which corresponds to the non-expanded repeat length. Lines carrying an expanded CAG repeat, 3aL73.1, 3aS73.1 and 3aS73.16 show multiple transcript amplicons. Line 3c73.2 shows a weak amplicon which is smaller in size than those for the non-expanded lines. MJD mouse control lines ms-2285 (29 and 66 CAG) and ms-2904 (60, 65 and 80 CAG) confirm the expression of transcripts with non-expanded and expanded CAG-repeats.

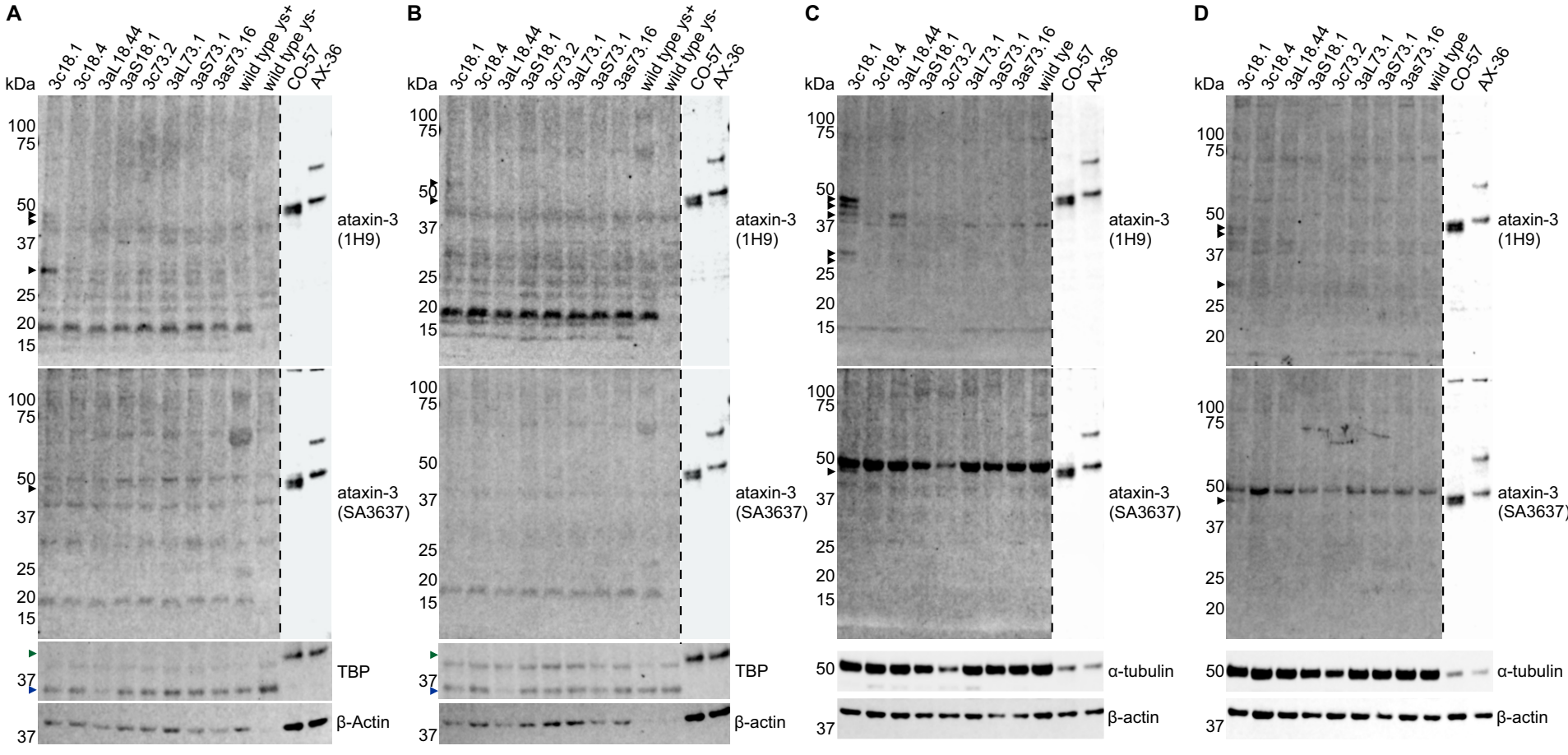

Figure 4.36. Analysis of ataxin-3 expression in transgenic MJD zebrafish larvae. (A) Immunostaining of Ataxin-3 using the antibody 1H9. Zebrafish larvae (5 dpf to 6 dpf) lysate samples were electrophoretically separated. All eight zebrafish lines showed multiple signals. Line 3c18.1 showed a weak signal of the ataxin-3 corresponding size (►) as well as an intense band at around 30 kDa which all could also be detected with the 3c-specific SA3637 antibody. WT zebrafish larvae (3 dpf) with yolk sac (ys+) and without (ys-) were used as controls. Human induced pluripotent stem cell control lines CO-57 (control) and AX-36 (MJD) are shown with reduced exposure time due to the strong signal. TATA-box-binding protein (TBP) (► human; ► zebrafish) and β-actin were used as loading controls. **(B)** Analysis of larvae homogenates (5 dpf to 6 dpf). Membrane was stained using the antibody 1H9 and SA3637. Both detections showed multiple signals for all eight zebrafish lines. Line 3c18.1 showed two weak signals with an approximate size of around 50 kDa (►) which could not be detected with the SA3637 antibody. **(C)** Adult zebrafish brain lysates were analyzed by SDS-PAGE and western blot and proteins were immunostained using the antibody 1H9 and SA3637. Expression could be confirmed in the zebrafish lines 3c18.1 and 3aL18.44. 3c18.1 showed a clear ataxin-3 signal (►) which

Figure 4.36 Analysis of ataxin-3 expression in transgenic *MJD* zebrafish larvae - *continued from previous page*
corresponded in size to the ataxin-3 signal of the healthy control cell line CO-57 and could also be detected using the antibody SA3637. This line additionally showed ataxin-3 fragments of around 30 kDa which could only be detected using the antibody 1H9. Ataxin-3 of line 3aL18.44 showed the characteristic smaller signal at 40 kDa). Expression of ataxin-3 could not be confirmed for the other lines using brain lysates. α-tubulin and β-actin were used as loading controls. **(D)** Brain homogenates were analyzed by SDS-PAGE and western blot and proteins were immunostained using the antibody 1H9. An expression of ataxin-3 in brain homogenates could only be confirmed for line 3c18.1 which shows full-length and fragment bands of ataxin-3 (►). The full-length ataxin-3 could also be detected using the antibody SA3637.

In order to exclude the possibility that other isoforms are insoluble in zebrafish, homogenates were generated from zebrafish larvae because these samples also contain insoluble components such as aggregates. Analysis of protein homogenates basically showed identical results (Figure 4.36 B). No expression could be confirmed for the other transgene MJD zebrafish lines.

Expression of CAG-expanded mRNA of correct size could be confirmed in seven out of eight lines (Figure 4.35 D). Therefore, it is unlikely that those lines do not translate the mRNA into proteins. One possible problem could be that ataxin-3 expression is controlled by the HuC promoter which results in a sole expression in neurons (Park et al., 2000). In lysates or homogenates of whole larvae the protein ratio between total protein a neuronal protein may be derogatory and impedes a specific detection of ataxin-3. Therefore, ataxin-3 protein levels were analyzed in adult (4 mpf) brain samples of MJD zebrafish. The brain lysates confirmed the expression of ataxin-3c in line 3c18.1 and additionally showed a transgene expression in line 3aL18.44 which fitted well the observed smaller size of ataxin-3aL in western blot (Figure 4.3, page 79) and could not be detected with the 3c-specific antibody SA3637 (Figure 4.36 C). An expression of ataxin-3 in line 3aL18.44 could not be observed in brain homogenates (Figure 4.36 D). As before, additional signals observed in both cases seemed to be N-terminal protein fragments.

These analyses endorse that the transgene is expressed in lines 3c18.1 and 3aL18.44. Other lines did not show an expression of ataxin-3 on protein level, although the expression could be confirmed on mRNA level (Figure 4.35 D).

One explanation for the absence of specific ataxin-3 signals in the western blot could be that the transgene ataxin-3 itself is insoluble, e. g. due to aggregation. Being SDS-insoluble, this protein fraction would not be analyzed by western blot. Further ataxin-3 isoforms showed differences in aggregation and solubility *in vitro* (see 4.2.1, page 97). This raised the interest to also analyze the isoform-specific aggregation characteristics *in vivo*. Therefore, larvae and brain homogenates (5 dpf to 6 dpf and 4 mpf) were analyzed for SDS-insoluble ataxin-3 using a filter trap assay. A low amount of insoluble proteins could be identified for all MJD lines (Figure 4.37 A). However, a clear sign of SDS-insoluble aggregates could not be identified for any line. In addition, line 3c18.1 which showed a clear signal in western blot also showed the highest amount of insoluble ataxin-3 among all eight lines. This suggests, that insolubility of ataxin-3 is not the cause for the absence of a clear signal in the western blot analysis.

Insoluble ataxin-3 was also analyzed in 4 mpf old zebrafish brain homogenates (Figure 4.37 B). Adult fish at this age neither showed a clear sign of protein aggregation. A recent MJD zebrafish model also suggests, that the aggregation process is not triggered within the first twelve months

of age (Watchon et al., 2017).

Generally, signals in the western blot analysis were weak and background was high, which suggests that the expression level in general is comparably low. The fact, that expression of ataxin-3 in line 3aL18.44 could not be seen in brain homogenates further corroborates the hypothesis that proteins are expressed but scarce. Therefore it was assumed that ataxin-3 is expressed in all lines; however, due to the low expression level, the high background and the unspecific signals in western blot a specific detection is hindered. In order to overcome these obstacles the ataxin-3 protein expression status of all lines should be assessed on a cellular level using immunohistochemical staining of brain sections from 4 mpf old MJD zebrafish. Cerebellar sections were used as this region represents the predominant area of MJD pathogenesis (Sudarsky and Coutinho, 1995). Direct ataxin-3 staining of cerebellar brain slides allows an assessment of ataxin-3 expression within a single cell and an analysis of the subcellular distribution of ataxin-3. Further, immunohistochemical staining also allows the analysis of ataxin-3 aggregates. Due to the fact that ataxin-3 is also involved in the ubiquitin-proteasome system and is itself a deubiquitinating enzyme (Doss-Pepe et al., 2003; Burnett et al., 2003; Mao et al., 2005), staining of ubiquitin was performed as well.

Staining of sections for ataxin-3 showed a clear, prevailing cytoplasmic staining of cells independent of the isoform and polyQ expansion, (Figure 4.38). Interestingly, WT zebrafish showed a weaker ataxin-3 staining which indicates an expression of the transgene ataxin-3 in all zebrafish lines. Ubiquitin staining showed a ubiquitous cell stain with a stronger presence of ubiquitin in the nuclei of transgene animals. This suggests an accumulation of ubiquitin or ubiquitinated proteins in the nucleus after expression of ataxin-3 in these animals. Interestingly, other brain regions of the zebrafish did not show this nuclear accumulation (van Beek, 2019). Aggregates could neither be identified by ataxin-3 nor by the ubiquitin staining.

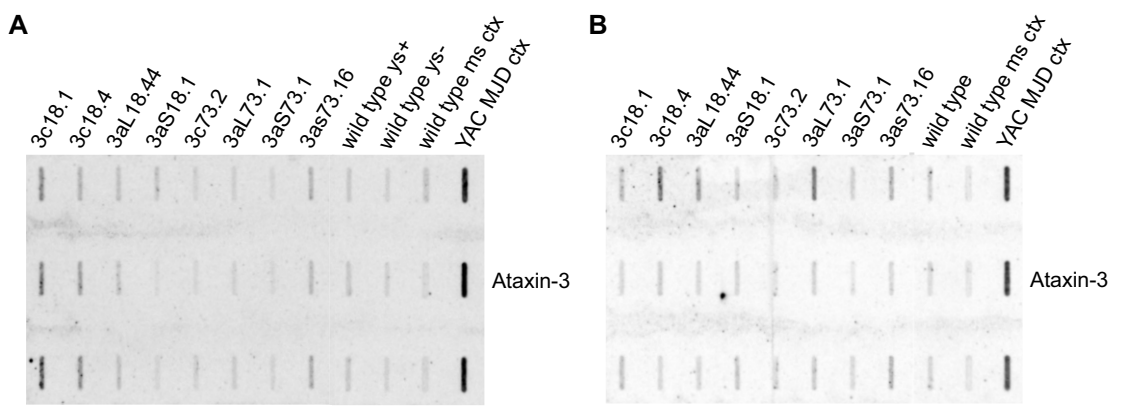

Figure 4.37. Analysis of ataxin-3 aggregation in transgenic zebrafish. (A) Filter trap analysis of MJD larvae homogenates (5 dpf to 6 dpf). Proteins were blotted onto a nitrocellulose membrane (0.45 µm) and immunodetection was performed using the antibody 1H9. Transgenic larvae show slightly more insoluble protein than control larvae with (ys+) and without (ys-) yolk sac, 3 dpf. Line 3c18.1 shows the highest amount of insoluble protein among the eight MJD zebrafish lines. Cortex samples of a WT mouse (C57/BL6) show a comparable background signal, while the transgenic yeast artificial chromosome (YAC) MJD mouse (MJD64-84) shows strong aggregation (15 months). Shown are technical triplicates. **(B)** Filter trap analysis of MJD zebrafish brain homogenates (4 mpf). Proteins were blotted onto a nitrocellulose membrane (0.45 µm) and detected using the antibody 1H9. No clear sign of ataxin-3 aggregation in the zebrafish could be detected. The amount of insoluble protein in all MJD zebrafish lines is comparable to the zebrafish controls (16 mpf). Shown are technical triplicates.

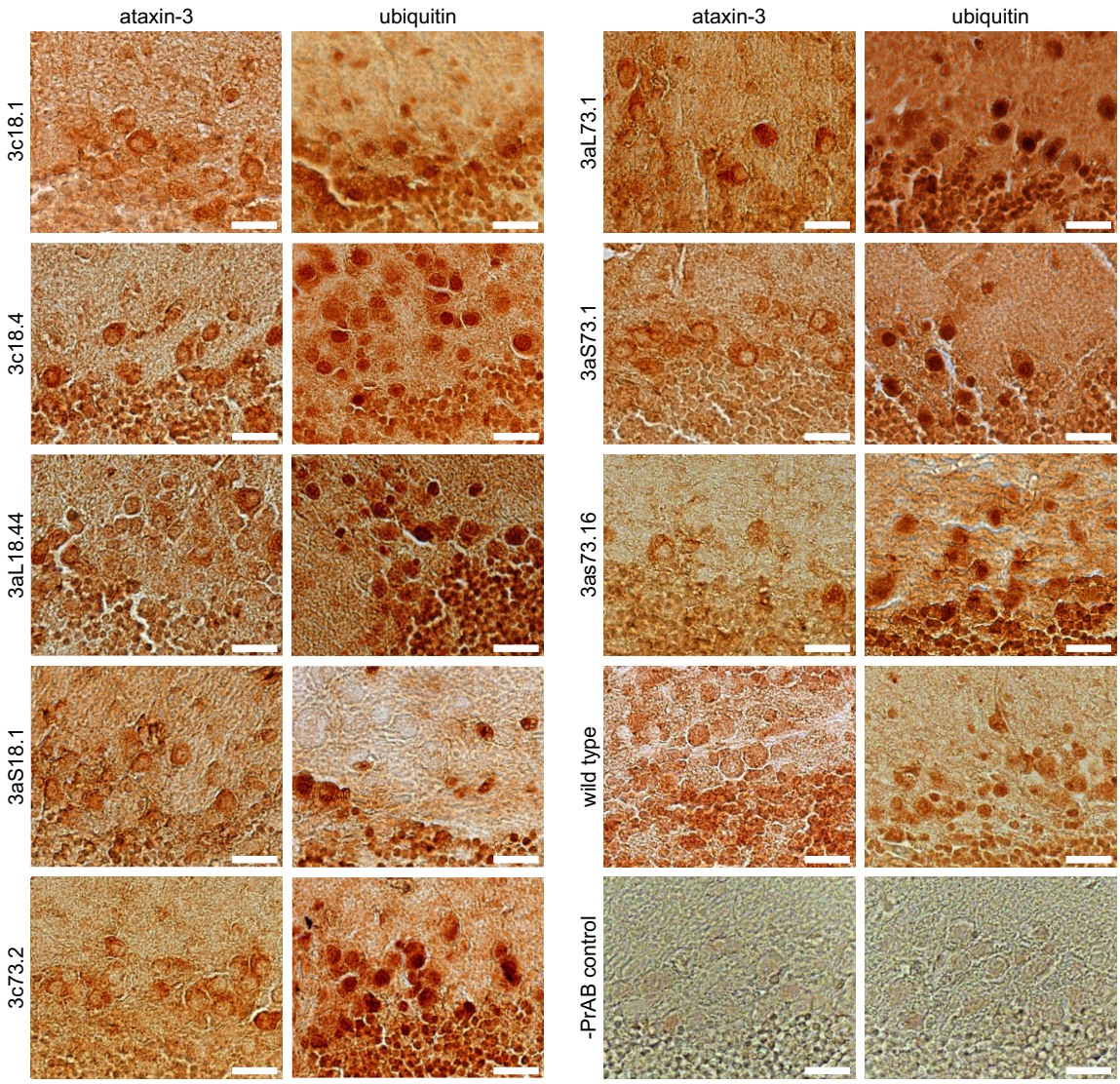

Figure 4.38. Immunohistochemical analysis of ataxin-3 expression and aggregation in the cerebellum of zebrafish. Cerebellar brain slides of zebrafish (WT, 16 mpf; transgenic, 4 mpf) were stained for ataxin-3 (1H9) and ubiquitin. A clear, predominantly cytoplasmic staining of ataxin-3 could be identified for the transgenic lines in comparison to the WT zebrafish line which confirms the expression of ataxin-3 in all lines. Intracellular or intranuclear aggregates were absent. Transgenic zebrafish showed a strong nuclear ubiquitin-staining which could not be found for the WT fish. The Staining control without primary antibody (-PrAB control) confirmed a specific staining with both antibodies.

In summary, zebrafish were injected with PhiC31 mRNA and pDestAttB-HuC-*hMJD1* isoform constructs for 18 and 73 CAG repeats. Offspring of all fish were raised and transgene founders could be identified for all lines. Integration of the construct into the zebrafish genome could be verified and CAG repeat length could be confirmed. Both 3aS73 lines proved to show a poly CAG mosaic. Expression of ataxin-3 mRNA could be confirmed for all lines but 3c73.2. Expression on western blot could only be confirmed for lines 3c18.1 and 3aL18.44. Immunohistochemical analysis of brain sections showed an expression of ataxin-3 in all eight lines, including the one without confirmed mRNA expression. Aggregates could not be found. Table 4.2 summarizes the results of all MJD zebrafish lines.

Table 4.2. Overview of MJD transgenic zebrafish. This table summarizes the results of the generation of MJD transgenic zebrafish. Protein indicates the confirmed ataxin-3 expression in western blot/immunohistochemistry.

Line	Integration	Expression		Aggregation
		mRNA	Protein	
*hMJD1*c18CAG$_{GG}$.1	yes	yes	yes/yes	no
*hMJD1*c18CAG$_{GG}$.4	yes	yes	no/yes	no
*hMJD1*aL18CAG$_{GGC}$.44	yes	yes	yes/yes	no
*hMJD1*aS18CAG$_{GGA}$.1	yes	yes	no/yes	no
*hMJD1*c73CAG$_{AC}$.2	yes	no	no/yes	no
*hMJD1*aL73CAG$_{ACC}$.1	yes	yes	no/yes	no
*hMJD1*aS73CAG$_{ACA}$.1	yes	yes	no/yes	no
*hMJD1*aS73CAG$_{ACA}$.16	yes	yes	no/yes	no

4.6 Evaluation of a read-through approach as a potential therapy for MJD

MJD is a fatal neurodegenerative disease that, despite intensive research, cannot be treated or cured so far. Current studies are investigating RNAi approaches (Alves et al., 2008b; Hu et al., 2009a; Liu et al., 2013; Magner et al., 2015; Evers et al., 2013b; Toonen et al., 2017; Moore et al., 2017; Rodríguez-Lebrón et al., 2013), target protein aggregation (Bonanomi et al., 2014b; Fujikake et al., 2008; Furusho et al., 2005; Chang et al., 2013; Chen et al., 2014; Tower et al., 2011; Nagai et al., 2003; Ito et al., 2016; Yoshida et al., 2002; Wang et al., 2018b), proteolytic cleavage (Haacke et al., 2007; Watchon et al., 2017), the degradation pathways UPS (Matsumoto et al., 2004; Jana et al., 2005; Wang et al., 2007) and autophagy (Menzies et al., 2010; Silva-Fernandes et al., 2014; Cunha-Santos et al., 2016; Watchon et al., 2017; Nascimento-Ferreira et al., 2013) as well as transcriptional dysregulation (Jung and Bonini, 2007; Chou et al., 2011, 2014; Yi et al., 2013; Lei et al., 2016) and antisense oligonucleotides (Hauser et al., 2022).

The nonsense SNP in *ATXN3*a, which is leading to the short isoform ataxin-3aS creates a protein isoform which is characterized by a strong aggregation phenotype (see 4.2.1, page 99), a phenomenon that is discussed to be the toxic cause of neurodegeneration in polyQ diseases (Bucciantini et al., 2002; Bates, 2003; Ross and Poirier, 2005; Lajoie and Snapp, 2010; Invernizzi et al., 2012). Aggregation of this isoform is accompanied by a dominant nuclear localization (see 4.1.7, page 97) which is associated with a stronger toxicity of ataxin-3 (Sowa et al., 2018). Further, it was previously reported that nonsense SNP in *ATXN3*a is linked to an earlier age at onset in MJD (Dengler, 2018). Taken together, it can be concluded that the nonsense SNP creates a highly toxic protein species that aggravates MJD pathology. This especially highlights to date unstudied therapeutic approaches that target single protein isoforms such as splice modulation therapy (reviewed in Arechavala-Gomeza et al., 2014) which could allow a shift in the expression from *ATXN3*a to *ATXN3*c. Other possibilities are approaches with agents to induce read-through of PTCs (reviewed in Keeling et al., 2014) which were studied in cystic fibrosis (Howard et al., 1996), congenital muscular dystrophy (Allamand et al., 2008), Duchenne muscular dystrophy (Arakawa et al., 2003; Heier and DiDonato, 2009; Malik et al., 2010), Rett-syndrom (Brendel et al., 2011) and cancer (Floquet et al., 2011; Bidou et al., 2017). As the nonsense SNP in *ATXN3*a creates a TAA stop codon, this therapy would directly allow a read-through from ataxin-3aS to ataxin-3aL. These therapies may not cure MJD; however, they may be able to delay disease progression and aao in order to improve life quality for those suffering from this fatal disease.

Roughly 2400 different disorders are caused by nonsense mutations (Karijolich and Yu, 2014; Peltz et al., 2013) leading to a PTC which accounts for around 10 % to 15 % of genetic disorder (Mort et al., 2008; Finkel, 2010). Three types of stop codons – and therefore also nonsense mutations leading to PTCs – exist: UAA (*ochre*), UAG (*amber*) and UGA (*opal*; Finkel, 2010). Usually, translation of mRNA at the ribosomes stops when a termination codon is recognized by class 1 release factors at the ribosomal A-site which leads to translational termination by eRF1/eRF3 mediated peptidyl-tRNA hydrolysis at the ribosomal P-site (Karijolich and Yu, 2014; Dever and Green, 2012; Pisareva et al., 2006; Mitkevich et al., 2006). However, when the

ribosome makes a mistake and accidentally incorporates an AA at the termination codon a read-through happens into the otherwise untranslated 3' UTR, thereby C-terminally expanding the protein, until the next stop codon is reached (von der Haar and Tuite, 2007; Li and Zhang, 2019). Small molecules are able to induce conformational changes at the 3' end of the rRNA which, during translation, enables the ribosome to insert a AA at an stop codon instead of initiating translational termination (Bedwell et al., 1997; Mendell and Dietz, 2001; Amrani et al., 2004; Welch et al., 2007). Translational read-through, however, is not necessarily an artificially induced phenomenon. The same principle is also applied by viruses (Firth and Brierley, 2012; Honigman et al., 1991) and known in eukaryotes as well (Loughran et al., 2014).

The aim of a translational read-through therapy is therefore to increase the likelihood of decoding the stop codon by a near-cognate tRNA instead of recognition by eukaryotic release factor 1 which leads to the production of full-length protein (Karijolich and Yu, 2014).

Drug induced PTC read-through was first described by Gorini and Kataja (1964) who used streptomycin, an antibiotic belonging to the class of aminoglycosides. Aminoglycosides specifically block prokaryotic protein synthesis by binding the 16S rRNA. Binding induces a conformational change and thereby the misincorporation of AAs (Purohit and Stern, 1994; Carter et al., 2000; Fan-Minogue and Bedwell, 2008; Keeling and Bedwell, 2005). This enables aminoglycosides to induce translational read-through (Gorini and Kataja, 1964; Palmer et al., 1979; Singh et al., 1979; Howard et al., 2000). They bind to the 16S rRNA decoding site and interfere with its proofreading function which causes increased rates of false incorporations of tRNAs instead of a translational termination (Moazed and Noller, 1987; Karijolich and Yu, 2014). Although aminoglycosides are highly specific for prokaryotes and require much lower concentrations for interference with ribosomal function (Keeling and Bedwell, 2005) a subset of them is also able to disturb eukaryotic proofreading functions and therefore cause translational read-through (Keeling and Bedwell, 2005; Fan-Minogue and Bedwell, 2008; Karijolich and Yu, 2014).

In order to evaluate the possibility of performing a read-through from ataxin-3aS to ataxin-3aL, two aminoglycosides were tested, Gentamicin and G418. Both are substances that can be used to perform a read-through of a stop codon (Howard et al., 1996). In order to test the effectiveness of these drugs the rs7158733 TAC_{991} was replaced by a TAA_{991} ochre stop codon in the pEGFP-N2-*hMJD1*aL18CAG_{AGC} and pEGFP-N2-*hMJD1*aL151CAG_{ACC} vectors (Figure 4.39 A). Therefore, a gBlock containing the TAA nonsense SNP was introduced between the PpuMI and ApaI restriction sites of the pEGFP-N2-*hMJD1*aL18CAG_{AGC} construct and sequence verified using the primers I866 and T527 resulting in the final construct pEGFP-N2-*hMJD1*aL18CAG_{AGA}. This fragment was afterwards excised and cloned into the 151CAG vector resulting in the pEGFP-N2-*hMJD1*aL151-CAG_{ACA} construct. This construct usually allows the expression of ataxin-3aS; however, upon a read-through of the PTC, ataxin-3aL-EGFP is being expressed (Figure 4.39 B).

In order to elucidate the concentration-dependent effects of G418 on correcting the PTC in *ATXN3*a HEK 293T *ATXN3* KO cells were transfected with this construct and grown for 24 h. Cells were then treated with G418 in concentrations varying between 25 µg/ml to 400 µg/ml for two days before EGFP expression was analyzed by fluorescence microscopy. According to

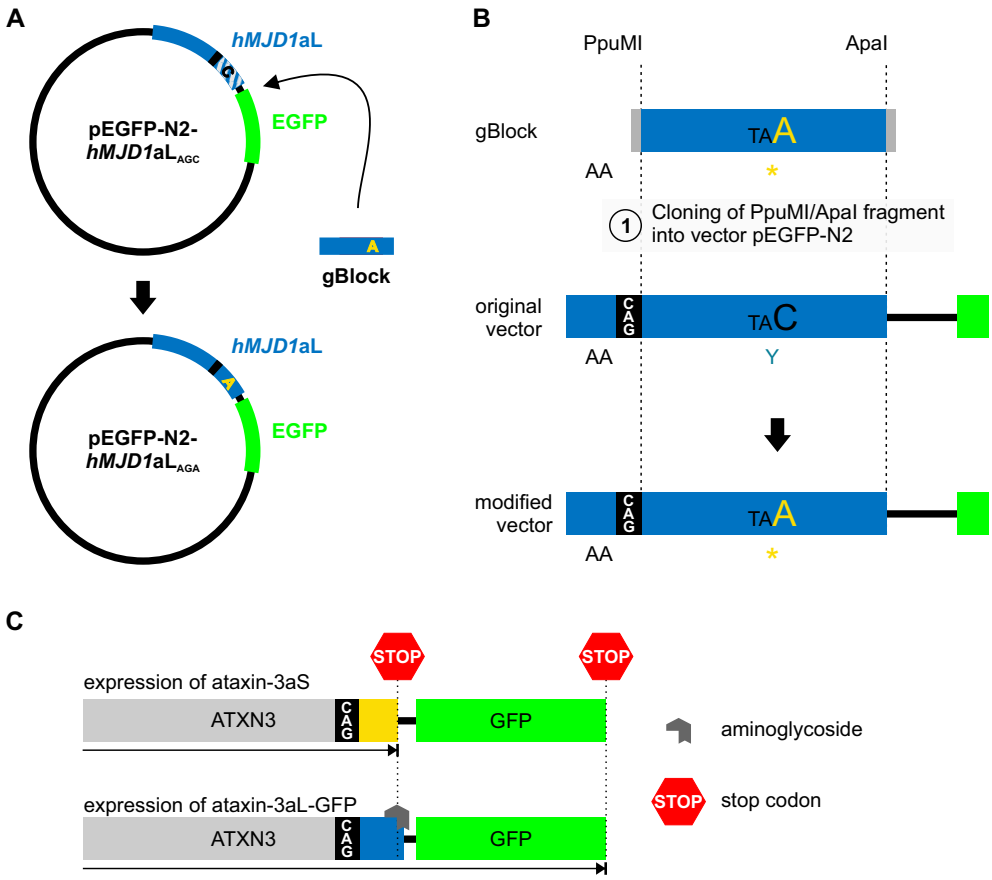

Figure 4.39. Cloning strategy for the introduction of the ochre stop SNP rs7158733 into the pEGFP-N2-*hMJD1*aL$_{AGC}$ vector. (A & B) Cloning of read-through constructs. In order to allow a read-through of the ochre stop codon in ataxin-3a rs7158733 was changed from TAC$_{991}$ to TAA$_{991}$ in the pEGFP-N2-*hMJD1*a18CAG$_{AGC}$ and -151CAG$_{ACC}$ constructs. A gBlock with the ataxin-3aL specific sequence and the nonsense SNP was digested with PpuMI and ApaI and the resulting fragment was cloned into the pEGFP-N2 vector. Due to the C-terminal EGFP-tag, a read-through allows the expression of ataxin-3aL-EGFP instead of -3aS. Therefore, EGFP expression can be used as a direct readout of the read-through rate. **(C)** Principle of the premature stop codon read-through approach. Ataxin-3aS is being expressed from the construct. Upon an induction of the stop codon read-through using G418 or Gentamicin, the translation continues to the stop codon of ataxin-3aL-EGFP.

the literature, these concentrations should result in 1 % to 3 % of GFP-positive cells (Halvey et al., 2012). It could be found that all cells show a basal EGFP expression independent of an aminoglycoside treatment (Figure 4.40). Visually it could be observed that the EGFP expression increased mildly in G418 treated cells. Toxic effects of these high concentrations could not be observed.

Microscopic analysis after aminoglycoside treatment showed that a basal EGFP expression occurs in transfected cells independent of a treatment. This impedes the evaluation of the read-through approach, especially when a small effect size is expected. In order to overcome this obstacle, treatment effectiveness was analyzed by western blot after a 48 h treatment of transfected HEK 293T *ATXN3* KO cells with G418 and Gentamicin in concentrations varying from 50 µg/ml to 400 µg/ml and 100 µg/ml to 500 µg/ml respectively. Immunostaining showed that a G418 treatment mildly increases the expression of normal 18Q and expanded 151Q ataxin-3aL-EGFP by around 10 % (Figure 4.41 A - D). However, this small effect size could not be confirmed statistically. A treatment of ataxin-3 expressing cells with Gentamicin also mildly increased the

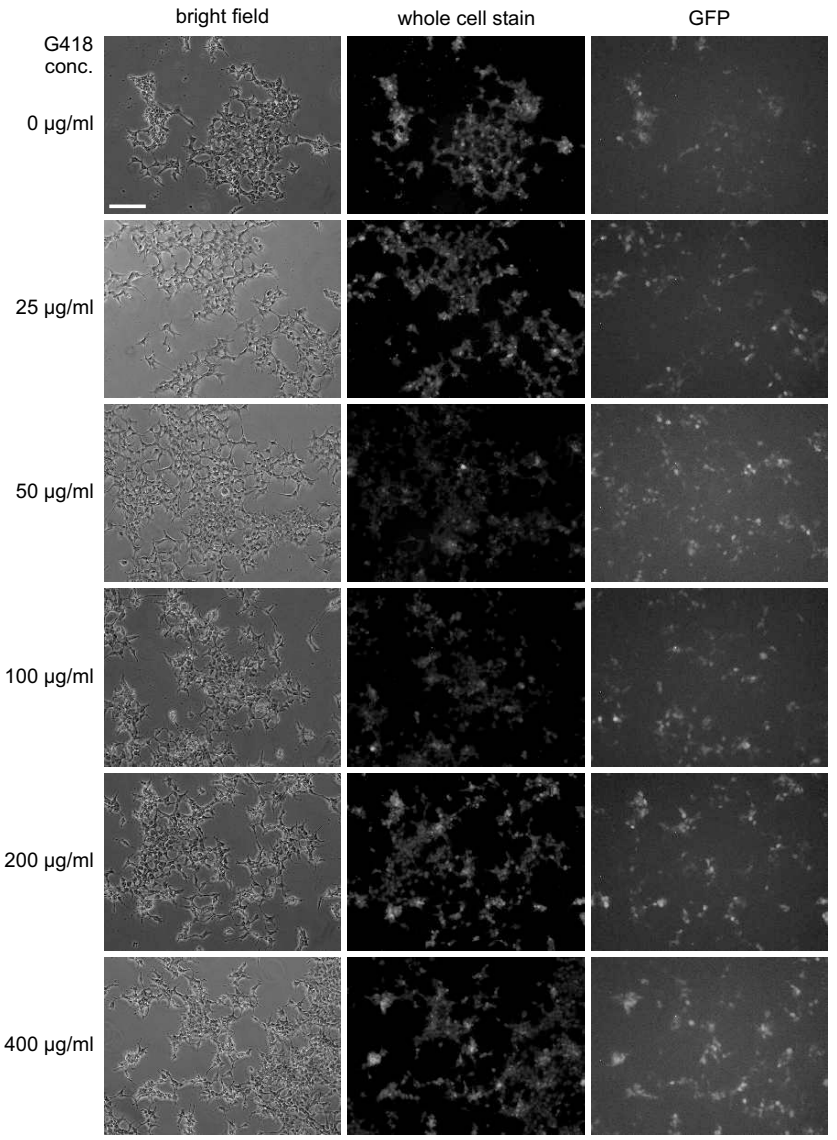

Figure 4.40. Microscopic analysis of GFP expression after treatment of pEGFP-N2-*hMJD1*aL18CAG$_{AGA}$ expressing cells with G418. HEK 293T *ATXN3* KO cells were transfected with pEGFP-N2-*hMJD1*aL18CAG$_{AGA}$ constructs and grown for 24 h before cells were treated with different amounts of G418 ranging from 25 µg/ml to 400 µg/ml. Due to the ochre stop codon in this construct untreated cells should express untagged ataxin-3aS while the G418 treatment should allow a read-through of this codon and therefore, leads to an expression of EGFP-tagged ataxin-3aL. PFA-fixation was performed after 48 h and total cells were stained using Cyto Paint Orange. Cells were analyzed for their EGFP expression. It could be observed that a basal read-through occurs in the untreated cells. Visually, a G418 treatment mildly increased the EGFP signal. Toxic effects of the G418 treatment could not be observed. Bar, 500 µm.

expression of ataxin-3aL-EGFP between 10 % to 25 % (Figure 4.41 E - H). Gentamicin thereby proved to be most efficient in 18Q ataxin-3 in concentrations between 300 µg/ml to 400 µg/ml. The effect on 151Q ataxin-3 could not be confirmed statistically.

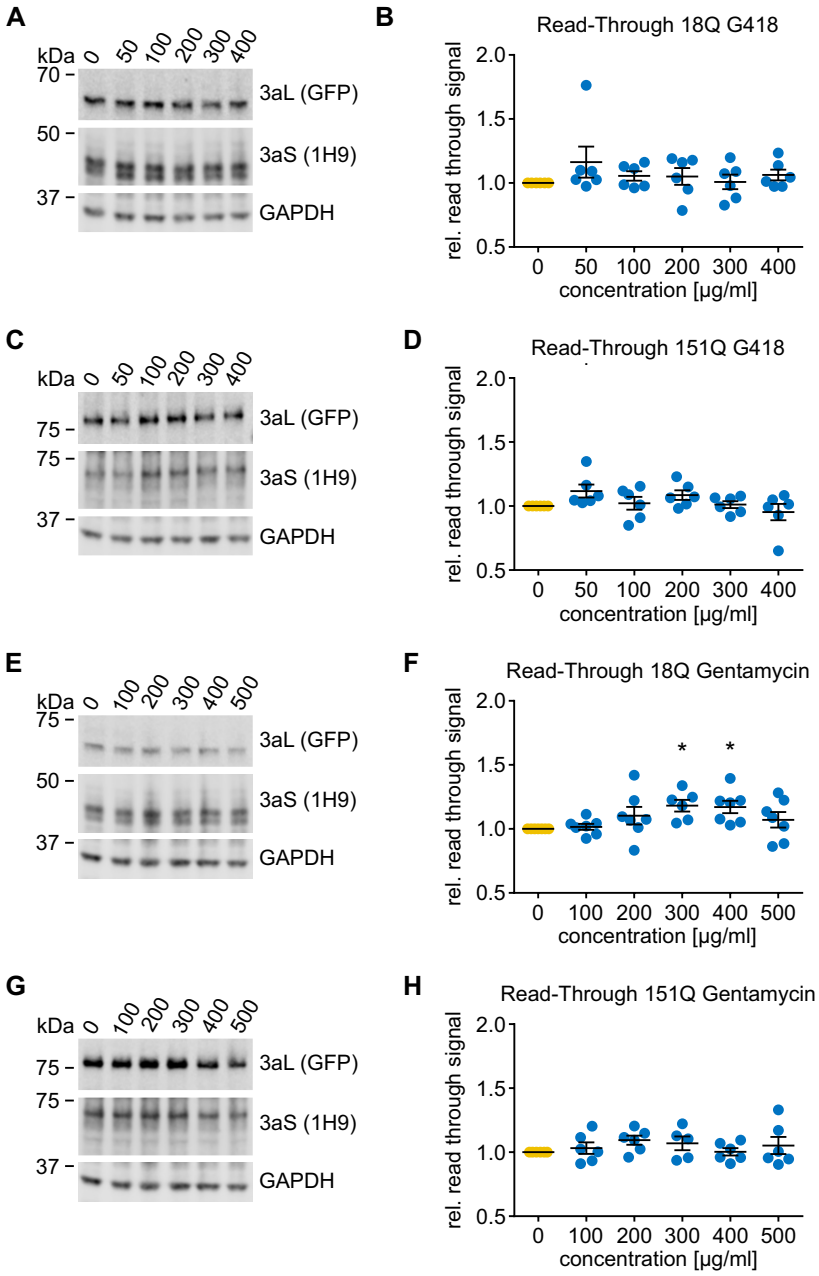

Figure 4.41. Evaluation of a read-through of ataxin-3aS to ataxin-3aL after treatment with G418 and Gentamicin. **(A)** HEK 293T *ATXN3* KO cells were transfected with pEGFP-N2-*hMJD1*aL18CAG$_{AGA}$ constructs and grown for 24 h. Cells were then treated with G418 at the indicated concentrations for 48 h. Cells were harvested and samples were processed for western blot. Membranes were immunostained for ataxin-3aL-EGFP (GFP), ataxin-3aS (1H9) and GAPDH. **(B)** The relative read-through signal from ataxin-3aS to -3aL was calculated for the G418 treatment. No difference in the ataxin-3aL-EGFP signal could be observed after the G418 treatment (Wilcoxon Signed Rank test with Hommel-adjustment, n = 6-7). **(C & D)** No statistical difference could be found for expanded ataxin-3a (pEGFP-N2-*hMJD1*aL151CAG$_{ACA}$) after the G418 treatment (Wilcoxon Signed Rank test with Hommel-adjustment, n = 6). **(E & F)** Treatment of 18Q ataxin-3a expressing cells (pEGFP-N2-*hMJD1*aL18CAG$_{AGA}$) with Gentamicin led to an increase in the ataxin-3aL-EGFP signal of around 10 % compared to untreated cells (Wilcoxon Signed Rank test with Hommel-adjustment, n = 6-7, * $p \leq 0.05$). **(G & H)** No statistical difference could be found for expanded ataxin-3a (pEGFP-N2-*hMJD1*aL151CAG$_{ACA}$) after the Gentamicin treatment (Wilcoxon Signed Rank test with Hommel-adjustment, n = 5-6). Data is represented as arithmetic mean ±SEM.

As the nonsense SNP causes ataxin-3a to undergo strong aggregation (see 4.2.1 Ataxin-3 isoforms show differences in protein aggregation) the effect of G418 and Gentamicin on aggregation was assessed in the next step. Though the total effect size for a read-through after a G418 treatment is low, it could have an effect on the aggregate formation of ataxin-3 when the formation of an aggregation seed is postponed by the treatment. Therefore, transfected cells were treated with both aminoglycoside drugs and lysed after 48 h. Samples were processed for filter retardation assay (Figure 4.42 A). Immunostaining of ataxin-3 showed that a G418 treatment of cells significantly reduced the amount of aggregates for 100 µg/ml, 200 µg/ml and 400 µg/ml by up to 25 % (Figure 4.42 B). Cells were also treated with Gentamicin for 48 h. It could be observed that this treatment also reduced the amount of aggregates up to 22 % for 300 µg/ml and 500 µg/ml but did not reach statistical significance (Figure 4.42 C & D).

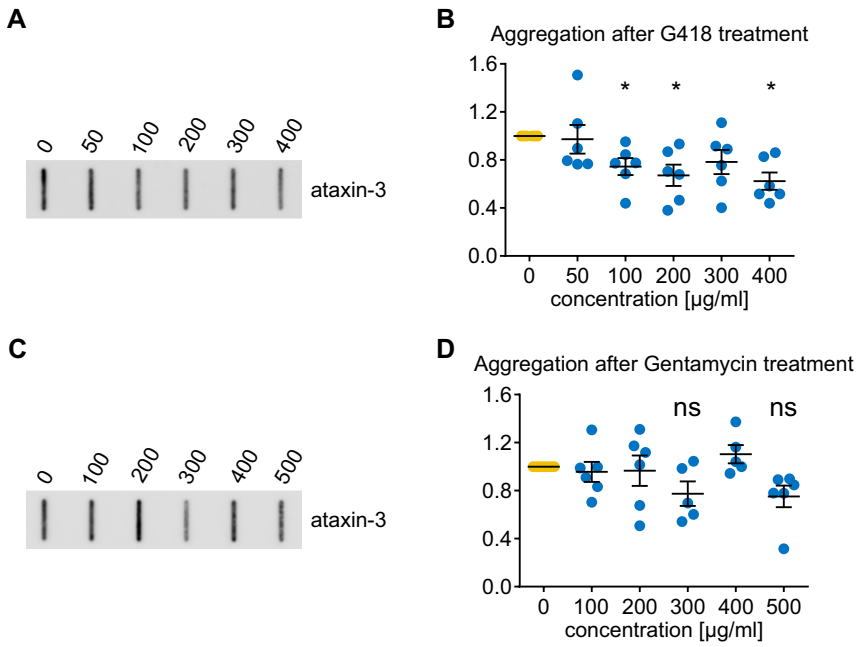

Figure 4.42. The effect of read-through on aggregation of ataxin-3aL. (A & B) HEK 293T *ATXN3* KO cells were transfected with pEGFP-N2-*hMJD1*aL151CAG$_{ACA}$ constructs and grown for 24 h. Cells were then treated with G418 at the indicated concentrations for 48 h. Cells were harvested and samples were processed for filter retardation assay. Membranes were immunostained for total ataxin-3 aggregates (1H9). Quantification of the aggregate signals showed that a G418 treatment led to a reduction of ataxin-3 aggregation (Wilcoxon Signed Rank test with Hommel-adjustment, n = 6, * $p \leq 0.05$). **(C & D)** Cells were treated with Gentamicin at the indicated concentrations for 48 h before they were harvested and processed for filter retardation assay. Membranes were immunostained for total ataxin-3 aggregates (1H9). Quantification of the aggregate signals showed that a Gentamicin treatment led to an insignificant reduction of ataxin-3 aggregation (Wilcoxon Signed Rank test with Hommel-adjustment, n = 5-6). Data is represented as arithmetic mean ±SEM.

4.7 Summary

In summary, it was found that ataxin-3 isoforms show differences in the protein half-live and that these differences are caused by the underlying degradation pathway of isoforms and their enzymatic activity (Figure 4.43 A). Further, ataxin-3 isoforms partially have a different subcellular localization and they display their specific interaction network. Alternative splicing together with the stop SNP lead to a loss or an increase in interaction strength depending on the protein partner. A pathological expansion of the polyQ causes a stabilization of ataxin-3 and an increase in insolubility. Aggregates were formed by all ataxin-3 isoforms but they differ in the amount/number of aggregates, aggregate size and aggregation kinetics. It could be shown that ataxin-3 isoforms have a mutual influence on each other by changing ataxin-3's protein stability and its aggregation phenotype. On one hand, the nonsense SNP in *ATXN3*a leads to an increased degradation rate and a degradation of ataxin-3aS by the UPS. On the other hand, the generated PTC also aggravates ataxin-3 aggregation and modifies interactions with protein partners (Weishäupl et al., 2019). Due to the presumably high toxicity of ataxin-3aS a read-through approach could be used as a potential therapy for MJD patients. It could be proven that a read-through reduces the amount of aggregates formed by ataxin-3a indicating that such a therapy would be beneficial. In general, the nonsense SNP in *ATXN3* creates a protein species which, despite sharing many characteristics, is different from ataxin-3c and ataxin-3aL in multiple aspects (Figure 4.43 B). A full summary of ataxin-3 characteristics is listed in Table A.2.

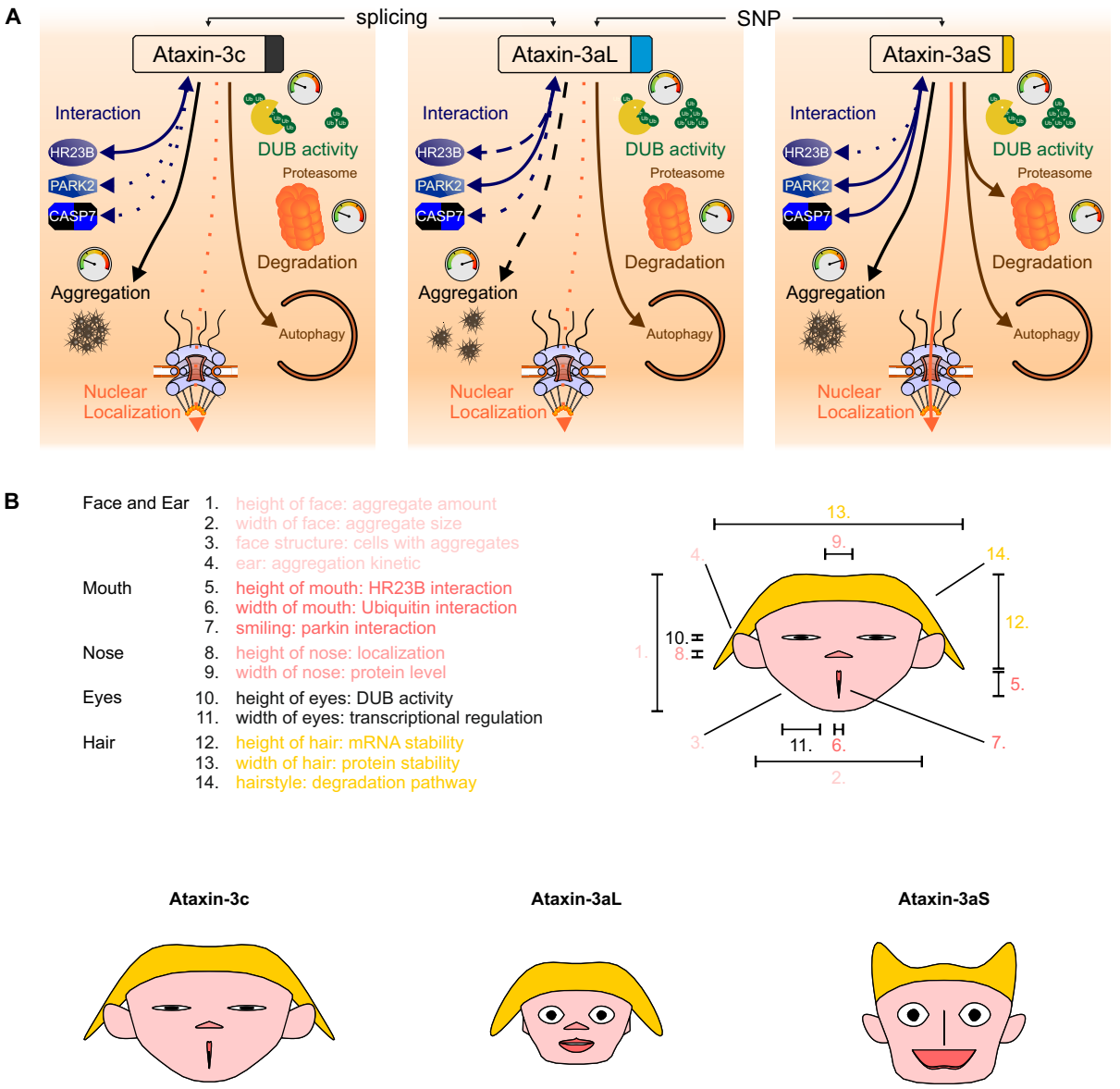

Figure 4.43. Summary of ataxin-3 isoform-specific characteristics. **(A)** Isoforms of ataxin-3 show various differences in their physiological and pathophysiological characteristics. Line type shows effect strength or amount, tachometer is an indicator of the kinetic (10 o'clock/green: slow; 12 o'clock/yellow: middle; 2 o'clock/red: fast). **(B)** Chernoff faces of ataxin-3 isoforms. The faces reveal, that ataxin-3 isoforms share common characteristics; however, the isoforms are three different protein species with their very own properties. Especially ataxin-3aS differs from the other two isoforms, although it shares interaction and general protein properties with ataxin-3aL. Subfigure A was modified from Weishäupl et al. (2019) available for use via `https://doi.org/10.1074/jbc.RA118.005801` under the CC BY 4.0 license (`https://creativecommons.org/licenses/by/4.0/`).

5 | Discussion

Protein diversity and thereby complexity in higher organisms is achieved on the transcriptional and protein level by alternative splicing and PTMs (reviewed in Lee and Rio, 2015; Spoel, 2018). It was found that 95 % to 100 % of multi-exon genes are spliced alternatively with at least two isoforms (Pan et al., 2008; Lee and Rio, 2015). Genes can be spliced differentially between tissues and cells and alternative splicing is especially applied in the brain where it plays a crucial role for both function and development of the CNS (Yeo et al., 2004; Johnson et al., 2009; Su et al., 2018). For this reason it is not surprising that alternative splicing dysfunctions frequently cause neurodegenerative diseases (reviewed in Mills and Janitz, 2012; Nik and Bowman, 2019). Nonetheless, alternative splicing can as well act as a modifier of disease (Nissim-Rafinia and Kerem, 2005; Howell et al., 2007; Bondy-Chorney et al., 2016) as it is the case for some polyQ disorders (Tsunemi et al., 2008; Hu et al., 2009b; Harris et al., 2010; Aikawa et al., 2017; Johnson et al., 2019). Genes responsible for polyQ disorders are partially spliced alternatively. Alternative splicing is known for DRPLA (Tadokoro et al., 2005; Beitel et al., 2013), SBMA (Dehm and Tindall, 2011; Lu and Luo, 2013; Jagla et al., 2007; Hu et al., 2009b; Guo et al., 2009; Yu et al., 2009b; Kallio et al., 2018; Wang et al., 2015; Shaman, 2015), SCA2 (Sahba et al., 1998; Nechiporuk et al., 1998; Affaitati et al., 2001; Welzel et al., 2012; Lastres-Becker et al., 2019), SCA3 (Goto et al., 1997; Bettencourt et al., 2010), SCA6 (Tsunemi et al., 2008; Aikawa et al., 2017), SCA7 (Einum et al., 2003; Ota et al., 2004) and SCA17 (UniProt # VSP_045488 and Ota et al., 2004). Partially, alternative splicing for these diseases has a relevance for the normal protein characteristics and disease pathology (Sahba et al., 1998; Nechiporuk et al., 1998; Affaitati et al., 2001; Einum et al., 2003; Ota et al., 2004; Tadokoro et al., 2005; Tsunemi et al., 2008; Dehm and Tindall, 2011; Lu and Luo, 2013; Lastres-Becker et al., 2019). Alternative splicing of the *ATN1* gene was reported to affect the subcellular localization of atrophin-1 and leads to a prominent nuclear localization of one isoform when a single glutamine is added to the protein apart from the polyQ repeat (Tadokoro et al., 2005). Although nuclear translocation of atrophin-1 is part of the DRPLA pathogenesis (Beitel et al., 2013) the consequence of this splice variant seem not to be studied yet. For the androgen receptor a total of twelve isoforms were described (reviewed in Dehm and Tindall, 2011; Lu and Luo, 2013) which mainly play a role in prostate cancer (Jagla et al., 2007; Hu et al., 2009b; Guo et al., 2009; Kallio et al., 2018) and polycystic ovary syndrome (Wang et al., 2015; Shaman, 2015). Alternative splicing here can lead to a truncated and constitutively active variants lacking the ligand-binding domain which leads to ligand-independent androgen recepor signaling (Hu et al., 2009b). Altered mRNA splicing also plays a role in SBMA due to the interaction of androgen receptor with splicing factors (Yu et al., 2009b). Six different splice variants have been described for the SCA2 causing gene *ATXN2* which lack certain exons in human, mouse and fibroblasts from SCA2

patients (Sahba et al., 1998; Nechiporuk et al., 1998; Affaitati et al., 2001; Lastres-Becker et al., 2019) and for which alternative splicing is modulated by the SCA1 disease protein ataxin-1 (Welzel et al., 2012). For the gene *CACNA1A* responsible for SCA6 two main isoforms were described which differ in their splice acceptor sites. Only one isoform contains the polyQ repeat due to a disruption of the otherwise present stop codon. Alternative splicing of *CACNA1A* therefore seems to play a major role in SCA6 pathogenesis as it was reported that the selective neurodegeneration may be a consequence of a specific increase in the expression of the polyQ containing isoform in Purkinje cells (Tsunemi et al., 2008). Both isoforms show similar channel properties but the polyQ isoform engages in multiple protein-interactions which are essential for its toxicity (Aikawa et al., 2017). Alternative splicing also could contribute to the pathology of SCA7. Three protein isoforms of different size could be identified which show varying expression patterns with one isoform being predominantly expressed in the CNS (Einum et al., 2003; Ota et al., 2004). Lastly, also *TBP*, the gene affected in SCA17, is known to be spliced alternatively (UniProt # VSP_045488 and Ota et al., 2004), however, no further information is available about the function or consequence of these variants.

In summary, alternative splicing is well described in seven out of nine genes of the polyQ proteins and certain isoforms are known to trigger pathology and/or substantially modify disease-relevant protein characteristics. Further, these examples show that already subtle changes in a protein can have a huge impact on its characteristics which modifies physiological and pathophysiological functions of the protein. Together, this highlights the possibility that alternative splicing together with the haplotype greatly modifies physiological ataxin-3 characteristics and contributes to the pathology of MJD (Harris et al., 2010; Bettencourt et al., 2010).

Isoforms of ataxin-3 were initially described only three years after the identification of the *ATXN3* gene (Kawaguchi et al., 1994; Goto et al., 1997). Despite intensive research on the molecular function of ataxin-3, little is known about the *ATXN3* transcript diversity (Bettencourt et al., 2010, 2013) or the differences between ataxin-3 isoforms regarding their physiological function or their contribution to MJD (Schmidt et al., 1998; Harris et al., 2010; Ramani et al., 2015; Johnson et al., 2019). It is known that at least two different protein isoforms - ataxin-3a and -3c - are translated (Kawaguchi et al., 1994; Goto et al., 1997) from alternatively spliced transcripts into proteins. A third one is generated by a nonsense SNP in *ATXN3*a leading to a shorter ataxin-3 isoform. Therefore, this isoform exists in two variants, ataxin-3aL (long) and ataxin-3aS (short, see 1.2, page 27, Weishäupl et al., 2019). It is generally considered that ataxin-3c is the predominant isoform in murine and human brain (Harris et al., 2010; Ramani et al., 2015). The presence of ataxin-3a and especially the nonsense SNP, however, has great impact on MJD pathology as shown here and in different studies. It is known that ataxin-3a shows a stronger aggregation phenotype (Harris et al., 2010) while the PTC in *ATXN3*3aS leads to a reduction of the aao and therefore a worsening of the phenotype (Dengler, 2018). Interestingly, the nonsense SNP is highly correlated with the expanded allele in MJD and is distributed worldwide with only two enclaves of non-stop carriers on islands - São Miguel and Graciosa (Azores, Portugal, Gaspar et al., 2002). Goto et al. (1997) proposed that the C-terminus of ataxin-3 causes isoform-specific functional differences. Despite this initial proposal was more than 20 years ago, the impact of alternative splicing and the PTC on MJD still remain elusive.

In order to close this knowledge gap, ataxin-3 isoforms were compared and characterized in the present work regarding their physiological function, their contribution to MJD pathology as well as their potential of a mutual influence which modifies their physiological and pathophysiological characteristics. A detailed description of expected differences can be found in chapter 1.2.

5.1 Physiological characteristics of ataxin-3 isoforms

5.1.1 Verification of a HEK 293T *ATXN3* knockout cell line

The gold standard of studying neurodegenerative disorders in a cellular model is with no doubt the usage of induced pluripotent stem cells, as they are as close to human neurons as they can be. Nonetheless, HEK 293T cells were used in the present study. The usage of this artificial kidney cell model may look arbitrary at the first glance. Nonetheless, it is validated by the primary interest of this work which was not to investigate the role of ataxin-3 in the neuronal functionality but to investigate biochemical differences of isolated protein species, i. e. the comparison of different ataxin-3 isoforms in their protein-specific physiological and pathophysiological characteristics which are mainly independent of the cell type. Further, this study required a model that shows high transfection efficiency and strong protein expression as transfections of cells with two or three plasmids at the same time at equal efficiency were required. Both are great advantages of HEK cells, which are also widely applied in the field of MJD and other neurodegenerative disorders (e. g. Durcan et al., 2011; Araujo et al., 2011; Rodríguez-Lebrón et al., 2013; Hübener et al., 2013; Zhou et al., 2013; Sowa et al., 2018; Tsai et al., 2003; Durcan et al., 2012; Mueller et al., 2009; Zeng et al., 2015; Yi et al., 2013; Matsumoto et al., 2004; Weber, 2017; Harmuth et al., 2018; Weber et al., 2018; Cullen et al., 2004; Nascimento-Ferreira et al., 2013; La Spada et al., 2001; Harris et al., 2010; Tsou et al., 2011) and the reason why this cell line was used.

Studying physiological and pathophysiological characteristics of single protein isoforms required a functional KO of endogenous ataxin-3 in order to be able to diminish both its endogenous and its possible mutual effects and acquire valid results. This is of special importance, as it is already known that ataxin-3 entities physically interact with each other (Todi et al., 2007). The KO was performed in the HEK 293T model using TALENs (Dold, 2014). TALENs (Boch et al., 2009) are, next to clustered regularly interspaced short palindromic repeats (CRISPR)/CRISPR-associated protein 9 (Cas9) (Cong et al., 2013) and zinc finger nucleases (reviewed in Urnov et al., 2010), a straight forward tool for genome editing. After introducing a frameshift mutation in exon 2 analysis of ataxin-3 protein levels by western blotting confirmed that ataxin-3 was no longer expressed and therefore renders the KO cell line a suitable model for the study of ataxin-3 isoform characteristics and their mutual interaction.

5.1.2 Ataxin-3 isoforms show differences in their protein level

Studying the protein level of polyQ diseases is important due to the monogenetic disease cause and previously reported gene dosage effects for some polyQ diseases (Zühlke et al., 2003; Toyoshima et al., 2004; Soga et al., 2017a,b; Tojima et al., 2018), although it is a matter of discussion in HD (Wexler et al., 1987; Squitieri et al., 2003). The protein level of ataxin-3 is an important factor in MJD pathology and homozygous patients show a more severe phenotype

(Lang et al., 1994; Sobue et al., 1996; Wang, 2018).

Ataxin-3c is considered to be the main isoform of ataxin-3 within the brain (Harris et al., 2010). However, no information was available about the expression and protein level of ataxin-3a isoforms. Therefore, the mRNA and protein levels of ataxin-3 transcripts/isoforms were analyzed in the present work upon expression from the same backbone vector in order to exclude vector dependent effects. It could be shown that all ataxin-3 isoforms are expressed from the vector. Ataxin-3 mRNA levels were unchanged between isoforms and CAG expansion but it could be shown that ataxin-3aS shows strongly reduced protein levels in comparison to ataxin-3c and ataxin-3aL. Upon an pathologic increase of the polyQ repeat the protein level of ataxin-3c increased (50 %) while the 3aL level dropped by about 70 %. Interestingly, the protein level of ataxin-3aS was unaffected by the polyQ repeat expansion.

Overall, ataxin-3c was found to show the highest protein level in all experiments which fits well to previous reports and confirms that this isoform may have the highest impact on disease pathogenesis and contributes most to the mutational load. Nonetheless, it is unclear whether there are tissue-specific splicing differences within the brain. Harris et al. (2010) showed that the ataxin-3a isoforms could not be detected in murine and human brain samples while their transcripts could be detected. The fact that ataxin-3aL and ataxin-3c show equal protein levels upon expression from the same backbone vector in the present study but ataxin-3aL could not be detected in murine brain samples suggests tissue-specific splice-variants as already proposed by Harris et al. (2010). Although, ataxin-3 shows a high protein level in virtually all tissues (endocrine tissues, bone marrow, immune system, lung, liver, gallbladder, pancreas, gastrointestinal tract, kidney, urinary bladder, male and female tissues, adipose and soft tissue and skin[1], Thul et al., 2017), no detailed information is available regarding isoform differences between these tissues.

The strong ataxin-3aL protein decrease upon a pathological polyQ expansion was surprising because mRNA levels were unchanged. This clearly shows that there is no correlation between mRNA and protein level in the present study. The human protein atlas also confirms, that there seems to be no direct correlation between the protein level and the mRNA expression level of *ATXN3*. Tissues with a low mRNA level showed a high protein level and vice versa (Thul et al., 2017). This lack of correlation is well described in the literature for various proteins and also between protein isoforms (Lichtinghagen et al., 2002; Chen et al., 2002a; Greenbaum et al., 2003).

5.1.3 Ataxin-3 isoforms differ in their stability and degradation pathway

Analyzing ataxin-3 protein levels revealed differences between ataxin-3 isoforms (see 4.1.2, page 78). Without a direct correlation between mRNA and protein level, these differences could be explained by differing protein half-lives. Isoform-specific differences in protein stability can be expected for the isoforms because two important phosphorylation sites, S335 and S347, which regulate the protein turnover are only present in ataxin-3c (Mueller et al., 2009, S340 and S352 due to 19 glutamine repeats). Analysis of ataxin-3's half-life showed that the isoforms indeed differ in their degradation rate. Ataxin-3c and -3aL showed half-lives of around 27 h and 31 h

[1]Human Protein Atlas for *ATXN3* available from https://v18.proteinatlas.org/

without a significant difference. Interestingly, the nonsense SNP in *ATXN3*a caused the isoform 3aS to be unstable compared to both other ataxin-3 isoforms with a half-life of around 13 hours. This isoform also shows a reduced protein level which therefore can at least partially be explained by its protein stability.

In general, the here determined half-life of ataxin-3c and 3aL fits well to the N-end rule predicted half-life of 30 h for peptides starting with a methionine (Gonda et al., 1989) and confirm the results by Berke et al. (2005) who also reported that ataxin-3c and ataxin-3aL show a similar stability. Also Mueller et al. (2009) reported a half-life for ataxin-3c that correlates well to the observed half-lives of ataxin-3c and -3aL. However, the results differ from those reported by Harris et al. (2010). They showed that ataxin-3aL has a shorter half-life than ataxin-3c. An explanation for the observed stability differences could be the different approaches and cellular systems which were used for assessing protein degradation. Harris et al. (2010) used Cycloheximide, an inhibitor of protein translation. Translational inhibition, however, contradicts protein degradation studies because it inhibits autophagy (Watanabe-Asano et al., 2014; Kovács, 1974; Papadopoulos and Pfeifer, 1986; Lawrence and Brown, 1993; Rez et al., 1991) and reduces proteasomal proteolysis (Zhao et al., 2015) and ubiquitination (Shenkman et al., 2007). Further, Harris et al. (2010) used tagged constructs, although it is known that a tag can influence protein stability (Deller et al., 2016). For this reason, a different approach was followed and untagged constructs were used while the Tet-Off system superseded the need for translational inhibition (e. g. by Cycloheximide) which increases the reliability of the results.

After termination of ataxin-3 expression using the Tet-Off system, neither differences in the mRNA stability nor in protein insolubility could be found. Therefore, it can be concluded that the measured protein half-lives reflect the physiological ataxin-3 degradation rates. Altogether, this clearly shows that the SNP and the polyQ expansion are able to directly modulate protein characteristics of ataxin-3 and presumably changes its degradation pathway which results in either vast degradation or a prolonged stability.

Although ataxin-3c has an additional UIM compared to 3aL, their stability did not differ. This shows that the protein-stabilizing effect of functional UIMs within ataxin-3 (Blount et al., 2014) only applies for functional UIMs within ataxin-3 (i. e. functional vs. non-functional) and not for an alternative splicing-induced substitution of the third UIM by a hydrophobic C-terminus.

The analysis of ataxin-3 stability showed that a length-increase of the polyQ expansion is accompanied by an increase in protein stability independent of the isoform (Weishäupl et al., 2019). While the effect for ataxin-3a isoforms was only mild (increase by 7 h and 11 h), ataxin-3c almost doubled its half-life (27 h vs. 53 h). This clearly shows that the polyQ expansion alters protein characteristics in a way that impedes protein clearance and thereby augments stability. The increase in ataxin-3c stability was also reflected by an increased total protein level of polyQ expanded ataxin-3c (Figure 4.3). This protein-level increase could be especially dramatic in MJD due to the increasing mutation load (Lang et al., 1994; Sobue et al., 1996; Wang, 2018). Interestingly, both ataxin-3a isoforms did not show an increase in their protein level upon polyQ expansion. The results obtained here confirm previous studies which report an increase in protein stability for expanded ataxin-3 (Zhou et al., 2013; Matsumoto et al., 2004) as well as

for other polyQ proteins, such as ataxin-1 (Riley et al., 2004), TATA-binding protein (Cullen et al., 2004; Bailey et al., 2002) and huntingtin (Roscic et al., 2011). These reports show that a stability-increase upon polyQ-expansion is a common effect observed for polyglutamine proteins.

After observing different half-lives for ataxin-3 isoforms, it was hypothesized that the vast degradation of ataxin-3aS results from different degradation pathways. Inhibition of either autophagy or UPS with two different inhibitors each confirmed this hypothesis. Western blot showed that ataxin-3c and ataxin-3aL are both degraded by autophagy. Ataxin-3aS instead is degraded by the UPS (Weishäupl et al., 2019). This can well explain the observed shorter half-life of ataxin-3aS as this pathway is thought to be the primary degradation mechanism for short-lived proteins (Zhang et al., 2017a). Although previous studies already analyzed the degradation pathway of ataxin-3 (Blount et al., 2014; Harris et al., 2010; Kristensen et al., 2017; Matsumoto et al., 2004; Wang et al., 2007), information about specific ataxin-3 isoforms were only presented for ataxin-3aL (Harris et al., 2010). For this reason and the partially ineligible experimental conditions it was necessary to determine the degradation pathway of ataxin-3aS and verify the partially conflictive results. Harris et al. (2010) reported that ataxin-3c is degraded by autophagy while ataxin-3a is degraded by the UPS. Kristensen et al. (2017) found that ataxin-3c is degraded by both pathways and Matsumoto et al. (2004) and Wang et al. (2007) reported a degradation by the UPS but neither did they mention the isoform under investigation nor did they analyze the autophagic pathway at all.

The observed differences can be explained by the isoform under investigation as well as experimental conditions. All mentioned authors used tagged constructs although they are known to change protein characteristics (Alvarez-Castelao et al., 2012; Majorek et al., 2014) and especially its N- or C-terminal position can affect the N-end rule (Bachmair et al., 1986; Deller et al., 2016). Further translational inhibition as performed by Harris et al. (2010) and Wang et al. (2007) especially inhibits autophagy (see above) and is thus explicitly inappropriate for degradation pathway studies. The usage of such inhibitors falsifies all obtained results. Moreover, the inhibitor itself and its concentration can greatly affect the results. Different proteasome and autophagy inhibitors used by the above mentioned ataxin-3 degradation studies are known to have severe side effects compared to Lactacystin and Bafilomycin A1 used in the present study and makes the results obtained here more reliable:

(1) MG-132 is known to inhibit calpains in a concentration dependent manner (Tsubuki et al., 1996) and acts as an activator of NF-κB (Fiedler et al., 1998). Even further, it causes a dose-dependent inhibition of cell growth by a cell cycle arrest and induces apoptosis (Han et al., 2009). Lactacystin used in the present study in contrast is the most specific proteasome inhibitor and considered a gold standard in proteasomal inhibition (Fenteany et al., 1995; Ōmura and Crump, 2019).

(2) Chloroquine, as an autophagy inhibitor, only inhibits starvation induced but not Torin-1 induced autophagy (Watanabe-Asano et al., 2014). Further, autolysosomes are still capable of degrading already endocytosed material because Chloroquine solely blocks autophagosome-lysosome fusion (Mauthe et al., 2018) whereas Bafilomycin A1 blocks their fusion and increases the autolysosomal pH in order to block degradation (Yamamoto et al., 1998; Jahreiss et al., 2008; Mauthe et al., 2018).

(3) 3-Methyladenine, anoher autophagy inhibitor, blocks the formation of autophagosomes (Seglen and Gordon, 1982) but also acts as an inhibitor of phosphoinositide 3-kinase (PI3K) (Ito et al., 2007; Wu et al., 2010) and therefore greatly affects normal cellular pathways.

5.1.4 Ataxin-3 isoforms differ in their enzymatic deubiquitination activity

Todi et al. (2009) reported that an inactivation of the JD by a C14A mutation resulted in an increased protein stability which also manifested in an increase of the ataxin-3 protein level. Therefore, an increased DUB-activity of ataxin-3aS could also explain the observed lower half-life and steady state level. Performing kinetic assays using a Rhodamine-110 labeled ubiquitin shows that all isoforms are able to cleave the Ubiquitin-Rhodamine-110 substrate although ataxin-3 is known to preferentially bind ubiquitin chains containing four or more ubiquitins via its UIMs (Burnett et al., 2003). Ataxin-3 thereby shows a comparably slow DUB kinetic compared to other DUB enzymes (Nicastro et al., 2010). Unexpectedly, it was found that alternative splicing but not the SNP rs7158733 affects ataxin-3's DUB activity. Ataxin-3 showed an initial velocity of around 16.500 RFU/min while ataxin-3aL and -3aS had an initial velocity of 36.000 RFU/min. Therefore, the catalytic activity is not able to explain the reduced stability of ataxin-3aS. However, the higher steady-state level of ataxin-3c could be explained by the lower enzymatic activity (Weishäupl et al., 2019).

The DUB activity of ataxin-3 isoforms was also previously investigated by Harris et al. (2010). Harris et al. (2010) reported that ataxin-3c and -3a do not differ in their enzymatic activity. However – in line with the results presented here - they also found a reduced relative fluorescence signal for ataxin-3c as well as an insignificant trend towards a lower initial velocity of ataxin-3c. The results presented in the present work are more reliable due to their experimental setup. It is known that the initial velocity of a protein depends on the substrate concentration as long as the concentration is low. Under conditions with a high substrate excess the initial velocity is nearly independent of the substrate concentration (Berg, Jeremy et al., 2015). According to the Michaelis-Menten kinetic the maximum conversion rate is reached under conditions of a high substrate excess. Therefore, the DUB analysis in the present study was performed using a 5-fold excess while Harris and colleagues used equimolar concentrations in this assay (Harris et al., 2010).

It is known that ataxin-3 activity is regulated by different means. Ataxin-3 is ubiquitinated in mammalian cells and in *Drosophila*. Interestingly, ubiquitination at K117 enhances its DUB activity (Todi et al., 2009, 2010; Scaglione et al., 2011; Tsou et al., 2013) and monoubiquitination is increased by proteotoxic stress (Todi et al., 2009). Due to the expression of ataxin-3 in a prokaryotic host, PTMs of ataxin-3 may not reflect the physiological situation in human cells. Further, ataxin-3's interaction with CHIP and VCP is capable of modifying its activity (Todi et al., 2009, 2010; Scaglione et al., 2011; Laço et al., 2012a). While no data is available about the interaction between ataxin-3 isoforms and CHIP it could be shown in the present study that all ataxin-3 isoforms interact with VCP similarly (see 4.1.5, page 87). The *in vitro* assay did not allow a interaction-induced modification of ataxin-3 activity. Therefore, a possible effect of the host system on the experimental results cannot be neglected in the results presented here. However, the results represent the basal ataxin-3 activity against short ubiquitin chains without

modification by PTMs and ataxin-3 interaction.

Normal and polyQ expanded ataxin-3 have a similar DUB activity *in vitro* (Burnett et al., 2003; Burnett and Pittman, 2005). However, Burnett and Pittman (2005) suggested that possible differences in substrate specificity exist between normal and expanded ataxin-3 as a result of altered protein interactions. The measured activity difference between ataxin-3 isoforms (see 4.1.4, page 84) could as well suggest that ataxin-3 isoforms edit different protein substrates which would directly affect the isoforms' interaction with protein partners.

5.1.5 Ataxin-3 isoforms differ in their interaction with protein partners

It is known that ataxin-3 interacts with various proteins (reviewed in doCarmo Costa and Paulson, 2012). However, information about the interaction of particular proteins with the individual ataxin-3 isoforms is limited as usually the isoform under investigation is not stated and if so, one cannot distinguish between ataxin-3aL and -3aS. Identification of interaction partners is crucial for understanding MJD because interaction partners of polyQ proteins can be genetic modifiers of pathogenesis (Williams and Paulson, 2008; Weishäupl et al., 2019). One such example is the alternative splicing of *CACNA1A* in SCA6. It was reported that the selective neurodegeneration may be a consequence of a specific increase in the expression of the polyQ containing isoform in Purkinje cells (Tsunemi et al., 2008). Both protein isoforms show similar channel properties but the polyQ isoform engages in multiple protein-interactions which are essential for its toxicity (Aikawa et al., 2017). Changes in interaction upon the presence of the nonsense SNP in *ATXN3*a may therefore be of special interest. This polymorphism reduces the aao in the Flores genotype of MJD (present in the expanded allele) compared to the São Miguel genotype (absence of the SNP, Dengler, 2018; Gaspar et al., 2002). The presence of SNP rs7158733 on both alleles - the expanded and the normal one - causes an even stronger reduction of the age at onset (Dengler, 2018).

In the present work, it could be shown that ataxin-3 isoforms share major parts of their interactomes, but also have individual partners with stronger or weaker interactions. The differences in interaction networks between the ataxin-3 isoforms suggest that they have their own specific interaction network whereby they take over functions in different cellular pathways. In total 330 binding partners could be identified in the present project by a SILAC tandem MS approach from which 32 were listed already in the primary Biological General Repository for Interaction Datasets (BioGRID; without two-hybrid results, Chatr-Aryamontri et al., 2017), or in the meta databases Agile Protein Interactomes DataServer (APID; Alonso-López et al., 2019) and Protein Interaction Network Analysis (PINA) 2 (Cowley et al., 2012; Weishäupl et al., 2019). Six of those 330 interactions presented here were additionally tested using GFP-trap assays in order to verify their validity.

Ataxin-3's interaction with various other proteins may be of high importance for the protein as its is believed that the interaction stabilizes the fold of its C-terminus and gives it a more compact structure (Masino et al., 2003). In general, ataxin-3a isoforms showed stronger interactions with most protein binding partners than ataxin-3c, whereas ataxin-3c showed strong interactions only with distinct proteins. Four out of seven proteins which primarily interact with ataxin-3c

were found to be either directly (HR23B and NGLY1) or indirectly (E3 ubiquitin-protein ligase UBR2 and hnRNP L) associated to the ERAD system. This could indicate that ataxin-3c could play a more important role in ERAD than ataxin-3a. Ataxin-3 interacts with VCP which was reported to be involved in ERAD as well (Zhong and Pittman, 2006; Wang et al., 2000). Ataxin-3 is also able to directly deubiquitinate ERAD proteins like TCPα. Sowa et al. (2009) suggested that this would lead to an increased E3 ligase activity and therefore to an increased protein turnover and a higher flux through the ERAD system. According to Laço et al. (2012a), the higher affinity of ataxin-3c (and ataxin-3aL) to HR23B could result in a reduced *in vivo* activity of this isoforms due to the lack of VCP-mediated activation. Indeed, ataxin-3c showed a reduced enzymatic activity (see 4.1.4, page 84); however, this reduction cannot be associated to a reduced activation of this isoform due to the *in vitro* conditions.

In general different known and unknown protein partners could be identified in the present studies. Among the known partners HR23A/B, VCP, parkin, tubulin and ubiquitin probably were the most relevant ones and will be discussed in detail.

5.1.5.1 Known interaction partners

5.1.5.1.1 Human homolog Rad23A/B

The interaction of ataxin-3 with HR23A/B was first described by Wang et al. (2000). HR23A/B are both human orthologs of the yeast DNA repair protein RAD23. The interaction is specific to ataxin-3 and does not involve the polyQ tract. HR23A/B interacts with both, normal and polyQ expanded ataxin-3 (Wang et al., 2000) and is involved in the regulation of the eukaryotic cell cycle (Kumar et al., 1999; Gragerov et al., 1998) as well as in the proteolytic pathway (Hiyama et al., 1999). It also interacts with the 26S proteasome via its ubiquitin-like domain which is also the site of interaction with ataxin-3 (Wang et al., 2000). Further, it was reported that HR23A/B is involved in nucleotide excision repair by an interaction with XPC (Sugasawa et al., 1997) and that HR23A/B could control DnaJ-1 transcription together with ataxin-3 (Tsou et al., 2015). Interestingly HR23A/B is recruited to ataxin-3 aggregates which may affect the normal function of HR23A/B (Wang et al., 2000; Yang et al., 2018). In the present study, it could be found, that the interaction of ataxin-3aS with HR23A/B is weaker than that of ataxin-3aL and ataxin-3c. This weaker interaction could explain observations on the ataxin-3aS's degradation rate and protein level and also indicate an increased toxicity of this isoform as described below.

Ataxin-3aS shows a lower protein level and a faster degradation rate compared to ataxin-3aL and ataxin-3c (see 4.1.2, page 78 and 4.1.3, page 80). According to a model proposed by Blount et al. (2014), the protein level and degradation rate of ataxin-3 is regulated by its interaction with HR23A/B: ataxin-3 binds ubiquitinated substrates which are shuttled to the proteasome by HR23A/B. When the complex reaches the proteasome, the interaction with HR23A/B prevents ataxin-3 degradation as it is believed that its association to the proteasome is weaker than the interaction with HR23A/B (Blount et al., 2014). According to this model it can be concluded that the weaker interaction of ataxin-3aS with HR23A/B results in a reduced rescue from proteasomal degradation and thereby explains the lower protein level and faster proteasomal degradation rate of ataxin-3aS.

Even further, the weaker interaction of ataxin-3aS with HR23A/B could also lead to a

possible loss of ataxin-3's neuroprotective function. It was reported that the disruption of ataxin-3's interaction with HR23A/B not only affects ataxin-3's protein level but also enhances its toxicity (Sutton et al., 2017). In this study a mild inhibition of interaction with HR23A/B - as observed for ataxin-3aS - was more toxic than a strong inhibition (Sutton et al., 2017). This is of particular interest as this attracts notice to the normal allele as a modifier of MJD pathology with a protective function against its polyQ-expanded pathogenic counterpart which can explain the strong clinical variability of MJD. Due to the mildly weaker interaction of ataxin-3aS with HR23A/B the neuroprotective function of this isoform could be reduced. Such an inhibition of ataxin-3 neuroprotective function could explain the earlier aao in patients carrying the *ATXN3*aS nonsense rs7158733 on the normal allele as reported by Dengler (2018).

5.1.5.1.2 Valosin Containing Protein/ATPase p93

Another well studied interaction partner is VCP (Doss-Pepe et al., 2003; Wang et al., 2006; Boeddrich et al., 2006). Both, VCP and HR23A/B are involved in protein quality control pathways (Dantuma et al., 2009; Raasi et al., 2004; Madsen et al., 2009) and targeting the VCP-binding motif in an MJD *Drosophila* model improves the phenotype (Johnson et al., 2021). VCP targets proteins from the endoplasmic reticulum for proteasomal degradation either by transferring these substrates directly to the proteasome or to other shuttling factors like HR23A/B or PLIC1 (Wang et al., 2000; Doss-Pepe et al., 2003; Heir et al., 2006; Zhong and Pittman, 2006; doCarmo Costa and Paulson, 2012) and acts as a scaffold protein (Madsen et al., 2009). The interaction site for VCP is well mapped and takes place via an arginine/lysine motif in the region of AA 277-291 of ataxin-3 which is located between the second UIM and the polyQ repeat (Doss-Pepe et al., 2003; Wang et al., 2006; Boeddrich et al., 2006) which is present in all three isoforms. Consequently, all three isoforms could be found to interact equally with VCP in the present study. Nonetheless, the interaction of ataxin-3aS with VCP could enhance its DUB activity in comparison to ataxin-3aL and ataxin-3c. Laço et al. (2012a) reported that VCP is able to selectively enhance the activity of WT ataxin-3. This enhancement on the other hand is negated by HR23A (Laço et al., 2012a). The activation, however, was reported to be limited to normal ataxin-3, although ataxin-3 with a pathological polyQ expansion shows a stronger interaction with VCP (Hirabayashi et al., 2001; Laço et al., 2012a). Based on this model, a stronger VCP-induced activation of normal ataxin-3aS can be expected as the inhibition is reduced due to the weaker interaction between ataxin-3aS and HR23A/B. This proposed activity increase again could assist explaining the reduced stability of ataxin-3aS. Enzymatically active ataxin-3 is known to be less stable than inactive entities (Todi et al., 2009). Analyzing ataxin-3's DUB activity in the present study did not reveal a particularly increased DUB activity of ataxin-3aS but instead showed that the activity of ataxin-3c is reduced in comparison to ataxin-3aL and ataxin-3aS. However, these assays were performed fully *in vitro* therefore modulatory effects of VCP and HR23A could not be assessed.

5.1.5.1.3 Parkin

Ataxin-3 was the first described DUB partner for parkin and WT as well as polyQ expanded ataxin-3 are known to interact with parkin (Gwinn-Hardy et al., 2001; Bettencourt et al., 2011;

Durcan et al., 2011; Durcan and Fon, 2011). Clinically, MJD shows a parkinsonian phenotype in the rare subtype IV (Park et al., 2015; Bettencourt et al., 2011; Tuite et al., 1995). The interaction between ataxin-3 and parkin, mediated by ataxin-3's UIMs, is well studied and known to causes a reduction in parkin ubiquitination. Parkin undergoes mainly K27 and K29-linked polyubiquitin autoubiquitination *in vitro* (Fallon et al., 2006; Joch et al., 2007; Durcan et al., 2011). Ataxin-3 itself is unable to hydrolyze previously assembled ubiquitin chains on parkin (Durcan et al., 2012). Instead, ataxin-3 forms and stabilizes a complex with parkin and an E2 ligase which prevents parkin autoubiquitination (Durcan et al., 2012). This mechanism requires a functional cysteine of the JD which is in stark contrast to other DUB enzymes with a similar mechanism (Nakada et al., 2010; Scortegagna et al., 2011; Durcan et al., 2012).

The SILAC tandem MS approach of the present study revealed that the nonsense SNP rs7158733 in *ATXN3*aS reduced the proteins ability to interact with parkin compared to ataxin-3aL and ataxin-3c. This weakening of interaction potentially has fatal consequences for the regulation of parkins neuroprotective function, the cellular parkin protein level and apoptosis: due to the weaker interaction of ataxin-3aS with this protein, parkin autoubiquitination could either be increased in presence of SNP rs7158733 which results in an activation of parkin (Durcan et al., 2011, 2012) or dysregulated. Due to the neuroprotective function of parkin, such an activation could be beneficial (Lonskaya et al., 2013; He et al., 2018) and reduce apoptosis (Kemeny et al., 2012). A lack of parkin's regulation, however, would be deleterious. Parkin is known to clear expanded ataxin-3 fragments and therefore prevent aggregation and cytotoxicity (Tsai et al., 2003). A dysregulation of parkin activity or induction of parkin degradation therefore may lead to a disruption of cell stress pathways (Durcan et al., 2012). Parkin further promotes the clearance of mitochondria which lost their membrane potential (Narendra et al., 2008) in a manner which is accompanied by parkin autoubiquitination and ubiquitination of other proteins associated with mitochondria (Geisler et al., 2010; Tanaka et al., 2010; Chan et al., 2011). As mentioned before, the reduced interaction between ataxin-3aS and parkin may not only affect parkin autoregulation but may also cause parkin clearance. Expanded ataxin-3 for example is not able to regulate parkins autoubiquitination and promotes parkin clearance via autophagy (Durcan et al., 2011) and also pathogenic mutations in parkin which interfere with parkins autoinhibition show a fast degradation (Chaugule et al., 2011). However, the report that ataxin-3c with a physiological polyQ expansion does not regulate parkin stability (Durcan et al., 2011; Durcan and Fon, 2011) is contradictory to this hypothesis. Nonetheless, the reduced ability to interact with parkin suggests a potential effect on parkin stability with all dysregulatory consequences.

Lastly, the interaction between ataxin-3 and parkin directly links ataxin-3 to apoptosis regulation. It was reported that parkin regulates the levels of the pro-apoptotic protein Apoptosis Related protein in the TGF-β Signaling pathway (ARTS) in order to prevent unwanted apoptosis (Kemeny et al., 2012). The above-mentioned increased parkin clearance would result in elevated ARTS levels accompanied by ARTS and X-linked inhibitor of apoptosis[2] (XIAP) regulated B-cell lymphoma 2 (Bcl-2) degradation which would result in apoptosis (Edison et al., 2017).

Further research will be necessary to clarify the significance of the interaction of ataxin-3aS

[2]Newly identified ataxin-3 interactor, see 4.1.5, page 87 and 5.1.5.2.3, page 157.

with parkin and their resulting consequence in pathology. The results presented in the present study together with the published literature suggest an increased toxicity of ataxin-3aS compared to ataxin-3c and -3aL (Gaspar et al., 2002; Dengler, 2018). This increased toxicity may be partially explained by the reduced interaction between ataxin-3aS and parkin.

5.1.5.1.4 Tubulin

Ataxin-3 was first reported to interact with tubulin by Mazzucchelli et al. (2009). Differences in ataxin-3's interaction with tubulin may play an important role in microtubule filament network organization (Mazzucchelli et al., 2009; Rodrigues et al., 2010; Bonanomi et al., 2014a) as well as ataxin-3's proposed role in directing aggregated proteins to aggresomes and aggresome formation (Burnett and Pittman, 2005; Mazzucchelli et al., 2009; Bonanomi et al., 2014a). Rodrigues et al. (2010) reported that ataxin-3 depletion leads to a microtubule network disorganization without an obvious effect on filament polymerization. Important for this process is the motor protein dynein, another binding partner of ataxin-3 (Ligon et al., 2001; Burnett and Pittman, 2005; Rodrigues et al., 2010). The previously reported interaction of ataxin-3 and tubulin (Mazzucchelli et al., 2009; Bonanomi et al., 2014a) as well as ataxin-3 and dynein (Burnett and Pittman, 2005) could be confirmed for all ataxin-3 isoforms in the present work. Further, the reported stronger interaction of tubulin with ataxin-3a isoforms compared to ataxin-3c (Bonanomi et al., 2014a) could be verified as well. Therefore it is clear that it is mainly ataxin-3aL and ataxin-3aS which is involved in the interaction with microtubules as already proposed by Bonanomi et al. (2014a). The lower affinity can be a cause of the loss or modification of tubulin binding region 3 which is located C-terminal of the polyQ repeat and which was reported to be essential for tubulin binding (Bonanomi et al., 2014a). Interestingly, the SILAC tandem MS results presented here showed that the SNP rs7158733 variant even tightened the interaction between ataxin-3aS and tubulin (see 4.1.5, page 87). However, the special role of ataxin-3aL and possible changes by ataxin-3aS remain elusive so far and require more detailed investigations. Nonetheless, the importance of ataxin-3aL and also ataxin-3aS for cytoskeletal organization remains untouched by this knowledge gap and is underlined by a study from Costa et al. (2010). It could be shown that ataxin-3 is important for the initial differentiation steps in myogenesis, to organize the cytoskeleton and also regulates integrin subunit levels as well as the levels of other proteins of the integrin-mediated signaling pathway (Rodrigues et al., 2010; doCarmo Costa and Paulson, 2012). The effect of a cytoskeletal disorganization however, is not limited to the microtubule network (Costa et al., 2010; Rodrigues et al., 2010). Rodrigues et al. (2010) hypothesized that the absence of ataxin-3 may first lead to microtubule disorganization which in turn affects the other cytoskeletal components. This is an effect that could previously be seen for microtubule disturbing drugs (Forry-Schaudies et al., 1986; Rodrigues et al., 2010).

The interaction of ataxin-3 with tubulin and dynein may also be important for shuttling aggregated proteins to aggresomes and regulating aggresome formation (Burnett and Pittman, 2005; Mazzucchelli et al., 2009; Rodrigues et al., 2010; Bonanomi et al., 2014a). When the protein degradation machinery is overwhelmed or impaired in eukaryotic cells, aggresomes, a kind of inclusion bodies in which these proteins accumulate, are formed around the MTOC (Ligon et al., 2001). Aggresomes seem to be a protective response of the cell which sequesters aggregates

to protect itself from their potential toxicity and also acts as a center for a potential autophagic clearance (Kawaguchi et al., 2003; Olanow et al., 2004; Ross and Poirier, 2005). Burnett and Pittman (2005) suggested that the participation of ataxin-3 in aggresome formation creates a dangerous situation because a protein which itself can misfold and aggregate takes part in a cellular process where it is exposed to misfolded and aggregated proteins. This observation is of special importance because ataxin-3a isoforms are the main interactor with tubulin (see 4.1.5, page 87, Bonanomi et al., 2014a). In the present study, ataxin-3aL was found to show microscopic protein foci and an increased relative amount of SDS-soluble ataxin-3 even without carrying a polyQ expansion (4.2.1). This can be explained by the two-stage pathway of ataxin-3 fibrillization where ataxin-3 di-/oligomerization is initiated by the JD domain and therefore, in the first step, independent of the polyQ domain (Ellisdon et al., 2006). Even further, the SNP rs7158733 induced shift from ataxin-3aL to ataxin-3aS induces an even increased propensity to form protein aggregates and therefor leads to the exposure of a highly aggregation prone protein to other proteins in this pathway. This supports the hypothesis that SNP rs7158733 is highly associated with the toxicity of ataxin-3 (Gaspar et al., 2002; Dengler, 2018)

5.1.5.1.5 Ubiquitin

Ataxin-3 seems to regulate protein ubiquitination of various different proteins (Schmitt et al., 2007; Scaglione et al., 2011) via ubiquitin binding by its UIMs (Berke et al., 2005). However, in the present study, it was found that ataxin-3c co-precipitates lower amounts of high-molecular-weight ubiquitinated proteins compared to the ataxin-3a isoforms. These results are consistent with a previous report by Berke et al. (2005). The reduced precipitation of ubiquitinated proteins shows that ataxin-3c either has a lower binding affinity to ubiquitin in general or that it binds ubiquitins more selective. It was reported previously that ataxin-3 acts as a molecular ruler selecting proteins marked with ubiquitins of a certain length (Nicastro et al., 2009). Therefore a more specific binding of ataxin-3c to ubiquitins seems more likely, especially because this isoform also shows a lower enzymatic activity against Ubiquitin-Rhodamine-110 (see 4.1.4, page 84) and fewer strong interactions in the SILAC tandem MS analysis (see 4.1.5, page 87). Ataxin-3c may be a protein of higher specialization, directed against more specific substrates instead of acting as a broad-spectrum deubiquitinating enzyme. This again shows, that ataxin-3 isoforms are different proteins which at least partially take over unequal functions within the cell.

5.1.5.2 Newly identified ataxin-3 interactors

Next to already well known interaction partners of ataxin-3 the SILAC tandem MS analysis also revealed a multitude of previously unknown interaction partners. Among the newly identified interaction partners many showed minor differences of their interaction with ataxin-3 isoforms. However, UBR2, caspase-7, X-linked inhibitor of apoptosis (XIAP) and diablo homolog showed the most prominent differences between them and will be introduced and discussed in more detail.

5.1.5.2.1 E3 ubiquitin-protein ligase UBR2

UBR2 could be identified as a new ataxin-3 interactor in the present study which interacts with all three isoforms but seems to show a stronger interaction with ataxin-3c. Ataxin-3 and UBR2 share common protein functions and pathways, because both are involved in the UPS pathway and are commonly involved in degradation of misfolded proteins, maintaining genome integrity and apoptosis: (1) UBR2 is an E3 ligase carrying a RING domain (Kwon et al., 1998, cf. parkin) and as an N-recognin participates as a major component of the N-end rule proteolytic pathway (Tasaki et al., 2005). This pathway is a ubiquitination dependent proteolytic pathway in which N-recognins recognize destabilizing N-terminal residues of short-lived proteins or peptides (so called N-degrons) and promote their degradation (reviewed in Tasaki and Kwon, 2007; Eldeeb et al., 2018). (2) In *S. cerevisiae* Ubr2 was also reported promoting the degradation of misfolded and unfolded polypeptides (Nillegoda et al., 2010). It is possible that ataxin-3 and UBR2 either target such proteins for degradation together or UBR2 targets ataxin-3 for degradation because the N-terminal methionine acts as a primary destabilizing residue in the Arg-N-end rule pathway (Eldeeb et al., 2018). (3) Further, it was reported that UBR2 is also involved in maintaining genome integrity (Ouyang et al., 2006; An et al., 2012) and plays an important role in chromatin inactivation and transcriptional silencing via ubiquitination of histone H2A and H2B (An et al., 2010, 2012) which was also observed for ataxin-3 by histone deacetylation (Evert et al., 2006). (4) Lastly, PINK1 is degraded by the N-end rule pathway upon recognition by UBR2 (Yamano and Youle, 2013). PINK1 together with the ataxin-3 interactor parkin plays an important role in mitophagy induction (Narendra et al., 2008). UBR2 could be an important modifier of MJD because many proteolytic protein fragments from the apoptosis signaling cascade which seems to be involved in MJD (Tsai et al., 2004b; Yi et al., 2013; Gao et al., 2015; Liu et al., 2016) are short lived-substrates of the Arg-N-end rule. The N-end rule pathway which targets these fragments for degradation clearly counteracts this caspase-mediated apoptosis-activation (Eldeeb et al., 2018).

5.1.5.2.2 Caspase-7

Another newly identified ataxin-3 interactor is caspase-7. The protein shows an increased interaction with ataxin-3aS compared to ataxin-3aL and ataxin-3c. This protein, like ataxin-3, is a cysteine protease (Lamkanfi et al., 2002) known to act as executioner caspase in apoptosis and is also involved in inflammation (Lamkanfi and Kanneganti, 2010). Therefore, caspase-7 together with X-linked inhibitor of apoptosis (XIAP) and diablo homolog (see 5.1.5.2.3 and 5.1.5.2.4, page 157) links ataxin-3, and hereby especially ataxin-3aS, directly to the apoptosis pathway (Lamkanfi and Kanneganti, 2010).

Interestingly, caspase-7 is known to cleave other polyQ proteins like huntingtin, androgen receptor, atrophin-1 (Shoesmith Berke et al., 2004) and ataxin-7 and thereby modulate the toxicity of the protein (Young et al., 2007). Despite it was previously reported that caspase-1 is a primary mediator of ataxin-3 cleavage (Wellington et al., 1998; Shoesmith Berke et al., 2004), a potential increase in ataxin-3aS cleavage by caspase-7 and the formation of polyQ containing, highly hydrophobic C-terminal fragments (see Figure 4.24) could explain a more severe phenotype in patients with this SNP. On the other hand, it seems plausible as well that ataxin-3

could act as an inhibitor of caspase-7 activation in a similar way as it was previously reported for huntingtin and caspase-3 activation (Zhang et al., 2006).

5.1.5.2.3 X-linked inhibitor of apoptosis

Interestingly, caspase-7 is not the only connector of ataxin-3 to apoptosis. In the present work it could be shown for the first time that ataxin-3 isoforms also interact with XIAP, suggesting a role of ataxin-3 in apoptosis regulation. XIAP is the X-linked inhibitor of apoptosis (IAP) and as other IAPs plays an important role in apoptosis regulation (Cryns and Yuan, 1998; Miller, 1999) and other cellular processes (reviewed in Holcik and Korneluk, 2001; Obexer and Ausserlechner, 2014). Among all IAPs, XIAP is the most potent inhibitor and the only one which is able to inhibit caspases by a direct physical interaction (Deveraux and Reed, 1999; Holcik and Korneluk, 2001; Eckelman et al., 2006). In its function as an apoptosis inhibitor XIAP binds and inhibits the effector caspases -3 (Huang et al., 2001; Riedl et al., 2001) and -7 (Chai et al., 2001a) and the initiator caspase-9 (Deveraux et al., 1997, 1998; Sun et al., 2000; Shiozaki et al., 2003; Obexer and Ausserlechner, 2014). Interestingly, caspase-7 was found to be another interactor of ataxin-3 in the present work (see Figure 4.11 and above). While XIAP interacts and regulates caspases by its baculoviral IAP repeat domains, its RING domain functions as an E3 ligase for recognition and ubiquitination of protein substrates as well as regulation of its own stability (Obexer and Ausserlechner, 2014; Suzuki et al., 2001; MacFarlane et al., 2002). The ring domain thereby is able to conjugate different types of ubiquitin chains to its target proteins (Damgaard et al., 2012; Oberoi et al., 2012; Obexer and Ausserlechner, 2014). A RING domain can also be found in other ataxin-3 interactors like parkin (Riley et al., 2013; Seirafi et al., 2015) and UBR2 (Kwon et al., 1998). The way of XIAP autoregulation and the RING domain show high similarity to parkin. XIAP and other IAPs attenuate their anti-apoptotic effect by autoubiquitination which causes a self-degradation upon apoptotic stimuli (Yang et al., 2000; Suzuki et al., 2001). It was suggested that blocking this autoubiquitination may enhance their activity (Suzuki et al., 2001). Although, it was reported that XIAP is deubiquitinated and stabilized by USP11 (Zhou et al., 2017), it would be interesting to see if ataxin-3 is also able to attenuate XIAP autoubiquitination in a similar way as it was reported for parkin (Durcan et al., 2012) and thereby assists XIAP-mediated apoptosis inhibition. A dysfunction in this interaction upon a polyQ expansion in ataxin-3 as observed for parkin (Durcan et al., 2012) could support ataxin-3 induced neurodegeneration.

5.1.5.2.4 Diablo homolog

Lastly, the interaction of ataxin-3 with Diablo homolog additionally supports ataxin-3's potential role in apoptosis regulation. Diablo homolog was found to interact equally with all isoforms. The protein is released from mitochondria upon apoptosis induction together with cytochrome c and interacts with several IAP proteins (Du et al., 2000; Verhagen et al., 2000). Its proteasomal degradation was reported to be regulated by XIAP via its RING domain (Suzuki et al., 2001; MacFarlane et al., 2002). Interestingly, it seems like Diablo homolog is also able to interact with XIAP's baculoviral IAP repeat 2 and 3 and thereby competes with caspase binding which ultimately leads to a release of already processed caspases from XIAP (Chai et al., 2000; Srinivasula

et al., 2001; Obexer and Ausserlechner, 2014). This also leads to a decreased affinity of XIAP for caspase-3 and caspase-7 (Huang et al., 2001). Thereby, the amount of initiator and effector caspases is increased which promotes apoptosis (Obexer and Ausserlechner, 2014).

5.1.5.3 Summary of ataxin-3 interaction partners

The interaction of ataxin-3 with caspase-7, XIAP and Diablo homolog support a new functional role of ataxin-3 in apoptosis regulation. It would be interesting to analyze how a polyQ expansion changes these interaction networks for ataxin-3 isoforms as an expansion affects protein interactions of ataxin-3 as suggested by Duvick et al. (2010); Nedelsky et al. (2010) and observed by Kristensen et al. (2018). In general, proteins showing a stronger interaction with ataxin-3c were less frequent and related to the parkinson's disease, huntington's disease and oxidative phosphorylation KEGG pathway. In contrast to this, proteins showing a strong interaction with ataxin-3aL and ataxin-3aS were more diverse and related to several different KEGG pathways whereby the spliceosome, proteasome, calcium signaling, gap junction, huntington's disease and parkinson's disease pathway were the most frequent ones (Weishäupl et al., 2019).

5.1.6 Ataxin-3 isoforms do not differ in their transcriptional regulation

Multiple studies reported that ataxin-3 is involved in transcriptional regulation (Evert et al., 2001; Chai et al., 2001b; Li et al., 2002; Evert et al., 2003, 2006; Chou et al., 2008; Reina et al., 2012). Therefore, it was analyzed whether cells show differences in the transcription of selected genes which were previously described to be ataxin-3-regulated. Upon expression of the isoforms in the HEK 293T *ATXN3* KO model, significant changes could not be observed. A possible explanation for this could be that the experimental setup was not suitable for a detection of transcriptional changes and it may be that transcriptional regulation of ataxin-3 requires a neuronal cell model, longer expression time or different growth temperatures. Evert et al. (2001, 2003) used neuronal CSM14.1 cells instead of HEK cells. Further, transcription was analyzed after 2 days of ataxin-3 expression, whereas Evert et al. (2001, 2003) analyzed transcription after 7 days and also used a different growth temperature 37 °C vs. 33 °C. Due to the different experimental setups, a comparison of these results is difficult. Nonetheless, the ability of ataxin-3 to directly regulate transcription remains without a doubt.

Li et al. (2002) reported that there are different mechanisms which were proposed to lead to transcriptional repression induced by polyQ proteins: inhibition of coactivator activity (Steffan et al., 2001), direct corepressor activity (Wood et al., 2000; Zhang et al., 2002) and sequestration of transcription factors into protein aggregates (Chai et al., 2001b; McCampbell, 2000; Nucifora et al., 2001; Steffan et al., 2000; Chai et al., 2001b; Riley and Orr, 2006). While it can be concluded that ataxin-3 isoforms may not show major differences in their ability to actively regulate transcription, it is likely that they show strong differences in their ability to sequester transcription factors into protein aggregates and thereby enforce transcriptional dysregulation. Ataxin-3 is known to sequester the transcriptional coactivators TATA-box-binding protein, CREB-binding protein and Protein PML into aggregates (Perez et al., 1998; McCampbell, 2000; Chai et al., 2001b, 2002). Interestingly, aggregates composed of full-length or C-terminal polyQ-containing

fragments sequester different proteins and also different transcriptional regulators which shows that the protein context and interactors play an important role in protein sequestration (Chai et al., 2001b). Therefore, it can be assumed that ataxin-3 isoforms sequester different proteins and that the presence of ataxin-3aS in contrast to ataxin-3aL may lead to further sequestration induced changes (1) due to the interactional changes between these isoforms (see 4.1.5, page 87), (2) because of the increased aggregation propensity in contrast to ataxin-3aL (see 4.2.1, page 99) and (3) because of the increased nuclear localization of ataxin-3a isoforms and especially ataxin-3aS (see 4.1.7, page 97). Especially the nuclear localization may be critical for the pathology of MJD (Schmidt et al., 1998; Bichelmeier et al., 2007; Sowa et al., 2018) which indicates that the transcriptional dysregulation could also be an important part of the pathogenic mechanism (Evert et al., 2003). As suggested by Riley and Orr (2006), transcriptional dysregulation plays an important role in MJD pathogenesis and indeed may be modified by ataxin-3 isoforms.

5.1.7 Ataxin-3 isoforms differ in their subcellular localization

The subcellular localization of a protein is an important determinator of its cellular function due to the cellular microenvironment in different compartments and the availability of different interactors. Therefore, it was of great interest to see whether ataxin-3 isoforms are differentially distributed between the two main compartments, nucleus and cytoplasm. This is of special interest because the nucleus was previously reported to be an essential site for MJD pathology (Schmidt et al., 1998; Bichelmeier et al., 2007; Sowa et al., 2018). Nuclear localization of ataxin-3 was required for phenotype manifestation (Bichelmeier et al., 2007) and ataxin-3 is known to be strongly located to the nucleus in the especially affected Purkinje cells whereas other cell types do not show this localization (Trottier et al., 1998; Weishäupl et al., 2019).

In the present study, it could be shown that all isoforms are located in both compartments, cytoplasm and nucleus. However, while ataxin-3c was almost exclusively cytoplasmic, ataxin-3aL and especially ataxin-3aS were strongly enriched in the nucleus compared to ataxin-3c. Thereby, most of the previous studies which reported a major localization in the nucleus (Tait et al., 1998) as well as in the cytoplasm (Paulson et al., 1997a; Trottier et al., 1998; Schmidt et al., 1998; Macedo-Ribeiro et al., 2009; Pozzi et al., 2008) could be confirmed. Some studies also reported an equal distribution (Wang et al., 1997) and localization inside the mitochondria (Trottier et al., 1998; Pozzi et al., 2008). In concordance with the results presented here, the only study reporting a mainly nuclear localization (Tait et al., 1998) studied ataxin-3a. Although it was reported that upon polyQ expansion ataxin-3 is translocated into the nucleus where it also forms nuclear inclusions (Paulson et al., 1997a,b; Schmidt et al., 1998; Riess et al., 2008), differences between normal and polyQ expanded ataxin-3 isoforms could not be observed in the present study. This conforms to Tait et al. (1998) who reported that neither proteolytic cleavage nor an expansion of the polyQ repeat are necessary for nuclear localization. Eventually, the localization of ataxin-3 is dependent on the cell type studied (Macedo-Ribeiro et al., 2009) whereby HEK 293T cells were reported to show a mainly cytoplasmic localization of ataxin-3 (Tait et al., 1998) which is in line with the results of the HEK 293T *ATXN3* KO model presented here. In addition to the nuclear localization of ataxin-3aS, a putative N-terminal S256 calpain cleavage fragment of ataxin-3 being enriched in the nucleus for all isoforms could be identified in the present work. This is of special interest as it was previously reported that ataxin-3 as part

of the toxic fragment hypothesis is cleaved by caspases (Wellington et al., 1998) and calpains (Hübener et al., 2013; Weber et al., 2017; Weber, 2017) and this fragment was shown to cause mitochondrial dysfunction (Harmuth et al., 2018).

The heterogeneous intracellular distribution of ataxin-3 suggests that the specific localization may be of critical importance for ataxin-3‘s protein function (Trottier et al., 1998). The ability of ataxin-3 to translocate between nucleus and cytosol affirms this suggestion. Shuttling of a protein between nucleus and cytosol depends on localization signals, interaction with specific transport proteins and certain cellular conditions as described in the following.

Ataxin-3’ shuttling is partially dependent on specific stimuli (Pozzi et al., 2008; Macedo-Ribeiro et al., 2009; Reina et al., 2010; Chai et al., 2002) and its subcellular localization is regulated by at least three nuclear export/import signals. Two functional NES were found to be located within the JD (AA 78-85 and 147-158, Antony et al., 2009; Albrecht et al., 2004) whereas one NLS was found to be in close proximity to the polyQ repeat (AA 273-286, Antony et al., 2009; Tait et al., 1998; Albrecht et al., 2004; Macedo-Ribeiro et al., 2009). These signals are all located in regions which are not alternatively spliced between ataxin-3c and -3a. However, it is known that the nuclear localization of ataxin-3 is regulated by CK2-mediated phosphorylation of ataxin-3 at S236 (first UIM) and S340/S352 (third UIM) (Mueller et al., 2009). The latter two serines are only present in ataxin-3c which suggests that ataxin-3c is only translocated to the nucleus upon phosphorylation while both ataxin-3a isoforms may also be capable of a translocation without PTM. This could explain the reduced nuclear localization of ataxin-3c in the present study.

Further, differences between ataxin-3 isoforms could also be explained by a differential interaction with transport proteins. It is known that ataxin-3 can be exported from the nucleus in a protein exportin 1A/chromosomal region maintenance 1 (XPO1/CRM1) dependent and independent mechanism (Macedo-Ribeiro et al., 2009). Protein exportin 1A could be identified as an interactor of ataxin-3 isoforms in the SILAC tandem MS analysis (see 4.1.5, page 87), however, no differences in interaction strength could be found. Another possible shuttling factor in regulating ataxin-3‘s nuclear localization is karyopherin subunit α 3 (KPNA3). A karyopherin subunit α 3 knockout can successfully prevent nuclear localization and toxicity of ataxin-3 but nothing is known about the interaction with ataxin-3 (Sowa et al., 2018). On the other hand, macromolecules, until they reach a critical mass of approximately 70 kDa, can diffuse into the nucleus. Larger macromolecules or proteins need to be actively imported (Seksek et al., 1997). Therefore, it is also possible that ataxin-3 is still capable of diffusion and does not require an active import into the nucleus.

Lastly, different forms of stress (proteotoxic, heat shock, oxidative) were reported to trigger a nuclear shuttling of ataxin-3. This could suggest a functional role of ataxin-3a isoforms in stress response, e. g. in transcriptional regulation (Reina et al., 2010). Differences in transcriptional regulation, however, could not be observed between ataxin-3 isoforms (see 4.1.6, page 95) but the experiments also were not conducted under stress conditions. Nonetheless, differences in stress-induced translocation between ataxin-3 isoforms can be expected as heat-shock dependent nuclear translocation of ataxin-3 is regulated by the JD (including S111 phosphorylation) together with the C-terminus (Reina et al., 2010).

Independent of the translocation mechanism, once inside the nucleus ataxin-3 could undergo a conformational change due to the interaction with the nuclear matrix which could enable new interactions with specific nuclear proteins and therefore enable the nuclear function of ataxin-3 (Tait et al., 1998; Perez et al., 1999). This conformational change happens either by the association to the matrix itself or, once ataxin-3 is in the nucleus, the protein undergoes a conformation change and then binds to the nuclear matrix (Perez et al., 1999). The increased localization of ataxin-3aL and especially -3aS inside the nucleus described here could be explained by this matrix association. It was previously reported that (1) exposure of hydrophobic groups increases the binding to the nuclear matrix (Lepock et al., 2001) and (2) other proteins that are associated to the nuclear membrane contain hydrophobic sequences which are important for the association and interaction (Stoppin et al., 1994). The C-terminus of ataxin-3a isoforms is highly hydrophobic and therefore could facilitate the interaction with the nuclear matrix whereas it is possible that this interaction does not happen for ataxin-3c or happens to a lesser extent, explaining the lower levels in the nucleus. Such a matrix association was also described previously for ataxin-1 (Skinner et al., 1997). Another explanation for the increased nuclear localization is oligomerization of ataxin-3. Di-/trimerizations are able to mask NES which prevents a nuclear export and therefore traps the protein inside this compartment (Reina et al., 2010; Stommel, 1999). Aggregation analysis of ataxin-3 (4.2.1) showed that ataxin-3a isoforms are prone to form protein aggregates and Harris et al. (2010) reported that oligomerization of this isoform is promoted by the hydrophobic C-terminus. According to Macedo-Ribeiro et al. (2009) nuclear export of ataxin-3 requires the JD as well as the UIM. Upon di-/trimerization those regions could be masked as well.

The nuclear localization of ataxin-3 is of high importance for ataxin-3's toxicity and there is a positive correlation of the nuclear localization with polyQ mediated toxicity (Perez et al., 1998; Bichelmeier et al., 2007; Sowa et al., 2018; Wang et al., 2018b). The same is true for other polyQ proteins like ataxin-1 (Burright et al., 1995; Klement et al., 1998), ataxin-7 (Kaytor et al., 1999), huntingtin (Saudou et al., 1998; Peters et al., 1999; Yang, 2002), androgen receptor (Katsuno et al., 2002) and atrophin-1 (Nucifora et al., 2003). Consequently, the nucleus was reported to be the main site of MJD pathology (Paulson et al., 1997b; Schmidt et al., 1998). Ataxin-3's adoption of an abnormal conformation in the nucleus could be an early event in MJD pathogenesis which exposes the polyQ domain (Perez et al., 1999) and could allow a rapid aggregation especially of ataxin-3a isoforms as described in section 5.2.1. Further, it was reported that expanded polyQ stretches are able to form membrane channels (Hirakura et al., 2000). The hydrophobic C-terminus of ataxin-3 could assist this formation.

In summary, the nuclear localization of polyQ proteins in general and ataxin-3 in detail is critical for the pathogenesis and ataxin-3aS shows a strongly increased nuclear localization. Further, the stronger nuclear localization of ataxin-3a isoforms suggests an important function inside the nucleus (Weishäupl et al., 2019).

5.2 Pathophysiological characteristics of ataxin-3 isoforms

5.2.1 Ataxin-3 isoforms show differences in protein aggregation

Aggregation of the respective polyQ expanded protein is a hallmark of all nine polyQ and many other inherited or acquired neurodegenerative diseases like α-synucleinopathies (e. g. PD, multiple systems atrophy, dementia with lewy bodies), tauopathies (e. g. AD, chronic traumatic encephalopathy, Frontotemporal dementia and parkinsonism linked to chromosome 17 (FTDP-17)) or prion diseases (Davies et al., 1997; Hayashi et al., 1998; Li et al., 1998; Skinner et al., 1997; Koyano et al., 1999; Paulson et al., 1997b; Ishikawa et al., 1999; Holmberg et al., 1998; Nakamura, 2001; Goedert et al., 2017; Orr et al., 2017; Sigurdson et al., 2019). Consistent with these previous reports the present study showed that all three isoforms of ataxin-3 are able to form aggregates. It was reported that aggregation happens in a two-step process which firstly generates SDS-soluble oligomers and by sequestration forms SDS-insoluble fibrils (Invernizzi et al., 2012; Bonanomi et al., 2015) whereby it is believed that toxicity is rather induced by oligomeric species generated in the initial phase of fibrillogenesis than by late stage insoluble aggregates (Lajoie and Snapp, 2010; Olshina et al., 2010; Tomic et al., 2009; Takahashi et al., 2008; Bucciantini et al., 2002; Baglioni et al., 2006; Campioni et al., 2010; Invernizzi et al., 2012). Kinetic analysis of ataxin-3 aggregation in the present study confirmed that the amount of SDS-insoluble fibrils increases over time in an isoform-independent manner. Normal ataxin-3 also formed SDS-soluble oligomers but not SDS-insoluble aggregates which confirms a previous report by Invernizzi et al. (2012) as well.

While all isoforms showed increasing aggregation over time numerous differences could be identified between ataxin-3 isoforms. Cells expressing ataxin-3aL and ataxin-3aS more frequently showed aggregate foci than those cells expressing ataxin-3c which suggests that ataxin-3a isoforms generally are more aggregation prone. Nonetheless, numerous differences could also be observed between ataxin-3aL and ataxin-3aS. Both isoforms differed in the amount of SDS-insoluble ataxin-3, *in vitro* aggregation kinetics, aggregate size and the number of aggregates per cell. This clearly shows that the SNP rs7158733 introduced PTC in *ATXN3*aS has a huge impact on aggregate formation. The nature of aggregates formed by ataxin-3aL suggests that these aggregates are more soluble than those of ataxin-3c and -3aS which could be of particular importance as toxicity of aggregates was associated to their size and density. It could be observed that tight aggregates are usually non-toxic while amorphous aggregates can be toxic (Duennwald et al., 2006b; Gruber et al., 2018). It is possible that small oligomers as well as amorphous aggregates are interacting with other proteins more efficiently than amyloid deposits and therefore induce toxic interactions as well as protein sequestration (Treusch et al., 2009). On the contrary, ataxin-3aL is associated with an increased aao, whereas patients, carrying the SNP rs7158733 which leads to ataxin-3aS show an earlier aao (Dengler, 2018). The SNP rs7158733 leading to ataxin-3aS converged most aggregation characteristics of ataxin-3aL towards that of ataxin-3c. In addition ataxin-3aS showed a faster aggregation kinetic than ataxin-3aL and ataxin-3c. This fact could make it harder for cells to cope with aggregates formed by this isoform as a faster aggregation can bypass cellular defense mechanisms (Duennwald et al., 2006b). Although ataxin-3c required more time to form visible inclusions the total number of cells with aggregates as well as total SDS-insoluble protein was comparable to ataxin-3aS. This suggests that

ataxin-3c is less likely to form aggregation seeds, nonetheless, when initial seeds are formed it aggregates fast. This is not surprising, as calculations showed that a single misfolded monomer is enough to act as a seed for the growth of larger oligomers and finally fibrils (Chen et al., 2002c,b).

Aggregation of ataxin-3 isoforms was previously analyzed *in vitro* and *in vivo* by Harris et al. (2010) and Johnson et al. (2019), however, both studies did not investigate the aggregation properties of ataxin-3aS. Harris et al. (2010) reported that ataxin-3aL is more aggregation prone than ataxin-3c and suggested that the presence of a highly aggregation prone isoform in certain subpopulations of neurons may contribute to the selective neuronal toxicity. The authors also describe a model of ataxin-3 aggregation according to which ataxin-3aL oligomerization is assisted by the hydrophobic C-terminus of the protein and therefore is predominantly forming insoluble fibrillar aggregates, whereas ataxin-3c is forming fewer insoluble aggregates. Harris et al. (2010) reported that ataxin-3aL generally showed more puncta per cell than ataxin-3c and also showed aggregates in almost all cells. This observation indeed could be confirmed in the present study. Ataxin-3aL in comparison to ataxin-3c usually formed multiple aggregates within a cell and more cells carried aggregates. Nonetheless, in contrast to the work of Harris et al. (2010) the total amount of SDS-insoluble ataxin-3 was reduced compared to ataxin-3c. A possible explanation could be given by the usage of protein tags which modify protein context. Usage of tagged constructs provides biased results due to the modifying effects of changing the polyQ flanking regions (Nozaki et al., 2001; Duennwald et al., 2006b; Invernizzi et al., 2012). The frequently used FLAG-epitope which was used by Harris et al. (2010), independent of its position, was found to modify aggregation and induce toxicity even when attached to non-toxic huntingtin (Duennwald et al., 2006b). SUMO-modification and a FLAG-tag both share a prominent feature: amino acids with a negative charge. A SUMO-1 modification at K166 of ataxin-3 increases ataxin-3's cytotoxicity (Zhou et al., 2013). Together, this suggests that a FLAG-tag could act similar to a SUMO-1 modification and is not suitable for aggregation and toxicity studies and renders the results of the present study to be more precise and reliable. The addition of a C-terminal EGFP-tag, as used in the present study, did not affect aggregation and toxicity as reported by Bonanomi et al. (2015).

The other study performed by Johnson et al. (2019) which analyzed a *Drosophila* model of MJD, reported that ataxin-3c shows a more prominent aggregation phenotype than ataxin-3aL together with an increased toxicity which is the opposite of the results presented by Harris et al. (2010). The authors reported that the reduced aggregation is a consequence of the observed lower protein level and, when expressed at identical levels, both isoforms neither differ in aggregation nor toxicity, which led them to the conclusion that ataxin-3aL does not have a significance for MJD pathogenesis (Johnson et al., 2019). Contrary, another study showed that a KI mouse model of MJD shows a CAG expansion dependent increase in the expression of the *ATXN3*a transcript compared to the *ATXN3*c transcript. This model shows a strong aggregation phenotype with region specific intranuclear and extranuclear inclusions although the expression level of ataxin-3 is only modest (Ramani et al., 2015). This clearly shows that definitely an expression of ataxin-3aL or ataxin-3aS could be of special importance for the pathogenesis of MJD and that the cellular as well as the protein context plays a crucial role in ataxin-3's aggregation characteristics. One important factor of the ataxin-3 protein context regarding aggregation is

common to all ataxin-3 isoforms, the N-terminal JD (Masino et al., 2011).

5.2.1.1 The JD is important for ataxin-3 aggregation and may be involved in differences between ataxin-3 isoforms

Though the C-terminus obviously has an impact on aggregation properties, the initial aggregation step is mediated by the JD which is identical between ataxin-3aL, ataxin-3aS and ataxin-3c. Therefore, all isoforms should follow a two-step aggregation process (Harris et al., 2010). The JD plays an important role in modulating ataxin-3 aggregation propensity by determining its stability and self-association ability whereas the polyQ repeat is only involved in the second aggregation step (Ellisdon et al., 2006; Masino et al., 2011; Matos et al., 2011). The JD contains two highly conserved regions which are responsible for substrate recognition but at the same time are also highly aggregation-prone making josephins proteins which are able to aggregate under native conditions (Masino et al., 2011). Interestingly, interaction of the JD with ubiquitin reduces its autoaggregation which led to the conclusion that josephin function and aggregation are encoded by identical regions of the protein (Masino et al., 2011). Ataxin-3c has a reduced ubiquitin affinity (see 4.1.5, page 87) which could therefore explain a stronger aggregation propensity of this isoform compared to ataxin-3a. It is possible that non-expanded ataxin-3, by interacting with other proteins via the JD, masks the aggregation-prone regions and therefore stabilizes itself. This tight balance could be disturbed by the addition of an aggregation prone element (e. g. a hydrophobic C-terminus) or hindrance of interactions (due to a different C-terminus, Masino et al., 2011). In the present study, it could be observed that in general ataxin-3c shows weaker interactions with many molecular partners than both ataxin-3a isoforms which could indicate that such aggregation prone regions are exposed more frequently in ataxin-3c which leads to the strong aggregation phenotype. Nonetheless, the observed conversion in aggregation properties between ataxin-3aL and -3aS can be associated solely to the changes induced by the differing C-termini.

5.2.1.2 Differences in aggregation between ataxin-3 isoforms can be explained by the protein context

The diverging aggregation properties of ataxin-3 isoforms with its partially minor and partially major disparities can be explained by different means which are all determined by the protein context of the respective isoform. This principle also applied to polyQ proteins in general (Gatchel and Zoghbi, 2005; Riley and Orr, 2006; Harris et al., 2010; Paulson, 2018; Lieberman et al., 2019). All nine polyQ proteins share the same phenomenon – aggregation. However, they entirely differ in their polyQ flanking regions (Zoghbi and Orr, 2000; Duennwald et al., 2006b) which ultimately causes distinct pathologies and phenotypes. It was previously reported that the polyQ flanking regions are a crucial part of such proteins (Totzeck et al., 2017) and that they are able to modify the protein's aggregation behavior (Crick et al., 2013; Eftekharzadeh et al., 2016). Alternative splicing of the *ATXN3* gene as well as the SNP rs7158733 may only change a small fraction compared to the total protein, nonetheless they cause significant changes which largely impact physiological protein functions (see 4.1, page 75). This made a direct impact of the C-terminus expectable as the modification is in close proximity to the polyQ repeat and

(1) changes the AA composition of the whole C-terminus and therefore also the biochemical properties of this region (i. e. hydrophobic amino acids in ataxin-3aL/ataxin-3aS compared to more hydrophilic one's in ataxin-3c), (2) changes molecular interactions (see 4.1.5, page 87) and (3) affects protein localization.

5.2.1.2.1 The hydrophobic C-terminus of ataxin-3aL and ataxin-3aS may increase aggregate formation via hydrophobic interactions

The mainly hydrophobic AA of the ataxin-3aL and ataxin-3aS C-terminus close to the polyQ repeat may greatly change the properties of the whole C-terminus. While the C-terminus of ataxin-3c is disordered (Lambrughi et al., 2021), it was previously reported that the C-terminus of ataxin-3a isoforms is largely unstructured (Goto et al., 1997) which seems to be a general fact for tertiary structures which surround polyQ regions (Albrecht et al., 2004). Ataxin-3a proteins are not the only proteins harboring folded domains flanked by intrinsically unstructured regions and a polyQ tract. Ataxin-3 shares this feature with ataxin-1 (SCA1), -2 (SCA2), -7 (SCA7) Voltage-dependent P/Q-type calcium channel subunit alpha-1A (SCA6), TBP (SCA17) and atrophin-1 (SBMA) (De Chiara et al., 2003; Albrecht et al., 2004; Uversky, 2010; Masino et al., 2011). This lack of structure, however, may explain the high aggregation propensity of these proteins (Albrecht et al., 2004). While polyQ repeats are able to form β-strands that can be linked together between main- and side-chain hydrogen bonds between amides (Perutz et al., 1994), the hydrophobic sequence in ataxin-3a isoforms may add an additional instability to the protein. It was reported that hydrophobic interactions can lead to aberrant interactions and thereby cause protein aggregation (Pechmann et al., 2009). Such regions may usually be stabilized within the protein (Pechmann et al., 2009), however, it is unclear if this stabilization still succeeds upon a pathological expansion of the polyQ repeat. Biochemical properties of the ataxin-3 C-terminus may therefore explain the observed higher aggregation propensity of both ataxin-3a isoforms.

5.2.1.2.2 Differences in protein-protein interactions are likely to contribute to the the individual ataxin-3 aggregation characteristics

Interactions are able to mask aggregation prone motifs and therefore stabilize a protein (Pechmann et al., 2009; Masino et al., 2011). Thus, differences in protein-protein interactions between the isoforms can contribute to the explanation of the observed variations in aggregation.

Numerous differences in molecular interactions could be identified for ataxin-3 isoforms (see 4.1.5, page 87), among them HR23A/B. HR23A/B is known to stabilize ataxin-3 and prevent its aggregation and toxicity by interacting with ataxin-3's Ubiquitin binding site 2. A weakening of this interaction was shown to cause faster aggregation and increase ataxin-3's toxicity in a *Drosophila* model (Sutton et al., 2017). Interestingly, both ataxin-3aL and ataxin-3c interact with HR23A/B but ataxin-3aS showed a weaker interaction with HR23B in the present study. A loss of stabilizing interactions could therefore explain the observed stronger aggregation behavior of ataxin-3aS in comparison to ataxin-3aL and shows that protein interactions may contribute to the individual aggregation phenotype of ataxin-3 isoforms. Thereby interactions may not only affect aggregation propensity but also ataxin-3 aggregate morphology by sequestration of different proteins like prion-proteins, chaperones or proteasome components.

Among prion-like proteins (Cascarina and Ross, 2019) heterogeneous nuclear ribonucleoprotein A1 (hnRNP A1) and heterogeneous nuclear ribonucleoprotein D-like (hnRNP D-like) could be identified as interactors of ataxin-3 using the SILAC tandem MS approach presented here. Among these two, hnRNP D-like shows a stronger interaction with ataxin-3c compared to ataxin-3aL and ataxin-3aS suggesting that their molecular interaction could change ataxin-3c aggregation and toxicity. It was reported that deletion or knockdown of prion-like proteins has a protective effect on polyQ-mediated toxicity, whereas an overexpression has toxic effects depending on the flanking regions of the polyQ protein (Duennwald et al., 2006a). Another protein class with direct impact on aggregation are chaperones that interact with polyQ proteins which either mediate their degradation or disposal (i. e. formation of inclusions, Schaffar et al., 2004). Multiple chaperones could be identified in the present study. The co-chaperone DNA-J together with chaperones was shown to prevent ataxin-3 aggregation and toxicity in *Drosophila* (Sutton et al., 2017; Tsou et al., 2015). Despite ataxin-3aL and ataxin-3aS show a stronger interaction with DNA-JA1, -A2, -B3, -B6 and -B7, ataxin-3aL indeed is less likely to form SDS-insoluble aggregates whereby such an DNA-J-mediated protective effect could be lost in ataxin-3aS. Next to chaperones, it was also reported that components of the proteasome complex co-aggregate with ataxin-3 and proteasome-inhibition increases this formation (Chai et al., 1999a,b). Further, polyQ expanded ataxin-3 is considered to directly inhibit proteasome function (Díaz-Hernández et al., 2006; Venkatraman et al., 2004). This is of special importance as ataxin-3aS was found to be degraded by the proteasome (see 4.1.3, page 80). Therefore, an inhibition of proteasomal degradation by polyQ expanded ataxin-3 may increase the aggregation of this specific isoform.

5.2.1.2.3 Protein localization of ataxin-3 isoforms may modify aggregate characteristics and toxicity

Lastly, protein localization may affect ataxin-3 aggregation. The cellular microenvironment has a big impact on aggregation properties due to (1) local protein concentration, (2) presence of stabilizing (e. g. chaperones) and destabilizing (e. g. proteases) factors and (3) constant protein supply (Invernizzi et al., 2012). Interestingly, extended naked polyQ peptides aggregate in the cytoplasm of a cell and are solely transported to the nucleus under presence of an NLS (Kazantsev et al., 2002) showing that the protein context is strikingly important for aggregate localization. Ataxin-3aL and especially ataxin-3aS was found to be located in the nucleus to a greater extent than ataxin-3c (see 4.1.7, page 97). This could suggest that localization of aggregates also differs between ataxin-3 isoforms. This is of importance, as aggregate localization was reported to be a better indicator for aggregate-induced toxicity than size or composition (Weiss et al., 2008). However, no differences could be found in aggregate localization; aggregates were exclusively cytoplasmic. This is in contrast to the reported aggregate localization in patients and animal models. It was reported that protein aggregates form primarily in the nucleus (Paulson et al., 1997b; Schmidt et al., 1998; Chai et al., 2001b; Bichelmeier et al., 2007) which shows that nuclear ataxin-3 is particularly aggregation prone (Chai et al., 2001b). Nuclear aggregation was reported to be part of the later stage of MJD pathogenesis (Pozzi et al., 2008) and was shown as well for SCA1, SCA2, SCA7, SCA17, DRPLA, SBMA and HD (Saudou et al., 1998; Schöls et al., 2004). Cytoplasmic aggregates, however, were also shown in SCA2, SCA6 and HD (Huynh et al., 2000; Ishikawa et al., 1999; Lunkes et al., 2002) and also reported in SCA3

(Hübener et al., 2011; Nguyen et al., 2013).

5.2.2 Ataxin-3 isoforms show minor differences in aggregation after cleavage

Ataxin-3 is subject to proteolytic cleavage by caspases (Wellington et al., 1998; Shoesmith Berke et al., 2004; Haacke et al., 2007), calpains (Hübener et al., 2013; Weber et al., 2017) and by autoproteolysis (Mauri et al., 2006). Ataxin-3 cleavage triggers cytotoxicity and aggregation which induces or emphasizes neurodegeneration (Ikeda et al., 1996; Paulson et al., 1997b; Haacke et al., 2006; Pozzi et al., 2008; Breuer et al., 2010; Matos et al., 2017; Weber et al., 2017). On the other side, calpain inhibition showed protective effects (Haacke et al., 2007; Weber et al., 2019; Robinson et al., 2021). In the present work it could be found that the C-terminus of ataxin-3c contains different predicted calpain cleavage sites, which do not exist in ataxin-3a. Cleavage at these positions together with cleavage at positions D208 and S256 (two sites important for pathogenesis, Weber et al., 2017), would lead to even smaller polyQ containing fragments that lack the non-polyQ C-terminus of ataxin-3 and therefore could be especially aggregation prone. Indeed, ataxin-3c showed a trend towards an increased aggregation propensity upon calpain induction which could not be observed for ataxin-3aL and -3aS. This increase accords to the toxic fragment hypothesis where small fragments containing the polyQ tract are more aggregation prone (Ikeda et al., 1996; Paulson et al., 1997b; Haacke et al., 2006; Breuer et al., 2010; Koch et al., 2011; Matos et al., 2017). It was suggested that the toxicity of these fragments results from (1) increasing ataxin-3's aggregation tendency and accumulation in the cell nucleus, (2) enabling co-aggregation even with non-expanded ataxin-3 and (3) altering the normal ataxin-3 function and turnover (Matos et al., 2017). Such a toxic fragment may only be critical for an initial seeding step and later on fragments are no longer necessary in order to drive the aggregation cascade (Paulson et al., 1997b; Pozzi et al., 2008). As it could be observed that ataxin-3c's initial induction of aggregation is slower than that of both ataxin-3a isoforms it is plausible that cleavage is accelerating seed generation and thereby aggregation of this specific isoform. However, cleavage is not required and ataxin-3 is able to aggregate without cleavage induction as well (see 4.2.1, page 99).

5.2.3 Ataxin-3 isoforms do not affect the mitochondrial potential and cell cycle

Proteins showing an expanded polyQ repeat are known to be toxic (Parker et al., 2001; Bates, 2003; Duennwald et al., 2006b; Hübener et al., 2011; Invernizzi et al., 2012) and the processes underlying polyQ mediated toxicity are essentially conserved throughout different species (Invernizzi et al., 2012). Harris et al. (2010) suggested that ataxin-3aL and ataxin-3c could proof to show a different toxicity. Later on Johnson et al. (2019) reported that ataxin-3c shows a higher toxicity in *Drosophila* due to the higher expression level but toxicity does not differ when ataxin-3aL and ataxin-3c are expressed in equal amounts. However, the authors did not study the effect of SNP rs7158733 which leads to ataxin-3aS and was observed to reduce the aao in patients (Dengler, 2018). Therefore, ataxin-3aS could proof to be a more toxic isoform in MJD. In order to clarify whether ataxin-3 isoforms show a differential toxic potential their toxicity was assessed by two means: analysis of the cells mitochondrial membrane potential and the

cell cycle. Membrane integrity is a part of MJD pathogenesis (Pellistri et al., 2013; Richter, 1987; Butterfield et al., 2002; Bonanomi et al., 2015; Harmuth et al., 2018) and it was suggested that age-related recurring oxidative stress could be the driving factor in MJD pathogenesis (Reina et al., 2010). Aggregates of expanded polyQ proteins are able to interact with membranes and induce membrane permeabilization (Lindgren and Hammarström, 2010; McLaurin and Chakrabartty, 1997; Jayasinghe and Langen, 2007; Zhang et al., 2017b). Formation of SDS-soluble aggregates is accompanied by an increase in reactive oxygen species levels due to the induction of mitochondrial dysfunctions (Lashuel et al., 2002; Bonanomi et al., 2015). Therefore, both, increased reactive oxygen species levels and ataxin-3 aggregates could potentially affect membrane integrity (Bonanomi et al., 2015). Due to the differential nature of the isoform-specific aggregates it seemed likely that the isoforms show a differential toxicity in *ATXN3* KO cells as. However, it could be found that membrane depolarization does not differ between ataxin-3 isoforms or transfected/non-transfected cells. Next to a mitochondrial phenotype, it was also reported that normal cell cycle progression is affected in ataxin-3 expressing cells and expression of polyQ expanded ataxin-3 has a growth-inhibitory effect (Invernizzi et al., 2012; Bonanomi et al., 2015). This can be explained by ataxin-3's interaction with HR23A/B and VCP. During cell cycle progression the protein level of HR23A is controlled by an Ubiquitin-protein ligase E3A mediated ubiquitination which regulates HR23A function during the cell cycle (Kumar et al., 1999). Further, VCP plays an important role in cell cycle progression by mediating degradation of important factors (Fu et al., 2003; Raman et al., 2011; Meyer and Weihl, 2014; Riemer et al., 2014). Investigating the cell cycle in ataxin-3 transfected cells in the present study showed that upon ataxin-3 expression cells do not display major differences between cell cycle subpopulations and an increase in the apoptosis associated SubG1 population (Yoshino et al., 2017; Grechowa et al., 2017; Chang et al., 2019) could not be observed. In summary, toxic potential as assessed by the mitochondrial membrane potential and cell cycle could not be identified for ataxin-3 isoforms independent of their polyQ expansion size. Both assays were performed on all cells without the possibility of discriminating between transfected and non-transfected cells. Therefore, possible effects in transfected cells could be masked by the presence of a high amount of non-transfected cells. Further, MJD is a disease of the adult and chronic stress by the polyQ expanded ataxin-3 may over time cause effects that could not be observed during the short experimental setup. Bonanomi et al. (2015) concordantly noted that membrane integrity may be corrupted on a long term. Utilizing a model with a stable expression of ataxin-3 isoforms would approach both problems as virtually all cells carry the transgene and expression is secured over a long period of time.

Despite no toxic effects could be observed for ataxin-3 isoforms it is likely that the isoforms differ in their toxic potential based on differing aggregation characteristics and due to their differences in molecular interactions. Most progressive neurodegenerative diseases are characterized by protein aggregation (Treusch et al., 2009). However, it still is a matter of discussion whether protein aggregates are the primary pathogenic entity or a byproduct of the pathogenic process or even a protective response of the cell (Arrasate et al., 2004; Rub et al., 2006; Slow et al., 2005; Saudou et al., 1998; Klement et al., 1998; Saudou et al., 1998; Olshina et al., 2010; Lajoie and Snapp, 2010; Arrasate et al., 2004; Miller et al., 2010; Sánchez et al., 2011; Xue et al., 2009; Lambert et al., 1998; Treusch et al., 2009; Haass and Selkoe, 2007). Neither expression level nor

visible protein aggregation of many polyQ proteins correlates with toxicity (Sharp et al., 1995; Schilling et al., 1995; Nishiyama et al., 1996, 1997; Saudou et al., 1998; Gutekunst et al., 1999; Kuemmerle et al., 1999; Simeoni, 2000; Duennwald et al., 2006b) although a strong correlation exists between polyQ-expansion size required for aggregation and the pathogenic threshold of polyQ diseases (Scherzinger et al., 1999). This fact suggests that at least initiation of the aggregation pathway acts as a pathological trigger (Scherzinger et al., 1999). Aggregation initiation was triggered faster in cells expressing ataxin-3aL and especially ataxin-3aS compared to ataxin-3c. Therefore, it is likely that cytotoxic processes are initiated earlier in presence of ataxin-3aS which could explain the reduced aao. Further, using the SILAC tandem MS approach, different interactors could be identified which are modulators of ataxin-3 toxicity. Protein exportin 1A/chromosomal region maintenance 1 (XPO1/CRM1). DnaJ homolog subfamily C member 7 (DNAJC7) and polyubiquitin-C (UBC) are mild to strong suppressors of MJD pathology (Bilen and Bonini, 2007) which could be proven to interact with all ataxin-3 isoforms DnaJ homolog subfamily B member 6 (DNAJB6), another strong suppressor of MJD toxicity (Bilen and Bonini, 2007) shows a significant stronger interaction with ataxin-3a. Interestingly, Bilen and Bonini (2007) reported that DnaJ homolog subfamily B member 6 induces autophagy. This fact, again, could lead to a differential toxicity of ataxin-3aL and -3aS as an autophagy induction may reduce ataxin-3aL protein levels but would not affect ataxin-3aS levels because this isoform is degraded by the proteasome (see 4.1.3, page 80).

Based on the observed haplotype-induced differences in the aao and the fact that ataxin-3 isoforms show differences in aggregation and their interaction with modulators of ataxin-3 toxicity it is likely that ataxin-3 isoforms and especially ataxin-3aS show differences in their cellular toxicity although these differences could not be assessed in the present work.

5.3 Mutual interaction of ataxin-3 isoforms

5.3.1 Ataxin-3 isoforms can have an influence on each other's stability

People sharing the same CAG expansion length show a wide variation in their aao (Slepko et al., 2006). Therefore, factors must exist which modify the aao. The normal allele is known to be one such modifier (Warrick et al., 2005; França et al., 2012; Sutton et al., 2017; Dengler, 2018). Ataxin-3 is able to interact with itself, whereby the exact mechanism is unknown (Masino et al., 2004; Todi et al., 2007). Nonetheless, the presence of different ataxin-3 isoforms in one single cell make a mutual influence of different ataxin-3 isoforms likely. In order to analyze this effect, physiological and pathophysiological characteristics (i. e. stability and aggregation) of ataxin-3 were analyzed. Isoform combinations were chosen in a way that they are likely to occur in MJD patients (Gaspar et al., 2002; Martins et al., 2006).

Indeed, the presence of a second ataxin-3 protein impacted ataxin-3 characteristics. Depending on the isoform combination, expression of a second ataxin-3 isoform was able to change the stability of ataxin-3. These results confirm a previous report that ataxin-3 is able to increase the degradation of inactive and otherwise slowly degraded ataxin-3 in trans (Todi et al., 2007). This change in stability is not a consequence of DUB of one ataxin-3 isoform by another because it was reported that ataxin-3 is not deubiquitinating other ataxin-3 proteins (Todi et al.,

2007; Weishäupl et al., 2019). Interestingly, in contrast to the results presented here, Todi et al. (2007) described an increase in degradation. These differences possibly arise due to the fact that inactive ataxin-3 was analyzed by Todi et al. (2007) whereas active ataxin-3 was studied in the present work. Enzymatic inactivation itself already impacts ataxin-3 stability (Todi et al., 2007). Therefore, it can be expected that active ataxin-3 shows different results upon co-expression. The stability increase could be explained by the fact that ataxin-3 is capable of rescuing itself from degradation. A similar mechanism was for example described for parkin which is known to be rescued from its degradation by ataxin-3 (Durcan et al., 2012). Further, an interaction between two ataxin-3 molecules could mask binding sites for other proteins which mitigate ataxin-3 degradation or it prevents an activation of ataxin-3 by VCP (Laço et al., 2012a). Both would result in a stabilization of the protein. Stabilization of ataxin-3aS, however, could be problematic as this variant in the normal allele is associated with an earlier aao (Dengler, 2018) and a stabilization of the protein could lead to an accumulation (Matsumoto et al., 2004) of this, presumably more toxic or less protective, variant.

These results show that experiments should be conducted in a KO background in order to prevent an experimental bias by the presence of a second allele. This is especially important for studies of minor protein isoforms or when two different alleles carry different haplotypes or mutations (Weishäupl et al., 2019).

5.3.2 Ataxin-3 isoforms have an influence on each other's aggregation

On a pathological level the present study analyzed the effect of ataxin-3 with a physiological polyQ repeat on aggregation of pathologically expanded ataxin-3. It could be found that co-expression of WT ataxin-3 prevents polyQ expanded ataxin-3 from aggregation independent of the isoform combination. These results confirm the assumption that ataxin-3 reduces the accumulation of protein aggregates (Warrick et al., 2005; Tsou et al., 2013, 2015). A WT *ATXN3* allele was previously shown to rescue the disease phenotype in *Drosophila* (Warrick et al., 2005; Tsou et al., 2013, 2015; Burr et al., 2014; Sutton et al., 2017). It is unclear whether a direct interaction of ataxin-3 isoforms is required for this protective function but it is known that it requires the physiological ubiquitin associated activities of ataxin-3 (Warrick et al., 2005; Tsou et al., 2013; Sutton et al., 2017). Further, the interaction with Rad23 as well as transcriptional regulation of DnaJ-1 also seems to play an important role for the protective function in *Drosophila* (Tsou et al., 2013, 2015; Sutton et al., 2017). Human homologs of both proteins exist. Therefore, it is possible that similar protective mechanisms also exist in humans. Even further, a neuroprotective function of ataxin-3 against other polyQ disorders is likely as well because DnaJ-1 is also able to suppress huntingtin toxicity (Kazemi-Esfarjani and Benzer, 2000). Surprisingly, results from a double-transgenic MJD model contradicted the reports from *Drosophila*. The presence of a WT allele did not mitigate the neurodegenerative phenotype of these mice and the authors hypothesized that only slowly progressing disease phenotypes could be influenced by the WT allele (Hübener and Riess, 2010).

Altogether, these results clearly show that ataxin-3 isoforms indeed have an impact on each other's physiological and pathophysiological characteristics. However, further studies investigating the details of this interaction and the potential neuroprotective mechanisms will be important

to fully clarify the role of the WT allele in MJD pathogenesis (Weishäupl et al., 2019).

5.4 Generation of a ataxin-3a isoform-specific antibody

5.4.1 An ataxin-3a isoform-specific antibody would allow further insights into ataxin-3 characteristics

Currently, no direct discrimination between ataxin-3c and ataxin-3a isoforms is possible. An ataxin-3c specific antibody was generated by Schmidt et al. (1998) and could successfully be used to detect ataxin-3c in nuclear inclusions of MJD patients and since then is widely used for different applications like analyzing the nuclear localization of ataxin-3 (Bichelmeier et al., 2007) or dissecting cleavage fragments (Weber et al., 2017; Harmuth et al., 2018) which requires antibodies specific for various protein regions. However, due to the inability of specifically discriminating between ataxin-3aL/ataxin-3aS and ataxin-3c without the use of a protein tag attached to ataxin-3 (e. g. in an animal model or human) important questions regarding the isoforms cannot be addressed. The availability of an ataxin-3aL/ataxin-3aS specific antibody on the other hand would enable different studies which will be described in more details below: (1) investigating the relative protein level of ataxin-3 isoforms, (2) analyzing the spatial distribution of ataxin-3 isoforms within the brain, (3) discrimination of ataxin-3 isoforms within a single cell and (4) determining ataxin-3aL/ataxin-3aS C-terminal cleavage sites.

Harris et al. (2010) tried to quantify ataxin-3aL and ataxin-3c protein levels by using the 3c-specific antibody generated by Schmidt et al. (1998). The authors claimed that ataxin-3c is the major protein isoform in brain as they could not identify an ataxin-3 signal which they could specifically relate to ataxin-3a. Using an isoform-specific antibody for ataxin-3a isoforms would finally allow to analyze the exact relative protein levels of ataxin-3 isoforms. Further, such an antibody would finally allow a screening of different neuronal cell populations for their expression of ataxin-3 isoforms and possibly identify certain populations which oppose the general expression pattern. This assumption is likely; ataxin-3 was reported to be located to the nucleus in Purkinje cells whereas this localization could not be observed in other cell types (Trottier et al., 1998). Although different brain regions were previously screened for their expression pattern (Thul et al., 2017)[3], to date, no information is available yet about the expression of specific ataxin-3 isoforms in certain types of tissue or certain cell types (Johnson et al., 2019). Analyses of *ATXN3* transcript diversity were performed (Bettencourt et al., 2010, 2013); however, it is of striking importance to perform such analyses on protein level as there is no simple correlation between mRNA and protein levels (Chusainow et al., 2009). This becomes especially obvious when one looks at the mRNA and protein level of *ATXN3*/ataxin-3 in the affected brain region *cerebellum* (Thul et al., 2017). Next, an ataxin-3aL/ataxin-3aS specific antibody would allow a discrimination between the isoforms within a single cell which would enable further studies on how ataxin-3 isoforms interact and behave within their cellular environment. Schmidt et al. (1998) showed that ataxin-3c aggregates in the nucleus of neurons. Ataxin-3a isoforms instead could show a differential behavior. Lastly, such an antibody would allow studying ataxin-3 cleavage as the identification of cleavage sites as well as the specific detection of fragments requires antibodies which are able to recognize those. No doubt, the

[3]Human Protein Atlas for *ATXN3* available from https://v18.proteinatlas.org/

described experiments can partially also be performed using cellular or animal models when appropriate protein tags are employed. Nonetheless, a protein tag always disturbs the natural protein context and greatly affects experimental outcomes (Nozaki et al., 2001; Duennwald et al., 2006b; Invernizzi et al., 2012).

5.4.2 The ataxin-3a C-terminus lacks important requirements of an antigen

In order to generate an ataxin-3aL/ataxin-3aS-specific antibody peptides were synthesized containing the C-terminal sequence of these isoforms followed by subsequent immunization of rabbits and purification of antibodies. Peptide-specific antibodies have a major advantage against those raised against purified proteins. They enable the generation of antibodies against proteins that cannot be purified, that were only identified based on cDNA sequence or against specific regions of a protein (Angeletti, 1999), e. g. the C-terminus of ataxin-3. On the other hand, small peptides act as haptens and therefore are weakly or non-immunogenic and require a carrier protein like keyhole limpet hemocyanin or tetanus toxoid which induces a strong immune response (Yano et al., 2005; Greenfield et al., 2018).

The usage of the C-terminal ataxin-3a peptides allows a direct immunization against the only region where ataxin-3 isoforms differ between each other and therefore are also the only regions that could be used as an immunogen for a discriminatory antibody. This, however, was problematic. In general antigenicity is a product of (1) composition, (2) secondary structure, (3) accessibility and (4) evolutionary conservation (Wang et al., 2011). The ataxin-3aL/ataxin-3aS C-terminus lacks most of these requirements. Firstly, the AA composition of a peptide used for immunization must allow a proper immune reaction of the host. Good immunogens are among others characterized by a high hydrophilicity value (Hopp and Woods, 1981) and a paratope usually is enriched with aromatic side chains and hydrophilic residues (reviewed in Novotny et al., 1986). This shows that a good immunogen should contain enough hydrophilic AAs to provide suitable antigenic determinants. This is not only necessary for the immunogen to act as such but also regarding solubility. In the case of peptide antibodies, it is obvious that a good immunogen must be soluble under the specific experimental conditions, i. e. purification and immunization (Angeletti, 1999). The synthesized peptide was highly insoluble as a result of the C-terminal AA composition of ataxin-3aL/ataxin-3aS rendering it a generally poor immunogen without antigenic determinants. One problem about peptides is their inability to fold in a way like longer polypeptides or proteins do. This makes them unable to bury hydrophobic stretches within the structure, which could happen under physiological conditions (Zaluzec et al., 1994). The C-terminus of ataxin-3a isoforms is not compactly folded but flexible and carries hydrophobic residues which are solvent-exposed (Masino et al., 2003; Sicorello et al., 2018). This renders the C-terminus accessible, however, due to their length restrictions, already small clusters of hydrophobic AA are able to change the general solubility of a peptide and render them insoluble (Angeletti, 1999). This was a problem that could be observed whenever the peptide was handled and was also previously observed by Sicorello et al. (2018).

Secondly, the C-terminus of ataxin-3 has a secondary structure composed of α-helices, β-sheets, turn and random coil. Whereas the C terminal region is mainly unstructured for ataxin-3aL and ataxin-3aS (Goto et al., 1997; Masino et al., 2004), the third UIM in ataxin-3c, as well as the other two UIMs, form an α-helical secondary structure (Sicorello et al., 2018). It is

generally assumed that the secondary structure of the whole C-terminus of ataxin-3 could be stabilized by protein-protein interactions (Masino et al., 2004) and this interaction may also be crucial in order to prevent ataxin-3 aggregation (Masino et al., 2004).

Thirdly, a defined tertiary structure is absent (Masino et al., 2004; Sicorello et al., 2018). This suggests, that ataxin-3, although carrying solvent-exposed hydrophobic stretches under the experimental conditions (Masino et al., 2003), tries to bury its hydrophobic residues inside a hydrophobic structure in order to prevent its exposure to the aqueous surrounding which would mask the epitope under physiological conditions (Zaluzec et al., 1994). Generally, the same masking effect also applies after denaturation and binding to a membrane as interaction of a protein with a membrane involves hydrophobic forces (Gershoni and Palade, 1982, 1983; Tovey and Baldo, 1989; Beeskow et al., 1997).

Lastly, the requirement of a lack of evolutionary conservation is fulfilled. While the N terminal JD shows a conserved sequence (Albrecht et al., 2003), the ataxin-3a C termini are not evolutionary conserved (Masino et al., 2003).

5.4.3 The specificity and sensitivity of the anti-3a antibody could be improved

The anti-3a antibody showed multiple protein bands on western blot and a lack of specificity among crude samples independent of denaturation (western blot) or physiological folding (fluorescence microscopy) whereby antibody dilution, detergents, sample denaturation/loading dye or the membrane used did not affect the binding capabilities of the antibody. Therefore, the antibody did neither show a high specificity nor sensitivity. A lack of specificity may be explained by the antibody itself and the ataxin-3 sample and partially by the fact that antibodies are often multi-specific and show cross reactivity due to molecular mimicry (Jain and Salunke, 2019). Concerning the antibody a possible reason could be the long immunization and therefore maturation time of the antibody. Germline antibody complementarity determining regions show a low amount of arginine (Birtalan et al., 2008; Burkovitz et al., 2014). However, maturation increases the number of arginine mutations in the complementarity determining regions of an antibody (Tiller et al., 2017). This is associated with a reduced specificity, presumably due to its high interactivity (Birtalan et al., 2008; Tiller et al., 2017). Antibodies with a high specificity against a hydrophobic Alzheimer's amyloid β peptide showed lower amounts of such mutations compared to those with a low specificity (Tiller et al., 2017). The long immunization time – which was necessary due to the low immunogenicity – therefore could explain the lack of specificity. However, the ataxin-3 sample could be the root cause of the problem as well. The inability of the purified antibody, to detect low amounts of ataxin-3aL and ataxin-3aS in crude lysates may be explained by the above mentioned masking of epitopes within the lysates. Usage of larger amounts of purified protein makes it more likely to have minimal amounts of protein epitopes accessible that are suitable for antibody binding. On the other hand, a lack of immunoreactivity can also be a result of PTMs of the protein in the cellular host (Angeletti, 1999). Hardly anything is known about modifications of the ataxin-3a C-termini but it known that, while the N terminus is protease-resistant, the C-terminus is protease accessible (Masino et al., 2003) and most ataxin-3 cleavage products contain C terminal fragments (Nicastro et al.,

2010). Therefore, small modifications of the ataxin-3a C termini may not be observed under most experimental conditions but render the ataxin-3 C-terminus undetectable using this antibody. Interestingly, this is not the first report of the inability of detecting ataxin-3 using an antibody. Perez et al. (1999) reported that ataxin-3 cannot be detected by the 1C2 antibody in absence of the nuclear environment, e. g. purified in solution or bound to ELISA plates.

Despite the fact that the antibody is not able to specifically and sensitively detect ataxin-3 in presence of large amounts of unrelated proteins, the experiments showed that the anti-3a antibody mostly is capable of discriminating between the ataxin-3 C termini under purified conditions. Therefore, a specific detection of ataxin-3a isoforms using this antibody seems to require more or less purified samples. This can be achieved by different means such as affinity purification or chromatography. However, all these techniques would rely on the sole use of the anti-3a antibody. Techniques like a sandwich-ELISA that makes use of two different antibodies for the detection show a great increase in specificity as the protein of interest is detected by two different antibodies (Kemeny et al., 1985). Another technique that uses two different antibodies is a TR-FRET. In this assay two different antibodies are used which are coupled with a donor and an acceptor fluorophore (Baldo et al., 2012). If both antibodies are in close spatial proximity an excitation of the donor triggers an energy transfer to the acceptor fluorophore which then in turn emits a fluorescence signal which can be measured. The usage of two different antibodies which require a close spatial proximity strongly improves the specificity of a TR-FRET assay while the micro assay design allows a high sensitivity (Baldo et al., 2012). It could be shown that this assay already is suitable for the specific detection of ataxin-3c in the present study; however, a discrimination of the ataxin-3aL/ataxin-3aS C-terminus was not possible so far and the assay requires further development.

Although various methods have been tested in order to improve the specificity and sensitivity of the antibody there are still more options to test. Detergents were used during immunodetections in order to increase antibody specificity. However, the detergent used did not improve the specificity. Instead, a more complex mixture like milk could be utilized during immunodetection. Usage of increased concentrations of Triton X-100 were reported to be insufficient for increasing specificity at least against a hydrophobic Alzheimer's amyloid β peptide while addition of milk increased the specificity (Tiller et al., 2017). Further, a cross-linking between antigen and epitope could be applied. Namiki et al. (2008) reported that employing the biuret reaction with cupric ions at high pH is able to enhance antigen-antibody specificity and thereby improves the performance of some poorly reacting antibodies. The authors stated, that the signals for 20 % of antibodies against membrane-bound proteins could be improved in that study. Among them, was an antibody that only reacted at high titers but hardly detected the protein using a conventional western blot technique which is a similar situation compared to the anti-3a antibody.

In summary, different measures can be applied in order to possibly improve the suitability of the generated antibody. Therefore, the antibody should be tested with the here mentioned improvements in order to see whether this has an beneficial effect on its specificity and sensitivity and therefore allows a reliable detection of ataxin-3a isoforms in crude samples.

5.4.4 Outlook

As mentioned above, it is difficult to generate antibodies against hydrophobic epitopes; however, it is not impossible. Antibodies against extracellular regions of claudin-5, a multi-spanning membrane protein, could be generated successfully. Extracellular regions of such membrane proteins show poor immunogenicity due to their high conservation. Hashimoto et al. (2018) used a wheat cell-free protein synthesis system that produced the antigens as proteoliposomes for generation of the immunogen. The liposomes thereby act as a peptide-carrier to antigen presenting cells. Further, lipid A, which is contained in the liposomes, acts as a strong adjuvants (Alving, Carl et al., 1995). Using a wheat system, however, is not the only suitable way to generate antibodies against such problematic proteins. Immunization with antigen-pulsed dendritic cells also leads to an efficient generation of antibodies (Sornasse et al., 1992). Tamura and Chiba (2009) successfully used this approach and generated antibodies against different transmembrane proteins by stable transduction of dendritic cells with antigens, immunization of mice using these cells and subsequent boostering using plasmids expressing the antigen. These two examples show that conventional methods for peptide antibody production reach their limits when antibodies against low/none immunogenic peptides should be produced.

If the above mentioned procedures fail to improve antibody specificity, the only possibility to generate an ataxin-3a-specific antibody may be a different approach for the generation of antibodies. Ideally, wheat expression with a lipid adjuvants may be utilized for immunogen production. Due to the low immunogenicity, ataxin-3 KO mice may be used for the generation of antisera against the peptides to increase the immune response (Declerck et al., 1995). If necessary, these mice could then be used for the generation of monoclonal antibodies and the production of a phage display library that allows further antibody maturation and selection (Sommavilla et al., 2010). The generation of a library from immunized animals is beneficial as antibodies usually show a higher affinity compared to those with a synthetic, semi-synthetic or native (non-immunized) origin (Solemani Zadeh et al., 2019). Sensitivity, specificity and affinity of an antibody against such difficult regions could then be increased by affinity maturation when necessary (Bostrom et al., 2009; Wang et al., 2019).

5.5 Generation of an isoform-specific MJD zebrafish model

To date, different animal models for studying MJD were generated. Next to *Mus musculus* models (Ikeda et al., 1996; Cemal et al., 2002; Goti et al., 2004; Bichelmeier et al., 2007; Chou et al., 2008; Boy et al., 2009, 2010; Silva-Fernandes et al., 2010; Hübener and Riess, 2010; Switonski et al., 2015; Ramani et al., 2015) also *Rattus norvegicus* (Alves et al., 2008a,b), *Drosophila melanogaster* (Warrick et al., 1998, 2005; Johnson et al., 2019) and *Caenorhabditis elegans* models (Christie et al., 2014) were generated. Recently, Watchon et al. (2017) described the first MJD *Danio rerio* model. Animal models frequently use an ataxin-3aS normal allele (Schmidt and Schmidt, 2018) and this may also be true for many cell models. Though, the normal allele usually does not carry the stop variant and is therefore not capable of producing ataxin-3aS (Maciel et al., 1999; Gaspar et al., 2002). Using an uncommon normal allele will create conflicting results and makes the interpretation and translation of results even more difficult. The negative effect of this variant on the aao when present on the normal allele (Gaspar et al., 2002; Dengler, 2018) further renders this isoform inadequate for a standard disease model. This fact underscores how important it is to be aware of the exact isoform and haplotype of the protein studied and shows that other animal models are required in order to model the actual situation in the majority of MJD patients.

Detailed studies of the pathophysiological characteristics of ataxin-3 isoforms *in vivo* require animal models with the same genetic background (Johnson et al., 2019). Although animal models of the same species expressing different ataxin-3 isoforms may exist, a comparison of those models may result in false conclusions. Ideally, the animal models share the same promoter and genetic locus of integration in order to allow a comparable *ATXN3* expression level. Unfortunately, no existing model fulfills these requirements. Due to the number of isoforms and CAG expansions a new model is required which is facile to generate, raise and expand. For these reasons the first ataxin-3 isoform-specific *Danio rerio* model was generated. Zebrafish are widely used for research in movement disorders and other neurodegenerative diseases (McWhorter et al., 2003; Miller, 2005; Schiffer et al., 2007; Flinn et al., 2008; Xi et al., 2011; Meshalkina et al., 2017; Saleem and Kannan, 2018) and are increasingly employed in drug discovery studies (Schiffer et al., 2007; Vaz et al., 2018; Pitchai et al., 2019). Zebrafish are vertebrates (in contrast to *C. elegans* and *D. melanogaster*) which allows a more proper translation of results to the human situation. Further, they combine a couple of big advantages. Their small size allows inexpensive housing of large numbers in a single tank. The comparatively short generation time of three months and the high number of offspring speed up research and the external development allows straightforward genetic manipulation (Fishman, 2001; Flinn et al., 2008). In addition, the zebrafish CNS has extensively been correlated to the human one which makes them especially eligible for research on neurological disorders. Lastly, antisense morpholino strategies which readily allow a gene knockdown during development enable the study of altered gene functions in a disease (Flinn et al., 2008).

Altogether, this makes zebrafish an ideal model for the generation of multiple MJD lines. Therefore, zebrafish expressing the ataxin-3 isoforms ataxin-3c, ataxin-3aL and ataxin-3aS with the polyQ expansion sizes 18Q and 73Q were created. In this study, expression of ataxin-3 was controlled by the HuC promoter which is a homolog to *Drosophila* elavl3. This promoter

allows a neuron-specific expression and identification of early neurons (Park et al., 2000). The integration of the transgene into the zebrafish genome was verified, followed by an analysis of the respective *ATXN3* mRNA expression level, the level of ataxin-3 protein and ataxin-3 aggregation in the zebrafish.

Integration of the full construct could be confirmed for all lines. Expression of ataxin-3 isoforms could be verified for seven out of eight lines. One of two ataxin-3c lines with a polyQ expansion size of 18Q did not show a clear transgene *ATXN3* mRNA signal although the construct successfully integrated into the zebrafish genome. In order to allow a direct comparison of different MJD zebrafish lines, an integration of the transgene into the zebrafish should be accomplished by usage of the PhiC3 integrase system (Mosimann et al., 2013). However, due to a misinterpretation of the annotation the required AttB site of the integration vector was lost during cloning. This circumstance prevented a site-directed integration into the zebrafish genome and caused a random integration. Such a random integration may be problematic due to the lack of comparability of isoforms, when they show different ataxin-3 expression levels. This could happen due to integration into a heterochromatin area (Hahn et al., 2010) and for example could also explain the lack of detectable mRNA in the above-mentioned ataxin-3c line. The unplanned random integration though may not necessarily be a general disadvantage of the model. The protein level of ataxin-3 was found not to be identical between the isoforms *in vitro* (see 4.3, page 79). Even further, it could be found that ataxin-3c and 3aL have similar mRNA levels *in vivo* although they markedly differ in their protein level (Johnson et al., 2019). This is in line with previous reports from Harris et al. (2010) who reported that ataxin-3c is the predominant isoform in murine brain. Adversely however is the fact that an integration may not only affect the transgene expression level itself. It can also change global or specific expression levels of various genes dependent on where the integration happens (e. g. regulatory element vs. a single gene). This complicates comparability of MJD pathology within the zebrafish lines and, depending on the integration site, would forbid drawing a conclusion, e. g. when an important interactor of ataxin-3 would be affected.

Protein expression could be confirmed for two lines expressing ataxin-3c and ataxin-3aL on western blot and for all lines using immunohistochemical staining of brain sections from adult zebrafish. Generally, the expression levels of the transgene ataxin-3 as analyzed by western blot were low in both lines, while all samples showed a high background staining. Due to the sole expression in neurons, the general protein level of ataxin-3 is low in larvae, but was believed to be higher in brain samples due to the sample nature. Therefore, those samples could be expected to have a better signal to noise ratio due to the reduced sample complexity. A low expression level was unexpected, as the first MJD zebrafish model generated by Watchon et al. (2017) also used a HuC promoter which enabled a clearly visible ataxin-3 expression. Nevertheless, specific detection of ataxin-3 expression in the majority of samples was not possible by western blotting independent of the underlying mRNA levels. This clearly highlights the partially lacking correlation between mRNA and protein level (Lichtinghagen et al., 2002; Chen et al., 2002a; Greenbaum et al., 2003). One reason for this lack of correlation can be the stability of the protein (Greenbaum et al., 2003). Protein turnover differs for ataxin-3 isoforms with ataxin-3aS being the least stable (see 4.1.3, page 80). The reduced protein stability of ataxin-3aS can

explain the lower protein level of this isoform but also the observed absence in western blot in the ataxin3-aS zebrafish line although the mRNA level was comparable to that of the ataxin-3c and ataxin-3aL lines. Another reason for the lack in correlation can be PTMs (Chen et al., 2002a; Greenbaum et al., 2003). Ataxin-3 is known to be subject to PTMs. It is cleaved by caspases (Wellington et al., 1998; Berke et al., 2004) and calpains (Haacke et al., 2007; Simoes et al., 2012; Weber et al., 2017; Weber, 2017) and modified by ubiquitination (Todi et al., 2009, 2010; Tsou et al., 2013; Carvalho et al., 2018), phosphorylation (Tao et al., 2008; Mueller et al., 2009) and SUMOylation (Zhou et al., 2013). However, it is unclear so far whether such modifications differ between ataxin-3 isoforms.

Lastly, zebrafish brain samples were analyzed for the presence of ataxin-3 aggregates. The well described cytoplasmic (Hübener et al., 2011; Nguyen et al., 2013) or intranuclear (Paulson et al., 1997b; Schmidt et al., 1998; Chai et al., 2001b; Bichelmeier et al., 2007) aggregates could not be identified using immunohistochemical staining of brain sections or filter trap assays. Depending on the disease model and the polyQ expansion, aggregates do not necessarily appear in an animal model (Ikeda et al., 1996; Bichelmeier et al., 2007; Silva-Fernandes et al., 2010; Watchon et al., 2017) and are age dependent. Watchon et al. (2017) reported no aggregation phenotype in 1 year old transgenic MJD zebrafish. The animals studied here were partially 4 mpf. Therefore, no aggregates could be expected unless a specific isoform shows a vast stronger aggregation phenotype. This could have been expected for ataxin-3aS as this isoform was especially aggregation prone (see 4.2.1, page 99) but was not observed.

In a next step it will be important to clarify the expression status of all lines concludingly. The inability of detecting ataxin-3 in western blot leaves doubt about the expression of ataxin-3 in all lines although immunohistochemical stainings of brain sections including parallel control staining indicate an expression. While western blot still allows a size comparison to a standard, immunostainings of slides fully rely on the specificity of the antibody. After confirming the expression status, founders which show a comparable protein level are required. Due to the random integration one cannot be sure whether a reduced protein level reflects the physiological situation or is attributable to the integration site. This is a strong disadvantage of the model as the expression level can greatly affect the experimental outcome (Johnson et al., 2019). After confirming the expression status the integration sites need to be determined in order to exclude the risk of an accidental inactivation of a disease related gene before the fish could be used for a detailed investigation of the impact of ataxin-3 isoforms on the pathology of MJD in zebrafish.

The newly generated zebrafish model is not the first model for comparing ataxin-3 isoforms *in vivo*, but it is the first isoform-specific MJD zebrafish model that enables a comparison of all three ataxin-3 isoforms. Despite numerous animal models for MJD exist (reviewed in Schmidt and Schmidt, 2018) there is only a single *Drosophila* model which compared ataxin-3 isoforms (Johnson et al., 2019) and a MJD KI mouse model that allows the expression of both isoforms (Ramani et al., 2015) and thereby showed interesting insights into alternative splicing in MJD. However, the *Drosophila* model only investigated ataxin-3c and ataxin-3aL but not ataxin-3aS and the KI model does not allow an isolated analysis of ataxin-3 isoforms.

The comparison of ataxin-3 isoforms in *Drosophila* showed that ataxin-3c is more toxic than

ataxin-3aL and flies expressing ataxin-3c showed reduced survival. Further, ataxin-3aL and -3c expressing flies showed a reduced ability to climb compared to control cells but climbing impairment was observed at a later time point in flies expressing ataxin-3aL than in flies expressing ataxin-3c. Lastly, Johnson et al. (2019) reported that ataxin-3c showed a more pronounced aggregation phenotype than ataxin-3aL. But looking at the ataxin-3 level, ataxin-3aL showed a lower protein level. Therefore, when ataxin-3aL was expressed at similar levels to ataxin-3c, both showed equal toxicity (Johnson et al., 2019). These results differ partially from the results presented here as well as from previous results published by Harris et al. (2010) showing that the studied model as well as modifications of the protein (e. g. protein tags) and the usage of certain inhibitors greatly affects experimental outcomes (see 5.1.3, page 146). Further, the study did not consider that ataxin-3aL only can be expressed from a minority of expanded ataxin-3 alleles worldwide due to the SNP rs7158733 (Gaspar et al., 2002; Dengler, 2018).

As mentioned above, Ramani et al. (2015) described an interesting KI mouse model of MJD with 82 Q-repeats which could be used to study ataxin-3 isoforms in more detail. Despite a modest ataxin-3 expression level, the KI model shows a strong aggregation phenotype with region specific intranuclear and extranuclear inclusions. Most interestingly, increasing CAG repeat lengths correlated with an increase in the relative number of *ATXN3*a transcripts in the KI mouse model (Ramani et al., 2015). This shift in expression suggests, that the main pathogenic protein in MJD could be ataxin-3aS as SNP rs7158733 with the TAA stop is the major variant worldwide (Maciel et al., 1999; Gaspar et al., 2002). Interestingly, a similar mechanism also leads to a polyQ induced change in gene splicing in SCA 6 (Tsou et al., 2011) and could also be observed for intron 1 in *HTT* transcripts that is followed by the CAG containing exon 1. This could suggest an aberrant splicing of mutant transcripts caused by an affected binding of splicing factors in CAG containing transcripts (Gipson et al., 2013; Sathasivam et al., 2013). Niblock et al. (2016) also reported this effect for intron 1 of normal and expanded *C9orf72* which, upon expansion, is the genetic cause for Amyotrophic lateral sclerosis (ALS) and Frontotemporal dementia (FTD). This suggests that repeat expansion induced splice modulation is a common effect in tri- and hexa-nucleotide repeat expanded transcripts (Baralle et al., 2008) and that ataxin-3aS plays an important role in the pathogenesis of MJD.

5.6 Evaluation of a read-through approach as a potential therapy for MJD

The haplotype of the *ATXN3* gene is known to have an impact on the aao of MJD. The exon 8/10 haplotype ACA in the expanded allele is associated to a significantly earlier aao compared to the haplotype GGC (Dengler, 2018). The SNP rs7158733 which is leading to the PTC and generates ataxin-3aS instead of ataxin-3aL seems to have the highest impact on the aao (Dengler, 2018) which shows that the expression of expanded ataxin-3aS is detrimental while the expression of ataxin-3aL has beneficial effects. This fact highlights to date unstudied therapeutic approaches such as splice modulation therapy (successfully applied in Duchenne muscular dystrophy, Wood et al., 2010) in order to suppress *ATXN3*a expression or PTC read-through approaches. A read-through which would generate ataxin-3aL despite the presence of the SNP rs7158733 induced PTC would reduce the amount of ataxin-3aS in patients carrying this variant.

Introduction of PTC into a gene whose open reading frame is transcribed into mRNA causes the release factors to recognize the stop codon when it enters the aminoacyl (A)-site at the ribosome (Schueren and Thoms, 2016). The ribosome then prematurely terminates the translation of the mRNA which leads to the production of a premature peptide or protein which eventually undergoes nonsense-mediated decay (Finkel, 2010; Hug et al., 2015). In case of a PTC read-through, the stop codon is not recognized by the release factors, instead an AA is added to the polypeptide chain (Li and Zhang, 2019). Translational read-through occurs naturally (Li and Zhang, 2019) and can as well be triggered using pharmaceutical agents such as aminoglycosides (Howard et al., 1996; Barton-Davis et al., 1999; Manuvakhova et al., 2000; Finkel, 2010). These agents are able to interfere with the process of the ribosomal proof-reading and thereby allow pairing of a near-cognate tRNA with the stop codon instead of the release factors so that translation continues until the next stop codon is reached (Keeling and Bedwell, 2005; Karijolich and Yu, 2014).

Different factors have an impact on the efficiency of a translational PTC read-through. Read-through primarily happens in non-conserved sequences and with an increase in gene expression the read-through level decreases (Li and Zhang, 2019). Both indicates a good chance for an effective read-through of the *ATXN3*aS mRNA. Further, the termination triplet as well as the base right after also have a big impact on the read-through capacity (Kopelowitz et al., 1992; Mccaughan et al., 1995; Manuvakhova et al., 2000; Karijolich and Yu, 2014). While the UAA triplet (which is the PTC leading to ataxin-3aS) was shown to be more stringent regarding a translational read-through compared to the UGA codon (Kopelowitz et al., 1992) the base after the UAA triplet in *ATXN3* (G) predicts a high read-through efficiency (Kopelowitz et al., 1992). However, the hydrophobicity of the ataxin-3aL C-terminus could be problematic as hydrophobicity impacts read-through capacity. Li and Zhang (2019) reported that genes which show lower levels of read-through show a translation of an extended hydrophobic peptide after the stop codon (Li and Zhang, 2019). Such a read-through may be naturally disfavored and deleterious (Arribere et al., 2016; Li and Zhang, 2019). In summary these results show, that a read-through of the *ATXN3*aS mRNA should be possible although the hydrophobic C-terminus of ataxin-3aL might have a negative impact on the efficiency.

In order to test whether a PTC read-through is actually possible, cells were treated with the aminoglycosides Gentamicin or G418 after transfection with an ataxin-3aL-EGFP construct carrying the SNP rs7158733 variant leading to the PTC. Upon a successful read-through EGFP-tagged ataxin-3aL should be expressed by the cells whereas no EGFP expression should be observed when read-through fails and ataxin-3aS is expressed. Cells were then either analyzed for their ataxin-3 protein level or aggregation. It could be observed that a PTC read-through is possible using G418 and Gentamicin. However, the cells also showed a basal expression of ataxin-3aL-EGFP without treatment.

Increasing G418 and Gentamicin concentrations resulted in a mild increase in EGFP-ataxin-3aL expression. Generally, the increase in protein level was about 10 % to 25 % above basal read-through levels. This seems to be a normal rate which can be achieved using these substances. Halvey et al. (2012) was able to achieve a comparable read-through rate of around 20 % using G418. Although only a modest read-through could be achieved in the experiments described here, even a low level of read-through could accumulate by a continued treatment (Atanasova et al., 2017). This is especially true due to the longer half-life of ataxin-3aL compared to ataxin-3aS and thereby could cause a switch of both protein levels.

Next to the total read-through capacity, also aggregation of ataxin-3 was measured after G418 and Gentamicin treatment. In both cases the total amount of insoluble ataxin-3 decreased by around 20 %. A reduction in aggregation after read-through from ataxin-3aS to ataxin-3aL could be expected as ataxin-3aL proved to form lower amounts of SDS-insoluble aggregates (see 4.2.1, page 99). However, a reduction in aggregation could also be observed for those concentrations of G418 and Gentamicin which did not show a read-through effect. Therefore, it is unlikely that the total reduction in aggregation by around 20 % solely bases on a read-through. Selection by both aminoglycoside antibiotics or simply apoptosis by other means of cellular stress could also result in a reduced aggregation profile. However, increased cell death could not be observed for increasing concentrations of G418 and Gentamicin, presumably due to the *neo* resistance gene present on the expression plasmid. Presumably, one could also expect a higher read-through levels without the presence of *neo*.

As mentioned above, a basal EGFP expression was observed, although EGFP is located C-terminal to the stop codon and can only be expressed upon read-through. This is not surprising. Low read-through levels can be observed for every stop codon (Karijolich and Yu, 2014). Translational read-through occurs naturally as no biological system is perfect and increases under cellular stress conditions (Tyedmers et al., 2008; Gerashchenko et al., 2012). The likelihood depends on the ability of release factors to recognize the termination codon and initiate termination on one hand and close tRNA which are able to decode it on the other (Karijolich and Yu, 2014). The likelihood also depends on the nucleotide sequence following the termination codon (Brenner et al., 1965; Bonetti et al., 1995) as well as the stop codon itself (Bonetti et al., 1995). Generally, stop codon read-through is not a rare event. Ribosomal-profiling showed that it can be observed for hundreds of genes at a detectable rate (Artieri and Fraser, 2014; Dunn et al., 2013). While it was long discussed whether read-through has a biological function (Dunn et al., 2013; Baranov et al., 2015; Stiebler et al., 2014; Pancsa et al., 2016; Tyedmers et al., 2008; Gerashchenko et al., 2012) or just reflects an error, recently growing evidence supports

the hypothesis that these events are non-adaptive errors (Li and Zhang, 2019; Xu and Zhang, 2014, 2018; Liu and Zhang, 2018; Liu et al., 2018; Saudemont et al., 2017; Warnecke and Hurst, 2011).

The proof of principle of a read-through of the *ATXN3*aL mRNA presented here shows that it is generally possible to induce a translational read-through within the *ATXN3*aS mRNA and thereby correct the PTC. Such a therapy may not cure MJD; however, it may be able to delay disease progression and aao. Importantly, while translational read-through was so far not discussed as a potential therapy for MJD, the induction of this process is a matter of research for different genetic disorders (reviewed in Karijolich and Yu, 2014) which are caused by nonsense mutations, e. g. hailey-hailey disease (Kellermayer et al., 2006) and hemophilia A and B (James et al., 2005). Further, it has been previously tested in clinical trials for Duchenne/Becker muscular dystrophy (Finkel et al., 2013; Bushby et al., 2014; McDonald et al., 2017), cystic fibrosis (Wilschanski et al., 2003; Hirawat et al., 2007; Kerem et al., 2008; Sermet-Gaudelus et al., 2010; Wilschanski et al., 2011; Kerem et al., 2014; Aslam et al., 2017) and recessive dystrophic epidermolysis bullosa (Atanasova et al., 2017) where these drugs partially proved to be beneficial. Ataluren (also known as PTC124) for example holds a conditional approval for Duchenne/Becker muscular dystrophy within the European Union as it was suggested that it inhibits disease progression by restoring dystrophin levels (Shimizu-Motohashi et al., 2019). Therefore important clinical data is available on the ability of different substances to achieve a read-through. Nonetheless, it is important to note that although different studies investigated various molecules inducing a PTC read-through, it may prove that so far studied therapeutic substances may not be efficient in restoring ataxin-3aL. Karijolich and Yu (2014) highlighted that the molecule has to be chosen on an individual basis. Therefore, a screening approach would be necessary in order to identify an ideal candidate for an SNP rs7158733 read through. Such a screening assay could be based on luciferase activity in order to easily detect and measure the read-through efficiency. However, when applying a luciferase based screening assay, it would be important to rely on a *Renilla* luciferase as firefly luciferase can lead to false positive results (Karijolich and Yu, 2014; Auld et al., 2009, 2010).

Lastly, it is important to consider side effects of the agents used to induce translational read-through. Although different studies have been performed which tested the effect of a PTC read-through therapy clinically, the long-term safety of these substances is not fully understood by now. Aminoglycosides like G418 and Gentamicin are taken up by the megalin receptor (Moestrup et al., 1995) and cause nephrotoxicity and ototoxicity (Turnidge, 2003; Fischel-Ghodsian, 2005; Guthrie, 2008; Mingeot-Leclercq and Tulkens, 1999; Avent et al., 2011). Applied systemically, a long term treatment with aminoglycosides showed severe side effects (Tokgoz et al., 2010; Walker and Shah, 1987). Gentamicin, in specific, shows a narrow therapeutic window combined with a complex administration (Finkel, 2010; Karpati and Lochmuller, 2001). Today, also other molecules are known to induce translational read-through even more efficient. Ataluren for example proved to be able to read-through the ochre (UAA), opal (UGA) and amber (UAG) stop codon starting at concentrations as low as 0.01 µM while 10.000 times higher concentrations of Gentamicin failed to do so (Welch et al., 2007). Further, pseudouridine Ψ-mediated suppression is a novel strategy developed by Karijolich and Yu (2012) which is based on directly target-

ing the PTC by nucleotide modification. Further, newer drugs like Ataluren also allow for an oral administration and additionally show a better safety profile compared to aminoglycosides (Finkel, 2010; Löscher et al., 2009). Therefore, despite beneficial effects could be observed, it is clear that translational read-through is not limited to the gene of interest and application of read-through inducing drugs is accompanied by side-effects. Nonetheless, with the development of newer substances the severity of side-effects may be reduced and in future may allow for a safe administration of these drugs for a treatment of diseases induced or severely modified by a PTC.

5.7 Summary and outlook

In summary, the present study found that ataxin-3 isoforms show major differences in their physiological and pathophysiological characteristics (Figure 4.43, page 141). Ataxin-3 isoforms presumably are different proteins with specific functions and interaction networks. Even further, the data presented here suggests that ataxin-3 isoforms contribute differently to the pathogenesis of MJD. Evidence could be found that the observed differences in the aao between patients with different ataxin-3 haplotypes are mainly determined by the presence of SNP rs7158733 in ataxin-3 which leads to aggravation of MJD pathology. Further, different studies suggest a neuroprotective function of the normal ataxin-3 allele that could be affected by the presence of this SNP. The polyQ induced shift in expression from *ATXN3*c to *ATXN3*a also highlights the relevance of this isoform for MJD and shows that this could be the major isoform driving MJD pathogenesis. Therefore, a precise annotation of protein isoforms studied in neurodegenerative diseases, ideally also of the haplotype used, is necessary to understand disease pathogenesis (Weishäupl et al., 2019).

Importantly, MJD patients depending on the underlying haplotype show differing ataxin-3 isoform combinations which impacts the physiological function as well as pathological characteristics of ataxin-3. This especially highlights the importance of polymorphisms within isoforms of disease-causing proteins as genetic modifiers in MJD and autosomal-dominantly inherited disorders in general. Taking this into consideration will help to understand the pathological differences between genetic subtypes varying in disease severity and aao (Weishäupl et al., 2019).

Lastly, the PTC leading to the isoform ataxin-3aS enables new therapy approaches like translational read-through of the stop codon. While such a treatment may not cure MJD the therapy may be able to delay disease progression and aao in order to improve life quality for those suffering from this fatal disease.

6 | References

Abeliovich, A., Schmitz, Y., Fariñas, I., Choi-Lundberg, D., Ho, W. H., Castillo, P. E., Shinsky, N., Verdugo, J. M., Armanini, M., Ryan, A., Hynes, M., Phillips, H., Sulzer, D., and Rosenthal, A. Mice lacking alpha-synuclein display functional deficits in the nigrostriatal dopamine system. *Neuron*, 25(1):239–52, jan 2000. ISSN 0896-6273.

Affaitati, A., De Cristofaro, T., Feliciello, A., and Varrone, S. Identification of alternative splicing of spinocerebellar ataxia type 2 gene. *Gene*, 267(1):89–93, apr 2001. ISSN 03781119.

Aikawa, T., Watanabe, T., Miyazaki, T., Mikuni, T., Wakamori, M., Sakurai, M., Aizawa, H., Ishizu, N., Watanabe, M., Kano, M., Mizusawa, H., and Watase, K. Alternative splicing in the C-terminal tail of Cav2.1 is essential for preventing a neurological disease in mice. *Hum. Mol. Genet.*, 26(16):3094–3104, may 2017. ISSN 0964-6906.

Albrecht, M., Hoffmann, D., Evert, B. O., Schmitt, I., Wüllner, U., and Lengauer, T. Structural modeling of ataxin-3 reveals distant homology to adaptins. *Proteins Struct. Funct. Genet.*, 50(2):355–370, dec 2003. ISSN 08873585.

Albrecht, M., Golatta, M., Wüllner, U., and Lengauer, T. Structural and functional analysis of ataxin-2 and ataxin-3. *Eur. J. Biochem.*, 271(15):3155–3170, jul 2004. ISSN 00142956.

Allamand, V., Bidou, L., Arakawa, M., Floquet, C., Shiozuka, M., Paturneau-Jouas, M., Gartioux, C., Butler-Browne, G. S., Mouly, V., Rousset, J. P., Matsuda, R., Ikeda, D., and Guicheney, P. Drug-induced readthrough of premature stop codons leads to the stabilization of laminin α2 chain mRNA in CMD myotubes. *J. Gene Med.*, 10(2):217–224, feb 2008. ISSN 15212254.

Allan, J. A., Docherty, A. J., Barker, P. J., Huskisson, N. S., Reynolds, J. J., and Murphy, G. Binding of gelatinases A and B to type-I collagen and other matrix components. *Biochem. J.*, 309 (Pt 1(Pt 1):299–306, jul 1995. ISSN 0264-6021.

Alluri, R. V., Komandur, S., Wagheray, A., Chaudhuri, J. R., Sitajayalakshmi, Meena, A. K., Jabeen, A., Chawda, K., Subhash, K., Krishnaveni, A., and Hasan, Q. Molecular analysis of CAG repeats at five different spinocerebellar ataxia loci: Correlation and alternative explanations for disease pathogenesis. *Mol. Cells*, 24(3):338–342, 2007. ISSN 10168478.

Almeida, B., Abreu, I. A., Matos, C. A., Fraga, J. S., Fernandes, S., Macedo, M. G., Gutiérrez-Gallego, R., Pereira, P. J. B., Carvalho, A. L., and Macedo-Ribeiro, S. SUMOylation of the brain-predominant Ataxin-3 isoform modulates its interaction with p97. *Biochim. Biophys. Acta - Mol. Basis Dis.*, 1852(9):1950–1959, sep 2015. ISSN 1879260X.

Alonso, E., Martínez-Ruano, L., De Biase, I., Mader, C., Ochoa, A., Yescas, P., Gutiérrez, R., White, M., Ruano, L., Fragoso-Benítez, M., Ashizawa, T., Bidichandani, S. I., and Rasmussen, A. Distinct distribution of autosomal dominant spinocerebellar ataxia in the Mexican population. *Mov. Disord.*, 22(7):1050–1053, 2007. ISSN 08853185.

Alonso-López, D., Campos-Laborie, F. J., Gutiérrez, M. A., Lambourne, L., Calderwood, M. A., Vidal, M., and De Las Rivas, J. APID database: Redefining protein-protein interaction experimental evidences and binary interactomes. *Database*, 2019, jan 2019. ISSN 17580463.

Alvarez-Castelao, B., Ruiz-Rivas, C., and Castaño, J. G. A critical appraisal of quantitative studies of protein degradation in the framework of cellular proteostasis. *Biochem. Res. Int.*, 2012:823597, jan 2012. ISSN 2090-2255.

Alves, S., Nascimento-Ferreira, I., Auregan, G., Hassig, R., Dufour, N., Brouillet, E., Pedroso de Lima, M. C., Hantraye, P., de Almeida, L. P., and Déglon, N. Allele-specific RNA silencing of mutant ataxin-3 mediates neuroprotection in a rat model of Machado-Joseph disease. *PLoS One*, 2008a. ISSN 19326203.

Alves, S., Régulier, E., Nascimento-Ferreira, I., Hassig, R., Dufour, N., Koeppen, A., Carvalho, A. L., Simões, S., De Lima, M. C., Brouillet, E., Gould, V. C., Déglon, N., and De Almeida, L. P. Striatal and nigral pathology in a lentiviral rat model of Machado-Joseph disease. *Hum. Mol. Genet.*, 2008b. ISSN 09646906.

Alves, S., Nascimento-Ferreira, I., Dufour, N., Hassig, R., Auregan, G., Nóbrega, C., Brouillet, E., Hantraye, P., Pedroso de Lima, M. C., Déglon, N., and de Almeida, L. P. Silencing ataxin-3 mitigates degeneration in a rat model of Machado-Joseph disease: No role for wild-type ataxin-3? *Hum. Mol. Genet.*, 19(12):2380–2394, jun 2010. ISSN 09646906.

Alving, Carl, R., Koulchin, V., Glenn, G. M., and Rao, M. Liposomes as Carriers of Peptide Antigens: Induction of Antibodies and Cytotoxic T Lymphocytes to Conjugated and Unconjugated Peptides. *Immunol. Rev.*, 145(1):5–31, jun 1995. ISSN 1600065X.

Amrani, N., Ganesan, R., Kervestin, S., Mangus, D. A., Ghosh, S., and Jacobson, A. A faux 3'-UTR promotes aberrant termination and triggers nonsense-mediated mRNA decay. *Nature*, 432(7013):112–118, nov 2004. ISSN 00280836.

Amselem, S., Duquesnoy, P., Attree, O., Novelli, G., Bousnina, S., Postel-Vinay, M.-C., and Goossens, M. Laron Dwarfism and Mutations of the Growth Hormone–Receptor Gene. *N. Engl. J. Med.*, 321(15):989–995, oct 1989. ISSN 0028-4793.

An, J. Y., Kim, E.-A., Jiang, Y., Zakrzewska, A., Kim, D. E., Lee, M. J., Mook-Jung, I., Zhang, Y., and Kwon, Y. T. UBR2 mediates transcriptional silencing during spermatogenesis via histone ubiquitination. *Proc. Natl. Acad. Sci.*, 107(5):1912–1917, feb 2010. ISSN 0027-8424.

An, J. Y., Kim, E., Zakrzewska, A., Yoo, Y. D., Jang, J. M., Han, D. H., Lee, M. J., Seo, J. W., Lee, Y. J., Kim, T. Y., de Rooij, D. G., Kim, B. Y., and Kwon, Y. T. UBR2 of the N-end rule pathway is required for chromosome stability via histone ubiquitylation in spermatocytes and somatic cells. *PLoS One*, 7(5):e37414, 2012. ISSN 19326203.

Angeletti, R. H. Design of useful peptide antigens, mar 1999. ISSN 15240215.

Antenora, A., Rinaldi, C., Roca, A., Pane, C., Lieto, M., Saccà, F., Peluso, S., De Michele, G., and Filla, A. The Multiple Faces of Spinocerebellar Ataxia type 2, sep 2017. ISSN 23289503.

Antony, P. M. A., Mäntele, S., Mollenkopf, P., Boy, J., Kehlenbach, R. H., Riess, O., and Schmidt, T. Identification and functional dissection of localization signals within ataxin-3. *Neurobiol. Dis.*, 36(2):280–92, nov 2009. ISSN 1095-953X.

Appel-Cresswell, S., Vilarino-Guell, C., Encarnacion, M., Sherman, H., Yu, I., Shah, B., Weir, D., Thompson, C., Szu-Tu, C., Trinh, J., Aasly, J. O., Rajput, A., Rajput, A. H., Jon Stoessl, A., and Farrer, M. J. Alpha-synuclein p.H50Q, a novel pathogenic mutation for Parkinson's disease. *Mov. Disord.*, 28(6):811–813, jun 2013. ISSN 08853185.

Arakawa, M., Shiozuka, M., Nakayama, Y., Hara, T., Hamada, M., Kondo, S., Ikeda, D., Takahashi, Y., Sawa, R., Nonomura, Y., Sheykholeslami, K., Kondo, K., Kaga, K., Kitamura, T., Suzuki-Miyagoe, Y., Takeda, S., and Matsuda, R. Negamycin Restores Dystrophin Expression in Skeletal and Cardiac Muscles of mdx Mice. *J. Biochem.*, 134(5):751–758, nov 2003. ISSN 0021924X.

Araujo, J., Breuer, P., Dieringer, S., Krauss, S., Dorn, S., Zimmermann, K., Pfeifer, A., Klockgether, T., Wuellner, U., and Evert, B. O. FOXO4-dependent upregulation of superoxide dismutase-2 in response to oxidative stress is impaired in spinocerebellar ataxia type 3. *Hum. Mol. Genet.*, 20(15):2928–2941, aug 2011. ISSN 1460-2083.

Arechavala-Gomeza, V., Khoo, B., and Aartsma-Rus, A. Splicing modulation therapy in the treatment of genetic diseases. *Appl. Clin. Genet.*, 7:245–52, 2014. ISSN 1178-704X.

Arrasate, M., Mitra, S., Schweitzer, E. S., Segal, M. R., and Finkbeiner, S. Inclusion body formation reduces levels of mutant huntingtin and the risk of neuronal death. *Nature*, 431 (7010):805–810, oct 2004. ISSN 0028-0836.

Arribere, J. A., Cenik, E. S., Jain, N., Hess, G. T., Lee, C. H., Bassik, M. C., and Fire, A. Z. Translation readthrough mitigation. *Nature*, 534(7609):719–723, jun 2016. ISSN 14764687.

Artieri, C. G. and Fraser, H. B. Evolution at two levels of gene expression in yeast. *Genome Res.*, 24(3):411–421, mar 2014. ISSN 15495469.

Ashkenazi, A., Bento, C. F., Ricketts, T., Vicinanza, M., Siddiqi, F., Pavel, M., Squitieri, F., Hardenberg, M. C., Imarisio, S., Menzies, F. M., and Rubinsztein, D. C. Polyglutamine tracts regulate beclin 1-dependent autophagy. *Nature*, 545(7652):108–111, may 2017. ISSN 14764687.

Aslam, A., Jahnke, N., Remmington, T., and Southern, K. W. Ataluren and similar compounds (specific therapies for premature termination codon class I mutations) for cystic fibrosis. *Paediatr. Respir. Rev.*, 24(1):32–34, 2017. ISSN 15260550.

Asselin-Mullen, P., Chauvin, A., Dubois, M. L., Drissi, R., Lévesque, D., and Boisvert, F. M. Protein interaction network of alternatively spliced NudCD1 isoforms. *Sci. Rep.*, 7(1):1–11, dec 2017. ISSN 20452322.

Atanasova, V. S., Jiang, Q., Prisco, M., Gruber, C., Piñón Hofbauer, J., Chen, M., Has, C., Bruckner-Tuderman, L., McGrath, J. A., Uitto, J., and South, A. P. Amlexanox Enhances Premature Termination Codon Read-Through in COL7A1 and Expression of Full Length Type VII Collagen: Potential Therapy for Recessive Dystrophic Epidermolysis Bullosa. *J. Invest. Dermatol.*, 137(9):1842–1849, 2017. ISSN 15231747.

Atsuta, N., Watanabe, H., Ito, M., Banno, H., Suzuki, K., Katsuno, M., Tanaka, F., Tamakoshi, A., and Sobue, G. Natural history of spinal and bulbar muscular atrophy (SBMA): A study of 223 Japanese patients. *Brain*, 129(6):1446–1455, 2006. ISSN 00068950.

Auld, D. S., Thorne, N., Maguire, W. F., and Inglese, J. Mechanism of PTC124 activity in cell-based luciferase assays of nonsense codon suppression. *Proc. Natl. Acad. Sci. U. S. A.*, 106(9):3585–90, mar 2009. ISSN 1091-6490.

Auld, D. S., Lovell, S., Thorne, N., Lea, W. A., Maloney, D. J., Shen, M., Rai, G., Battaile, K. P., Thomas, C. J., Simeonov, A., Hanzlik, R. P., and Inglese, J. Molecular basis for the high-affinity binding and stabilization of firefly luciferase by PTC124. *Proc. Natl. Acad. Sci. U. S. A.*, 107(11):4878–83, mar 2010. ISSN 1091-6490.

Avendano, M. and Cylus, J. *Working at Older Ages: Why it's important, how it affects health, and the policy options to support health capacity for work.* European Observatory on Health Systems and Policies, Copenhagen, 2019.

Avent, M. L., Rogers, B. A., Cheng, A. C., and Paterson, D. L. Current use of aminoglycosides: Indications, pharmacokinetics and monitoring for toxicity, jun 2011. ISSN 14440903.

Babovic-Vuksanovic, D., Snow, K., Patterson, M. C., and Michels, V. V. Spinocerebellar ataxia type 2 (SCA 2) in an infant with extreme CAG repeat expansion. *Am. J. Med. Genet.*, 79 (5):383–387, 1998. ISSN 01487299.

Bachmair, A., Finley, D., and Varshavsky, A. In vivo half-life of a protein is a function of its amino-terminal residue. *Science*, 234(4773):179–86, oct 1986. ISSN 0036-8075.

Baglioni, S., Bucciantini, M., Taddei, N., Chiti, F., Stefani, M., Casamenti, F., Luheshi, L. M., and Dobson, C. M. Prefibrillar amyloid aggregates could be generic toxins in higher organisms. *J. Neurosci.*, 26(31):8160–8167, aug 2006. ISSN 0270-6474.

Bailey, C. K., Andriola, I. F. M., Kampinga, H. H., and Merry, D. E. Molecular chaperones enhance the degradation of expanded polyglutamine repeat androgen receptor in a cellular model of spinal and bulbar muscular atrophy. *Hum. Mol. Genet.*, 11(5):515–523, 2002. ISSN 0964-6906.

Baldo, B., Paganetti, P., Grueninger, S., Marcellin, D., Kaltenbach, L. S., Lo, D. C., Semmelroth, M., Zivanovic, A., Abramowski, D., Smith, D., Lotz, G. P., Bates, G. P., and Weiss, A. TR-FRET-based duplex immunoassay reveals an inverse correlation of soluble and aggregated mutant huntingtin in Huntington's disease. *Chem. Biol.*, 19(2):264–275, feb 2012. ISSN 10745521.

Banich, M. T. and Compton, R. J. *Cognitive Neuroscience*. Cambridge University Press, 4 edition, apr 2018. ISBN 9781316664018.

Baralle, M., Pastor, T., Bussani, E., and Pagani, F. Influence of Friedreich Ataxia GAA Noncoding Repeat Expansions on Pre-mRNA Processing. *Am. J. Hum. Genet.*, 83(1):77–88, jul 2008. ISSN 00029297.

Baranov, P. V., Atkins, J. F., and Yordanova, M. M. Augmented genetic decoding: Global, local and temporal alterations of decoding processes and codon meaning, sep 2015. ISSN 14710064.

Barton-Davis, E. R., Cordier, L., Shoturma, D. I., Leland, S. E., and Sweeney, H. L. Aminoglycoside antibiotics restore dystrophin function to skeletal muscles of mdx mice. *J. Clin. Invest.*, 104(4):375–381, aug 1999. ISSN 00219738.

Bates, G. Huntingtin aggregation and toxicity in Huntington's disease, may 2003. ISSN 01406736.

Bauer, P. O., Zumrova, A., Matoska, V., Marikova, T., Krilova, S., Boday, A., Singh, B., and Goetz, P. Absence of spinocerebellar ataxia type 3/Machado-Joseph disease within ataxic patients in the Czech population. *Eur. J. Neurol.*, 12(11):851–857, 2005. ISSN 13515101.

Bedwell, D. M., Kaenjak, A., Benos, D. J., Bebok, Z., Bubien, J. K., Hong, J., Tousson, A., Clancy, J. P., and Sorscher, E. J. Suppression of a CFTR premature stop mutation in a bronchial epithelial cell line. *Nat. Med.*, 3(11):1280–1284, nov 1997. ISSN 10788956.

Beeskow, T., Kroner, K. H., and Anspach, F. B. Nylon-based affinity membranes: Impacts of surface modification on protein adsorption. *J. Colloid Interface Sci.*, 196(2):278–291, 1997. ISSN 00219797.

Beitel, L. K., Alvarado, C., Mokhtar, S., Paliouras, M., and Trifiro, M. Mechanisms mediating spinal and bulbar muscular atrophy: Investigations into polyglutamine-expanded androgen receptor function and dysfunction. *Front. Neurol.*, 4 MAY, 2013. ISSN 16642295.

Berg, Jeremy, M., Tymoczko, J. L., Gatto, G. J., and Stryer, L. *Biochemistry 8th Edition*. 2015. ISBN 978-1-4641-2610-9.

Bergers, G., Brekken, R., McMahon, G., Vu, T. H., Itoh, T., Tamaki, K., Tanzawa, K., Thorpe, P., Itohara, S., Werb, Z., and Hanahan, D. Matrix metalloproteinase-9 triggers the angiogenic switch during carcinogenesis. *Nat. Cell Biol.*, 2(10):737–744, oct 2000. ISSN 1465-7392.

Berke, S. J. S., Schmied, F. A. F., Brunt, E. R., Ellerby, L. M., and Paulson, H. L. Caspase-mediated proteolysis of the polyglutamine disease protein ataxin-3. *J. Neurochem.*, 89(4): 908–918, may 2004. ISSN 0022-3042.

Berke, S. J. S., Chai, Y., Marrs, G. L., Wen, H., and Paulson, H. L. Defining the role of ubiquitin-interacting motifs in the polyglutamine disease protein, ataxin-3. *J. Biol. Chem.*, 280(36):32026–32034, sep 2005. ISSN 00219258.

Bettencourt, C., Santos, C., Montiel, R., Costa, M. D. C., Cruz-Morales, P., Santos, L. R., Simões, N., Kay, T., Vasconcelos, J., Maciel, P., and Lima, M. Increased transcript diversity: novel splicing variants of Machado-Joseph disease gene (ATXN3). *Neurogenetics*, 11(2):193–202, 2010. ISSN 1364-6753.

Bettencourt, C., Santos, C., Coutinho, P., Rizzu, P., Vasconcelos, J., Kay, T., Cymbron, T., Raposo, M., Heutink, P., and Lima, M. Parkinsonian phenotype in Machado-Joseph disease (MJD/SCA3): A two-case report. *BMC Neurol.*, 11:131, oct 2011. ISSN 14712377.

Bettencourt, C., Raposo, M., Ros, R., Montiel, R., Bruges-Armas, J., and Lima, M. Transcript Diversity of Machado-Joseph Disease Gene (ATXN3) Is Not Directly Determined by SNPs in Exonic or Flanking Intronic Regions. *J. Mol. Neurosci.*, 49(3):539–543, 2013. ISSN 08958696.

Bichelmeier, U., Schmidt, T., Hübener, J., Boy, J., Rüttiger, L., Häbig, K., Poths, S., Bonin, M., Knipper, M., Schmidt, W. J., Wilbertz, J., Wolburg, H., Laccone, F., and Riess, O. Nuclear localization of ataxin-3 is required for the manifestation of symptoms in SCA3: in vivo evidence. *J. Neurosci.*, 27(28):7418–28, jul 2007. ISSN 1529-2401.

Bidou, L., Bugaud, O., Belakhov, V., Baasov, T., and Namy, O. Characterization of new-generation aminoglycoside promoting premature termination codon readthrough in cancer cells. *RNA Biol.*, 14(3):378–388, 2017. ISSN 15558584.

Bilen, J. and Bonini, N. M. Genome-wide screen for modifiers of ataxin-3 neurodegeneration in Drosophila. *PLoS Genet.*, 3(10):1950–1964, 2007. ISSN 15537390.

Bird, T. D. *Hereditary Ataxia Overview*. University of Washington, Seattle, jul 1993.

Birtalan, S., Zhang, Y., Fellouse, F. A., Shao, L., Schaefer, G., and Sidhu, S. S. The Intrinsic Contributions of Tyrosine, Serine, Glycine and Arginine to the Affinity and Specificity of Antibodies. *J. Mol. Biol.*, 377(5):1518–1528, apr 2008. ISSN 00222836.

Blount, J. R., Tsou, W.-L., Ristic, G., Burr, A. A., Ouyang, M., Galante, H., Scaglione, K. M., and Todi, S. V. Ubiquitin-binding site 2 of ataxin-3 prevents its proteasomal degradation by interacting with Rad23. *Nat. Commun.*, 5:4638, jan 2014. ISSN 2041-1723.

Boch, J., Scholze, H., Schornack, S., Landgraf, A., Hahn, S., Kay, S., Lahaye, T., Nickstadt, A., and Bonas, U. Breaking the code of DNA binding specificity of TAL-type III effectors. *Science*, 326(5959):1509–12, dec 2009. ISSN 1095-9203.

Boeddrich, A., Gaumer, S., Haacke, A., Tzvetkov, N., Albrecht, M., Evert, B. O., Müller, E. C., Lurz, R., Breuer, P., Schugardt, N., Plassmann, S., Xu, K., Warrick, J. M., Suopanki, J., Wüllner, U., Frank, R., Hartl, U. F., Bonini, N. M., and Wanker, E. E. An arginine/lysine-rich motif is crucial for VCP/p97-mediated modulation of ataxin-3 fibrillogenesis. *EMBO J.*, 25(7):1547–58, apr 2006. ISSN 0261-4189.

Bokeh Development Team. Bokeh: Python library for interactive visualization, 2018.

Bonanomi, M., Mazzucchelli, S., D'Urzo, A., Nardini, M., Konarev, P. V., Invernizzi, G., Svergun, D. I., Vanoni, M., Regonesi, M. E., and Tortora, P. Interactions of ataxin-3 with its

molecular partners in the protein machinery that sorts protein aggregates to the aggresome. *Int. J. Biochem. Cell Biol.*, 51(1):58–64, 2014a. ISSN 18785875.

Bonanomi, M., Natalello, A., Visentin, C., Pastori, V., Penco, A., Cornelli, G., Colombo, G., Malabarba, M. G., Doglia, S. M., Relini, A., Regonesi, M. E., and Tortora, P. Epigallocatechin-3-gallate and tetracycline differently affect ataxin-3 fibrillogenesis and reduce toxicity in spinocerebellar ataxia type 3 model. *Hum. Mol. Genet.*, 2014b. ISSN 14602083.

Bonanomi, M., Visentin, C., Invernizzi, G., Tortora, P., and Regonesi, M. E. The toxic effects of pathogenic ataxin-3 variants in a yeast cellular model. *PLoS One*, 10(6):e0129727, jun 2015. ISSN 19326203.

Bondy-Chorney, E., Crawford Parks, T. E., Ravel-Chapuis, A., Jasmin, B. J., and Côté, J. Staufen1s role as a splicing factor and a disease modifier in Myotonic Dystrophy Type I. *Rare Dis.*, 4(1):e1225644, jan 2016. ISSN 2167-5511.

Bonetti, B., Fu, L., Moon, J., and Bedwell, D. M. The efficiency of translation termination is determined by a synergistic interplay between upstream and downstream sequences in Saccharomyces cerevisiae. *J. Mol. Biol.*, 251(3):334–345, aug 1995. ISSN 00222836.

Bostrom, J., Lee, C. V., Haber, L., and Fuh, G. Improving Antibody Binding Affinity and Specificity for Therapeutic Development. In *Methods Mol. Biol.*, volume 525, pages 353–376. Humana Press, 2009.

Bouillet, P. and Strasser, A. BH3-only proteins - evolutionarily conserved proapoptotic Bcl-2 family members essential for initiating programmed cell death. *J. Cell Sci.*, 115(Pt 8):1567–74, apr 2002. ISSN 0021-9533.

Boy, J., Schmidt, T., Wolburg, H., Mack, A., Nuber, S., Böttcher, M., Schmitt, I., Holzmann, C., Zimmermann, F., Servadio, A., and Riess, O. Reversibility of symptoms in a conditional mouse model of spinocerebellar ataxia type 3. *Hum. Mol. Genet.*, 18(22):4282–4295, 2009. ISSN 09646906.

Boy, J., Schmidt, T., Schumann, U., Grasshoff, U., Unser, S., Holzmann, C., Schmitt, I., Karl, T., Laccone, F., Wolburg, H., Ibrahim, S., and Riess, O. A transgenic mouse model of spinocerebellar ataxia type 3 resembling late disease onset and gender-specific instability of CAG repeats. *Neurobiol. Dis.*, 37(2):284–293, feb 2010. ISSN 09699961.

Bradley, W. G., Andrew, A. S., Traynor, B. J., Chiò, A., Butt, T. H., and Stommel, E. W. Gene-Environment-Time Interactions in Neurodegenerative Diseases: Hypotheses and Research Approaches. *Ann. Neurosci.*, 25(4):261–267, apr 2019. ISSN 09763260.

Brendel, C., Belakhov, V., Werner, H., Wegener, E., Gärtner, J., Nudelman, I., Baasov, T., and Huppke, P. Readthrough of nonsense mutations in Rett syndrome: evaluation of novel aminoglycosides and generation of a new mouse model. *J. Mol. Med.*, 89(4):389–398, apr 2011. ISSN 0946-2716.

Brenner, S., Stretton, A. O., and Kaplan, S. Genetic code: The 'nonsense' triplets for chain termination and their suppression. *Nature*, 206(4988):994–998, jun 1965. ISSN 00280836.

Breuer, P., Haacke, A., Evert, B. O., and Wüllner, U. Nuclear aggregation of polyglutamine-expanded ataxin-3: fragments escape the cytoplasmic quality control. *J. Biol. Chem.*, 285(9): 6532–7, feb 2010. ISSN 1083-351X.

Brignone, C., Bradley, K. E., Kisselev, A. F., and Grossman, S. R. A post-ubiquitination role for MDM2 and hHR23A in the p53 degradation pathway. *Oncogene*, 23(23):4121–4129, 2004. ISSN 09509232.

Brusco, A., Gellera, C., Cagnoli, C., Saluto, A., Castucci, A., Michielotto, C., Fetoni, V., Mariotti, C., Migone, N., Di Donato, S., and Taroni, F. Molecular Genetics of Hereditary Spinocerebellar Ataxia: Mutation Analysis of Spinocerebellar Ataxia Genes and CAG/CTG Repeat Expansion Detection in 225 Italian Families. *Arch. Neurol.*, 61(5):727–733, 2004. ISSN 00039942.

Bryer, A., Krause, A., Bill, P., Davids, V., Bryant, D., Butler, J., Heckmann, J., Ramesar, R., and Greenberg, J. The hereditary adult-onset ataxias in South Africa. *J. Neurol. Sci.*, 216 (1):47–54, 2003. ISSN 0022510X.

Bucciantini, M., Giannoni, E., Chiti, F., Baroni, F., Taddei, N., Ramponi, G., Dobson, C. M., and Stefani, M. Inherent toxicity of aggregates implies a common mechanism for protein misfolding diseases. *Nature*, 416(6880):507–511, apr 2002. ISSN 00280836.

Burkovitz, A., Sela-Culang, I., and Ofran, Y. Large-scale analysis of somatic hypermutations in antibodies reveals which structural regions, positions and amino acids are modified to improve affinity. *FEBS J.*, 281(1):306–319, jan 2014. ISSN 1742464X.

Burnett, B., Li, F., and Pittman, R. N. The polyglutamine neurodegenerative protein ataxin-3 binds polyubiquitylated proteins and has ubiquitin protease activity. *Hum. Mol. Genet.*, 12 (23):3195–3205, 2003. ISSN 09646906.

Burnett, B. G. and Pittman, R. N. The polyglutamine neurodegenerative protein ataxin 3 regulates aggresome formation. *Proc. Natl. Acad. Sci. U. S. A.*, 102(12):4330–4335, 2005.

Burr, A. A., Tsou, W. L., Ristic, G., and Todi, S. V. Using membrane-targeted green fluorescent protein to monitor neurotoxic protein-dependent degeneration of Drosophila eyes. *J. Neurosci. Res.*, 92(9):1100–1109, 2014. ISSN 10974547.

Burright, E. N., Brent Clark, H., Servadio, A., Matilla, T., Feddersen, R. M., Yunis, W. S., Duvick, L. A., Zoghbi, H. Y., and Orr, H. T. SCA1 transgenic mice: A model for neurodegeneration caused by an expanded CAG trinucleotide repeat. *Cell*, 82(6):937–948, sep 1995. ISSN 00928674.

Bushby, K., Finkel, R., Wong, B., Barohn, R., Campbell, C., Comi, G. P., Connolly, A. M., Day, J. W., Flanigan, K. M., Goemans, N., Jones, K. J., Mercuri, E., Quinlivan, R., Renfroe, J. B., Russman, B., Ryan, M. M., Tulinius, M., Voit, T., Moore, S. A., Lee Sweeney, H., Abresch, R. T., Coleman, K. L., Eagle, M., Florence, J., Gappmaier, E., Glanzman, A. M., Henricson, E., Barth, J., Elfring, G. L., Reha, A., Spiegel, R. J., O'donnell, M. W., Peltz, S. W., McDonald, C. M., Kornberg, A. J., Wray, A., Carroll, K., Kennedy, R., Villano, D.,

de Valle, K., North, K. N., Dexter, M., Wicks, S., Rose, K., Buyse, G. M., van den Hauwe, M., Vrijsen, B., Janmohammad, A., Scholtes, C., Mah, J. K., Wright, C. J., Chiu, A., Walker, L. M., Sarnat, H. B., Selby, K., King, C., Meisner, L., Doppler, V., De Castro, D., Decostre, V., Chabrol, B., Levy, N., Halbert, C., Pereon, Y., Magot, A., Perrier, J., Mahe, J. Y., Perrau, A. S., Chasserieau, R., Schara, U., Lutz, S., Busse, M., Della Marina, A., Bosbach, T., Kirschner, J., Stanescu, A., Pohl, A., Rensing-Zimmerman, C., Eisele, U., Fetzer, I., Vogt, S., Bertini, E., D'Amico, A., Kofler, A., Gesu, P. B., Carlesi, A., Bonetti, A. M., Gagliardi, M. G., Santecchia, L., Emma, F., Bergami, G., Vasco, G., Bianco, F., Mazzone, E. S., Pane, M., De Sanctis, R., Magri, F., Lucchini, V., Corti, S. P., Moggio, M. G., Sciacco, M., Govoni, A., Bresolin, N., Nevo, Y., Dor-Wollman, T., Bar-Lev, A., Krojanker-Yaffe, D., Weisband, E., Vilchez, J. J., Muelas, N., Sevilla, T., Smeyers, P., Calle, F., González, M., de la Osa, A., Colomer, J., Ortez, C. I., Nascimento, A., Febrer, A., Medina, J., Muni, R., Thorarinsdottir, B., Darin, N., Sterky, U., Kroksmark, A. K., Berglund, L., Sejersen, T., Hovmöller, M., Trulsson, E., Hök, A., Kipping, P., Guglieri, M., Straub, V., Sàrközy, A., Willis, T., Mayhew, A., McCallum, M., Smith, L., Bell, G., Muntoni, F., Manzur, A. Y., Robb, S. A., Main, M., Ash, M., Scoto, M., Cirak, S., Smith, M. R., Pandey, R., James, S., Emery, N., Groves, L., Kulshrestha, R., Collins, J., McGuire, M., McCormick, A., Morehart, P., Hu, S., Brown, R., Bonnemann, C. G., Yang, M. L., Foley, A. R., Murphy-Kotzer, L., Dorsey, L., Estilow, T., Paisley, A., Yum, S., Thomas, T., Smith, K., Bromberg, M. B., McGerty, B., Heidarian, L. L., Swoboda, K., Gappmaier, V., Karachunski, P. I., Margolis, M., Naughton, C., Buser, K. K., Dalton, J., Matthews, K. D., Stephan, C. M., Laubenthal, K. S., Darras, B. T., Kang, P. B., Riley, S. O., Quigley, J., Butler, H., Parsons, J., Apkon, S. D., Gibbons, M., Carey, T., Dasouki, M. J., Anderson, H. S., Arthur, A., Burns, J. M., Dimachkie, M. M., Pasnoor, M., Wang, Y. I., Herbelin, L., Myles, R., Ciafaloni, E., Heatwole, C., Eichinger, K., Pandya, S., Pestronk, A., Al-Lozi, M., Lopate, G., Golumbek, P., Sommerville, R. B., Wang, L., Wojcicka-Mitchell, A., Godbey, A., Malkus, B., Schierbecker, J., Siener, C., Lu, M., Harms, M., Varadachary, A., Iyadurai, S., Rojas, L., Iannacone, S. T., Gilbreath, H., Khonghatithum, C., Merryman, R., Nelson, L., Andersen, M., Greene, M., Kern, S., Sproule, D. M., Kaufmann, P., De Vivo, D., Battista, V., Constantinescu, A., Montes, J., Dunaway, S., Montgomery, M., Marra, J., Han, J., Joyce, N., Goude, E., Johnson, L., Nicorici, A., Cregan, M., Bougher, G., Keohane, T., Sussman, M. D., Zilke, K., del Rosario, E., Wechsler, S. B., Juel, V. C., Hobson-Webb, L., Smith, E. C., Mackey, J., Case, L., and Ollendick, K. Ataluren treatment of patients with nonsense mutation dystrophinopathy. *Muscle and Nerve*, 50(4):477–487, oct 2014. ISSN 10974598.

Butterfield, D. A., Castegna, A., Lauderback, C. M., and Drake, J. Evidence that amyloid beta-peptide-induced lipid peroxidation and its sequelae in Alzheimer's disease brain contribute to neuronal death. *Neurobiol. Aging*, 23(5):655–64, 2002. ISSN 0197-4580.

Calvisi, D. F., Pinna, F., Meloni, F., Ladu, S., Pellegrino, R., Sini, M., Daino, L., Simile, M. M., De Miglio, M. R., Virdis, P., Frau, M., Tomasi, M. L., Seddaiu, M. A., Muroni, M. R., Feo, F., and Pascale, R. M. Dual-Specificity Phosphatase 1 Ubiquitination in Extracellular Signal-Regulated Kinase-Mediated Control of Growth in Human Hepatocellular Carcinoma. *Cancer Res.*, 68(11):4192–4200, jun 2008. ISSN 0008-5472.

Campioni, S., Mannini, B., Zampagni, M., Pensalfini, A., Parrini, C., Evangelisti, E., Relini, A., Stefani, M., Dobson, C. M., Cecchi, C., and Chiti, F. A causative link between the structure of aberrant protein oligomers and their toxicity. *Nat. Chem. Biol.*, 6(2):140–147, feb 2010. ISSN 15524469.

Carmo, S. M. *Interaction of ataxin-2 and ataxin-3 in Machado- Joseph disease*. Dissertation, Universidade de Aveiro, 2011.

Carroll, L. S., Massey, T. H., Wardle, M., and Peall, K. J. Dentatorubral-pallidoluysian atrophy: An update, 2018. ISSN 21608288.

Carter, A. P., Clemons, W. M., Brodersen, D. E., Morgan-Warren, R. J., Wimberly, B. T., and Ramakrishnan, V. Functional insights from the structure of the 30S ribosomal subunit and its interactions with antibiotics. *Nature*, 407(6802):340–348, sep 2000. ISSN 00280836.

Carvalho, A. L., Silva, A., and Macedo-Ribeiro, S. Polyglutamine-Independent Features in Ataxin-3 Aggregation and Pathogenesis of Machado-Joseph Disease. In *Adv. Exp. Med. Biol.*, volume 1049, pages 275–288. Springer, Cham, 2018.

Carvalho, D. R., La Rocque-Ferreira, A., Rizzo, I. M., Imamura, E. U., and Speck-Martins, C. E. Homozygosity Enhances Severity in Spinocerebellar Ataxia Type 3. *Pediatr. Neurol.*, 38(4):296–299, apr 2008. ISSN 08878994.

Cascarina, S. M. and Ross, E. D. Natural and Pathogenic Protein Sequence Variation Affecting Prion-Like Domains Within and Across Human Proteomes. *bioRxiv*, page 626648, may 2019.

Casey, H. L. and Gomez, C. M. Spinocerebellar Ataxia Type 6. In *Pagon RA, Bird TD, Dolan CR, al., Ed. GeneReviews [Internet]. Univ. Washington, Seattle; Initial Post. Oct. 23, 1998; Last Updat. June 16, 2008.* 1998.

Castillo-Carranza, D. L., Guerrero-Muñoz, M. J., Sengupta, U., Gerson, J. E., and Kayed, R. α-Synuclein Oligomers Induce a Unique Toxic Tau Strain. *Biol. Psychiatry*, 84(7):499–508, 2018. ISSN 18732402.

Cecchin, C. R., Pires, A. P., Rieder, C. R., Monte, T. L., Silveira, I., Carvalho, T., Saraiva-Pereira, M. L., Sequeiros, J., and Jardim, L. B. Depressive symptoms in Machado-Joseph disease (SCA3) patients and their relatives. *Community Genet.*, 10(1):19–26, dec 2006. ISSN 14222795.

Cemal, C. K., Carroll, C. J., Lawrence, L., Lowrie, M. B., Ruddle, P., Al-Mahdawi, S., King, R. H. M., Pook, M. A., Huxley, C., and Chamberlain, S. YAC transgenic mice carrying pathological alleles of the MJD1 locus exhibit a mild and slowly progressive cerebellar deficit. *Hum. Mol. Genet.*, 11(9):1075–1094, may 2002. ISSN 14602083.

Chai, J., Du, C., Wu, J.-W., Kyin, S., Wang, X., and Shi, Y. Structural and biochemical basis of apoptotic activation by Smac/DIABLO. *Nature*, 406(6798):855–862, aug 2000. ISSN 0028-0836.

Chai, J., Shiozaki, E., Srinivasula, S. M., Wu, Q., Datta, P., Alnemri, E. S., Shi, Y., and Dataa, P. Structural basis of caspase-7 inhibition by XIAP. *Cell*, 104(5):769–80, mar 2001a. ISSN 0092-8674.

Chai, Y., Koppenhafer, S. L., Bonini, N. M., and Paulson, H. L. Analysis of the role of heat shock protein (Hsp) molecular chaperones in polyglutamine disease. *J. Neurosci.*, 19(23): 10338–47, dec 1999a. ISSN 0270-6474.

Chai, Y., Koppenhafer, S. L., Shoesmith, S. J., Perez, M. K., and Paulson, H. L. Evidence for Proteasome Involvement in Polyglutamine Disease: Localization to Nuclear Inclusions in SCA3/MJD and Suppression of Polyglutamine Aggregation in vitro. *Hum. Mol. Genet.*, 8(4): 673–682, apr 1999b. ISSN 0964-6906.

Chai, Y., Wu, L., Griffin, J. D., and Paulson, H. L. The Role of Protein Composition in Specifying Nuclear Inclusion Formation in Polyglutamine Disease. *J. Biol. Chem.*, 276(48): 44889–44897, nov 2001b. ISSN 00219258.

Chai, Y., Shao, J., Miller, V. M., Williams, A., and Paulson, H. L. Live-cell imaging reveals divergent intracellular dynamics of polyglutamine disease proteins and supports a sequestration model of pathogenesis. *Proc. Natl. Acad. Sci.*, 99(14):9310–9315, jul 2002. ISSN 0027-8424.

Chai, Y., Berke, S. S., Cohen, R. E., and Paulson, H. L. Poly-ubiquitin binding by the polyglutamine disease protein ataxin-3 links its normal function to protein surveillance pathways. *J. Biol. Chem.*, 279(5):3605–11, jan 2004. ISSN 0021-9258.

Chan, N. C., Salazar, A. M., Pham, A. H., Sweredoski, M. J., Kolawa, N. J., Graham, R. L. J., Hess, S., and Chan, D. C. Broad activation of the ubiquitin-proteasome system by Parkin is critical for mitophagy. *Hum. Mol. Genet.*, 20(9):1726–37, may 2011. ISSN 1460-2083.

Chandler, J. H., Reed, T. E., and Dejong, R. N. Huntington's chorea in Michigan: III. Clinical observations. *Neurology*, 10(2):148–153, feb 1960. ISSN 1526632X.

Chang, K. H., Chen, W. L., Lee, L. C., Lin, C. H., Kung, P. J., Lin, T. H., Wu, Y. C., Wu, Y. R., Chen, Y. C., Lee-Chen, G. J., and Chen, C. M. Aqueous extract of paeonia lactiflora and paeoniflorin as aggregation reducers targeting chaperones in cell models of spinocerebellar ataxia 3. *Evidence-based Complement. Altern. Med.*, 2013, 2013.

Chang, M., Pan, B., Wang, C., and Huang, B. Cordycepin-induced unfolded protein response-dependent cell death, and AKT/MAPK-mediated drug resistance in mouse testicular tumor cells. *Cancer Med.*, 8(8):cam4.2285, may 2019. ISSN 2045-7634.

Chatr-Aryamontri, A., Oughtred, R., Boucher, L., Rust, J., Chang, C., Kolas, N. K., O'Donnell, L., Oster, S., Theesfeld, C., Sellam, A., Stark, C., Breitkreutz, B. J., Dolinski, K., and Tyers, M. The BioGRID interaction database: 2017 update. *Nucleic Acids Res.*, 45(D1):D369–D379, 2017. ISSN 13624962.

Chatterjee, A., Saha, S., Chakraborty, A., Silva-Fernandes, A., Mandal, S. M., Neves-Carvalho, A., Liu, Y., Pandita, R. K., Hegde, M. L., Hegde, P. M., Boldogh, I., Ashizawa, T., Koeppen, A. H., Pandita, T. K., Maciel, P., Sarkar, P. S., and Hazra, T. K. The Role of the Mammalian

DNA End-processing Enzyme Polynucleotide Kinase 3'-Phosphatase in Spinocerebellar Ataxia Type 3 Pathogenesis. *PLOS Genet.*, 11(1):e1004749, jan 2015. ISSN 1553-7404.

Chattopadhyay, B., Basu, P., Gangopadhyay, P. K., Mukherjee, S. C., Sinha, K. K., Chakraborty, A., Roy, T., Roychoudhury, S., Majumder, P. P., and Bhattacharyya, N. P. Variation of CAG repeats and two intragenic polymorphisms at SCA3 locus among Machado-Joseph disease/SCA3 patients and diverse normal populations from eastern India. *Acta Neurol. Scand.*, 108(6):407–414, 2003. ISSN 00016314.

Chaugule, V. K., Burchell, L., Barber, K. R., Sidhu, A., Leslie, S. J., Shaw, G. S., and Walden, H. Autoregulation of Parkin activity through its ubiquitin-like domain. *EMBO J.*, 30(14): 2853–2867, jul 2011. ISSN 02614189.

Chen, C. M., Weng, Y. T., Chen, W. L., Lin, T. H., Chao, C. Y., Lin, C. H., Chen, I. C., Lee, L. C., Lin, H. Y., Wu, Y. R., Chen, Y. C., Chang, K. H., Tang, H. Y., Cheng, M. L., Lee-Chen, G. J., and Lin, J. Y. Aqueous extract of Glycyrrhiza inflata inhibits aggregation by upregulating PPARGC1A and NFE2L2-ARE pathways in cell models of spinocerebellar ataxia 3. *Free Radic. Biol. Med.*, 2014. ISSN 18734596.

Chen, G., Gharib, T. G., Huang, C.-C., Taylor, J. M. G., Misek, D. E., Kardia, S. L. R., Giordano, T. J., Iannettoni, M. D., Orringer, M. B., Hanash, S. M., and Beer, D. G. Discordant protein and mRNA expression in lung adenocarcinomas. *Mol. Cell. Proteomics*, 1(4):304–13, apr 2002a. ISSN 1535-9476.

Chen, S., Berthelier, V., Hamilton, J. B., O'Nuallain, B., and Wetzel, R. Amyloid-like features of polyglutamine aggregates and their assembly kinetics. *Biochemistry*, 41(23):7391–7399, 2002b. ISSN 00062960.

Chen, S., Ferrone, F. A., and Wetzel, R. Huntington's disease age-of-onset linked to polyglutamine aggregation nucleation. *Proc. Natl. Acad. Sci. U. S. A.*, 99(18):11884–9, sep 2002c. ISSN 0027-8424.

Chinery, R., Brockman, J. A., Dransfield, D. T., and Coffey, R. J. Antioxidant-induced nuclear translocation of CCAAT/enhancer-binding protein β. A critical role for protein kinase A-mediated phosphorylation of Ser299. *J. Biol. Chem.*, 272(48):30356–30361, nov 1997. ISSN 00219258.

Chiti, F. and Dobson, C. M. Amyloid formation by globular proteins under native conditions, dec 2009. ISSN 15524469.

Chong, S. S., McCall, A. E., Cota, J., Subramony, S. H., Orr, H. T., Hughes, M. R., and Zoghbi, H. Y. Gametic and somatic tissue–specific heterogeneity of the expanded SCA1 CAG repeat in spinocerebellar ataxia type 1. *Nat. Genet.*, 10(3):344–350, 1995. ISSN 15461718.

Chou, A.-H., Yeh, T.-H., Ouyang, P., Chen, Y.-L., Chen, S.-Y., and Wang, H.-L. Polyglutamine-expanded ataxin-3 causes cerebellar dysfunction of SCA3 transgenic mice by inducing transcriptional dysregulation. *Neurobiol. Dis.*, 31(1):89–101, jul 2008. ISSN 1095-953X.

Chou, A. H., Chen, S. Y., Yeh, T. H., Weng, Y. H., and Wang, H. L. HDAC inhibitor sodium butyrate reverses transcriptional downregulation and ameliorates ataxic symptoms in a transgenic mouse model of SCA3. *Neurobiol. Dis.*, 2011. ISSN 09699961.

Chou, A. H., Chen, Y. L., Hu, S. H., Chang, Y. M., and Wang, H. L. Polyglutamine-expanded ataxin-3impairslong-term depression in Purkinjeneurons of SCA3 transgenic mouse byinhibiting HAT andimpairing histone acetylation. *Brain Res.*, 2014. ISSN 18726240.

Chow, M. K., Ellisdon, A. M., Cabrita, L. D., and Bottomley, S. P. Polyglutamine expansion in ataxin-3 does not affect protein stability: Implications for misfolding and disease. *J. Biol. Chem.*, 279(46):47643–47651, nov 2004a. ISSN 00219258.

Chow, M. K., Paulson, H. L., and Bottomley, S. P. Destabilization of a non-pathological variant of ataxin-3 results in fibrillogenesis via a partially folded intermediate: A model for misfolding in polyglutamine disease. *J. Mol. Biol.*, 335(1):333–341, jan 2004b. ISSN 00222836.

Christian, M., Cermak, T., Doyle, E. L., Schmidt, C., Zhang, F., Hummel, A., Bogdanove, A. J., and Voytas, D. F. Targeting DNA double-strand breaks with TAL effector nucleases. *Genetics*, 186(2):757–61, oct 2010. ISSN 1943-2631.

Christie, N. T. M., Lee, A. L., Fay, H. G., Gray, A. a., and Kikis, E. a. Novel polyglutamine model uncouples proteotoxicity from aging. *PLoS One*, 9(5):e96835, 2014. ISSN 1932-6203.

Chung, C. H. and Baek, S. H. Deubiquitinating Enzymes: Their Diversity and Emerging Roles. *Biochem. Biophys. Res. Commun.*, 266(3):633–640, dec 1999. ISSN 0006291X.

Chusainow, J., Yang, Y. S., Yeo, J. H., Ton, P. C., Asvadi, P., Wong, N. S., and Yap, M. G. A study of monoclonal antibody-producing CHO cell lines: What makes a stable high producer? *Biotechnol. Bioeng.*, 102(4):1182–1196, mar 2009. ISSN 00063592.

Ciftci, K. and Levy, R. J. Enhanced plasmid DNA transfection with lysosomotropic agents in cultured fibroblasts. *Int. J. Pharm.*, 218(1-2):81–92, may 2001. ISSN 0378-5173.

Colomer Gould, V. F., Goti, D., Pearce, D., Gonzalez, G. A., Gao, H., Bermudez de Leon, M., Jenkins, N. A., Copeland, N. G., Ross, C. A., and Brown, D. R. A Mutant ataxin-3 fragment results from processing at a site N-terminal to amino acid 190 in brain of Machado-Joseph disease-like transgenic mice. *Neurobiol. Dis.*, 27(3):362–369, 2007. ISSN 09699961.

Cong, L., Ran, F. A., Cox, D., Lin, S., Barretto, R., Habib, N., Hsu, P. D., Wu, X., Jiang, W., Marraffini, L. A., and Zhang, F. Multiplex genome engineering using CRISPR/Cas systems. *Science (80-.).*, 339(6121):819–823, feb 2013. ISSN 10959203.

Costa, M. d. C., Bajanca, F., Rodrigues, A. J., Tomé, R. J., Corthals, G., Macedo-Ribeiro, S., Paulson, H. L., Logarinho, E., and Maciel, P. Ataxin-3 plays a role in mouse myogenic differentiation through regulation of integrin subunit levels. *PLoS One*, 5(7):e11728, jan 2010. ISSN 19326203.

Coutinho, P. and Andrade, C. Autosomal dominant system degeneration in Portuguese families of the Azores Islands. A new genetic disorder involving cerebellar, pyramidal, extrapyramidal and spinal cord motor functions. *Neurology*, 28(7):703–9, jul 1978. ISSN 0028-3878.

Coutinho, P., Ruano, L., Loureiro, J. L., Cruz, V. T., Barros, J., Tuna, A., Barbot, C., Guimarães, J., Alonso, I., Silveira, I., Sequeiros, J., Neves, J. M., Serrano, P., and Silva, M. C. Hereditary ataxia and spastic paraplegia in Portugal: A population-based prevalence study. *JAMA Neurol.*, 70(6):746–755, 2013. ISSN 21686149.

Cowley, M. J., Pinese, M., Kassahn, K. S., Waddell, N., Pearson, J. V., Grimmond, S. M., Biankin, A. V., Hautaniemi, S., and Wu, J. PINA v2.0: Mining interactome modules. *Nucleic Acids Res.*, 40(D1), jan 2012. ISSN 03051048.

Cox, J., Matic, I., Hilger, M., Nagaraj, N., Selbach, M., Olsen, J. V., and Mann, M. A practical guide to the maxquant computational platform for silac-based quantitative proteomics. *Nat. Protoc.*, 4(5):698–705, 2009. ISSN 17502799.

Craig, K., Keers, S. M., Walls, T. J., Curtis, A., and Chinnery, P. F. Minimum prevalence of spinocerebellar ataxia 17 in the north east of England. *J. Neurol. Sci.*, 239(1):105–109, dec 2005. ISSN 0022510X.

Creagh, E. M., Murphy, B. M., Duriez, P. J., Duckett, C. S., and Martin, S. J. Smac/Diablo antagonizes ubiquitin ligase activity of inhibitor of apoptosis proteins. *J. Biol. Chem.*, 279 (26):26906–14, jun 2004. ISSN 0021-9258.

Crick, S. L., Ruff, K. M., Garai, K., Frieden, C., and Pappu, R. V. Unmasking the roles of N- and C-terminal flanking sequences from exon 1 of huntingtin as modulators of polyglutamine aggregation. *Proc. Natl. Acad. Sci. U. S. A.*, 110(50):20075–20080, dec 2013. ISSN 00278424.

Cristofani, R., Crippa, V., Rusmini, P., Cicardi, M. E., Meroni, M., Licata, N. V., Sala, G., Giorgetti, E., Grunseich, C., Galbiati, M., Piccolella, M., Messi, E., Ferrarese, C., Carra, S., and Poletti, A. Inhibition of retrograde transport modulates misfolded protein accumulation and clearance in motoneuron diseases. *Autophagy*, 13(8):1280–1303, 2017. ISSN 15548635.

Cryns, V. and Yuan, J. Proteases to die for. *Genes Dev.*, 12(11):1551–1570, jun 1998. ISSN 0890-9369.

Cullen, D. A., Leigh, P. N., and Gallo, J. M. Degradation properties of polyglutamine-expanded human androgen receptor in transfected cells. *Neurosci. Lett.*, 357(3):175–178, 2004. ISSN 03043940.

Cummings, C. J. Fourteen and counting: unraveling trinucleotide repeat diseases. *Hum. Mol. Genet.*, 9(6):909–916, apr 2000. ISSN 0964-6906.

Cunha-Santos, J., Duarte-Neves, J., Carmona, V., Guarente, L., De Almeida, L. P., and Cavadas, C. Caloric restriction blocks neuropathology and motor deficits in Machado-Joseph disease mouse models through SIRT1 pathway. *Nat. Commun.*, 2016. ISSN 20411723.

Damgaard, R. B., Nachbur, U., Yabal, M., Wong, W. W.-L., Fiil, B. K., Kastirr, M., Rieser, E., Rickard, J. A., Bankovacki, A., Peschel, C., Ruland, J., Bekker-Jensen, S., Mailand, N., Kaufmann, T., Strasser, A., Walczak, H., Silke, J., Jost, P. J., and Gyrd-Hansen, M. The ubiquitin ligase XIAP recruits LUBAC for NOD2 signaling in inflammation and innate immunity. *Mol. Cell*, 46(6):746–58, jun 2012. ISSN 1097-4164.

Dantuma, N. P., Heinen, C., and Hoogstraten, D. The ubiquitin receptor Rad23: At the crossroads of nucleotide excision repair and proteasomal degradation, apr 2009. ISSN 15687864.

Davies, S. W., Turmaine, M., Cozens, B. A., DiFiglia, M., Sharp, A. H., Ross, C. A., Scherzinger, E., Wanker, E. E., Mangiarini, L., and Bates, G. P. Formation of neuronal intranuclear inclusions underlies the neurological dysfunction in mice transgenic for the HD mutation. *Cell*, 90(3):537–548, aug 1997. ISSN 00928674.

De Castilhos, R. M., Furtado, G. V., Gheno, T. C., Schaeffer, P., Russo, A., Barsottini, O., Pedroso, J. L., Salarini, D. Z., Vargas, F. R., De Lima, M. A. D. F. D., Godeiro, C., Santana-da Silva, L. C., Toralles, M. B. P., Santos, S., Van Der Linden, H., Wanderley, H. Y., De Medeiros, P. F. V., Pereira, E. T., Ribeiro, E., Saraiva-Pereira, M. L., and Jardim, L. B. Spinocerebellar ataxias in Brazil - Frequencies and modulating effects of related genes. *Cerebellum*, 13(1):17–28, 2014a. ISSN 14734230.

De Castilhos, R. M., Furtado, G. V., Gheno, T. C., Schaeffer, P., Russo, A., Barsottini, O., Pedroso, J. L., Salarini, D. Z., Vargas, F. R., De Lima, M. A. D. F. D., Godeiro, C., Santana-da Silva, L. C., Toralles, M. B. P., Santos, S., Van Der Linden, H., Wanderley, H. Y., De Medeiros, P. F. V., Pereira, E. T., Ribeiro, E., Saraiva-Pereira, M. L., and Jardim, L. B. Spinocerebellar ataxias in Brazil - Frequencies and modulating effects of related genes. *Cerebellum*, 13(1):17–28, 2014b. ISSN 14734230.

De Chiara, C., Giannini, C., Adinolfi, S., De Boer, J., Guida, S., Ramos, A., Jodice, C., Kioussis, D., and Pastore, A. The AXH module: An independently folded domain common to ataxin-1 and HBP1. *FEBS Lett.*, 551(1-3):107–112, sep 2003. ISSN 00145793.

Declerck, P. J., Carmeliet, P., Verstreken, M., De Cock, F., and Collen, D. Generation of monoclonal antibodies against autologous proteins in gene- inactivated mice. *J. Biol. Chem.*, 270(15):8397–8400, apr 1995. ISSN 00219258.

Dehm, S. M. and Tindall, D. J. Alternatively spliced androgen receptor variants. *Endocr. Relat. Cancer*, 18(5):R183, oct 2011. ISSN 13510088.

Deller, M. C., Kong, L., and Rupp, B. Protein stability: A crystallographer's perspective. *Acta Crystallogr. Sect. Struct. Biol. Commun.*, 72:72–95, 2016. ISSN 2053230X.

Dengler, L. *Analyse genetischer Polymorphismen und ihr Einfluss auf das Erkrankungsalter bei der Spinozerebellaren Ataxie Typ 3*. PhD thesis, Eberhard Karls Universität Tübingen, 2018.

Dever, T. E. and Green, R. The elongation, termination, and recycling phases of translation in eukaryotes. *Cold Spring Harb. Perspect. Biol.*, 4(7):1–16, jul 2012. ISSN 19430264.

Deveraux, Q. L. and Reed, J. C. IAP family proteins–suppressors of apoptosis. *Genes Dev.*, 13 (3):239–52, feb 1999. ISSN 0890-9369.

Deveraux, Q. L., Takahashi, R., Salvesen, G. S., and Reed, J. C. X-linked IAP is a direct inhibitor of cell-death proteases. *Nature*, 388(6639):300–304, jul 1997. ISSN 0028-0836.

Deveraux, Q. L., Roy, N., Stennicke, H. R., Arsdale, T. V., Zhou, Q., Srinivasula, S. M., Alnemri, E. S., Salvesen, G. S., and Reed, J. C. IAPs block apoptotic events induced by caspase-8 and cytochrome c by direct inhibition of distinct caspases. *EMBO J.*, 17(8):2215–2223, apr 1998. ISSN 14602075.

Díaz-Hernández, M., Valera, A. G., Morán, M. A., Gómez-Ramos, P., Alvarez-Castelao, B., Castaño, J. G., Hernández, F., and Lucas, J. J. Inhibition of 26S proteasome activity by huntingtin filaments but not inclusion bodies isolated from mouse and human brain. *J. Neurochem.*, 98(5):1585–1596, sep 2006. ISSN 00223042.

Dick, T. P., Ruppert, T., Groettrup, M., Kloetzel, P. M., Kuehn, L., Koszinowski, U. H., Stevanovic, S., Schild, H., and Rammensee, H.-G. Coordinated Dual Cleavages Induced by the Proteasome Regulator PA28 Lead to Dominant MHC Ligands. *Cell*, 86(2):253–262, jul 1996. ISSN 0092-8674.

doCarmo Costa, M. and Paulson, H. L. Toward understanding Machado-Joseph Disease. *Prog. Neurobiol.*, 97(2):239–257, 2012.

Dold, S. M. *Generierung einer humanen Ataxin-3-Knockout Zelllinie mit Hilfe von TALEN's, einer neuen Nuklease-Technologie*. Bachelor-thesis, Hochschule Furtwangen, 2014.

Donaldson, K. M., Li, W., Ching, K. A., Batalov, S., Tsai, C.-C., and Joazeiro, C. A. P. Ubiquitin-mediated sequestration of normal cellular proteins into polyglutamine aggregates. *Proc. Natl. Acad. Sci.*, 100(15):8892–8897, 2003. ISSN 0027-8424.

Doss-Pepe, E. W., Stenroos, E. S., Johnson, W. G., and Madura, K. Ataxin-3 interactions with rad23 and valosin-containing protein and its associations with ubiquitin chains and the proteasome are consistent with a role in ubiquitin-mediated proteolysis. *Mol. Cell. Biol.*, 23 (18):6469–83, sep 2003. ISSN 0270-7306.

Dragašević, N. T., Čuljković, B., Klein, C., Ristić, A., Keckarević, M., Topisirović, I., Vukosavić, S., Svetel, M., Kock, N., Stefanova, E., Romac, S., and Kostić, V. S. Frequency analysis and clinical characterization of different types of spinocerebellar ataxia in Serbian patients. *Mov. Disord.*, 21(2):187–191, 2006. ISSN 08853185.

Du, C., Fang, M., Li, Y., Li, L., and Wang, X. Smac, a mitochondrial protein that promotes cytochrome c-dependent caspase activation by eliminating IAP inhibition. *Cell*, 102(1):33–42, jul 2000. ISSN 0092-8674.

Du, X. and Gomez, C. M. Spinocerebellum ataxia type 6: Molecular mechanisms and calcium channel genetics. In *Adv. Exp. Med. Biol.*, volume 1049, pages 147–173. Springer New York LLC, 2018.

Duennwald, M. L., Jagadish, S., Giorgini, F., Muchowski, P. J., and Lindquist, S. A network of protein interactions determines polyglutamine toxicity. *Proc. Natl. Acad. Sci. U. S. A.*, 103 (29):11051–11056, jul 2006a. ISSN 00278424.

Duennwald, M. L., Jagadish, S., Muchowski, P. J., and Lindquist, S. Flanking sequences profoundly alter polyglutamine toxicity in yeast. *Proc. Natl. Acad. Sci.*, 103(29):11045–11050, jul 2006b. ISSN 0027-8424.

Dunn, J. G., Foo, C. K., Belletier, N. G., Gavis, E. R., and Weissman, J. S. Ribosome profiling reveals pervasive and regulated stop codon readthrough in Drosophila melanogaster. *Elife*, 2013(2), dec 2013. ISSN 2050084X.

Durcan, T. M. and Fon, E. A. Mutant ataxin-3 promotes the autophagic degradation of parkin. *Autophagy*, 7(2):233–234, feb 2011. ISSN 1554-8627.

Durcan, T. M., Kontogiannea, M., Thorarinsdottir, T., Fallon, L., Williams, A. J., Djarmati, A., Fantaneanu, T., Paulson, H. L., and Fon, E. a. The Machado-Joseph disease-associated mutant form of ataxin-3 regulates parkin ubiquitination and stability. *Hum. Mol. Genet.*, 20 (1):141–154, 2011. ISSN 1460-2083.

Durcan, T. M., Kontogiannea, M., Bedard, N., Wing, S. S., and Fon, E. A. Ataxin-3 deubiquitination is coupled to parkin ubiquitination via E2 ubiquitin-conjugating enzyme. *J. Biol. Chem.*, 287(1):531–541, 2012. ISSN 00219258.

Durr, A., Stevanin, G., Cancel, G., Duyckaerts, C., Abbas, N., Didierjean, O., Benomar, A., Lyon-caen, O., Julien, J., Serdaru, M., Penet, C., Agid, Y., and Brice, A. Spinocerebellar ataxia 3 and Machado-Joseph disease: Clinical, molecular, and neuropathological features. *Ann. Neurol.*, 39(4):490–499, 1996.

Duvick, L., Barnes, J., Ebner, B., Agrawal, S., Andresen, M., Lim, J., Giesler, G. J., Zoghbi, H. Y., and Orr, H. T. SCA1-like disease in mice expressing wild-type ataxin-1 with a serine to aspartic acid replacement at residue 776. *Neuron*, 67(6):929–35, sep 2010. ISSN 1097-4199.

Duyao, M., Ambrose, C., Myers, R., Novelletto, A., Persichetti, F., Frontali, M., Folstein, S., Ross, C., Franz, M., Abbott, M., Gray, J., Conneally, P., Young, A., Penney, J., Hollingsworth, Z., Shoulson, I., Lazzarini, A., Falek, A., Koroshetz, W., Sax, D., Bird, E., Vonsattel, J., Bonilla, E., Alvir, J., Conde, J. B., Cha, J. H., Dure, L., Gomez, F., Ramos, M., Sanchez-Ramos, J., Snodgrass, S., De-Young, M., Wexler, N., Moscowitz, C., Penchaszadeh, G., Macfarlane, H., Anderson, M., Jenkins, B., Srinidhi, J., Barnes, G., Gusella, J., and Macdonald, M. Trinucleotide repeat length instability and age of onset in Huntington's disease. *Nat. Genet.*, 4(4):387–392, 1993. ISSN 15461718.

Eckelman, B. P., Salvesen, G. S., and Scott, F. L. Human inhibitor of apoptosis proteins: why XIAP is the black sheep of the family. *EMBO Rep.*, 7(10):988–994, oct 2006. ISSN 1469-221X.

Edison, N., Curtz, Y., Paland, N., Mamriev, D., Chorubczyk, N., Haviv-Reingewertz, T., Kfir, N., Morgenstern, D., Kupervaser, M., Kagan, J., Kim, H. T., and Larisch, S. Degradation of Bcl-2 by XIAP and ARTS Promotes Apoptosis. *Cell Rep.*, 21(2):442–454, oct 2017. ISSN 22111247.

Eftekharzadeh, B., Piai, A., Chiesa, G., Mungianu, D., García, J., Pierattelli, R., Felli, I. C., and Salvatella, X. Sequence Context Influences the Structure and Aggregation Behavior of a PolyQ Tract. *Biophys. J.*, 110(11):2361–2366, jun 2016. ISSN 15420086.

Egeblad, M. and Werb, Z. New functions for the matrix metalloproteinases in cancer progression. *Nat. Rev. Cancer*, 2(3):161–174, mar 2002. ISSN 1474-175X.

Einum, D. D., Clark, A. M., Townsend, J. J., Ptacek, L. J., and Fu, Y. H. A novel central nervous system-enriched spinocerebellar ataxia type 7 gene product. *Arch. Neurol.*, 60(1): 97–103, jan 2003. ISSN 00039942.

El Seblani, N., Welleford, A. S., Quintero, J. E., van Horne, C. G., and Gerhardt, G. A. Invited review: Utilizing peripheral nerve regenerative elements to repair damage in the CNS, apr 2020. ISSN 1872678X.

Elbaz, A., Dufouil, C., and Alpérovitch, A. Interaction between genes and environment in neurodegenerative diseases, apr 2007. ISSN 16310691.

Eldeeb, M. A., Fahlman, R. P., Esmaili, M., and Ragheb, M. A. Regulating apoptosis by degradation: The n-end rule-mediated regulation of apoptotic proteolytic fragments in mammalian cells, oct 2018. ISSN 14220067.

Ellegren, H. Microsatellites: Simple sequences with complex evolution, jun 2004. ISSN 14710056.

Ellisdon, A. M., Thomas, B., and Bottomley, S. P. The two-stage pathway of ataxin-3 fibrillogenesis involves a polyglutamine-independent step. *J. Biol. Chem.*, 281(25):16888–16896, 2006. ISSN 00219258.

Evers, M. M., Toonen, L. J. A., and van Roon-Mom, W. M. C. Ataxin-3 Protein and RNA Toxicity in Spinocerebellar Ataxia Type 3: Current Insights and Emerging Therapeutic Strategies. *Mol. Neurobiol.*, nov 2013a. ISSN 0893-7648.

Evers, M. M., Tran, H. D., Zalachoras, I., Pepers, B. a., Meijer, O. C., den Dunnen, J. T., van Ommen, G. J. B., Aartsma-Rus, A., and van Roon-Mom, W. M. C. Ataxin-3 protein modification as a treatment strategy for spinocerebellar ataxia type 3: Removal of the CAG containing exon. *Neurobiol. Dis.*, 58:49–56, oct 2013b. ISSN 1095-953X.

Evers, M. M., Toonen, L. J., and Van Roon-Mom, W. M. Ataxin-3 protein and RNA toxicity in spinocerebellar ataxia type 3: Current insights and emerging therapeutic strategies, jun 2014. ISSN 15591182.

Evert, B. O., Vogt, I. R., Kindermann, C., Ozimek, L., de Vos, R. A. I., Brunt, E. R. P., Schmitt, I., Klockgether, T., and Wüllner, U. Inflammatory Genes Are Upregulated in Expanded Ataxin-3-Expressing Cell Lines and Spinocerebellar Ataxia Type 3 Brains. *J. Neurosci.*, 21 (15):5389–5396, aug 2001. ISSN 0270-6474.

Evert, B. O., Vogt, I. R., Vieira-Saecker, A. M., Ozimek, L., De Vos, R. A., Brunt, E. R., Klockgether, T., and Wüllner, U. Gene expression profiling in ataxin-3 expressing cell lines reveals distinct effects of normal and mutant ataxin-3. *J. Neuropathol. Exp. Neurol.*, 62(10): 1006–1018, 2003. ISSN 00223069.

Evert, B. O., Araujo, J., Vieira-Saecker, A. M., de Vos, R. A. I., Harendza, S., Klockgether, T., and Wullner, U. Ataxin-3 Represses Transcription via Chromatin Binding, Interaction with Histone Deacetylase 3, and Histone Deacetylation. *J. Neurosci.*, 26(44):11474–11486, nov 2006. ISSN 0270-6474.

Fallon, L., Bélanger, C. M., Corera, A. T., Kontogiannea, M., Regan-Klapisz, E., Moreau, F., Voortman, J., Haber, M., Rouleau, G., Thorarinsdottir, T., Brice, A., van Bergen en Henegouwen, P. M., and Fon, E. A. A regulated interaction with the UIM protein Eps15 implicates parkin in EGF receptor trafficking and PI(3)K–Akt signalling. *Nat. Cell Biol.*, 8 (8):834–842, aug 2006. ISSN 1465-7392.

Fan-Minogue, H. and Bedwell, D. M. Eukaryotic ribosomal RNA determinants of aminoglycoside resistance and their role in translational fidelity. *RNA*, 14(1):148–157, jan 2008. ISSN 13558382.

Fang, J., Shing, Y., Wiederschain, D., Yan, L., Butterfield, C., Jackson, G., Harper, J., Tamvakopoulos, G., and Moses, M. A. Matrix metalloproteinase-2 is required for the switch to the angiogenic phenotype in a tumor model. *Proc. Natl. Acad. Sci. U. S. A.*, 97(8):3884–9, apr 2000. ISSN 0027-8424.

Fei, E., Jia, N., Zhang, T., Ma, X., Wang, H., Liu, C., Zhang, W., Ding, L., Nukina, N., and Wang, G. Phosphorylation of ataxin-3 by glycogen synthase kinase 3β at serine 256 regulates the aggregation of ataxin-3. *Biochem. Biophys. Res. Commun.*, 357(2):487–492, jun 2007. ISSN 0006291X.

Fenteany, G., Standaert, R. F., Lane, W. S., Choi, S., Corey, E. J., and Schreiber, S. L. Inhibition of proteasome activities and subunit-specific amino-terminal threonine modification by lactacystin. *Science*, 268(5211):726–731, 1995. ISSN 0036-8075.

Fernandez, M., McClain, M. E., Martinez, R. A., Snow, K., Lipe, H., Ravits, J., Bird, T. D., and La Spada, A. R. Late-onset SCA2: 33 CAG repeats are sufficient to cause disease. *Neurology*, 55(4):569–572, 2000. ISSN 00283878.

Fiedler, M. A., Wernke-Dollries, K., and Stark, J. M. Inhibition of TNF-α-induced NF-κB activation and IL-8 release in A549 cells with the proteasome inhibitor MG-132. *Am. J. Respir. Cell Mol. Biol.*, 19(2):259–268, aug 1998. ISSN 10441549.

Filla, A., De Michele, G., Campanella, G., Perretti, A., Santoro, L., Serlenga, L., Ragno, M., Calabrese, O., Castaldo, I., De Joanna, G., and Cocozza, S. Autosomal dominant cerebellar ataxia type I. Clinical and molecular study in 36 Italian families including a comparison between SCA1 and SCA2 phenotypes. *J. Neurol. Sci.*, 142(1-2):140–147, 1996. ISSN 0022510X.

Finkel, R. S. Read-through strategies for suppression of nonsense mutations in Duchenne/Becker muscular dystrophy: Aminoglycosides and ataluren (PTC124), sep 2010. ISSN 08830738.

Finkel, R. S., Flanigan, K. M., Wong, B., Bönnemann, C., Sampson, J., Sweeney, H. L., Reha, A., Northcutt, V. J., Elfring, G., Barth, J., and Peltz, S. W. Phase 2a study of ataluren-mediated dystrophin production in patients with nonsense mutation Duchenne muscular dystrophy. *PLoS One*, 8(12):e81302, dec 2013. ISSN 19326203.

Firth, A. E. and Brierley, I. Non-canonical translation in RNA viruses, jul 2012. ISSN 00221317.

Fischbeck, K. H. Kennedy disease. *J. Inherit. Metab. Dis.*, 20(2):152–158, jun 1997. ISSN 01418955.

Fischel-Ghodsian, N. Genetic factors in aminoglycoside toxicity, jan 2005. ISSN 14622416.

Fishman, M. C. Zebrafish–the canonical vertebrate. *Science (80-.).*, 294(5545):1290–1, nov 2001. ISSN 0036-8075.

Flinn, L., Bretaud, S., Lo, C., Ingham, P. W., and Bandmann, O. Zebrafish as a new animal model for movement disorders, sep 2008. ISSN 00223042.

Floquet, C., Rousset, J.-P., and Bidou, L. Readthrough of Premature Termination Codons in the Adenomatous Polyposis Coli Gene Restores Its Biological Activity in Human Cancer Cells. *PLoS One*, 6(8):e24125, aug 2011. ISSN 1932-6203.

Forry-Schaudies, S., Murray, J. M., Toyama, Y., and Holtzer, H. Effects of colcemid and taxol on microtubules and intermediate filaments in chick embryo fibroblasts. *Cell Motil. Cytoskeleton*, 6(3):324–338, 1986. ISSN 0886-1544.

França, M. C., Emmel, V. E., D'Abreu, A., Maurer-Morelli, C. V., Secolin, R., Bonadia, L. C., da Silva, M. S., Nucci, A., Jardim, L. B., Saraiva-Pereira, M. L., Marques, W., Paulson, H., and Lopes-Cendes, I. Normal ATXN3 Allele but Not CHIP Polymorphisms Modulates Age at Onset in Machado-Joseph Disease. *Front. Neurol.*, 3(November):164, jan 2012. ISSN 1664-2295.

Fu, X., Ng, C., Feng, D., and Liang, C. Cdc48p is required for the cell cycle commitment point at Start via degradation of the G1-CDK inhibitor Far1p. *J. Cell Biol.*, 163(1):21–26, oct 2003. ISSN 00219525.

Fujigasaki, H., Uchihara, T., Koyano, S., Iwabuchi, K., Yagishita, S., Makifuchi, T., Nakamura, A., Ishida, K., Toru, S., Hirai, S., Ishikawa, K., Tanabe, T., and Mizusawa, H. Ataxin-3 is translocated into the nucleus for the formation of intranuclear inclusions in normal and Machado-Joseph disease brains. *Exp. Neurol.*, 165(2):248–256, oct 2000. ISSN 00144886.

Fujikake, N., Nagai, Y., Popiel, H. A., Okamoto, Y., Yamaguchi, M., and Toda, T. Heat shock transcription factor 1-activating compounds suppress polyglutamine-induced neurodegeneration through induction of multiple molecular chaperones. *J. Biol. Chem.*, 2008. ISSN 00219258.

Furusho, K., Yoshizawa, T., and Shoji, S. Ectoine alters subcellular localization of inclusions and reduces apoptotic cell death induced by the truncated Machado-Joseph disease gene product with an expanded polyglutamine stretch. *Neurobiol. Dis.*, 2005. ISSN 09699961.

Gan, S. R., Shi, S. S., Wu, J. J., Wang, N., Zhao, G. X., Weng, S. T., Murong, S. X., Lu, C. Z., and Wu, Z. Y. High frequency of Machado-Joseph disease identified in Southeastern Chinese kindreds with spinocerebellar ataxia. *BMC Med. Genet.*, 11(1):47, mar 2010. ISSN 14712350.

Gao, R., Liu, Y., Silva-Fernandes, A., Fang, X., Paulucci-Holthauzen, A., Chatterjee, A., Zhang, H. L., Matsuura, T., Choudhary, S., Ashizawa, T., Koeppen, A. H., Maciel, P., Hazra, T. K., and Sarkar, P. S. Inactivation of PNKP by Mutant ATXN3 Triggers Apoptosis by Activating the DNA Damage-Response Pathway in SCA3. *PLOS Genet.*, 11(1):e1004834, jan 2015. ISSN 1553-7404.

Gao, X., Fan, L., Li, H., Li, J., Liu, X., Sun, R., and Yu, Z. Hepatic injury is associated with cell cycle arrest and apoptosis with alteration of cyclin A and D1 in ammonium chloride-induced hyperammonemic rats. *Exp. Ther. Med.*, 11(2):427–434, feb 2016. ISSN 17921015.

Gaspar, C., Lopes-Cendes, I., Hayes, S., Goto, J., Arvidsson, K., Dias, A., Silveira, I., Maciel, P., Coutinho, P., Lima, M., Zhou, Y.-X., Soong, B.-W., Watanabe, M., Giunti, P., Stevanin, G., Riess, O., Sasaki, H., Hsieh, M., Nicholson, G., Brunt, E., Higgins, J., Lauritzen, M., Tranebjaerg, L., Volpini, V., Wood, N., Ranum, L., Tsuji, S., Brice, A., Sequeiros, J., and Rouleau, G. Ancestral Origins of the Machado-Joseph Disease Mutation: A Worldwide Haplotype Study. *Am. J. Hum. Genet.*, 68(2):523–528, 2002. ISSN 00029297.

Gasteiger, E., Gattiker, A., Hoogland, C., Ivanyi, I., Appel, R. D., and Bairoch, A. ExPASy: The proteomics server for in-depth protein knowledge and analysis. *Nucleic Acids Res.*, 31 (13):3784–3788, jul 2003. ISSN 03051048.

Gatchel, J. R. and Zoghbi, H. Y. Diseases of Unstable Repeat Expansion: Mechanisms and Common Principles. *Nat. Rev. Genet.*, 6(10):743–755, oct 2005. ISSN 1471-0056.

Geisler, S., Holmström, K. M., Skujat, D., Fiesel, F. C., Rothfuss, O. C., Kahle, P. J., and Springer, W. PINK1/Parkin-mediated mitophagy is dependent on VDAC1 and p62/SQSTM1. *Nat. Cell Biol.*, 12(2):119–131, feb 2010. ISSN 1465-7392.

Geiss-Friedlander, R. and Melchior, F. Concepts in sumoylation: A decade on, dec 2007. ISSN 14710072.

Gerashchenko, M. V., Lobanov, A. V., and Gladyshev, V. N. Genome-wide ribosome profiling reveals complex translational regulation in response to oxidative stress. *Proc. Natl. Acad. Sci. U. S. A.*, 109(43):17394–17399, 2012. ISSN 00278424.

Gershoni, J. M. and Palade, G. E. Electrophoretic transfer of proteins from sodium dodecyl sulfate-polyacrylamide gels to a positively charged membrane filter. *Anal. Biochem.*, 124(2): 396–405, 1982. ISSN 10960309.

Gershoni, J. M. and Palade, G. E. Protein blotting: Principles and applications, 1983. ISSN 10960309.

Gil-Parrado, S., Fernández-Montalván, A., Assfalg-Machleidt, I., Popp, O., Bestvater, F., Holloschi, A., Knoch, T. A., Auerswald, E. A., Welsh, K., Reed, J. C., Fritz, H., Fuentes-Prior, P., Spiess, E., Salvesen, G. S., and Machleidt, W. Ionomycin-activated calpain triggers apoptosis. A probable role for Bcl-2 family members. *J. Biol. Chem.*, 277(30):27217–26, jul 2002. ISSN 0021-9258.

Giorgetti, E. and Lieberman, A. P. Polyglutamine androgen receptor-mediated neuromuscular disease, may 2016. ISSN 14209071.

Gipson, T. A., Neueder, A., Wexler, N. S., Bates, G. P., and Housman, D. Aberrantly spliced HTT, a new player in Huntington's disease pathogenesis, nov 2013. ISSN 15476286.

Gitler, A. D., Dhillon, P., and Shorter, J. Neurodegenerative disease: models, mechanisms, and a new hope. *Dis. Model. Mech.*, 10(5):499–502, may 2017. ISSN 1754-8403.

Globas, C., du Montcel, S. T., Baliko, L., Boesch, S., Depondt, C., DiDonato, S., Durr, A., Filla, A., Klockgether, T., Mariotti, C., Melegh, B., Rakowicz, M., Ribai, P., Rola, R., Schmitz-Hubsch, T., Szymanski, S., Timmann, D., Van de Warrenburg, B. P., Bauer, P., and Schols, L. Early symptoms in spinocerebellar ataxia type 1, 2, 3, and 6. *Mov. Disord.*, 23(15):2232–2238, 2008. ISSN 15318257.

Gloeckner, C. J., Boldt, K., and Ueffing, M. Strep/FLAG tandem affinity purification (SF-TAP) to study protein interactions. *Curr. Protoc. Protein Sci.*, Chapter 19(SUPPL. 57):Unit19.20, aug 2009. ISSN 19343655.

Goedert, M., Jakes, R., and Spillantini, M. G. The Synucleinopathies: Twenty Years on, 2017. ISSN 1877718X.

Gonda, D. K., Bachmair, A., Wunning, I., Tobias, J. W., Lane, W. S., and Varshavsky, A. Universality and stucture of the N-end rule. *J. Biol. Chem.*, 264(28):16700–16712, oct 1989. ISSN 00219258.

Gorczyca, W., Bruno, S., Darzynkiewicz, R., Gong, J., and Darzynkiewicz, Z. DNA strand breaks occurring during apoptosis - their early insitu detection by the terminal deoxynucleotidyl transferase and nick translation assays and prevention by serine protease inhibitors. *Int. J. Oncol.*, 1(6):639–48, nov 1992. ISSN 1019-6439.

Gorini, L. and Kataja, E. Phenotypic Repair by Streptomycin of Defective Genotypes in E. coli. *Proc. Natl. Acad. Sci. U. S. A.*, 51(3):487–93, mar 1964. ISSN 0027-8424.

Goti, D., Katzen, S. M., Mez, J., Kurtis, N., Kiluk, J., Ben-Haïem, L., Jenkins, N. A., Copeland, N. G., Kakizuka, A., Sharp, A. H., Ross, C. A., Mouton, P. R., and Colomer, V. A mutant ataxin-3 putative-cleavage fragment in brains of Machado-Joseph disease patients and transgenic mice is cytotoxic above a critical concentration. *J. Neurosci.*, 24(45):10266–79, nov 2004. ISSN 1529-2401.

Goto, J., Watanabe, M., Ichikawa, Y., Yee, S. B., Ihara, N., Endo, K., Igarashi, S., Takiyama, Y., Gaspar, C., Maciel, P., Tsuji, S., Rouleau, G. A., and Kanazawa, I. Machado-Joseph disease gene products carrying different carboxyl termini. *Neurosci. Res.*, 28(4):373–7, aug 1997. ISSN 0168-0102.

Gragerov, A., Kino, T., Ilyina-Gragerova, G., Chrousos, G. P., and Pavlakis, G. N. HHR23A, the human homologue of the yeast repair protein RAD23, interacts specifically with Vpr protein and prevents cell cycle arrest but not the transcriptional effects of Vpr. *Virology*, 245(2): 323–330, 1998. ISSN 00426822.

Grechowa, I., Horke, S., Wallrath, A., Vahl, C. F., and Dorweiler, B. Human neutrophil elastase induces endothelial cell apoptosis by activating the PERK-CHOP branch of the unfolded protein response. *FASEB J.*, 31(9):3868–3881, sep 2017. ISSN 15306860.

Greenbaum, D., Colangelo, C., Williams, K., and Gerstein, M. Comparing protein abundance and mRNA expression levels on a genomic scale. *Genome Biol.*, 4(9):117, 2003. ISSN 1474-760X.

Greenfield, E. A., DeCaprio, J., and Brahmandam, M. Making weak antigens strong: Cross-linking peptides to KLH with maleimide. *Cold Spring Harb. Protoc.*, 2018(10):810–811, oct 2018. ISSN 15596095.

Gruber, A., Hornburg, D., Antonin, M., Krahmer, N., Collado, J., Schaffer, M., Zubaite, G., Lüchtenborg, C., Sachsenheimer, T., Brügger, B., Mann, M., Baumeister, W., Hartl, F. U., Hipp, M. S., and Fernández-Busnadiego, R. Molecular and structural architecture of polyQ aggregates in yeast. *Proc. Natl. Acad. Sci. U. S. A.*, 115(15):E3446–E3453, apr 2018. ISSN 10916490.

Grunseich, C., Rinaldi, C., and Fischbeck, K. Spinal and bulbar muscular atrophy: Pathogenesis and clinical management. *Oral Dis.*, 20(1):6–9, 2014. ISSN 1354523X.

Gunawardena, S., Her, L. S., Brusch, R. G., Laymon, R. A., Niesman, I. R., Gordesky-Gold, B., Sintasath, L., Bonini, N. M., and Goldstein, L. S. Disruption of axonal transport by loss of huntingtin or expression of pathogenic polyQ proteins in Drosophila. *Neuron*, 40(1):25–40, sep 2003. ISSN 08966273.

Guo, Z., Yang, X., Sun, F., Jiang, R., Linn, D. E., Chen, H., Chen, H., Kong, X., Melamed, J., Tepper, C. G., Kung, H. J., Brodie, A. M., Edwards, J., and Qiu, Y. A novel androgen receptor splice variant is up-regulated during prostate cancer progression and promotes androgen depletion-resistant growth. *Cancer Res.*, 69(6):2305–2313, mar 2009. ISSN 00085472.

Gutekunst, C. A., Li, S. H., Yi, H., Mulroy, J. S., Kuemmerle, S., Jones, R., Rye, D., Ferrante, R. J., Hersch, S. M., and Li, X. J. Nuclear and neuropil aggregates in Huntington's disease: Relationship to neuropathology. *J. Neurosci.*, 19(7):2522–2534, apr 1999. ISSN 02706474.

Guthrie, O. W. Aminoglycoside induced ototoxicity, jul 2008. ISSN 0300483X.

Gwinn-Hardy, K., Singleton, a., O'Suilleabhain, P., Boss, M., Nicholl, D., Adam, a., Hussey, J., Critchley, P., Hardy, J., and Farrer, M. Spinocerebellar ataxia type 3 phenotypically resembling parkinson disease in a black family. *Arch. Neurol.*, 58:296–299, 2001. ISSN 00039942.

Haacke, A. Aggregationsverhalten des Polyglutaminproteins Ataxin-3 in vitro und in Zellkultur Erklärung Ehrenwörtliche Versicherung. *Arbeit*, 2006.

Haacke, A., Broadley, S. A., Boteva, R., Tzvetkov, N., Hartl, F. U., and Breuer, P. Proteolytic cleavage of polyglutamine-expanded ataxin-3 is critical for aggregation and sequestration of non-expanded ataxin-3. *Hum. Mol. Genet.*, 15(4):555–568, feb 2006. ISSN 09646906.

Haacke, A., Hartl, F. U., and Breuer, P. Calpain inhibition is sufficient to suppress aggregation of polyglutamine-expanded ataxin-3. *J. Biol. Chem.*, 2007. ISSN 00219258.

Haas, E., Incebacak, R., Hentrich, T., Maringer, Y., Schmidt, T., Zimmermann, F., Casadei, N., Mills, J., Aronica, E., Riess, O., Schulze-Hentrich, J., and Huebener-Schmid, J. A novel Ataxin-3 knock-in mouse model mimics the human SCA3 disease phenotype including neuropathological, behavioral, and transcriptional abnormalities. *bioRxiv*, page 2020.02.28.968024, mar 2020.

Haass, C. and Selkoe, D. J. Soluble protein oligomers in neurodegeneration: Lessons from the Alzheimer's amyloid β-peptide. *Nat. Rev. Mol. Cell Biol.*, 8(2):101–112, feb 2007. ISSN 14710072.

Haberhausen, G., Damian, M. S., Leweke, F., and Müller, U. Spinocerebellar ataxia, type 3 (SCA3) is genetically identical to Machado-Joseph disease (MJD). *J. Neurol. Sci.*, 132(1): 71–75, 1995. ISSN 0022510X.

Hahn, M., Dambacher, S., and Schotta, G. Heterochromatin dysregulation in human diseases. *J. Appl. Physiol.*, 109(1):232–242, jul 2010. ISSN 8750-7587.

Hakak, Y., Walker, J. R., Li, C., Wong, W. H., Davis, K. L., Buxbaum, J. D., Haroutunian, V., and Fienberg, A. A. Genome-wide expression analysis reveals dysregulation of myelination-related genes in chronic schizophrenia. *Proc. Natl. Acad. Sci.*, 98(8):4746–4751, apr 2001. ISSN 0027-8424.

Halvey, P. J., Liebler, D. C., and Slebos, R. J. A reporter system for translational readthrough of stop codons in human cells. *FEBS Open Bio*, 2:56–59, jan 2012. ISSN 22115463.

Hamm, A., Krott, N., Breibach, I., Blindt, R., and Bosserhoff, A. K. Efficient Transfection Method for Primary Cells. *Tissue Eng.*, 8(2):235–245, apr 2002. ISSN 1076-3279.

Hampe, C., Ardila-Osorio, H., Fournier, M., Brice, A., and Corti, O. Biochemical analysis of Parkinson's disease-causing variants of Parkin, an E3 ubiquitin-protein ligase with monoubiquitylation capacity. *Hum. Mol. Genet.*, 15(13):2059–75, jul 2006. ISSN 0964-6906.

Han, Y. H., Moon, H. J., You, B. R., and Park, W. H. The effect of MG132, a proteasome inhibitor on HeLa cells in relation to cell growth, reactive oxygen species and GSH. *Oncol. Rep.*, 22(1):215–21, jul 2009. ISSN 1021-335X.

Harding, A. E., Thomas, P. K., Baraitser, M., Bradbury, P. G., Morgan-Hughes, J. A., and Ponsford, J. R. X-linked recessive bulbospinal neuronopathy: A report of ten cases. *J. Neurol. Neurosurg. Psychiatry*, 45(11):1012–1019, 1982. ISSN 00223050.

Harmuth, T., Prell-Schicker, C., Weber, J. J., Gellerich, F., Funke, C., Drießen, S., Magg, J. C. D., Krebiehl, G., Wolburg, H., Hayer, S. N., Hauser, S., Krüger, R., Schöls, L., Riess, O., and Hübener-Schmid, J. Mitochondrial Morphology, Function and Homeostasis Are Impaired by Expression of an N-terminal Calpain Cleavage Fragment of Ataxin-3. *Front. Mol. Neurosci.*, 11:368, oct 2018. ISSN 1662-5099.

Harper, P. S. The epidemiology of Huntington's disease, jun 1992. ISSN 03406717.

Harris, G. M., Dodelzon, K., Gong, L., Gonzalez-Alegre, P., and Paulson, H. L. Splice isoforms of the polyglutamine disease protein ataxin-3 exhibit similar enzymatic yet different aggregation properties. *PLoS One*, 5(10):e13695, jan 2010. ISSN 1932-6203.

Hashimoto, Y., Zhou, W., Hamauchi, K., Shirakura, K., Doi, T., Yagi, K., Sawasaki, T., Okada, Y., Kondoh, M., and Takeda, H. Engineered membrane protein antigens successfully induce antibodies against extracellular regions of claudin-5. *Sci. Rep.*, 8(1):8383, dec 2018. ISSN 20452322.

Hauser, S., Helm, J., Kraft, M., Korneck, M., Hübener-Schmid, J., and Schöls, L. Allele-specific targeting of mutant ataxin-3 by antisense oligonucleotides in SCA3-iPSC-derived neurons. *Mol. Ther. - Nucleic Acids*, 27:99–108, mar 2022. ISSN 21622531.

Havugimana, P. C., Hart, G. T., Nepusz, T., Yang, H., Turinsky, A. L., Li, Z., Wang, P. I., Boutz, D. R., Fong, V., Phanse, S., Babu, M., Craig, S. A., Hu, P., Wan, C., Vlasblom, J., Dar, V. U. N., Bezginov, A., Clark, G. W., Wu, G. C., Wodak, S. J., Tillier, E. R., Paccanaro, A., Marcotte, E. M., and Emili, A. A census of human soluble protein complexes. *Cell*, 150 (5):1068–1081, 2012. ISSN 00928674.

Hayashi, M., Saito, Y., and Kawashima, S. Calpain activation is essential for membrane fusion of erythrocytes in the presence of exogenous Ca2+. *Biochem. Biophys. Res. Commun.*, 182 (2):939–46, jan 1992. ISSN 0006-291X.

Hayashi, Y., Kakita, A., Yamada, M., Egawa, S., Oyanagi, S., Naito, H., Tsuji, S., and Takahashi, H. Hereditary dentatorubral-pallidoluysian atrophy: ubiquitinated filamentous inclusions in the cerebellar dentate nucleus neurons. *Acta Neuropathol.*, 95(5):479–482, may 1998. ISSN 00016322.

He, J., Xia, M., Yeung, P. K., Li, J., Li, Z., Chung, K. K., Chung, S. K., and Xia, J. PICK1 inhibits the E3 ubiquitin ligase activity of Parkin and reduces its neuronal protective effect. *Proc. Natl. Acad. Sci. U. S. A.*, 115(30):E7193–E7201, jul 2018. ISSN 10916490.

Heathfield, K. W. Huntington's chorea: a centenary review. *Postgrad. Med. J.*, 49(567):32–45, 1973. ISSN 00325473.

Heemels, M.-T. Neurodegenerative diseases. *Nature*, 539(7628):437–453, 2014.

Heier, C. R. and DiDonato, C. J. Translational readthrough by the aminoglycoside geneticin (G418) modulates SMN stability in vitro and improves motor function in SMA mice in vivo. *Hum. Mol. Genet.*, 18(7):1310–1322, apr 2009. ISSN 09646906.

Heir, R., Ablasou, C., Dumontier, E., Elliott, M., Fagotto-Kaufmann, C., and Bedford, F. K. The UBL domain of PLIC-1 regulates aggresome formation. *EMBO Rep.*, 7(12):1252–1258, 2006. ISSN 1469-221X.

Herzog, L. K., Kevei, É., Marchante, R., Böttcher, C., Bindesbøll, C., Lystad, A. H., Pfeiffer, A., Gierisch, M. E., Salomons, F. A., Simonsen, A., Hoppe, T., and Dantuma, N. P. The Machado–Joseph disease deubiquitylase ataxin-3 interacts with LC3C/GABARAP and promotes autophagy. *Aging Cell*, 19(1), jan 2020. ISSN 14749726.

Hirabayashi, M., Inoue, K., Tanaka, K., Nakadate, K., Ohsawa, Y., Kamei, Y., Popiel, A. H., Sinohara, A., Iwamatsu, A., Kimura, Y., Uchiyama, Y., Hori, S., and Kakizuka, A. VCP/p97 in abnormal protein aggregates, cytoplasmic vacuoles, and cell death, phenotypes relevant to neurodegeneration. *Cell Death Differ. 2001 810*, 8(10):977, oct 2001. ISSN 1476-5403.

Hirakura, Y., Azimov, R., Azimova, R., and Kagan, B. L. Polyglutamine-induced ion channels: A possible mechanism for the neurotoxicity of huntington and other CAG repeat diseases. *J. Neurosci. Res.*, 60(4):490–494, may 2000. ISSN 03604012.

Hirawat, S., Welch, E. M., Elfring, G. L., Northcutt, V. J., Paushkin, S., Hwang, S., Leonard, E. M., Almstead, N. G., Ju, W., Peltz, S. W., and Miller, L. L. Safety, tolerability, and pharmacokinetics of PTC124, a nonaminoglycoside nonsense mutation suppressor, following single- and multiple-dose administration to healthy male and female adult volunteers. *J. Clin. Pharmacol.*, 47(4):430–444, apr 2007. ISSN 00912700.

Hirokawa, N., Sato-Yoshitake, R., Yoshida, T., and Kawashima, T. Brain dynein (MAP1C) localizes on both anterogradely and retrogradely transported membranous organelles in vivo. *J. Cell Biol.*, 111(3):1027–37, sep 1990. ISSN 0021-9525.

Hiyama, H., Yokoi, M., Masutani, C., Sugasawa, K., Maekawa, T., Tanaka, K., Hoeijmakers, J. H., and Hanaoka, F. Interaction of hHR23 with S5a. The ubiquitin-like domain of hHR23 mediates interaction with S5a subunit of 26 S proteasome. *J. Biol. Chem.*, 274(39):28019–28025, sep 1999. ISSN 00219258.

Hofmann, K. and Falquet, L. A ubiquitin-interacting motif conserved in components of the proteasomal and lysosomal protein degradation systems. *Trends Biochem. Sci.*, 26(6):347–50, jun 2001. ISSN 0968-0004.

Holcik, M. and Korneluk, R. G. XIAP, the guardian angel. *Nat. Rev. Mol. Cell Biol.*, 2(7): 550–556, 2001. ISSN 14710072.

Holmberg, M., Duyckaerts, C., Dürr, A., Cancel, G., Gourfinkel-An, I., Damier, P., Faucheux, B., Trottier, Y., Hirsch, E. C., Agid, Y., and Brice, A. Spinocerebellar ataxia type 7 (SCA7): A neurodegenerative disorder with neuronal intranuclear inclusions. *Hum. Mol. Genet.*, 7(5): 913–918, 1998. ISSN 09646906.

Hommel, G. A stagewise rejective multiple test procedure based on a modified bonferroni test. *Biometrika*, 75(2):383–386, jun 1988. ISSN 00063444.

Honigman, A., Wolf, D., Yaish, S., Falk, H., and Panet, A. cis acting RNA sequences control the gag-pol translation readthrough in murine leukemia virus. *Virology*, 183(1):313–319, jul 1991. ISSN 10960341.

Hopp, T. P. and Woods, K. R. Prediction of protein antigenic determinants from amino acid sequences. *Proc. Natl. Acad. Sci. U. S. A.*, 78(6 I):3824–3828, jun 1981. ISSN 00278424.

Howard, M., Frizzell, R. A., and Bedwell, D. M. Aminoglycoside antibiotics restore CFTR function by overcoming premature stop mutations. *Nat. Med.*, 2(4):467–469, 1996. ISSN 10788956.

Howard, M. T., Shirts, B. H., Petros, L. M., Flanigan, K. M., Gesteland, R. F., and Atkins, J. F. Sequence specificity of aminoglycoside-induced stop codon readthrough: Potential implications for treatment of Duchenne muscular dystrophy. *Ann. Neurol.*, 48(2):164–169, aug 2000. ISSN 03645134.

Howell, V. M., Jones, J. M., Bergren, S. K., Li, L., Billi, A. C., Avenarius, M. R., and Meisler, M. H. Evidence for a direct role of the disease modifier SCNM1 in splicing. *Hum. Mol. Genet.*, 16(20):2506–2516, 2007. ISSN 09646906.

Hsu, J. Y., Jhang, Y. L., Cheng, P. H., Chang, Y. F., Mao, S. H., Yang, H. I., Lin, C. W., Chen, C. M., and Yang, S. H. The truncated C-terminal fragment of mutant ATXN3 disrupts mitochondria dynamics in spinocerebellar ataxia type 3 models. *Front. Mol. Neurosci.*, 10: 196, jun 2017. ISSN 16625099.

Hu, J., Matsui, M., Gagnon, K. T., Schwartz, J. C., Gabillet, S., Arar, K., Wu, J., Bezprozvanny, I., and Corey, D. R. Allele-specific silencing of mutant huntingtin and ataxin-3 genes by targeting expanded CAG repeats in mRNAs. *Nat. Biotechnol.*, 2009a. ISSN 10870156.

Hu, R., Dunn, T. A., Wei, S., Isharwal, S., Veltri, R. W., Humphreys, E., Han, M., Partin, A. W., Vessella, R. L., Isaacs, W. B., Bova, G. S., and Luo, J. Ligand-independent androgen receptor variants derived from splicing of cryptic exons signify hormone-refractory prostate cancer. *Cancer Res.*, 69(1):16–22, jan 2009b. ISSN 00085472.

Huang, D. W., Sherman, B. T., and Lempicki, R. A. Systematic and integrative analysis of large gene lists using DAVID bioinformatics resources. *Nat. Protoc.*, 4(1):44–57, 2009. ISSN 17542189.

Huang, Y., Park, Y. C., Rich, R. L., Segal, D., Myszka, D. G., and Wu, H. Structural basis of caspase inhibition by XIAP: differential roles of the linker versus the BIR domain. *Cell*, 104 (5):781–90, mar 2001. ISSN 0092-8674.

Hübener, J. and Riess, O. Polyglutamine-induced neurodegeneration in SCA3 is not mitigated by non-expanded ataxin-3: Conclusions from double-transgenic mouse models. *Neurobiol. Dis.*, 38(1):116–124, 2010. ISSN 09699961.

Hübener, J., Vauti, F., Funke, C., Wolburg, H., Ye, Y., Schmidt, T., Wolburg-Buchholz, K., Schmitt, I., Gardyan, A., Drießen, S., Arnold, H. H., Nguyen, H. P., and Riess, O. N-terminal ataxin-3 causes neurological symptoms with inclusions, endoplasmic reticulum stress and ribosomal dislocation. *Brain*, 134(7):1925–1942, jul 2011. ISSN 14602156.

Hübener, J., Weber, J. J., Richter, C., Honold, L., Weiss, A., Murad, F., Breuer, P., Wüllner, U., Bellstedt, P., Paquet-Durand, F., Takano, J., Saido, T. C., Riess, O., and Nguyen, H. P. Calpain-mediated ataxin-3 cleavage in the molecular pathogenesis of spinocerebellar ataxia type 3 (SCA3). *Hum. Mol. Genet.*, 22(3):508–518, 2013. ISSN 1460-2083.

Hug, N., Longman, D., and Cáceres, J. F. Mechanism and regulation of the nonsense-mediated decay pathway, feb 2015. ISSN 13624962.

Huynh, D. P., Figueroa, K., Hoang, N., and Pulst, S. M. Nuclear localization or inclusion body formation of ataxin-2 are not necessary for SCA2 pathogenesis in mouse or human. *Nat. Genet.*, 26(1):44–50, sep 2000. ISSN 10614036.

Ichikawa, Y., Goto, J., Hattori, M., Toyoda, A., Ishii, K., Jeong, S. Y., Hashida, H., Masuda, N., Ogata, K., Kasai, F., Hirai, M., Maciel, P., Rouleau, G. a., Sakaki, Y., and Kanazawa, I. The genomic structure and expression of MJD, the Machado-Joseph disease gene. *J Hum Genet*, 46(7):413–422, 2001.

Igarashi, S., Takiyama, Y., Cancel, G., Rogaeva, E. A., Sasaki, H., Wakisaka, A., Zhou, Y. X., Takano, H., Endo, K., Sanpei, K., Oyake, M., Tanaka, H., Stevanin, G., Abbas, N., Dürr, A., Rogaev, E. I., Sherrington, R., Tsuda, T., Ikeda, M., Cassa, E., Nishizawa, M., Benomar, A., Julien, J., Weissenbach, J., Wang, G. X., Agid, Y., St. George-Hyslop, P. H., Brice, A., and Tsuji, S. Intergenerational instability of the CAG repeat of the gene for Machado-Joseph disease (MJD1) is affected by the genotype of the normal chromosome: Implications for the molecular mechanisms of the instability of the CAG repeat. *Hum. Mol. Genet.*, 5(7):923–932, jul 1996. ISSN 09646906.

Ikeda, H., Yamaguchi, M., Sugai, S., Aze, Y., Narumiya, S., and Kakizuka, A. Expanded polyglutamine in the machado-joseph disease protein induces cell death in vitro and in vivo. *Nat. Genet.*, 13(2):196–202, jun 1996. ISSN 15461718.

Invernizzi, G., Aprile, F. A., Natalello, A., and Ghisleni, A. The relationship between aggregation and toxicity of polyglutamine-containing ataxin-3 in the intracellular environment of escherichia coli. *PLoS One*, 7(12):e51890, 2012. ISSN 1932-6203.

Ishikawa, K., Fujigasaki, H., Saegusa, H., Ohwada, K., Fujita, T., Iwamoto, H., Komatsuzaki, Y., Toru, S., Toriyama, H., Watanabe, M., Ohkoshi, N., Shoji, S., Kanazawa, I., Tanabe, T., and Mizusawa, H. Abundant expression and cytoplasmic aggregations of α1A voltage-dependent calcium channel protein associated with neurodegeneration in spinocerebellar ataxia type 6. *Hum. Mol. Genet.*, 8(7):1185–1193, 1999. ISSN 09646906.

Ito, N., Kamiguchi, K., Nakanishi, K., Sokolovskya, A., Hirohashi, Y., Tamura, Y., Murai, A., Yamamoto, E., Kanaseki, T., Tsukahara, T., Kochin, V., Chiba, S., Shimohama, S., Sato, N., and Torigoe, T. A novel nuclear DnaJ protein, DNAJC8, can suppress the formation of spinocerebellar ataxia 3 polyglutamine aggregation in a J-domain independent manner. *Biochem. Biophys. Res. Commun.*, 2016. ISSN 10902104.

Ito, S., Koshikawa, N., Mochizuki, S., and Takenaga, K. 3-Methyladenine suppresses cell migration and invasion of HT1080 fibrosarcoma cells through inhibiting phosphoinositide 3-kinases independently of autophagy inhibition. *Int. J. Oncol.*, 31(2):261–268, aug 2007. ISSN 10196439.

Iughetti, P., Zatz, M., Bueno, M. R., and Marie, S. K. Different origins of mutations at the Machado-Joseph locus (MJD1), may 1996. ISSN 00222593.

Iwabuchi, K., Tsuchiya, K., Uchihara, T., and Yagishita, S. Autosomal dominant spinocerebellar degenerations. Clinical, pathological, and genetic correlations. *Rev. Neurol. (Paris).*, 155(4): 255–270, 1999. ISSN 00353787.

Jagla, M., Fève, M., Kessler, P., Lapouge, G., Erdmann, E., Serra, S., Bergerat, J. P., and Céraline, J. A splicing variant of the androgen receptor detected in a metastatic prostate cancer exhibits exclusively cytoplasmic actions. *Endocrinology*, 148(9):4334–4343, sep 2007. ISSN 00137227.

Jahreiss, L., Menzies, F. M., and Rubinsztein, D. C. The itinerary of autophagosomes: From peripheral formation to kiss-and-run fusion with lysosomes. *Traffic*, 9(4):574–587, apr 2008. ISSN 13989219.

Jain, D. and Salunke, D. M. Antibody specificity and promiscuity, feb 2019. ISSN 14708728.

James, P. D., Raut, S., Rivard, G. E., Poon, M.-C., Warner, M., McKenna, S., Leggo, J., and Lillicrap, D. Aminoglycoside suppression of nonsense mutations in severe hemophilia. *Blood*, 106(9):3043–8, nov 2005. ISSN 0006-4971.

Jana, N. R., Dikshit, P., Goswami, A., Kotliarova, S., Murata, S., Tanaka, K., and Nukina, N. Co-chaperone CHIP associates with expanded polyglutamine protein and promotes their degradation by proteasomes. *J. Biol. Chem.*, 280(12):11635–11640, 2005. ISSN 00219258.

Jardim, L. B., Pereira, M. L., Silveira, I., Ferro, A., Sequeiros, J., and Giugliani, R. Neurologic findings in Machado-Joseph disease: Relation with disease duration, subtypes, and (CAG)n. *Arch. Neurol.*, 58(6):899–904, jun 2001. ISSN 00039942.

Jayasinghe, S. A. and Langen, R. Membrane interaction of islet amyloid polypeptide, aug 2007. ISSN 00052736.

Jeremiasz, J. *Analyse der Rolle von Parkin in der Pathogenese der Spinozerebellären Ataxie Typ 3*. PhD thesis, Universität Tübingen, 2011.

Jin, D. K., Oh, M. R., Song, S. M., Koh, S. W., Lee, M., Kim, G. M., Lee, W. Y., Chung, C. S., Lee, K. H., Im, J. H., Lee, M. J., Kim, J. W., and Lee, M. S. Frequency of spinocerebellar ataxia types 1, 2, 3, 6, 7 and dentatorubral pallidoluysian atrophy mutations in Korean patients with spinocerebellar ataxia. *J. Neurol.*, 246(3):207–210, 1999. ISSN 03405354.

Jin, J.-L., Liu, Z., Lu, Z.-J., Guan, D.-N., Wang, C., Chen, Z.-B., Zhang, J., Zhang, W.-Y., Wu, J.-Y., and Xu, Y. Safety and Efficacy of Umbilical Cord Mesenchymal Stem Cell Therapy in Hereditary Spinocerebellar Ataxia. *Curr. Neurovasc. Res.*, 10(1):11–20, jan 2013. ISSN 15672026.

Joch, M., Ase, A. R., Chen, C. X.-Q., MacDonald, P. A., Kontogiannea, M., Corera, A. T., Brice, A., Séguéla, P., and Fon, E. A. Parkin-mediated monoubiquitination of the PDZ protein PICK1 regulates the activity of acid-sensing ion channels. *Mol. Biol. Cell*, 18(8): 3105–3118, aug 2007. ISSN 1059-1524.

Johnson, M. B., Kawasawa, Y. I., Mason, C. E., Krsnik, Ž., Coppola, G., Bogdanović, D., Geschwind, D. H., Mane, S. M., State, M. W., and Šestan, N. Functional and Evolutionary Insights into Human Brain Development through Global Transcriptome Analysis. *Neuron*, 62 (4):494–509, may 2009. ISSN 08966273.

Johnson, S. L., Blount, J. R., Libohova, K., Ranxhi, B., Paulson, H. L., Tsou, W.-L., and Todi, S. V. Differential toxicity of ataxin-3 isoforms in Drosophila models of Spinocerebellar Ataxia Type 3. *Neurobiol. Dis.*, page 104535, jul 2019. ISSN 09699961.

Johnson, S. L., Libohova, K., Blount, J. R., Sujkowski, A. L., Prifti, M. V., Tsou, W. L., and Todi, S. V. Targeting the VCP-binding motif of ataxin-3 improves phenotypes in Drosophila models of Spinocerebellar Ataxia Type 3. *Neurobiol. Dis.*, 160:105516, dec 2021. ISSN 1095953X.

Johnston, J. A., Ward, C. L., and Kopito, R. R. Aggresomes: a cellular response to misfolded proteins. *J. Cell Biol.*, 143(7):1883–98, dec 1998. ISSN 0021-9525.

Johnston, S. C., Riddle, S. M., Cohen, R. E., and Hill, C. P. Structural basis for the specificity of ubiquitin C-terminal hydrolases. *EMBO J.*, 18(14):3877–3887, jul 1999. ISSN 02614189.

Johri, A. and Beal, M. F. Mitochondrial dysfunction in neurodegenerative diseases, sep 2012. ISSN 00223565.

Jonasson, J., Juvonen, V., Sistonen, P., Ignatius, J., Johansson, D., Björck, E. J., Wahlström, J., Melberg, A., Holmgren, G., Forsgren, L., and Holmberg, M. Evidence for a common Spinocerebellar ataxia type 7 (SCA7) founder mutation in Scandinavia. *Eur. J. Hum. Genet.*, 8(12):918–922, 2000. ISSN 10184813.

Jung, J. and Bonini, N. CREB-binding protein modulates repeat instability in a Drosophila model for polyQ disease. *Science (80-.).*, 2007. ISSN 00368075.

Jung, J., Xu, K., Lessing, D., and Bonini, N. M. Preventing Ataxin-3 protein cleavage mitigates degeneration in a Drosophila model of SCA3. *Hum. Mol. Genet.*, 18(24):4843–4852, 2009. ISSN 09646906.

Juvonen, V., Hietala, M., Kairisito, V., and Savontaus, M. L. The occurrence of dominant spinocerebellar ataxias among 251 Finnish ataxia patients and the role of predisposing large normal alleles in a genetically isolated population. *Acta Neurol. Scand.*, 111(3):154–162, 2005. ISSN 00016314.

Kallio, H. M., Hieta, R., Latonen, L., Brofeldt, A., Annala, M., Kivinummi, K., Tammela, T. L., Nykter, M., Isaacs, W. B., Lilja, H. G., Bova, G. S., and Visakorpi, T. Constitutively active androgen receptor splice variants AR-V3, AR-V7 and AR-V9 are co-expressed in castration-resistant prostate cancer metastases. *Br. J. Cancer*, 119(3):347–356, aug 2018. ISSN 15321827.

Kang, D., Gho, Y. S., Suh, M., and Kang, C. Highly sensitive and fast protein detection with Coomassie brilliant blue in sodium dodecyl sulfate-polyacrylamide gel electrophoresis [5], nov 2002. ISSN 02532964.

Kann, O. and Kovács, R. Mitochondria and neuronal activity, feb 2007. ISSN 03636143.

Kantarci, S., Al-Gazali, L., Hill, R. S., Donnai, D., Black, G. C. M., Bieth, E., Chassaing, N., Lacombe, D., Devriendt, K., Teebi, A., Loscertales, M., Robson, C., Liu, T., MacLaughlin, D. T., Noonan, K. M., Russell, M. K., Walsh, C. A., Donahoe, P. K., and Pober, B. R. Mutations in LRP2, which encodes the multiligand receptor megalin, cause Donnai-Barrow and facio-oculo-acoustico-renal syndromes. *Nat. Genet.*, 39(8):957–9, aug 2007. ISSN 1061-4036.

Karijolich, J. and Yu, Y.-T. Modifying the genetic code: Converting nonsense codons into sense codons by targeted pseudouridylation. *Nature*, 474(7351):395–398, 2012. ISSN 0028-0836.

Karijolich, J. and Yu, Y. T. Therapeutic suppression of premature termination codons: Mechanisms and clinical considerations (Review), aug 2014. ISSN 1791244X.

Karpati, G. and Lochmuller, H. When running a stop sign may be a good thing, jun 2001. ISSN 03645134.

Karra, D. and Dahm, R. Transfection Techniques for Neuronal Cells. *J. Neurosci.*, 30(18): 6171–6177, may 2010. ISSN 0270-6474.

Katayama, T., Ogura, Y., Aizawa, H., Kuroda, H., Suzuki, Y., Kuroda, K., and Kikuchi, K. Nineteen CAG repeats of the SCA6 gene in a Japanese patient presenting with ataxia [3], 2000. ISSN 03405354.

Katsuno, M., Adachi, H., Kume, A., Li, M., Nakagomi, Y., Niwa, H., Sang, C., Kobayashi, Y., Doyu, M., and Sobue, G. Testosterone reduction prevents phenotypic expression in a transgenic mouse model of spinal and bulbar muscular atrophy. *Neuron*, 35(5):843–854, aug 2002. ISSN 08966273.

Kawaguchi, Y., Okamoto, T., Taniwaki, M., Aizawa, M., Inoue, M., Katayama, S., Kawakami, H., Nakamura, S., Nishimura, M., Akiguchi, I., Kimura, J., Narumiya, S., and Kakizuka, A. CAG expansions in a novel gene for Machado-Joseph disease at chromosome 14q32.1. *Nat. Genet.*, 8(3):221–228, 1994. ISSN 15461718.

Kawaguchi, Y., Kovacs, J. J., McLaurin, A., Vance, J. M., Ito, A., and Yao, T. P. The deacetylase HDAC6 regulates aggresome formation and cell viability in response to misfolded protein stress. *Cell*, 115(6):727–38, dec 2003. ISSN 0092-8674.

Kaytor, M. D., Duvick, L. A., Skinner, P. J., Koob, M. D., Ranum, L. P. W., and Orr, H. T. Nuclear localization of the spinocerebellar ataxia type 7 protein, ataxin-7. *Hum. Mol. Genet.*, 8(9):1657–1664, sep 1999. ISSN 09646906.

Kazachkova, N., Raposo, M., Montiel, R., Cymbron, T., Bettencourt, C., Silva-Fernandes, A., Silva, S., MacIel, P., and Lima, M. Patterns of mitochondrial DNA damage in blood and brain tissues of a transgenic mouse model of machado-joseph disease. *Neurodegener. Dis.*, 11 (4):206–214, apr 2013. ISSN 16602854.

Kazantsev, A., Preisinger, E., Dranovsky, A., Goldgaber, D., and Housman, D. Insoluble detergent-resistant aggregates form between pathological and nonpathological lengths of polyglutamine in mammalian cells. *Proc. Natl. Acad. Sci.*, 96(20):11404–11409, sep 2002. ISSN 0027-8424.

Kazemi-Esfarjani, P. and Benzer, S. Genetic suppression of polyglutamine toxicity in Drosophila. *Science (80-.).*, 287(5459):1837–1840, mar 2000. ISSN 00368075.

Keeling, K. M. and Bedwell, D. M. Pharmacological suppression of premature stop mutations that cause genetic diseases, dec 2005. ISSN 15701603.

Keeling, K. M., Xue, X., Gunn, G., and Bedwell, D. M. Therapeutics Based on Stop Codon Readthrough. *Annu. Rev. Genomics Hum. Genet.*, 15(1):371–394, 2014. ISSN 1527-8204.

Kellermayer, R., Szigeti, R., Keeling, K. M., Bedekovics, T., and Bedwell, D. M. Aminoglycosides as potential pharmacogenetic agents in the treatment of Hailey-Hailey disease. *J. Invest. Dermatol.*, 126(1):229–31, jan 2006. ISSN 0022-202X.

Kemeny, D. M., Urbanek, R., Samuel, D., and Richards, D. Increased sensitivity and specificity of a sandwich ELISA for measurement of IgE antibodies. *J. Immunol. Methods*, 78(2):217–226, apr 1985. ISSN 00221759.

Kemeny, S., Dery, D., Loboda, Y., Rovner, M., Lev, T., Zuri, D., Finberg, J. P., and Larisch, S. Parkin promotes degradation of the mitochondrial pro-apoptotic ARTS protein. *PLoS One*, 7(7):e38837, jul 2012. ISSN 19326203.

Kennedy, W. R., Alter, M., and Sung, J. H. Progressive proximal spinal and bulbar muscular atrophy of late onset: A sex-linked recessive trait. *Neurology*, 18(7):671–680, 1968. ISSN 1526632X.

Kerem, E., Hirawat, S., Armoni, S., Yaakov, Y., Shoseyov, D., Cohen, M., Nissim-Rafinia, M., Blau, H., Rivlin, J., Aviram, M., Elfring, G. L., Northcutt, V. J., Miller, L. L., Kerem, B., and Wilschanski, M. Effectiveness of PTC124 treatment of cystic fibrosis caused by nonsense mutations: a prospective phase II trial. *Lancet*, 372(9640):719–727, aug 2008. ISSN 01406736.

Kerem, E., Konstan, M. W., De Boeck, K., Accurso, F. J., Sermet-Gaudelus, I., Wilschanski, M., Elborn, J. S., Melotti, P., Bronsveld, I., Fajac, I., Malfroot, A., Rosenbluth, D. B., Walker, P. A., McColley, S. A., Knoop, C., Quattrucci, S., Rietschel, E., Zeitlin, P. L., Barth, J., Elfring, G. L., Welch, E. M., Branstrom, A., Spiegel, R. J., Peltz, S. W., Ajayi, T., and Rowe, S. M. Ataluren for the treatment of nonsense-mutation cystic fibrosis: A randomised, double-blind, placebo-controlled phase 3 trial. *Lancet Respir. Med.*, 2(7):539–547, 2014. ISSN 22132619.

Khan, L. A., Bauer, P. O., Miyazaki, H., Lindenberg, K. S., Landwehrmeyer, B. G., and Nukina, N. Expanded polyglutamines impair synaptic transmission and ubiquitin-proteasome system in Caenorhabditis elegans. *J. Neurochem.*, 98(2):576–587, jul 2006. ISSN 00223042.

Kieling, C., Prestes, P. R., Saraiva-Pereira, M. L., and Jardim, L. B. Survival estimates for patients with Machado-Joseph disease (SCA3). *Clin. Genet.*, 72(6):543–545, dec 2007. ISSN 00099163.

Kinoshita, S., Akira, S., and Kishimoto, T. A member of the C/EBP family, NF-IL6 beta, forms a heterodimer and transcriptionally synergizes with NF-IL6. *Proc. Natl. Acad. Sci.*, 89(4): 1473–1476, feb 1992. ISSN 0027-8424.

Kitada, T., Asakawa, S., Hattori, N., Matsumine, H., Yamamura, Y., Minoshima, S., Yokochi, M., Mizuno, Y., and Shimizu, N. Mutations in the parkin gene cause autosomal recessive juvenile parkinsonism. *Nature*, 392(6676):605–608, apr 1998. ISSN 00280836.

Klement, I. A., Skinner, P. J., Kaytor, M. D., Yi, H., Hersch, S. M., Clark, H. B., Zoghbi, H. Y., and Orr, H. T. Ataxin-1 nuclear localization and aggregation: role in polyglutamine-induced disease in SCA1 transgenic mice. *Cell*, 95(1):41–53, oct 1998. ISSN 0092-8674.

Klinke, I., Minnerop, M., Schmitz-Hübsch, T., Hendriks, M., Klockgether, T., Wüllner, U., and Helmstaedter, C. Neuropsychological features of patients with spinocerebellar ataxia (SCA) types 1, 2, 3, and 6. *Cerebellum*, 9(3):433–442, sep 2010. ISSN 14734222.

Ko, J., Ou, S., and Patterson, P. H. New anti-huntingtin monoclonal antibodies: implications for huntingtin conformation and its binding proteins. *Brain Res. Bull.*, 56(3-4):319–29, 2001. ISSN 0361-9230.

Koch, P., Breuer, P., Peitz, M., Jungverdorben, J., Kesavan, J., Poppe, D., Doerr, J., Ladewig, J., Mertens, J., Tüting, T., Hoffmann, P., Klockgether, T., Evert, B. O., Wüllner, U., and Brüstle, O. Excitation-induced ataxin-3 aggregation in neurons from patients with Machado-Joseph disease. *Nature*, 480(7378):543–546, dec 2011. ISSN 00280836.

Koht, J. and Tallaksen, C. M. Cerebellar ataxia in the eastern and southern parts of Norway. *Acta Neurol. Scand.*, 115(SUPPL.187):76–79, 2007. ISSN 00016314.

Koide, R., Ikeuchi, T., Onodera, O., Tanaka, H., Igarashi, S., Endo, K., Takahashi, H., Kondo, R., Ishikawa, A., Hayashi, T., Saito, M., Tomoda, A., Miike, T., Naito, H., Ikuta, F., and Tsuji, S. Unstable expansion of CAG repeat in hereditary dentatorubral–pallidoluysian atrophy (DRPLA). *Nat. Genet.*, 6(1):9–13, 1994. ISSN 15461718.

Koide, R., Kobayashi, S., Shimohata, T., Ikeuchi, T., Maruyama, M., Saito, M., Yamada, M., Takahashi, H., and Tsuji, S. A neurological disease caused by an expanded CAG trinucleotide repeat in the TATA-binding protein gene: A new polyglutamine disease? *Hum. Mol. Genet.*, 8(11):2047–2053, 1999. ISSN 09646906.

Kopelowitz, J., Hampe, C., Goldman, R., Reches, M., and Engelberg-Kulka, H. Influence of codon context on UGA suppression and readthrough. *J. Mol. Biol.*, 225(2):261–269, may 1992. ISSN 00222836.

Kovács, J. Effect of cycloheximide on induced autophagy in epithelial cells of the seminal vesicle of mice. *Acta Morphol Acad Sci Hung.*, 22(1):69–75, 1974.

Koyano, S., Uchihara, T., Fujigasaki, H., Nakamura, A., Yagishita, S., and Iwabuchi, K. Neuronal intranuclear inclusions in spinocerebellar ataxia type 2: triple-labeling immunofluorescent study. *Neurosci. Lett.*, 273(2):117–120, oct 1999. ISSN 03043940.

Kretzschmar, D., Tschäpe, J., Bettencourt Da Cruz, A., Asan, E., Poeck, B., Strauss, R., and Pflugfelder, G. O. Glial and neuronal expression of polyglutamine proteins induce behavioral changes and aggregate formation in Drosophila. *Glia*, 49(1):59–72, jan 2005. ISSN 08941491.

Krishan, A. Rapid flow cytofluorometric analysis of mammalian cell cycle by propidium iodide staining. *J. Cell Biol.*, 66(1):188–93, jul 1975. ISSN 0021-9525.

Krishna, N., Mohan, S., Yashavantha, B. S., Rammurthy, A., Kiran Kumar, H. B., Mittal, U., Tyagi, S., Mukerji, M., Jain, S., Pal, P. K., and Purushottam, M. SCA 1, SCA 2 & SCA 3/MJD mutations in ataxia syndromes in southern India. *Indian J. Med. Res.*, 126(5): 465–470, 2007. ISSN 09715916.

Kristensen, L. V., Oppermann, F. S., Rauen, M. J., Hartmann-Petersen, R., and Thirstrup, K. Polyglutamine expansion of ataxin-3 alters its degree of ubiquitination and phosphorylation at specific sites. *Neurochem. Int.*, 105:42–50, 2017. ISSN 18729754.

Kristensen, L. V., Oppermann, F. S., Rauen, M. J., Fog, K., Schmidt, T., Schmidt, J., Harmuth, T., Hartmann-Petersen, R., and Thirstrup, K. Mass spectrometry analyses of normal and polyglutamine expanded ataxin-3 reveal novel interaction partners involved in mitochondrial function. *Neurochem. Int.*, 112:5–17, 2018. ISSN 18729754.

Krüger, R., Kuhn, W., Müller, T., Woitalla, D., Graeber, M., Kösel, S., Przuntek, H., Epplen, J. T., Schols, L., and Riess, O. AlaSOPro mutation in the gene encoding α-synuclein in Parkinson's disease. *Nat. Genet.*, 18(2):106–108, feb 1998. ISSN 1061-4036.

Kuemmerle, S., Gutekunst, C. A., Klein, A. M., Li, X. J., Li, S. H., Beal, M. F., Hersch, S. M., and Ferrante, R. J. Huntington aggregates may not predict neuronal death in Huntington's disease. *Ann. Neurol.*, 46(6):842–9, dec 1999. ISSN 0364-5134.

Kumar, S., Talis, A. L., and Howley, P. M. Identification of HHR23A as a substrate for E6-associated protein-mediated ubiquitination. *J. Biol. Chem.*, 274(26):18785–92, jun 1999. ISSN 0021-9258.

Kwon, Y. T., Reiss, Y., Fried, V. A., Hershko, A., Yoon, J. K., Gonda, D. K., Sangan, P., Copeland, N. G., Jenkins, N. A., and Varshavsky, A. The mouse and human genes encoding the recognition component of the N-end rule pathway. *Proc. Natl. Acad. Sci. U. S. A.*, 95 (14):7898–7903, jul 1998. ISSN 00278424.

Kyte, J. and Doolittle, R. F. A simple method for displaying the hydropathic character of a protein. *J. Mol. Biol.*, 157(1):105–132, may 1982. ISSN 00222836.

La Spada, A. R. and Taylor, J. P. Polyglutamines placed into context. *Neuron*, 38(5):681–4, jun 2003. ISSN 0896-6273.

La Spada, A. R., Wilson, E. M., Lubahn, D. B., Harding, A. E., and Fischbeck, K. H. Androgen receptor gene mutations in X-linked spinal and bulbar muscular atrophy. *Nature*, 352(6330): 77–79, 1991. ISSN 00280836.

La Spada, A. R., Fu, Y. H., Sopher, B. L., Libby, R. T., Wang, X., Li, L. Y., Einum, D. D., Huang, J., Possin, D. E., Smith, A. C., Martinez, R. A., Koszdin, K. L., Treuting, P. M., Ware, C. B., Hurley, J. B., Ptáček, L. J., and Chen, S. Polyglutamine-expanded ataxin-7 antagonizes CRX function and induces cone-rod dystrophy in a mouse model of SCA7. *Neuron*, 31(6): 913–927, sep 2001. ISSN 08966273.

Laço, M. N., Cortes, L., Travis, S. M., Paulson, H. L., and Rego, a. C. Valosin-Containing Protein (VCP/p97) Is an Activator of Wild-Type Ataxin-3. *PLoS One*, 7(9):e43563, jan 2012a. ISSN 19326203.

Laço, M. N., Oliveira, C. R., Paulson, H. L., and Rego, A. C. Compromised mitochondrial complex II in models of Machado–Joseph disease. *Biochim. Biophys. Acta - Mol. Basis Dis.*, 1822(2):139–149, feb 2012b. ISSN 09254439.

Laffita-Mesa, J. M., Rodríguez Pupo, J. M., Moreno Sera, R., Vázquez Mojena, Y., Kourí, V., Laguna-Salvia, L., Martínez-Godales, M., Valdevila Figueira, J. A., Bauer, P. O., Rodríguez-Labrada, R., Zaldívar, Y. G., Paucar, M., Svenningsson, P., and Pérez, L. V. De Novo Mutations in Ataxin-2 Gene and ALS Risk. *PLoS One*, 8(8):e70560, aug 2013. ISSN 19326203.

Lajoie, P. and Snapp, E. L. Formation and toxicity of soluble polyglutamine oligomers in living cells. *PLoS One*, 5(12):e15245, dec 2010. ISSN 19326203.

Lakhani, S. A., Masud, A., Kuida, K., Porter, G. A., Booth, C. J., Mehal, W. Z., Inayat, I., and Flavell, R. A. Caspases 3 and 7: Key Mediators of Mitochondrial Events of Apoptosis. *Science (80-.).*, 311(5762):847–851, feb 2006. ISSN 0036-8075.

Lambert, M. P., Barlow, A. K., Chromy, B. A., Edwards, C., Freed, R., Liosatos, M., Morgan, T. E., Rozovsky, I., Trommer, B., Viola, K. L., Wals, P., Zhang, C., Finch, C. E., Krafft, G. A., and Klein, W. L. Diffusible, nonfibrillar ligands derived from A 1-42 are potent central nervous system neurotoxins. *Proc. Natl. Acad. Sci.*, 95(11):6448–6453, may 1998. ISSN 0027-8424.

Lambrughi, M., Maiani, E., Aykac Fas, B., Shaw, G. S., Kragelund, B. B., Lindorff-Larsen, K., Teilum, K., Invernizzi, G., and Papaleo, E. Ubiquitin Interacting Motifs: Duality Between Structured and Disordered Motifs. *Front. Mol. Biosci.*, 8, jun 2021. ISSN 2296889X.

Lamkanfi, M. and Kanneganti, T. D. Caspase-7: A protease involved in apoptosis and inflammation. *Int. J. Biochem. Cell Biol.*, 42(1):21–24, 2010. ISSN 13572725.

Lamkanfi, M., Declercq, W., Kalai, M., Saelens, X., and Vandenabeele, P. Alice in caspase land. A phylogenetic analysis of caspases from worm to man. *Cell Death Differ.*, 9(4):358–361, 2002. ISSN 13509047.

Lang, A. E., Rogaeva, E. A., Tsuda, T., Hutterer, J., and St George-Hyslop, P. Homozygous inheritance of the Machado-Joseph disease gene. *Ann. Neurol.*, 36(3):443–447, sep 1994. ISSN 15318249.

Laron, Z., Pertzelan, A., and Mannheimer, S. Genetic pituitary dwarfism with high serum concentation of growth hormone–a new inborn error of metabolism? *Isr. J. Med. Sci.*, 2(2): 152–5, 1966. ISSN 0021-2180.

Lashuel, H. A., Hartley, D., Petre, B. M., Walz, T., and Lansbury, P. T. Neurodegenerative disease: Amyloid pores from pathogenic mutations. *Nature*, 418(6895):291, jul 2002. ISSN 00280836.

Lastres-Becker, I., Nonis, D., Nowock, J., and Auburger, G. New alternative splicing variants of the ATXN2 transcript. *Neurol. Res. Pract.*, 1(1):22, dec 2019. ISSN 2524-3489.

Lawrence, B. and Brown, W. Inhibition of protein synthesis separates autophagic sequestration from the delivery of lysosomal enzymes. *J Cell Sci.*, 105:473–80, 1993.

Lecker, S. H., Goldberg, A. L., and Mitch, W. E. Protein degradation by the ubiquitin-proteasome pathway in normal and disease states. *J. Am. Soc. Nephrol.*, 17(7):1807–19, jul 2006. ISSN 1046-6673.

Leduc, E. H., Scott, G. B., and Avrameas, S. Ultrastructural localization of intracellular immune globulins in plasma cells and lymphoblasts by enzyme-labeled antibodies. *J. Histochem. Cytochem.*, 17(4):211–224, apr 1969. ISSN 0022-1554.

Lee, W. Y., Jin, D. K., Oh, M. R., Lee, J. E., Song, S. M., Lee, E. A., Kim, G. M., Chung, J. S., and Lee, K. H. Frequency analysis and clinical characterization of spinocerebellar ataxia types 1, 2, 3, 6, and 7 in Korean patients. *Arch. Neurol.*, 60(6):858–863, 2003. ISSN 00039942.

Lee, Y. and Rio, D. C. Mechanisms and regulation of alternative Pre-mRNA splicing, jun 2015. ISSN 15454509.

Leggo, J., Dalton, A., Morrison, P. J., Dodge, A., Connarty, M., Kotze, M. J., and Rubinsztein, D. C. Analysis of spinocerebellar ataxia types 1, 2, 3, and 6, dentatorubral-pallidoluysian atrophy, and Friedreich's ataxia genes in spinocerebellar ataxia patients in the UK. *J. Med. Genet.*, 34(12):982–985, 1997. ISSN 00222593.

Lei, L. F., Yang, G. P., Wang, J. L., Chuang, D. M., Song, W. H., Tang, B. S., and Jiang, H. Safety and efficacy of valproic acid treatment in SCA3/MJD patients. *Park. Relat. Disord.*, 2016. ISSN 18735126.

Leisman, G., Melillo, R., and R., F. Clinical Motor and Cognitive Neurobehavioral Relationships in the Basal Ganglia. In *Basal Ganglia - An Integr. View*. InTech, jan 2013.

Lepock, J. R., Frey, H. E., Heynen, M. L., Senisterra, G. A., and Warters, R. L. The nuclear matrix is a thermolabile cellular structure. *Cell Stress Chaperones*, 6(2):136–147, apr 2001. ISSN 13558145.

Lerer, I. Machado-Joseph disease: Correlation between the clinical features, the CAG repeat length and homozygosity for the mutation. *Eur. J. Hum. Genet.*, 4(1):3–7, 1996. ISSN 10184813.

Lesage, S., Anheim, M., Letournel, F., Bousset, L., Honoré, A., Rozas, N., Pieri, L., Madiona, K., Dürr, A., Melki, R., Verny, C., Brice, A., and French Parkinson's Disease Genetics Study Group. G51D α-synuclein mutation causes a novel Parkinsonian-pyramidal syndrome. *Ann. Neurol.*, 73(4):459–471, apr 2013. ISSN 03645134.

Lessing, D. and Bonini, N. M. Polyglutamine genes interact to modulate the severity and progression of neurodegeneration in Drosophila. *PLoS Biol.*, 6(2):0266–0274, feb 2008. ISSN 15449173.

Li, C. and Zhang, J. Stop-codon read-through arises largely from molecular errors and is generally nonadaptive. *PLoS Genet.*, 15(5):e1008141, may 2019. ISSN 15537404.

Li, F., Macfarlan, T., Pittman, R. N., and Chakravarti, D. Ataxin-3 is a histone-binding protein with two independent transcriptional corepressor activities. *J. Biol. Chem.*, 277(47):45004–45012, nov 2002. ISSN 00219258.

Li, M., Miwa, S., Kobayashi, Y., Merry, D. E., Yamamoto, M., Tanaka, F., Doyu, M., Hashizume, Y., Fischbeck, K. H., and Sobue, G. Nuclear inclusions of the androgen receptor protein in spinal and bulbar muscular atrophy. *Ann. Neurol.*, 44(2):249–254, 1998. ISSN 03645134.

Li, T., Martins, S., Peng, Y., Wang, P., Hou, X., Chen, Z., Wang, C., Tang, Z., Qiu, R., Chen, C., Hu, Z., Xia, K., Tang, B., Sequeiros, J., and Jiang, H. Is the high frequency of machado-joseph disease in China due to new mutational orignis? *Front. Genet.*, 10(FEB):740, feb 2019. ISSN 16648021.

Li, X., Liu, H., Fischhaber, P. L., and Tang, T. S. Toward therapeutic targets for SCA3: Insight into the role of Machado-Joseph disease protein ataxin-3 in misfolded proteins clearance, sep 2015. ISSN 18735118.

Lichtinghagen, R., Musholt, P. B., Lein, M., Römer, A., Rudolph, B., Kristiansen, G., Hauptmann, S., Schnorr, D., Loening, S. A., and Jung, K. Different mRNA and protein expression of matrix metalloproteinases 2 and 9 and tissue inhibitor of metalloproteinases 1 in benign and malignant prostate tissue. *Eur. Urol.*, 42(4):398–406, oct 2002. ISSN 0302-2838.

Lieberman, A. P., Shakkottai, V. G., and Albin, R. L. Polyglutamine Repeats in Neurodegenerative Diseases. *Annu. Rev. Pathol. Mech. Dis.*, 14(1):1–27, jan 2019. ISSN 1553-4006.

Ligon, L. A., Karki, S., Tokito, M., and Holzbaur, E. L. F. Dynein binds to β-catenin and may tether microtubules at adherens junctions. *Nat. Cell Biol.*, 3(10):913–917, oct 2001. ISSN 1465-7392.

Limprasert, P., Nouri, N., Heyman, R. A., Nopparatana, C., Kamonsilp, M., Deininger, P. L., and Keats, B. J. Analysis of CAG repeat of the Machado-Joseph gene in human, chimpanzee and monkey populations: A variant nucleotide is associated with the number of CAG repeats. *Hum. Mol. Genet.*, 5(2):207–213, feb 1996. ISSN 09646906.

Lindblad, K., Savontaus, M. L., Stevanin, G., Holmberg, M., Digre, K., Zander, C., Ehrsson, H., David, G., Benomar, A., Nikoskelainen, E., Trottier, Y., Holmgren, G., Ptacek, L. J., Anttinen, A., Brice, A., and Schalling, M. An expanded CAG repeat sequence in spinocerebellar ataxia type 7. *Genome Res.*, 6(10):965–971, 1996. ISSN 10549803.

Lindgren, M. and Hammarström, P. Amyloid oligomers: Spectroscopic characterization of amyloidogenic protein states, mar 2010. ISSN 1742464X.

Liu, H., Li, X., Ning, G., Zhu, S., Ma, X., Liu, X., Liu, C., Huang, M., Schmitt, I., Wüllner, U., Niu, Y., Guo, C., Wang, Q., and Tang, T.-S. The Machado–Joseph Disease Deubiquitinase Ataxin-3 Regulates the Stability and Apoptotic Function of p53. *PLOS Biol.*, 14(11):e2000733, nov 2016. ISSN 1545-7885.

Liu, J., Pendergraff, H., Narayanannair, K. J., Lackey, J. G., Kuchimanchi, S., Rajeev, K. G., Manoharan, M., Hu, J., and Corey, D. R. RNA duplexes with abasic substitutions are potent and allele-selective inhibitors of huntingtin and ataxin-3 expression. *Nucleic Acids Res.*, 2013. ISSN 03051048.

Liu, W. C., Slusarchyk, D. S., Astle, G., Trejo, W. H., Brown, W. E., and Meyers, E. Ionomycin, a new polyether antibiotic. *J. Antibiot. (Tokyo).*, 31(9):815–9, sep 1978. ISSN 0021-8820.

Liu, Y.-X., Wang, J., Guo, J., Wu, J., Lieberman, H. B., and Yin, Y. DUSP1 is controlled by p53 during the cellular response to oxidative stress. *Mol. Cancer Res.*, 6(4):624–33, apr 2008. ISSN 1541-7786.

Liu, Z. and Zhang, J. Human C-to-U coding RNA editing is largely nonadaptive. *Mol. Biol. Evol.*, 35(4):963–969, apr 2018. ISSN 15371719.

Liu, Z., Cao, J., Gao, X., Ma, Q., Ren, J., and Xue, Y. GPS-CCD: A novel computational program for the prediction of calpain cleavage sites. *PLoS One*, 6(4):e19001, apr 2011. ISSN 19326203.

Liu, Z., Zhang, J., and Yeager, M. Most m6A RNA Modifications in Protein-Coding Regions Are Evolutionary Unconserved and Likely Nonfunctional. *Mol. Biol. Evol.*, 35(3):666–675, mar 2018. ISSN 15371719.

Lonskaya, I., Desforges, N. M., Hebron, M. L., and Moussa, C. E.-H. Ubiquitination increases parkin activity to promote autophagic α-synuclein clearance. *PLoS One*, 8(12):e83914, dec 2013. ISSN 1932-6203.

Lopes, T. M., D'Abreu, A., Junior, M. C. F., Yasuda, C. L., Betting, L. E., Samara, A. B., Castellano, G., Somazz, J. C., Balthazar, M. L. F., Lopes-Cendes, I., and Cendes, F. Widespread neuronal damage and cognitive dysfunction in spinocerebellar ataxia type 3. *J. Neurol.*, 260(9):2370–2379, sep 2013. ISSN 0340-5354.

López-Bastida, J., Perestelo-Pérez, L., Montón-Álvarez, F., and Serrano-Aguilar, P. Social economic costs and health-related quality of life in patients with degenerative cerebellar ataxia in Spain. *Mov. Disord.*, 23(2):212–217, jan 2008. ISSN 08853185.

Löscher, W., Klotz, U., Zimprich, F., and Schmidt, D. The clinical impact of pharmacogenetics on the treatment of epilepsy. *Epilepsia*, 50(1):1–23, 2009. ISSN 00139580.

Loughran, G., Chou, M. Y., Ivanov, I. P., Jungreis, I., Kellis, M., Kiran, A. M., Baranov, P. V., and Atkins, J. F. Evidence of efficient stop codon readthrough in four mammalian genes. *Nucleic Acids Res.*, 42(14):8928–8938, aug 2014. ISSN 13624962.

Lu, C. and Luo, J. Decoding the androgen receptor splice variants, 2013. ISSN 22234691.

Lunkes, A., Lindenberg, K. S., Ben-Haem, L., Weber, C., Devys, D., Landwehrmeyer, G. B., Mandel, J. L., and Trottier, Y. Proteases acting on mutant huntingtin generate cleaved products that differentially build up cytoplasmic and nuclear inclusions. *Mol. Cell*, 10(2): 259–269, aug 2002. ISSN 10972765.

Macagno, A., Gilliet, M., Sallusto, F., Lanzavecchia, A., Nestle, F. O., and Groettrup, M. Dendritic cells up-regulate immunoproteasomes and the proteasome regulator PA28 during maturation. *Eur. J. Immunol.*, 29(12):4037–4042, dec 1999. ISSN 0014-2980.

MacDonald, M. E., Ambrose, C. M., Duyao, M. P., Myers, R. H., Lin, C., Srinidhi, L., Barnes, G., Taylor, S. A., James, M., Groot, N., MacFarlane, H., Jenkins, B., Anderson, M. A., Wexler, N. S., Gusella, J. F., Bates, G. P., Baxendale, S., Hummerich, H., Kirby, S., North, M., Youngman, S., Mott, R., Zehetner, G., Sedlacek, Z., Poustka, A., Frischauf, A. M., Lehrach, H., Buckler, A. J., Church, D., Doucette-Stamm, L., O'Donovan, M. C., Riba-Ramirez, L., Shah, M., Stanton, V. P., Strobel, S. A., Draths, K. M., Wales, J. L., Dervan, P., Housman, D. E., Altherr, M., Shiang, R., Thompson, L., Fielder, T., Wasmuth, J. J., Tagle, D., Valdes, J., Elmer, L., Allard, M., Castilla, L., Swaroop, M., Blanchard, K., Collins, F. S., Snell, R., Holloway, T., Gillespie, K., Datson, N., Shaw, D., and Harper, P. S. A novel gene containing a trinucleotide repeat that is expanded and unstable on Huntington's disease chromosomes. *Cell*, 72(6):971–983, mar 1993. ISSN 00928674.

Macedo-Ribeiro, S., Cortes, L., Maciel, P., and Carvalho, A. L. Nucleocytoplasmic shuttling activity of ataxin-3. *PLoS One*, 4(6):e5834, jun 2009. ISSN 19326203.

MacFarlane, M., Merrison, W., Bratton, S. B., and Cohen, G. M. Proteasome-mediated Degradation of Smac during Apoptosis: XIAP Promotes Smac Ubiquitination in Vitro. *J. Biol. Chem.*, 277(39):36611–36616, sep 2002. ISSN 0021-9258.

Maciel, P., Gaspar, C., DeStefano, A. L., Silveira, I., Coutinho, P., Radvany, J., Dawson, D. M., Sudarsky, L., Guimarães, J., and Loureiro, J. E. Correlation between CAG repeat length and clinical features in Machado-Joseph disease. *Am. J. Hum. Genet.*, 57(1):54–61, jul 1995. ISSN 0002-9297.

Maciel, P., Caspar, C., Guimarães, L., Goto, J., Lopes-Cendes, I., Hayes, S., Arvidsson, K., Dias, A., Sequeiros, J., Sousa, A., and Rouleau, G. A. Study of three intragenic polymorphisms in the Machado-Joseph disease gene (MJD1) in relation to genetic instability of the (CAG)(n) tract. *Eur. J. Hum. Genet.*, 7(2):147–156, 1999. ISSN 10184813.

Maciel, P., Do Carmo Costa, M., Ferro, A., Rousseau, M., Santos, C. S., Gaspar, C., Barros, J., Rouleau, G. A., Coutinho, P., and Sequeiros, J. Improvement in the molecular diagnosis of Machado-Joseph disease. *Arch. Neurol.*, 58(11):1821–1827, 2001. ISSN 00039942.

Madsen, L., Seeger, M., Semple, C. A., and Hartmann-Petersen, R. New ATPase regulators-p97 goes to the PUB, dec 2009. ISSN 13572725.

Maejima, Y., Isobe, M., and Sadoshima, J. Regulation of autophagy by Beclin 1 in the heart, jun 2016. ISSN 10958584.

Magner, D., Biala, E., Lisowiec-Wachnicka, J., Kierzek, E., and Kierzek, R. A tandem oligonucleotide approach for snpselective RNA degradation using modified Antisense oligonucleotides. *PLoS One*, 2015. ISSN 19326203.

Majorek, K. A., Kuhn, M. L., Chruszcz, M., Anderson, W. F., and Minor, W. Double trouble - Buffer selection and his-tag presence may be responsible for nonreproducibility of biomedical experiments. *Protein Sci.*, 23(10):1359–1368, 2014. ISSN 1469896X.

Malik, V., Rodino-Klapac, L. R., Viollet, L., and Mendell, J. R. Aminoglycoside-induced mutation suppression (stop codon readthrough) as a therapeutic strategy for Duchenne muscular dystrophy. *Ther. Adv. Neurol. Disord.*, 3(6):379–89, nov 2010. ISSN 1756-2864.

Maltecca, F., Filla, A., Castaldo, I., Coppola, G., Fragassi, N. A., Carella, M., Bruni, A., Cocozza, S., Casari, G., Servadio, A., and De Michele, G. Intergenerational instability and marked anticipation in SCA-17. *Neurology*, 61(10):1441–1443, nov 2003. ISSN 00283878.

Mandal, A. and Drerup, C. M. Axonal Transport and Mitochondrial Function in Neurons, aug 2019. ISSN 16625102.

Manuvakhova, M., Keeling, K., and Bedwell, D. M. Aminoglycoside antibiotics mediate context-dependent suppression of termination codons in a mammalian translation system. *RNA*, 6 (7):1044–1055, 2000. ISSN 13558382.

Mao, Y., Senic-Matuglia, F., Di Fiore, P. P., Polo, S., Hodsdon, M. E., and De Camilli, P. Deubiquitinating function of ataxin-3: insights from the solution structure of the Josephin domain. *Proc. Natl. Acad. Sci. U. S. A.*, 102(36):12700–12705, 2005.

Marcelo, A., Brito, F., Carmo-Silva, S., Matos, C. A., Alves-Cruzeiro, J., Vasconcelos-Ferreira, A., Koppenol, R., Mendonça, L., De Almeida, L. P., and Nóbrega, C. Cordycepin activates autophagy through AMPK phosphorylation to reduce abnormalities in Machado-Joseph disease models. *Hum. Mol. Genet.*, 28(1):51–63, 2019. ISSN 14602083.

Marchal, S., Shehi, E., Harricane, M. C., Fusi, P., Heitz, F., Tortora, P., and Lange, R. Structural instability and fibrillar aggregation of non-expanded human ataxin-3 revealed under high pressure and temperature. *J. Biol. Chem.*, 278(34):31554–31563, aug 2003. ISSN 00219258.

Mariotti, C., Gellera, C., Grisoli, M., Mineri, R., Castucci, A., and Di Donato, S. Pathogenic effect of an intermediate-size SCA-6 allele (CAG)19 in a homozygous patient. *Neurology*, 57 (8):1502–1504, oct 2001. ISSN 00283878.

Martin, M., Iyadurai, S. J., Gassman, A., Gindhart, J. G., Hays, T. S., Saxton, W. M., and Saxton, W. M. Cytoplasmic dynein, the dynactin complex, and kinesin are interdependent and essential for fast axonal transport. *Mol. Biol. Cell*, 10(11):3717–28, nov 1999. ISSN 1059-1524.

Martins, S. and Sequeiros, J. Origins and spread of machado-joseph disease ancestral mutations events. In *Adv. Exp. Med. Biol.*, volume 1049, pages 243–254. Springer New York LLC, 2018.

Martins, S., Calafell, F., Wong, V. C., Sequeiros, J., and Amorim, A. A multistep mutation mechanism drives the evolution of the CAG repeat at MJD/SCA3 locus. *Eur. J. Hum. Genet.*, 14(8):932–940, aug 2006. ISSN 10184813.

Martins, S., Calafell, F., Gaspar, C., Wong, V. C., Silveira, I., Nicholson, G. A., Brunt, E. R., Tranebjaerg, L., Stevanin, G., Hsieh, M., Soong, B. W., Loureiro, L., Dürr, A., Tsuji, S., Watanabe, M., Jardim, L. B., Giunti, P., Riess, O., Ranum P, L. P., Brice, A., Rouleau, G. A., Coutinho, P., Amorim, A., and Sequeiros, J. Asian origin for the worldwide-spread

mutational event in Machado-Joseph disease. *Arch. Neurol.*, 64(10):1502–1508, 2007. ISSN 00039942.

Martins, S., Coutinho, P., Silveira, I., Giunti, P., Jardim, L. B., Calafell, F., Sequeiros, J., and Amorim, A. Cis-acting factors promoting the CAG intergenerational instability in Machado-Joseph disease. *Am. J. Med. Genet. Part B Neuropsychiatr. Genet.*, 147(4):439–446, jun 2008. ISSN 15524841.

Martins Junior, C. R., de Borba, F. C., Martinez, A. R. M., de Rezende, T. J. R., Cendes, I. L., Pedroso, J. L., Barsottini, O. G. P., and França Júnior, M. C. Twenty-five years since the identification the first SCA gene: History, clinical featureand perspectives for SCA1, aug 2018. ISSN 16784227.

Maruyama, H., Nakamura, S., Matsuyama, Z., Sakai, T., Doyu, M., Sobue, G., Seto, M., Tsujihata, M., Oh-i, T., Nishio, T., Sunohara, N., Takahashi, R., Hayashi, M., Nishino, I., Ohtake, T., Oda, T., Nishimura, M., Saida, T., Matsumoto, H., Baba, M., Kawaguchi, Y., Kakizuka, A., and Kawakami, H. Molecular features of the CAG repeats and clinical manifestation of machado-joseph disease. *Hum. Mol. Genet.*, 4(5):807–812, 1995. ISSN 09646906.

Maruyama, H., Izumi, Y., Morino, H., Oda, M., Toji, H., Nakamura, S., and Kawakami, H. Difference in disease-free survival curve and regional distribution according to subtype of spinocerebellar ataxia: A study of 1,286 Japanese patients. *Am. J. Med. Genet.*, 114(5): 578–583, jul 2002. ISSN 0148-7299.

Masino, L., Musi, V., Menon, R. P., Fusi, P., Kelly, G., Frenkiel, T. A., Trottier, Y., and Pastore, A. Domain architecture of the polyglutamine protein ataxin-3: A globular domain followed by a flexible tail. *FEBS Lett.*, 549(1-3):21–25, 2003. ISSN 00145793.

Masino, L., Nicastro, G., Menon, R. P., Piaz, F. D., Calder, L., and Pastore, A. Characterization of the structure and the amyloidogenic properties of the Josephin domain of the polyglutamine-containing protein ataxin-3. *J. Mol. Biol.*, 344(4):1021–1035, dec 2004. ISSN 00222836.

Masino, L., Nicastro, G., Calder, L., Vendruscolo, M., and Pastore, A. Functional interactions as a survival strategy against abnormal aggregation. *FASEB J.*, 25(1):45–54, jan 2011. ISSN 1530-6860.

Matilla, T., McCall, A., Subramony, S. H., and Zoghbi, H. Y. Molecular and clinical correlations in spinocerebellar ataxia type 3 and Machado-Joseph disease. *Ann. Neurol.*, 38(1):68–72, 1995. ISSN 15318249.

Matos, C. A. *Regulation of ataxin-3 by phosphorylation: Relevance for Machado-Joseph disease.* PhD thesis, Universidade de Coimbra, 2014.

Matos, C. A., de Macedo-Ribeiro, S., and Carvalho, A. L. Polyglutamine diseases: the special case of ataxin-3 and Machado-Joseph disease. *Prog. Neurobiol.*, 95(1):26–48, sep 2011. ISSN 1873-5118.

Matos, C. A., Pereira de Almeida, L., and Nobrega, C. Proteolytic Cleavage of Polyglutamine Disease-Causing Proteins: Revisiting the Toxic Fragment Hypothesis. *Curr. Pharm. Des.*, 23 (5):753–775, mar 2017. ISSN 13816128.

Matos, C. A., de Almeida, L. P., and Nóbrega, C. Machado–Joseph disease/spinocerebellar ataxia type 3: lessons from disease pathogenesis and clues into therapy, jan 2019. ISSN 14714159.

Matsumine, H., Saito, M., Shimoda-Matsubayashi, S., Tanaka, H., Ishikawa, A., Nakagawa-Hattori, Y., Yokochi, M., Kobayashi, T., Igarashi, S., Takano, H., Sanpei, K., Koike, R., Mori, H., Kondo, T., Mizutani, Y., Schäffer, A. A., Yamamura, Y., Nakamura, S., Kuzuhara, S., Tsuji, S., and Mizuno, Y. Localization of a gene for an autosomal recessive form of juvenile Parkinsonism to chromosome 6q25.2-27. *Am. J. Hum. Genet.*, 60(3):588–96, mar 1997. ISSN 0002-9297.

Matsumoto, M., Yada, M., Hatakeyama, S., Ishimoto, H., Tanimura, T., Tsuji, S., Kakizuka, A., Kitagawa, M., and Nakayama, K. I. Molecular clearance of ataxin-3 is regulated by a mammalian E4. *EMBO J.*, 23(3):659–669, feb 2004. ISSN 02614189.

Matsumura, R., Takayanagi, T., Murata, K., Futamura, N., Hirano, M., and Ueno, S. Relationship of (CAG)nC configuration to repeat instability of the Machado-Joseph disease gene. *Hum. Genet.*, 98(6):643–645, dec 1996. ISSN 03406717.

Mauri, P. L., Riva, M., Ambu, D., De Palma, A., Secundo, F., Benazzi, L., Valtorta, M., Tortora, P., and Fusi, P. Ataxin-3 is subject to autolytic cleavage. *FEBS J.*, 273(18):4277–4286, sep 2006. ISSN 1742-464X.

Mauthe, M., Orhon, I., Rocchi, C., Zhou, X., Luhr, M., Hijlkema, K.-J., Coppes, R. P., Engedal, N., Mari, M., and Reggiori, F. Chloroquine inhibits autophagic flux by decreasing autophagosome-lysosome fusion. *Autophagy*, 14(8):1435–1455, aug 2018. ISSN 1554-8627.

Mayeux, R. and Stern, Y. Epidemiology of Alzheimer disease. *Cold Spring Harb. Perspect. Med.*, 2(8), 2012. ISSN 21571422.

Mazzucchelli, S., De Palma, A., Riva, M., D'Urzo, A., Pozzi, C., Pastori, V., Comelli, F., Fusi, P., Vanoni, M., Tortora, P., Mauri, P., and Regonesi, M. E. Proteomic and biochemical analyses unveil tight interaction of ataxin-3 with tubulin. *Int. J. Biochem. Cell Biol.*, 41(12): 2485–2492, dec 2009. ISSN 1357-2725.

McCampbell, A. CREB-binding protein sequestration by expanded polyglutamine. *Hum. Mol. Genet.*, 9(14):2197–2202, sep 2000. ISSN 14602083.

Mccaughan, K. K., Brown, C. M., Dalphin, M. E., Berry, M. J., and Tate, W. P. Translational termination efficiency in mammals is influenced by the base following the stop codon. *Proc. Natl. Acad. Sci. U. S. A.*, 92(12):5431–5435, jun 1995. ISSN 00278424.

McDonald, C. M., Campbell, C., Torricelli, R. E., Finkel, R. S., Flanigan, K. M., Goemans, N., Heydemann, P., Kaminska, A., Kirschner, J., Muntoni, F., Osorio, A. N., Schara, U., Sejersen, T., Shieh, P. B., Sweeney, H. L., Topaloglu, H., Tulinius, M., Vilchez, J. J., Voit, T., Wong, B., Elfring, G., Kroger, H., Luo, X., McIntosh, J., Ong, T., Riebling, P., Souza, M., Spiegel, R. J., Peltz, S. W., Mercuri, E., Alfano, L. N., Eagle, M., James, M. K., Lowes, L., Mayhew, A., Mazzone, E. S., Nelson, L., Rose, K. J., Abdel-Hamid, H. Z., Apkon, S. D.,

Barohn, R. J., Bertini, E., Bloetzer, C., de Vaud, L. C., Butterfield, R. J., Chabrol, B., Chae, J. H., ro Jongno-gu, D., Comi, G. P., Darras, B. T., Dastgir, J., Desguerre, I., Escobar, R. G., Finanger, E., Guglieri, M., Hughes, I., Iannaccone, S. T., Jones, K. J., Karachunski, P., Kudr, M., Lotze, T., Mah, J. K., Mathews, K., Nevo, Y., Parsons, J., Péréon, Y., de Queiroz Campos Araujo, A. P., Renfroe, J. B., de Resende, M. B. D., Ryan, M., Selby, K., Tennekoon, G., and Vita, G. Ataluren in patients with nonsense mutation Duchenne muscular dystrophy (ACT DMD): a multicentre, randomised, double-blind, placebo-controlled, phase 3 trial. *Lancet*, 390 (10101):1489–1498, sep 2017. ISSN 1474547X.

McGuire, J. L., Depasquale, E. A., Funk, A. J., O'Donnovan, S. M., Hasselfeld, K., Marwaha, S., Hammond, J. H., Hartounian, V., Meador-Woodruff, J. H., Meller, J., and McCullumsmith, R. E. Abnormalities of signal transduction networks in chronic schizophrenia. *NPJ Schizophr.*, 3(1):30, sep 2017. ISSN 2334-265X.

McLaurin, J. A. and Chakrabartty, A. Characterization of the interactions of Alzheimer β-amyloid peptides with phospholipid membranes. *Eur. J. Biochem.*, 245(2):355–363, apr 1997. ISSN 00142956.

McLean, I. W. and Nakane, P. K. Periodate-lysine-paraformaldehyde fixative a new fixative for immunoelectron microscopy. *J. Histochem. Cytochem.*, 22(12):1077–1083, dec 1974. ISSN 0022-1554.

McLoughlin, H. S., Moore, L. R., and Paulson, H. L. Pathogenesis of SCA3 and implications for other polyglutamine diseases, feb 2020. ISSN 1095953X.

McWhorter, M. L., Monani, U. R., Burghes, A. H., and Beattie, C. E. Knockdown of the survival motor neuron (Smn) protein in zebrafish causes defects in motor axon outgrowth and pathfinding. *J. Cell Biol.*, 162(5):919–932, sep 2003. ISSN 1540-8140.

Medicherla, B., Kostova, Z., Schaefer, A., and Wolf, D. H. A genomic screen identifies Dsk2p and Rad23p as essential components of ER-associated degradation. *EMBO Rep.*, 5(7):692–697, 2004. ISSN 1469221X.

Mendell, J. T. and Dietz, H. C. When the message goes awry: Disease-producing mutations that influence mRNA content and performance, nov 2001. ISSN 00928674.

Menon, V. and Povirk, L. Involvement of p53 in the repair of DNA double strand breaks: Multifaceted roles of p53 in homologous recombination repair (HRR) and non-homologous end joining (NHEJ). *Subcell. Biochem.*, 85:321–336, 2014. ISSN 03060225.

Menzies, F. M., Huebener, J., Renna, M., Bonin, M., Riess, O., and Rubinsztein, D. C. Autophagy induction reduces mutant ataxin-3 levels and toxicity in a mouse model of spinocerebellar ataxia type 3. *Brain*, 133(1):93–104, 2010. ISSN 00068950.

Meshalkina, D. A., Kysil, E. V., Warnick, J. E., Demin, K. A., and Kalueff, A. V. Adult zebrafish in CNS disease modeling: a tank that's half-full, not half-empty, and still filling. *Lab Anim. (NY).*, 46(10):378–387, oct 2017. ISSN 0093-7355.

Meyer, H. and Weihl, C. C. The VCP/p97 system at a glance: connecting cellular function to disease pathogenesis. *J. Cell Sci.*, 127(18):3877–3883, 2014. ISSN 0021-9533.

Michalik, A., Martin, J. J., and Van Broeckhoven, C. Spinocerebellar ataxia type 7 associated with pigmentary retinal dystrophy, jan 2004. ISSN 10184813.

Miller, J., Arrasate, M., Shaby, B. A., Mitra, S., Masliah, E., and Finkbeiner, S. Quantitative Relationships between Huntingtin Levels, Polyglutamine Length, Inclusion Body Formation, and Neuronal Death Provide Novel Insight into Huntington's Disease Molecular Pathogenesis. *J. Neurosci.*, 30(31):10541–10550, aug 2010. ISSN 0270-6474.

Miller, L. K. An exegesis of IAPs: salvation and surprises from BIR motifs. *Trends Cell Biol.*, 9(8):323–8, aug 1999. ISSN 0962-8924.

Miller, V. M. CHIP Suppresses Polyglutamine Aggregation and Toxicity In Vitro and In Vivo. *J. Neurosci.*, 25(40):9152–9161, oct 2005. ISSN 0270-6474.

Mills, J. D. and Janitz, M. Alternative splicing of mRNA in the molecular pathology of neurodegenerative diseases. *Neurobiol. Aging*, 33(5):1012.e11–1012.e24, 2012. ISSN 01974580.

Mingeot-Leclercq, M. P. and Tulkens, P. M. Aminoglycosides: nephrotoxicity. *Antimicrob. Agents Chemother.*, 43(5):1003–12, may 1999. ISSN 0066-4804.

Mitkevich, V. A., Kononenko, A. V., Petrushanko, I. Y., Yanvarev, D. V., Makarov, A. A., and Kisselev, L. L. Termination of translation in eukaryotes is mediated by the quaternary eRF1 • eRF3 • GTP • Mg2+ complex. The biological roles of eRF3 and prokaryotic RF3 are profoundly distinct. *Nucleic Acids Res.*, 34(14):3947–3954, 2006. ISSN 13624962.

Mittal, U., Srivastava, A. K., Jain, S., Jain, S., and Mukerji, M. Founder Haplotype for Machado-Joseph Disease in the Indian Population. *Arch. Neurol.*, 62(4):637, 2005. ISSN 0003-9942.

Miyashita, T., Nagao, K., Ohmi, K., Yanagisawa, H., Okamura-Oho, Y., and Yamada, M. Intracellular aggregate formation of dentatorubral-pallidoluysian atrophy (DRPLA) protein with the extended polyglutamine. *Biochem. Biophys. Res. Commun.*, 249(1):96–102, aug 1998. ISSN 0006291X.

Moazed, D. and Noller, H. F. Interaction of antibiotics with functional sites in 16S ribosomal RNA. *Nature*, 327(6121):389–394, jun 1987. ISSN 00280836.

Moestrup, S. K., Cui, S., Vorum, H., Bregengård, C., Bjørn, S. E., Norris, K., Gliemann, J., and Christensen, E. I. Evidence that epithelial glycoprotein 330/megalin mediates uptake of polybasic drugs. *J. Clin. Invest.*, 96(3):1404–1413, 1995. ISSN 00219738.

Monaco, S., Sparano, V., Gioia, M., Sbardella, D., Di Pierro, D., Marini, S., and Coletta, M. Enzymatic processing of collagen IV by MMP-2 (gelatinase A) affects neutrophil migration and it is modulated by extracatalytic domains. *Protein Sci.*, 15(12):2805–15, dec 2006. ISSN 0961-8368.

Moore, L. R., Rajpal, G., Dillingham, I. T., Qutob, M., Blumenstein, K. G., Gattis, D., Hung, G., Kordasiewicz, H. B., Paulson, H. L., and McLoughlin, H. S. Evaluation of Antisense Oligonucleotides Targeting ATXN3 in SCA3 Mouse Models. *Mol. Ther. - Nucleic Acids*, 2017. ISSN 21622531.

Moretti, P., Blazo, M., Garcia, L., Armstrong, D., Lewis, R. A., Roa, B., and Scaglia, F. Spinocerebellar ataxia type 2 (SCA2) presenting with ophthalmoplegia and developmental delay in infancy. *Am. J. Med. Genet.*, 124A(4):392–396, feb 2004. ISSN 0148-7299.

Morfini, G., Pigino, G., and Brady, S. T. Polyglutamine expansion diseases: failing to deliver. *Trends Mol. Med.*, 11(2):64–70, feb 2005. ISSN 1471-4914.

Morizane, Y., Honda, R., Fukami, K., and Yasuda, H. X-Linked Inhibitor of Apoptosis Functions as Ubiquitin Ligase toward Mature Caspase-9 and Cytosolic Smac/DIABLO. *J. Biochem.*, 137(2):125–132, feb 2005. ISSN 0021-924X.

Moro, A., Munhoz, R. P., Arruda, W. O., Raskin, S., Moscovich, M., and Teive, H. A. Spinocerebellar ataxia type 3: subphenotypes in a cohort of brazilian patients. *Arq. Neuropsiquiatr.*, 72(9):659–662, sep 2014. ISSN 16784227.

Morris, A. M., Watzky, M. A., and Finke, R. G. Protein aggregation kinetics, mechanism, and curve-fitting: A review of the literature, mar 2009. ISSN 15709639.

Mort, M., Ivanov, D., Cooper, D. N., and Chuzhanova, N. A. A meta-analysis of nonsense mutations causing human genetic disease. *Hum. Mutat.*, 29(8):1037–1047, aug 2008. ISSN 10597794.

Mosimann, C., Puller, A.-C., Lawson, K. L., Tschopp, P., Amsterdam, A., and Zon, L. I. Site-directed zebrafish transgenesis into single landing sites with the phiC31 integrase system. *Dev. Dyn.*, 242(8):949–63, aug 2013. ISSN 1097-0177.

Mueller, T., Breuer, P., Schmitt, I., Walter, J., Evert, B. O., and Wüllner, U. CK2-dependent phosphorylation determines cellular localization and stability of ataxin-3. *Hum. Mol. Genet.*, 18(17):3334–3343, sep 2009. ISSN 09646906.

Muñoz, E., Rey, M. J., Milà, M., Cardozo, A., Ribalta, T., Tolosa, E., and Ferrer, I. Intranuclear inclusions, neuronal loss and CAG mosaicism in two patients with Machado-Joseph disease. *J. Neurol. Sci.*, 200(1-2):19–25, aug 2002. ISSN 0022510X.

Myers, R. H., Macdonald, M. E., Koroshetz, W. J., Duyao, M. P., Ambrose, C. M., Taylor, S. A., Barnes, G., Srinidhi, J., Lin, C. S., Whaley, W. L., Lazzarini, A. M., Schwarz, M., Wolff, G., Bird, E. D., Vonsattel, J. P., and Gusella, J. F. De novo expansion of a (CAG)n repeat in sporadic Huntington's disease. *Nat. Genet.*, 5(2):168–173, 1993. ISSN 15461718.

Nagai, Y., Fujikake, N., Ohno, K., Higashiyama, H., Popiel, H. A., Rahadian, J., Yamaguchi, M., Strittmatter, W. J., Burke, J. R., and Toda, T. Prevention of polyglutamine oligomerization and neurodegeneration by the peptide inhibitor QBP1 in Drosophila. *Hum. Mol. Genet.*, 2003. ISSN 09646906.

Nakada, S., Tai, I., Panier, S., Al-Hakim, A., Iemura, S.-i., Juang, Y.-C., O'Donnell, L., Kumakubo, A., Munro, M., Sicheri, F., Gingras, A.-C., Natsume, T., Suda, T., and Durocher, D. Non-canonical inhibition of DNA damage-dependent ubiquitination by OTUB1. *Nature*, 466(7309):941–946, aug 2010. ISSN 0028-0836.

Nakamura, K. SCA17, a novel autosomal dominant cerebellar ataxia caused by an expanded polyglutamine in TATA-binding protein. *Hum. Mol. Genet.*, 10(14):1441–1448, jul 2001. ISSN 14602083.

Nakano, K. K., Dawson, D. M., and Spence, A. Machado disease: A hereditary ataxia in portuguese emigrants to massachusetts. *Neurology*, 22(1):49–55, 1972. ISSN 1526632X.

Namiki, T., Valencia, J. C., Hall, M. D., and Hearing, V. J. A novel approach to enhance antibody sensitivity and specificity by peptide cross-linking. *Anal. Biochem.*, 383(2):265–269, dec 2008. ISSN 00032697.

Nardacchione, A., Orsi, L., Brusco, A., Franco, A., Grosso, E., Dragone, E., Mortara, P., Schiffer, D., and De Marchi, M. Definition of the smallest pathological CAG expansion in SCA7, 1999. ISSN 00099163.

Narendra, D., Tanaka, A., Suen, D.-F., and Youle, R. J. Parkin is recruited selectively to impaired mitochondria and promotes their autophagy. *J. Cell Biol.*, 183(5):795–803, dec 2008. ISSN 1540-8140.

Nascimento-Ferreira, I., Nóbrega, C., Vasconcelos-Ferreira, A., Onofre, I., Albuquerque, D., Aveleira, C., Hirai, H., Déglon, N., and Pereira de Almeida, L. Beclin 1 mitigates motor and neuropathological deficits in genetic mouse models of Machado-Joseph disease. *Brain*, 136(Pt 7):2173–2188, 2013. ISSN 1460-2156.

Nechiporuk, T., Huynh, D. P., Figueroa, K., Sahba, S., Nechiporuk, A., and Pulst, S. M. The mouse SCA2 gene: cDNA sequence, alternative splicing and protein expression. *Hum. Mol. Genet.*, 7(8):1301–1309, 1998. ISSN 09646906.

Nedelsky, N. B., Todd, P. K., and Taylor, J. P. Autophagy and the ubiquitin-proteasome system: Collaborators in neuroprotection, dec 2008. ISSN 09254439.

Nedelsky, N. B., Pennuto, M., Smith, R. B., Palazzolo, I., Moore, J., Nie, Z., Neale, G., and Taylor, J. P. Native functions of the androgen receptor are essential to pathogenesis in a drosophila model of spinobulbar muscular atrophy. *Neuron*, 67(6):936–952, sep 2010. ISSN 08966273.

Nelson, D. L., Orr, H. T., and Warren, S. T. The unstable repeats-Three evolving faces of neurological disease, 2013. ISSN 10974199.

Nguyen, H. H. P. and Weydt, P. Huntington disease, jun 2018. ISSN 18635490.

Nguyen, H. P., Hübener, J., Weber, J. J., Grueninger, S., Riess, O., and Weiss, A. Cerebellar Soluble Mutant Ataxin-3 Level Decreases during Disease Progression in Spinocerebellar Ataxia Type 3 Mice. *PLoS One*, 8(4):e62043, jan 2013. ISSN 19326203.

Niblock, M., Smith, B. N., Lee, Y. B., Sardone, V., Topp, S., Troakes, C., Al-Sarraj, S., Leblond, C. S., Dion, P. A., Rouleau, G. A., Shaw, C. E., and Gallo, J. M. Retention of hexanucleotide repeat-containing intron in C9orf72 mRNA: implications for the pathogenesis of ALS/FTD. *Acta Neuropathol. Commun.*, 4(1):18, dec 2016. ISSN 20515960.

Nicastro, G., Menon, R. P., Masino, L., Knowles, P. P., McDonald, N. Q., and Pastore, A. The solution structure of the Josephin domain of ataxin-3: Structural determinants for molecular recognition. *Proc. Natl. Acad. Sci.*, 102(30):10493–10498, jul 2005. ISSN 0027-8424.

Nicastro, G., Masino, L., Esposito, V., Menon, R. P., De Simone, A., Fraternali, F., and Pastore, A. Josephin domain of ataxin-3 contains two distinct ubiquitin-binding sites. *Biopolym. - Pept. Sci. Sect.*, 91(12):1203–1214, 2009. ISSN 00063525.

Nicastro, G., Todi, S. V., Karaca, E., Bonvin, A. M., Paulson, H. L., and Pastore, A. Understanding the role of the josephin domain in the polyub binding and cleavage properties of ataxin-3. *PLoS One*, 5(8):e12430, aug 2010. ISSN 19326203.

Niemann, S., Zhao, C., Pascu, F., Stahl, U., Aulepp, U., Niswander, L., Weber, J. L., and Müller, U. Homozygous WNT3 mutation causes tetra-amelia in a large consanguineous family. *Am. J. Hum. Genet.*, 74(3):558–63, mar 2004. ISSN 0002-9297.

Nijman, S. M. B., Luna-Vargas, M. P. A., Velds, A., Brummelkamp, T. R., Dirac, A. M. G., Sixma, T. K., and Bernards, R. A genomic and functional inventory of deubiquitinating enzymes. *Cell*, 123(5):773–86, dec 2005. ISSN 0092-8674.

Nik, S. and Bowman, T. V. Splicing and neurodegeneration: Insights and mechanisms, mar 2019. ISSN 17577012.

Nillegoda, N. B., Theodoraki, M. A., Mandal, A. K., Mayo, K. J., Ren, H. Y., Sultana, R., Wu, K., Johnson, J., Cyr, D. M., and Caplan, A. J. Ubr1 and Ubr2 Function in a Quality Control Pathway for Degradation of Unfolded Cytosolic Proteins. *Mol. Biol. Cell*, 21(13):2102–2116, jul 2010. ISSN 1059-1524.

Nishiyama, K., Murayama, S., Goto, J., Watanabe, M., Hashida, H., Katayama, S., Nomura, Y., Nakamura, S., and Kanazawa, I. Regional and cellular expression of the Machado-Joseph disease gene in brains of normal and affected individuals. *Ann. Neurol.*, 40(5):776–781, nov 1996. ISSN 03645134.

Nishiyama, K., Nakamura, K., Murayama, S., Yamada, M., and Kanazawa, I. Regional and cellular expression of the dentatorubral-pallidoluysian atrophy gene m brains of normal and affected individuals. *Ann. Neurol.*, 41(5):599–605, may 1997. ISSN 03645134.

Nissim-Rafinia, M. and Kerem, B. The splicing machinery is a genetic modifier of disease severity, sep 2005. ISSN 01689525.

Nóbrega, C., Mendonça, L., Marcelo, A., Lamazière, A., Tomé, S., Despres, G., Matos, C. A., Mechmet, F., Langui, D., den Dunnen, W., de Almeida, L. P., Cartier, N., and Alves, S. Restoring brain cholesterol turnover improves autophagy and has therapeutic potential in

mouse models of spinocerebellar ataxia. *Acta Neuropathol.*, 138(5):837–858, nov 2019. ISSN 14320533.

Norsk Helseinformatikk. Substantia nigra, 2016.

Novotny, J., Handschumacher, M., Haber, E., Bruccoleri, R. E., Carlson, W. B., Fanning, D. W., Smith, J. A., and Rose, G. D. Antigenic determinants in proteins coincide with surface regions accessible to large probes (antibody domains). *Proc. Natl. Acad. Sci. U. S. A.*, 83(2):226–230, jan 1986. ISSN 00278424.

Nozaki, K., Onodera, O., Takano, H., and Tsuji, S. Amino acid sequences flanking polyglutamine stretches influence their potential for aggregate formation. *Neuroreport*, 12(15):3357–3364, oct 2001. ISSN 09594965.

Nucifora, F. C., Ellerby, L. M., Wellington, C. L., Wood, J. D., Herring, W. J., Sawa, A., Hayden, M. R., Dawson, V. L., Dawson, T. M., and Ross, C. A. Nuclear localization of a non-caspase truncation product of atrophin-1, with an expanded polyglutamine repeat, increases cellular toxicity. *J. Biol. Chem.*, 278(15):13047–13055, apr 2003. ISSN 00219258.

Nucifora, J., Sasaki, M., Peters, M. F., Huang, H., Cooper, J. K., Yamada, M., Takahashi, H., Tsuji, S., Troncoso, J., Dawson, V. L., Dawson, T. M., and Ross, C. A. Interference by huntingtin and atrophin-1 with CBP-mediated transcription leading to cellular toxicity. *Science (80-.).*, 291(5512):2423–2428, mar 2001. ISSN 00368075.

Oberoi, T. K., Dogan, T., Hocking, J. C., Scholz, R.-P., Mooz, J., Anderson, C. L., Karreman, C., Meyer zu Heringdorf, D., Schmidt, G., Ruonala, M., Namikawa, K., Harms, G. S., Carpy, A., Macek, B., Köster, R. W., and Rajalingam, K. IAPs regulate the plasticity of cell migration by directly targeting Rac1 for degradation. *EMBO J.*, 31(1):14–28, jan 2012. ISSN 02614189.

Obexer, P. and Ausserlechner, M. J. X-linked inhibitor of apoptosis protein - a critical death resistance regulator and therapeutic target for personalized cancer therapy. *Front. Oncol.*, 4: 197, 2014. ISSN 2234-943X.

Ogun, S. A., Martins, S., Adebayo, P. B., Dawodu, C. O., Sequeiros, J., and Finkel, M. F. Machado-Joseph disease in a Nigerian family: Mutational origin and review of the literature. *Eur. J. Hum. Genet.*, 23(2):271–273, 2015. ISSN 14765438.

Ohlmeier, C., Saum, K. U., Galetzka, W., Beier, D., and Gothe, H. Epidemiology and health care utilization of patients suffering from Huntington's disease in Germany: Real world evidence based on German claims data. *BMC Neurol.*, 19(1):318, dec 2019. ISSN 14712377.

Olanow, C. W., Perl, D. P., DeMartino, G. N., and McNaught, K. S. P. Lewy-body formation is an aggresome-related process: a hypothesis. *Lancet. Neurol.*, 3(8):496–503, aug 2004. ISSN 1474-4422.

Olshina, M. A., Angley, L. M., Ramdzan, Y. M., Tang, J., Bailey, M. F., Hill, A. F., and Hatters, D. M. Tracking mutant huntingtin aggregation kinetics in cells reveals three major populations that include an invariant oligomer pool. *J. Biol. Chem.*, 285(28):21807–21816, jul 2010. ISSN 00219258.

Ong, S.-E., Blagoev, B., Kratchmarova, I., Kristensen, D. B., Steen, H., Pandey, A., and Mann, M. Stable isotope labeling by amino acids in cell culture, SILAC, as a simple and accurate approach to expression proteomics. *Mol. Cell. Proteomics*, 1(5):376–386, 2002. ISSN 15359476.

Onofre, I., Mendonça, N., Lopes, S., Nobre, R., De Melo, J. B., Carreira, I. M., Januário, C., Gonçalves, A. F., and De Almeida, L. P. Fibroblasts of Machado Joseph Disease patients reveal autophagy impairment. *Sci. Rep.*, 6(1):1–10, jun 2016. ISSN 20452322.

Ooms, J. magick: Advanced Graphics and Image-Processing in R. 2017.

Ordway, J. M., Tallaksen-Greene, S., Gutekunst, C. A., Bernstein, E. M., Cearley, J. A., Wiener, H. W., Dure IV, L. S., Lindsey, R., Hersch, S. M., Jope, R. S., Albin, R. L., and Detloff, P. J. Ectopically expressed CAG repeats cause intranuclear inclusions and a progressive late onset neurological phenotype in the mouse. *Cell*, 91(6):753–763, dec 1997. ISSN 00928674.

Orr, H. T., yi Chung, M., Banfi, S., Kwiatkowski, T. J., Servadio, A., Beaudet, A. L., McCall, A. E., Duvick, L. A., Ranum, L. P., and Zoghbi, H. Y. Expansion of an unstable trinucleotide CAG repeat in spinocerebellar ataxia type 1. *Nat. Genet.*, 4(3):221–226, 1993. ISSN 15461718.

Orr, M. E., Sullivan, A. C., and Frost, B. A Brief Overview of Tauopathy: Causes, Consequences, and Therapeutic Strategies, 2017. ISSN 18733735.

Ota, T., Suzuki, Y., Nishikawa, T., Otsuki, T., Sugiyama, T., Irie, R., Wakamatsu, A., Hayashi, K., Sato, H., Nagai, K., Kimura, K., Makita, H., Sekine, M., Obayashi, M., Nishi, T., Shibahara, T., Tanaka, T., Ishii, S., ichi Yamamoto, J., Saito, K., Kawai, Y., Isono, Y., Nakamura, Y., Nagahari, K., Murakami, K., Yasuda, T., Iwayanagi, T., Wagatsuma, M., Shiratori, A., Sudo, H., Hosoiri, T., Kaku, Y., Kodaira, H., Kondo, H., Sugawara, M., Takahashi, M., Kanda, K., Yokoi, T., Furuya, T., Kikkawa, E., Omura, Y., Abe, K., Kamihara, K., Katsuta, N., Sato, K., Tanikawa, M., Yamazaki, M., Ninomiya, K., Ishibashi, T., Yamashita, H., Murakawa, K., Fujimori, K., Tanai, H., Kimata, M., Watanabe, M., Hiraoka, S., Chiba, Y., Ishida, S., Ono, Y., Takiguchi, S., Watanabe, S., Yosida, M., Hotuta, T., Kusano, J., Kanehori, K., Takahashi-Fujii, A., Hara, H., Tanase, T. o., Nomura, Y., Togiya, S., Komai, F., Hara, R., Takeuchi, K., Arita, M., Imose, N., Musashino, K., Yuuki, H., Oshima, A., Sasaki, N., Aotsuka, S., Yoshikawa, Y., Matsunawa, H., Ichihara, T., Shiohata, N., Sano, S., Moriya, S., Momiyama, H., Satoh, N., Takami, S., Terashima, Y., Suzuki, O., Nakagawa, S., Senoh, A., Mizoguchi, H., Goto, Y., Shimizu, F., Wakebe, H., Hishigaki, H., Watanabe, T., Sugiyama, A., Takemoto, M., Kawakami, B., Yamazaki, M., Watanabe, K., Kumagai, A., Itakura, S., Fukuzumi, Y., Fujimori, Y., Komiyama, M., Tashiro, H., Tanigami, A., Fujiwara, T., Ono, T., Yamada, K., Fujii, Y., Ozaki, K., Hirao, M., Ohmori, Y., Kawabata, A., Hikiji, T., Kobatake, N., Inagaki, H., Ikema, Y., Okamoto, S., Okitani, R., Kawakami, T., Noguchi, S., Itoh, T., Shigeta, K., Senba, T., Matsumura, K., Nakajima, Y., Mizuno, T., Morinaga, M., Sasaki, M., Togashi, T., Oyama, M., Hata, H., Watanabe, M., Komatsu, T., Mizushima-Sugano, J., Satoh, T., Shirai, Y., Takahashi, Y., Nakagawa, K., Okumura, K., Nagase, T., Nomura, N., Kikuchi, H., Masuho, Y., Yamashita, R., Nakai, K., Yada, T., Nakamura, Y., Ohara, O., Isogai, T., and Sugano, S. Complete sequencing and characterization of 21,243 full-length human cDNAs. *Nat. Genet.*, 36(1):40–45, jan 2004. ISSN 10614036.

Ouyang, Y., Kwon, Y. T., An, J. Y., Eller, D., Tsai, S. C., Diaz-Perez, S., Troke, J. J., Teitell, M. A., and Marahrens, Y. Loss of Ubr2, an E3 ubiquitin ligase, leads to chromosome fragility and impaired homologous recombinational repair. *Mutat. Res. - Fundam. Mol. Mech. Mutagen.*, 596(1-2 SPEC. ISS.):64–75, apr 2006. ISSN 00275107.

Padiath, Q. S., Srivastava, A. K., Roy, S., Jain, S., and Brahmachari, S. K. Identification of a novel 45 repeat unstable allele associated with a disease phenotype at the MJD1/SCA3 locus. *Am. J. Med. Genet. - Neuropsychiatr. Genet.*, 133 B(1):124–126, feb 2005. ISSN 15524841.

Page-McCaw, A., Ewald, A. J., and Werb, Z. Matrix metalloproteinases and the regulation of tissue remodelling. *Nat. Rev. Mol. Cell Biol.*, 8(3):221–233, mar 2007. ISSN 1471-0072.

Palmer, E., Wilhelm, J. M., and Sherman, F. Phenotypic suppression of nonsense mutants in yeast by aminoglycoside antibiotics, jan 1979. ISSN 00280836.

Pan, Q., Shai, O., Lee, L. J., Frey, B. J., and Blencowe, B. J. Deep surveying of alternative splicing complexity in the human transcriptome by high-throughput sequencing. *Nat. Genet.*, 40(12):1413–1415, dec 2008. ISSN 10614036.

Pancsa, R., MacOssay-Castillo, M., Kosol, S., and Tompa, P. Computational analysis of translational readthrough proteins in Drosophila and yeast reveals parallels to alternative splicing. *Sci. Rep.*, 6(1):32142, aug 2016. ISSN 20452322.

Pandey, M. and Rajamma, U. Huntington's disease: the coming of age. *J. Genet.*, 97(3): 649–664, 2018. ISSN 09737731.

Papadopoulos, T. and Pfeifer, U. Regression of rat liver autophagic vacuoles by locally applied cycloheximide. *Lab Invest.*, 54(1):100–7, 1986.

Paradisi, I., Ikonomu, V., and Arias, S. Spinocerebellar ataxias in Venezuela: Genetic epidemiology and their most likely ethnic descent. *J. Hum. Genet.*, 61(3):215–222, 2015. ISSN 1435232X.

Park, H., Suzuki, T., and Lennarz, W. J. Identification of proteins that interact with mammalian peptide:N-glycanase and implicate this hydrolase in the proteasome-dependent pathway for protein degradation. *Proc. Natl. Acad. Sci.*, 98(20):11163–11168, 2001. ISSN 0027-8424.

Park, H., Kim, H.-J., and Jeon, B. S. Parkinsonism in Spinocerebellar Ataxia. *Biomed Res. Int.*, 2015:1–11, mar 2015. ISSN 2314-6133.

Park, H. C., Kim, C. H., Bae, Y. K., Yeo, S. Y., Kim, S. H., Hong, S. K., Shin, J., Yoo, K. W., Hibi, M., Hirano, T., Miki, N., Chitnis, A. B., and Huh, T. L. Analysis of upstream elements in the HuC promoter leads to the establishment of transgenic zebrafish with fluorescent neurons. *Dev. Biol.*, 227(2):279–93, nov 2000. ISSN 0012-1606.

Parker, J. A., Connolly, J. B., Wellington, C., Hayden, M., Dausset, J., and Neri, C. Expanded polyglutamines in Caenorhabditis elegans cause axonal abnormalities and severe dysfunction of PLM mechanosensory neurons without cell death. *Proc. Natl. Acad. Sci.*, 98(23):13318–13323, nov 2001. ISSN 0027-8424.

Parks, W. C., Wilson, C. L., and López-Boado, Y. S. Matrix metalloproteinases as modulators of inflammation and innate immunity. *Nat. Rev. Immunol.*, 4(8):617–629, aug 2004. ISSN 1474-1733.

Paschal, B. M. and Vallee, R. B. Retrograde transport by the microtubule-associated protein MAP 1C. *Nature*, 330(6144):181–183, nov 1987. ISSN 0028-0836.

Pau, G., Fuchs, F., Sklyar, O., Boutros, M., and Huber, W. EBImage-an R package for image processing with applications to cellular phenotypes. *Bioinformatics*, 26(7):979–981, 2010. ISSN 13674803.

Paulsen, F. and Waschke, J. *Sobotta, Atlas der Anatomie Band 3*. Urban & Fischer Verlag/Elsevier GmbH, 24 edition, 2017.

Paulson, H. Repeat expansion diseases. In *Handb. Clin. Neurol.*, volume 147, pages 105–123. Elsevier B.V., 2018.

Paulson, H. L. and Bonini, N. M. Spinocerebellar ataxia type 3, 2000. ISSN 10276599.

Paulson, H. L., Das, S. S., Crino, P. B., Perez, M. K., Patel, S. C., Gotsdiner, D., Fischbeck, K. H., and Pittman, R. N. Machado-Joseph disease gene product is a cytoplasmic protein widely expressed in brain. *Ann. Neurol.*, 41(4):453–62, apr 1997a. ISSN 0364-5134.

Paulson, H. L., Perez, M. K., Trottier, Y., Trojanowski, J. Q., Subramony, S. H., Das, S. S., Vig, P., Mandel, J. L., Fischbeck, K. H., and Pittman, R. N. Intranuclear inclusions of expanded polyglutamine protein in spinocerebellar ataxia type 3. *Neuron*, 19(2):333–344, 1997b. ISSN 08966273.

Pechmann, S., Levy, E. D., Tartaglia, G. G., and Vendruscolo, M. Physicochemical principles that regulate the competition between functional and dysfunctional association of proteins. *Proc. Natl. Acad. Sci. U. S. A.*, 106(25):10159–10164, jun 2009. ISSN 00278424.

Pellistri, F., Bucciantini, M., Invernizzi, G., Gatta, E., Penco, A., Frana, A. M., Nosi, D., Relini, A., Regonesi, M. E., Gliozzi, A., Tortora, P., Robello, M., and Stefani, M. Different ataxin-3 amyloid aggregates induce intracellular Ca 2+ deregulation by different mechanisms in cerebellar granule cells. *Biochim. Biophys. Acta - Mol. Cell Res.*, 1833(12):3155–3165, dec 2013. ISSN 01674889.

Peltz, S. W., Morsy, M., Welch, E. M., and Jacobson, A. Ataluren as an Agent for Therapeutic Nonsense Suppression. *Annu. Rev. Med.*, 64(1):407–425, 2013. ISSN 0066-4219.

Pereira Sena, P., Weber, J. J., Watchon, M., Robinson, K. J., Wassouf, Z., Hauser, S., Helm, J., Abeditashi, M., Schmidt, J., Hübener-Schmid, J., Schöls, L., Laird, A. S., Riess, O., and Schmidt, T. Pathophysiological interplay between O -GlcNAc transferase and the Machado–Joseph disease protein ataxin-3. *Proc. Natl. Acad. Sci.*, 118(47):e2025810118, nov 2021. ISSN 0027-8424.

Perez, M. K., Paulson, H. L., Pendse, S. J., Saionz, S. J., Bonini, N. M., and Pittman, R. N. Recruitment and the role of nuclear localization in polyglutamine-mediated aggregation. *J. Cell Biol.*, 143(6):1457–70, dec 1998. ISSN 0021-9525.

Perez, M. K., Paulson, H. L., and Pittman, R. N. Ataxin-3 with an altered conformation that exposes the polyglutamine domain is associated with the nuclear matrix. *Hum. Mol. Genet.*, 8(13):2377–2385, dec 1999. ISSN 09646906.

Perutz, M. F., Johnson, T., Suzuki, M., and Finch, J. T. Glutamine repeats as polar zippers: Their possible role in inherited neurodegenerative diseases. *Proc. Natl. Acad. Sci. U. S. A.*, 91(12):5355–5358, jun 1994. ISSN 00278424.

Peters, M. F., Nucifora, F. C., Kushi, J., Seaman, H. C., Cooper, J. K., Herring, W. J., Dawson, V. L., Dawson, T. M., and Ross, C. A. Nuclear targeting of mutant huntingtin increases toxicity. *Mol. Cell. Neurosci.*, 14(2):121–128, aug 1999. ISSN 10447431.

Pfeiffer, A., Luijsterburg, M. S., Acs, K., Wiegant, W. W., Helfricht, A., Herzog, L. K., Minoia, M., Böttcher, C., Salomons, F. A., Attikum, H., and Dantuma, N. P. Ataxin-3 consolidates the MDC 1-dependent DNA double-strand break response by counteracting the SUMO -targeted ubiquitin ligase RNF 4. *EMBO J.*, 36(8):1066–1083, apr 2017. ISSN 0261-4189.

Pisareva, V. P., Pisarev, A. V., Hellen, C. U., Rodnina, M. V., and Pestova, T. V. Kinetic analysis of interaction of eukaryotic release factor 3 with guanine nucleotides. *J. Biol. Chem.*, 281(52):40224–40235, dec 2006. ISSN 00219258.

Pitchai, A., Rajaretinam, R. K., and Freeman, J. L. Zebrafish as an Emerging Model for Bioassay-Guided Natural Product Drug Discovery for Neurological Disorders. *Medicines*, 6 (2):61, may 2019. ISSN 2305-6320.

Pless, O., Kowenz-Leutz, E., Knoblich, M., Lausen, J., Beyermann, M., Walsh, M. J., and Leutz, A. G9a-mediated Lysine Methylation Alters the Function of CCAAT/Enhancer-binding Protein-β. *J. Biol. Chem.*, 283(39):26357–26363, sep 2008. ISSN 0021-9258.

Polymeropoulos, M. H., Lavedan, C., Leroy, E., Ide, S. E., Dehejia, A., Dutra, A., Pike, B., Root, H., Rubenstein, J., Boyer, R., Stenroos, E. S., Chandrasekharappa, S., Athanassiadou, A., Papapetropoulos, T., Johnson, W. G., Lazzarini, A. M., Duvoisin, R. C., Di Iorio, G., Golbe, L. I., and Nussbaum, R. L. Mutation in the alpha-synuclein gene identified in families with Parkinson's disease. *Science*, 276(5321):2045–7, jun 1997. ISSN 0036-8075.

Pozzi, C., Valtorta, M., Tedeschi, G., Galbusera, E., Pastori, V., Bigi, A., Nonnis, S., Grassi, E., and Fusi, P. Study of subcellular localization and proteolysis of ataxin-3. *Neurobiol. Dis.*, 30(2):190–200, 2008. ISSN 09699961.

Preckel, T., Fung-Leung, W. P., Cai, Z., Vitiello, A., Salter-Cid, L., Winqvist, O., Wolfe, T. G., Von Herrath, M., Angulo, A., Ghazal, P., Lee, J. D., Fourie, A. M., Wu, Y., Pang, J., Ngo, K., Peterson, P. A., Früh, K., and Yang, Y. Impaired immunoproteasome assembly and immune responses in PA28-/- mice. *Science*, 286(5447):2162–5, dec 1999. ISSN 0036-8075.

Price, D. L. New order from neurological disorders, jun 1999. ISSN 00280836.

Przedborski, S., Vila, M., and Jackson-Lewis, V. Neurodegeneration: what is it and where are we? *J. Clin. Invest.*, 111(1):3–10, jan 2003. ISSN 0021-9738.

Puente, X. S. and López-Otín, C. A genomic analysis of rat proteases and protease inhibitors, apr 2004. ISSN 10889051.

Puente, X. S., Sánchez, L. M., Gutiérrez-Fernández, A., Velasco, G., and López-Otín, C. A genomic view of the complexity of mammalian proteolytic systems. *Biochem. Soc. Trans.*, 33 (2):331–334, apr 2005. ISSN 03005127.

Pujana, M. A., Corral, J., Gratacòs, M., Combarros, O., Berciano, J., Genís, D., Banchs, I., Estivill, X., Volpini, V., Sánchez, A., Calopa, M., Rosell, J., Cervera, C., Escudero, D., Molina, M., Guitart, M., Gabau, E., Gutiérrez, J. A., Benítez, J., Perez De Colosia, V., and Villanueva, P. Spinocerebellar ataxias in Spanish patients: Genetic analysis of familial and sporadic cases. *Hum. Genet.*, 104(6):516–522, 1999. ISSN 03406717.

Pulst, S. M., Nechiporuk, A., Nechiporuk, T., Gispert, S., Chen, X. N., Lopes-Cendes, I., Pearlman, S., Starkman, S., Orozco-Diaz, G., Lunkes, A., Dejong, P., Rouleau, G. A., Auburger, G., Korenberg, J. R., Figueroa, C., and Sahba, S. Moderate expansion of a normally biallelic trinucleotide repeat in spinooerebellar ataxia type. *Nat. Genet.*, 14(3):269–276, 1996. ISSN 10614036.

Purohit, P. and Stern, S. Interactions of a small RNA with antibiotic and RNA ligands of the 30S subunit. *Nature*, 370(6491):659–662, aug 1994. ISSN 00280836.

R Core Team. R Core Team (2017). R: A language and environment for statistical computing. *R Found. Stat. Comput. Vienna, Austria. URL http//www.R-project.org/.*, page R Foundation for Statistical Computing, 2017.

Raasi, S., Orlov, I., Fleming, K. G., and Pickart, C. M. Binding of polyubiquitin chains to ubiquitin-associated (UBA) domains of HHR23A. *J. Mol. Biol.*, 341(5):1367–1379, aug 2004. ISSN 00222836.

Raman, M., Havens, C. G., Walter, J. C., and Harper, J. W. A Genome-wide Screen Identifies p97 as an Essential Regulator of DNA Damage-Dependent CDT1 Destruction. *Mol. Cell*, 44 (1):72–84, oct 2011. ISSN 10972765.

Ramani, B., Harris, G. M., Huang, R., Seki, T., Murphy, G. G., Do Carmo Costa, M., Fischer, S., Saunders, T. L., Xia, G., McEachin, R. C., and Paulson, H. L. A knockin mouse model of spinocerebellar ataxia type 3 exhibits prominent aggregate pathology and aberrant splicing of the disease gene transcript. *Hum. Mol. Genet.*, 24(5):1211–1224, 2015. ISSN 14602083.

Ranum, L. P., Lundgren, J. K., Schut, L. J., Ahrens, M. J., Perlman, S., Aita, J., Bird, T. D., Gomez, C., and Orr, H. T. Spinocerebellar ataxia type 1 and Machado-Joseph disease: Incidence of CAG expansions among adult-onset ataxia patients from 311 families with dominant, recessive, or sporadic ataxia. *Am. J. Hum. Genet.*, 57(3):603–608, 1995. ISSN 00029297.

Ravikumar, B., Duden, R., and Rubinsztein, D. C. Aggregate-prone proteins with polyglutamine and polyalanine expansions are degraded by autophagy. *Hum. Mol. Genet.*, 11(9):1107–1117, may 2002. ISSN 14602083.

Read, A. P. Huntington's disease: Testing the test. *Nat. Genet.*, 4(4):329–330, 1993. ISSN 15461718.

Rédei, G. P. DRPLA. In *Encycl. Genet. Genomics, Proteomics Informatics*, pages 563–563. Springer Netherlands, jun 2008.

Reina, C. P., Zhong, X., and Pittman, R. N. Proteotoxic stress increases nuclear localization of ataxin-3. *Hum. Mol. Genet.*, 19(2):235–249, jan 2010. ISSN 09646906.

Reina, C. P., Nabet, B. Y., Young, P. D., and Pittman, R. N. Basal and stress-induced Hsp70 are modulated by ataxin-3. *Cell Stress Chaperones*, 17(6):729–42, nov 2012. ISSN 1466-1268.

Reyes-Turcu, F. E. and Wilkinson, K. D. Polyubiquitin binding and disassembly by deubiquitinating enzymes, apr 2009. ISSN 00092665.

Rez, G., Palfia, Z., and Fellinger, E. Occurrence and inhibition by cycloheximide of apoptosis in vinblastine-treated murine pancreas. A role for autophagy? *Acta Biol. Hung.*, 42(1-3): 133–140, 1991. ISSN 0236-5383.

Rhodes, L. E., Freeman, B. K., Auh, S., Kokkinis, A. D., La Pean, A., Chen, C., Lehky, T. J., Shrader, J. A., Levy, E. W., Harris-Love, M., Di Prospero, N. A., and Fischbeck, K. H. Clinical features of spinal and bulbar muscular atrophy. *Brain*, 132(12):3242–3251, 2009. ISSN 00068950.

Riccardi, C. and Nicoletti, I. Analysis of apoptosis by propidium iodide staining and flow cytometry. *Nat. Protoc.*, 1(3):1458–1461, nov 2006. ISSN 1754-2189.

Richter, C. Biophysical consequences of lipid peroxidation in membranes. *Chem. Phys. Lipids*, 44(2-4):175–89, 1987. ISSN 0009-3084.

Riedl, S. J., Renatus, M., Schwarzenbacher, R., Zhou, Q., Sun, C., Fesik, S. W., Liddington, R. C., and Salvesen, G. S. Structural basis for the inhibition of caspase-3 by XIAP. *Cell*, 104 (5):791–800, mar 2001. ISSN 0092-8674.

Riemer, A., Dobrynin, G., Dressler, A., Bremer, S., Soni, A., Iliakis, G., and Meyer, H. The p97-Ufd1-Npl4 ATPase complex ensures robustness of the G2/M checkpoint by facilitating CDC25A degradation. *Cell Cycle*, 13(6):919–927, mar 2014. ISSN 15514005.

Riess, O., Rüb, U., Pastore, A., Bauer, P., and Schöls, L. SCA3: neurological features, pathogenesis and animal models., jun 2008. ISSN 14734230.

Riley, B. E. and Orr, H. T. Polyglutamine neurodegenerative diseases and regulation of transcription: assembling the puzzle. *Genes Dev.*, 20(16):2183–92, aug 2006. ISSN 0890-9369.

Riley, B. E., Xu, Y., Zoghbi, H. Y., and Orr, H. T. The effects of the polyglutamine repeat protein ataxin-1 on the UbL-UBA protein A1UP. *J. Biol. Chem.*, 279(40):42290–42301, 2004. ISSN 00219258.

Riley, B. E., Lougheed, J. C., Callaway, K., Velasquez, M., Brecht, E., Nguyen, L., Shaler, T., Walker, D., Yang, Y., Regnstrom, K., Diep, L., Zhang, Z., Chiou, S., Bova, M., Artis, D. R.,

Yao, N., Baker, J., Yednock, T., and Johnston, J. A. Structure and function of Parkin E3 ubiquitin ligase reveals aspects of RING and HECT ligases. *Nat. Commun.*, 4(1):1–9, jun 2013. ISSN 20411723.

Roberts, E. A. and Deretic, V. Autophagic proteolysis of long-lived proteins in nonliver cells. *Methods Mol. Biol.*, 445:111–7, jan 2008. ISSN 1064-3745.

Robinson, J. T., Thorvaldsdóttir, H., Winckler, W., Guttman, M., Lander, E. S., Getz, G., and Mesirov, J. P. Integrative genomics viewer, jan 2011. ISSN 10870156.

Robinson, J. T., Thorvaldsdóttir, H., Wenger, A. M., Zehir, A., and Mesirov, J. P. Variant review with the integrative genomics viewer, nov 2017. ISSN 15387445.

Robinson, K. J., Yuan, K., Plenderleith, S. K., Watchon, M., and Laird, A. S. A novel calpain inhibitor compound has protective effects on a zebrafish model of spinocerebellar ataxia type 3. *Cells*, 10(10), oct 2021. ISSN 20734409.

Rodrigues, A.-J., Coppola, G., Santos, C., Costa, M. d. C., Ailion, M., Sequeiros, J., Geschwind, D. H., and Maciel, P. Functional genomics and biochemical characterization of the C. elegans orthologue of the Machado-Joseph disease protein ataxin-3. *FASEB J.*, 21(4):1126–1136, apr 2007. ISSN 0892-6638.

Rodrigues, A. J., Neves-Carvalho, A., Ferro, A., Rokka, A., Corthals, G., Logarinho, E., and Maciel, P. ATX-3, CDC-48 and UBXN-5: A new trimolecular complex in Caenorhabditis elegans. *Biochem. Biophys. Res. Commun.*, 386(4):575–581, sep 2009. ISSN 0006291X.

Rodrigues, A. J., do Carmo Costa, M., Silva, T. L., Ferreira, D., Bajanca, F., Logarinho, E., and Maciel, P. Absence of ataxin-3 leads to cytoskeletal disorganization and increased cell death. *Biochim. Biophys. Acta - Mol. Cell Res.*, 1803(10):1154–1163, oct 2010. ISSN 01674889.

Rodrigues, A. J., Neves-Carvalho, A., Teixeira-Castro, A., Rokka, A., Corthals, G., Logarinho, E., and Maciel, P. Absence of ataxin-3 leads to enhanced stress response in c. elegans. *PLoS One*, 6(4):e18512, apr 2011. ISSN 19326203.

Rodriguez, C. I. and Dymecki, S. M. Origin of the precerebellar system. *Neuron*, 27(3):475–486, sep 2000. ISSN 08966273.

Rodríguez-Lebrón, E., Costa, M. D., Luna-Cancalon, K., Peron, T. M., Fischer, S., Boudreau, R. L., Davidson, B. L., and Paulson, H. L. Silencing mutant ATXN3 expression resolves molecular phenotypes in SCA3 transgenic mice. *Mol. Ther.*, 2013. ISSN 15250024.

Rojiani, M. V., Alidina, J., Esposito, N., and Rojiani, A. M. Expression of MMP-2 correlates with increased angiogenesis in CNS metastasis of lung carcinoma. *Int. J. Clin. Exp. Pathol.*, 3(8):775–81, oct 2010. ISSN 1936-2625.

Romanul, F. C., Fowler, H. L., Radvany, J., Feldman, R. G., and Feingold, M. Azorean Disease of the Nervous System. *N. Engl. J. Med.*, 296(26):1505–1508, jun 1977. ISSN 15334406.

Roscic, A., Baldo, B., Crochemore, C., Marcellin, D., and Paganetti, P. Induction of autophagy with catalytic mTOR inhibitors reduces huntingtin aggregates in a neuronal cell model. *J. Neurochem.*, 119(2):398–407, 2011. ISSN 00223042.

Rosenberg, R. N., Nyhan, W. L., Bay, C., and Shore, P. Autosomal dominant striatonigral degeneration: A ctinical, pathologic, and biochemical study of a new genetic disorder. *Neurology*, 26(8):703–714, 1976. ISSN 1526632X.

Ross, C. A. and Poirier, M. A. What is the role of protein aggregation in neurodegeneration? *Nat. Rev. Mol. Cell Biol. 2005 611*, 6(11):891, sep 2005. ISSN 1471-0080.

Ross, C. A., Poirier, M. A., Wanker, E. E., and Amzel, M. Polyglutamine fibrillogenesis: The pathway unfolds, jan 2003. ISSN 00278424.

Roy, S. K., Hu, J., Meng, Q., Xia, Y., Shapiro, P. S., Reddy, S. P., Platanias, L. C., Lindner, D. J., Johnson, P. F., Pritchard, C., Pagés, G., Pouyssegur, J., and Kalvakolanu, D. V. MEKK1 plays a critical role in activating the transcription factor C/EBP-β-dependent gene expression in response to IFN-γ. *Proc. Natl. Acad. Sci. U. S. A.*, 99(12):7945–7950, jun 2002. ISSN 00278424.

Ruano, L., Melo, C., Silva, M. C., and Coutinho, P. The global epidemiology of hereditary ataxia and spastic paraplegia: A systematic review of prevalence studies, 2014. ISSN 14230208.

Rüb, U., Bruntt, E. R., Del Turco, D., De Vos, R. A., Gierga, K., Paulson, H., and Braak, H. Guidelines for the pathoanatomical examination of the lower brain stem in ingestive and swallowing disorders and its application to a dysphagic spinocerebellar ataxia type 3 patient. *Neuropathol. Appl. Neurobiol.*, 29(1):1–13, feb 2003. ISSN 03051846.

Rub, U., de Vos, R. A., Brunt, E. R., Sebesteny, T., Schols, L., Auburger, G., Bohl, J., Ghebremedhin, E., Gierga, K., Seidel, K., den Dunnen, W., Heinsen, H., Paulson, H., and Deller, T. Spinocerebellar Ataxia Type 3 (SCA3): Thalamic Neurodegeneration Occurs Independently from Thalamic Ataxin-3 Immunopositive Neuronal Intranuclear Inclusions. *Brain Pathol.*, 16(3):218–227, jul 2006. ISSN 1015-6305.

Rüb, U., Brunt, E. R., and Deller, T. New insights into the pathoanatomy of spinocerebellar ataxia type 3 (Machado-Joseph disease), apr 2008. ISSN 13507540.

Rüb, U., Schöls, L., Paulson, H., Auburger, G., Kermer, P., Jen, J. C., Seidel, K., Korf, H. W., and Deller, T. Clinical features, neurogenetics and neuropathology of the polyglutamine spinocerebellar ataxias type 1, 2, 3, 6 and 7, may 2013. ISSN 03010082.

Rudich, P. and Lamitina, T. Models and mechanisms of repeat expansion disorders: a worm's eye view, jul 2018. ISSN 09737731.

Sacco, J. J., Yau, T. Y., Darling, S., Patel, V., Liu, H., Urbé, S., Clague, M. J., and Coulson, J. M. The deubiquitylase Ataxin-3 restricts PTEN transcription in lung cancer cells. *Oncogene*, 33(33):4265–4272, aug 2014. ISSN 14765594.

Sahba, S., Nechiporuk, A., Figueroa, K. P., Nechiporuk, T., and Pulst, S. M. Genomic structure of the human gene for spinocerebellar ataxia type 2 (SCA2) on chromosome 12q24.1. *Genomics*, 47(3):359–364, feb 1998. ISSN 08887543.

Saleem, S. and Kannan, R. R. Zebrafish: an emerging real-time model system to study Alzheimer's disease and neurospecific drug discovery. *Cell Death Discov.*, 4(1):45, dec 2018. ISSN 2058-7716.

Sambataro, F. and Pennuto, M. Post-translational modifications and protein quality control in motor neuron and polyglutamine diseases, mar 2017. ISSN 16625099.

Sánchez, L., Madurga, S., Pukala, T., Vilaseca, M., López-Iglesias, C., Robinson, C. V., Giralt, E., and Carulla, N. Aβ40 and Aβ42 amyloid fibrils exhibit distinct molecular recycling properties. *J. Am. Chem. Soc.*, 133(17):6505–6508, may 2011. ISSN 00027863.

Sariyer, I. K. Transfection of neuronal cultures. *Methods Mol. Biol.*, 1078:133–139, 2013. ISSN 10643745.

Sasaki, H., Yabe, I., and Tashiro, K. The hereditary spinocerebellar ataxias in Japan, 2003. ISSN 14248581.

Sasaki, H., Fukazawa, T., Yanagihara, T., Hamada, T., Shima, K., Matsumoto, A., Hashimoto, K., Ito, N., Wakisaka, A., and Tashiro, K. Clinical features and natural history of spinocerebellar ataxia type 1. *Acta Neurol. Scand.*, 93(1):64–71, jan 2009. ISSN 0001-6314.

Sathasivam, K., Neueder, A., Gipson, T. A., Landles, C., Benjamin, A. C., Bondulich, M. K., Smith, D. L., Faull, R. L. M., Roos, R. A. C., Howland, D., Detloff, P. J., Housman, D. E., and Bates, G. P. Aberrant splicing of HTT generates the pathogenic exon 1 protein in Huntington disease. *Proc. Natl. Acad. Sci. U. S. A.*, 110(6):2366–2370, feb 2013. ISSN 00278424.

Saudemont, B., Popa, A., Parmley, J. L., Rocher, V., Blugeon, C., Necsulea, A., Meyer, E., and Duret, L. The fitness cost of mis-splicing is the main determinant of alternative splicing patterns. *Genome Biol.*, 18(1):208, dec 2017. ISSN 1474760X.

Saudou, F., Finkbeiner, S., Devys, D., and Greenberg, M. E. Huntingtin acts in the nucleus to induce apoptosis but death does not correlate with the formation of intranuclear inclusions. *Cell*, 95(1):55–66, oct 1998. ISSN 00928674.

Saute, J. A. M. and Jardim, L. B. Machado Joseph disease: Clinical and genetic aspects, and current treatment, may 2015. ISSN 21678707.

Saute, J. A. M., de Castilhos, R. M., Monte, T. L., Schumacher-Schuh, A. F., Donis, K. C., D'Ávila, R., Souza, G. N., Russo, A. D., Furtado, G. V., Gheno, T. C., de Souza, D. O. G., Portela, L. V. C., Saraiva-Pereira, M. L., Camey, S. A., Torman, V. B. L., de Mello Rieder, C. R., and Jardim, L. B. A randomized, phase 2 clinical trial of lithium carbonate in Machado-Joseph disease. *Mov. Disord.*, 29(4):568–573, 2014. ISSN 15318257.

Scaglione, K. M., Zavodszky, E., Todi, S. V., and Patury, S. Ube2w and ataxin-3 coordinately regulate the ubiquitin ligase CHIP. *Mol. Cell*, 43(4):599–612, 2011.

Schaffar, G., Breuer, P., Boteva, R., Behrends, C., Tzvetkov, N., Strippel, N., Sakahira, H., Siegers, K., Hayer-Hartl, M., and Hartl, F. U. Cellular toxicity of polyglutamine expansion proteins: Mechanism of transcription factor deactivation. *Mol. Cell*, 15(1):95–105, jul 2004. ISSN 10972765.

Scheel, H., Tomiuk, S., and Hofmann, K. Elucidation of ataxin-3 and ataxin-7 function by integrative bioinformatics. *Hum. Mol. Genet.*, 12(21):2845–2852, sep 2003. ISSN 1460-2083.

Scherzinger, E., Sittler, A., Schweiger, K., Heiser, V., Lurz, R., Hasenbank, R., Bates, G. P., Lehrach, H., and Wanker, E. E. Self-assembly of polyglutamine-containing huntingtin fragments into amyloid-like fibrils: Implications for Huntington's disease pathology. *Proc. Natl. Acad. Sci. U. S. A.*, 96(8):4604–4609, apr 1999. ISSN 00278424.

Schiffer, N. W., Broadley, S. A., Hirschberger, T., Tavan, P., Kretzschmar, H. A., Giese, A., Haass, C., Hartl, F. U., and Schmid, B. Identification of anti-prion compounds as efficient inhibitors of polyglutamine protein aggregation in a zebrafish model. *J. Biol. Chem.*, 282(12): 9195–9203, mar 2007. ISSN 00219258.

Schilling, G., Sharp, A. H., Loev, S. J., Wagster, M. V., Li, S. H., Stine, O. C., and Ross, C. A. Expression of the huntington's disease (IT15) protein product in HD patients. *Hum. Mol. Genet.*, 4(8):1365–1371, aug 1995. ISSN 09646906.

Schmidt, J. and Schmidt, T. Animal models of Machado-Joseph disease. In *Adv. Exp. Med. Biol.*, volume 1049, pages 289–308. Springer New York LLC, 2018.

Schmidt, J., Mayer, A. K., Bakula, D., Freude, J., Weber, J. J., Weiss, A., Riess, O., and Schmidt, T. Vulnerability of frontal brain neurons for the toxicity of expanded ataxin-3. *Hum. Mol. Genet.*, 28(9):1463–1473, 2019. ISSN 14602083.

Schmidt, T., Bernhard Landwehrmeyer, G., Schmitt, I., Trottier, Y., Auburger, G., Laccone, F., Klockgether, T., Völpel, M., Epplen, J. T., Schöls, L., and Riess, O. An isoform of ataxin-3 accumulates in the nucleus of neuronal cells in affected brain regions of SCA3 patients. *Brain Pathol.*, 8(4):669–679, 1998. ISSN 10156305.

Schmidt, T., Lindenberg, K. S., Krebs, A., Schöls, L., Laccone, F., Herms, J., Rechsteiner, M., Riess, O., and Landwehrmeyer, B. Protein surveillance machinery in brains with spinocerebellar ataxia type 3: Redistribution and differential recruitment of 26S proteasome subunits and chaperones to neuronal intranuclear inclusions. *Ann. Neurol.*, 51(3):302–310, 2002. ISSN 03645134.

Schmitt, I., Brattig, T., Gossen, M., and Riess, O. Characterization of the rat spinocerebellar ataxia type 3 gene. *Neurogenetics*, 1(2):103–112, 1997. ISSN 13646745.

Schmitt, I., Evert, B. O., Khazneh, H., Klockgether, T., and Wuellner, U. The human MJD gene: Genomic structure and functional characterization of the promoter region. *Gene*, 314 (1-2):81–88, sep 2003. ISSN 03781119.

Schmitt, I., Linden, M., Khazneh, H., Evert, B. O., Breuer, P., Klockgether, T., and Wuellner, U. Inactivation of the mouse Atxn3 (ataxin-3) gene increases protein ubiquitination. *Biochem. Biophys. Res. Commun.*, 362(3):734–9, oct 2007. ISSN 0006-291X.

Schöls, L., Vieira-saecker, A. M. M., Schöls, S., Przuntek, H., Epplen, J. T., and Riess, O. Trinucleotide expansion within the MJD1 gene presents clinically as spinocerebellar ataxia and occurs most frequently in german SCA patients. *Hum. Mol. Genet.*, 4(6):1001–1005, 1995. ISSN 09646906.

Schöls, L., Amoiridis, G., Epplen, J. T., Langkafel, M., Przuntek, H., and Riess, O. Relations between genotype and phenotype in German patients with the Machado-Joseph disease mutation. *J. Neurol. Neurosurg. Psychiatry*, 61(5):466–470, nov 1996. ISSN 00223050.

Schöls, L., Haan, J., Riess, O., Amoiridis, G., and Przuntek, H. Sleep disturbance in spinocerebellar ataxias: Is the SCA3 mutation a cause of restless legs syndrome? *Neurology*, 51(6): 1603–1607, 1998. ISSN 00283878.

Schöls, L., Bauer, P., Schmidt, T., Schulte, T., and Riess, O. Autosomal dominant cerebellar ataxias: Clinical features, genetics, and pathogenesis, may 2004. ISSN 14744422.

Schroeder, J. J. *Die Rolle der Isoformen von Ataxin 3 für die Pathogenese der Spinozerebellären Ataxie Typ 3*. PhD thesis, Eberhard Karls Universität Tübingen, 2011.

Schubert, U., Antón, L. C., Gibbs, J., Norbury, C. C., Yewdell, J. W., and Bennink, J. R. Rapid degradation of a large fraction of newly synthesized proteins by proteasomes. *Nature*, 404(6779):770–774, apr 2000. ISSN 00280836.

Schueren, F. and Thoms, S. Functional Translational Readthrough: A Systems Biology Perspective, aug 2016. ISSN 15537404.

Schuler-Faccini, L., Osorio, C. M., Romariz, F., Paneque, M., Sequeiros, J., and Jardim, L. B. Genetic counseling and presymptomatic testing programs for Machado-Joseph disease: Lessons from Brazil and Portugal. *Genet. Mol. Biol.*, 37(1 SUPPL. 1):263–270, 2014. ISSN 16784685.

Scortegagna, M., Subtil, T., Qi, J., Kim, H., Zhao, W., Gu, W., Kluger, H., and Ronai, Z. A. USP13 enzyme regulates Siah2 ligase stability and activity via noncatalytic ubiquitin-binding domains. *J. Biol. Chem.*, 286(31):27333–41, aug 2011. ISSN 1083-351X.

See, K. and Winkler, C. Live Ca2+ imaging reveals reduced excitability of motor axons and Schwann cells in a zebrafish model for Spinal Muscular Atrophy. *Hum. Mol. Genet.*, 2013.

Seglen, P. O. and Gordon, P. B. 3-Methyladenine: specific inhibitor of autophagic/lysosomal protein degradation in isolated rat hepatocytes. *Proc. Natl. Acad. Sci. U. S. A.*, 79(6):1889–92, mar 1982. ISSN 0027-8424.

Seidel, K., den Dunnen, W. F. A., Schultz, C., Paulson, H., Frank, S., de Vos, R. A., Brunt, E. R., Deller, T., Kampinga, H. H., and Rüb, U. Axonal inclusions in spinocerebellar ataxia type 3. *Acta Neuropathol.*, 120(4):449–60, oct 2010. ISSN 1432-0533.

Seidel, K., Meister, M., Dugbartey, G. J., Zijlstra, M. P., Vinet, J., Brunt, E. R. P., van Leeuwen, F. W., Rüb, U., Kampinga, H. H., and den Dunnen, W. F. A. Cellular protein quality control and the evolution of aggregates in spinocerebellar ataxia type 3 (SCA3). *Neuropathol. Appl. Neurobiol.*, 38(6):548–558, oct 2012. ISSN 03051846.

Seirafi, M., Kozlov, G., and Gehring, K. Parkin structure and function, jun 2015. ISSN 17424658.

Seksek, O., Biwersi, J., and Verkman, A. S. Translational diffusion of macromolecule-sized solutes in cytoplasm and nucleus. *J. Cell Biol.*, 138(1):131–142, jul 1997. ISSN 00219525.

Sermet-Gaudelus, I., De Boeck, K., Casimir, G. J., Vermeulen, F., Leal, T., Mogenet, A., Roussel, D., Fritsch, J., Hanssens, L., Hirawat, S., Miller, N. L., Constantine, S., Reha, A., Ajayi, T., Elfring, G. L., and Miller, L. L. Ataluren (PTC124) induces cystic fibrosis transmembrane conductance regulator protein expression and activity in children with nonsense mutation cystic fibrosis. *Am. J. Respir. Crit. Care Med.*, 182(10):1262–1272, 2010. ISSN 1073449X.

Shaman, A. A. Metabolic syndrome and cardiovascular risk assessment among women with polycystic ovary syndrome attending King Khalid Hospital in Tabuk. *Endocrinol. Metab. Syndr.*, 04(04), 2015.

Sharp, A. H., Loev, S. J., Schilling, G., Li, S. H., Li, X. J., Bao, J., Wagster, M. V., Kotzuk, J. A., Steiner, J. P., Lo, A., Hedreen, J., Sisodia, S., Snyder, S. H., Dawson, T. M., Ryugo, D. K., and Ross, C. A. Widespread expression of Huntington's disease gene (IT15) protein product. *Neuron*, 14(5):1065–1074, may 1995. ISSN 08966273.

Shehi, E., Fusi, P., Secundo, F., Pozzuolo, S., Bairati, A., and Tortora, P. Temperature-Dependent, Irreversible Formation of Amyloid Fibrils by a Soluble Human Ataxin-3 Carrying a Moderately Expanded Polyglutamine Stretch (Q36). *Biochemistry*, 42(49):14626–14632, 2003. ISSN 00062960.

Shenkman, M., Tolchinsky, S., Kondratyev, M., and Lederkremer, G. Z. Transient arrest in proteasomal degradation during inhibition of translation in the unfolded protein response. *Biochem. J.*, 404(3):509–516, 2007. ISSN 0264-6021.

Shimizu, H., Yamada, M., Toyoshima, Y., Ikeuchi, T., Onodera, O., and Takahashi, H. Involvement of Onuf's nucleus in Machado-Joseph disease: A morphometric and immunohistochemical study. *Acta Neuropathol.*, 120(4):439–448, oct 2010. ISSN 00016322.

Shimizu, Y., Yoshida, K., Okano, T., Ohara, S., Hashimoto, T., Fukushima, Y., and Ikeda, S. I. Regional features of autosomal-dominant cerebellar ataxia in Nagano: Clinical and molecular genetic analysis of 86 families. *J. Hum. Genet.*, 49(11):610–616, 2004. ISSN 14345161.

Shimizu-Motohashi, Y., Komaki, H., Motohashi, N., Takeda, S., Yokota, T., and Aoki, Y. Restoring dystrophin expression in duchenne muscular dystrophy: Current status of therapeutic approaches, jan 2019. ISSN 20754426.

Shiozaki, E. N., Chai, J., Rigotti, D. J., Riedl, S. J., Li, P., Srinivasula, S. M., Alnemri, E. S., Fairman, R., and Shi, Y. Mechanism of XIAP-mediated inhibition of caspase-9. *Mol. Cell*, 11 (2):519–27, feb 2003. ISSN 1097-2765.

Shizuka, M., Watanabe, M., Ikeda, Y., Mizushima, K., Okamoto, K., and Shoji, M. Molecular analysis of a de novo mutation for spinocerebellar ataxia type 6 and (CAG)n repeat units in normal elder controls. *J. Neurol. Sci.*, 161(1):85–87, nov 1998. ISSN 0022510X.

Shoesmith Berke, S. J., Flores Schmied, F. A., Brunt, E. R., Ellerby, L. M., and Paulson, H. L. Caspase-mediated proteolysis of the polyglutamine disease protein ataxin-3. *J. Neurochem.*, 89(4):908–918, 2004. ISSN 00223042.

Sicorello, A., Kelly, G., Oregioni, A., Nováček, J., Sklenář, V., and Pastore, A. The Structural Properties in Solution of the Intrinsically Mixed Folded Protein Ataxin-3. *Biophys. J.*, 115 (1):59–71, 2018. ISSN 15420086.

Sigurdson, C. J., Bartz, J. C., and Glatzel, M. Cellular and Molecular Mechanisms of Prion Disease. *Annu. Rev. Pathol. Mech. Dis.*, 14(1):497–516, jan 2019. ISSN 1553-4006.

Silva-Fernandes, A. *Development and characterization of transgenic mouse models for Machado-Joseph disease*. PhD thesis, Universidade do Minho, Braga - Portugal., 2010.

Silva-Fernandes, A., Costa, M. d. C., Duarte-Silva, S., Oliveira, P., Botelho, C. M., Martins, L., Mariz, J. A., Ferreira, T., Ribeiro, F., Correia-Neves, M., Costa, C., and Maciel, P. Motor uncoordination and neuropathology in a transgenic mouse model of Machado–Joseph disease lacking intranuclear inclusions and ataxin-3 cleavage products. *Neurobiol. Dis.*, 40(1):163–176, oct 2010. ISSN 09699961.

Silva-Fernandes, A., Duarte-Silva, S., Neves-Carvalho, A., Amorim, M., Soares-Cunha, C., Oliveira, P., Thirstrup, K., Teixeira-Castro, A., and Maciel, P. Chronic Treatment with 17-DMAG Improves Balance and Coordination in A New Mouse Model of Machado-Joseph Disease. *Neurotherapeutics*, 11(2):433–449, 2014. ISSN 18787479.

Silveira, I., Lopes-Cendes, Kish, S., Maciel, P., Gaspar, C., Coutinho, P., Botez, M. I., Teive, H., Arruda, W., Steiner, C. E., Pinto-Junior, W., Maciel, J. A., Jain, S., Sack, G., Andermann, E., Sudarsky, L., Rosenberg, R., MacLeod, P., Chitayat, D., Babul, R., Sequeiros, J., and Rouleau, G. A. Frequency of spinocerebellar ataxia type 1, dentatorubropallidoluysian atrophy, and Machado-Joseph disease mutations in a large group of spinocerebellar ataxia patients. *Neurology*, 46(1):214–218, 1996. ISSN 00283878.

Simeoni, S. Motoneuronal cell death is not correlated with aggregate formation of androgen receptors containing an elongated polyglutamine tract. *Hum. Mol. Genet.*, 9(1):133–144, jan 2000. ISSN 14602083.

Simoes, A. T., Goncalves, N., Koeppen, A., Deglon, N., Kugler, S., Duarte, C. B., and Pereira de Almeida, L. Calpastatin-mediated inhibition of calpains in the mouse brain prevents mutant ataxin 3 proteolysis, nuclear localization and aggregation, relieving Machado-Joseph disease. *Brain*, 135(8):2428–2439, aug 2012. ISSN 0006-8950.

Singh, A., Ursic, D., and Davies, J. Phenotypic suppression and misreading in Saccharomyces cerevisiae, jan 1979. ISSN 00280836.

Singh, A. N., Oehler, J., Torrecilla, I., Kilgas, S., Li, S., Vaz, B., Guérillon, C., Fielden, J., Hernandez-Carralero, E., Cabrera, E., Tullis, I. D., Meerang, M., Barber, P. R., Freire, R., Parsons, J., Vojnovic, B., Kiltie, A. E., Mailand, N., and Ramadan, K. The p97–Ataxin 3 complex regulates homeostasis of the DNA damage response E3 ubiquitin ligase RNF 8. *EMBO J.*, 38(21), nov 2019. ISSN 0261-4189.

Sittler, A., Muriel, M. P., Marinello, M., Brice, A., den Dunnen, W., and Alves, S. Deregulation of autophagy in postmortem brains of Machado-Joseph disease patients. *Neuropathology*, 38 (2):113–124, apr 2018. ISSN 14401789.

Skinner, P. J., Koshy, B. T., Cummings, C. J., Klement, I. A., Helin, K., Servadio, A., Zoghbi, H. Y., and Orr, H. T. Ataxin-1 with an expanded glutamine tract alters nuclear matrix-associated structures. *Nature*, 389(6654):971–974, 1997. ISSN 00280836.

Slack, D. N., Seternes, O.-M., Gabrielsen, M., and Keyse, S. M. Distinct Binding Determinants for ERK2/p38α and JNK MAP Kinases Mediate Catalytic Activation and Substrate Selectivity of MAP Kinase Phosphatase-1. *J. Biol. Chem.*, 276(19):16491–16500, may 2001. ISSN 0021-9258.

Slepko, N., Bhattacharyya, A. M., Jackson, G. R., Steffan, J. S., Marsh, J. L., Thompson, L. M., and Wetzel, R. Normal-repeat-length polyglutamine peptides accelerate aggregation nucleation and cytotoxicity of expanded polyglutamine proteins. *Proc. Natl. Acad. Sci. U. S. A.*, 103(39):14367–14372, 2006.

Slow, E. J., Graham, R. K., Osmand, A. P., Devon, R. S., Lu, G., Deng, Y., Pearson, J., Vaid, K., Bissada, N., Wetzel, R., Leavitt, B. R., and Hayden, M. R. Absence of behavioral abnormalities and neurodegeneration in vivo despite widespread neuronal huntingtin inclusions. *Proc. Natl. Acad. Sci. U. S. A.*, 102(32):11402–7, aug 2005. ISSN 0027-8424.

Snel, B. STRING: a web-server to retrieve and display the repeatedly occurring neighbourhood of a gene. *Nucleic Acids Res.*, 28(18):3442–3444, 2000. ISSN 13624962.

Sobue, G., Doyu, M., Nakao, N., Shimada, N., Mitsuma, T., Maruyama, H., Kawakami, S., and Nakamura, S. Homozygosity for Machado-Joseph disease gene enhances phenotypic severity. *J. Neurol. Neurosurg. Psychiatry*, 60(3):354–6, mar 1996. ISSN 0022-3050.

Soga, K., Ishikawa, K., Furuya, T., Iida, T., Yamada, T., Ando, N., Ota, K., Kanno-Okada, H., Tanaka, S., Shintaku, M., Eishi, Y., Mizusawa, H., and Yokota, T. Gene dosage effect in spinocerebellar ataxia type 6 homozygotes: A clinical and neuropathological study. *J. Neurol. Sci.*, 373:321–328, feb 2017a. ISSN 18785883.

Soga, K., Ishikawa, K., Furuya, T., Iida, T., Yamada, T., Ando, N., Ota, K., Kanno-Okada, H., Tanaka, S., Shintaku, M., Eishi, Y., Mizusawa, H., and Yokota, T. Gene dosage effect in spinocerebellar ataxia type 6 homozygotes: A clinical and neuropathological study. *J. Neurol. Sci.*, 373:321–328, feb 2017b. ISSN 18785883.

Solemani Zadeh, A., Grässer, A., Dinter, H., Hermes, M., and Schindowski, K. Efficient Construction and Effective Screening of Synthetic Domain Antibody Libraries. *Methods Protoc.*, 2(1):17, feb 2019. ISSN 2409-9279.

Sommavilla, R., Lovato, V., Villa, A., Sgier, D., and Neri, D. Design and construction of a naïve mouse antibody phage display library. *J. Immunol. Methods*, 353(1-2):31–43, feb 2010. ISSN 00221759.

Soong, B. W. and Liu, R. S. Positron emission tomography in asymptomatic gene carriers of Machado-Joseph disease. *J. Neurol. Neurosurg. Psychiatry*, 64(4):499–504, apr 1998. ISSN 00223050.

Soong, B.-w., Lu, Y.-c., Choo, K.-b., and Lee, H.-y. Frequency Analysis of Autosomal Dominant Cerebellar Ataxias in Taiwanese Patients and Clinical and Molecular Characterization of Spinocerebellar Ataxia Type 6. *Arch. Neurol.*, 58(7):1105, jul 2001. ISSN 0003-9942.

Sornasse, T., Flamand, V., De Becker, G., Bazin, H., Tielemans, F., Thielemans, K., Urbain, J., Leo, O., and Moser, M. Antigen-pulsed dendritic cells can efficiently induce an antibody response in vivo. *J. Exp. Med.*, 175(1):15–21, jan 1992. ISSN 15409538.

Sowa, A. S., Martin, E., Martins, I. M., Schmidt, J., Depping, R., Weber, J. J., Rother, F., Hartmann, E., Bader, M., Riess, O., Tricoire, H., and Schmidt, T. Karyopherin α-3 is a key protein in the pathogenesis of spinocerebellar ataxia type 3 controlling the nuclear localization of ataxin-3. *Proc. Natl. Acad. Sci.*, 115(11):201716071, 2018. ISSN 0027-8424.

Sowa, A. S., Popova, T. G., Harmuth, T., Weber, J. J., Pereira Sena, P., Schmidt, J., Hübener-Schmid, J., and Schmidt, T. Neurodegenerative phosphoprotein signaling landscape in models of SCA3. *Mol. Brain*, 14(1), dec 2021. ISSN 17566606.

Sowa, A. S., Haas, E., Hübener-Schmid, J., and Lorentz, A. Ataxin-3, The Spinocerebellar Ataxia Type 3 Neurodegenerative Disorder Protein, Affects Mast Cell Functions. *Front. Immunol.*, 13, apr 2022. ISSN 16643224.

Sowa, M. E., Bennett, E. J., Gygi, S. P., and Harper, J. W. Defining the Human Deubiquitinating Enzyme Interaction Landscape. *Cell*, 138(2):389–403, 2009. ISSN 1097-4172.

Spillantini, M. G., Schmidt, M. L., Lee, V. M.-Y., Trojanowski, J. Q., Jakes, R., and Goedert, M. α-Synuclein in Lewy bodies. *Nature*, 388(6645):839–840, aug 1997. ISSN 0028-0836.

Spires, T. L. and Hannan, A. J. Nature, nurture and neurology: Gene-environment interactions in neurodegenerative disease. FEBS Anniversary Prize Lecture delivered on 27 June 2004 at the 29th FEBS Congress in Warsaw. *FEBS J.*, 272(10):2347–2361, apr 2005. ISSN 1742464X.

Spoel, S. H. Orchestrating the proteome with post-translational modifications. *J. Exp. Bot.*, 69 (19):4499–4503, aug 2018. ISSN 14602431.

Squitieri, F., Gellera, C., Cannella, M., Mariotti, C., Cislaghi, G., Rubinsztein, D. C., Almqvist, E. W., Turner, D., Bachoud-Lévi, A. C., Simpson, S. A., Delatycki, M., Maglione, V., Hayden, M. R., and Di Donato, S. Homozygosity for CAG mutation in Huntington disease is associated with a more severe clinical course. *Brain*, 126(4):946–955, apr 2003. ISSN 00068950.

Srinivasula, S. M., Hegde, R., Saleh, A., Datta, P., Shiozaki, E., Chai, J., Lee, R. A., Robbins, P. D., Fernandes-Alnemri, T., Shi, Y., and Alnemri, E. S. A conserved XIAP-interaction motif in caspase-9 and Smac/DIABLO regulates caspase activity and apoptosis. *Nature*, 410 (6824):112–116, mar 2001. ISSN 00280836.

St-Laurent, J., Boulay, M.-E., Prince, P., Bissonnette, E., and Boulet, L.-P. Comparison of cell fixation methods of induced sputum specimens: An immunocytochemical analysis. *J. Immunol. Methods*, 308(1-2):36–42, jan 2006. ISSN 0022-1759.

Steffan, J. S., Kazantsev, A., Spasic-Boskovic, O., Greenwald, M., Zhu, Y.-Z., Gohler, H., Wanker, E. E., Bates, G. P., Housman, D. E., and Thompson, L. M. The Huntington's disease protein interacts with p53 and CREB-binding protein and represses transcription. *Proc. Natl. Acad. Sci.*, 97(12):6763–6768, jun 2000. ISSN 0027-8424.

Steffan, J. S., Bodai, L., Pallos, J., Poelman, M., McCampbell, A., Apostol, B. L., Kazantsev, A., Schmidt, E., Zhu, Y. Z., Greenwald, M., Kurokawa, R., Housman, D. E., Jackson, G. R., Marsh, J. L., and Thompson, L. M. Histone deacetylase inhibitors arrest polyglutamine-dependent neurodegeneration in Drosophila. *Nature*, 413(6857):739–743, oct 2001. ISSN 00280836.

Stetler, R. A., Gan, Y., Zhang, W., Liou, A. K., Gao, Y., Cao, G., and Chen, J. Heat shock proteins: cellular and molecular mechanisms in the central nervous system. *Prog. Neurobiol.*, 92(2):184–211, oct 2010. ISSN 1873-5118.

Stevanin, G. and Brice, A. Spinocerebellar ataxia 17 (SCA17) and Huntington's disease-like 4 (HDL4), jun 2008. ISSN 14734230.

Stevanin, G., Cancel, G., Didierjean, O., Durr, A., Abbas, N., Cassa, E., Feingold, J., Agid, Y., and Brice, A. Linkage disequilibrium at the Machado-Joseph disease/spinal cerebellar ataxia 3 locus: Evidence for a common founder effect in French and Portuguese-Brazilian families as well as a second ancestral Portuguese- Azorean mutation [3], 1995. ISSN 00029297.

Stevanin, G., Lebre, A. S., Mathieux, C., Cancel, G., Abbas, N., Didierjean, O., Dürr, A., Trottier, Y., Agid, Y., and Brice, A. Linkage disequilibrium between the spinocerebellar ataxia 3/Machado-Joseph disease mutation and two intragenic polymorphisms, one of which, X359Y, affects the stop codon. *Am. J. Hum. Genet.*, 60(6):1548–52, jun 1997. ISSN 0002-9297.

Stevanin, G., Giunti, P., David, G., Belal, S., Dürr, A., Ruberg, M., Wood, N., and Brice, A. De novo expansion of intermediate alleles in spinocerebellar ataxia 7. *Hum. Mol. Genet.*, 7 (11):1809–1813, 1998. ISSN 09646906.

Stiebler, A. C., Freitag, J., Schink, K. O., Stehlik, T., Tillmann, B. A., Ast, J., and Bölker, M. Ribosomal Readthrough at a Short UGA Stop Codon Context Triggers Dual Localization of Metabolic Enzymes in Fungi and Animals. *PLoS Genet.*, 10(10):e1004685, oct 2014. ISSN 15537404.

Stommel, J. M. A leucine-rich nuclear export signal in the p53 tetramerization domain: regulation of subcellular localization and p53 activity by NES masking. *EMBO J.*, 18(6):1660–1672, mar 1999. ISSN 0261-4189.

Stoppin, V., Vantard, M., Schmit, A. C., Lambert, A. M., Schneider, D., Weissinger, A., and Thompson, W. Isolated plant nuclei nucleate microtubule assembly: The nuclear surface in higher plants has centrosome-like activity. *Plant Cell*, 6(8):1099–1106, aug 1994. ISSN 1040-4651.

Storey, E., Du Sart, D., Shaw, J. H., Lorentzos, P., Kelly, L., McKinley Gardner, R. J., Forrest, S. M., Biros, I., and Nicholson, G. A. Frequency of spinocerebellar ataxia types 1, 2, 3, 6, and 7 in Australian patients with spinoeerebellar ataxia. *Am. J. Med. Genet.*, 95(4):351–358, 2000. ISSN 01487299.

Su, C. H., Dhananjaya, D., and Tarn, W. Y. Alternative splicing in neurogenesis and brain development, feb 2018. ISSN 2296889X.

Subramanian, S., Mishra, R. K., and Singh, L. Genome-wide analysis of microsatellite repeats in humans: their abundance and density in specific genomic regions. *Genome Biol.*, 4(2):R13, 2003. ISSN 14656914.

Sudarsky, L. and Coutinho, P. Machado-Joseph disease. *Clin. Neurosci.*, 3(1):17–22, 1995. ISSN 1065-6766.

Sugasawa, K., Ng, J. M., Masutani, C., Maekawa, T., Uchida, A., van der Spek, P. J., Eker, A. P., Rademakers, S., Visser, C., Aboussekhra, A., Wood, R. D., Hanaoka, F., Bootsma, D., and Hoeijmakers, J. H. Two human homologs of Rad23 are functionally interchangeable in complex formation and stimulation of XPC repair activity. *Mol. Cell. Biol.*, 17(12):6924–31, dec 1997. ISSN 0270-7306.

Sullivan, R., Yau, W. Y., O'Connor, E., and Houlden, H. Spinocerebellar ataxia: an update. *J. Neurol.*, 266(2):533–544, feb 2019. ISSN 14321459.

Sun, C., Cai, M., Meadows, R. P., Xu, N., Gunasekera, A. H., Herrmann, J., Wu, J. C., and Fesik, S. W. NMR structure and mutagenesis of the third Bir domain of the inhibitor of apoptosis protein XIAP. *J. Biol. Chem.*, 275(43):33777–81, oct 2000. ISSN 0021-9258.

Sura, T., Eu-Ahsunthornwattana, J., Youngcharoen, S., Busabaratana, M., Dejsuphong, D., Trachoo, O., Theerasasawat, S., Tunteeratum, A., Noparutchanodom, C., and Tunlayadechanont, S. Frequencies of spinocerebellar ataxia subtypes in Thailand: Window to the population history. *J. Hum. Genet.*, 54(5):284–288, 2009. ISSN 14345161.

Sutton, J. R., Blount, J. R., Libohova, K., Tsou, W. L., Joshi, G. S., Paulson, H. L., Costa, M. C., Scaglione, K. M., and Todi, S. V. Interaction of the polyglutamine protein ataxin-3 with Rad23 regulates toxicity in drosophila models of Spinocerebellar Ataxia Type 3. *Hum. Mol. Genet.*, 26(8):1419–1431, 2017. ISSN 14602083.

Suzuki, K., Bose, P., Leong-Quong, R. Y., Fujita, D. J., and Riabowol, K. REAP: A two minute cell fractionation method. *BMC Res. Notes*, 3(1):294, 2010. ISSN 17560500.

Suzuki, Y., Nakabayashi, Y., and Takahashi, R. Ubiquitin-protein ligase activity of X-linked inhibitor of apoptosis protein promotes proteasomal degradation of caspase-3 and enhances its anti-apoptotic effect in Fas-induced cell death. *Proc. Natl. Acad. Sci.*, 98(15):8662–8667, 2001. ISSN 0027-8424.

Switonski, P. M., Fiszer, A., Kazmierska, K., Kurpisz, M., Krzyzosiak, W. J., and Figiel, M. Mouse ataxin-3 functional knock-out model. *NeuroMolecular Med.*, 13(1):54–65, mar 2011. ISSN 15351084.

Switonski, P. M., Szlachcic, W. J., Krzyzosiak, W. J., and Figiel, M. A new humanized ataxin-3 knock-in mouse model combines the genetic features, pathogenesis of neurons and glia and late disease onset of SCA3/MJD. *Neurobiol. Dis.*, 73:174–188, jan 2015. ISSN 1095953X.

Szklarczyk, D., Franceschini, A., Wyder, S., Forslund, K., Heller, D., Huerta-Cepas, J., Simonovic, M., Roth, A., Santos, A., Tsafou, K. P., Kuhn, M., Bork, P., Jensen, L. J., and Von Mering, C. STRING v10: Protein-protein interaction networks, integrated over the tree of life. *Nucleic Acids Res.*, 43(D1):D447–D452, 2015. ISSN 13624962.

Szklarczyk, D., Morris, J. H., Cook, H., Kuhn, M., Wyder, S., Simonovic, M., Santos, A., Doncheva, N. T., Roth, A., Bork, P., Jensen, L. J., and Von Mering, C. The STRING database in 2017: Quality-controlled protein-protein association networks, made broadly accessible. *Nucleic Acids Res.*, 45(D1):D362–D368, 2017. ISSN 13624962.

Tadokoro, K., Yamazaki-Inoue, M., Tachibana, M., Fujishiro, M., Nagao, K., Toyoda, M., Ozaki, M., Ono, M., Miki, N., Miyashita, T., and Yamada, M. Frequent occurrence of protein isoforms with or without a single amino acid residue by subtle alternative splicing: The case of Gln in DRPLA affects subcellular localization of the products. *J. Hum. Genet.*, 50(8):382–394, sep 2005. ISSN 14345161.

Tait, D., Riccio, M., Sittler, A., Scherzinger, E., Santi, S., Ognibene, A., Maraldi, N. M., Lehrach, H., and Wanker, E. E. Ataxin-3 is transported into the nucleus and associates with the nuclear matrix. *Hum. Mol. Genet.*, 7(6):991–7, jun 1998. ISSN 0964-6906.

Takahashi, T., Kikuchi, S., Katada, S., Nagai, Y., Nishizawa, M., and Onodera, O. Soluble polyglutamine oligomers formed prior to inclusion body formation are cytotoxic. *Hum. Mol. Genet.*, 17(3):345–356, feb 2008. ISSN 09646906.

Takahashi, T., Katada, S., and Onodera, O. Polyglutamine diseases: Where does toxicity come from? What is toxicity? Where are we going?, 2010. ISSN 16742788.

Takeyama, K. I., Ito, S., Yamamoto, A., Tanimoto, H., Furutani, T., Kanuka, H., Miura, M., Tabata, T., and Kato, S. Androgen-dependent neurodegeneration by polyglutamine-expanded human androgen receptor in Drosophila. *Neuron*, 35(5):855–864, aug 2002. ISSN 08966273.

Takiyama, Y., Nishizawa, M., Tanaka, H., Kawashima, S., Sakamoto, H., Karube, Y., Shimazaki, H., Soutome, M., Endo, K., Ohta, S., Kagawa, Y., Kanazawa, I., Mizuno, Y., Yoshida, M., Yuasa, T., Horikawa, Y., Oyanagi, K., Nagai, H., Kondo, T., Inuzuka, T., Onodera, O., and Tsuji, S. The gene for Machado-Joseph disease maps to human chromosome 14q. *Nat. Genet.*, 4(3):300–304, 1993. ISSN 15461718.

Takiyama, Y., Igasrashi, S., Rogaeva, E. A., Endo, K., Rogaev, E. I., Tanaka, H., Sherrington, R., Sanpei, K., Liang, Y., Saito, M., Tsuda, T., Takano, H., Ikeda, M., Lin, C., Chi, H., Kennedy, J. L., Lang, A. E., Wherrett, J. R., Segawa, M., Nomura, Y., Yuasa, T., Weissenbach, J., Yoshida, M., Nishizawa, M., Kidd, K. K., Tsuji, S., and St George-hyslop, P. H. Evidence for inter-generational instability in the CAG repeat in the MJD1 gene and for conserved haplotypes at flanking markers amongst japanese and caucasian subjects with machado-joseph disease. *Hum. Mol. Genet.*, 4(7):1137–1146, 1995. ISSN 09646906.

Tallaksen-Greene, S. J., Ordway, J. M., Crouse, A. B., Jackson, W. S., Detloff, P. J., and Albin, R. L. Hprt(CAG)146 mice: Age of onset of behavioral abnormalities, time course of neuronal intranuclear inclusion accumulation, neurotransmitter marker alterations, mitochondrial function markers, and susceptibility to 1-Methyl-4-phenyl-1,2,3,6-tetrahydropyridi. *J. Comp. Neurol.*, 465(2):205–219, oct 2003. ISSN 00219967.

Tamura, T. and Chiba, J. Production of antibodies against multipass membrane proteins expressed in human tumor cells using dendritic cell immunization. *J. Biomed. Biotechnol.*, 2009: 673098, apr 2009. ISSN 11107243.

Tanaka, A., Cleland, M. M., Xu, S., Narendra, D. P., Suen, D.-F., Karbowski, M., and Youle, R. J. Proteasome and p97 mediate mitophagy and degradation of mitofusins induced by Parkin. *J. Cell Biol.*, 191(7):1367–80, dec 2010. ISSN 1540-8140.

Tang, B., Liu, C., Shen, L., Dai, H., Pan, Q., Jing, L., Ouyang, S., and Xia, J. Frequency of SCA1, SCA2, SCA3/MJD, SCA6, SCA7, and DRPLA CAG trinucleotide repeat expansion in patients with hereditary spinocerebellar ataxia from Chinese kindreds. *Arch. Neurol.*, 57 (4):540–544, 2000. ISSN 00039942.

Tao, R. S., Fei, E. K., Ying, Z., Wang, H. F., and Wang, G. H. Casein kinase 2 interacts with and phosphorylates ataxin-3. *Neurosci. Bull.*, 24(5):271–277, oct 2008. ISSN 16737067.

Taroni, F. and DiDonato, S. Pathways to motor incoordination: The inherited ataxias, 2004. ISSN 1471003X.

Tasaki, T. and Kwon, Y. T. The mammalian N-end rule pathway: new insights into its components and physiological roles. *Trends Biochem. Sci.*, 32(11):520–528, nov 2007. ISSN 09680004.

Tasaki, T., Lee, M. J., Kwon, Y. T., Mulder, L. C. F., Muesing, M., Iwamatsu, A., Davydov, I. V., and Varshavsky, A. A family of mammalian E3 ubiquitin ligases that contain the UBR box motif and recognize N-degrons. *Mol. Cell. Biol.*, 25(16):7120–7136, aug 2005. ISSN 0270-7306.

Teixeira-Castro, A., Ailion, M., Jalles, A., Brignull, H. R., Vilacã, J. L., Dias, N., Rodrigues, P., Oliveira, J. F., Neves-Carvalho, A., Morimoto, R. I., and Maciel, P. Neuron-specific proteotoxicity of mutant ataxin-3 in C. elegans: Rescue by the DAF-16 and HSF-1 pathways. *Hum. Mol. Genet.*, 20(15):2996–3009, aug 2011. ISSN 09646906.

Telenius, H., Kremer, B., Goldberg, Y. P., Theilmann, J., Andrew, S. E., Zeisler, J., Adam, S., Greenberg, C., Ives, E. J., Clarke, L. A., and Hayden, M. R. Somatic and gonadal mosaicism of the Huntington disease gene CAG repeat in brain and sperm. *Nat. Genet.*, 6(4):409–414, 1994. ISSN 15461718.

The UniProt Consortium. UniProt: a worldwide hub of protein knowledge. *Nucleic Acids Res.*, 47(D1):D506–D515, jan 2019. ISSN 0305-1048.

Thomas, P. and Smart, T. G. HEK293 cell line: A vehicle for the expression of recombinant proteins. *J. Pharmacol. Toxicol. Methods*, 51(3 SPEC. ISS.):187–200, may 2005. ISSN 10568719.

Thorvaldsdóttir, H., Robinson, J. T., and Mesirov, J. P. Integrative Genomics Viewer (IGV): High-performance genomics data visualization and exploration. *Brief. Bioinform.*, 14(2):178–192, 2013. ISSN 14675463.

Thul, P. J., Akesson, L., Wiking, M., Mahdessian, D., Geladaki, A., Ait Blal, H., Alm, T., Asplund, A., Björk, L., Breckels, L. M., Bäckström, A., Danielsson, F., Fagerberg, L., Fall, J., Gatto, L., Gnann, C., Hober, S., Hjelmare, M., Johansson, F., Lee, S., Lindskog, C., Mulder, J., Mulvey, C. M., Nilsson, P., Oksvold, P., Rockberg, J., Schutten, R., Schwenk, J. M., Sivertsson, A., Sjöstedt, E., Skogs, M., Stadler, C., Sullivan, D. P., Tegel, H., Winsnes, C., Zhang, C., Zwahlen, M., Mardinoglu, A., Pontén, F., Von Feilitzen, K., Lilley, K. S., Uhlén, M., and Lundberg, E. A subcellular map of the human proteome. *Science (80-.).*, 356(6340): eaal3321, may 2017. ISSN 10959203.

Tien, C.-L., Wen, F.-C., and Hsieh, M. The polyglutamine-expanded protein ataxin-3 decreases bcl-2 mRNA stability. *Biochem. Biophys. Res. Commun.*, 365(2):232–238, jan 2008. ISSN 0006291X.

Tiller, K. E., Li, L., Kumar, S., Julian, M. C., Garde, S., and Tessier, P. M. Arginine mutations in antibody complementarity-determining regions display context-dependent affinity/specificity trade-offs. *J. Biol. Chem.*, 292(40):16638–16652, 2017. ISSN 1083351X.

Timmons, S., Coakley, M. F., Moloney, A. M., and O' Neill, C. Akt signal transduction dysfunction in Parkinson's disease. *Neurosci. Lett.*, 467(1):30–35, dec 2009. ISSN 03043940.

Tobey, R. A. and Crissman, H. A. Use of flow microfluorometry in detailed analysis of effects of chemical agents on cell cycle progression. *Cancer Res.*, 32(12):2726–32, dec 1972. ISSN 0008-5472.

Todi, S. V., Laco, M. N., Winborn, B. J., Travis, S. M., Wen, H. M., and Paulson, H. L. Cellular turnover of the polyglutamine disease protein ataxin-3 is regulated by its catalytic activity. *J. Biol. Chem.*, 282(40):29348–29358, 2007. ISSN 0021-9258.

Todi, S. V., Winborn, B. J., Scaglione, K. M., Blount, J. R., Travis, S. M., and Paulson, H. L. Ubiquitination directly enhances activity of the deubiquitinating enzyme ataxin-3. *EMBO J.*, 28(4):372–382, feb 2009. ISSN 02614189.

Todi, S. V., Scaglione, K. M., Blount, J. R., Basrur, V., Conlon, K. P., Pastore, A., Elenitoba-Johnson, K., and Paulson, H. L. Activity and cellular functions of the deubiquitinating enzyme and polyglutamine disease protein ataxin-3 are regulated by ubiquitination at lysine 117. *J. Biol. Chem.*, 285(50):39303–13, dec 2010. ISSN 1083-351X.

Tojima, M., Murakami, G., Hikawa, R., Yamakado, H., Yamashita, H., Takahashi, R., and Matsui, M. Homozygous 31 trinucleotide repeats in the SCA2 allele are pathogenic for cerebellar ataxia. *Neurol. Genet.*, 4(6), dec 2018. ISSN 23767839.

Tokgoz, B., Somdas, M. A., Ucar, C., Kocyigit, I., Unal, A., Sipahioglu, M. H., Oymak, O., and Utas, C. Correlation between hearing loss and peritonitis frequency and administration of ototoxic intraperitoneal antibiotics in patients with CAPD. *Ren. Fail.*, 32(2):179–184, 2010. ISSN 0886022X.

Tomic, J. L., Pensalfini, A., Head, E., and Glabe, C. G. Soluble fibrillar oligomer levels are elevated in Alzheimer's disease brain and correlate with cognitive dysfunction. *Neurobiol. Dis.*, 35(3):352–358, sep 2009. ISSN 09699961.

Tomioka, I., Ishibashi, H., Minakawa, E. N., Motohashi, H. H., Takayama, O., Saito, Y., Popiel, H. A., Puentes, S., Owari, K., Nakatani, T., Nogami, N., Yamamoto, K., Noguchi, S., Yonekawa, T., Tanaka, Y., Fujita, N., Suzuki, H., Kikuchi, H., Aizawa, S., Nagano, S., Yamada, D., Nishino, I., Ichinohe, N., Wada, K., Kohsaka, S., Nagai, Y., and Seki, K. Transgenic monkey model of the polyglutamine diseases recapitulating progressive neurological symptoms. *eNeuro*, 4(2), 2017. ISSN 23732822.

Toonen, L. J., Rigo, F., van Attikum, H., and van Roon-Mom, W. M. Antisense Oligonucleotide-Mediated Removal of the Polyglutamine Repeat in Spinocerebellar Ataxia Type 3 Mice. *Mol. Ther. - Nucleic Acids*, 2017. ISSN 21622531.

Torashima, T., Koyama, C., Iizuka, A., Mitsumura, K., Takayama, K., Yanagi, S., Oue, M., Yamaguchi, H., and Hirai, H. Lentivector-mediated rescue from cerebellar ataxia in a mouse model of spinocerebellar ataxia. *EMBO Rep.*, 9(4):393–399, apr 2008. ISSN 1469-221X.

Totzeck, F., Andrade-Navarro, M. A., and Mier, P. The protein structure context of polyQ regions. *PLoS One*, 12(1):e0170801, jan 2017. ISSN 19326203.

Tovey, E. R. and Baldo, B. A. Protein binding to nitrocellulose, nylon and PVDF membranes in immunoassays and electroblotting. *J. Biochem. Biophys. Methods*, 19(2-3):169–183, aug 1989. ISSN 0165-022X.

Tower, C., Fu, L., Gill, R., Prichard, M., Lesort, M., and Sztul, E. Human cytomegalovirus UL97 kinase prevents the deposition of mutant protein aggregates in cellular models of Huntington's disease and Ataxia. *Neurobiol. Dis.*, 2011. ISSN 09699961.

Toyoshima, Y. and Takahashi, H. Spinocerebellar ataxia type 17 (SCA17). In *Adv. Exp. Med. Biol.*, volume 1049, pages 219–231. Springer New York LLC, 2018.

Toyoshima, Y., Onodera, O., Yamada, M., Tsuji, S., and Takahashi, H. Spinocerebellar Ataxia Type 17. In *Pagon RA, Bird TD, Dolan CR, al., Ed. GeneReviews [Internet]. Univ. Washington, Seattle; Initial Post. March 29, 2005; Last Updat. Sept. 12, 2019.*

Toyoshima, Y., Yamada, M., Onodera, O., Shimohata, M., Inenaga, C., Fujita, N., Morita, M., Tsuji, S., and Takahashi, H. SCA17 Homozygote Showing Huntington's Disease-like Phenotype. *Ann. Neurol.*, 55(2):281–286, feb 2004. ISSN 03645134.

Treusch, S., Cyr, D. M., and Lindquist, S. Amyloid deposits: Protection against toxic protein species? *Cell Cycle*, 8(11):1668–1674, jun 2009. ISSN 15514005.

Trott, A., Jardim, L. B., Ludwig, H. T., Saute, J. A., Artigalás, O., Kieling, C., Wanderley, H. Y., Rieder, C. R., Monte, T. L., Socal, M., Alonso, I., Ferro, A., Carvalho, T., do Céu Moreira, M., Mendonça, P., Ferreirinha, F., Silveira, I., Sequeiros, J., Giugliani, R., and Saraiva-Pereira, M. L. Spinocerebellar ataxias in 114 Brazilian families: Clinical and molecular findings, 2006. ISSN 00099163.

Trottier, Y., Lutz, Y., Stevanin, G., Imbert, G., Devys, D., Cancel, G., Saudou, F., Weber, C., David, G., Tora, L., Agid, Y., Brice, A., and Mandel, J. L. Polyglutamine expansion as a pathological epitope in huntington's disease and four dominant cerebellar ataxias. *Nature*, 378(6555):403–406, nov 1995. ISSN 00280836.

Trottier, Y., Cancel, G., An-Gourfinkel, I., Lutz, Y., Weber, C., Brice, A., Hirsch, E., and Mandel, J. L. Heterogeneous intracellular localization and expression of ataxin-3. *Neurobiol. Dis.*, 5(5):335–347, 1998. ISSN 09699961.

Tsai, H. F., Liu, C. S., Leu, T. M., Wen, F. C., Lin, S. J., Liu, C. C., Yang, D. K., Li, C., and Hsieh, M. Analysis of trinucleotide repeats in different SCA loci in spinocerebellar ataxia patients and in normal population of Taiwan. *Acta Neurol. Scand.*, 109(5):355–360, 2004a. ISSN 00016314.

Tsai, H. F., Tsai, H. J., and Hsieh, M. Full-length expanded ataxin-3 enhances mitochondrial-mediated cell death and decreases Bcl-2 expression in human neuroblastoma cells. *Biochem. Biophys. Res. Commun.*, 324(4):1274–1282, nov 2004b. ISSN 0006291X.

Tsai, Y. C., Fishman, P. S., Thakor, N. V., and Oyler, G. a. Parkin facilitates the elimination of expanded polyglutamine proteins and leads to preservation of proteasome function. *J. Biol. Chem.*, 278(24):22044–22055, 2003. ISSN 0021-9258.

Tsou, W.-L., Soong, B.-W., Paulson, H. L., and Rodríguez-Lebrón, E. Splice isoform-specific suppression of the Cav2.1 variant underlying spinocerebellar ataxia type 6. *Neurobiol. Dis.*, 43(3):533–42, sep 2011. ISSN 1095-953X.

Tsou, W.-L., Burr, A. a., Ouyang, M., Blount, J. R., Scaglione, K. M., and Todi, S. V. Ubiquitination regulates the neuroprotective function of the deubiquitinase ataxin-3 in vivo. *J. Biol. Chem.*, 288(48):34460–34469, nov 2013. ISSN 1083-351X.

Tsou, W.-L., Ouyang, M., Hosking, R. R., Sutton, J. R., Blount, J. R., Burr, A. A., and Todi, S. V. The deubiquitinase ataxin-3 requires Rad23 and DnaJ-1 for its neuroprotective role in Drosophila melanogaster. *Neurobiol. Dis.*, 82:12–21, oct 2015. ISSN 1095-953X.

Tsubuki, S., Saito, Y., Tomioka, M., Ito, H., and Kawashima, S. Differential inhibition of calpain and proteasome activities by peptidyl aldehydes of di-leucine and tri-leucine. *J. Biochem.*, 119(3):572–576, mar 1996. ISSN 0021924X.

Tsuji, S. Unstable expansion of triplet repeats as a new disease mechanism for neurodegenerative diseases, sep 1996. ISSN 09168478.

Tsunemi, T., Ishikawa, K., Jin, H., and Mizusawa, H. Cell-type-specific alternative splicing in spinocerebellar ataxia type 6. *Neurosci. Lett.*, 447(1):78–81, dec 2008. ISSN 03043940.

Tu, Y., Liu, H., Zhu, X., Shen, H., Ma, X., Wang, F., Huang, M., Gong, J., Li, X., Wang, Y., Guo, C., and Tang, T. S. Ataxin-3 promotes genome integrity by stabilizing Chk1. *Nucleic Acids Res.*, 45(8):4532–4549, may 2017. ISSN 13624962.

Tuite, P. J., Rogaeva, E. A., George-Hyslop, P. H. S., and Lang, A. E. Dopa-responsive parkinsonism phenotype of Machado-Joseph disease: Confirmation of 14q CAG expansion. *Ann. Neurol.*, 38(4):684–687, oct 1995. ISSN 1531-8249.

Turnidge, J. Pharmacodynamics and dosing of aminoglycosides, sep 2003. ISSN 08915520.

Tyanova, S., Temu, T., Sinitcyn, P., Carlson, A., Hein, M. Y., Geiger, T., Mann, M., and Cox, J. The Perseus computational platform for comprehensive analysis of (prote)omics data, 2016. ISSN 15487105.

Tyedmers, J., Madariaga, M. L., and Lindquist, S. Prion switching in response to environmental stress. *PLoS Biol.*, 6(11):2605–2613, nov 2008. ISSN 15449173.

Tysnes, O. B. and Storstein, A. Epidemiology of Parkinson's disease, aug 2017. ISSN 14351463.

Tzvetkov, N. and Breuer, P. Josephin domain-containing proteins from a variety of species are active de-ubiquitination enzymes. *Biol. Chem.*, 388(9):973–8, sep 2007. ISSN 1431-6730.

Ueno, S., Kondoh, K., Komure, Y., Komure, O., Kuno, S., Kawai, J., Hazama, F., and Sano, A. Somatic mosaicism of CAG repeat in dentatorubral-pallidoluysian atrophy (DRPLA). *Hum. Mol. Genet.*, 4(4):663–666, apr 1995. ISSN 09646906.

Urnov, F. D., Rebar, E. J., Holmes, M. C., Zhang, H. S., and Gregory, P. D. Genome editing with engineered zinc finger nucleases, sep 2010. ISSN 14710056.

Uversky, V. N. Targeting intrinsically disordered proteins in neurodegenerative and protein dysfunction diseases: Another illustration of the D 2 concept, aug 2010. ISSN 14789450.

Vale, J., Bugalho, P., Silveira, I., Sequeiros, J., Guimarães, J., and Coutinho, P. Autosomal dominant cerebellar ataxia: Frequency analysis and clinical characterization of 45 families from Portugal. *Eur. J. Neurol.*, 17(1):124–128, 2010. ISSN 13515101.

Valenzuela-Fernández, A., Cabrero, J. R., Serrador, J. M., and Sánchez-Madrid, F. HDAC6: a key regulator of cytoskeleton, cell migration and cell-cell interactions, jun 2008. ISSN 09628924.

van Beek, H. *Charakterisierung Ataxin-3-isoformspezifischer Zebrafisch- modelle für die spinocerebelläre Ataxie Typ 3.* Master thesis, University of Applied Sciences Albstadt-Sigmaringen, 2019.

Van De Warrenburg, B. P., Frenken, C. W., Ausems, M. G., Kleefstra, T., Sinke, R. J., Knoers, N. V., and Kremer, H. P. Striking anticipation in spinocerebellar ataxia type 7: The infantile phenotype, 2001. ISSN 03405354.

Van De Warrenburg, B. P., Sinke, R. J., Verschuuren-Bemelmans, C. C., Scheffer, H., Brunt, E. R., Ippel, P. F., Maat-Kievit, J. A., Dooijes, D., Notermans, N. C., Lindhout, D., Knoers, N. V., and Kremer, H. P. Spinocerebellar ataxias in the Netherlands: Prevalence and age at onset variance analysis. *Neurology*, 58(5):702–708, mar 2002. ISSN 00283878.

van Nocker, S. and Vierstra, R. D. Multiubiquitin chains linked through lysine 48 are abundant in vivo and are competent intermediates in the ubiquitin proteolytic pathway. *J. Biol. Chem.*, 268(33):24766–73, nov 1993. ISSN 0021-9258.

Vaz, R. L., Outeiro, T. F., and Ferreira, J. J. Zebrafish as an Animal Model for Drug Discovery in Parkinson's Disease and Other Movement Disorders: A Systematic Review. *Front. Neurol.*, 9(JUN):347, jun 2018. ISSN 1664-2295.

Velázquez-Pérez, L. C., Rodríguez-Labrada, R., and Fernandez-Ruiz, J. Spinocerebellar ataxia type 2: Clinicogenetic aspects, mechanistic insights, and management approaches, sep 2017. ISSN 16642295.

Veneziano, L. and Frontali, M. DRPLA. In *Pagon RA, Bird TD, Dolan CR, al., Ed. GeneReviews [Internet]. Univ. Washington, Seattle; Initial Post. August 6, 1999; Last Updat. June 9, 2016.* Seattle (WA): University of Washington, Seattle.

Venkatraman, P., Wetzel, R., Tanaka, M., Nukina, N., and Goldberg, A. L. Eukaryotic proteasomes cannot digest polyglutamine sequences and release them during degradation of polyglutamine-containing proteins. *Mol. Cell*, 14(1):95–104, apr 2004. ISSN 10972765.

Verhagen, A. M., Ekert, P. G., Pakusch, M., Silke, J., Connolly, L. M., Reid, G. E., Moritz, R. L., Simpson, R. J., and Vaux, D. L. Identification of DIABLO, a mammalian protein that promotes apoptosis by binding to and antagonizing IAP proteins. *Cell*, 102(1):43–53, jul 2000. ISSN 0092-8674.

Verkerk, A. J., Pieretti, M., Sutcliffe, J. S., Fu, Y. H., Kuhl, D. P., Pizzuti, A., Reiner, O., Richards, S., Victoria, M. F., Zhang, F., Eussen, B. E., van Ommen, G. J. B., Blonden, L. A., Riggins, G. J., Chastain, J. L., Kunst, C. B., Galjaard, H., Thomas Caskey, C., Nelson, D. L., Oostra, B. A., and Warran, S. T. Identification of a gene (FMR-1) containing a CGG repeat coincident with a breakpoint cluster region exhibiting length variation in fragile X syndrome. *Cell*, 65(5):905–914, may 1991. ISSN 00928674.

von der Haar, T. and Tuite, M. F. Regulated translational bypass of stop codons in yeast, feb 2007. ISSN 0966842X.

von Mering, C., Huynen, M., Jaeggi, D., Schmidt, S., Bork, P., and Snel, B. STRING: A database of predicted functional associations between proteins, 2003. ISSN 03051048.

von Mering, C., Jensen, L. J., Snel, B., Hooper, S. D., Krupp, M., Foglierini, M., Jouffre, N., Huynen, M. A., and Bork, P. STRING: Known and predicted protein-protein associations, integrated and transferred across organisms. *Nucleic Acids Res.*, 33(DATABASE ISS.), 2005. ISSN 03051048.

Vucic, D., Deshayes, K., Ackerly, H., Pisabarro, M. T., Kadkhodayan, S., Fairbrother, W. J., and Dixit, V. M. SMAC Negatively Regulates the Anti-apoptotic Activity of Melanoma Inhibitor of Apoptosis (ML-IAP). *J. Biol. Chem.*, 277(14):12275–12279, apr 2002. ISSN 0021-9258.

Walker, P. D. and Shah, S. V. Gentamicin enhanced production of hydrogen peroxide by renal cortical mitochondria. *Am. J. Physiol. - Cell Physiol.*, 253(4):C495–9, oct 1987. ISSN 00029513.

Wan, L., Xu, K., Chen, Z., Tang, B., and Jiang, H. Roles of Post-translational Modifications in Spinocerebellar Ataxias. *Front. Cell. Neurosci.*, 12:290, sep 2018. ISSN 1662-5102.

Wang, F., Pan, J., Liu, Y., Meng, Q., Lv, P., Qu, F., Ding, G. L., Klausen, C., Leung, P. C., Chan, H. C., Yao, W., Zhou, C. Y., Shi, B., Zhang, J., Sheng, J., and Huang, H. Alternative splicing of the androgen receptor in polycystic ovary syndrome. *Proc. Natl. Acad. Sci. U. S. A.*, 112(15):4743–4748, apr 2015. ISSN 10916490.

Wang, G., Ide, K., Nukina, N., Goto, J., Ichikawa, Y., Uchida, K., Sakamoto, T., and Kanazawa, I. Machado-Joseph disease gene product identified in lymphocytes and brain. *Biochem. Biophys. Res. Commun.*, 233(2):476–479, apr 1997. ISSN 0006291X.

Wang, G., Sawai, N., Kotliarova, S., Kanazawa, I., and Nukina, N. Ataxin-3, the MJD1 gene product, interacts with the two human homologs of yeast DNA repair protein RAD23, HHR23A and HHR23B. *Hum. Mol. Genet.*, 9(12):1795–1803, 2000.

Wang, H., Jia, N., Fei, E., Wang, Z., Liu, C., Zhang, T., Fan, J., Wu, M., Chen, L., Nukina, N., Zhou, J., and Wang, G. p45, an ATPase subunit of the 19S proteasome, targets the polyglutamine disease protein ataxin-3 to the proteasome. *J. Neurochem.*, 101(6):1651–1661, jun 2007. ISSN 0022-3042.

Wang, J., An, L., Zhao, Y., Zhang, C., Li, S., Ye, C., Jing, S., and Hang, H. In vitro affinity maturation of antibody against membrane-bound GPCR molecules. *Appl. Microbiol. Biotechnol.*, 103(18):7703–7717, sep 2019. ISSN 0175-7598.

Wang, Q., Li, L., and Ye, Y. Regulation of retrotranslocation by p97-associated deubiquitinating enzyme ataxin-3. *J. Cell Biol.*, 174(7):963–971, sep 2006. ISSN 0021-9525.

Wang, X.-Z., Huang, X.-Y., Yao, J.-G., Wang, C., Xia, Q., and Long, X.-D. Genetic polymorphisms in ataxin-3 and liver cirrhosis risk related to aflatoxin B1. *Oncotarget*, 9(44): 27321–27332, jun 2018a. ISSN 1949-2553.

Wang, Y., Wu, W., Negre, N. N., White, K. P., Li, C., and Shah, P. K. Determinants of antigenicity and specificity in immune response for protein sequences. *BMC Bioinformatics*, 12(1):251, jun 2011. ISSN 14712105.

Wang, Z. Experimental and Clinical Strategies for Treating Spinocerebellar Ataxia Type 3, 2018. ISSN 18737544.

Wang, Z. J., Hanet, A., Weishäupl, D., Martins, I. M., Sowa, A. S., Riess, O., and Schmidt, T. Divalproex sodium modulates nuclear localization of ataxin-3 and prevents cellular toxicity caused by expanded ataxin-3. *CNS Neurosci. Ther.*, 2018b. ISSN 17555949.

Warnecke, T. and Hurst, L. D. Error prevention and mitigation as forces in the evolution of genes and genomes, dec 2011. ISSN 14710056.

Warrick, J. M., Paulson, H. L., Gray-Board, G. L., Bui, Q. T., Fischbeck, K. H., Pittman, R. N., and Bonini, N. M. Expanded polyglutamine protein forms nuclear inclusions and causes neural degeneration in Drosophila. *Cell*, 93(6):939–949, jun 1998. ISSN 00928674.

Warrick, J. M., Morabito, L. M., Bilen, J., Gordesky-Gold, B., Faust, L. Z., Paulson, H. L., and Bonini, N. M. Ataxin-3 suppresses polyglutamine neurodegeneration in Drosophila by a ubiquitin-associated mechanism. *Mol. Cell*, 18(1):37–48, 2005. ISSN 10972765.

Watanabe-Asano, T., Kuma, A., and Mizushima, N. Cycloheximide inhibits starvation-induced autophagy through mTORC1 activation. *Biochem. Biophys. Res. Commun.*, 445(2):334–339, 2014. ISSN 10902104.

Watchon, M., Yuan, K. C., Mackovski, N., Svahn, A. J., Cole, N. J., Goldsbury, C., Rinkwitz, S., Becker, T. S., Nicholson, G. A., and Laird, A. S. Calpain Inhibition Is Protective in Machado–Joseph Disease Zebrafish Due to Induction of Autophagy. *J. Neurosci.*, 2017. ISSN 0270-6474.

Weber, J. J. *Calpains in the Molecular Pathogenesis of Polyglutamine Disorders and their Potential as a Therapeutic Target.* Dissertation, University of Tübingen, 2017.

Weber, J. J., Golla, M., Guaitoli, G., Wanichawan, P., Hayer, S. N., Hauser, S., Krahl, A. C., Nagel, M., Samer, S., Aronica, E., Carlson, C. R., Schöls, L., Riess, O., Gloeckner, C. J., Nguyen, H. P., and Hübener-Schmid, J. A combinatorial approach to identify calpain cleavage sites in the Machado-Joseph disease protein ataxin-3. *Brain*, 140(5):1280–1299, may 2017. ISSN 14602156.

Weber, J. J., Kloock, S. J., Nagel, M., Ortiz-Rios, M. M., Hofmann, J., Riess, O., and Nguyen, H. P. Calpastatin ablation aggravates the molecular phenotype in cell and animal models of Huntington disease. *Neuropharmacology*, 133:94–106, may 2018. ISSN 18737064.

Weber, J. J., Pereira Sena, P., Singer, E., and Nguyen, H. P. Killing Two Angry Birds with One Stone: Autophagy Activation by Inhibiting Calpains in Neurodegenerative Diseases and beyond, feb 2019. ISSN 23146141.

Weishäupl, D. *Analysen zur Bedeutung der Isoformen von Ataxin-3 für die Pathogenese der Spinocerebellären Ataxie Typ 3.* Master thesis, Hochschule Albstadt-Sigmaringen, 2012.

Weishäupl, D., Schneider, J., Peixoto Pinheiro, B., Ruess, C., Dold, S. M., von Zweydorf, F., Gloeckner, C. J., Schmidt, J., Riess, O., and Schmidt, T. Physiological and pathophysiological characteristics of ataxin-3 isoforms. *J. Biol. Chem.*, 294(2):644–661, nov 2019. ISSN 1083-351X.

Weiss, A., Klein, C., Woodman, B., Sathasivam, K., Bibel, M., Régulier, E., Bates, G. P., and Paganetti, P. Sensitive biochemical aggregate detection reveals aggregation onset before symptom development in cellular and murine models of Huntington's disease. *J. Neurochem.*, 104(3):846–858, nov 2008. ISSN 00223042.

Weiss, A., Abramowski, D., Bibel, M., Bodner, R., Chopra, V., DiFiglia, M., Fox, J., Kegel, K., Klein, C., Grueninger, S., Hersch, S., Housman, D., Régulier, E., Rosas, H. D., Stefani, M., Zeitlin, S., Bilbe, G., and Paganetti, P. Single-step detection of mutant huntingtin in animal and human tissues: A bioassay for Huntington's disease. *Anal. Biochem.*, 395(1):8–15, dec 2009. ISSN 10960309.

Welch, E. M., Barton, E. R., Zhuo, J., Tomizawa, Y., Friesen, W. J., Trifillis, P., Paushkin, S., Patel, M., Trotta, C. R., Hwang, S., Wilde, R. G., Karp, G., Takasugi, J., Chen, G., Jones, S., Ren, H., Moon, Y. C., Corson, D., Turpoff, A. A., Campbell, J. A., Conn, M. M., Khan, A., Almstead, N. G., Hedrick, J., Mollin, A., Risher, N., Weetall, M., Yeh, S., Branstrom, A. A., Colacino, J. M., Babiak, J., Ju, W. D., Hirawat, S., Northcutt, V. J., Miller, L. L., Spatrick, P., He, F., Kawana, M., Feng, H., Jacobson, A., Peltz, S. W., and Sweeney, H. L. PTC124 targets genetic disorders caused by nonsense mutations. *Nature*, 447(7140):87–91, may 2007. ISSN 14764687.

Wellington, C. L., Ellerby, L. M., Hackam, A. S., Margolis, R. L., Trifiro, M. A., Singaraja, R., McCutcheon, K., Salvesen, G. S., Propp, S. S., Bromm, M., Rowland, K. J., Zhang, T., Rasper, D., Roy, S., Thornberry, N., Pinsky, L., Kakizuka, A., Ross, C. A., Nicholson, D. W., Bredesen, D. E., and Hayden, M. R. Caspase cleavage of gene products associated with triplet expansion disorders generates truncated fragments containing the polyglutamine tract. *J. Biol. Chem.*, 273(15):9158–67, apr 1998. ISSN 0021-9258.

Welzel, F., Kaehler, C., Isau, M., Hallen, L., Lehrach, H., and Krobitsch, S. FOX-2 dependent splicing of ataxin-2 transcript is affected by ataxin-1 overexpression. *PLoS One*, 7(5):e37985, may 2012. ISSN 19326203.

Wessel, D. and Flügge, U. I. A method for the quantitative recovery of protein in dilute solution in the presence of detergents and lipids. *Anal. Biochem.*, 138(1):141–143, apr 1984. ISSN 10960309.

Wexler, N. S., Young, A. B., Tanzi, R. E., Travers, H., Starosta-Rubinstein, S., Penney, J. B., Snodgrass, S. R., Shoulson, I., Gomez, F., Arroyo, M. A., Penchaszadeh, G. K., Moreno, H., Gibbons, K., Faryniarz, A., Hobbs, W., Anderson, M. A., Bonilla, E., Conneally, P. M., and Gusella, J. F. Homozygotes for huntington's disease. *Nature*, 326(6109):194–197, 1987. ISSN 00280836.

Wilkinson, K. D. Ubiquitination and deubiquitination: Targeting of proteins for degradation by the proteasome. *Semin. Cell Dev. Biol.*, 11(3):141–148, jun 2000. ISSN 10849521.

Williams, A. J. and Paulson, H. L. Polyglutamine neurodegeneration: protein misfolding revisited. *Trends Neurosci.*, 31(10):521–8, oct 2008. ISSN 0166-2236.

Wilschanski, M., Yahav, Y., Yaacov, Y., Blau, H., Bentur, L., Rivlin, J., Aviram, M., Bdolah-Abram, T., Bebok, Z., Shushi, L., Kerem, B., and Kerem, E. Gentamicin-induced correction of CFTR function in patients with cystic fibrosis and CFTR stop mutations. *N. Engl. J. Med.*, 349(15):1433–41, oct 2003. ISSN 1533-4406.

Wilschanski, M., Miller, L. L., Shoseyov, D., Blau, H., Rivlin, J., Aviram, M., Cohen, M., Armoni, S., Yaakov, Y., Pugatch, T., Cohen-Cymberknoh, M., Miller, N. L., Reha, A., Northcutt, V. J., Hirawat, S., Donnelly, K., Elfring, G. L., Ajayi, T., and Kerem, E. Chronic ataluren (PTC124) treatment of nonsense mutation cystic fibrosis. *Eur. Respir. J.*, 38(1): 59–69, 2011. ISSN 09031936.

Winborn, B. J., Travis, S. M., Todi, S. V., Scaglione, K. M., Xu, P., Williams, A. J., Cohen, R. E., Peng, J., and Paulson, H. L. The deubiquitinating enzyme ataxin-3, a polyglutamine disease protein, edits Lys63 linkages in mixed linkage ubiquitin chains. *J. Biol. Chem.*, 283 (39):26436–26443, sep 2008. ISSN 00219258.

Wiseman, B. S., Sternlicht, M. D., Lund, L. R., Alexander, C. M., Mott, J., Bissell, M. J., Soloway, P., Itohara, S., and Werb, Z. Site-specific inductive and inhibitory activities of MMP-2 and MMP-3 orchestrate mammary gland branching morphogenesis. *J. Cell Biol.*, 162 (6):1123–1133, sep 2003. ISSN 0021-9525.

Wood, A., Krogan, N. J., Dover, J., Schneider, J., Heidt, J., Boateng, M. A., Dean, K., Golshani, A., Zhang, Y., Greenblatt, J. F., Johnston, M., Shilatifard, A., Louis, S., Hill, C., and Carolina, N. Bre1 , an E3 Ubiquitin Ligase Short Article Required for Recruitment and Substrate Selection of Rad6 at a Promoter 1402 South Grand Boulevard University of North Carolina at Chapel Hill. *Compass*, 11:267–274, 2003.

Wood, J. D., Nucifora, F. C., Duan, K., Zhang, C., Wang, J., Kim, Y., Schilling, G., Sacchi, N., Liu, J. M., and Ross, C. A. Atrophin-1, the dentato-rubral and pallido-luysian atrophy gene product, interacts with ETO/MTG8 in the nuclear matrix and represses transcription. *J. Cell Biol.*, 150(5):939–948, sep 2000. ISSN 00219525.

Wood, M. J., Gait, M. J., and Yin, H. RNA-targeted splice-correction therapy for neuromuscular disease. *Brain*, 133(4):957–972, 2010. ISSN 14602156.

Woods, B. T. and Schaumburg, H. H. Nigro-spino-dentatal degeneration with nuclear ophthalmoplegia. A unique and partially treatable clinico-pathological entity. *J. Neurol. Sci.*, 17(2): 149–166, 1972. ISSN 0022510X.

Wu, Y. R., Lin, H. Y., Chen, C. M., Gwinn-Hardy, K., Ro, L. S., Wang, Y. C., Li, S. H., Hwang, J. C., Fang, K., Hsieh-Li, H. M., Li, M. L., Tung, L. C., Su, M. T., Lu, K. T., and Lee-Chen, G. J. Genetic testing in spinocerebellar ataxia in Taiwan: Expansions of trinucleotide repeats in SCA8 and SCA17 are associated with typical Parkinson's disease. *Clin. Genet.*, 65(3): 209–214, 2004. ISSN 00099163.

Wu, Y. T., Tan, H. L., Shui, G., Bauvy, C., Huang, Q., Wenk, M. R., Ong, C. N., Codogno, P., and Shen, H. M. Dual role of 3-methyladenine in modulation of autophagy via different temporal patterns of inhibition on class I and III phosphoinositide 3-kinase. *J. Biol. Chem.*, 285(14):10850–10861, apr 2010. ISSN 00219258.

Wüllner, U., Reimold, M., Abele, M., Bürk, K., Minnerop, M., Dohmen, B. M., Machulla, H. J., Bares, R., and Klockgether, T. Dopamine transporter positron emission tomography in spinocerebellar ataxias type 1, 2, 3, and 6. *Arch. Neurol.*, 62(8):1280–1285, aug 2005. ISSN 00039942.

Wyllie, A. H. Glucocorticoid-induced thymocyte apoptosis is associated with endogenous endonuclease activation. *Nature*, 284(5756):555–556, 1980. ISSN 00280836.

Wyttenbach, A., Sauvageot, O., Carmichael, J., Diaz-Latoud, C., Arrigo, A.-P., and Rubinsztein, D. C. Heat shock protein 27 prevents cellular polyglutamine toxicity and suppresses the increase of reactive oxygen species caused by huntingtin. *Hum. Mol. Genet.*, 11(9):1137–51, may 2002. ISSN 0964-6906.

Xi, Y., Noble, S., and Ekker, M. Modeling neurodegeneration in zebrafish, jun 2011. ISSN 15284042.

Xu, C. and Zhang, J. Alternative Polyadenylation of Mammalian Transcripts Is Generally Deleterious, Not Adaptive. *Cell Syst.*, 6(6):734–742.e4, 2018. ISSN 24054720.

Xu, G. and Zhang, J. Human coding RNA editing is generally nonadaptive. *Proc. Natl. Acad. Sci. U. S. A.*, 111(10):3769–3774, 2014. ISSN 10916490.

Xue, W. F., Hellewell, A. L., Gosal, W. S., Homans, S. W., Hewitt, E. W., and Radford, S. E. Fibril fragmentation enhances amyloid cytotoxicity. *J. Biol. Chem.*, 284(49):34272–34282, dec 2009. ISSN 00219258.

Yabe, I., Sasaki, H., Matsuura, T., Takada, A., Akemi Wakisaka, Suzuki, Y., Fukazawa, T., Hamada, T., Oda, T., Ohnishi, A., and Tashiro, K. SCA6 mutation analysis in a large cohort of the Japanese patients with late-onset pure cerebellar ataxia. *J. Neurol. Sci.*, 156(1):89–95, mar 1998. ISSN 0022510X.

Yamada, M., Sato, T., Tsuji, S., and Takahashi, H. CAG repeat disorder models and human neuropathology: Similarities and differences, jan 2008. ISSN 00016322.

Yamamoto, A., Tagawa, Y., Yoshimori, T., Moriyama, Y., Masaki, R., and Tashiro, Y. Bafilomycin A1 prevents maturation of autophagic vacuoles by inhibiting fusion between autophagosomes and lysosomes in rat hepatoma cell line, H-4-II-E cells. *Cell Struct. Funct.*, 23 (1):33–42, feb 1998. ISSN 0386-7196.

Yamano, K. and Youle, R. J. PINK1 is degraded through the N-end rule pathway. *Autophagy*, 9(11):1758–1769, nov 2013. ISSN 15548635.

Yang, H., Yue, H.-W., He, W.-T., Hong, J.-Y., Jiang, L.-L., and Hu, H.-Y. PolyQ-expanded huntingtin and ataxin-3 sequester ubiquitin adaptors hHR23B and UBQLN2 into aggregates via conjugated ubiquitin. *FASEB J.*, 32(6):2923–2933, jun 2018. ISSN 0892-6638.

Yang, W. Aggregated polyglutamine peptides delivered to nuclei are toxic to mammalian cells. *Hum. Mol. Genet.*, 11(23):2905–2917, nov 2002. ISSN 14602083.

Yang, W. Z., Zhang, Y., Wu, F., Zhang, M., Cho, S. C., Li, C. Z., Li, S. H., Shu, G. J., Sheng, Y. X., Zhao, N., Tang, Y., Jiang, S., Jiang, S., Gandjian, M., Ichim, T. E., and Hu, X. Human umbilical cord blood-derived mononuclear cell transplantation: Case series of 30 subjects with Hereditary Ataxia. *J. Transl. Med.*, 9, may 2011. ISSN 14795876.

Yang, Y., Fang, S., Jensen, J. P., Weissman, A. M., and Ashwell, J. D. Ubiquitin protein ligase activity of IAPs and their degradation in proteasomes in response to apoptotic stimuli. *Science*, 288(5467):874–7, may 2000. ISSN 0036-8075.

Yano, A., Onozuka, A., Asahi-Ozaki, Y., Imai, S., Hanada, N., Miwa, Y., and Nisizawa, T. An ingenious design for peptide vaccines. *Vaccine*, 23(17-18):2322–2326, 2005. ISSN 0264410X.

Yeo, G., Holste, D., Kreiman, G., and Burge, C. B. Variation in alternative splicing across human tissues. *Genome Biol.*, 5(10), 2004. ISSN 14656914.

Yi, J., Zhang, L., Tang, B., Han, W., Zhou, Y., Chen, Z., Jia, D., and Jiang, H. Sodium Valproate Alleviates Neurodegeneration in SCA3/MJD via Suppressing Apoptosis and Rescuing the Hypoacetylation Levels of Histone H3 and H4. *PLoS One*, 8(1):e54792, jan 2013. ISSN 1932-6203.

Yoshida, H., Yoshizawa, T., Shibasaki, F., Shoji, S., and Kanazawa, I. Chemical chaperones reduce aggregate formation and cell death caused by the truncated Machado-Joseph disease gene product with an expanded polyglutamine stretch. *Neurobiol. Dis.*, 2002. ISSN 09699961.

Yoshino, H., Kumai, Y., and Kashiwakura, I. Effects of endoplasmic reticulum stress on apoptosis induction in radioresistant macrophages. *Mol. Med. Rep.*, 15(5):2867–2872, may 2017. ISSN 17913004.

Yoshizawa, T., Yamagishi, Y., Koseki, N., Goto, J., Yoshida, H., Shibasaki, F., Shoji, S., and Kanazawa, I. Cell cycle arrest enhances the in vitro cellular toxicity of the truncated Machado-Joseph disease gene product with an expanded polyglutamine stretch. *Hum. Mol. Genet.*, 9 (1):69–78, jan 2000. ISSN 14602083.

Young, J. E., Gouw, L., Propp, S., Sopher, B. L., Taylor, J., Lin, A., Hermel, E., Logvinova, A., Chen, S. F., Chen, S., Bredesen, D. E., Truant, R., Ptacek, L. J., La Spada, A. R., and Ellerby, L. M. Proteolytic cleavage of ataxin-7 by caspase-7 modulates cellular toxicity and transcriptional dysregulation. *J. Biol. Chem.*, 282(41):30150–30160, 2007. ISSN 00219258.

Yu, Y.-C., Kuo, C.-L., Cheng, W.-L., Liu, C.-S., and Hsieh, M. Decreased antioxidant enzyme activity and increased mitochondrial DNA damage in cellular models of Machado-Joseph disease. *J. Neurosci. Res.*, 87(8):1884–1891, jun 2009a. ISSN 03604012.

Yu, Z., Wang, A. M., Robins, D. M., and Lieberman, A. P. Altered RNA splicing contributes to skeletal muscle pathology in Kennedy disease knock-in mice. *DMM Dis. Model. Mech.*, 2 (9-10):500–507, sep 2009b. ISSN 17548403.

Zalk, R. and Shoshan-Barmatz, V. ATP-binding sites in brain p97/VCP (valosin-containing protein), a multifunctional AAA ATPase. *Biochem. J.*, 374(Pt 2):473–80, sep 2003. ISSN 1470-8728.

Zaluzec, E. J., Gage, D. A., Allison, J., and Throck Watson, J. Direct matrix-assisted laser desorption ionization mass spectrometric analysis of proteins immobilized on nylon-based membranes. *J. Am. Soc. Mass Spectrom.*, 5(4):230–237, apr 1994. ISSN 18791123.

Zambusi, A. and Ninkovic, J. Regeneration of the central nervous system-principles from brain regeneration in adult zebrafish, jan 2020. ISSN 19480210.

Zarraga, I. G., Zhang, L., Stump, M. R., Gong, Q., Vincent, G. M., and Zhou, Z. Nonsense-mediated mRNA decay caused by a frameshift mutation in a large kindred of type 2 long QT syndrome. *Hear. Rhythm*, 8(8):1200–1206, aug 2011. ISSN 15475271.

Zarranz, J. J., Alegre, J., Gómez-Esteban, J. C., Lezcano, E., Ros, R., Ampuero, I., Vidal, L., Hoenicka, J., Rodriguez, O., Atarés, B., Llorens, V., Tortosa, E. G., del Ser, T., Muñoz, D. G., and de Yebenes, J. G. The new mutation, E46K, of α-synuclein causes parkinson and Lewy body dementia. *Ann. Neurol.*, 55(2):164–173, feb 2004. ISSN 03645134.

Zeng, L., Tallaksen-Greene, S. J., Wang, B., Albin, R. L., and Paulson, H. L. The de-ubiquitinating enzyme ataxin-3 does not modulate disease progression in a knock-in mouse model of Huntington disease. *J. Huntingtons. Dis.*, 2(2):201–15, 2013. ISSN 1879-6397.

Zeng, L., Wang, B., Merillat, S. A., Minakawa, E. N., Perkins, M. D., Ramani, B., Tallaksen-Greene, S. J., Costa, M. d. C., Albin, R. L., and Paulson, H. L. Differential recruitment of UBQLN2 to nuclear inclusions in the polyglutamine diseases HD and SCA3. *Neurobiol. Dis.*, 82:281–288, 2015. ISSN 1095953X.

Zeng, L.-X., Tang, Y., and Ma, Y. Ataxin-3 expression correlates with the clinicopathologic features of gastric cancer. *Int. J. Clin. Exp. Med.*, 7(4):973, 2014.

Zhang, J., Rowe, W. L., Clark, A. G., and Buetow, K. H. Genomewide Distribution of High-Frequency, Completely Mismatching SNP Haplotype Pairs Observed To Be Common across Human Populations. *Am. J. Hum. Genet.*, 73(5):1073–1081, nov 2003. ISSN 00029297.

Zhang, S., Xu, L., Lee, J., and Xu, T. Drosophila Atrophin homolog functions as a transcriptional corepressor in multiple developmental processes. *Cell*, 108(1):45–56, jan 2002. ISSN 00928674.

Zhang, T., Wolfe, C., Pierle, A., Welle, K. A., Hryhorenko, J. R., and Ghaemmaghami, S. Proteome-wide modulation of degradation dynamics in response to growth arrest. *Proc. Natl. Acad. Sci. U. S. A.*, 114(48):E10329–E10338, nov 2017a. ISSN 10916490.

Zhang, X., St Clair, J. R., London, E., and Raleigh, D. P. Islet amyloid polypeptide membrane interactions: Effects of membrane composition. *Biochemistry*, 56(2):376–390, jan 2017b. ISSN 15204995.

Zhang, Y., Leavitt, B. R., Van Raamsdonk, J. M., Dragatsis, I., Goldowitz, D., MacDonald, M. E., Hayden, M. R., and Friedlander, R. M. Huntingtin inhibits caspase-3 activation. *EMBO J.*, 25(24):5896–5906, dec 2006. ISSN 02614189.

Zhao, J., Zhai, B., Gygi, S. P., and Goldberg, A. L. mTOR inhibition activates overall protein degradation by the ubiquitin proteasome system as well as by autophagy. *Proc. Natl. Acad. Sci.*, 112(52):15790–15797, 2015. ISSN 0027-8424.

Zhao, Y., Tan, E. K., Law, H. Y., Yoon, C. S., Wong, M. C., and Ng, I. Prevalence and ethnic differences of autosomal-dominant cerebellar ataxia in Singapore. *Clin. Genet.*, 62(6):478–481, 2002. ISSN 00099163.

Zhong, X. and Pittman, R. N. Ataxin-3 binds VCP/p97 and regulates retrotranslocation of ERAD substrates. *Hum. Mol. Genet.*, 15(16):2409–2420, aug 2006. ISSN 0964-6906.

Zhou, Y. F., Liao, S. S., Luo, Y. Y., Tang, J. G., Wang, J. L., Lei, L. F., Chi, J. W., Du, J., Jiang, H., Xia, K., Tang, B. S., and Shen, L. SUMO-1 Modification on K166 of PolyQ-Expanded aTaxin-3 Strengthens Its Stability and Increases Its Cytotoxicity. *PLoS One*, 8(1): e54214, jan 2013. ISSN 19326203.

Zhou, Y.-X., Qiao, W.-H., Gu, W.-H., Xie, H., Tang, B.-S., Zhou, L.-S., Yang, B.-X., Takiyama, Y., Tsuji, S., He, H.-Y., Deng, C.-X., Goldfarb, L. G., and Wang, G.-X. Spinocerebellar Ataxia Type 1 in China. *Arch. Neurol.*, 58(5):789, may 2001. ISSN 0003-9942.

Zhou, Z., Luo, A., Shrivastava, I., He, M., Huang, Y., Bahar, I., Liu, Z., and Wan, Y. Regulation of XIAP Turnover Reveals a Role for USP11 in Promotion of Tumorigenesis. *EBioMedicine*, 15:48–61, feb 2017. ISSN 2352-3964.

Zhuchenko, O., Bailey, J., Bonnen, P., Ashizawa, T., Stockton, D. W., Amos, C., Dobyns, W. B., Subramony, S. H., Zoghbi, H. Y., and Lee, C. C. Autosomal dominant cerebellar ataxia (SCA6) associated with small polyglutamine expansions in the α(1A)-voltage-dependent calcium channel, jan 1997. ISSN 10614036.

Zoghbi, H. Y. and Orr, H. T. Glutamine Repeats and Neurodegeneration. *Annu. Rev. Neurosci.*, 23(1):217–247, mar 2000. ISSN 0147-006X.

Zühlke, C. H., Spranger, M., Spranger, S., Voigt, R., Lanz, M., Gehlken, U., Hinrichs, F., and Schwinger, E. SCA17 caused by homozygous repeat expansion in TBP due to partial isodisomy 6. *Eur. J. Hum. Genet.*, 11(8):629–632, aug 2003. ISSN 10184813.

Ōmura, S. and Crump, A. Lactacystin: first-in-class proteasome inhibitor still excelling and an exemplar for future antibiotic research, apr 2019. ISSN 18811469.

A | Supplementary results

A.1 Detailed results of the interaction of ataxin-3 isoforms with other proteins

Table A.1. Interaction of ataxin-3 isoforms with other proteins. This table lists detailed results of the SILAC tandem MS analysis for isoform-specific ataxin-3 interaction partners. All results are displayed as pair-wise comparisons between ataxin-3c and ataxin-3aL, ataxin-3c and ataxin-3aS and ataxin-3aL and ataxin-3aS. If more than one gene name ist listed, the SILAC tandem MS approach did not allow for a more specific identification. Table modified from Weishäupl et al. (2019), available for use via `https://doi.org/10.1074/jbc.RA118.005801` under the CC BY 4.0 license (`https://creativecommons.org/licenses/by/4.0/`).

Gene	**ataxin-3c vs. ataxin-3aL**		**ataxin-3c vs. ataxin-3aS**		**ataxin-3aL vs. ataxin-3aS**	
name	-log p-value	difference	-log p-value	difference	-log p-value	difference
ACACA	2.61	1.04	3.38	1.94	3.70	0.82
ACLY	0.73	0.24	0.61	0.36	0.34	0.16
ACOT9	1.51	-1.50	1.31	-2.27	0.65	-0.56
ACTA1;ACTC1;ACTG2	0.65	0.43	0.21	0.49	0.05	0.09
ACTA2	2.82	0.55	2.17	0.93	1.33	0.24
ACTG1;ACTB	3.45	0.57	3.55	1.00	2.69	0.43
ACTN1	1.55	0.37	1.55	0.89	1.89	0.40
ACTN4	1.06	0.41	1.34	0.81	2.84	0.42
ACTR1A	0.36	0.26	0.06	0.02	0.61	-0.17
AHCY	4.55	1.31	3.02	2.18	3.09	0.93
AIFM1	1.17	0.16	1.30	0.33	1.39	0.27
AIMP2	0.65	0.23	0.39	0.37	0.07	0.04
ALDOA	0.29	0.06	1.31	0.57	2.30	0.51
AMOT	1.24	0.94	1.27	1.24	1.00	0.37
ANP32A;ANP32B	1.43	0.12	0.49	0.42	0.47	0.28
ARCN1	3.14	1.46	2.59	1.29	0.10	-0.01
ASNA1	3.50	1.26	2.61	2.26	2.94	1.13
ATP1A1	1.45	1.11	0.95	1.54	0.72	0.58
ATP2A2;ATP2A3	3.92	0.97	3.93	1.39	3.21	0.32

Continued on next page

Table A.1. Interaction of ataxin-3 isoforms with other proteins. – *Continued from previous page*

Gene	**ataxin-3c vs. ataxin-3aL**		**ataxin-3c vs. ataxin-3aS**		**ataxin-3aL vs. ataxin-3aS**	
name	-log p-value	difference	-log p-value	difference	-log p-value	difference
ATP5A1	3.64	0.97	4.73	1.25	3.22	0.29
ATP5B	4.60	0.69	3.75	0.57	0.96	-0.09
ATP5C1	3.35	0.52	0.01	-0.01	0.57	-0.28
ATP5F1	5.39	0.75	1.70	0.89	0.32	0.04
ATP5J2	1.31	0.66	0.93	0.67	0.21	-0.28
ATP5O	2.98	0.94	3.08	1.92	3.04	0.79
ATXN2L	4.02	-0.07	1.10	-0.08	1.23	-0.10
ATXN3	4.97	1.94	1.96	1.54	1.12	-0.60
BAG2	0.64	1.15	0.46	0.35	1.49	-0.66
BAG5	3.95	1.59	2.38	1.75	0.09	0.01
BAG6	0.80	0.80	0.87	1.50	0.47	0.35
BCAP31	1.48	-0.83	1.00	-0.98	0.39	0.10
BIRC2	1.83	-0.91	2.06	-1.29	0.35	-0.31
BYSL	1.01	0.15	0.04	0.01	0.39	-0.13
C14orf166	2.36	0.64	2.67	0.93	3.71	0.50
C1QBP	1.87	1.84	0.93	1.07	0.80	-0.75
C2orf47	3.74	0.91	3.69	2.07	3.18	1.17
CAD	5.28	0.98	4.03	1.34	2.26	0.39
CANX	0.25	0.19	4.29	4.40	2.95	5.25
CASP7	2.22	0.42	3.37	1.00	3.35	0.40
CCT2	2.61	0.48	2.41	0.83	2.25	0.35
CCT3	2.18	0.44	4.68	0.97	3.61	0.50
CCT4	2.12	0.53	2.76	0.97	2.44	0.43

Continued on next page

Table A.1. Interaction of ataxin-3 isoforms with other proteins. – *Continued from previous page*

Gene	**ataxin-3c vs. ataxin-3aL**		**ataxin-3c vs. ataxin-3aS**		**ataxin-3aL vs. ataxin-3aS**	
name	-log p-value	difference	-log p-value	difference	-log p-value	difference
CCT5	2.36	0.48	3.69	1.09	2.82	0.46
CCT6A	2.19	0.43	3.30	0.83	3.47	0.42
CCT7	2.38	0.48	3.52	0.98	3.16	0.44
CCT8	0.07	-0.10	0.98	0.79	0.42	0.19
CFL1	0.03	0.04	0.20	0.31	1.75	0.23
CKB	1.97	0.78	3.11	1.25	3.15	0.55
CLTC	0.89	0.23	1.33	0.67	1.47	0.41
COPA	1.92	0.51	1.90	0.60	0.89	0.17
CSE1L	2.28	2.72	1.07	2.54	0.19	0.45
CYC1	3.63	0.71	2.46	1.03	1.35	0.25
CYFIP1	1.31	0.29	1.93	0.53	2.29	0.20
DARS	1.72	1.47	2.70	3.55	5.77	1.67
DBT	0.93	0.14	0.72	0.34	0.78	0.15
DCTN2	0.27	0.32	0.55	1.35	0.47	0.59
DDB1	6.35	1.17	2.39	1.78	1.11	0.59
DDX6	1.32	-0.68	0.17	-0.21	0.91	0.40
DIABLO	1.82	0.64	2.35	1.99	5.59	1.19
DLD	1.35	0.54	3.09	1.97	4.50	1.41
DLST	2.90	1.63	2.57	2.16	2.69	0.61
DNAJA1	1.91	1.67	1.63	2.39	1.36	0.62
DNAJA2	0.87	1.68	1.30	2.71	3.44	0.65
DNAJA3	4.94	2.46	3.26	3.18	2.46	0.73
DNAJB6;DNAJB3;DNAJB7	0.18	0.36	1.24	-0.73	0.10	-0.24

Continued on next page

Table A.1. Interaction of ataxin-3 isoforms with other proteins. – *Continued from previous page*

Gene	**ataxin-3c vs. ataxin-3aL**		**ataxin-3c vs. ataxin-3aS**		**ataxin-3aL vs. ataxin-3aS**	
name	-log p-value	difference	-log p-value	difference	-log p-value	difference
DNAJC7	4.21	1.27	1.89	2.28	1.46	0.74
DPM1	1.92	2.56	1.57	3.43	1.02	0.56
DSG1	0.69	0.39	0.31	0.22	0.01	-0.01
DSP	1.02	-2.53	0.01	-0.16	1.68	-2.16
DYNC1H1	3.03	0.80	3.75	1.94	3.74	0.97
EEF1A1P5;EEF1A1	1.46	0.45	2.33	1.05	3.89	0.59
EEF1A2	1.47	0.47	2.65	1.16	2.32	0.61
EEF1B2	1.93	0.58	2.27	1.29	3.25	0.54
EEF1D	1.07	0.47	1.95	1.05	1.92	0.24
EEF1G	0.58	-0.29	0.46	-0.27	0.08	0.05
EEF2	1.68	0.44	2.59	1.03	2.18	0.41
EFTUD2	1.27	0.75	0.24	0.35	0.70	-0.42
EIF3A	1.41	0.57	1.24	1.16	1.32	0.76
EIF4A1;EIF4A2	0.31	0.12	0.25	0.24	0.19	0.05
EIF4G1	0.57	0.38	0.54	0.53	0.38	0.12
ENAH	2.30	0.55	3.60	1.11	3.35	0.56
ENO1	1.11	0.71	0.62	0.82	0.10	0.04
EPRS	0.08	-0.09	0.02	-0.10	0.12	-0.28
FAF2	2.27	1.13	1.78	1.64	3.12	0.67
FAM115A	0.88	1.27	1.47	3.49	1.74	1.62
FAM195B	1.64	0.45	1.75	0.86	1.00	0.27
FANCI	1.96	0.54	1.83	0.76	0.94	0.51
FASN	1.08	0.71	1.29	1.30	1.02	0.45

Continued on next page

Table A.1. Interaction of ataxin-3 isoforms with other proteins. – *Continued from previous page*

Gene	ataxin-3c vs. ataxin-3aL		ataxin-3c vs. ataxin-3aS		ataxin-3aL vs. ataxin-3aS	
name	-log p-value	difference	-log p-value	difference	-log p-value	difference
FLNA	0.55	0.26	0.39	0.39	0.00	0.00
GANAB	1.78	0.75	1.85	1.37	1.27	0.58
GAPDH	1.47	0.56	0.98	0.53	0.62	0.17
GART	2.12	1.45	1.73	1.37	1.73	-0.24
GCN1L1	0.81	0.38	0.39	0.46	0.12	0.06
GET4	0.61	0.15	0.04	0.02	0.23	0.07
GNB2L1	1.70	0.98	1.51	1.07	0.58	0.36
GRPEL1	2.60	0.28	2.96	0.79	3.88	0.49
GTF2I	1.69	2.41	1.55	3.15	1.47	0.54
HAGH	0.23	0.34	0.28	0.55	0.79	0.37
HAX1	0.61	1.89	0.23	0.93	1.87	-0.67
HNRNPA1;HNRNPA1L2	2.91	0.69	1.30	0.95	0.12	0.05
HNRNPA2B1	0.11	-0.14	0.05	-0.12	0.01	-0.01
HNRNPH1;HNRNPH2	1.23	-1.55	1.60	-1.68	0.35	-0.03
HNRNPK	0.26	-0.37	0.16	-0.33	0.68	0.16
HNRNPL	2.26	0.61	2.83	1.22	2.61	0.52
HNRNPM	2.61	1.89	2.48	2.43	2.16	0.43
HNRNPU	2.69	0.45	3.44	0.93	2.79	0.35
HSD17B12	3.94	0.64	5.08	1.17	3.56	0.49
HSP90AA1	1.84	0.35	1.95	0.57	2.15	0.22
HSP90AB1	0.66	0.56	1.48	0.31	0.15	-0.19
HSP90AB2P	0.90	0.28	1.17	0.32	0.02	-0.01
HSP90B1	0.47	0.39	0.89	-0.20	0.45	-0.41

Continued on next page

Table A.1. Interaction of ataxin-3 isoforms with other proteins. – *Continued from previous page*

Gene	**ataxin-3c vs. ataxin-3aL**		**ataxin-3c vs. ataxin-3aS**		**ataxin-3aL vs. ataxin-3aS**	
name	-log p-value	difference	-log p-value	difference	-log p-value	difference
HSPA1A	1.81	0.24	2.01	0.51	0.97	0.09
HSPA1L	2.42	0.14	0.56	0.15	0.51	-0.07
HSPA4	2.33	0.21	2.49	0.23	3.43	-0.13
HSPA4L	0.04	-0.01	0.95	0.48	0.44	0.24
HSPA5	2.31	0.23	2.13	0.62	1.25	0.30
HSPA6	0.01	0.00	0.01	0.00	1.69	-0.12
HSPA8	2.88	1.91	2.21	2.04	0.03	-0.02
HSPA9	1.70	0.57	0.88	0.52	0.52	-0.07
HSPB1	1.35	1.00	0.86	1.56	1.31	0.32
HSPD1	1.86	0.23	2.40	0.36	0.38	0.05
HSPE1	0.31	0.49	0.48	0.75	0.57	0.21
HSPH1	2.25	0.36	3.14	0.78	2.11	0.44
HUWE1	2.00	0.40	1.70	1.81	1.37	1.42
IARS	1.29	0.81	0.55	0.99	0.02	-0.01
IMPDH2	0.44	0.18	1.53	0.76	1.63	0.46
IPO7	0.95	2.06	1.35	2.98	1.32	0.22
IQGAP1	1.53	0.57	0.92	0.90	0.89	0.47
IRS4	0.87	0.83	0.39	1.15	0.36	0.29
KARS	0.60	0.42	0.92	0.99	0.45	0.57
KDELR1	0.24	0.91	0.50	1.76	0.10	0.50
KPNB1	0.00	0.00	0.90	0.07	0.07	-0.02
KRT2	1.54	1.44	1.46	2.95	1.34	1.04
LAMA4	2.19	0.46	1.21	1.12	2.20	0.73

Continued on next page

Table A.1. Interaction of ataxin-3 isoforms with other proteins. – *Continued from previous page*

Gene	ataxin-3c vs. ataxin-3aL		ataxin-3c vs. ataxin-3aS		ataxin-3aL vs. ataxin-3aS	
name	-log p-value	difference	-log p-value	difference	-log p-value	difference
LAMP2	2.06	0.28	2.67	0.58	1.26	0.28
LANCL1	2.07	0.92	1.92	1.90	0.77	0.35
LARS	3.38	1.04	3.57	1.89	3.15	0.82
LDHB	1.64	1.71	1.84	2.23	0.99	0.58
LSM12	0.74	1.06	0.93	1.67	1.42	0.56
MAD2L1	2.34	0.66	2.96	1.09	1.72	0.34
MAGED1	0.30	-0.08	0.08	0.11	0.25	0.26
MARS	5.46	0.83	4.47	1.65	4.22	0.83
MCMBP	0.02	0.01	0.86	0.23	1.26	0.41
MIF	2.08	0.39	2.25	0.63	1.77	0.24
MYH10	1.74	0.42	1.99	0.66	0.72	0.30
MYH9	3.06	0.92	2.28	1.68	2.27	0.77
MYL12A;MYL12B	1.28	0.44	1.53	0.54	0.24	0.09
MYL9	3.95	1.49	4.55	2.19	5.83	0.86
NAP1L1	2.49	-1.80	1.31	-2.02	0.43	-0.21
NCKAP1	0.45	0.18	1.40	0.69	1.62	0.38
NDUFA4	2.80	0.58	3.13	0.77	0.77	0.27
NGLY1	1.57	0.47	0.80	0.69	0.80	0.21
NME1	0.61	0.40	1.27	1.01	3.30	0.62
NME2;NME2P1	1.63	0.54	1.60	1.12	3.55	0.44
NONO	0.48	0.17	4.26	1.44	3.81	1.24
NPM1	0.13	0.05	0.31	-0.23	0.19	-0.04
NUFIP2	0.05	-0.06	0.18	0.29	1.97	0.34

Continued on next page

Table A.1. Interaction of ataxin-3 isoforms with other proteins. – *Continued from previous page*

Gene	**ataxin-3c vs. ataxin-3aL**		**ataxin-3c vs. ataxin-3aS**		**ataxin-3aL vs. ataxin-3aS**	
name	-log p-value	difference	-log p-value	difference	-log p-value	difference
OGDH	0.81	0.69	1.58	1.35	1.09	0.61
PAICS	3.63	1.48	4.36	3.11	4.33	1.50
PARP1	1.81	0.67	3.15	1.71	5.56	0.89
PC	1.11	0.55	0.96	1.13	1.17	0.79
PCBP1	0.40	0.30	0.13	0.18	0.18	-0.08
PCMT1	0.06	0.31	0.39	1.90	1.31	1.58
PDIA6	1.23	0.55	0.72	0.75	0.35	0.09
PFN1	3.71	0.71	2.55	1.21	1.84	0.45
PGAM5	3.83	0.50	3.61	1.11	2.86	0.43
PGK1	4.21	1.40	4.02	1.84	3.32	0.36
PHB	0.61	0.35	0.47	0.48	1.30	0.18
PHB2	0.20	0.13	0.60	0.38	0.24	0.09
PHGDH	1.04	0.42	0.63	0.46	0.04	0.01
PKM	0.92	0.28	1.15	0.56	0.74	0.14
POLDIP3	1.00	0.50	0.65	1.15	1.91	0.60
PPIA	2.56	0.38	1.03	0.60	0.35	0.12
PRDX1	0.66	0.57	0.87	0.95	1.80	0.43
PRDX2	5.72	0.60	2.69	1.17	3.50	0.58
PRDX3	0.98	0.47	1.11	0.88	0.80	0.31
PRDX4	2.16	0.32	1.82	0.59	0.85	0.20
PRKDC	0.24	-0.17	0.46	-0.41	0.01	-0.01
PRMT1	1.76	0.32	0.69	0.74	0.72	0.29
PRPF40A	2.04	0.69	1.92	1.32	2.56	0.85

Continued on next page

Table A.1. Interaction of ataxin-3 isoforms with other proteins. – *Continued from previous page*

Gene	ataxin-3c vs. ataxin-3aL		ataxin-3c vs. ataxin-3aS		ataxin-3aL vs. ataxin-3aS	
name	-log p-value	difference	-log p-value	difference	-log p-value	difference
PRPF8	0.32	0.11	0.31	0.23	1.74	0.18
PSAT1	0.91	0.13	2.02	0.48	2.56	0.36
PSMA1	2.40	0.23	1.66	0.65	1.65	0.35
PSMA4	1.32	0.28	4.89	0.73	1.67	0.30
PSMA5	1.34	0.23	1.61	0.48	1.59	0.31
PSMA6	2.35	0.72	2.80	1.40	3.73	0.65
PSMA7;PSMA8	0.25	0.12	0.50	0.41	0.82	0.20
PSMB1	0.96	0.27	1.81	0.53	1.79	0.35
PSMB2	1.56	0.50	1.32	1.08	2.73	0.37
PSMB4	0.66	0.28	0.63	0.60	0.12	0.08
PSMB5	1.18	0.19	0.53	0.44	1.28	0.49
PSMB6	0.83	-0.15	0.16	-0.12	0.05	-0.01
PSMC1	0.74	0.34	0.97	0.80	1.44	0.33
PSMC2	0.46	0.28	2.31	0.79	1.19	0.47
PSMC3	0.46	0.12	1.46	0.31	0.62	0.18
PSMC4	1.59	0.38	1.45	0.69	2.00	0.24
PSMC5	0.35	0.06	1.40	0.42	2.04	0.25
PSMC6	0.32	-0.20	0.47	-0.26	0.37	0.07
PSMD1	1.94	0.58	2.43	0.83	0.81	0.09
PSMD11	0.88	0.35	0.97	0.49	0.56	0.16
PSMD12	1.15	0.27	1.06	0.27	2.67	0.22
PSMD13	1.42	0.21	3.22	0.55	1.59	0.29
PSMD14	0.48	0.23	0.91	0.23	0.36	0.25

Continued on next page

Table A.1. Interaction of ataxin-3 isoforms with other proteins. – *Continued from previous page*

Gene	**ataxin-3c vs. ataxin-3aL**		**ataxin-3c vs. ataxin-3aS**		**ataxin-3aL vs. ataxin-3aS**	
name	-log p-value	difference	-log p-value	difference	-log p-value	difference
PSMD2	1.34	0.30	2.10	0.79	3.15	0.69
PSMD3	0.69	-0.12	0.61	0.20	1.11	0.25
PSMD4	1.74	0.89	1.12	1.38	1.41	0.53
PSMD6	0.82	-0.83	2.44	-1.82	2.60	-1.08
PSMD7	0.23	0.17	0.42	0.45	0.53	0.18
PTPLAD1	1.55	0.86	0.77	1.52	1.19	0.62
RAD23B	0.71	0.42	0.66	0.67	1.65	0.06
RAN	0.70	0.22	1.28	0.64	1.16	0.35
RANBP1	1.11	1.47	0.84	1.49	0.26	-0.30
RARS	2.12	0.77	3.14	1.46	1.74	0.54
RBBP4	0.71	0.21	0.91	0.39	1.87	0.33
RBFOX2;RBFOX1	0.14	0.14	0.70	0.99	0.78	0.78
RBFOX3	1.34	0.17	1.74	0.54	2.84	0.34
RBM25	2.14	0.28	3.39	0.89	3.13	0.42
RELA	1.08	0.46	1.55	1.03	0.74	0.52
RNF126	1.68	1.21	0.89	0.81	0.31	0.22
RPA1	1.55	0.61	3.81	1.65	3.34	0.83
RPA2	1.54	0.95	2.24	1.78	4.16	0.93
RPA3	2.94	0.58	2.35	1.30	1.39	0.35
RPL15	0.04	-0.02	0.66	0.80	1.44	0.89
RPL23	0.59	0.45	2.32	1.49	2.97	1.02
RPL38	0.56	0.41	2.89	1.17	2.30	0.78
RPN1	0.63	0.40	3.15	0.98	1.48	0.52

Continued on next page

Table A.1. Interaction of ataxin-3 isoforms with other proteins. – *Continued from previous page*

Gene	ataxin-3c vs. ataxin-3aL		ataxin-3c vs. ataxin-3aS		ataxin-3aL vs. ataxin-3aS	
name	-log p-value	difference	-log p-value	difference	-log p-value	difference
RPS10;RPS10P5	0.76	-0.34	4.08	0.97	1.45	1.06
RPS12	2.32	-0.27	1.62	0.69	1.18	0.80
RPS13	0.25	-0.44	0.40	0.40	1.65	0.82
RPS14	0.07	-0.09	0.91	0.83	1.19	0.82
RPS15A	0.55	0.35	2.13	1.15	3.61	0.90
RPS16	0.26	0.76	1.19	1.97	0.53	1.14
RPS19	0.97	0.42	2.21	1.26	3.54	0.64
RPS2	0.10	-0.10	2.04	0.51	1.20	0.68
RPS20	0.47	0.34	2.14	1.07	2.48	0.81
RPS27	0.01	-0.01	0.96	0.78	0.91	0.55
RPS3	0.41	0.42	3.01	1.16	1.63	0.64
RPS3A	0.03	0.08	2.60	0.80	0.17	0.39
RPS4X	2.18	0.83	2.82	1.66	3.98	0.76
RPS6	0.61	0.19	1.25	0.42	2.67	0.24
RPS8	0.14	0.51	0.68	-0.84	0.60	-1.52
RPS9	0.28	0.20	0.88	0.01	0.00	0.00
RPSA	0.61	-0.49	1.06	-0.88	0.60	-0.43
RUVBL1	0.91	1.64	1.17	3.26	1.16	1.23
S100A8	0.62	0.38	2.25	3.70	1.59	3.42
SARS	5.18	0.90	4.78	1.59	1.80	0.53
SDHA	0.95	0.35	1.65	0.45	2.12	0.18
SEC61A1	1.62	0.45	1.53	0.79	1.26	0.26
SEMG2	1.59	0.42	1.42	0.71	1.26	0.28

Continued on next page

Table A.1. Interaction of ataxin-3 isoforms with other proteins. – *Continued from previous page*

Gene	**ataxin-3c vs. ataxin-3aL**		**ataxin-3c vs. ataxin-3aS**		**ataxin-3aL vs. ataxin-3aS**	
name	-log p-value	difference	-log p-value	difference	-log p-value	difference
SET;SETSIP	3.40	0.73	1.91	0.62	1.66	0.18
SF3A3	1.77	0.53	0.54	0.91	0.03	-0.01
SF3B1	0.28	-0.36	0.23	-0.37	1.47	0.40
SF3B2	0.57	0.49	1.36	1.44	1.47	0.83
SF3B3	2.86	1.88	1.99	2.87	1.68	0.91
SF3B6	1.82	2.82	1.69	3.90	2.07	1.09
SFPQ	4.09	2.23	4.52	3.27	4.44	0.87
SLC1A5	4.25	2.16	4.29	3.05	3.81	0.84
SLC25A11	4.22	1.89	3.25	2.50	2.43	0.51
SLC25A22	3.66	1.36	2.55	2.04	2.23	0.80
SLC25A3	1.03	0.43	1.41	0.88	0.65	0.25
SLC25A5	0.22	0.29	0.10	0.32	0.15	-0.18
SLC25A6	2.06	0.67	1.46	1.23	1.19	0.59
SLC3A2	2.67	0.57	3.54	1.11	2.52	0.45
SNAP23	1.78	0.41	3.06	0.86	2.07	0.37
SNRNP200	0.85	-0.64	0.02	-0.03	0.31	-0.06
SNRPD2	1.74	1.50	1.01	2.07	0.94	0.82
SNRPD3	1.69	0.65	1.02	1.02	0.26	0.15
SNRPN;SNRPB	2.73	0.62	5.74	1.17	3.81	0.47
SSBP1	1.41	1.50	1.91	2.52	2.59	0.92
SSR4	1.25	0.34	2.65	0.93	2.33	0.32
STIP1	1.27	2.17	2.94	3.55	0.97	1.05
TCP1	1.09	0.73	0.68	0.78	0.77	0.21

Continued on next page

Table A.1. Interaction of ataxin-3 isoforms with other proteins. – *Continued from previous page*

Gene	ataxin-3c vs. ataxin-3aL		ataxin-3c vs. ataxin-3aS		ataxin-3aL vs. ataxin-3aS	
name	-log p-value	difference	-log p-value	difference	-log p-value	difference
TECR	0.74	0.79	0.60	0.80	0.40	0.18
TFG	1.44	-0.97	0.92	-1.19	0.25	0.17
TIMM50	1.52	0.50	1.78	0.97	2.88	0.35
TKT	2.38	2.07	3.56	2.93	1.92	0.79
TPI1	4.35	2.02	4.65	4.06	4.62	1.99
TRAF2	2.80	1.27	5.01	3.11	3.96	1.79
TRIM28	3.86	1.83	4.73	4.04	5.19	2.19
TUBA1A;TUBA3C	1.76	0.77	2.93	1.91	3.76	1.26
TUBA1B;TUBA4A	4.18	1.94	4.61	4.07	5.02	2.11
TUBA1C	2.96	1.59	4.00	3.49	4.57	2.01
TUBA3E	1.48	2.12	1.75	3.69	1.76	1.52
TUBB	0.15	0.18	0.43	0.65	2.41	0.46
TUBB2B;TUBB2A	1.03	0.58	0.08	0.05	1.24	-0.18
TUBB4A	0.63	0.23	1.70	0.68	2.23	0.35
TUBB4B	1.57	1.20	0.75	0.73	0.85	-0.25
brave TUBB8	1.91	-1.08	1.18	-1.51	0.79	-0.32
TXN	0.03	0.01	0.23	0.09	0.22	0.08
UBA1	0.66	0.25	0.80	0.34	0.65	0.13
UBB;UBC;RPS27A	0.12	0.04	2.53	-0.30	2.10	-0.44
UBL4A	0.08	0.03	1.01	0.56	1.75	0.44
UBR2	2.83	-0.12	0.08	-0.03	0.59	-0.15
USP7	3.36	0.87	2.75	1.29	3.40	0.52
VARS	1.89	0.40	3.56	1.05	4.34	0.47

Continued on next page

Table A.1. Interaction of ataxin-3 isoforms with other proteins. – *Continued from previous page*

Gene	**ataxin-3c vs. ataxin-3aL**		**ataxin-3c vs. ataxin-3aS**		**ataxin-3aL vs. ataxin-3aS**	
name	-log p-value	difference	-log p-value	difference	-log p-value	difference
VCP	1.14	0.26	1.47	0.54	2.88	0.24
VIM	1.60	-0.38	1.08	-0.43	0.32	-0.07
WDR87	0.95	0.56	1.69	1.04	1.57	0.34
XPO1	2.45	0.67	1.68	1.06	1.51	0.29
XRCC5	1.89	0.40	3.56	1.05	4.34	0.47
XRCC6	1.14	0.26	1.47	0.54	2.88	0.24
YTHDF2	1.60	-0.38	1.08	-0.43	0.32	-0.07
YWHAE	0.95	0.56	1.69	1.04	1.57	0.34
YWHAZ;YWHAQ; YWHAB	2.45	0.67	1.68	1.06	1.51	0.29

A.2 Confirmation of ataxin-3c stability under co-expression of ataxin-3 isoforms

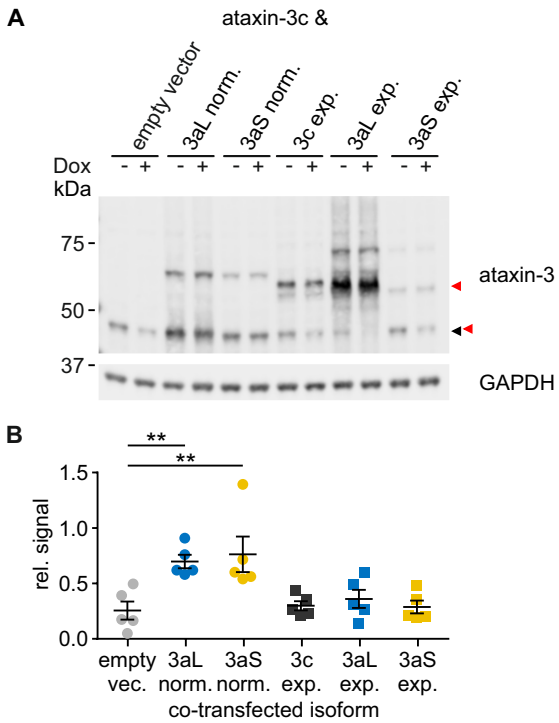

Figure A.1. Stability of ataxin-3c under co-expression with FLAG-V5-tagged ataxin-3 isoforms. (A) HEK293 *ATXN3* KO cells were transfected with pTRE-ataxin-3c (◀) and constitutively expressing ataxin-3 isoforms (pcDNA3.1-FLAG-ataixn-3-V5, ◀). Ataxin-3 expression was turned off using doxycycline at 24 h post transfection for 32 h. Cells were collected and samples were processed for western blot and immunostaining. Ataxin-3 was detected using the antibody 1H9. **(B)** Relative ataxin-3 signals after 32 h. Ataxin-3c is stabilized by an co-expression of ataxin-3aL and -3aS compared to an expression of ataxin-3c alone (Kruskal-Wallis test with Dunnett's test, ** $p < 0.01$, $n = 5$). Figure was modified from Weishäupl et al. (2019), available for use via `https://doi.org/10.1074/jbc.RA118.005801` under the CC BY 4.0 license (`https://creativecommons.org/licenses/by/4.0/`).

A.3 Detailed cloning strategy for the generation of zebrafish expression vectors

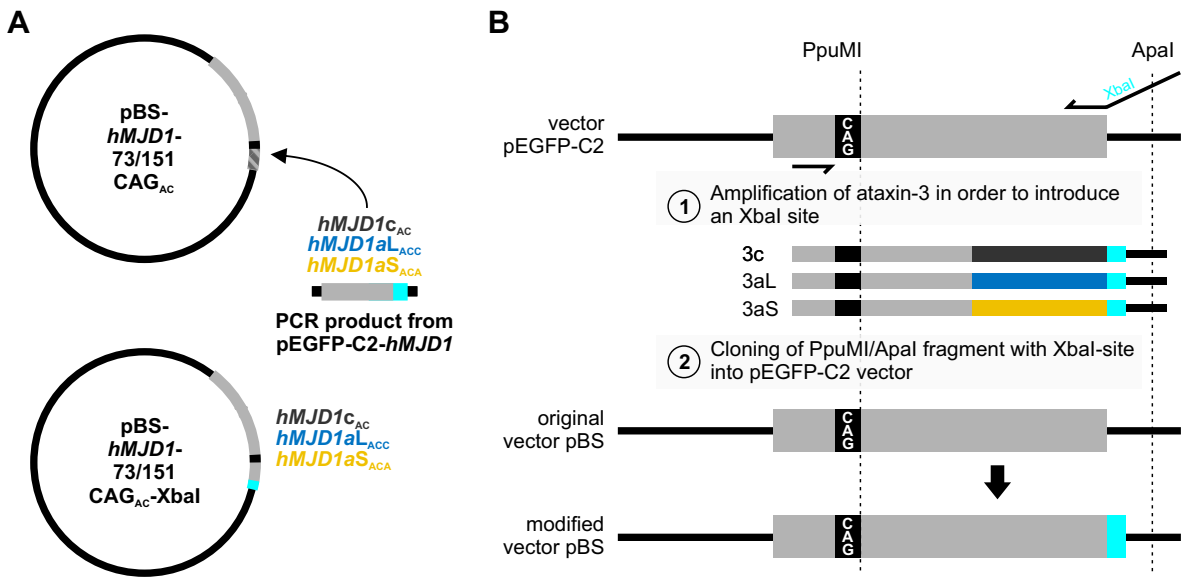

Figure A.2. Cloning strategy for the generation of expanded pBS-*hMJD* constructs.
A & B The XbaI site was introduced into the pBS*hMJD1*-73/151CAG$_{AC}$ constructs by the introduction of a PCR product containing the respective ataxin-3 isoform followed by the XbaI site. The 3' site of the ataxin-3 **cDNA!** (**cDNA!**) was amplified from pEGFP-C2-*hMJD1*-73/151CAG$_{AC}$ using the primers R058 and R059. The PCR product was then introduced into the pBluescript vector via the PpuMI/ApaI site in a subsequent step.

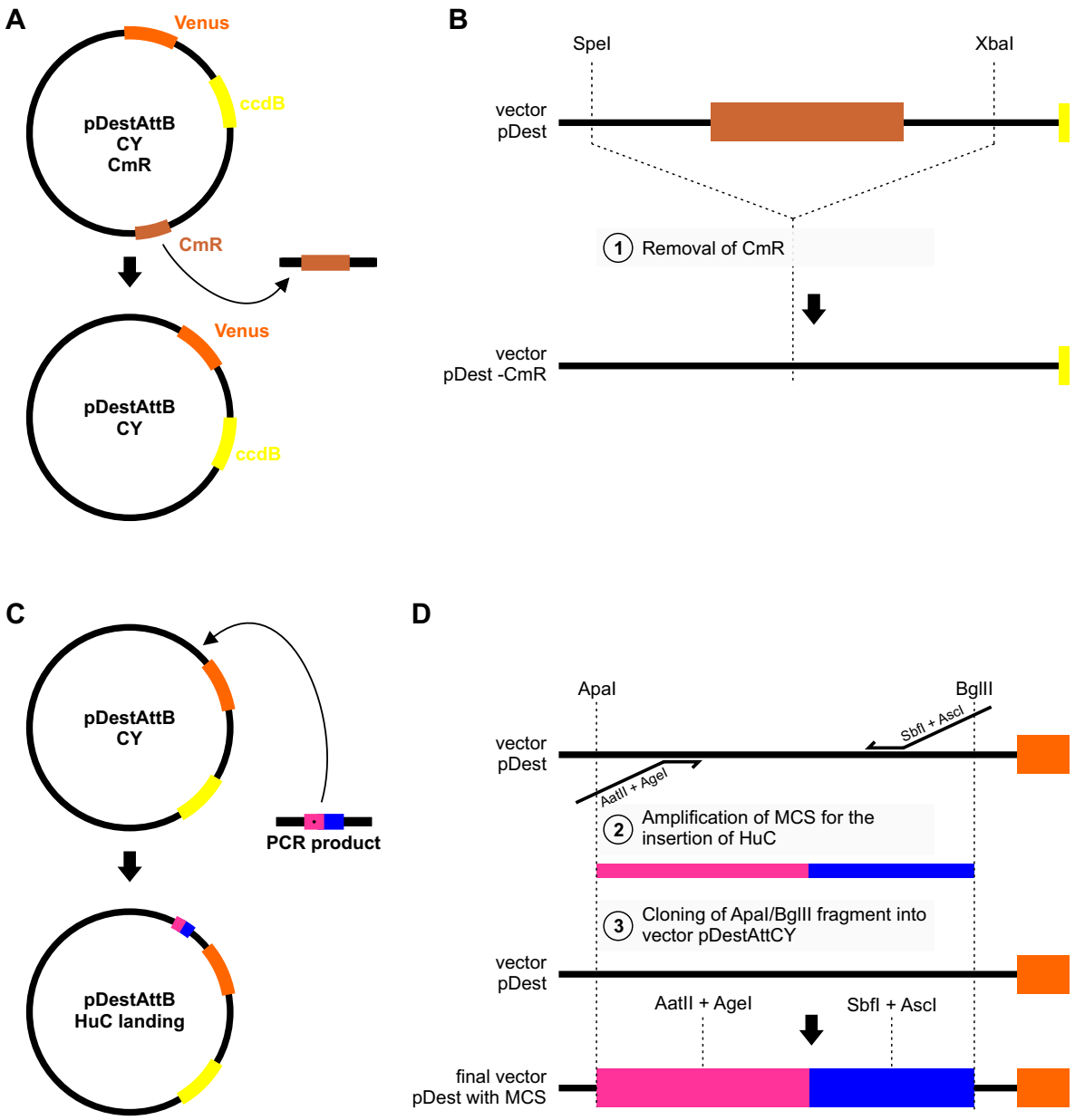

Figure A.3. Cloning strategy for the generation of vector pDestAttB-CY-HUC-insertion. **A & B** In order to introduce a multiple cloing site (MCS) containing a recognition motif for AatII, AgeI, SbfI and AscI into the pDestAttB-CY vector (CmR) was removed by a SpeI and XbaI digestion in a fist step. **C & D** The multiple cloning site was subsequently amplified from the vector using the primers Q436 und Q437 containing the respective recognition motifs. The PCR product was then introduced into the pDestAttB-CY vector using the ApaI and BglII sites resulting in the pDestAttB-HuC_landing vector.

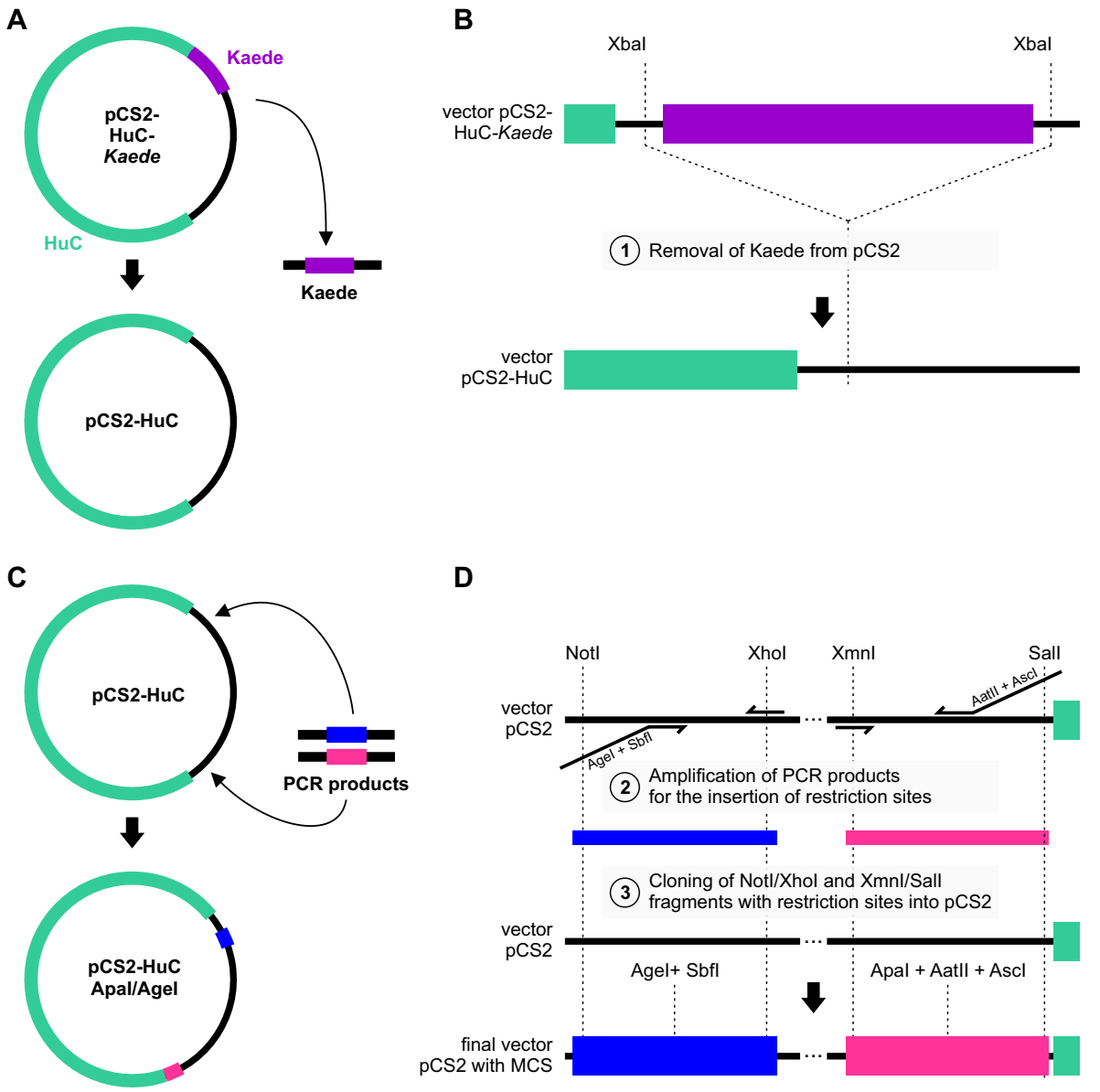

Figure A.4. Cloning strategy for the generation of vector pCS2-HuC A & B In order to transfer the HuC promoter from the pCS2 vector into the pDestAttB vector Kaede was removed in a first step using the XbaI site resulting in the vector pCS2-HuC. **C & D** Two multiple cloning sites (MCS) were introduced 5' and 3' of HuC in the pCS2-HuC vector. One site containing motifs for AgeI and SbfI and another site with motifs for AatII and AscI were amplified using the primers Q583/Q439 and Q517/Q518 from the pCS2-HuC vector and subsequently cloned into the vector using AgeI/SbfI and ApaI/AscI which created the pCS2-HuC-ApaI/AgeI vector for the cloning of HuC into the pDestAttB vector.

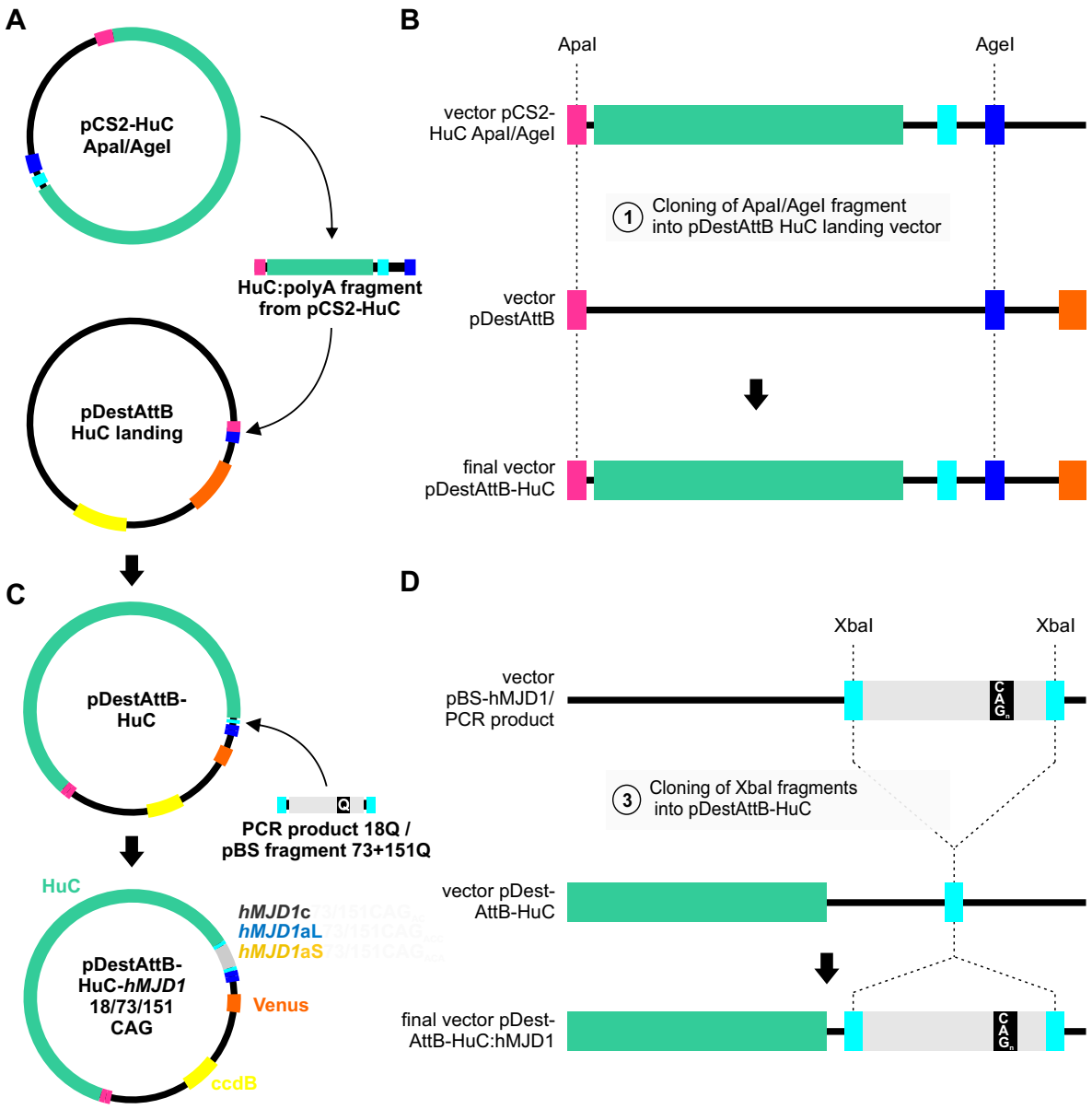

Figure A.5. Cloning strategy for the generation of vector pDestAttB-HuC:*hMJD1*. A & B HuC was introduced into the vector pDestAttB-HuC_landing vector from pCS2-HuC-ApaI/AgeI using the ApaI and AgeI site resulting in the vector pDestAttB-HuC. **C & D** Ataxin-3 was introduced into the vector pDestAttB-HuC as a PCR product for 18Q (primers Q822 und Q824) or a fragment from the vector pBS*hMJD1*-73/151CAG$_{AC}$ for 73Q and 151Q using the PCR-attached or introduced XbaI sites. Introduction of ataxin-3 into the vector pDestAttB-HuC resulted in the final expression vectors pDestAttB-HuC-*hMJD1*-18CAG$_{GG}$, pDestAttB-HuC-*hMJD1*-73CAG$_{AC}$ and pDestAttB-HuC-*hMJD1*-151CAG$_{AC}$

A.4 Analysis of the polyCAG repeat size of the MJD zebrafish model

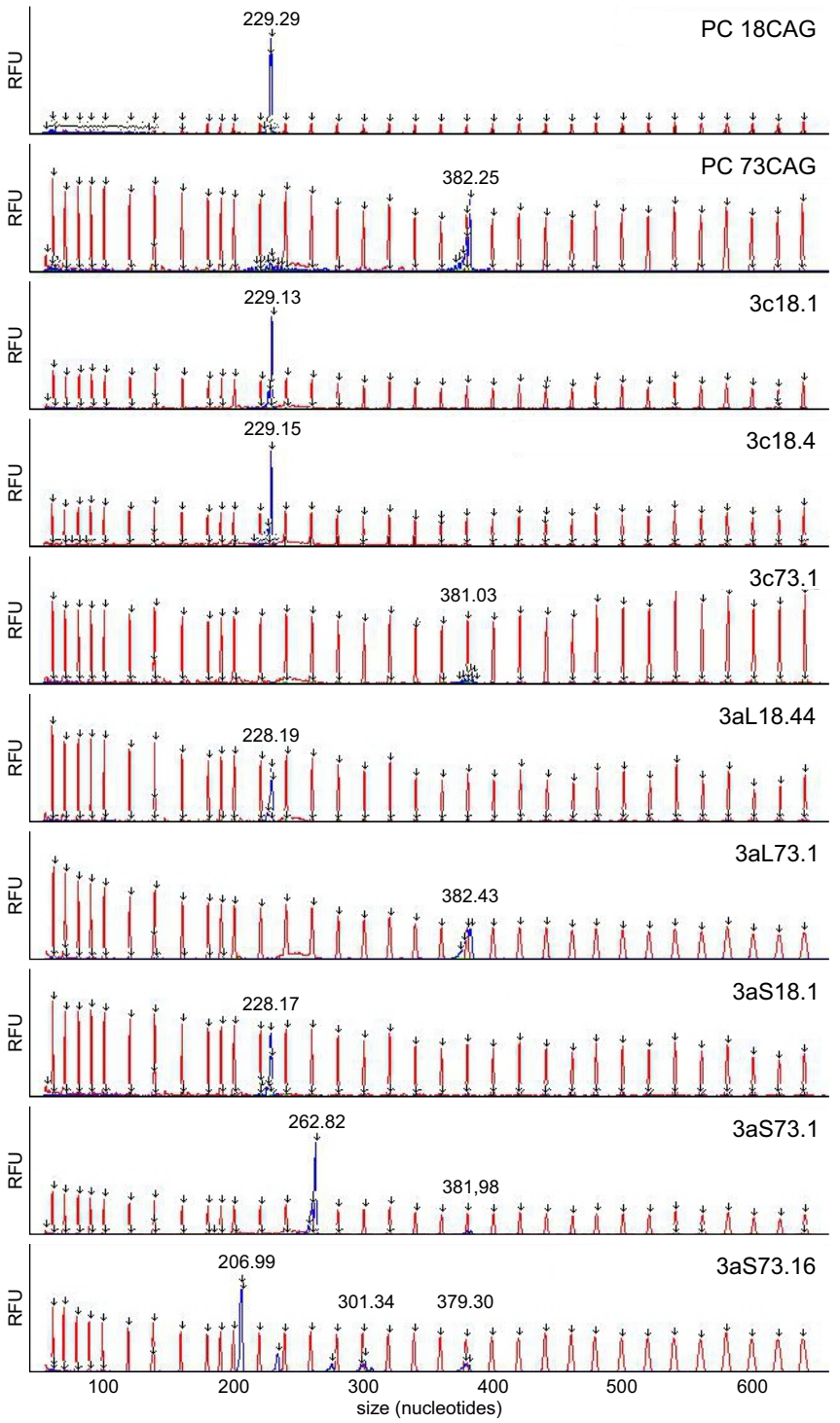

Figure A.6. Verification of the *ATXN3* CAG repeat length in transgenic zebrafish using fragment length analysis. The CAG repeat length of the zebrafish lines was analyzed by Fragment Length Analysis of the R100/R888 PCR products. 18 and 73CAG ataxin-3c and -3aL lines as well as the 18CAG ataxin-3aS line carry the expected CAG repeat length. Both 73CAG ataxin-3aS lines show a mixed CAG repeat length with a comparably weak peak for 72 or 73 CAG repeats. This indicates a mosaic of the CAG repeat length in these lines.

A.5 Summary of ataxin-3 isoform-specific characteristics

Table A.2. Summary of ataxin-3 characteristics. This table summarizes the ataxin-3 characteristics for normal and pathologically expanded ataxin-3 isoforms. A, autophagy; P, ubiquitin-proteasome system; n. d., not determined.

	normal			expanded		
Factor	3c	3aL	3aS	3c	3aL	3aS
Protein level	↑	↑	↓↓	↑	↓↓	↓↓
mRNA level	⟶	⟶	⟶	⟶	⟶	⟶
Half-life	⟶	⟶	↓	↑	↑	↑
Degradation pathway	A	A	A/P	n. d.	n. d.	n. d.
DUB activity	↓	⟶	⟶	n. d.	n. d.	n. d.
Nuclear localization	↓	↑	↑	↓	↑	↑
HR23B interaction	⟶	⟶	↓	n. d.	n. d.	n. d.
UBR2 interaction	↑	⟶	⟶	n. d.	n. d.	n. d.
α-tubulin interaction	↓	↑	↑↑	n. d.	n. d.	n. d.
caspase 7 interaction	⟶	⟶	↑↑	n. d.	n. d.	n. d.
VCP interaction	⟶	⟶	⟶	n. d.	n. d.	n. d.
ubiquitin interaction	↓	↑	↑	n. d.	n. d.	n. d.
XIAP interaction	⟶	⟶	⟶	n. d.	n. d.	n. d.
parkin interaction	↓	↑	↑	n. d.	n. d.	n. d.
Transcription regulation	⟶	⟶	⟶	⟶	⟶	⟶
Toxicity	⟶	⟶	⟶	⟶	⟶	⟶
Aggregation (amount)	⟶	⟶	⟶	↑↑	↑	↑↑
Aggregation (cinetic)	⟶	⟶	⟶	↑	↑↑	↑↑
Aggregation (size)	n. d.	n. d.	n. d.	↑	↓	↑
Aggregation (number)	n. d.	n. d.	n. d.	⟶	↑	⟶
Fragmentation by Ca^{2+} influx	⟶	⟶	⟶	⟶	⟶	⟶
Calpain-I substrate	⟶	⟶	⟶	⟶	⟶	⟶
Cleavage increases aggregation	n. d.	n. d.	n. d.	↑	⟶	⟶
Effect on co-degradation	↑	↑	↑	↑	⟶	⟶
Effect on co-aggregation	↓	↓	↓	n. d.	n. d.	n. d.

B | Scripts

B.1 Analysis of DUB activity

This Matlab code calculates the DUB acitivity of ataxin-3 isoforms from the data of the ubiquitin-rhodamine-110 assay (see 4.1.4, page 84). The code requires a text file with the data as well as a text file describing the sample positions called *WellsUsed.txt*)

```
function [ds] = UbRhoAssay_single_all(timepoints, export_status)
% This function plots the RFU over time and calculates the initial velocity
% by fitting a linear function to the datapoints of the first 2 minutes.
% It exports a graph without fit, a graph with the fit as well as a zoomed
% graph with the fit.
%
% timepoints: specify the timepoints for the measurement in the following
% order: [no. of measurements + 1, time between measurements],
% e.g. [181, 0.167] for a 30 min timeseries with a measurement every
% 10 seconds. Plus 1 is necessary due to the intital measurement at 0 seconds.
%
% export_status: 0 no export of data, 1 export data
%
% The function requires a text file (WellsUsex.txt) specifying the position of
% samples
% (including replicates) on the plate in the following example format:
% Protein1, Protein2, Protein3, Protein4
% A01, A03, A05, A07
% B01, B03, B05, B07
% C01, C03, C05, C07

% Select file to analyze
[datafile path] = uigetfile('*.txt', 'Select the datafile');
cd(path);

% Import data
Data = importdata(datafile, ',', 1);

% Assign values
Well = Data.textdata(2:end, 1);
Signal = Data.data;

% Load WellsUsed in order to assign the values to the protein
```

```
WellsUsed = readtable('WellsUsed.txt');
reads = height(WellsUsed);
WellsUsed = table2cell(WellsUsed);

% Create timestamp
Time = [0:timepoints(2):(timepoints(1)*timepoints(2)-timepoints(2))];

% Loop through values and assign the signal
for i = 1:6
for j = 1:reads
Well_IDs{j,i} = strmatch(WellsUsed(j,i), Well);
Result_Data{j, i} = Signal(Well_IDs{j, i});
end
end

% Create empty matrix
Data3c = [];
Data3alang = [];
Data3akurz = [];
DataBuffer = [];
DataGST = [];
DataUSP2Core = [];

% Assign data to the matrix for every read
for i = 1:reads
Data3c = [Data3c; Result_Data{i, 1}];
Data3alang = [Data3alang; Result_Data{i, 2}];
Data3akurz = [Data3akurz; Result_Data{i, 3}];
DataBuffer = [DataBuffer; Result_Data{i, 4}];
DataGST = [DataGST; Result_Data{i, 5}];
DataUSP2Core = [DataUSP2Core; Result_Data{i, 6}];
end

% Create a Dataset contaiing all assay conditions
Dataset = mat2dataset(Data3c);
Dataset.Data3alang = Data3alang;
Dataset.Data3akurz = Data3akurz;
Dataset.DataBuffer = DataBuffer;
Dataset.DataGST = DataGST;
Dataset.DataUSP2Core = DataUSP2Core;
Dataset.Timepoints = [Time'; Time'; Time'];

% Summarize data
summary = grpstats(Dataset, 'Timepoints', {'mean'});
summary.GroupCount = [];

% Rename columns in the summary
summary.Properties.VarNames = {'Timepoint' 'Ataxin3c_15Q_GG' 'Ataxin3a_long_15Q_GGC'
    'Ataxin3a_short_15Q_GGA' 'Assay_Buffer' 'GST' 'USP2Core'};
```

```
82
83 % Create a short summary with each 6th value (every minute)
84 summary_short = summary(1:6:181,:);
85
86 % Create an import summary for other plotting software
87 max_time = int8(Time(end)+1);
88 import_summary = [repeat({'Ataxin3c'}, max_time)'; repeat({'Ataxin3along'},
       max_time)'; repeat({'Ataxin3ashort'}, max_time)'; repeat({'Buffer'}, max_time)';
       repeat({'GST'}, max_time)'; repeat({'USP2Core'}, max_time)'];
89 import_summary(:,2) = [num2cell(round(summary_short.Ataxin3c_15Q_GG));
       num2cell(round(summary_short.Ataxin3a_long_15Q_GGC));
       num2cell(round(summary_short.Ataxin3a_short_15Q_GGA));
       num2cell(round(summary_short.Assay_Buffer)); num2cell(round(summary_short.GST));
       num2cell(round(summary_short.USP2Core))];
90 import_summary(:,3) = [num2cell(Time(1:6:181))' ; num2cell(Time(1:6:181))' ;
       num2cell(Time(1:6:181))'; num2cell(Time(1:6:181))'; num2cell(Time(1:6:181))';
       num2cell(Time(1:6:181))'];
91 import_summary = cell2table(import_summary);
92 import_summary.Properties.VariableNames = {'Sample', 'Signal', 'Timepoint'};
93
94
95 % Fit lines to initial values
96 Ataxin3c_fit_line = fit(summary.Timepoint(1:18), summary.Ataxin3c_15Q_GG(1:18),
       'poly1');
97 Ataxin3c_gradient = Ataxin3c_fit_line.p1;
98 Ataxin3alang_fit_line = fit(summary.Timepoint(1:18),
       summary.Ataxin3a_long_15Q_GGC(1:18), 'poly1');
99 Ataxin3alang_gradient = Ataxin3alang_fit_line.p1;
100 Ataxin3akurz_fit_line = fit(summary.Timepoint(1:18),
       summary.Ataxin3a_short_15Q_GGA(1:18), 'poly1');
101 Ataxin3akurz_gradient = Ataxin3akurz_fit_line.p1;
102
103 % Analyze gradients (initial velocity)
104 gradients = [Ataxin3c_gradient, Ataxin3alang_gradient, Ataxin3akurz_gradient];
105 gradients = mat2dataset(gradients);
106 gradients.Properties.VarNames = {'Ataxin3c_15Q_GG' 'Ataxin3a_long_15Q_GGC'
       'Ataxin3a_short_15Q_GGA'};
107
108 % Export of data
109 if export_status == 1
110
111 disp('Exporting data files...');
112 export(summary, 'File', 'Assay Summary.txt', 'WriteVarNames', true); % full annotated
       summary of the assay
113 export(summary_short, 'File', 'Assay Summary_short.txt', 'WriteVarNames', true); %
       short annotated summary of the assay
114 export(summary_short, 'XLSfile','Assay Summary_short.xlsx'); % Additional Excel-file
115 export(gradients, 'File', 'Assay gradients.txt', 'WriteVarNames', true); % calculated
       initial velocities
```

```
writetable(import_summary, 'Import Summary.txt'); % Summary for plotting in other
    software

end

% Plotting
% Create figure without fit
Colors = {[0 0 0], [237/256 45/256 46/256], [0 140/256 71/256], ...
[24/256 89/256 169/256], [243/256 125/256 34/256], ...
[102/256 44/256 145/256], [161/256 29/256 32/256], ...
[179/256 56/256 147/256]}

disp('Create figure without fit')
h.figure = figure;
plot(summary.Timepoint, summary.Ataxin3c_15Q_GG, 'Color', Colors{2}, 'LineWidth', 2);
hold on
plot(summary.Timepoint, summary.Ataxin3a_long_15Q_GGC, 'Color', Colors{5},
    'LineWidth', 2);
plot(summary.Timepoint, summary.Ataxin3a_short_15Q_GGA, 'Color', Colors{4},
    'LineWidth', 2);
plot(summary.Timepoint, summary.Assay_Buffer, 'Color', Colors{8}, 'LineWidth', 2);
plot(summary.Timepoint, summary.GST, 'Color', Colors{3}, 'LineWidth', 2);
plot(summary.Timepoint, summary.USP2Core, 'Color', Colors{6}, 'LineWidth', 2);
legend('Ataxin3c 15Q GG', 'Ataxin3a long 15Q GGC', 'Ataxin3a short 15Q GGA', ...
'Assay Buffer', 'GST', 'USP2Core', 'Location', 'NorthWest');
ylabel('RFU [ ]');
xlabel('Time [min]');
box off
hold off
title('DUB activity of Ataxin-3 Isoforms', 'FontSize', 12, ...
'FontWeight', 'bold');

% Export
saveas(h.figure, datafile(1:end-4), 'fig');
print(gcf,'-depsc', strcat(datafile(1:end-4), '.eps'));

% Create figure with fit
disp('Create figure with fit')
h.figure = figure;
plot(summary.Timepoint, summary.Ataxin3c_15Q_GG, 'Color', Colors{2}, 'LineWidth', 2);
hold on
plot(summary.Timepoint, summary.Ataxin3a_long_15Q_GGC, 'Color', Colors{5},
    'LineWidth', 2);
plot(summary.Timepoint, summary.Ataxin3a_short_15Q_GGA, 'Color', Colors{4},
    'LineWidth', 2);
plot(summary.Timepoint, summary.Assay_Buffer, 'Color', Colors{8}, 'LineWidth', 2);
plot(summary.Timepoint, summary.GST, 'Color', Colors{3}, 'LineWidth', 2);
plot(summary.Timepoint, summary.USP2Core, 'Color', Colors{6}, 'LineWidth', 2);

```

```
% fit lines
p1 = plot(Ataxin3c_fit_line);
set(p1, 'Color',Colors{2}, 'LineWidth', 2); % hLegendEntry, 'IconDisplayStyle', 'off'

p2 = plot(Ataxin3alang_fit_line);
set(p2, 'Color', Colors{5}, 'LineWidth', 2);
p3 = plot(Ataxin3akurz_fit_line);
set(p3, 'Color', Colors{4}, 'LineWidth', 2);

legend('Ataxin3c 15Q GG', 'Ataxin3a long 15Q GGC', ...
'Ataxin3a short 15Q GGA', 'Assay Buffer', 'GST', 'USP2Core', 'Fit 3c', 'Fit long',
    'Fit short', 'Location', 'NorthWest');

% Define axis limits
xlim([0 30]);
ylabel('RFU [ ]');
xlabel('Time [min]');
box off
hold off
title('DUB activity of Ataxin-3 Isoforms', 'FontSize', 12, ...
'FontWeight', 'bold');

% Export
saveas(h.figure, strcat(datafile(1:end-4), '_fit'), 'fig');
print(gcf,'-depsc', strcat(datafile(1:end-4), '_fit', '.eps'));

% Zoomed image of the initial 10 timepoints with fit
disp('Create zoom image')
h.figure = figure;
plot(summary.Timepoint, summary.Ataxin3c_15Q_GG, 'Color', Colors{2}, 'LineWidth', 2);
hold on
plot(summary.Timepoint, summary.Ataxin3a_long_15Q_GGC, 'Color', Colors{5},
    'LineWidth', 2);
plot(summary.Timepoint, summary.Ataxin3a_short_15Q_GGA, 'Color', Colors{4},
    'LineWidth', 2);
plot(summary.Timepoint, summary.Assay_Buffer, 'Color', Colors{8}, 'LineWidth', 2);

% fit lines
p1 = plot(Ataxin3c_fit_line);
set(p1, 'Color',Colors{2}, 'LineWidth', 2) % hLegendEntry, 'IconDisplayStyle', 'off'

p2 = plot(Ataxin3alang_fit_line)
set(p2, 'Color', Colors{5}, 'LineWidth', 2)
p3 = plot(Ataxin3akurz_fit_line)
set(p3, 'Color', Colors{4}, 'LineWidth', 2)

legend('Ataxin3c 15Q GG', 'Ataxin3a long 15Q GGC', ...
'Ataxin3a short 15Q GGA', 'Assay Buffer', 'Fit 3c', 'Fit long', 'Fit short',
    'Location', 'NorthWest')
```

```
205
206 % Define axis limits
207 xlim([0 10])
208 ylabel('RFU [ ]');
209 xlabel('Time [min]');
210 box off
211 hold off
212 title('DUB activity of Ataxin-3 Isoforms', 'FontSize', 12, ...
213 'FontWeight', 'bold')
214
215 % Export
216 saveas(h.figure, strcat(datafile(1:end-4), '_zoom'), 'fig');
217 print(gcf,'-depsc', strcat(datafile(1:end-4), '_zoom', '.eps'));
```

B.2 Interactive plot of ataxin-3 interaction partners

In order to analyze the interaction of ataxin-3 isoforms with other proteins (see 4.1.5, page 4.1.5) an interactive plot was generated using the Python package Bokeh with the code below. This script requires a text file containing the the p-value and differences for the comparisons ataxin-3c/ataxin-3aL, ataxin-3c/ataxin-3aS, ataxin-3aL/ataxin-3aS, the gene, UniprotID, protein and information about the respective group within the comparison plots (stronger interaction with 3c, 3aL, 3aS, not significant or unchanged) for assigning the correct color. The code generates a html-file which can be viewd using a standard webrowser.

```
1  # Import required packages
2  import math
3  import numpy as np
4  import pandas as pd
5  from bokeh.io import show, output_file
6  from bokeh.plotting import figure
7  from bokeh.models.widgets import DataTable, TableColumn, NumberFormatter
8  from bokeh.layouts import row, gridplot, widgetbox
9  from bokeh.models import ColumnDataSource, CDSView, GroupFilter, HoverTool,
       BoxZoomTool, ResetTool, LassoSelectTool, WheelZoomTool, PanTool, SaveTool,
       BoxSelectTool, LassoSelectTool, TapTool, axes, Span
10 from bokeh.core.properties import Enum
11
12 # Load data, define column names and formats
13 MS = np.loadtxt('MS_data.txt', delimiter ='\t', skiprows = 1,
14     dtype={'names': ('pLc', 'dLc', 'pSc', 'dSc', 'pLS', 'dLS', 'Gene',
           'UniprotID', 'Protein', 'argLc', 'argSc', 'argLS'),
15        'formats': ('f4', 'f4', 'f4', 'f4', 'f4', 'f4', 'S50', 'S50', 'S50', 'S2','S2',
              'S2')
16     }
17 )
18
19 # MS_data.txt file contains the p-value and differences for the comparisons of
```

```
    ataxin-3 isoforms as well as the gene, UniprotID, protein and information about
    the respective group (stronger interaction with 3c, 3aL, 3aS, not significant or
    unchanged)

# Create DataFrame and source data
pMS = pd.DataFrame(MS)
source = ColumnDataSource(data=pMS)

# Define output file
output_file("MS-data_final.html", title = 'Interaction of ataxin-3 isoforms')

# Define tools
# Tools for ataxin-3c and ataxin-3aL
# Hover behaviour
hoverLc = HoverTool(tooltips=[
("Uniprot ID", "@UniprotID"),
      ("Gene", "@Gene"),
      ("- log p-value", "@pLc{(0.00)}"),
      ("t-test difference", "@dLc{0.00}")
])

# Available tools
toolsLc = [BoxZoomTool(), ResetTool(), WheelZoomTool(), PanTool(), SaveTool(),
    BoxSelectTool(), LassoSelectTool(), TapTool(), hoverLc]

# Tools for ataxin-3c and ataxin-3aS
# Hover behaviour
hoverSc = HoverTool(tooltips=[
("Uniprot ID", "@UniprotID"),
      ("Gene", "@Gene"),
      ("- log p-value", "@pSc{(0.00)}"),
      ("t-test difference", "@dSc{0.00}")
])

# Available tools
toolsSc = [BoxZoomTool(), ResetTool(), WheelZoomTool(), PanTool(), SaveTool(),
    BoxSelectTool(), LassoSelectTool(), TapTool(), hoverSc]

# Tools for ataxin-3aL and ataxin-3aS
# Hover behaviour
hoverLS = HoverTool(tooltips=[
("Uniprot ID", "@UniprotID"),
      ("Gene", "@Gene"),
      ("- log p-value", "@pLS{(0.00)}"),
      ("t-test difference", "@dLS{0.00}")
])

# Available tools
toolsLS = [BoxZoomTool(), ResetTool(), WheelZoomTool(), PanTool(), SaveTool(),
```

```
    BoxSelectTool(), LassoSelectTool(), TapTool(), hoverLS]

# Define the colormap for the plots
#fcolormap = {'c': '#333333', 'L': '#0073C2', 'S': '#EFC000', 'ns': '#FFFFFF', 'uc':
    '#d0d3d4'}
#lcolormap = {'c': '#333333', 'L': '#0073C2', 'S': '#EFC000', 'ns': '#d0d3d4', 'uc':
    '#d0d3d4'}
#fcolorsLc = [fcolormap[x] for x in pMS['argLc']]
#lcolorsLc = [lcolormap[x] for x in pMS['argLc']]
#fcolorsSc = [fcolormap[x] for x in pMS['argSc']]
#lcolorsSc = [lcolormap[x] for x in pMS['argSc']]
#fcolorsLS = [fcolormap[x] for x in pMS['argLS']]
#lcolorsLS = [lcolormap[x] for x in pMS['argLS']]

# Define grouping of variables
viewLc = {}
argsLc = ['c', 'L', 'uc', 'ns']
for i in argsLc:
viewLc[i] = CDSView(source=source, filters=[GroupFilter(column_name= 'argLc', group=
    i)])

viewSc = {}
argsSc = ['c', 'K', 'uc', 'ns']
for i in argsSc:
viewSc[i] = CDSView(source=source, filters=[GroupFilter(column_name= 'argSc', group=
    i)])

viewLS = {}
argsLS = ['K', 'L', 'uc', 'ns']
for i in argsLS:
 viewLS[i] = CDSView(source=source, filters=[GroupFilter(column_name= 'argLS', group=
     i)])

# Plotting
# General setup for plots
dots = 10
alpha = 1.0
vline = Span(location = 0, dimension = "height", line_color = "gray", line_width=1,
    line_alpha = 0.5, line_dash = 'dashed')
hline = Span(location = -math.log(0.05, 10), dimension = "width", line_color =
    "gray", line_width = 1, line_alpha = 0.5, line_dash = 'dashed')

# Plot the comparison of ataixn-3c and ataxin-3aL
Lc = figure(tools=toolsLc, title="Ataxin-3c vs. ataxin-3aL",
    sizing_mode='scale_both', plot_width=500, plot_height=500,
    x_axis_label='difference', y_axis_label = '-log p-value')
Lc.circle("dLc", "pLc", source = source, size=dots, line_color="#0073C2",
    fill_color="#0073C2", fill_alpha=1.0, legend = "stronger 3aL", view =
    viewLc['L']) #, hover_color="firebrick")
```

```
Lc.circle("dLc", "pLc", source = source, size=dots, line_color="#333333",
    fill_color="#333333", fill_alpha=1.0, legend = "stronger 3c", view = viewLc['c'])
    #, hover_color="firebrick")
Lc.circle("dLc", "pLc", source = source, size=dots, line_color="#d0d3d4",
    fill_color="#FFFFFF", fill_alpha=1.0, legend = "insignificant", view =
    viewLc['ns']) #, hover_color="firebrick")
Lc.circle("dLc", "pLc", source = source, size=dots, line_color="#d0d3d4",
    fill_color="#d0d3d4", fill_alpha=1.0, legend = "unchanged", view = viewLc['uc'])
    #, hover_color="firebrick")
Lc.circle("dLc", "pLc", source = source, size=dots, fill_color=None, line_color=None,
    hover_color="firebrick") #hover_line_color also possible
Lc.legend.orientation = "horizontal"
Lc.legend.click_policy="hide"
Lc.yaxis.axis_label_text_font_style = "normal"
Lc.xaxis.axis_label_text_font_style = "normal"
Lc.toolbar.active_tap = TapTool()
Lc.renderers.extend([vline, hline])

# Plot the comparison of ataixn-3c and ataxin-3aS
Sc = figure(tools=toolsSc, title="Ataxin-3c vs. ataxin-3aS",
    sizing_mode='scale_both', plot_width=500, plot_height=500,
    x_axis_label='difference', y_axis_label = '-log p-value', x_range = Lc.x_range,
    y_range = Lc.y_range)
Sc.circle("dSc", "pSc", source = source, size=dots, line_color="#EFC000",
    fill_color="#EFC000", fill_alpha=1.0, legend = "stronger 3aS", view =
    viewSc['K']) #, hover_color="firebrick")
Sc.circle("dSc", "pSc", source = source, size=dots, line_color="#333333",
    fill_color="#333333", fill_alpha=1.0, legend = "stronger 3c", view = viewSc['c'])
    #, hover_color="firebrick")
Sc.circle("dSc", "pSc", source = source, size=dots, line_color="#d0d3d4",
    fill_color="#FFFFFF", fill_alpha=1.0, legend = "insignificant", view =
    viewSc['ns']) #, hover_color="firebrick")
Sc.circle("dSc", "pSc", source = source, size=dots, line_color="#d0d3d4",
    fill_color="#d0d3d4", fill_alpha=1.0, legend = "unchanged", view = viewSc['uc'])
    #, hover_color="firebrick")
Sc.circle("dSc", "pSc", source = source, size=dots, fill_color=None, line_color=None,
    hover_color="firebrick")
Sc.legend.orientation = "horizontal"
Sc.legend.click_policy="hide"
Sc.yaxis.axis_label_text_font_style = "normal"
Sc.xaxis.axis_label_text_font_style = "normal"
Sc.toolbar.active_tap = TapTool()
Sc.renderers.extend([vline, hline])

# Plot the comparison of ataixn-3aL and ataxin-3aS
LS = figure(tools=toolsLS, title="Ataxin-3aL vs. ataxin-3aS",
    sizing_mode='scale_both', plot_width=500, plot_height=500,
    x_axis_label='difference', y_axis_label = '-log p-value', x_range = Lc.x_range,
    y_range = Lc.y_range)
```

```
LS.circle("dLS", "pLS", source = source, size=dots, line_color="#EFC000",
    fill_color="#EFC000", fill_alpha=1.0, legend = "stronger 3aS", view =
    viewLS['K']) #, hover_color="firebrick")
LS.circle("dLS", "pLS", source = source, size=dots, line_color="#0073C2",
    fill_color="#0073C2", fill_alpha=1.0, legend = "stronger 3aL", view =
    viewLS['L']) #, hover_color="firebrick")
LS.circle("dLS", "pLS", source = source, size=dots, line_color="#d0d3d4",
    fill_color="#FFFFFF", fill_alpha=1.0, legend = "insignificant", view =
    viewLS['ns']) #, hover_color="firebrick")
LS.circle("dLS", "pLS", source = source, size=dots, line_color="#d0d3d4",
    fill_color="#d0d3d4", fill_alpha=1.0, legend = "unchanged", view = viewLS['uc'])
    #, hover_color="firebrick")
LS.circle("dLS", "pLS", source = source, size=dots, fill_color=None, line_color=None,
    hover_color="firebrick")
LS.legend.orientation = "horizontal"
LS.legend.click_policy="hide"
LS.yaxis.axis_label_text_font_style = "normal"
LS.xaxis.axis_label_text_font_style = "normal"
LS.toolbar.active_tap = TapTool()
LS.renderers.extend([vline, hline])

# Create a Data Table below plots
columns = [
TableColumn(field="Gene", title="gene"),
TableColumn(field="UniprotID", title="Uniprot ID"),
TableColumn(field="Protein", title="Protein"),
TableColumn(field="pLc", title="-log p-value (3c vs. 3aL)", formatter =
    NumberFormatter(format = '0.000')),
TableColumn(field="dLc", title="t-test difference (3c vs. 3aL)", formatter =
    NumberFormatter(format = '0.000')),
TableColumn(field="pSc", title="-log p-value (3c vs. 3aS)", formatter =
    NumberFormatter(format = '0.000')),
TableColumn(field="dSc", title="t-test difference (3c vs. 3aS)", formatter =
    NumberFormatter(format = '0.000')),
TableColumn(field="pLS", title="-log p-value (3aL vs. 3aS)", formatter =
    NumberFormatter(format = '0.000')),
TableColumn(field="dLS", title="t-test difference (3aL vs. 3aS)", formatter =
    NumberFormatter(format = '0.000'))
]
data_table = DataTable(source=source, columns=columns, width=1720, height=280,
    fit_columns = False, selectable = True, scroll_to_selection = True)

# Set the layout and show the plot
layout = gridplot([[Lc, Sc, LS], [data_table]], merge_tools=True,
    sizing_mode='scale_width') #scale_width
show(layout)
```

B.3 Analysis of aggregate size

This R code was used in order to measure the aggregate size in fluorescence microscopy images (see 4.2.1 Ataxin-3 isoforms show differences in protein aggregation), page 102. Pictures were taken in a way that cells were hardly seen but aggregates were visible and not saturated. Upon start the script asks for a directory containing the pictures as *JPG* files. The script produces pictures with labeled aggregates, a *CSV* file with the picture ID, aggregate ID and aggreagte details as well as a density plot as *PDF*.

```
# Install necessary packages
install.packages("devtools")
install.packages("dlib")
install.packages("magick")
install.packages("svDialogs")
install.packages("ggplot2")
install.packages("ggppubr")
install.packages("plyr")
install.packages("FSA")
install.packages("DescTools")

source("http://bioconductor.org/biocLite.R")
biocLite("EBImage")

# Load necessary packages
library("EBImage"); # Image analysis
library("magick"); # Annotation
library("svDialogs"); # Dialog for choosing the work directory
library("ggplot2"); # Creating graphs
library("ggpubr"); # Combining graphs
library("plyr"); # Applying functions to data.frame
library("FSA") # dunnTest
library("DescTools") # Nemenyitest

# Create function for the analysis
aggregateAreaAnalysis <- function(){

# Select directory with pictures
setwd(dlgDir(default = getwd(), title = "In which directory are the pictures
    stored?")$res);
directory = getwd();
files <- list.files(directory); # Directory needs to just contain the image files

# Define the final data.frame
fts_table <- data.frame(Aggregate.ID = integer(),
area = double(),
perimeter = double(),
radius.mean = double(),
radius.sd = double(),
radius.min = double(),
```

```
radius.max = double(),
labeling = character());

# Apply the analysis for each image in the directory
for(i in 1:length(files)){
filename = strsplit(files[i], split = ".JPG")
(paste("Currently processing file no.", i, filename, sep = " "))
print(paste("Done to", round(100/(length(files)+3)*i, 0), "%", sep = " "))
# +3 for writing files, density and calculation

# Read image
img = readImage(files[i])
display(img, method="browser")

# Calculate background and make thresholding
disc_size = 31
disc = makeBrush(disc_size, "disc")
disc = disc / sum(disc)
offset = 0.04 # Can be varied between 0.03 and 0.05
nuc_bg = filter2(img, disc )
nuc_th = img > nuc_bg + offset
display(nuc_th, all=TRUE)
display(thresh(img, w=15, h=15, offset=0.05), all=TRUE )

# Peroform watershed and set colormode for color picture to color and export color
    picture
tol = 1
ext = 1
nmask = watershed(distmap(nuc_th), tol, ext)
nmaskl = colorLabels(nmask)
colorMode(nmaskl) = Color
display(nmaskl, all=TRUE, title = "Objects")
writeImage(nmaskl, files = paste(filename, "_object", ".jpeg", sep = "") ,type =
    "jpeg", quality = 100)

# Calculate features and export them
fts = computeFeatures.shape(nmask);
pos = computeFeatures.moment(nmask);

# Remove spots smaller than 10 pixels // fts[,1] ist s.area // fts[,2] ist s.perimeter
size_limit = fts[,2] >= 10
fts = fts[size_limit, ]
pos = pos[size_limit, ]

# Create table with data
img_name <- replicate(dim(fts)[1], filename[[1]]);
agg_id <- c(1:dim(fts)[1]);

fts <- data.frame(agg_id, fts, img_name);
```

```
fts_table <- rbind(fts_table, fts);

# Add annotation
annot_img <- image_read(paste(filename, "_object", ".jpeg", sep = ""))
for(j in 1:dim(pos)[1]){
annot_img <- image_annotate(annot_img, paste(j), size = 15, color = "white", location
    = paste("+", pos[j,1], "+", pos[j,2], sep = ""))
} # End of "j" for loop
image_write(annot_img, paste(filename, "_annotated", ".jpeg", sep = ""))

} # End of "i" for loop

# Write table with data
print("Creating the data table.");
print(paste("Done to", round(100/(length(files)+3)*(i+1), 0), "%", sep = " "))
fts_table_name <- tail(strsplit(directory, split = "[/]")[[1]], n = 1)
write.csv(fts_table, file = paste(fts_table_name, ".csv", sep = ""));

# Calculate density function, means and deviantions for s.area and s.perimeter
print("Calculating means and density.");
print(paste("Done to", round(100/(length(files)+3)*(i+2), 0), "%", sep = " "))
area_mean <- mean(fts_table$s.area)
area_sd <- sd(fts_table$s.area)
area_median <- median(fts_table$s.area)
area_mad <- mad(fts_table$s.area)
perimeter_mean <- mean(fts_table$s.perimeter)
perimeter_sd <- sd(fts_table$s.perimeter)
perimeter_median <- median(fts_table$s.perimeter)
perimeter_mad <- mad(fts_table$s.perimeter)
statistics <- data.frame(area_mean, area_sd, area_median, area_mad, perimeter_mean,
    perimeter_sd, perimeter_median, perimter_mad)
write.csv(statistics, file = paste(fts_table_name, "_statistics", ".csv", sep = ""));

# Create density plot
print("Creating density plot.");
print(paste("Done to", round(100/(length(files)+3)*(i+3), 0), "%", sep = " "))
area_density <- ggplot(fts_table, aes(s.area)) +
geom_density(colour = "black") +
theme_bw() +
theme(axis.title.x=element_blank(),
axis.text.x=element_blank(),
axis.ticks.x=element_blank()) +
ylab("Density [ ]")

# Export density plot
ggexport(area_density, filename = paste(filename, "_density", ".pdf", sep = ""),
    width = 20, height = 20, units = "cm", dpi = 300)
print("Finished");
}
```